



Proceedings

ICSET-23

ISBN-978- 969-23733-0-2



U.S.-Pakistan Center for Advanced Studies in **Energy**,
University Of Engineering & Technology Peshawar



*Proceedings of the 5th International Conference on Sustainable
Energy Technologies (ICSET 2023) Peshawar, Pakistan
14-15 December 2023*



5th International Conference on Sustainable Energy Technologies (ICSET 2023)



ICSET-23

Proceedings of 5th International Conference on Sustainable Energy
Technologies (ICSET 2023) Peshawar, Pakistan

14-15 December 2023

ISBN: 978-969-23733-0-2

Editor

Engr. Fahad Ullah Zafar



U.S.-Pakistan Center for Advanced Studies in **Energy** (USPCAS-E)
University of Engineering and Technology Peshawar

Forward

With great pleasure, I present the Proceedings for the 2023 International Conference on Sustainable Energy Technologies (ICSET-23) as the Conference Chair, which is the fifth of the series of international conferences on Sustainable Energy held at the U.S.-Pakistan Center for Advanced Studies in Energy (USPCAS-E), UET Peshawar. The primary goal of this flagship event is to establish a unique platform that brings together a diverse community comprising scholars, researchers, academicians, as well as personnel from the government and industry. The conference focus on alternative and renewable energy, thermal and electrical power systems, energy policy and planning, with emphases on innovation and development of the energy sector of the country, through exchange of information and ideas between different stakeholders. This not only holds promise for significant impacts on the business and social environment but also invites active participation from government bodies and relevant industries. By engaging governmental stakeholders and industry experts, the conference aims to foster collaboration, address challenges, and propel advancements in sustainable energy solutions, thus contributing to an environmentally friendly future.

The 5th International Conference on Sustainable Energy Technologies (ICSET-23) encompasses a range of topics related to sustainable energy, addressing key thematic areas including Renewable Energy Technologies, Energy, Environment, and Policy, Thermal Energy Systems, Electrical Energy Systems, and Energy Materials. USPCAS-E UET Peshawar is one of its kind center in the province, dedicated not only to research in the energy sector but also actively engaged in addressing energy-related issues in the country. Having successfully organized this event for the past four years, USPCAS-E has well-equipped infrastructure, a capable administration, highly qualified faculty, and motivated students, all contributing to the ongoing success of this international conference.

On behalf of the Conference Committees, I extend my appreciation to the Keynote Speakers, Session Chairs, and all the authors for their valuable contributions, which played a pivotal role in the success of this two-day event. Special thanks are due to the technical and financial sponsors for their support in making this event possible. Lastly, I would like to express gratitude to all my colleagues on various committees for their dedicated hard work in the successful organization of this International Conference.

Dr. Adnan Daud Khan
Conference Chair

Contents

Preface

Conference Committees

Sponsors Profiles

About the Conference

Keynote Speakers

Publications Section

Preface

Over the last two decades, Pakistan has encountered significant challenges in its energy sector, adversely impacting not only the lifestyle of its citizens but also the nation's economy and overall development. Despite possessing ample renewable energy resources, Pakistan has struggled to harness and effectively deploying these resources to meet the energy demands of its population.

In this regard, U.S.-Pakistan Center for Advanced Studies in **Energy** (USPCAS-E) UET Peshawar hosted 5th International Conference on Sustainable Energy Technologies (ICSET-23) on December 14-15, 2023 at USPCAS-E, Hayatabad Peshawar. This conferences not only brought together the key stakeholders from the government, academia and industry on a unified platform but also offered a forum for national and international energy professionals to contribute their insights to address issues in this sector as well as for the researchers to disseminate their research findings. More than 200 participants comprising of energy professionals and researchers, students and faculty members were gathered at this single venue providing their insights in thematic areas related to Renewable Energy Technologies, Energy, Environment and Policy, Thermal Energy Systems, Electrical Energy Systems, and Energy Materials. Beyond the exchange of research insights, the conference served as a comprehensive platform for knowledge sharing, identification of industry-relevant problems, fostering networking opportunities, and laying the groundwork for future collaborations.

The conference was augmented by the presence of distinguished professionals, researchers, and academicians from around the world who delivered keynote talks. The keynote speakers for the conference included Dr. Antonio D' Angola (University of Basilicata, Italy), Dr. Anamitra Pal (Arizona state University, USA), Mr. Pierre Pisterman (Hydropower Plant Nancy, France), Dr Zia Wadud (University of Leeds, UK), Dr. Muhammad Shakeel Ahmad (Kuala Lumpur University of Malaya, Malaysia), Dr. Abdul Sattar Nizami (Government College University, Pakistan), Prof. Dr. Abdullah Yasar (Government College University, Pakistan), Mr. Mian Arif Ali (Revgreen Pakistan), Dr. Muhammad Zahir Iqbal (Ghulam Ishaq Khan Institute of Engineering Sciences and Technology, Pakistan), Mr. Wajid Ali Chatha (National Transmission and Dispatch Company, Pakistan), Dr. Muhammad Tahir (Abdul Wali Khan University, Pakistan), Dr. Abdul Basit (National Transmission and Dispatch Company, Pakistan), and Mr. Muhammad Baber Zaman (Teklinx, Pakistan). In addition to the keynote speakers, researchers from all over Pakistan showcased their work in various thematic areas of the conference. The conference was co-sponsored by Higher Education Commission (HEC) of Pakistan, Pakistan Science Foundation (PSF), Directorate of Science and Technology (DOST) and Center for Building and Industrial Energy Assessments (CIBEA).

The proceedings of the ICSET-23 have been compiled to facilitate broader dissemination to those who might be interested in understanding the challenges and opportunities in Pakistan's energy sector, along with insights into the latest sustainable energy technologies. With our sincerest thanks to all the participants, speakers and of course the sponsors, we hope that these proceedings will be helpful to you.

Engr. Fahad Ullah Zafar
Editor

Dr. Adnan Daud Khan
Conference Chair

Acknowledgements

We would like to thank all the keynote speakers for their time and efforts for preparing and delivering the insightful talks. We also thank University of Engineering and Technology Peshawar for providing every possible support to make this conference a success. We sincerely appreciate the efforts of all those who were involved in the organizing and overseeing activities. Last but not least, we are thankful to Higher Education Commission (HEC) of Pakistan, Pakistan Science Foundation (PSF), Directorate of Science and Technology (DOST), and Center for Industrial and Building Energy Assessments (CIBEA) for their funding. Without their support it would not have been possible to hold such a unique and successful event.

Conference Management & Organizing Committees

Patron in Chief: Prof. Dr. Iftikhar Hussain

Vice Patron in Chief: Prof. Dr. Qaiser Ali

Patron: Prof. Dr. Sahar Noor

Conference Chair: Dr. Adnan Daud Khan

Treasurer UET Peshawar Prof. Dr. Misbahullah

Focal Person Technical: Engr. Fahad Ullah Zafar

Conference Advisory Committee

- Prof. Dr. Sahar Noor
- Prof. Dr. Misbah Ullah
- Dr. Adnan Daud Khan
- Director ORIC
- Director QEC
- Director Media
- Director IT/CMS
- Dr. Tanvir Ahmad (SAARC)
- Dr. Abdul Basit (NTDC)
- Dr. Abu Syed Mahajumi (University of Bedfordshire, UK)
- Dr. Arafat ur Rehman (University of Wolverhampton, UK)
- Dr. Muhammad Imran (NUST)
- Dr. Shakeel Ahmad (University of Malaya, Malaysia)
- Dr. Muhammad Amin (Taibah University, KSA)
- Dr. Immad Ullah (LUMS)
- Dr. Faisal Asfand (University of Huddersfield, UK)
- Dr. Ali Turab Jafry (GIKI)
- Dr. Khurshid Ahmad (UET Peshawar)
- Engr. Fahad Ullah Zafar (UET Peshawar)

Conference Editorial Board

- Dr. Adnan Daud Khan
- Dr. Muhammad Noman
- Engr. Fahad Ullah Zafar

Technical Committee

- Prof. Dr. Sahar Noor (UET Peshawar)
- Dr. Adnan Daud Khan (UET Peshawar)
- Dr. Muhammad Noman (UET Peshawar)
- Dr. Saeed Badshah (IIUI)
- Prof. Dr. Farid Ullah (UET Peshawar)

Organizing Committee

- Dr. Adnan Daud Khan
- Dr. Muhammad Noman
- Dr. Zohaib Ur Rehman



ICSET-23

*Proceedings of the 5th International Conference on Sustainable
Energy Technologies (ICSET 2023) Peshawar, Pakistan
14-15 December 2023*



UET Peshawar

- Dr. Muhammad Hassan
- Dr. Muhammad Arif
- Dr. Amir Naveed
- Dr. Muhammad Aslam
- Dr. Kaleem Ullah
- Engr. Noor Muhammad
- Engr. Atif Sardar
- Engr. Zafar Ullah
- Engr. Fahad Ullah Zafar
- Engr. Muhammad Saad Rehan
- Mr. Muhammad Naif
- Engr. Muhammad Ishaq Khan
- Ms. Haseena
- Mr. Waleed Zafar

Publicity and Publication

- Dr. Muhammad Noman
- Engr. Fahad Ullah Zafar
- Engr. Muhammad Saad Rehan
- Ms. Haseena
- Mr. Muhammad Naif

Registration Committee

- Dr. Zohaib Ur Rehman
- Dr. Noor Muhammad
- Engr. Fahad Ullah Zafar
- Mr. Muhammad Naif

Finance Committee

- Dr. Adnan Daud Khan
- Dr. Muhammad Noman
- Dr. Muhammad Arif
- Mr. Muhammad Naif

Local Arrangement Committee

- Mr. Muhammad Naif
- Dr. Atif Sardar
- Engr. Muhammad Ishaq Khan
- Mr. Waleed Zafar

Website Committee

- Ms. Haseena
- Engr. Muhammad Ishaq Khan
- Mr. Kamran Rasheed

Sponsors Profiles

Higher Education Commission

The Higher Education Commission (HEC) of Pakistan is an independent, autonomous, and constitutionally established institution of primary funding, overseeing, regulating, and accrediting the higher education efforts in Pakistan.

The HEC offers a wide range of programs for Universities, Faculty and Students. Several of HEC programs have supported establishment of laboratories, launching of new academic programs, faculty development and funding and fellowships for research and human resources capacity building.

The Commission in addition to other functions such as providing research funding, generously supports activities of science promotion and dissemination of research.



Pakistan Science Foundation

Pakistan Science Foundation (PSF) is the apex body for promotion and funding of scientific and technological research and science popularization in the country. PSF has two subsidiary organizations i.e. Pakistan Museum of Natural History (PMNH) and Pakistan Scientific and Technological Information Center (PASTIC).

The Foundation functions as a link of PMNH/PASTIC agency for the establishment of comprehensive scientific and technological information dissemination centers, promotion of research in the universities and other institutions, establishment of science centers, museums, promotion of scientific societies, organization of periodical science conferences, exchange of visits of scientists with other countries, prizes and fellowships to individuals engaged in developing processes of consequence to the economy of the country.



Directorate General of Science & Technology (DoST)

The Department of Science & Technology and Information & Technology was created in October 2003 under the National Policy on Science and Technology. In December 2006, the Directorate General of Science and Technology (DoST) was formally established, marking the joining of the startup team, including the





ICSET-23

*Proceedings of the 5th International Conference on Sustainable
Energy Technologies (ICSET 2023) Peshawar, Pakistan
14-15 December 2023*



UET Peshawar

Director, Deputy Director, and Assistant Director, along with initial support staff. Notably, the province of Khyber Pakhtunkhwa (KP) holds the distinction of being the first province to establish a dedicated department for science & technology.

Center for Industrial and Building Energy Assessments (CIBEA)

CIBEA is a successful faculty led spin-off in UET Peshawar, resulted by an HEC funded Technology Development Fund Project. It has invested in state-of-the-art Energy Audit Equipment. CIBEA helps industries save on their energy bills. CIBEA is led by a US Certified Energy Manager (CEM), with over 10 years of experience in Energy Audits.



The qualified team of MSc Electrical and MSc Thermal Engineers has experience in conducting energy audits in Lahore, KP, and Baluchistan. CIBEA has an expert team of consulting engineers who can conduct industrial and building energy audits, conduct carbon footprint studies for the industry and buildings, advice on reducing energy and carbon footprint, help in ISO 50001 implementation, conduct Building Information Modeling (BIM), design low-cost energy-efficient buildings, conduct EDGE certification of buildings and LEED certification of buildings. As a part of its social corporate responsibility activities, CIBEA generously support science and engineering promotion activities.

About the Conference

Conference Objectives

- Develop and further strengthen industry-academia-government linkages to address energy challenges
- Discuss and analyze challenges in Pakistan's energy sector with the scientific community, and policy makers with the aim of addressing the problems
- Disseminate research, and policy achievements and knowledge created by the researchers to the energy professionals
- Provide students and young researchers an opportunity to interact with the energy professionals
- Provide a platform to the energy professionals for future collaborations

Key Thematic Areas

The conference focused on the following thematic areas:

Renewable Energy Technologies

- Artificial Intelligence in Energy
- Biogas and Biomass
- Hydropower Technologies
- Wind Energy
- Hydrogen and Fuel Cells

Energy, Environment and Policy

- Sustainable Development Goals
- Energy Economics and Modelling
- Green Building
- Energy Efficiency
- Energy Policy and governance
- Low Carbon Economy
- Climate Change
- Energy Markets
- Energy for Transportation

Energy Materials

- Materials for Energy Applications
- Nanomaterials and characterization
- Electrochemistry

- Biomaterials
- Batteries and Storage Technology

Thermal Energy Systems

- Thermal Energy Technologies
- Clean Coal Technologies
- Heating, Ventilation and Air-Conditioning
- Solar Thermal Technologies
- Cogeneration
- Computational Fluid Dynamics
- Power plant and Internal Combustion Engine

Electrical Energy Systems

- Smart Grids
- FACTS Technologies
- Emerging Technologies for Electrical Energy Systems
- Control and optimization of Energy Systems
- Electric Transmission and Distribution



ICSET-23

*Proceedings of the 5th International Conference on Sustainable
Energy Technologies (ICSET 2023) Peshawar, Pakistan
14-15 December 2023*



UET Peshawar

Structure of the Conference

The two-day conference was a dynamic forum featuring thirteen (13) Keynote Talks and five (5) technical sessions, each dedicated to one of the conference's thematic areas. Renowned energy professionals and researchers, from both national and international institutions, delivered the Keynote Talks, offering profound insights into the latest developments and challenges within the energy sector.

The technical sessions, a vital component of the conference, provided a platform for researchers from various universities across the country to present their work. Within each technical session, a total of five (5) presenters had the opportunity to showcase their research findings to the audience. The floor was then opened for question and answer session by the moderator for participants and audience.

Research Articles Publications

One of the objectives of ICSET is to serve as a platform for researchers in the field of energy from across the country, providing them with an opportunity to showcase their research and disseminate their findings. This objective is fulfilled by inviting the researchers to submit their manuscripts for the conference, and publishing the research articles in the conference proceedings. For ICSET-23, a total of 85 manuscripts were submitted which underwent comprehensive review process, and after careful evaluation, 46 research articles were deemed of significant quality and merit, making them eligible for publication in the ICSET proceedings.

Keynote Speakers

Dr. Antonio D'Angola, Associate Professor University of Basilicata Italy

Dr. Antonio D'Angola is an Associate Professor at the University of Basilicata. His research activity focuses on the design and investigation of renewable energy systems and solutions. His talk was focused on **Enhancing Photovoltaic (PV) Efficiency and Harnessing Thermal Energy through PVT System Modeling**.

Dr. D'Angola discussed the impact of high temperature on the PV modules' performance and the utilization of modeling techniques for analyzing the PV-Thermal systems. He emphasized on how critical is this issue for a country like Pakistan where high temperatures during the summer season can badly affect the of PV modules' efficiency. The talk highlighted the integration of Photovoltaic-Thermal (PVT) systems, which can generate both electrical and thermal energy. Notably, this approach addresses the challenge of reduced PV efficiency in elevated temperatures by simultaneously providing thermal energy for use and cooling the PV systems.



Dr. Anamitra Pal, Professor Arizona State University, USA



Dr. Anamitra Pal is an Associate Professor at Arizona State University, USA. His research focuses on data analytics and AI applications in power systems, energy modeling in smart grids, and critical infrastructure resilience. His talk was focused on **Big Data Analytics for the Electric Power Grid of the 21st Century**.

Dr. Pal discussed the use of AI and Data Analytics to understand and improve the modern electric power grid. He emphasized using these advanced techniques to analyze large amounts of data generated by the power grid. In the context of the 21st century, characterized by a growing reliance on interconnected and technologically advanced power systems, the significance of employing big data analytics becomes paramount. Such analytics can offer solutions for optimizing grid operations, enhancing reliability, predicting maintenance needs, and ultimately facilitating the transition towards a more efficient and resilient power infrastructure.



ICSET-23



UET Peshawar

Mr. Pierre Pisterman, CEO Hydropower Plant Nancy, France

With a strong educational background in engineering and business administration, Mr. Pierre Pisterman is a visionary leader in the field of hydroelectric power, working as the CEO of Hydropower Plant (HPP) Nancy. Under his leadership, HPP has managed over 200 hydro-electric projects globally, ranging from 100 kW to 15,000 kW, and currently operates more than 500 MW of hydro turbines. His keynote talk centered around **Maintenance of Existing Small Hydro Power Stations, Covering a Spectrum from Light Maintenance to Complete Rehabilitation.**



The presentation included discussions on various technical cases, providing insights into the strategies and procedures involved in ensuring the efficient and reliable operation of the hydro power facilities. The talk aimed to provide a comprehensive understanding of the challenges and solutions associated with sustaining and optimizing small hydro power stations.

Dr. Zia Wadud, Associate Professor University of Leeds, UK



Dr. Zia Wadud is currently an Associate Professor in Transport and Energy at University of Leeds, UK. Prior to his appointment at University of Leeds, he was a Commonwealth Scholar at Imperial College London and held research positions at the University of Cambridge and Massachusetts Institute of Technology. He delivered a talk on **E-ride Hailing, Travel and the Environment: Tales from Developing and Emerging.**

Dr. Zia addressed different transportation challenges in the developing world and how they can be mitigated using the E-ride technologies. Dr. Zia also discussed the environmental aspect of the e-ride hailing focusing on its effect on carbon emissions. Furthermore, he explored the economic implications of adopting such services in emerging countries.

Dr. Muhammad Shakeel Ahmad, Assistant Professor Kuala Lumpur University of Malaya, Malaysia

Dr. Shakeel Ahmad is an Assistant Professor at UM Power Energy Dedicated Advanced Centre (UMPEDAC), University of Malaya, Malaysia, renowned for his academic and research background. With a focus on





ICSET-23

*Proceedings of the 5th International Conference on Sustainable
Energy Technologies (ICSET 2023) Peshawar, Pakistan
14-15 December 2023*



UET Peshawar

hydrogen production, electro-catalysis, combustion applications, and structural materials, Dr. Ahmad has filed patents in the USA and Malaysia. His talk revolved around an interesting topic ***Hydrogen: The Fuel of Future from the Past.***

Dr. Shakeel's addressed the historical applications and evolution of hydrogen as a fuel, and provided valuable insights into the various future applications of hydrogen. He emphasized that hydrogen can be a better alternative of the fossil fuels, which are hazardous to the environment, for use in the automobiles. Thus providing a greener and environmental friendly alternative. He also explored various research and application aspects of hydrogen as an alternative fuel in Pakistan.

Dr. Abdul Sattar Nizami, Associate Professor Government College University, Pakistan



Dr. Abdul-Sattar Nizami, an Associate Professor at Government College (GC) University Lahore, Pakistan, has a vast experience in the field of biofuels. He has a PhD in Sustainable Gaseous Biofuel from the University College Cork, Ireland and has worked at the University of Toronto, Canada as a Postdoctoral Fellow on alternative fuels and life cycle studies. His keynote talk was on ***Energy Sustainability and Recycling: Pathways to a Greener Future.***

Dr. Nizami addressed the pressing need for environmentally conscious practices, he explored the the interconnection between energy sustainability and recycling initiatives. Emphasizing the significance of recycling, he highlighted its impact on both the environment and energy conservation. Furthermore, Dr. Nizami explored the extensive scope of recycling opportunities in Pakistan, discussing how recycling can contribute in improving the country's climatic conditions.

Prof. Dr. Abdullah Yasar, Professor Government College University, Pakistan

Prof. Dr. Abdullah Yasar is Civil engineer and Professer at GC University Lahore, Pakistan, having vast experience in the field of environmental science. His research is focused on sustainable development, wastewater treatment, air pollution control, waste to product & waste to energy systems. Presently he is working and contributing on solutions to the





ICSET-23



UET Peshawar

national challenges and community issues. His keynote talk was focused on **Prices and Crises Scenarios of Pakistan Energy Sector**.

In his talk, Dr. Abdullah provided an in-depth analysis of the complexities regarding the energy pricing structure and shed light on the challenges and issues that the Pakistan energy sector faces. He explored the various factors that influence energy prices and elaborated on how the high prices can be mitigated. He also detailed strategies for addressing and handling the crises within Pakistan's energy sector, outlining ways to reduce or eliminate them. He highlighted the recommended actions that various stakeholders should undertake, which would be beneficial for Pakistan's energy sector and assist in resolving the energy sector issues.

Dr. Muhammad Zahir Iqbal, Associate Professor GIK Institute (GIKI) of Engineering Sciences and Technology, Pakistan



Dr. Muhammad Zahir Iqbal is an accomplished Associate Professor with a distinguished academic background, holding a Post Doctorate from Georgia State University, USA, and Ph.D. degrees from Sejong University, South Korea, and Universitat Politècnica de Catalunya, Spain. His talk focused on **The Future of Energy Storage Technology**.

Dr. Zahir in his talk discussed the forefront of technological advancements, his talk explored the evolving landscape of energy storage technologies. He illuminated on the current state of this field, and shed light on emerging technologies and innovative strategies set to shape the future of energy storage. From cutting-edge research to practical applications, Dr. Zia provided a comprehensive overview of energy storage, emphasizing its crucial role in advancing sustainable energy solutions and addressing the needs of a continually evolving energy landscape.

Dr. Abdul Basit, Manager R&D National Transmission and Dispatch Company (NTDC), Pakistan

Dr. Abdul Basit is a highly experienced and accomplished professional in Electrical Power Systems and Renewable Energy Systems. He is currently serving as the Manager of Research and Development at National Power Control Center under the National Transmission & Dispatch Company (NTDC), Pakistan. Dr. Basit's responsibilities include conducting studies on emerging phenomena, publishing white papers for system operators' future





ICSET-23



UET Peshawar

needs assessment, and engaging with academia and international forums. He presented keynote talk on **Control and Optimization of Energy Systems in the Power Electrical Network of Pakistan**.

Dr. Basit discussed the significance of optimizing the energy systems within the power network, particularly in Pakistan. Going into the details of Pakistan's power network, he explained the strategic management and enhancement of the various components within the power grid that is required to ensure efficient, reliable, and sustainable energy delivery. Furthermore, Dr. Basit emphasized on the importance of a robust and adaptive power infrastructure for the evolving needs of Pakistan's energy landscape.

Dr. Muhammad Tahir, Assistant Professor Abdul Wali Khan University, Pakistan



Dr. Muhammad Tahir, is an Assistant Professor of Physics and Principal Investigator at the Semiconductor Physics & Devices Lab in the Department of Physics, at Abdul Wali Khan University Mardan, Pakistan. He has extensive research experience, including Hybrid Organic- inorganic nanocomposites, Thermoelectric devices, Organic photovoltaics, Thin films growth for electronic and optoelectronic devices, and Spectroscopy of functional materials. His presentation focused on **Potential of Perovskite Tandem Solar Cells**.

Dr. Tahir's talk covered current trends in third-generation photovoltaic technology and the ongoing efforts to commercialize Perovskite solar cells. Regarding tandem solar cells, Dr. Tahir discussed the utilization of Perovskite as the top cells in tandem configurations due to its flexible bandgap. He emphasized that perovskite exhibits compatibility with silicon, CIGS, OPV as well as with other Perovskites. Dr. Tahir specifically highlighted the use of silicon solar cells in tandem with perovskite, due to their superior power conversion efficiency and higher stability. Furthermore, he provided insights into the commercialization prospects of these tandem solar cells, particularly in the context of Pakistan.



ICSET-23



UET Peshawar

*Mr. Wajid Ali Chatha, Manager Regulatory Affairs & Grid Code Compliance
NTDC, Pakistan*

With 14 years of experience in Project Management & Controls, Techno-Commercial Contracts, Stakeholder Management, and Energy Market Analysis, Mr. Wajid Ali Chatha is currently working as Manager Regulatory Affairs & Grid Code Compliance NTDC, Pakistan. He has a diverse career spanning various organizations, including National Power Control Centre (NPCC), China Power Hub Generation Company Ltd, Fatima Energy Limited, Reon Energy Limited, Presson Descon International Limited, and Pak American Fertilizers Limited. His expertise includes ensuring grid code compliance, managing power plant operations, contracts management, and overseeing safety. His talk centered around the **Power Sector: Regulatory Framework & Challenges**.



Mr. Chatha explored the structure of Pakistan's power sector, with a specific focus on electric power regulators and oversight bodies. Investigating the energy flow and value chain of the country's power sector, he provided insights into its operations and economic framework. Additionally, Mr. Chatha addressed the numerous challenges faced by the Pakistan's power sector which include seasonality, energy poverty, line losses, circular debt, infrastructure and energy mix and discussed the strategies in place to tackle these challenges.

Mr. Mian Arif Ali, Chief Executive Officer (CEO) Revgreen, Pakistan



With a 35 years' experience of working in different business sectors, Mr. Mian Arif Ali is the Founder and CEO of Revgreen Pakistan. Mr. Ali has a demonstrated history in the field of renewable energy and environment, specifically specializing in Biogas technology. His expertise span from establishing the large-scale biogas plants, rural energy development, environmental awareness and management, and biowaste recycling. He presented a very interesting and engaging keynote talk on **Biogas Technology in Pakistan-Applications, Benefits & Future**.

Mr. Ali explained how human activities are polluting the environment, leading to climate change, and specifically Pakistan experiencing significant consequences in recent years. He discussed the applications of biogas and highlighted the advantages of adopting it as an alternative energy source. Emphasizing that biogas not only serves as an alternative energy option but also mitigates greenhouse gas emissions and facilitates nutrient



ICSET-23



UET Peshawar

recovery, contributing to the natural nutrient cycle. Additionally, Mr. Ali explored the market opportunities in Pakistan, providing insights into various aspects of biogas plant production and operation in the country. He also addressed the biogas plant's yield corresponding to its size, the amount of fossil fuel it can substitute in mmBTUs, and the economic savings it can generate by the substitution. Furthermore, he discussed the future prospects of using the Biogas in Pakistan highlighting its potential integration with energy storage and the grid system for power production. He also explored how biogas can play a role in mitigating the energy crises by serving as a substitute for natural gas as well as being utilized in power production.

Mr. Muhammad Babar Zaman, TekLinx Lahore, Pakistan

Mr. Babar Zaman has 21 years of experience in the field of electronic design and development. He has been working on development and operation of the Solar Testing Equipment underscoring his commitment to ensuring the quality and functionality of Solar Panels through the development of rigorous testing mechanisms. He is currently working as the Director of Teklinx Pakistan. His talk was focused on ***Business Opportunities and Challenges for Indigenous Manufacturing of PV Reliability Testing Equipment.***

Mr. Babar discussed the importance of reliability analysis for PV modules in his presentation, focusing specifically on its relevance to Pakistan. He elaborated on how reliability analysis can be applied to screen out defective PV modules. Additionally, he emphasized on increasing the PV module testing in Pakistan and provided insights into indigenously developing the PV testing setups within the country. Moreover, Mr. Babar shed light on the market for PV modules testing setups and offered perspective on the technical and financial details, the challenges faced and the supply chain for the manufacturing of setups.



Publications Section

| Paper ID | Paper Title | Page No. |
|------------|---|----------|
| ICSET-2301 | Monitoring and controlling unaccounted-for gas (SNGPL) in Peshawar city of Pakistan | 01 |
| ICSET-2302 | Comparative analysis of heatsink's performance parameters under forced convection | 10 |
| ICSET-2303 | Relating the sustainable development goals with sustainable lean manufacturing and lean six sigma in spinning mills | 18 |
| ICSET-2304 | Enhancing the performance of perovskite solar cell through MoS ₂ interface layer | 33 |
| ICSET-2305 | Socio-economic impacts of micro hydro power (MHP) electrification on the rural community of Pakistan: a case study of 150 kw MHP plant at village Lalkoo (Swat) | 39 |
| ICSET-2306 | Intelligent demand-side management for integrated renewable energy in residential area smart grid: A pathway to sustainable energy use | 53 |
| ICSET-2307 | Design and sustainable fabrication of a PVC wind turbine for clean energy generation | 66 |
| ICSET-2308 | A reconfigurable circular patch antenna embedded with magneto-static responsive structures in multi-layer substrates for mmWave applications | 76 |
| ICSET-2309 | Pyrolysis reactor design and performance assessment for renewable energy production from bay leaves and beech wood | 85 |
| ICSET-2310 | Designing and optimization of on-grid hybrid renewable energy system for both irrigation and electrification of village in Khyber Pakhtunkhwa | 101 |
| ICSET-2311 | Design of a metamaterial broadband solar absorber based on a multilayer hollow flower shaped structure | 112 |
| ICSET-2312 | Case study: Analysing energy use intensity (EUI) for energy efficiency and optimization in an educational building | 120 |
| ICSET-2313 | Physics-Informed Neural Networks For Numerical Solution Of 1D Hyperbolic PDEs | 129 |
| ICSET-2314 | Identification and evaluation of risk assessment in steel manufacturing industry | 137 |
| ICSET-2315 | Dc micro-grid with the sliding mode control: Application of bi-directional buck/boost converter | 149 |
| ICSET-2316 | Portable eco-friendly seed germination system | 166 |
| ICSET-2317 | Estimating lithium-ion battery internal circuit parameters, open circuit voltage and ampere-hour capacity at different temperatures | 180 |
| ICSET-2318 | Climate change impacts on sustainable bioenergy generation in Pakistan | 190 |



ICSET-23

*Proceedings of the 5th International Conference on Sustainable
Energy Technologies (ICSET 2023) Peshawar, Pakistan
14-15 December 2023*



UET Peshawar

| | | |
|------------|--|-----|
| ICSET-2319 | ANFIS based evaluation of the microgrid resilience under multiple factors | 222 |
| ICSET-2320 | Natural gas flow optimization in gas transmission network using pressure profiling & isolation technique | 236 |
| ICSET-2321 | Energy efficient HVAC system selection for an educational building | 246 |
| ICSET-2322 | Gap analysis between academic research and policy making in energy sector of Pakistan | 254 |
| ICSET-2323 | Comparative study of renewable energy resources in rural areas of Khyber Pakhtunkhwa | 266 |
| ICSET-2324 | Integrated evacuated tube collector and heat storage to improve heating efficiency | 279 |
| ICSET-2325 | Pascal polynomial collocation method for inverse heat problem | 258 |
| ICSET-2326 | Techno-economic analysis of Aluminium busbar in low voltage electrical distribution panel | 293 |
| ICSET-2327 | Numerical solution of 1d parabolic PDES with integral boundary condition via Haar wavelets collocation method | 302 |
| ICSET-2328 | Investigations of different configurations of heat sink for thermal management of photovoltaic system via active cooling | 311 |
| ICSET-2329 | Wind turbine failure rate and downtime survey with special reference to Pakistan | 322 |
| ICSET-2330 | Chemical treatment of photovoltaic silicon solar cell through benzene- a step towards recycling | 331 |
| ICSET-2331 | Numerical solution of PDES model using physics informed neural networks | 336 |
| ICSET-2332 | Frequency control of micro grid through wind power and electric vehicles | 344 |
| ICSET-2333 | Synthesis of gold nanoparticles for solar cell applications | 354 |
| ICSET-2334 | Investigating the effect of high-temperature annealing on the optical properties of silicon Nano particles film at rear side of solar cell | 363 |
| ICSET-2335 | Thermal efficiency assessment, benchmarking and improvement measures for gas fired captive power plants in Pakistan | 372 |
| ICSET-2336 | A combined approach of computational fluid dynamics and experimental study on air jet interaction | 380 |
| ICSET-2337 | Analysis on homer software for energy modelling and forecasting: A case study | 394 |
| ICSET-2338 | Sustainable wheels in motion: Eco-transit, a review of three-wheeler reverse trike fun utility vehicle innovation | 408 |
| ICSET-2339 | Aerodynamic evaluation of NACA airfoils for wind turbines: insights from Qblade simulations | 415 |
| ICSET-2340 | Integration of electric-power grid with electric vehicles and renewable energy sources in Peshawar university for a sustainable campus | 424 |



ICSET-23

*Proceedings of the 5th International Conference on Sustainable
Energy Technologies (ICSET 2023) Peshawar, Pakistan
14-15 December 2023*



UET Peshawar

| | | |
|------------|--|-----|
| ICSET-2341 | Modelling of solid-state transformer for offshore wind turbine and high voltage DC transmission | 439 |
| ICSET-2342 | Design, analysis and fabrication of long endurance hybrid delta wing UAV | 446 |
| ICSET-2343 | Production improvement and enhancement in a manufacturing unit by implementing overall equipment effectiveness | 457 |
| ICSET-2344 | Techno-economic analysis of large-scale solar power plant in Peshawar | 468 |
| ICSET-2345 | Implementation/impact of solar energy system on a power grid system | 479 |
| ICSET-2346 | Machine learning based scheduling and load forecasting of energy management system for prosumer | 488 |
| ICSET-2347 | Life Cycle Assessment and Economics Sustainability of Renewable Energy Resources | 501 |



Paper ID: ICSET-2301

MONITORING AND CONTROLLING UNACCOUNTED-FOR GAS (SNGPL) IN PESHAWAR CITY OF PAKISTAN

Sehrish Shafiq Taj^{1,*}, Dr. Arif Khattak¹, and Muhammad Waqas Hanif²

¹US-Pakistan Center for Advanced Studies in Energy, University of Engineering and Technology Peshawar,
Pakistan

²University of Engineering and Technology Taxila, Punjab, Pakistan

**Corresponding author*

Email: ailia.taj@gmail.com

ABSTRACT

Monitoring unaccounted for gas (UFG) in the energy sector of Pakistan is challenging due to the sudden increase in demand and price of natural gas. Therefore, the aim of this research work is to analyze the technical and non-technical aspects of UFG in the Sui Norther Gas Pipeline (SNGPL) system of Peshawar City, Pakistan. Quantitative and qualitative methods have been used to analyze the data. Surveys and interviews have been conducted with consumers and staff at SNGPL Peshawar City to collect the data. The results indicated that measurement errors and low gas pressure make a significant contribution to the UFG. Furthermore, it has been suggested that proactive strategies are needed to address UFG systematically and sustainably in order to minimize losses and ensure the viability of Peshawar City.

Keywords: Unaccounted for Gas, Sui Norther Gas Pipeline, measurement errors, low gas pressure, quantitative and qualitative methods.

INTRODUCTION

Natural gas is a primary source of energy in the world; it is used for power generation, transportation, cooking and heating in homes. It is widely available around the world (found with or without oil reserves) and produces fewer greenhouse gas emissions as compared to other natural resources like oil, coal, etc [1]. In Pakistan, natural gas contributes approximately 46% of the primary energy mix due to Pakistan's heavy dependence on fossil fuels [2]. Pakistan is an energy-deficit country, and mostly energy resources are imported to eke out its energy needs. The natural gas in Pakistan is used for power generation, fertilizer manufacturing, transport, industries, cooking, and heating purposes [3].

Natural gas transmission and distribution network of Pakistan is highly developed due to Sui Northern Gas Pipeline Limited (SNGPL) and Sui Southern Gas Company Limited (SSGC). These two organizations are responsible for regulating the network, covering Punjab, Khyber Pakhtunkhwa, Karachi, Interior Sindh, and Baluchistan. SNGPL has approximately 6.1 million customers and an extensive transmission network. [4, 5]. Furthermore, SNGPL has 16 regional offices in Punjab and Khyber Pakhtunkhwa, each with a dedicated Unaccounted-for Gas (UFG) Management Department. They are responsible to reduce UFG in the Peshawar region, with 2018 having the highest percentage and volume [6]. UFG is the difference between metered gas injected into transmission networks and gas measured at the consumer's end [7]. Technical UFG are gas



ICSET-23



UET Peshawar

losses also known as contributing factors that normally occur in any system. These losses can be reduced through some technical maintenance or calculation etc. [8]. There are many numbers of technical loss in Peshawar City which are affecting both customers as well as the transmission and distribution of natural gas by SNGPL. On the other hand, non-technical unaccounted for gas are such losses that cannot be detected by the naked eye, but they cause loss in the system that can only be identified and reduced by looking them under the magnifying glass. Such losses are hard to identify and cause more problems in system than technical UFG [9].

However, researchers implemented the comprehensive strategies for UFG reduction in order to achieve the reliable and efficient natural gas supply in the Peshawar region [1, 4, 10, 11]. However, they face challenges to eliminate due to the involvement of several factors in natural gas transportation, especially in mitigating unaccounted-for gas (UFG) losses [12]. Fraser et al. concluded that mismanagement and inadequate policies are major problems to eliminate these losses [13]. Masood et al. reported that increases in Unaccounted for Gas for the OGDCL is due to the inefficient frameworks for price determination that prompting the government to seek World Bank assistance [4]. Furthermore, they concluded that gas theft, instability, minimum billing concerns, leakages, measurement errors, and sales patterns are major challenges that OGRA faced in Peshawar region. Therefore, optimal management and utilization of these resources have not been completely achieved. Additionally, UFG losses within transmission and distribution systems posed notable financial impacts for utilities, prompting apprehensions about revenue and operational efficiency.

It has been concluded from the compressive literature review that there is still gaped to study the technical and non-technical aspects of unaccounted for Gas in the Peshawar region. The conducting this study plays a significant role to resolve this crucial issue to achieve the sustainable growth in natural gas sector of Pakistan. Therefore, the aim of this research work is to analysis the technical and non-technical aspects of UFG in Sui Norther Gas Pipeline (SNGPL) system of Peshawar City, Pakistan. Furthermore, quantitative, and qualitative methods have been used to complete this research work. The questionnaire has been distributed to the customers and interview conducted to achieve the required data. It is also worthily mentioned that Mixed methods approach assists to achieve the goals of both qualitative and Quantitative methods [12].

RESEARCH METHODOLOGY

Mixed methodologies consisting of quantitative and qualitative approaches have been selected to perform the analysis. In order to develop the questionnaire, the data available on the OGRA and SNGPL has been analyzed. In this questionnaire, 11 questions have been asked about the technical aspects of the UFG, and 3 questions have been asked about the non-technical aspects of the UFG. After that, a questionnaire was developed and distributed to the employees, consumers, and staff of the SNGPL office located in Peshawar, Pakistan, in order to collect quantitative data. However, the response rate is observed as 80 percent of these questionnaires because 240 participants responded and filled them out of 300. In terms of qualitative aspects, only five employees from the OGRA and SNGPL agreed to the interview and suggested improvements. Furthermore, interviews have been conducted to collect qualitative data. Statistical Package for Social Science (SPSS) has been used to evaluate and analyze the statistical data and draw tables and graphs for each response, respectively. The flow diagram of the research methodology that was adopted in this research work is shown in Figure 1.



Figure 1: Research Methodology

RESULT AND DISCUSSION

The research examines Unaccounted Gas (UFG) levels in Peshawar City, focusing on the Sui Northern Gas Pipeline Limited (SNGPL) consumer base. It uses SPSS software analysis, surveys, interviews, and secondary data to analyze responses from over 200 customers and SNGPL Peshawar Office employees. The findings will inform discussions, recommendations, and strategies to combat UFG, improve gas supply system efficiency, and ensure better energy distribution in Peshawar City.

Technical Aspects of UFG

The questionnaires related to technical aspects of UFS is discussed in this section.

Customer Experience and Complaints

A survey found that 55.1% of customers experienced gas leakages, indicating a significant issue in the city as shown in figure 2. Customers mainly report leakages to the company for resolution, and around 127 customers have made complaints to the SNGPL Peshawar Office, suggesting that those who experience leaks are proactive in reporting them as shown in figure 3.

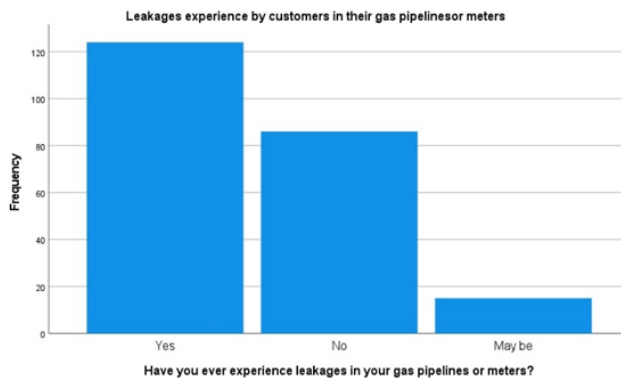


Figure 3: Leakages experience by customers

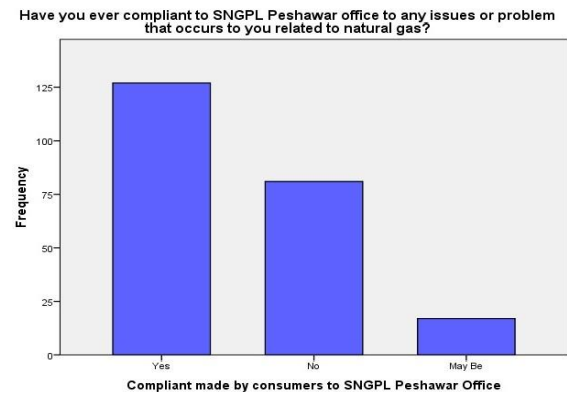


Figure 2: Compliant made by customers

Among the customers who lodged complaints, only 47 received a response from SNGPL, while 123 complaints went unanswered, highlighting a gap in the complaint management system as shown in figure 4.

Experts suggest implementing programs to address leakage problems, both above and underground. A survey showed that 183 out of 235 participants agreed that regular checking, monitoring, and pipe

replacement programs are effective, highlighting the need for regulatory commitment and company management involvement as shown in figure 5.

Infrastructure Development Impact

Peshawar's BRT projects have caused damage to the natural gas distribution network, causing unaccounted gas losses. A survey found that 148 respondents agreed that gas pipelines were damaged during BRT development, while 20 disagreed and 57 were uncertain about the occurrence as shown in figure 6.



Figure 4: Response of customers

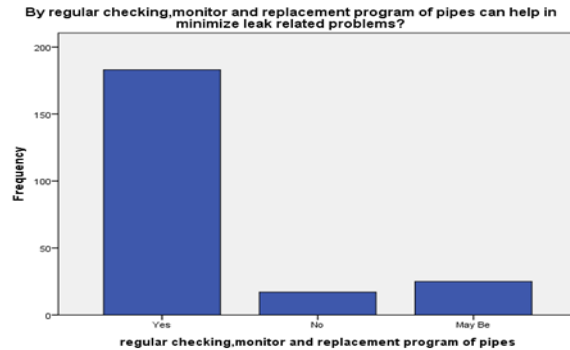


Figure 5: Regular checking and replacement program

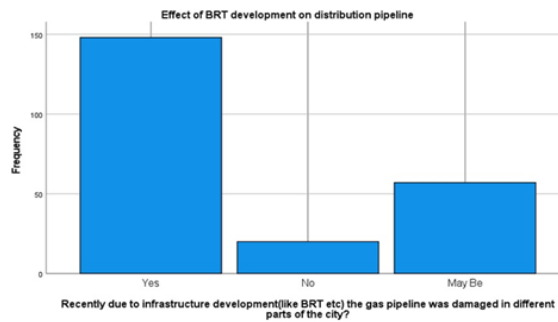


Figure 6: Recent Development

Third Party Damage

Gas leaks challenge customer experiences, highlighting areas for improvement in detection, resolution, and prevention strategies. To mitigate third-party damages in the future, the consensus is that parties involved in development projects should negotiate and communicate before initiating any work. This proactive approach aims to prevent accidental damage. A large majority (196 participants) agreed with this suggestion, while 10 disagreed and 19 were uncertain about its effectiveness as shown in figure 7.

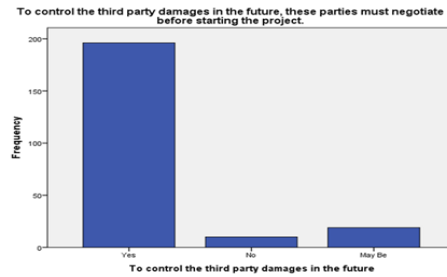


Figure 7: Control third party damages

Penalty System

Implementing a penalty system for parties that fail to cooperate or negotiate before starting a project could be a viable solution. Out of 24 SNGPL employees, 20 agreed that a penalty system should be in place, while 1 disagreed, and 3 were neutral on the matters as shown in figure 8.

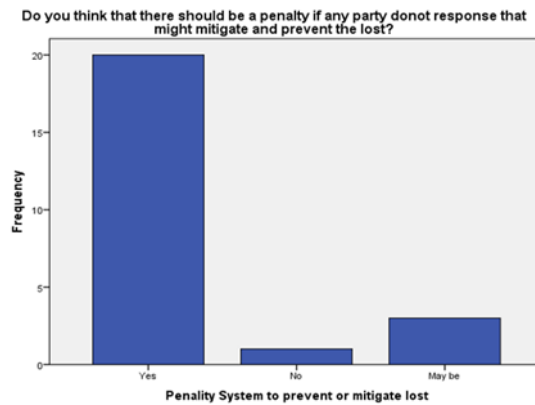


Figure 8: Penalty System

Training for Third-Party Employee

To minimize losses resulting from gas leaks during development when company representatives cannot promptly respond, third-party employees could be trained to calculate gas losses. Among SNGPL employees, 19 agreed with this suggestion, 2 disagreed, and 3 were neutral as shown in figure 9. Among customers, 182 agreed, 2 disagreed, and 40 were neutral on providing training to third-party employees as shown in figure 10.

Proactive measures

Proactive measures are crucial to preventing gas leaks and unaccounted losses from third-party damages during infrastructure development. The interview conducted with the employees of SNGPL suggested that SNGPL and third-party entities should engage in negotiations, implement a penalty system, and provide training to enhance the gas network's integrity. Drawing on lessons from other countries can guide Pakistan's policy development[14]. Accurate gas flow measurement is crucial for billing accuracy and operational efficiency. Errors can occur from temperature and pressure variations, as well as aging meters. Different meters, including diaphragm, rotary, turbine, and orifice, are used to measure gas flow [15]. Ensuring meter

accuracy within regulatory standards minimizes unaccounted-for-gas (UFG) [16]. Sui Northern Gas Pipeline Limited (SNGPL) has a meter replacement policy to maintain accurate billing and operational efficiency. The policy specifies replacement periods based on the type of connection such as industrial, commercial and special domestic [17]. Customers were surveyed to assess the implementation of the meter replacement policy. Table 1 in the appendix section indicates the age of customers meters compared to the replacement periods specified in the policy. Observed that out of 225 meters, 20 meters have exceeded their replacement period, potentially leading to inaccurate billing and UFG.

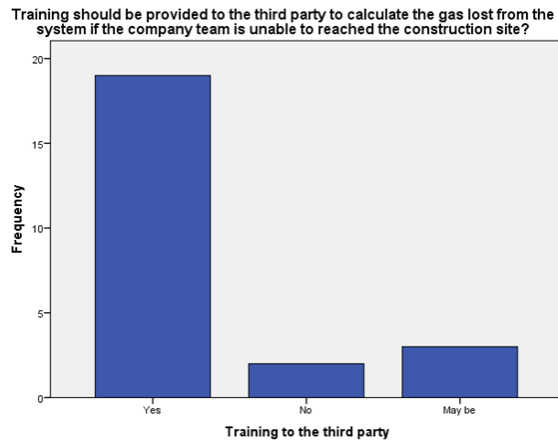


Figure 9: Training for third party

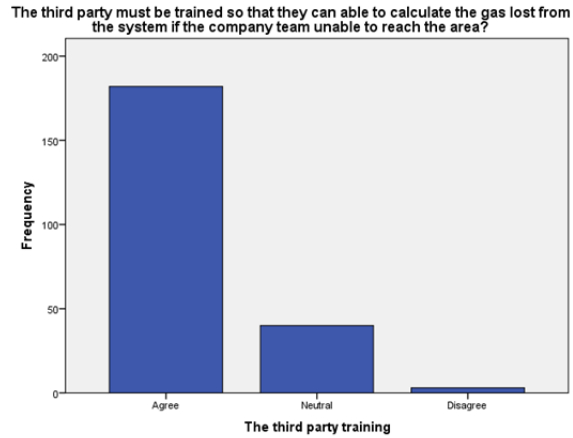


Figure 10: Responses of employees

Metering Achievement

SNGPL Peshawar Office provided information about the level of metering achieved in Peshawar city. Figure 4.13 shows that SNGPL Peshawar has achieved between 85% and 100% metering coverage in the city, indicating a relatively high level of meter installation and measurement accuracy.



Figure 11: Metering Achieved by SNGPL Peshawar

Non-technical UFG

In this section, analysis of responses related to the Non-technical UFG has been discussed.

Gas Theft

Gas theft significantly contributes to gas distribution system losses, resulting in higher Unaccounted-For-Gas (UFG) levels. Peshawar City faces a major issue in suburban areas, prompting investigations into its causes and potential solutions. According to the SNGPL Peshawar Office, gas theft is a notable problem involving both domestic and non-consumers. The areas most affected by gas theft are the suburbs of Peshawar City. An assessment of the percentage of gas theft in Peshawar revealed that it falls in 20% to 40% as shown in figure 12. Gas theft is influenced by economic conditions, infrastructure development, and the pandemic, leading to increased reliance on methods like tampering with meters and illegal connections. Customers and employees believe these factors drive more individuals to engage in these criminal activities as shown in figure 13.

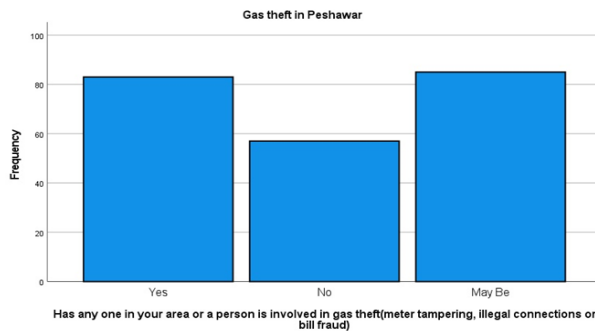


Figure 13: Number of percentages of gas theft

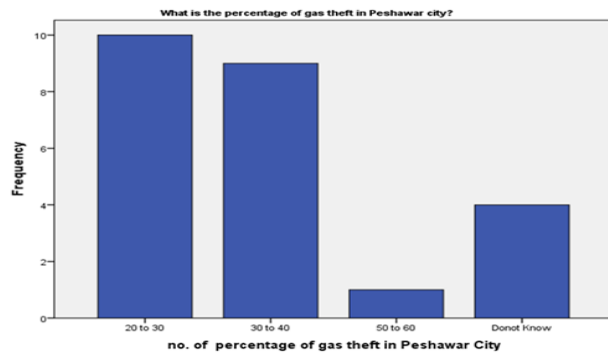


Figure 12: Number of thefts according to Customers

Addressing Employee Involvement

Addressing employee involvement in gas theft is crucial to maintaining the integrity of the gas distribution system. Establishing policies and laws to hold employees accountable and create a transparent, ethical work environment is essential as shown in figure 14. Customers and employees support creating laws or policies to hold employees accountable for gas theft or negligence in their duties.

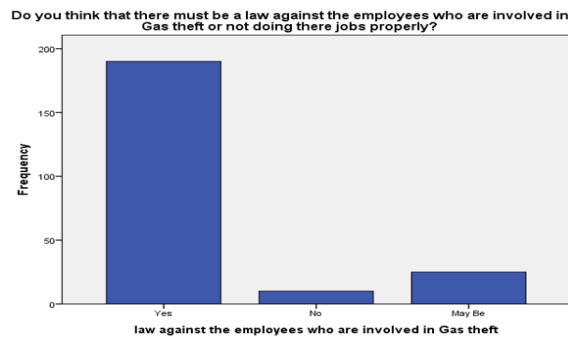


Figure 14: Law against employees against gas theft

CONCLUSION

It has been concluded that gas theft is a complex issue with various factors. Addressing it requires preventive measures, public awareness campaigns, enforcement efforts, and organizational accountability. SNGPL and



ICSET-23



UET Peshawar

authorities can reduce theft, minimize UFG, and ensure efficient natural gas distribution by implementing comprehensive strategies. Furthermore, 183 out of 235 participants agreed that regular checking, monitoring, and pipe replacement programs are effective, highlighting the need for regulatory commitment and company management involvement. It has been observed that measurement errors and low gas pressure are significant UFG contributors in Peshawar city of Pakistan. Despite regulatory measures, UFG detection relies on customer complaints. Proactive strategies are needed to address UFG systematically and sustainably, minimizing losses and ensuring the sector's viability.

ACKNOWLEDGMENT

I am grateful to staff of US Pakistan Center for Advanced Studies in Energy at University of Engineering and Technology Peshawar and Unites States Agency for International Development (USAID) for their assistance and guidance to carry out this research work.

REFERENCES

- [1] Bakht, K., et al., *LNG import contract in the perspective of associated technical and managerial challenges for the distribution companies of Pakistan*. International Journal of Advanced Computer Science and Applications, 2016. **7**(6).
- [2] Mir, K.A., P. Purohit, and S. Mehmood, *Sectoral assessment of greenhouse gas emissions in Pakistan*. Environmental Science and pollution research, 2017. **24**: p. 27345-27355.
- [3] Costello, K.W., *Lost and unaccounted-for gas: Challenges for public utility regulators*. Utilities Policy, 2014. **29**: p. 17-24.
- [4] Masood, A., *Pakistan's gas crisis due to gas theft & unaccounted for gas (UFG)*. International Journal of Renewable Energy Technology Research, 2013. **2**(2): p. 53-58.
- [5] Shafiq, M., et al., *Monitoring and controlling of unaccounted for gas (UFG) in distribution networks: A case study of Sui Northern Gas Pipelines Limited Pakistan*. IFAC-PapersOnLine, 2018. **51**(11): p. 253-258.
- [6] Grubert, E.A. and A.R. Brandt, *Three considerations for modeling natural gas system methane emissions in life cycle assessment*. Journal of Cleaner Production, 2019. **222**: p. 760-767.
- [7] Stephenson, T., J.E. Valle, and X. Riera-Palou, *Modeling the relative GHG emissions of conventional and shale gas production*. Environmental science & technology, 2011. **45**(24): p. 10757-10764.
- [8] Webb, R., *Lost but not forgotten: The hidden environmental costs of compensating pipelines for natural gas losses*. KBH Energy Center Research Paper, 2015(2015-04).
- [9] Balcombe, P., et al., *The natural gas supply chain: the importance of methane and carbon dioxide emissions*. ACS Sustainable Chemistry & Engineering, 2017. **5**(1): p. 3-20.
- [10] Kanshio, S. and S.M. Tahir. *Allocation of Processed Natural Gas Streams Under a Gas Tolling Arrangement*. in *SPE Nigeria Annual International Conference and Exhibition*. 2020. SPE.
- [11] Ranjah, Z.U., *Enforcing Foreign Arbitral Awards in Pakistan: Orient Power Company (Private) Limited v Sui Northern Gas Pipelines Limited PLD 2019 Lahore 607*. LUMS LJ, 2020. **7**: p. 189.
- [12] Eyisi, D., *The usefulness of qualitative and quantitative approaches and methods in researching problem-solving ability in science education curriculum*. Journal of education and practice, 2016. **7**(15): p. 91-100.
- [13] Fraser, J.M., *Lessons from the independent private power experience in Pakistan*. 2005: World Bank Group, Energy and Mining Sector Board.



ICSET-23

Proceedings of the 5th International Conference on Sustainable
Energy Technologies (ICSET 2023) Peshawar, Pakistan
14-15 December 2023



UET Peshawar

- [14] Arif, M., *Future of LNG in Pakistan*. Oil and Gas and Energy Law Intelligence, 2017. **15**: p. 4-5.
- [15] Mubin, S. and G. Mubin, *Risk analysis for construction and operation of gas pipeline projects in Pakistan*. Pakistan Journal of Engineering and Applied Sciences, 2008.
- [16] Qureshi, A.B., *Evolving LNG/RLNG Regime in Pakistan and the National Energy Security*. Policy Perspectives, 2018. **15**(3): p. 119-138.
- [17] Soltanisarvestani, A., A. Safavi, and M. Rahimi, *The Detection of Unaccounted for Gas in Residential Natural Gas Customers Using Particle Swarm Optimization-based Neural Networks*. Energy Sources, Part B: Economics, Planning, and Policy, 2023. **18**(1): p. 2154412.

APPENDIX A

Table 1: Questions related to age of meter

| Status of your connection | How old is meter of customers | | | | | | | |
|---------------------------|--------------------------------|--------------|--------------|------------------|-------------------|--------------------------|----------------|-------|
| | New (6 months to 1 year) | 2 to 4 years | 5 to 7 years | 8 to 10 years | 11 to 15 years | More than 15 years | Do not Know | Other |
| | | | | | | | | |
| Domestic | 2 | 76 | 40 | 33 | 16 | 20 | 28 | 0 |
| Special Domestic | 0 | 0 | 10 | 0 | 0 | 0 | 0 | 0 |
| Commercial | 0 | 0 | 0 | 0 | 0 | 0 | 0 | 0 |
| Industrial | 0 | 0 | 0 | 0 | 0 | 0 | 0 | 0 |

Paper ID: ICSET-2302

COMPARATIVE ANALYSIS OF HEAT SINK'S PERFORMANCE PARAMETERS UNDER FORCED CONVECTION

Umair Ahmad Khan *, Hamid Ullah, Ahmad Nawaz

Department of Mechanical Engineering, University of Engineering & Technology, Peshawar, Pakistan

**Corresponding author*

Email: umair.ahmad@uetpeshawar.edu.pk

ABSTRACT

Implementing heatsinks under forced convection have been the go-to methodology for cooling down electronic components like Central Processing Units. To ensure that the Central Processing Units consistently perform at their peak capabilities, it is imperative that their temperature does not rise to extreme levels. The cooling capability of a heatsink depends on various design parameters where fin profile and heatsink material play the most crucial role. Therefore, it is essential to comparatively analyse various configurations of these parameters to develop effective heatsink geometry and material capable of providing best possible cooling performance. Using CFD simulations with the use of ANSYS Fluent software, various configurations of aforementioned parameters were comparatively analysed in forced convection manner under the influence of 80 CFM airflow speed. For the analyses, a heatsink containing 15 fins each of 3 mm width and 65 mm height was used. A total of 6 fin profile and 8 most commonly available materials were examined. After careful analysis, it is determined that rectangular plate fins offer best cooling performance in terms of fin profile. Among the material options considered, Silicon Carbide exhibited the most effective cooling, yielding a processor's temperature as low as 98.11°C, followed by Silver at 100.25 °C and Copper at 102.094 °C.

KEYWORDS: Heatsink, Heatsink Materials, Forced Convection, Fin Profile

INTRODUCTION

Due to progress in the electronics sector, addressing the heat dissipation from electronic devices has emerged as a crucial concern in recent times. Over the past few years, significant effort have been dedicated to creating affordable cooling solutions that deliver optimal cooling efficiency [1]. The rise of cloud computing has brought about a requirement for computers with robust computing capabilities that can operate continuously in server and data centre environments. To ensure that computer's Central Processing Units (CPU) can sustain peak performance over extended periods, effective ventilation and cooling are essential. Without adequate cooling mechanisms, the performance of CPUs would degrade due to escalating temperatures. Thus, ensuring proper CPU ventilation and cooling holds utmost significance. The cause of the increased heat generation in CPU is due to exponentially increasing transistor count in an individual CPU for maximizing their computing performance. For instance, the CPU in first consumer personal computer, the Intel 8088 had 2900 transistors, which has risen to on average 4 billion transistors per CPU in recent times [2].



Various means of cooling the CPU to ensure temperature stays within safe limits have been proposed and implemented including air-cooled heatsinks, heat pipes and cold water cooling to nitrogen cooling [3]. Where air-cooled heatsink employing forced convection method of heat transfer have been determined to be the best option both in terms of effective cooling performance as well as cost and usability for general users. Air cooling methodology employs a heatsink that extracts the generated heat from the CPU and dissipates it into ambient environment under the influence of a fan blowing air over it, thus prohibiting the generated heat to elevate CPU temperature. The key component of such a CPU cooler is its heatsink, whose heat dissipation ability depends on various design parameters, most notably fin profile and material of the heatsink. Therefore, understanding the efficiency of various configurations in terms of heatsink's material and fin profiles is of paramount importance.

In the context of material selection for heatsinks, Aluminum and Copper have been the preferred choices for quite some time. Nonetheless, researchers have also examined the potential of alternative materials by analysing their conjugate heat transfer capability. Silver has been found to exhibit an exceptionally efficient heat transfer rate. Unfortunately, its elevated cost renders it impractical for widespread consumer use [4]. Other novel materials like Copper-Graphite composites have been analysed as well for heatsink materials and the results have been promising but because of their novelty, they have very high cost and are not appropriate to be used by general consumers [5]. Because of high costs and affordability, Aluminium and Copper have been the main choice of materials for the heatsinks. Conjugate heat transfer ability of certain basic fin profiles has been examined using CFD tools as well [4]. However, further detailed examination of more fin designs is required to develop sufficient heatsinks for CPUs of high computing performance and hence, high heat generation.

Convection is the method of heat transfer responsible for moving heat from a solid heatsink to the surrounding fluid air. The quantity of heat transferred through convection is governed by Newton's Law of Cooling (1), whereas conductive heat transfer is governed by Fourier's law of heat transfer (2).

$$Q = k.A(\Delta T) \quad (1)$$

$$Q = h.A(\Delta T) \quad (2)$$

Where Q is the amount of heat transferred, k and h are conductive and convective heat transfer coefficient, A is surface area through which heat transfer is occurring. ΔT is temperature difference between two bodies.

The aim of this research is to determine the best configurations of the aforementioned heatsink design parameters by implementing the numerical method of computational fluid dynamics (CFD). With that goal in mind, the heat transfer capability under forced convection of 6 fin profiles and 8 materials is analysed comparatively against a CPU generating 380 watts of heat.

RESEARCH METHODOLOGY

Comparative analyses were performed utilizing ANSYS Fluent 2021 R1, encompassing examinations of 6 distinct fin profiles and 8 different heatsink materials.

Reynolds-averaged formulation of Navier-Stokes equations (RANS) is implemented for the computation of flow velocity and pattern. RANS equation is given as follows:

$$\frac{\partial(\rho U)}{\partial t} + \nabla \cdot (\rho U U) = -\nabla p + \nabla \cdot [\mu(\nabla U + (\nabla U)^T)] + \rho F - \nabla \cdot \left(\frac{2}{3} \mu(\nabla \cdot U) \right) - \nabla \cdot (\rho \overline{U'U'}) \quad (3)$$

The Reynold stresses were evaluated using standard k-epsilon turbulent eddy viscosity model. The continuity equation for the coolant which in this case is air can be given as follows:

$$\nabla \cdot \mathbf{u} = 0 \quad (4)$$

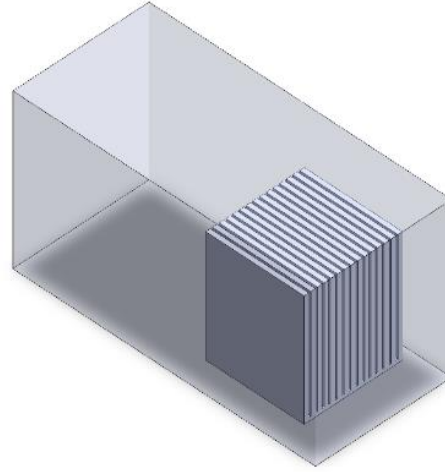


Figure 15: Heatsink inside Analysis Fluid Domain

Each simulation was run for a total of 1000 iterations. In most cases, convergence was achieved before reaching this iteration limit, with convergence factors set at "0.0001" for continuity and velocity equations and "10⁻⁹" for the energy equations involved in heat transfer calculations.

To investigate the influence of mesh density on the final results, three different mesh densities were initially created, all utilizing second-order tetrahedral meshes. The element size was kept relatively smaller in regions where the interaction between the heatsink and the surrounding air occurred, particularly in close proximity to the heatsink.

The analysis focused on a heatsink featuring 15 fins, each with a width of 3 mm, length of 75 mm and height of 65 mm. Initially the analysis was conducted using these three distinct mesh densities to understand the effect of mesh density on the results. The results were found to converge after mesh density of average 3.3 million elements and therefore, every individual analysis was conducted with this mesh density. Further details regarding these mesh densities are outlined in Table 1:

Table 1 Mesh Density Comparison

| Mesh Type | Number of Elements | CPU Temperature | Analysis Time |
|-----------|--------------------|-----------------|---------------|
| Course | 1,292,798 | 118.652 | 20 min 10 sec |
| Medium | 2,263,990 | 119.925 | 27 min 17 sec |
| Fine | 3,390,790 | 120.367 | 35 min 40 sec |

The analyses were carried out using a PC with "Intel (R) Core (TM) i5-4690 CPU @ 3.90 GHz with 4 cores ". The heatsink had to confine to constraints, both in terms of available space inside the Desktop PC Case and reasonable airflow speed. These design constraints given in Table 2 also acted as boundary conditions for the CFD simulations.

Table 2 Heatsink Design Parameters

| Parameter | Value |
|---------------------------|--------------------------------|
| Heatsink size (L x W x H) | 75mm x 75mm x 75mm |
| Fan Size (L x W x H) | 20mm x 90mm x 90mm |
| CPU Size (L x W x H) | 37.5 mm x 37mm x 5 mm |
| Airflow Speed | 80 CFM (Cubic Feet per Minute) |
| Heat Generation from CPU | 380 watts |
| Ambient Temperature | 25 °C |

RESULTS & DISCUSSION

Fin Profiles

A total of 6 fin profiles and configurations were subjected to a conjugate heat transfer simulation using ANSYS Fluent.

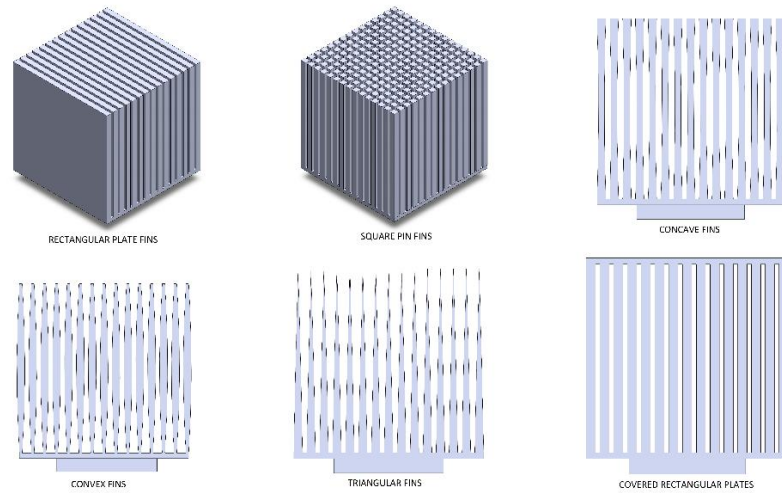


Figure 16: Fin Geometries

These analyses were performed on an Aluminum heatsink equipped with 15 fins for each profile. The outcomes for the chosen profiles are presented in Table 3.

Table 3 CPU Temperatures for Fin Profiles

| Fin Profile | CPU Temperature (°C) |
|----------------------------|----------------------|
| Rectangular Plates | 120.367 |
| Square Pin Fins | 138.264 |
| Concave Fins | 120.695 |
| Convex Fins | 133.854 |
| Triangular Plate Fins | 146.615 |
| Covered Rectangular Plates | 119.133 |

As seen in the table, the optimal fin profile is a rectangular plate yielding temperature as low as 120.367 °C. Concave fins are only slightly behind rectangular plate fins with 120.695 °C.

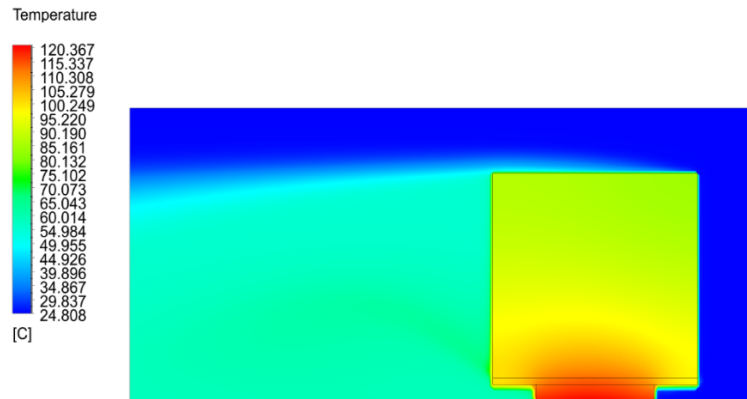


Figure 17: Temperature Contours of Rectangular Plate Fins

Moreover, covering the fins at top is determined to provide further improvement in cooling performance. In case of rectangular plate fins, providing a covering at the top resulted in decrease of temperature from 120.367 °C to 119.133 °C. This can be attributed to the additional surface area provided by the top covering through which heat dissipation can occur.

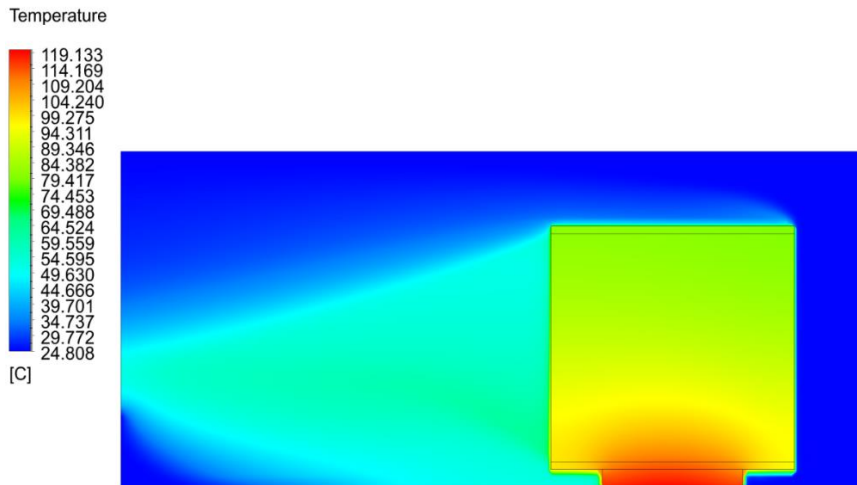


Figure 18: Temperature Contours for Covered Rectangular Plate Fins

Square pin fins were analyzed with a heatsink of total 225 square fins (15 x 15), each of 3mm to the outcome of 138.264 °C.

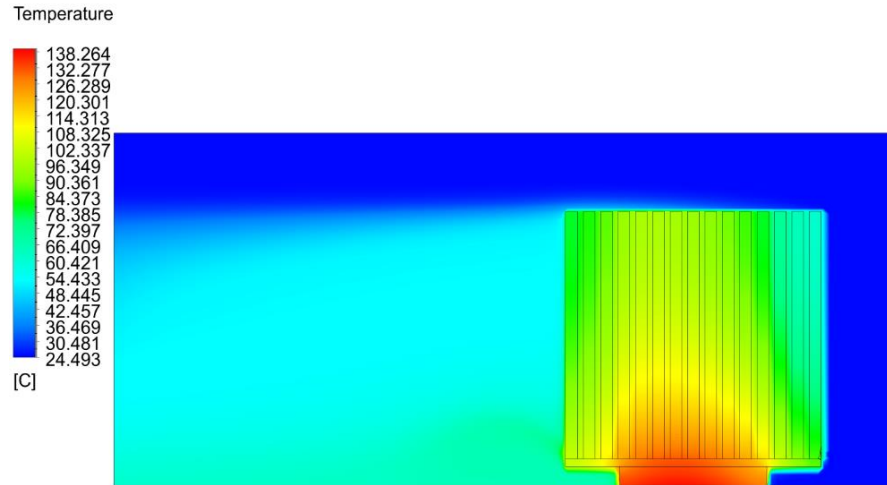


Figure 19: Temperature Contours for Square Pin Fins

Heatsink Materials

A total of 8 materials were analysed for heatsink. The assessment of heatsink materials extended beyond cooling performance, encompassing material cost as well. This aspect is crucial when determining the optimal material for the heatsink. Material analysis was carried out using a simple heatsink with 15 covered rectangular plate fins. The details of CPU temperatures are for various materials are shown in Table 4:

Table 4 CPU Temperatures for Heatsink Materials

| Material | CPU Temperatures (°C) | Material cost per Kg (USD) | Heatsink Cost (USD) |
|-----------------|-----------------------|----------------------------|---------------------|
| Aluminium | 119.133 | 2.40 | 1.36 |
| Copper | 102.094 | 8.22 | 14.80 |
| Silver | 100.25 | 729.5 | 1623.80 |
| Nickel | 159.778 | 26.93 | 46.3204 |
| Iron | 170.024 | 0.08 | 0.12 |
| Magnesium | 129.441 | 2.26 | 0.77 |
| Tungsten | 124.814 | 25.52 | 98.09 |
| Silicon Carbide | 98.11 | 36 | 23.40 |

As indicated in Table 4, the most favourable CPU temperature is achieved when utilizing silicon carbide, reaching as low as 98.11°C. The second-best performer is silver, with a temperature of 100.25°C, followed by copper at 102.094°C. Using Silver as the choice of material for the heatsink is not recommended due to its extremely high cost.

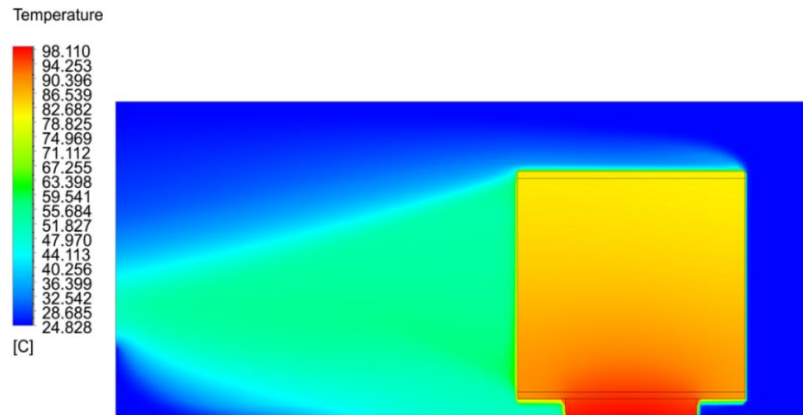


Figure 20: Temperature Contours for Silicon Carbide Heatsink

As mentioned previously, the covered rectangular configuration of fin profiles provides the best cooling performance. A heatsink with these fin profiles made of Silicon Carbide proved to be the best combination of fin profiles and heatsink materials in terms of cooling performance. In terms of the material cost, Silicon Carbide is comparatively an expensive choice. Therefore, when considering for both cost and optimum cooling performance, Copper heatsinks appear to be the most suitable option of obtaining the temperatures of 102.094 °C, which is only slightly behind the cooling performance of Silicon Carbide with 36 % lower cost.

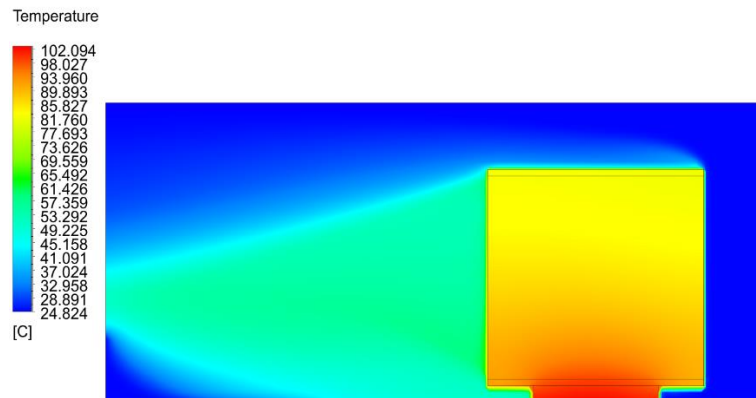


Figure 21: Temperature Contours for Copper Heatsink

CONCLUSION

Computational Fluid Dynamics (CFD) presents a robust and versatile framework for the purpose of designing heatsinks that can effectively cater to a wide range of cooling requirements. In this particular research investigation, CFD methodology was harnessed to discern the most optimal heatsink configuration with respect to temperature regulation for electronic components, such as the central processing unit (CPU). This encompassed an in-depth analysis of various heatsink materials and the selection of appropriate fin geometries. Among the different fin profiles evaluated, it was found that rectangular plate fins exhibited exceptional cooling performance, thereby positioning them as the preferred choice. Furthermore, the



ICSET-23



UET Peshawar

incorporation of a top cover over the fins was demonstrated to significantly enhance the cooling efficiency across all the fin profiles under consideration. In the realm of heatsink materials, Silicon Carbide emerged as the standout option, offering best cooling efficiency. However, it is noteworthy that copper, while slightly trailing behind Silicon Carbide in terms of cooling performance, provides a significantly more budget-friendly option. In contrast, silver exhibited good cooling performance but was ultimately deemed impractical due to its extremely high cost, rendering it an unviable choice as a heatsink material. In future research, it would be beneficial to explore additional heatsink design parameters, such as the number of fins and the configuration of their placement. These investigations could potentially unveil a broader array of possibilities for enhancing the cooling performance of heatsinks.

REFERENCES

- [1] A. Moradikazerouni, M. Afrand, J. Alsarraf, O. Mahian, S. Wongwises, and M. Tran, “Comparison of the effect of five different entrance channel shapes of a micro-channel heat sink in forced convection with application to cooling a supercomputer circuit board,” *Appl. Therm. Eng.*, vol. 150, Mar. 2019, doi: 10.1016/j.applthermaleng.2019.01.051.
- [2] S. K. Moore and D. Schneider, “The State of the Transistor: In 75 years, it’s become tiny, mighty, ubiquitous, and just plain weird,” *IEEE Spectr.*, vol. 59, no. 12, pp. 30–31, Dec. 2022, doi: 10.1109/MSPEC.2022.9976480.
- [3] A. Habibi Khalaj and S. K. Halgamuge, “A Review on efficient thermal management of air- and liquid-cooled data centers: From chip to the cooling system,” *Appl. Energy*, vol. 205, no. C, pp. 1165–1188, 2017.
- [4] H. Kepekci and A. Asma, “Comparative Analysis Of Heat Sink Performance Using Different,” *Am. J. Eng. Appl. Sci.*, vol. 9, pp. 204–210, Apr. 2020.
- [5] S. Lee, S. Son, J. Kim, J. Yesuraj, K. Kim, and S.-H. Rhi, “Heat conduction and thermal expansion of copper–graphite composite as a heat sink,” *Int. J. Energy Res.*, vol. 46, no. 8, pp. 10907–10918, 2022, doi: 10.1002/er.7891.

Paper ID: ICSET-2303

RELATING THE SUSTAINABLE DEVELOPMENT GOALS WITH SUSTAINABLE LEAN MANUFACTURING AND LEAN SIX SIGMA IN SPINNING MILLS

Muhammad Akram*, Rehman Akhtar, Muhammad Touseef Rahim
Industrial Engineering Department, University of Engineering & Technology, Peshawar 25000, Pakistan

**Corresponding author*
Email: akramkhan0310@gmail.com

ABSTRACT

Pakistan is the one of the largest exporter of fiber goods in Asia. It is the 6th largest producer and 3rd largest consumer of cotton. In manufacturing sector, 46% is from textile sector. The role of textile industries in the growth of Pakistan GDP is highly important as it provides employment to about 45% of the total labour force. It means that densely populated country like Pakistan is highly dependent on textile sectors. Now it is much crucial to get more revenue from this sector. For this purpose, the production line's efficiency and breakdowns should be optimized as much as possible. Nowadays majority of industries are moving towards green manufacturing with the application of lean manufacturing tools, because of major environmental concerns, and customer's policies. This technique not only help in reducing ecological impact but also helps to save overall production cost by reducing waste and efficiently usage of resources. The lean manufacturing tools, used in this research are Total Productive Maintenance (TPM), Kaizen, and Autonomous maintenance which contribute to achieve major Sustainable Development Goals (SDGs), by enhancing the Overall Equipment Efficiency (OEE), eliminating waste, and encouraging Eco-friendly actions. This study enhanced the OEE by 11.01% which reduced the breakdown of machines by 24%, also elaborated the approaches through which Sustainable Lean Manufacturing and Lean Six Sigma helps to achieve SDG8, SDG9, SDG12, and SDG 13.

INTRODUCTION

Sustainability is of utmost importance for business practices these days [1], as attaining SDGs will help human beings to live a better life, make their environment pleasant, and leads to economic prosperity [2]. Therefore, companies are attempting in order to improve their footprints and enhance their understanding about Sustainable Development Goals [3]. In 2016, United Nation's proposed the agenda of Sustainable Development Goals (SDGs), with 17 SDGs to be achieved by the end of 2030 [4]. This agenda demonstrated the major objectives of social, economic, and environmental development. Moreover, it is the responsibility of everyone to contribute towards these goals, including public, companies, government, and civil societies [5]. Although it was criticized and considered quite expensive and potentially inconsistent especially between economic and environmental SDG [6]. On the other hand, textile industries are also criticized for their over consumption of resources, large amount of waste generation, and a negative impact on the environment [7], because especially, apparel industries consumes significant amount of water, energy and other natural resources, and contributes towards significant amount of waste generation [8]. Various researches recorded that around 92M tons of waste was generated by textile sector in 2014, and it is will



ICSET-23



UET Peshawar

gradually increase by 60% every year from 2015 till 2030 [9], out of which a very least amount of waste is recycled & reused, and a considerable amount ended up into landfills [10]. Therefore, such business started focusing on Eco-friendly actions to control climate change [11], including small and medium enterprises (SMEs) [12]. Thus, Sustainable Lean Manufacturing and Lean Six Sigma are well known approaches which contribute towards sustainability by increasing the efficiency of the processes and waste reduction, respectively. It also optimizes inventory, resource consumptions and reduces their overall impact on the environment. Therefore, this lean manufacturing terminology has been modified to Sustainable Lean manufacturing, because it ensures to properly address the social, economic, and environmental aspect of manufacturing process. This lean manufacturing terminology has been modified to Sustainable Lean manufacturing, because it ensures to properly address the social, economic, and environmental aspect of manufacturing process [13]. In this sense, some of Lean manufacturing techniques, such as TPM (Total productive maintenance), & OEE (Overall Equipment Effectiveness) are used to align overall equipment & manufacturing setup with environmental responsibility, which also promotes environment friendly method for production processes [14]. Because, TPM technique has been used here to increase the maintenance performance and to decrease the down time. The main aim of the total productive maintenance is to increase the (OEE) [15] while, the sole purpose of Autonomous Maintenance is to provide the operators with more responsibilities and allow them to take charge of simple task like measuring pressure tension, sensor regulation, lubrication and cleaning. This should be prepared to notice any changes and trouble shoot them quickly [16].

In this study, it is shown that some major SDGs can be achieved by Sustainable Lean Manufacturing and Lean Six Sigma implementations. Here, increasing the efficiency of machine resulted in high productivity. On the other hand, waste proportion is also reduced, which decreased rework percentage and optimized resources thus, contributing towards sustainable practices.

METHODOLOGY

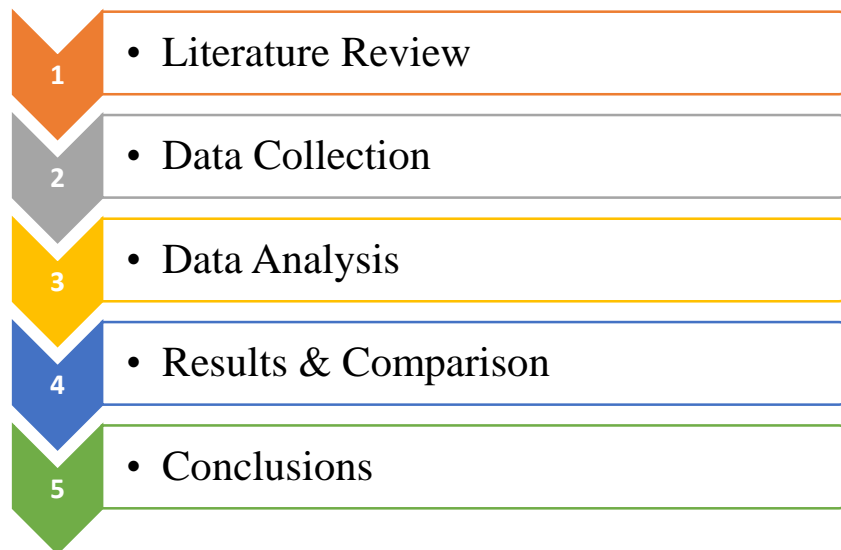


Figure 1: Research Methodology

The methodology used to complete this research has been elaborated in this section, which is divided into 5 steps, as shown in figure [Error! Reference source not found.](#) 1. First of all, literature is reviewed for this study, which is a very effective and important step before starting any research. Then, we selected the industry and the problem it was facing by inspecting all departments to find out which department is acting as bottleneck station. To find out what losses are occurring in the Bottleneck station, we used six losses lean tool. The six losses are idling and minor stoppage, yield loss, equipment failure, setup and adjustment, reduced speed and process defect. We inspected and found that the major defects were occurring in the ring frame section also taking help from literature. The data of ring section output per shift, defect per shift, operating time of 48 machine per shift, down time of each machine per shift, actual cycle time, actual processing time, and rate of quality was collected for 25 days, which was analysed and compared with the standards. Initially, primary & secondary data were collected by visiting the ring frame section, and from their records, respectively. Now, to analyse this data first we computed the time of each activity, frequency of each activity, calculation of OEE before TPM implementation. Then we made Pareto chart figure 2, to search out the major losses activities. Similarly, we made the fishbone diagram to search out the causes of these losses 3. After this, the Sustainable Lean Manufacturing technique was chosen to control these problems. When we applied the first two pillars of TPM i.e Autonomous maintenance and Kaizen, we again calculated output of the ring section per shift, defect per shift, product, operating speed rate, net operating rate, performance efficiency, and Overall Equipment Efficiency. The next step is data analysis in which, the operating time of machine per shift, down time of each machine per shift, actual cycle time, actual processing time, rate of quality product, operating speed rate, net operating rate, performance efficiency, and Overall Equipment Efficiency was analysed after tools implementation.

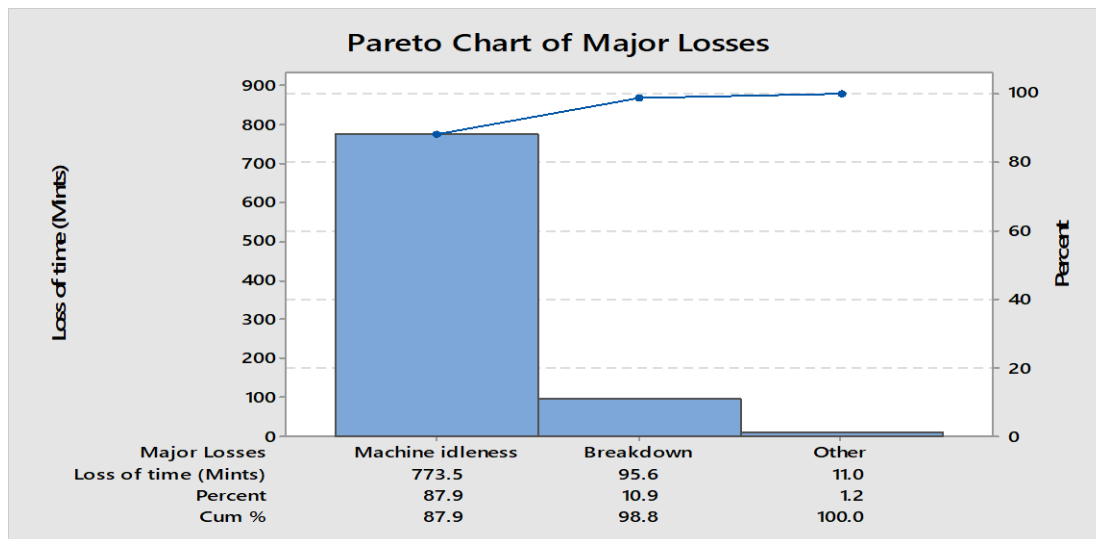


Figure 2: Pareto Analysis for Major Losses Identification

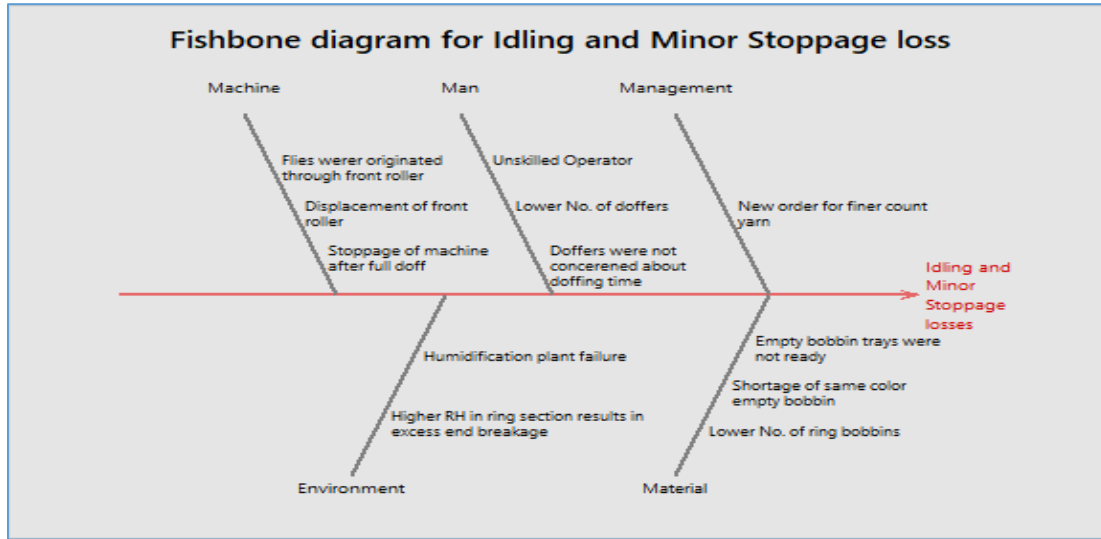


Figure 3: Fishbone Diagram for Idling and Minor Stoppage Losses

Calculation of Overall Equipment Efficiency

The goal of OEE is to calculate the Overall performance of a section in order to know whether the efficiency can be improved or not. OEE can be calculated by multiplying availability of equipment of, performance efficiency of the process and rate of quality product where

- Availability identifies the problem cause by the downtime losses.
- Performance indicates the losses cause by speed reduction and
- Quality Indicates the scrap and rework losses.

Availability

The availability is the ratio between the amount of time the machine is actually producing and the amount of time it was planned to produce. The availability [17] can be calculated as;

$$Availability = \frac{Actual\ operating\ time}{Required\ Availability} * 100 \quad (1)$$

OR

$$Availability = \frac{Required\ Availability - Downtime}{Required\ Availability} * 100 \quad (2)$$

So, Actual operating time = Required availability – Downtime

Actual operating = Planned operating time – unplanned downtime

The down time means the actual time for which the machines is stopped due to repair. This time is also known as Breakdown time. The output of this formula gives the true availability of the equipment.



The performance rate is defined as the ideal cycle time to produce the item multiplied by the output of the equipment and then divided by the actual cycle time. The formula [17] can be expressed as;

$$\text{Performance Rate} = \frac{\text{Total Numbered Produced}}{\text{Expected Production}} * 100 \quad (3)$$

Expected production [18] can be calculated as

$$\text{Expected Production} = \frac{\text{Actual Operating Time}}{\text{Theoretical Cycle Time}} \quad (4)$$

So,

$$\text{Performance Rate} = \frac{\text{Theoretical Cycle time} * \text{Units produced}}{\text{Theoretical Cycle time} * \text{Units produced}} * 100 \quad (5)$$

The theoretical cycle time or the production output will be in the unit of production, like parts per hour and the output will be the total output in the given time period interval.

Calculation of Cycle Time [17]:

Number of spindle per frame : 1048 Spindles
Doffing time for tensile yarn : 110 Minutes

$$\text{Idle cycle time} = \frac{\text{Ideal Cycle Time}}{\text{Number of Spindles}} \quad (6)$$

$$\text{Actual Cycle Time} = \frac{\text{Actual Doffing Time}}{\text{Number of Running Spindles}} \quad (7)$$

Similarly, the rate of quality product [17] can be calculated as;

$$\text{Quality Rate} = \frac{\text{Output Production} - \text{Defective Parts}}{\text{Output Production}} * 100 \quad (8)$$

Finally, results are compared before and after Sustainable Lean Manufacturing Implementations, and research is concluded along some recommendations at the end.

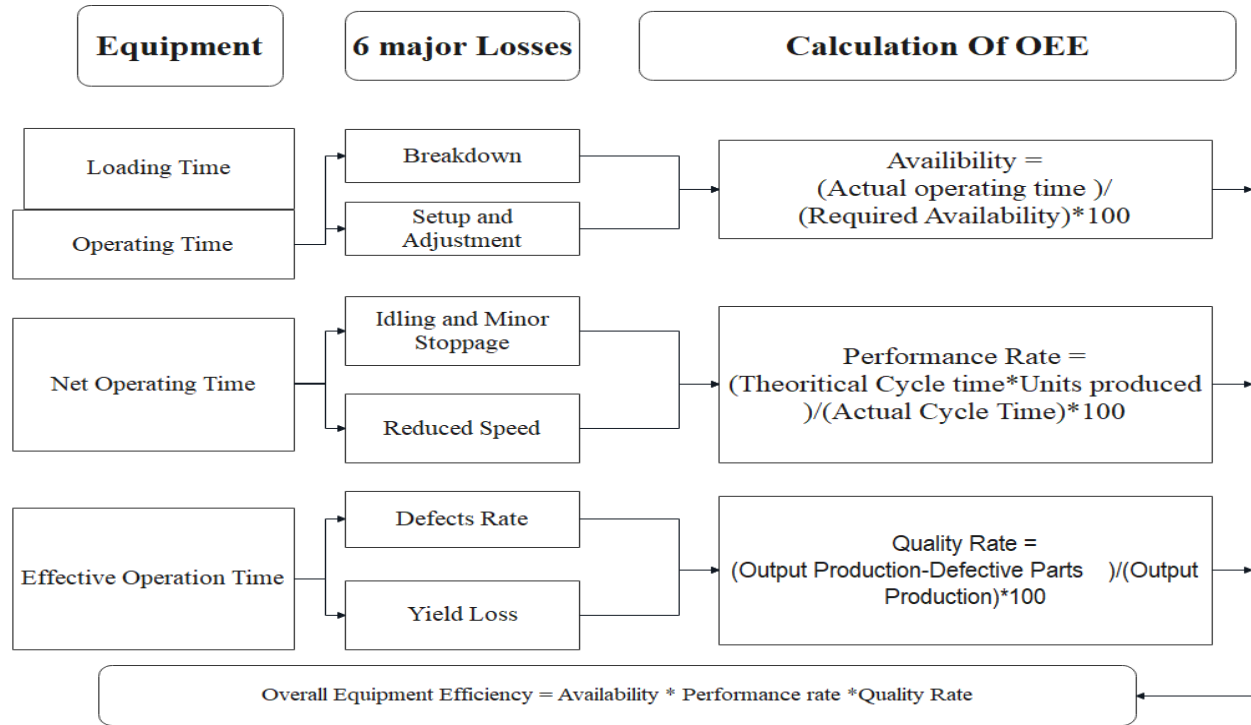


Figure 22: Calculation of OEE [17]

RESULTS & DISCUSSION

During production, some major stoppage losses were identified and classified as well as the OEE (Overall Equipment Efficiency) was calculated, initially. Once the data was studied and analyzed, the TPM (Total Productive Maintenance) tool implementation started. With the help of TPM tool implementation, a sudden decline was noticed in number of major stoppages losses, as a result the calculated OEE (Overall Equipment Efficiency) improved from 66.11% to 72.30%.

Comparison of Significant losses before & after stoppage losses

At last, it was determined that the major losses were only, idling and machine failure losses, which had a broad impact on OEE (Overall Equipment Efficiency). Thus, such stoppage losses were reduced and controlled successfully, with the help of training programs as well as, with implementation of Kaizen. In Table 5 some major stoppage losses are compared, before and after reducing them.

Table 5: Identified Significant Losses

| Losses due to | Before time loss (mins) | After time loss (mins) |
|------------------------------|----------------------------|------------------------|
| Idling and minor stoppage | 773.5 | 562.8 |
| Breakdown | 95.6 | 76.6 |
| Reduced speed | 11 | 9 |
| Yield loss | 0 | 0 |
| Changeover | 0 | 0 |
| Process defects | 0 | 0 |

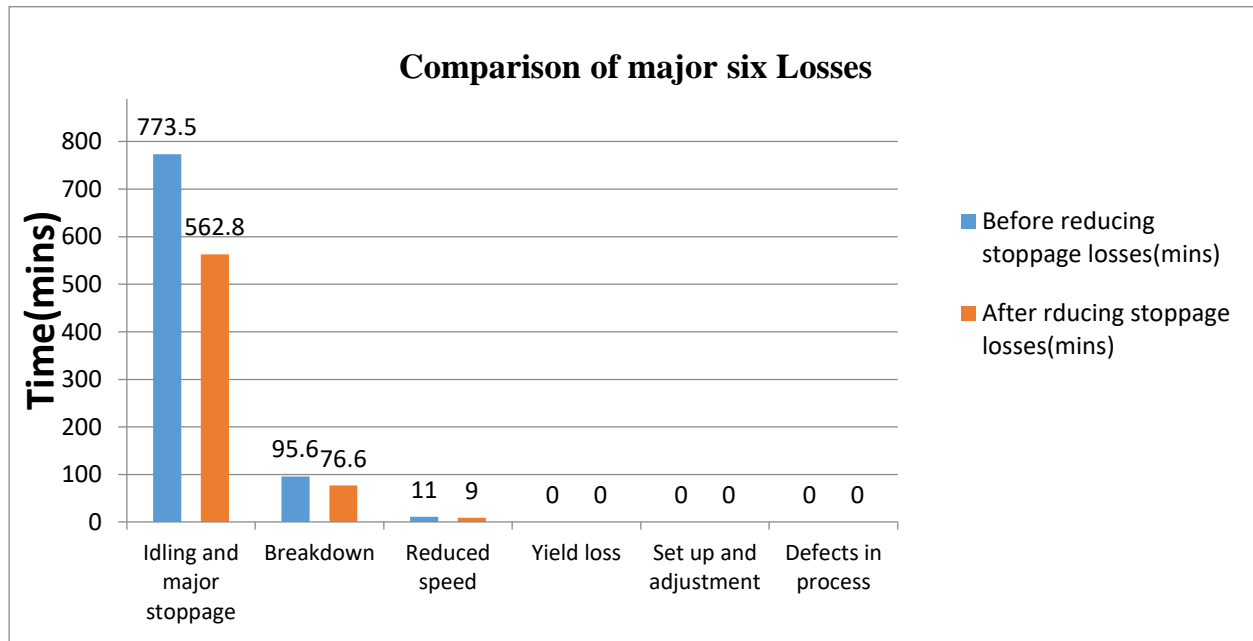


Figure 23: Six Losses Comparison before and after reducing stoppage losses

Comparison of Overall Equipment Efficiency before & after stoppage losses

The OEE (Overall Equipment Efficiency) of ring frame after reducing stoppage losses is compared in the Table 6. With the help of TPM (Total Productive Maintenance) tool implementation a significant increase is seen in OEE. As a result of TPM tool implementation almost 11% change is noticed, such that OEE jumped from 63% to 74%.

Table 6: OEE Comparison before and after Reducing Stoppage Losses

| S.No | OEE calculation before stoppage losses | OEE calculation after stoppage losses |
|------|---|--|
| 1 | 64.97 | 76.2 |
| 2 | 61.88 | 69.44 |
| 3 | 62.33 | 69.78 |
| 4 | 61.44 | 66.69 |
| 5 | 63.36 | 82.27 |
| 6 | 61.3 | 73.91 |
| 7 | 56.29 | 76.31 |
| 8 | 61.18 | 81.35 |
| 9 | 59.35 | 68.98 |
| 10 | 63.71 | 75.05 |
| 11 | 62.56 | 74.94 |
| 12 | 67.6 | 76.66 |
| 13 | 64.97 | 80.44 |
| 14 | 58.09 | 70.7 |
| 15 | 58.9 | 74.59 |
| 16 | 69.44 | 71.84 |
| 17 | 67.83 | 75.85 |
| 18 | 65.66 | 77.46 |
| 19 | 58.44 | 75.4 |
| 20 | 69.21 | 75.51 |
| 21 | 68.84 | 76.43 |
| 22 | 57.06 | 74.36 |
| 23 | 60.84 | 73.79 |
| 24 | 68.75 | 72.76 |
| 25 | 66.11 | 72.3 |

Comparisons of different factors

The overall production, Performance Efficiency, Overall Equipment Efficiency, Rate of Quality, and Percentage Availability are compared before and after reducing stoppage losses in Figure 24, Figure 25, Figure 26, Figure 27, Figure 28, respectively.

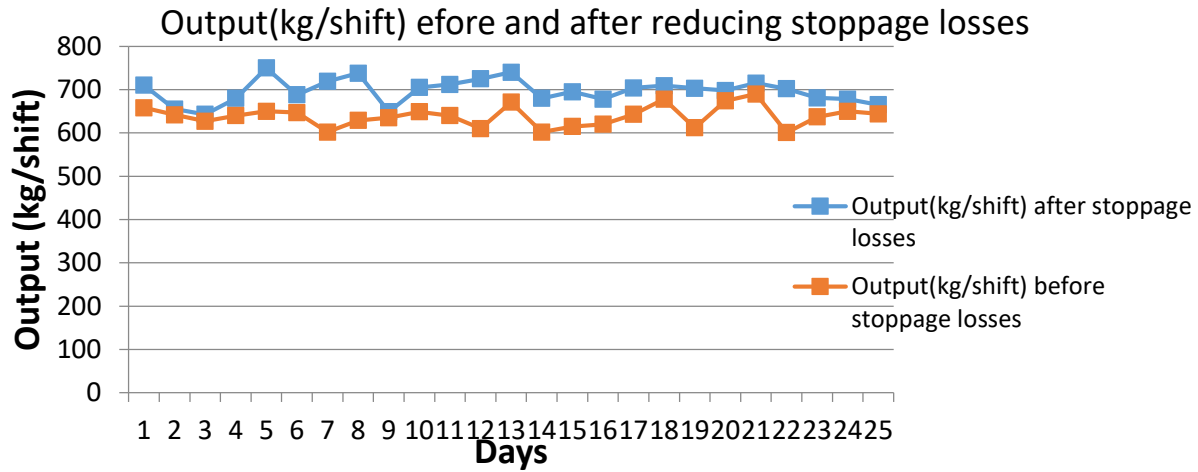


Figure 24: Comparison of Output before and after reducing stoppage losses

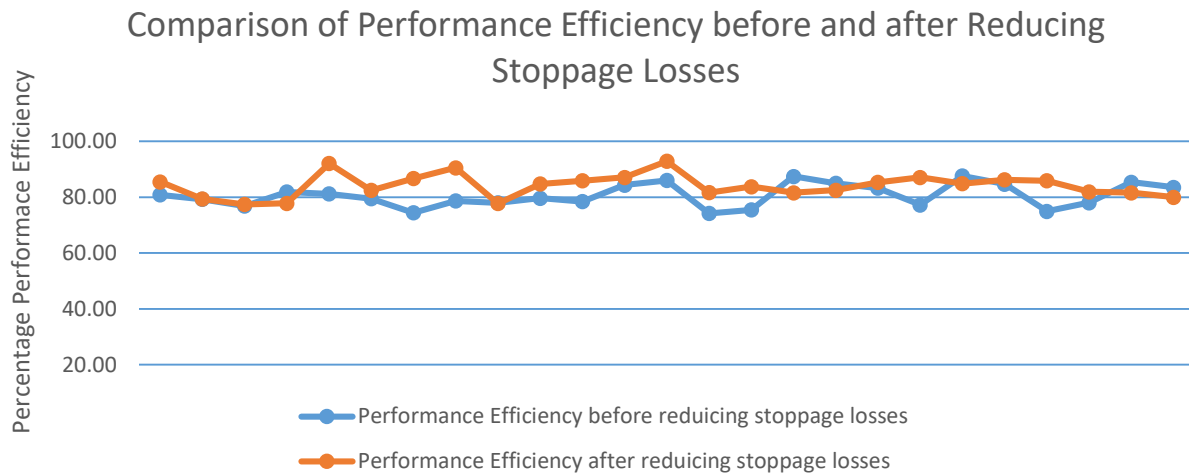


Figure 25: Comparison of Performance Efficiency before and after Reducing Stoppage Losses

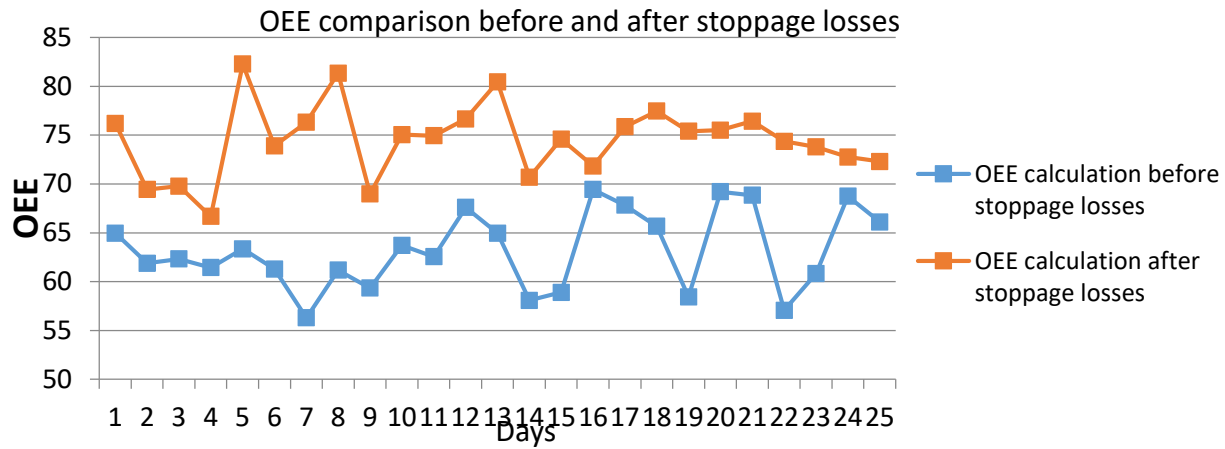


Figure 26: Comparison of OEE before and after reducing stoppage losses

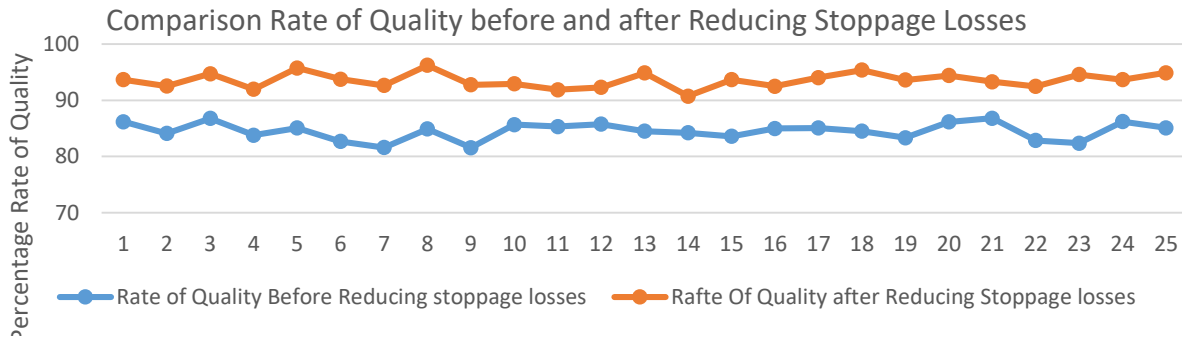


Figure 27: Comparison of Rate of Quality before and after reducing stoppage losses

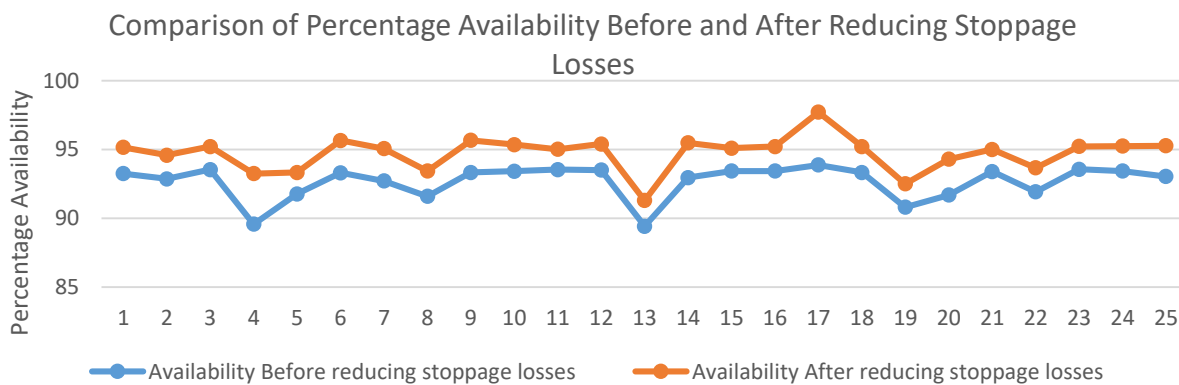


Figure 28: Comparison of Availability Percentage before and after reducing stoppage losses

Key findings

During this study, we did not witness any specific standard policy regarding developing or enhancing operator's skill, throughout research period. The operators and maintenance staff had very limited knowledge about examining and reducing stoppage losses, in order to evaluate the overall equipment efficiency (OEE).

In this study, some offline training programs were arranged in order to develop their skills. Thus, Kaizen, which is TPM's pillar, was implemented, which resulted in significant reduction of stoppage time of ring frame machine. Due to which throughput time was also decreased, resulting in increment of machine performance. It is clear that, there wasn't any interference of TPM implementation which helps in reducing the wastage of time and in increasing the production. Moreover, an opportunity was provided to the operators, to enhance their fundamental knowledge about maintenance operations in relevance to TPM.

The time loss due to machine stoppage before TPM implementation was an average of 35 minutes per shift. But, it was dropped to an average of 25 minutes per shift. Once, the causes of stoppage losses were analysed, the principal reasons were found out. Furthermore, fishbone diagram was constructed on the basis of identified root causes and their counter measures. The reduction of stoppage losses increased the number of productive spindles, which in turn reduced these defective shaped bobbins and thus, the production was increased. The principal findings are as follows.

1. Defective ring cops' reduction percentage is 55%.
2. Production is increased by 8.35%.
3. The Overall Equipment Efficiency (OEE) is increased from 63.20% to 74.52%.

Contribution of Sustainable Lean Manufacturing and Lean Sigma in SDGs

Sustainable Lean Manufacturing plays a vital role towards Sustainable Development Goals. In this research four major SDGs are achieved such that, SDG 8, SDG9, SDG12, and SDG 13 discussed as under;

The main objective of lean manufacturing tool is, to minimize and eliminate waste. In order to reduce waste, every step of production process was examined and the areas were identified where resources were utilized inefficiently. Thus, some sustainable actions were taken in order to optimize inventory, reduce defects, eliminate bottleneck, and optimize the layout in order to reduce unnecessary movements. This approach contributed towards Sustainable Development Goal of Responsible consumption and production i.e. SDG12, as it optimizes resources.

Similarly, Kaizen tool was used which focuses on continuous improvement. This approach created a culture of skill development to learn new skills in order to compete in the market, and improve their personal as well as economic growth. Thus, this approach supports SDG8. Similarly, by adapting new technology, innovation, and relevant skills, the process inefficiencies can be eliminated and the resources can also be used in Research & Development., which contribute towards SDG9.

Furthermore, Sustainable Lean Manufacturing also contributes towards SDG13 by aligning the industrial operations with sustainability of environment. This tool optimizes the utilization of energy and promotes those production processes which are more energy efficient. Thus, decreases the emissions of hazardous and greenhouse gases into the environment. In this way, Sustainable Lean manufacturing



ICSET-23

*Proceedings of the 5th International Conference on Sustainable
Energy Technologies (ICSET 2023) Peshawar, Pakistan
14-15 December 2023*



UET Peshawar

contributes towards SDG13 by introducing green manufacturing techniques and shaping industrial for greener future.

After elaborating the contributions of Sustainable Lean Manufacturing towards SDGs. We now discuss the ways Lean Six Sigma increase these impacts;

The Sustainable Lean manufacturing acts as a base in order to drive responsible production and efficient usage of resources. On the basis of this, Lean Six Sigma added an additional dimension of precision in production process, and continuous improvement. By integrating the methodologies of Six Sigma with Lean principles, companies gain a significant tool in order to refine production process, reduce process variability, and enhance overall product quality, which supports SDG8 by creating a competitive and economically viable environment for business, stimulates economic growth and development.

In addition, the problem solving approach of Lean Six Sigma not only refine the operations but also promotes industry growth and innovation, which contributes towards the 9th goal of SDGs. Moreover, it also helps to optimize the utilization of resources by conducting Root-Cause Analysis, and performing innovative improvements, in such a way achieves SDG12.

From environmental perspective, Lean Six Sigma also plays a vital role to reduce the environmental impact, systematically as, it optimizes energy consumption, reduces waste and emission of greenhouses gases into the environment, within the production processes. This approach contributes towards SDG13 by supporting the objective of bringing the organizations towards eco-friendly practices.



Figure 29: Targeted SDGs through Sustainable Lean Manufacturing and Lean Six Sigma

CONCLUSION

Manufacturing industries are moving towards green manufacturing by optimizing resources, reducing and increasing productivity via sustainable practices. This study is carried out to target a higher level economic stability along with the aim of spike in customer satisfaction through high quality. As we know that the spinning process is a continuous process. The OEE of the plant depends upon the availability of raw material and stable functionality of all machines. The goal of this study was to relate the Sustainable Lean



ICSET-23



UET Peshawar

Manufacturing and Lean Six Sigma with Sustainable Development Goals. For which, we calculated the current OEE and to identify current losses in ring frame section using six losses tool, afterwards lean tools and techniques were applied to enhance productivity and quality rate. The collection of data after implementation of TPM revealed that the Kaizen and Autonomous maintenance increased the OEE and the overall loss of time. Before implementation of lean tools and techniques, the overall equipment efficiency (OEE) of ring frame section was 63.20%. After applying TPM pillars, the overall equipment efficiency (OEE) improved up to 74.52%. Thus, this gives us information that combining the principles of Sustainable Lean Manufacturing and Lean Six Sigma methodologies contributes towards four major objectives of Sustainable Development Goals by reducing waste, optimizing production process, optimizing energy consumption, and usage of technology & resources, efficiently.

ACKNOWLEDGEMENTS

I am deeply grateful to my supervisor Dr. Rehman Akhtar who played a vital role in the success of this research. I would like to thank Engr. Muhammad Touseef Rahim for his invaluable input and support throughout the research process.

REFERENCES

- [1] Y. Wu, K. Zhang, and J. Xie. (2020). Bad greenwashing, good greenwashing: Corporate social responsibility and information transparency. *Management Science*, vol. 66, no. 7, pp. 3095–3112.
- [2] R. Agrawal, A. Majumdar, K. Majumdar, R. D. Raut, and B. E. Narkhede (2022). Attaining sustainable development goals (SDGs) through supply chain practices and business strategies: A systematic review with bibliometric and network analyses. *Business Strategy and the Environment*, vol. 31, no. 7, pp. 3669–3687.
- [3] S. Jørgensen, A. Mjøs, and L. J. T. Pedersen (2021). Sustainability reporting and approaches to materiality: tensions and potential resolutions. *Sustainability Accounting, Management and Policy Journal*, vol. 13, no. 2, pp. 341–361.
- [4] <https://www.un.org/sustainabledevelopment/sustainable-development-goals/>, accessed Aug. 20, 2023.
- [5] <https://www.un.org/ecosoc/en/2018-ECOSOC-Partnership-Forum>, accessed Aug. 20, 2023.
- [6] R. Bali Swain and F. Yang-Wallentin. (2020). Achieving sustainable development goals: predicaments and strategies,” *International Journal of Sustainable Development & World Ecology*, vol. 27, no. 2, pp. 96–106.
- [7] Kirsi Niinimäki, Greg Peters, Helena et.all (2020). The environmental price of fast fashion. pp. 189-200.
- [8] Vandana Gupta, Madhvi Arora, Jasmine Minhas. (2020). Innovating opportunities for fashion brands by using Textile Waste for better fashion. *Recycling from Waste in fashion and Textile: A Sustainable and Circular Economic Approach*. pp. 298-334.



ICSET-23

*Proceedings of the 5th International Conference on Sustainable
Energy Technologies (ICSET 2023) Peshawar, Pakistan
14-15 December 2023*



UET Peshawar

- [9] M. Md. Khairul Akter, U. N. Haq, Md. M. Islam, and M. A. Uddin. (2022). Textile-apparel manufacturing and material waste management in the circular economy: A conceptual model to achieve sustainable development goal (SDG) 12 for Bangladesh. *Cleaner Environmental Systems*, vol. 4, p. 100070.
- [10] Nattha Pensupa, Shao-yuan Leu and Cenyu Du. (2023). Recent trends in sustainable textile waste recycling methods: Current Situation and Future Prospects. *Chemistry and Chemical technologies in Waste valorization*, pp189-228.
- [11] Md Shamsuzzaman, Md. Abdul Kashem et. all. (2021). Quantifying environmental sustainability of denim garments washing factories through effluent analysis. *Journal of Cleaner Production*, vol. 290, 125740.
- [12] P. Castellani, C. Rossato, E. Giaretta, and A. Vargas-Sánchez. (2023). Partner selection strategies of SMEs for reaching the Sustainable Development Goals,” *Rev Manag Sci*. 228-323
- [13] B. Debnath, M. S. Shakur, A. B. M. M. Bari, and C. L. Karmaker. (2023). A Bayesian Best–Worst approach for assessing the critical success factors in sustainable lean manufacturing. *Decision Analytics Journal*, vol. 6, p. 100157.
- [14] J. L. García Alcaraz, A. S. Morales García, J. R. Díaz Reza, J. Blanco Fernández, E. Jiménez Macías, and R. Puig i Vidal. (2022). Machinery Lean Manufacturing Tools for Improved Sustainability: The Mexican Maquiladora Industry Experience. *Mathematics*, vol. 10, no. 9, Art. no. 9.
- [15] J. Gianfranco, M. I. Taufik, F. Hariadi, and M. Fauzi. (2022). PENGUKURAN TOTAL PRODUCTIVE MAINTENANCE (TPM) MENGGUNAKAN METODE OVERALL EQUIPMENT EFFECTIVENESS (OEE) PADA MESIN REAKTOR PRODUKSI. *Jurnal Lebesgue : Jurnal Ilmiah Pendidikan Matematika, Matematika dan Statistika*, vol. 3, no. 1, Art. no. 1.
- [16] K. Ramu, R. Manickam, and A. Murugan. (2022). Analysis of Autonomous Maintenance Activities Using FUZZY ARAS Method. *Journal on Electronic and Automation Engineering*, vol. 1, pp. 35–46.
- [17] A. K. Gupta and D. R. K. Garg. (2022). OEE Improvement by TPM Implementation: A Case Study,” vol. 1, no. 1.
- [18] A. J. deRon and J. E. Rooda. (2005). Equipment Effectiveness: OEE Revisited. *IEEE Trans. Semicond. Manufact.* vol. 18, no. 1, pp. 190–196.

Paper ID: ICSET-2304

ENHANCING THE PERFORMANCE OF PEROVSKITE SOLAR CELL THROUGH MoS₂ INTERFACE LAYER

Abdul Haseeb Hassan Khan*, Muhammad Noman, Abdul Basit
*Renewable Energy Engineering, US-Pakistan Centre for Advanced Studies in Energy, University of Engineering and
Technology Peshawar, Pakistan*

**Corresponding author*
Email: abdulhaseeb.ree@uetpeshawar.edu.pk

ABSTRACT

In light of the increasing popularity of Perovskite solar cells (PSCs) due to their affordability and performance, addressing issues like hysteresis and instability caused by trap states at interfaces is crucial for their economic viability. To mitigate these challenges, researchers have been actively developing passivation methods. In this study, we investigate the impact of introducing a MoS₂ interface layer into the Perovskite solar cell structure. Our research focuses on key performance parameters, including open circuit voltage (V_{oc}), short circuit current (J_{sc}), fill factor (FF), and power conversion efficiency (PCE), both with and without the MoS₂ interface layer. Through comprehensive simulations, our findings reveal significant improvements. Specifically, the addition of the MoS₂ interface layer enhances the PCE of the RbGeI₃ based PSC from 15.63% to 17.20%. Furthermore, our study demonstrates enhancements in J_{sc} and FF. This study addresses a critical research gap by providing a deeper understanding of how interface layers, such as MoS₂, can be harnessed to improve the performance of PSCs. Our contribution lies in elucidating the mechanisms behind these enhancements, shedding light on the potential of MoS₂, and offering insights into how such strategies can accelerate the growth and boost the performance of Perovskite solar cells. This work aims to drive advancements in renewable energy technology and facilitate the broader adoption of PSCs in the clean energy landscape.

KEYWORDS: MoS₂; Interface Layer; SCAPS-1D; Passivation

INTRODUCTION

The category of 3rd generation photovoltaic cells that show promise are the organic hybrid Perovskite solar cell (PSC) and inorganic hybrid PSC. These cells are anticipated to serve as viable alternatives for traditional silicon PV cells due to their easy manufacturing process and lower cost [1]. Various exchange-correlation function were used to assess the thermoelectric, optoelectronic, thermodynamic, structural as well as mechanical characteristics of RbGeI₃ perovskite [2]. Numerous investigations using Raman spectroscopy along with X-ray diffraction was carried out to study RbGeI₃ thermal behaviour [3]. Another work looked through the cubic RbGeI₃ and RbDyO₃ perovskites structural, magnetic, and electronic characteristics [4]. Additionally, the optical, electrical, as well as structural characteristics of RbGeI₃ perovskites were examined using first principles in a different work. The band gap, lattice constants, effective masses of electrons and holes high frequency dielectric constant, static dielectric constant, tolerance factor, and other characteristics were all included in this study using the PBEsol functional [5].



ICSET-23



UET Peshawar

Researchers are exploring 2D materials such as WS₂ and MoS₂ for their excellent solar cell capabilities, inspired by the discovery of graphene [6]. MoS₂ were utilized as interface among Hole transport layer (HTL) / CH₃NH₃PbI₃ and an active layer additive to improve perovskite solar cell (PSC) efficiency and stability [7].

This paper evaluates photovoltaic effectiveness of RbGeI₃ using SCAPS 1D. Hole transport layer (HTL) uses Spiro-OMeTAD, whereas electron transport layer (ETL) uses Titanium dioxide (TiO₂). Simulations will be done in two parts. We simulate the Photovoltaic Cell of PSC structures without an interface layer (IL) first. This will allow photovoltaic comparisons. Next, a MoS₂ passivation layer will be placed between the absorber and the hole transport layer (HTL) to test its impact on device performance. We study relevant literature to get material characteristics, layer thicknesses, and other simulation input parameters.

Simulation Methodology and Device Structure

SILVACO, COMSOL, SETFOS, ATLAS, and SCAPS are numerical modeling tools for solar cell performance study. Due of its controllability and user-friendliness, SCAPS-1D version 3.3.10 was used in this study. SCAPS can also simulate lighted and illuminated cells and construct a seven-layer heterostructure cells. Ghent University developed the Solar Cell Capacitance Simulator. This programme estimates power conversion efficiency (PCE), fill factor (FF), open circuit voltage (V_{oc}), short circuit current (J_{sc}), energy band alignment, as well as Current-Voltage (IV) Curve to evaluate solar cells.

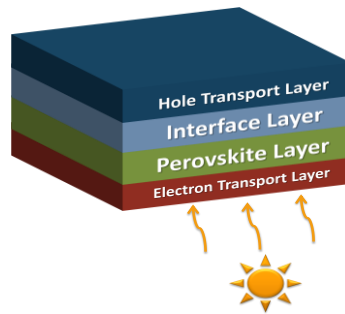


Figure 1: Perovskite solar cell with interface layer

RESULT AND DISCUSSION

IV Curve and Thickness Variation of RbGeI₃ With and Without MoS₂ IL

The introduction of the MoS₂ IL led to substantial improvements in key photovoltaic parameters, including an increase in open circuit voltage from 0.8V to 0.82V, short-circuit current from 30.7 to 31.6 mA/cm², fill factor FF from 62.58% to 66.30%, and power conversion efficiency (PCE) from 15.63% to 17.20%. Through SCAPS 1D simulations, we were able to dissect the mechanisms underlying these enhancements. These included the facilitation of efficient charge transport due to MoS₂ high carrier mobility, reducing recombination losses, as well as the favourable energy level alignment between MoS₂



and RbGeI_3 for improved charge separation and extraction. Additionally, we explored the impact of RbGeI_3 thickness variation with and without MoS_2 acting as an IL, and our simulations provided insights into the increase in PCE with thickness, attributing it to enhanced light collection and reduced recombination. The RbGeI_3 paired with a MoS_2 IL exhibited even higher PCE, indicating the enhanced charge carrier separation at the interface.

Table 1. Information about the primary Parameters used in the PSC modelling

| Parameters | TiO_2 | RbGeI_3 | MoS_2 | Spiro-OMeTAD |
|------------------------------------|----------------------|------------------------|----------------------|----------------------|
| Thickness (nm) | 150 | 400 | 50 | 150 |
| Bandgap (eV) | 3.2 | 1.310 | 1.290 | 3.0 |
| Electron affinity (eV) | 4.00 | 3.9 | 4.2 | 2.2 |
| Dielectric permittivity (relative) | 10 | 23.00 | 4.0 | 3.0 |
| CB effective density of states | 2×10^{18} | 1.4×10^{19} | 7.5×10^{17} | 2.2×10^{18} |
| VB effective density of states | 1.8×10^{19} | 2.8×10^{19} | 1.8×10^{18} | 1.8×10^9 |
| Electron mobility | 2×10^1 | 2.8×10^1 | 1×10^2 | 2×10^{-4} |
| Hole mobility | 1×10^1 | 2.7×10^1 | 1.5×10^2 | 2×10^{-4} |
| Shallow uniform donor density | 1×10^{17} | 1×10^9 | - | - |
| Shallow uniform acceptor density | - | 1×10^9 | 1×10^{21} | 1×10^{17} |
| Total Defect Density | 1×10^{15} | 1.000×10^{15} | 1×10^{15} | 1×10^{15} |

Table 2. Performance of RbGeI_3 Based PSC with & without MoS_2 as interface layer

| Structure | Voc | Jsc | FF | η |
|--|--------|------------------------------|---------|--------|
| $\text{TiO}_2/\text{RbGeI}_3/\text{Spiro-OMeTAD}$ | 0.8 V | 30.7 mA/cm^2 | 62.58 % | 15.63% |
| $\text{TiO}_2/\text{RbGeI}_3/\text{MoS}_2/\text{Spiro-OMeTAD}$ | 0.82 V | 31.6 mA/cm^2 | 66.30 % | 17.20% |

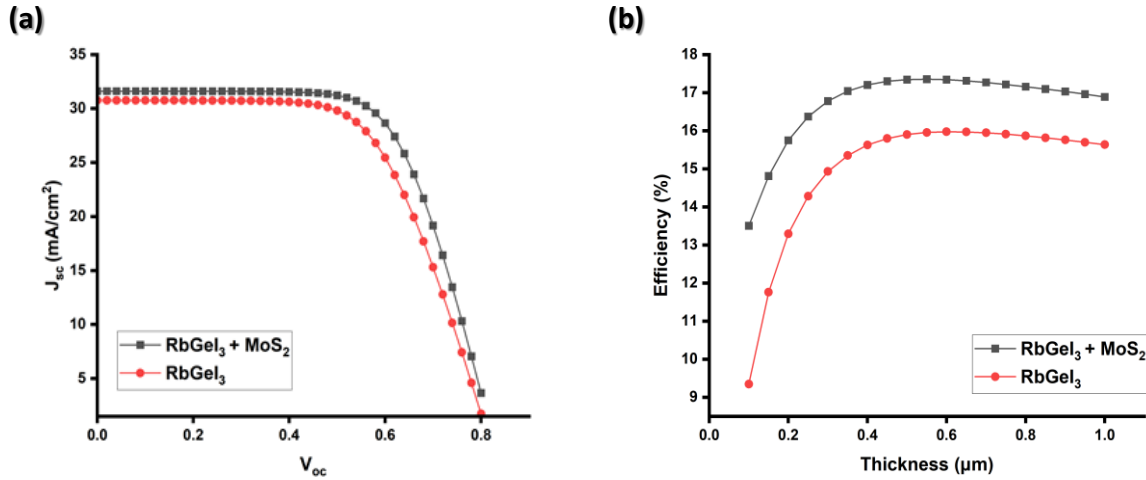


Figure 2. (a) IV Curve of RbGeI₃ PSC with and Without Interface Layer. (b) Impact of changing RbGeI₃ Thickness on Efficiency with and Without IL

Band Gap Alignment of RbGeI₃ with MoS₂ Interface Layer

The TiO₂/RbGeI₃ contact has 1.99 eV valance band offset (VBO) and -0.1 eV conduction band offset (CBO). This unique design maximises electron transmission to the electron transport layer (ETL) while minimising interface recombination losses. RbGeI₃/MoS₂ has a 0.28 eV valance band offset (VBO) and -0.3 eV conduction band offset (CBO). This alignment optimises electron-hole separation and transit to their layers. Ultimately, the MoS₂/Spiro-OMeTAD interface's 2 eV conduction band and -0.29 eV valance band optimise hole to the HTL as well as inhibit electron-hole recombinations. Band alignment throughout all interfaces creates a solar cell with efficient charge transport and low recombination, essential for high device efficiency. The positive VBO and slightly negative CBO at the TiO₂/RbGeI₃ interface promote electron transport from the absorber layer to the ETL. Effective electron transport reduces electron-hole recombination, increasing photocurrent and cell efficiency. The RbGeI₃/MoS₂ interface's reduced VBO and negative CBO aid electron-hole separation. This reduces recombination losses by directing produced charges to their transport layers. Reduced recombination increases open-circuit voltage (VOC), another important solar cell efficiency factor. The MoS₂/Spiro-OMeTAD interface's strong CBO and slightly negative VBO provide excellent hole transfer to the HTL. This prevents interface recombination, increasing cell production.

Table 3. VBO & CBO at Interfaces

| Interface | CBO | VBO |
|---------------------------------------|------|-------|
| TiO ₂ / RbGeI ₃ | -0.1 | 1.99 |
| RbGeI ₃ / MoS ₂ | -0.3 | 0.28 |
| MoS ₂ / Spiro-OMeTAD | 2 | -0.29 |

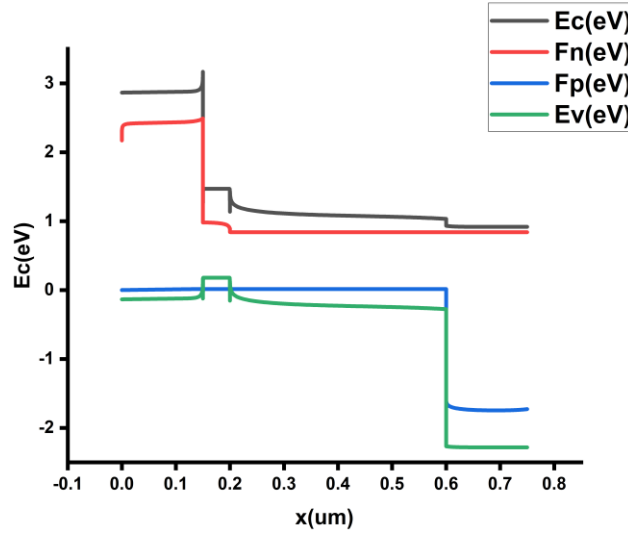


Figure 3. Band Gap Alignment of RbGeI₃ with MoS₂ Layer

CONCLUSION

In conclusion, SCAPS-1D simulations were used in this paper, to explore the photovoltaic performances of RbGeI₃. Titanium dioxides (TiO₂) along with Spiro-OMeTAD were utilized as ETL as well as HTL, accordingly. Along with HTL, 50 nm MoS₂ layer was inserted as an interface layer (IL) among the absorbers, which increases the cell's performance. A comparison of the data shows that MoS₂ inter face layer (IL) has a positive influence on the efficiency of perovskite solar cell (PSC) for RbGeI₃ absorber materials. RbGeI₃ also performed better with the MoS₂ layer, with the J_{sc} rising from 30.7 mA/cm² towards 31.6 mA/cm², the fill factor (FF) growing from 62.58% to 66.30%, and the PCE increases among 15.63% towards 17.20%. Future research in the area of perovskite solar cells should take into account a number of trends and techniques. First, more research into cutting-edge interface materials beyond MoS₂ may improve device performance. The creation of scalable manufacturing methods that preserve the quality of these materials during mass production is also essential for economic viability. In order to facilitate the general implementation of PSCs, research should continue to solve stability and hysteresis problems in PSCs. Future study should focus on investigating innovative production techniques and materials with increased environmental sustainability. Researchers can help Perovskite solar cell technology continues to advance and be successful in the field of renewable energy by tackling these issues and trends. This research gives useful insights for development as well as optimization of PSC among absorbers, emphasizing need of using an appropriate passivation layer, such as MoS₂, to ensure optimum device performance.

ACKNOWLEDGMENTS

We are grateful to Professor Marc Burgelman of the University of Gent in Belgium for providing the SCAPS 1-D.

REFERENCES



ICSET-23

Proceedings of the 5th International Conference on Sustainable
Energy Technologies (ICSET 2023) Peshawar, Pakistan
14-15 December 2023



UET Peshawar

- [1] P. Gao, M. Grätzel, and M. K. Nazeeruddin, "Organohalide lead perovskites for photovoltaic applications," *Energy & Environmental Science*, vol. 7, no. 8, pp. 2448-2463, 2014.
- [2] K. D. Jayan and V. Sebastian, "Ab initio DFT determination of structural, mechanical, optoelectronic, thermoelectric and thermodynamic properties of RbGeI₃ inorganic perovskite for different exchange-correlation functionals," *Materials Today Communications*, vol. 28, p. 102650, 2021.
- [3] G. Thiele, H. Rotter, and K. Schmidt, "Die Kristallstrukturen und phasentransformationen des tetramorphen RbGeI₃," *Zeitschrift für anorganische und allgemeine Chemie*, vol. 571, no. 1, pp. 60-68, 1989.
- [4] K. A. Parrey, T. Farooq, S. A. Khandy, U. Farooq, and A. Gupta, "First principle studies on structure, magneto-electronic and elastic properties of photovoltaic semiconductor halide (RbGeI₃) and ferromagnetic half metal oxide (RbDyO₃)," *Computational Condensed Matter*, vol. 19, p. e00381, 2019.
- [5] U.-G. Jong, C.-J. Yu, Y.-H. Kye, Y.-G. Choe, W. Hao, and S. Li, "First-principles study on structural, electronic, and optical properties of inorganic Ge-based halide perovskites," *Inorganic chemistry*, vol. 58, no. 7, pp. 4134-4140, 2019.
- [6] T. Wang *et al.*, "2D WSe₂ flakes for synergistic modulation of grain growth and charge transfer in tin-based perovskite solar cells," *Advanced Science*, vol. 8, no. 11, p. 2004315, 2021.
- [7] Z. Liu *et al.*, "CH₃NH₃PbI₃: MoS₂ heterostructure for stable and efficient inverted perovskite solar cell," *Solar Energy*, vol. 195, pp. 436-445, 2020.

Paper ID: ICSET-2305

SOCIO-ECONOMIC IMPACTS OF MICRO HYDRO POWER (MHP) ELECTRIFICATION ON THE RURAL COMMUNITY OF PAKISTAN: A CASE STUDY OF 150 KW MHP PLANT AT VILLAGE LALKOO (SWAT)

Bilal Ayaz Khan, Abeera A. Ansari*, Muhammad Yousif

*U. S-Pakistan Centre for Advanced Studies in Energy (USPCAS-E), National University of Sciences and Technology
(NUST), Sector H-12, Islamabad, Pakistan*

**Corresponding author*

Email: abeera@uspcase.nust.edu.pk

ABSTRACT

Electricity is an essential element in any country's socioeconomic development since it boosts welfare, raises living standards, and reduces poverty. While extending grid electricity is not feasible in some remote areas of Pakistan however, Micro-hydropower (MHP) is the most feasible, decentralized renewable energy option for providing reliable and affordable electricity to the remote and isolated areas of Pakistan. This study aimed to evaluate the socioeconomic impacts of the Micro hydro power (MHP) plant located in the village Lalkoo (Swat) Pakistan. A household questionnaire survey was used to collect the primary data. A total of 136 participants were selected using the simple random sampling procedure. Positive results were observed both in terms of social and economic areas. In terms of social impacts, MHP electrification had a positive impact on education indicating significant increase in children's study hours. The electrified household were also of the opinion that MHP produces smoke-free energy, so health-related difficulties lessened after its electrification. Additionally, electrification also increased respondents access to information and communication technologies. Another key social benefit of MHP electrification according to respondents was that the village security situation improved after its installation. One of the key reasons for security improvement was street light installation after village electrification. In terms of economic impacts, the participants reported significant decrease on the expenditure of kerosene and candles. The participants also expressed that their income increased after MHP electrification. Overall, the results showed that respondents were pleased with MHP's electrical service.

KEYWORDS: Micro hydropower (MHP), Socio-economic, Rural Electrification

INTRODUCTION

Energy, particularly electricity is worldwide acknowledged as one of the most basic input for financial and social growth [1], [2]. Electricity is necessary for a satisfactory level of life style because it meets necessary human needs by boosting education, health and construction of infrastructure[3]. The lack of power in faraway areas of evolving nations has been recognized as a critical element impeding on the road to a superior standard of living[4]. According to the statistics supplied by International Energy Agency (IEA), 770 million inhabitants worldwide do not have access to electricity in 2019 [5]. In Pakistan, more than 40 million inhabitants lack access to electric power[6]. Due to the rise in energy demand, Pakistan has



been experiencing an energy shortage for the past few decades, and it is only expected to get worse in the years to come. Due to country's expanding economy and population, the basic energy resources are unable to adequately fulfil the current energy demands [7]. Supply and demand differences in Pakistan in 2016 were 5298 MW. Later in 2017, though, it was raised to 6097 MW[8], [9]. Load shedding has consequently become a widespread action throughout Pakistan, resulting in enforced disruption of power in metropolitan region up to 8 to 12 hours per day while in rural regions up to 16 to 18 hours per day [10]. The continuously increasing energy demand is predicted to reach an all-time high of 142 MTOE by 2025 [11].

Pakistan is a country that massively depends on fossil fuels for its energy requirements[7], [12]. Fossil fuels are depletable energy resources that release greenhouse gases (GHG) upon utilization. The released GHG emissions have detrimental impact on the environment and ecosystem. Not only are fossil fuel-based power plants responsible for CO₂ emissions, but they also generate noise, warmth, and unleash sulphur dioxide (SO₂), carbon monoxide (CO), nitrogen oxide (NO_x), and particulate matter [13]. Renewable energy resources (RERs), on the other hand, are limitless, replenishable and release little to no GHG emissions or air pollutants [14].

Pakistan is blessed with enormous RERs reserves containing solar, hydro, wind[15]. Because of inadequate legislation and infrastructure, Pakistan's renewable energy capacity of 167.7 GW has not been efficiently harnessed up to this point [16]. Among the RERs, micro hydel and canal falls have high potential in Pakistan for effective utilization[17]. The overall potential of MHP available across Pakistan is 3100 MW[18]. For remote villages without access to national electrical grid, MHP projects can be a sustainable option for electricity generation. This is because the adoption of a MHP plant is more affordable alternative that has a smaller negative environmental effect as compared to a conventional fossil fuel generator[19], [20]. Small hydropower plants are typically managed by provisional governments in Pakistan. The provisional government of KPK province, through its Energy and Power department, has begun implementing 356 micro/mini hydropower facilities across 11 districts of the province. There were 356 projects in total, having an overall capacity of 34.7 MW. During the implementation phase, however, 24 MHP were left out because they were neither technically nor socially practicable. As a result, the total number of projects was amended to 332, with overall capacity of 32.5 MW[21]. The interim administration of KPK is currently utilizing another six micro hydro projects having total capability of 118 MW, while the Punjab local government is working tirelessly to implement four micro hydro projects having an overall capability of 20 MW[18], [22].

Substantial amount of literature suggest MHP electrification can aid community, especially in rural setting, through socio-economic development. [23]–[26]. However, in Pakistan there has been little to no research about socioeconomic implications of these MHP used for rural electrification. The main motivation of this paper is, therefore, to close this research gap, which has remained, unanswered in Pakistan. The main question addressed in this research is what are the socioeconomic impacts of MHP electrification in rural KPK region? We are optimistic that the results of this study will be of great importance to those researchers in Pakistan who are keen to understand the socioeconomic impacts MHP electrification on rural people. The implementers and policy makers of MHP projects will also benefit greatly from the results of this research. It will enable them to plan successfully for future projects.

RESEARCH METHODOLOGY AND STUDY AREA

Data Collection

Cross sectional survey approach was adopted in this research. Structured questionnaires were used to conduct surveys that involved face-to-face interaction with participants. Each respondent was informed



ICSET-23



UET Peshawar

about the study's goal and significance before the primary data collection. Secondary data was gathered for this study via reports, journals, and organizations in charge of implementing these projects. The questionnaire was designed based on the available literature. The questionnaire had a total of 38 questions, which addressed a variety of socioeconomic and demographic areas. It took 30 minutes to complete the questionnaire. The questionnaire was pretested on thirty respondents before the full-scale study, and based on comments from respondents, it was improved and made ready for the full-scale study.

Study Area

The study was administered in district Swat which is in north of Pakistan. It has a total population of 1.26 million and its capital is Saidu Sharif[27], [28]. District Swat reportedly receives an average rainfall of 1000 to 1200 mm per annum which makes the district fertile and rich in forestry and agricultural planes[29], [30]. It, therefore, comes as no surprise that the inhabitants of Swat are widely dependent upon these natural resources for livelihood[31], [32]. Reports show that agriculture is one of the principal source of income and 42% of the respondents are employed in the agricultural activities[33]. Likewise, majority of the people are also reliant on forest zones for fuel wood and fodder[34].

The studied village selected for this research was Lalkoo Village in district Swat. Lalkoo Village is located 58 kilometres from Mingora and 35 kilometres from Matta Tehsil. The condition of the road is fair, and is accessible by any car[35]. Figure 1 below shows the study area map.

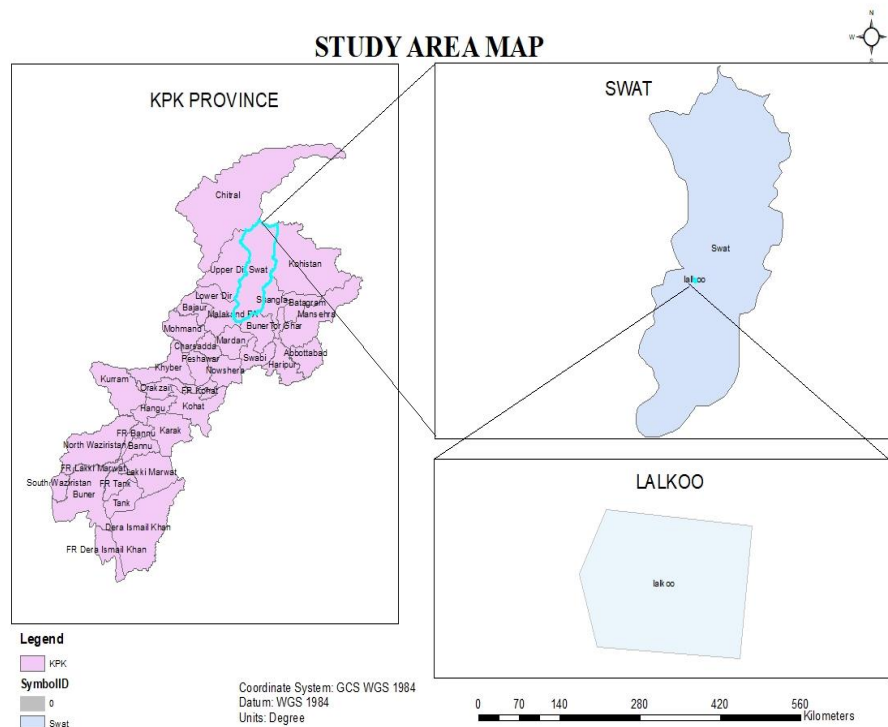


Figure 30: Study area Map



In this community, a 150 kW MHP plant has been erected on the cost of 40 million Pakistan Rupees (PKR). Pakhtunkhwa energy development organization (PEDO) and Sarhad program of rural support (SRSP) oversaw the project's development and implementation, which began in August 2016. This MHP operates for approximately 22 hours every day. Currently, each household is being charged a fixed monthly tariff of 300 PKR.

Sampling Size

In this study, the sample size was calculated using the Taro Yamane formula as shown in the Eqs. (1) [36]. The confidence interval chosen was 95% while the margin of error was set at 5% (0.05).

$$n = \frac{N}{(1 + Ne^2)} \quad (1)$$

Where,

n= sample size

N= total population

e= margin of error (0.05)

The total number of households connected to MHP was found to be 206. Based on the above formula, 136 sample participants were selected. A sample is a statistically selected part of a population about which the researcher wants to make observations and draw statistical conclusions. The best sample size can fully satisfy the requirements of representativeness, adjustability, efficacy, and dependability. It is, hence, very important for the researcher to determine a suitable margin of error and an adequate level of confidence when calculating the sample size. Moreover, the criteria of interest and budgetary restrictions must also be taken into account[37].

Sampling Approach

After calculating the sample size, a simple random sampling was performed to draw the survey sample. The sampling frame was the head of the households, which was obtained from the village head. The head of the household was also the survey respondent. However, if the person was unavailable or unable to respond, another senior member of the household was asked to complete the questionnaire.

Data Analysis

The collected data was coded and analyzed in Statistical Package for Social Sciences (SPSS, version 23). The analysis was carried out by opening the software's analyze window and selecting the descriptive statistics option. The information gathered was examined using frequency and percentage.

RESULTS AND DISCUSSION

Demographic Analysis

Table 1 illustrates the demographics of the respondents. In our survey, 66.2% of the respondents were male, and 33.8% were female. 34.6% of respondents in our study were in the age of 42-52. 88% of the



respondents in our study were married. 36% of the respondents have a family in the range of 6-7. Only 13.2% of the respondents have a family size in the range of 2-3. 26.5 % of the respondents were farmers by occupation in our survey. While 25% of the respondents were involved in business. 12.5 % of the respondents were daily wagers. 57.4% of the respondents had 3-5 male children in their household while 52.9% of the respondents had 3-5 female children in their household.

Table 1: Demography of the respondents

| Variable | Description | Frequency | Percentage |
|---------------------------|--------------|-----------|------------|
| Gender | Male | 90 | 66.2 |
| | Female | 46 | 33.8 |
| Age of respondent | <20 | 9 | 6.6 |
| | 20-30 | 18 | 13.2 |
| | 31-41 | 28 | 20.6 |
| | 42-52 | 47 | 34.6 |
| | >52 | 34 | 25 |
| Respondent marital status | Married | 119 | 87.5 |
| | Unmarried | 17 | 12.5 |
| Household size | 2-3 | 18 | 13.2 |
| | 4-5 | 43 | 31.6 |
| | 6-7 | 49 | 36 |
| | 7 plus | 26 | 19.1 |
| Occupation | Farmer | 36 | 26.5 |
| | Business | 34 | 25 |
| | Shopkeeper | 8 | 5.9 |
| | Govt servant | 7 | 5.1 |
| | Daily wager | 17 | 12.5 |
| | Unemployed | 1 | 0.7 |
| | Housewife | 33 | 24.3 |
| Male children | 0-2 | 53 | 39 |
| | 3-5 | 78 | 57.4 |
| | 5 plus | 5 | 3.7 |
| Female children | 0-2 | 63 | 46.3 |
| | 3-5 | 72 | 52.9 |
| | 5 plus | 1 | 0.7 |
| Elderly male | 0-1 | 101 | 74.3 |
| | 2-3 | 34 | 25 |
| | >3 | 1 | 0.7 |
| Elderly female | 0-1 | 93 | 68.4 |
| | 2-3 | 43 | 31.6 |

Fuel choice for lighting and cooking before and after electrification.

Table 2 shows the lighting sources used before and after the MHP installation. The most prevalent usage of electricity among the responders was for lights. The energy source for lighting has undergone a significant change after MHP installation. Kerosene, candles and firewood were only used as backup after



MHP installation. Kerosene and candles were the primary sources of lighting in the village prior to MHP. Prior to having access to MHP, around 110 households relied on kerosene for lighting. However, just 12 households used kerosene as a lighting source after being given access to MHP. Similarly, 80 households used candles prior to the installation of the MHP, but afterwards only 20 households used it as a lighting source.

The survey also revealed electricity-based lighting source to be more efficient and socially preferred. For instance, a light bulb could illuminate an entire room, whereas a candle would not do so to the same degree, hence making it impossible for more than one person to read at night[38], [39]. The findings showed that electrical lighting has replaced kerosene as the primary energy source. This has been indicated in previous reported study as well[40]. This finding shows that the people of the village used conventional energy sources because they were available, rather than because they were dependable.

However, unlike lighting sources, there is little evidence of the same movement in cooking fuels, implying that having access to modernized electric power does not imply having access to modernized cooking fuels as well. When compared to alternatives, firewood was the most widely used resource because it's easily available and is free of cost. Table 2 below shows that the primary source for cooking in the village was fuel wood. Fuel wood was primarily used for cooking before and after electrification. It is evident from the figure that all the respondents relied on fuel wood for their cooking purpose even after MHP electrification. Before MHP installation, 136 households used fuel wood as their cooking fuel and after MHP installation 134 homes used fuel wood as their cooking source. Even after MHP electricity, firewood continues to be the primary fuel for cooking. This observation is also supported in the previous study [41]. Therefore, this study's findings show that fuel choice used for cooking has not been significantly impacted by electrification.

Table 2: Fuel choice for lighting before and after Micro hydro electrification

| Energy choice for lighting | Frequency of respondents | |
|----------------------------|--------------------------|------------------------|
| | Before MHP installation | After MHP installation |
| Micro hydropower | 0 | 136 |
| Kerosene | 110 | 12 |
| Candles | 80 | 20 |
| Generator | 8 | 6 |
| Wood | 56 | 7 |
| Energy choice for cooking | Frequency of respondents | |
| | Before MHP installation | After MHP installation |
| Wood | 136 | 134 |
| Dung cake | 11 | 8 |
| Charcoal | 10 | 8 |
| Micro hydropower | 0 | 0 |

Social Impacts of Micro Hydropower

Electrification was found to have a noteworthy effect on youngster's education. Traditional kerosene light, which was ineffectual and harmful to children's health, was replaced by clean, bright, and economical electricity. Figure 2 shows that micro hydro systems also greatly benefited students by giving them more time to study which was agreed by almost 83.8% of respondents. Prior to electrification, the majority of the children studied in the range of 1-2 hours but after electrification it changed from 1-2 hours range to 3-4 hours as shown below in Figure 3. These positives results are also evident in literature[42], [43]. While



households can watch television as a form of pleasure thanks to electricity therefore we asked respondents about whether television hamper study time of children. 76.5% of the respondents disagree with the statement that television hampers the study time of children.

Before MHP residents had to rely on firewood, candles and kerosene for cooking and lighting. Unlike these resources, micro-hydroelectricity produces clean, smoke-free energy. As a result, installation of MHP plant aided in decreasing indoor air pollution, and significantly lowering the prevalence of visual and respiratory disorders. Around 75% of respondents agreed that health-related difficulties had lessened as a result of MHP electrification (Figure 2). This result is also validated by another published study[44]. The respondents were also asked about electrification's impact on health care services with 61.8% respondents agreeing that the health care services have improved after electrification. This positive result of electrification impact on health care service is evident from literature as well[45]. Electricity also increased their awareness regarding health issues according to 64.7% of the respondents. This observation is also supported in previous study [46]. The main source of knowledge regarding health issues according to the respondents was T.V with 51 respondents indicating T.V as the main source of knowledge.

Access to electricity also enhanced security, or more precisely, how people perceived security. Most of the respondents (83.1%) agreed that the security situation in their village has improved after electrification as shown in Figure 2. This is also evident in literature [45], [47]. The main cause of the security improvement was due to increased access to street lighting outside the house and having light all night in the home. 81 respondents reported that having streetlights outside their houses was one of the major reasons for feeling safer and secure. While 56 respondents suggested that having bright light all night in the home was the key reason for improved security in the community.

77.2% of the respondents agreed that access to information has increased after access to electricity. The finding is parallel with previous reported study [45]. It can be seen from Figure 4 below that ownership of information and communication technologies increased after MHP electrification. After electrification, more than 88% of households acquired radios compared to 66.9% percent before electrification. Use of mobile phones, in each household, also drastically increased up to 94% after MHP electrification. However, a major change was observed with respect to ownership of television sets, which rarely existed in the selected rural community before MHP electrification. This is evident from literature[48].

Economic Impacts

MHP also resulted in some positive economic impacts. The reduction in expenditure on supplemental energy sources, because of the quitting of kerosene and candle use, was one of the most significant effects. Before MHP installation, kerosene and candles were the primary fuel used for lighting. However, after MHP installation, there was major shift from kerosene and candle to electricity as the primary source of lighting which was supplied by MHP. This is evident in our findings where 75.7% of respondents agreed that their energy expenses decreased thanks to MHP electrification (Figure 5). Significant monetary reduction in terms of money spent on kerosene and candles after MHP installation is depicted in Table 3. Reduction on energy expenses after MHP electrification is also evident from literature[49].

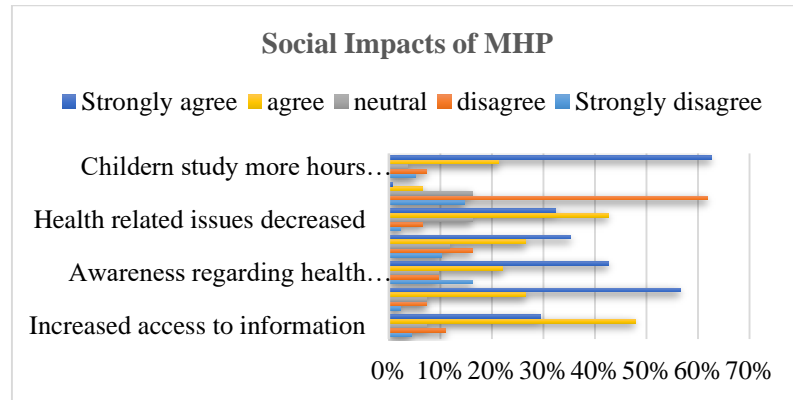


Figure 31: Opinion of respondents regarding social impacts of MHP

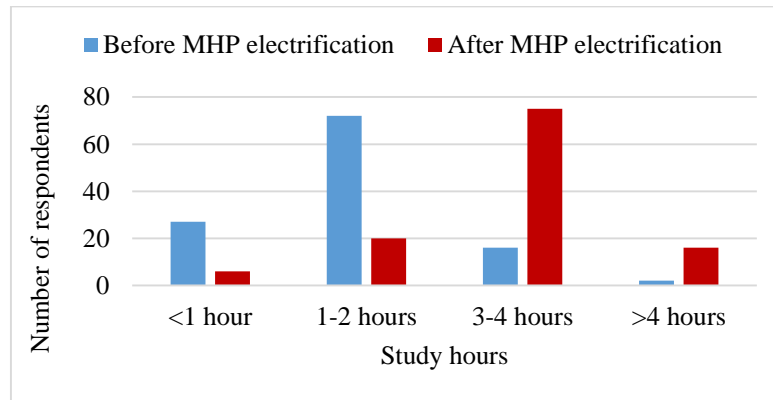


Figure 32: Study hours before and after MHP installation

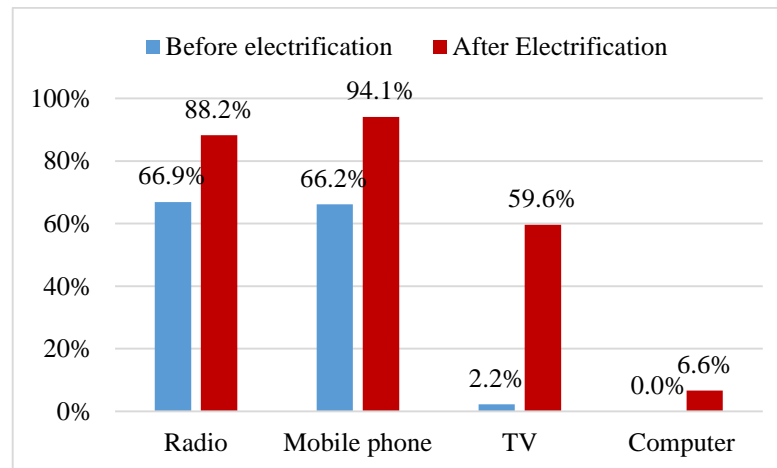


Figure 33: Access to information and communication technologies

Respondent's income also increased after MHP electrification as shown in Figure 6. Up to 37.50% respondents declared that their monthly income increased to 30,001-40,001 PKR after MHP electrification.



Before MHP, only 16.9% community members had income in that range which further shows the favorable influence of MHP initiative on the community of Lalkoo Village. The increase in income is supported by numerous studies [40], [44], [50].

The respondents were also asked about the electrification impact on income generation activities. Overall, electrification did not appear to have a substantial impact on the expansion of income-generating activities. Figure 7 shows that the number of homes with home-based income-generating enterprises was about the same before and after electricity. Sewing fabric, handicraft, and weaving remained the common home-based income generating activities in the studied area. So, electricity was not concluded as the primary driving element behind the formation of income-generating businesses. Literature also supports this finding that electrification alone has little to no impact on the initiation of income-generating activities and that additional conditions must be in place to facilitate the growth of income-generating activities[51].

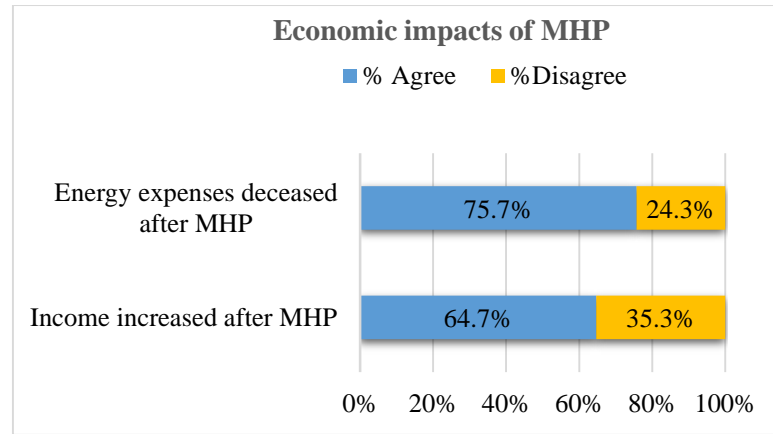


Figure 34: Opinion of respondents regarding Economic impacts

Table 3: Expenditure on kerosene and candles before and after MHP installation

| | | Frequency | |
|----------|--------------------|-----------|-------|
| Category | Expenditure in PKR | Before | After |
| Kerosene | 0-200 | 3 | 7 |
| | 200-400 | 13 | 3 |
| | 400-600 | 52 | 2 |
| | 600-800 | 24 | 0 |
| | 800-1000 | 15 | 0 |
| | >1000 | 3 | 0 |
| Candle | | Before | After |
| | 0-200 | 25 | 18 |
| | 200-400 | 45 | 2 |
| | 400-600 | 10 | 0 |

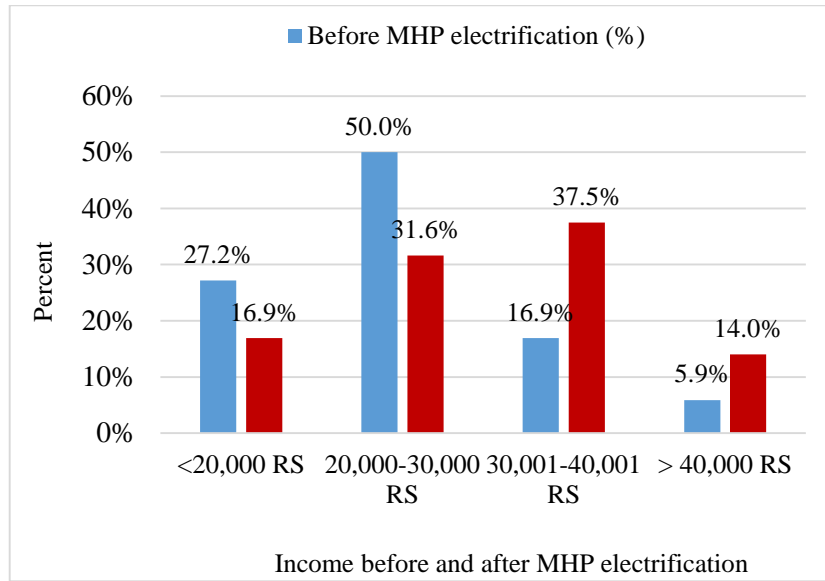


Figure 35: Income before and after MHP installation

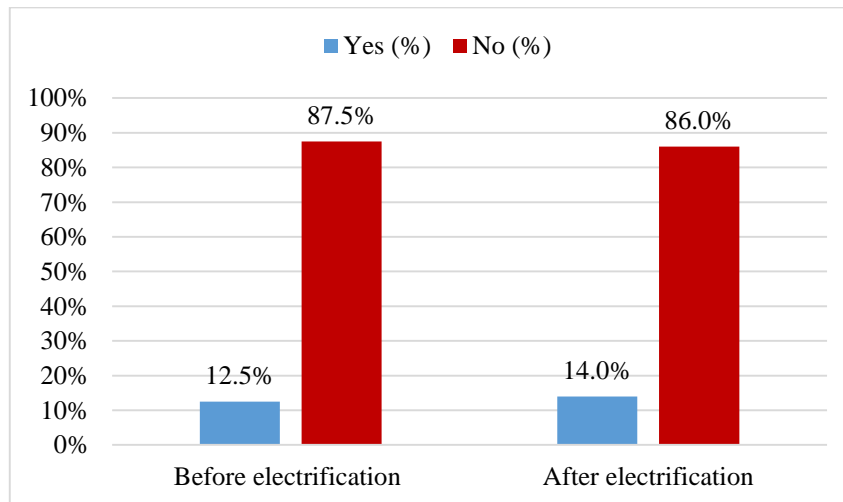


Figure 36: Home base income generation activities before and after electrification

CONCLUSION

Pakistan's energy requirements are mostly met by conventional fossil fuel-based energy sources. The government is making every effort to include clean energy in the total energy supply due to the hazards involved with using traditional energy sources, such as their rising costs, rapid decrease in supply, and negative environmental repercussions[52]. Options for renewable energy could help countries like Pakistan overcome their ongoing energy crisis. MHP is regarded as one of the most profitable ways to produce electric power. This research was conducted to understand the socioeconomic impact of MHP in the rural area of Lalkoo (Swat) using a survey approach.



ICSET-23



UET Peshawar

The findings of the research indicated that MHP installation has a favorable impact on rural people's lives. It improved the rural household's socioeconomic status. In terms of social impacts education, health, security and access to information and communication were greatly impacted. Education of the children was significantly improved in terms of increased study hours. 83.8% of respondents agreed with the statement that they had more time to study because of electrification. Health of the respondents also improved greatly with 75% of respondents reporting less health-related difficulties after electrification. Significant improvements in the village's security condition were also noted after electrification. According to 83.1% of the survey participants, electrification had increased security in their hamlet. The main cause of the security improvement according to the respondents was due to increased access to street lighting outside the house and having light all night in the home. Additionally, 77.2% of the respondents also agreed that access to information and communication has increased after access to electricity. In terms of economic impacts positive improvement were reported in terms of income and money spent on energy expenses. Up to 37.50% respondents declared that their monthly income increased to 30,001-40,001 PKR after MHP electrification. While 75.7% of respondents agreed that their energy expenses decreased thanks to MHP electrification. However, no significant influence on income-generating activities was reported. It is our expectation that implementers and policymakers of MHP projects will benefit greatly from this research, as it will enable them to plan successfully for future projects.

LIMITATION OF STUDY AND FUTURE RESEARCH

This research is grounded on the fundamental investigation carried out for educational purposes. Due to time and money restrictions, the study was only able to include one village, and only a small sample size was chosen from it. The results will be more representative and reliable if a large sample is chosen, even if we utilized a probabilistic sampling method and technically the results may be applied for comparable non-urban areas in Pakistan. A bias in the responses to the questions could be another drawback. Despite disclaimers of surveying team not representing a government agency, respondents may still have replied to the preferred option.

More research is needed to have a better grasp of the socioeconomic and environmental effects of these MHP projects on Pakistani rural communities. Future research should focus on the environmental consequence of these MHP projects, which might have significant policy conclusions in terms of extending MHP in the face of global climate change.

ACKNOWLEDGEMENTS

This research was supported and financed by U.S Pakistan Center for Advanced Studies in Energy (USPCAS-E), National University of Sciences and Technology (NUST), Sector H-12, Islamabad.

REFERENCES

- [1] Katuwal, H., & Bohara, A. K. (2009). Biogas: A promising renewable technology and its impact on rural households in Nepal. *Renew. Sustain. Energy Rev.*, 13(9), 2668–2674.
- [2] Mulder, P., & Tembe, J. (2020). Rural electrification in an imperfect world: A case study from Mozambique. *Energy*, 36(2008), 2785–2794.
- [3] Wazed, M. A., & Ahmed, S. (2009). A feasibility study of micro-hydroelectric power generation at Sapchari waterfall, Khagrachari, Bangladesh. *J. Appl. Sci.*, 9(2), 372–376.



- [4] Anup, G., Ian, B., & Sang-Eun, O. (2011). Micro-hydropower: A promising decentralized renewable technology and its impact on rural livelihoods. *Sci. Res. Essays*, 6(6), 1240–1248.
- [5] IEA. (2019). Access to electricity. [Online]. Available: <https://www.iea.org/reports/sdg7-data-and-projections/access-to-electricity>. [Accessed: 28-Jul-2022].
- [6] IEA. (2018). Pakistan. [Online]. Available: <https://www.iea.org/countries/Pakistan>. [Accessed: 28-Jul-2022].
- [7] Mirza, U. K., Ahmad, N., Majeed, T., & Harijan, K. (2007). Wind energy development in Pakistan. pp. 2179–2190.
- [8] NEPRA. (2016). State of industry report 2016.
- [9] NEPRA. (2019). State of Industry report 2019.
- [10] Das Valasai, G., Uqaili, M. A., Memon, H. U. R., Samoo, S. R., Mirjat, N. H., & Harijan, K. (2017). Overcoming electricity crisis in Pakistan: A review of sustainable electricity options. *Renew. Sustain. Energy Rev.*, 72, 734–745.
- [11] Ali, S., Fazal, T., Javed, F., Hafeez, A., Akhtar, M., & Haider, B. (2020). Investigating biodiesel production strategies as a sustainable energy resource for Pakistan. *J. Clean. Prod.*
- [12] Raheem, A., et al. (2016). Renewable energy deployment to combat energy crisis in Pakistan. *Energy, Sustainability and Society*, 6(1).
- [13] Carnino, A., & Niehaus, F. (1999). Health and environmental impacts of electricity generation: Targeting safety. *IAEA Bulletin*, 41(1), 7.
- [14] Singh, V. K., & Singal, S. K. (2017). Operation of hydro power plants-a review. *Renew. Sustain. Energy Rev.*, 69, 610–619.
- [15] Abdul, I., et al. (2020). Turn on the lights: Macroeconomic factors affecting renewable energy in Pakistan. *Renew. Sustain. Energy Rev.*, 38, 277–284.
- [16] Rafique, M. M., & Rehman, S. (2017). National energy scenario of Pakistan – Current status, future alternatives, and institutional infrastructure: An overview. *Renew. Sustain. Energy Rev.*, 69, 156–167.
- [17] Sheikh, M. A. (2010). Energy and renewable energy scenario of Pakistan. *Renew. Sustain. Energy Rev.*, 14(1), 354–363.
- [18] Kamran, M. (2018). Current status and future success of renewable energy in Pakistan. *Renew. Sustain. Energy Rev.*, 82, 609–617.
- [19] Huang, S. R., et al. (2014). Evaluating the productivity and financial feasibility of a vertical-axis micro-hydro energy generation project using operation simulations. *Renew. Energy*, 66, 241–250.
- [20] Mainali, B., & Silveira, S. (2013). Alternative pathways for providing access to electricity in developing countries. *Renew. Energy*, 57, 299–310.
- [21] Social Uplifts. [Online]. Available: <https://pedokp.gov.pk/socialUp/socialUpDetail/10>. [Accessed: 03-Jun-2022].
- [22] Ahsan, S., & Shah, A. (2019). Feasibility study of renewable energy sources for developing the hydrogen economy in Pakistan. *Int. J. Hydrogen Energy*, 45(32), 15841–15854.
- [23] Gurung, A., Gurung, O. P., & Oh, S. E. (2011). The potential of a renewable energy technology for rural electrification in Nepal: A case study from Tangting. *Renew. Energy*, 36(11), 3203–3210.
- [24] Gurung, A., et al. (2011). Socio-economic impacts of a micro-hydropower plant on rural livelihoods. *Sci. Res. Essays*, 6(19), 3964–3972.
- [25] Airaj, M., et al. (2020). Sustainable energy, 1(1), 1–7.
- [26] Karumba, M., & Muchapondwa, E. (2018). The impact of microhydroelectricity on household welfare indicators. *Energy Efficiency*, 11(3), 663–681.



- [27] Bangash, S. (2012). Socio-Economic Conditions of Post-Conflict Swat: A Critical Appraisal. *Tigah A J. Peace Dev.*, 2(December), 66–79.
- [28] Dahri, Z. H., et al. (2011). Satellite-based snowcover distribution and associated snowmelt runoff modeling in Swat River Basin of Pakistan. *Proc. Pakistan Acad. Sci.*, 48(1), 19–32.
- [29] ADP-Swat 1 - Atlas of the Natural Resources Evaluation. [Online]. Available: <https://studylib.net/doc/18778584/adp-swat-1---atlas-of-the-natural-resources-evaluation>. [Accessed: 12-Jul-2022].
- [30] Welcome to Pakistan Research Repository: evaluation of surface water resources and sediment load in indus and swat kohistan north pakistan. [Online]. Available: <http://pr.hec.gov.pk/jspui/handle/123456789/3687>. [Accessed: 12-Jul-2022].
- [31] Khan, S. R., & Khan, S. R. (2009). Assessing poverty-deforestation links: Evidence from Swat, Pakistan. *Ecol. Econ.*, 68(10), 2607–2618.
- [32] Becker, F. G., et al. (2015). Government of Khyber Pakhtunkhwa. Khyber Pakhtunkhwa Wildlife and Biodiversity (Protection, Preservation, Conservation and Management) Act. *Syria Stud.*, 7(1), 37–72.
- [33] Dir, D., et al. (2015). Application of Remote Sensing and GIS in Forest Cover Change in Tehsil Barawal. (June), 1501–1508.
- [34] Lalkoo village. (2021). [Online]. Available: <http://worldajuba.blogspot.com/2021/04/gabin-jabba-swat-valley-kalam-pakistan.html>. [Accessed: 30-Jul-2022].
- [35] Yamane, T. (1967). *Statistics: An Introductory Analysis* (2nd ed.). New York: Harper and Row.
- [36] Kothari, C. R. (2004). *Research Methodology: Methods and Techniques*. New Age International.
- [37] Howells, M. I., et al. (2005). A model of household energy services in a low-income rural African village. (33), 1833–1851.
- [38] Sector, T. R. (2013). A Survey of Energy Related Behaviour and Perceptions in South Africa.
- [39] González, A. H., et al. (2009). Micro Hydro Power Plants in Andean Bolivian communities: Impacts on development and environment, 1(7).
- [40] Bisaga, I., & Parikh, P. (2018). To climb or not to climb? Investigating energy use behaviour among Solar Home System adopters through energy ladder and social practice lens. *Energy Res. Soc. Sci.*, 44(May), 293–303.
- [41] Raj, R., Palit, D., & Mahapatra, S. (2014). Comparative Analysis of Solar Photovoltaic Lighting Systems in. *Energy Procedia*, 54, 680–689.
- [42] Arnaiz, M., Cochrane, T. A., Hastie, R., & Bellen, C. (2018). Micro-hydropower impact on communities' livelihood analysed with the capability approach. *Energy Sustain. Dev.*, 45, 206–210.
- [43] Shoaib, A., & Ariaratnam, S. (2016). A Study of Socioeconomic Impacts of Renewable Energy Projects in Afghanistan. *Procedia Eng.*, 145, 995–1003.
- [44] Patil, D. A. (2010). Connecting Power—Biomass Electrification, Social Change and Management in Indian Village. (November 2018).
- [45] Sarker, S. A., et al. (2020). Economic viability and socio-environmental impacts of solar home systems for off-grid rural electrification in Bangladesh. *Energies*, 13(3).
- [46] Gippner, O., Dhakal, S., & Sovacool, B. K. (2013). Microhydro electrification and climate change adaptation in Nepal: Socioeconomic lessons from the Rural Energy Development Program (REDP). *Mitig. Adapt. Strateg. Glob. Chang.*, 18(4), 407–427.
- [47] Sánchez, A., & Izzo, M. (2017). Micro hydropower: an alternative for climate change mitigation, adaptation, and development of marginalized local communities in Hispaniola Island. *Clim. Change*, pp. 79–87.



ICSET-23

*Proceedings of the 5th International Conference on Sustainable
Energy Technologies (ICSET 2023) Peshawar, Pakistan
14-15 December 2023*



UET Peshawar

- [48] Strategies, L., et al. (2019). Impact of Micro Hydropower Projects on Household Income, Expenditure and Diversification of Livelihood Strategies in Azad Jammu and Kashmir. (1), 45–63.
- [49] Wamukonya, N., & Davis, M. (2001). Socio-economic impacts of rural electrification in Namibia: comparisons between grid, solar and unelectrified households. *Energy Sustain. Dev.*, 5(3), 5–13.
- [50] IEA. (2019). Access to electricity. [Online]. Available: <https://www.iea.org/reports/sdg7-data-and-projections/access-to-electricity>. [Accessed: 28-Jul-2022].
- [51] Wamukonya, N., & Davis, M. (2001). Socio-economic impacts of rural electrification in Namibia: comparisons between grid, solar and unelectrified households. *Energy Sustain. Dev.*, 5(3), 5–13.
- [52] Jan, I., & Akram, W. (2018). Willingness of rural communities to adopt biogas systems in Pakistan: Critical factors and policy implications. *Renew. Sustain. Energy Rev.*, 81, 3178–3185.

Paper ID: ICSET-2306

INTELLIGENT DEMAND-SIDE MANAGEMENT FOR INTEGRATED RENEWABLE ENERGY IN RESIDENTIAL AREA SMART GRID: A PATHWAY TO SUSTAINABLE ENERGY USE

Abdullah Nawaz^{1,*}, Muhammad Sulaiman¹, Zohaib Ur Rehman¹, Amir Sohail Khan², Zainab Rasheed¹,
Habibatallah Saleh³, Muhammad Shoaib¹

¹Energy Management and Sustainability, Centre for Advance Studies in Energy, University of Engineering and
Technology Peshawar, Pakistan

²School of Information Engineering, Jiangxi University of Science and Technology, No 86, Hongqi Ave, Ganzhou,
Jiangxi, China

³Faculty of Energy and Environmental Engineering, The British University in Egypt (BUE), El-Sherouk City, Egypt

**Corresponding author*

Email: Kabdullahnawaz@gmail.com

ABSTRACT

Meeting the rapidly growing demand for electricity while facing limitations in grid expansion and constructing new conventional power plants has become a significant challenge. Demand-side management (DSM) in smart grids (SG) is being explored as a viable way to solve this problem. Using an energy management controller (EMC) based on heuristic algorithms, a novel method to DSM is described in this study that incorporates renewable energy into household load scheduling. The proposed EMC uses a day-ahead price-based demand response (DR) program to schedule residential loads using binary particle swarm optimisation (BPSO), bacterial foraging optimisation (BFO), and hybrid bacterial BPSO (HPBOA). This scheme's primary goals are to reduce electricity costs, the peak-to-average ratio (PAR), and CO₂ emissions, both with and without the use of solar panels and electric storage systems (ESS). According to our simulation results, the HPBOA-based EMC performs better in terms of management effectiveness than BPSO and BFOA-based EMC and effectively reduce not only PAR, electricity cost, CO₂ emission but also energy consumption and user comfort is taken into account. This suggested approach is ideal for managing residential services in real life. It is projected that it will close the supply-demand imbalance and support the development of a more sustainable energy future.

KEYWORDS: An Intelligent Controller Framework, smart grid, energy management controller, heuristic algorithm, carbon reduction

INTRODUCTION

The rising energy demand has led to a number of problems, including voltage instability, frequency drops, blackouts, and load shedding. Two strategies are now in use to solve these issues: By adopting a Home Energy Management (HEM) system to optimise the current power generation capacity, one may (i)



increase the capacity of power production and (ii) control energy consumption [1]. In the first strategy, adding additional substations serves as the main way for increasing the capacity of power generation. The second method, on the other hand, applies scheduling approaches while using Demand Side Management (DSM) program to control the demand based on the available generation capacity. These scheduling strategies take into account the requirements of both the user and the utility provider to control the load during peak and off-peak hours. To schedule home appliances, researchers have used Mixed Integer Linear Programming (MILP), a method that has been the subject of a substantial amount of research [2, 3, 4, 5, 6]. This method entails developing a mathematical model to assist in scheduling appliance usage as efficiently as possible.

Scientists have recently suggested a number of Demand Side Management (DSM) solutions to help consumers lower their energy usage. These strategies make use of off-peak load operation and renewable energy sources (RES) [7]. One study used a forward-backward algorithm to reduce the price of thermal appliances while accounting for the ability of thermostatic devices to store heat and the incorporation of photovoltaic (PV) panels with Energy Storage Systems (ESS). To avoid the occurrence of peaks in the electrical system, they also suggested a peak flattening method. The significance of optimal energy algorithms in enhancing end-user consumers (EUCs) performance, lowering consumer energy consumption, and delivering positive environmental effects was noted in [8]. The authors proposed the use of a genetic algorithm (GA) in two stages to reduce both electricity costs and human discomfort. The first stage involves lowering electricity expenses, and the second stage improved on that optimisation without raising the price of electricity that was purchased Fernandes et.al (18).

In case studies, the integration of numerous systems, including photovoltaic (PV), storage, lighting, heating, and air conditioning, has resulted in lower costs and Peak-to-Average Ratios (PAR). However, as a result, the system's complexity has grown. For scheduling appliances and lowering electricity expenditures, many studies have used Mixed Integer Non-Linear Programming (MINLP) or MILP and MINLP, such as in [10, 11, 12, 13]. To reduce power costs and PAR through appliance scheduling, the developers of [14] concentrated on residential users with integrated Energy Storage Systems (ESS) and PV. The particle swarm optimisation (PSO) technique was applied to reduce PAR and electricity costs by integrating Renewable Energy Sources (RES) and Electric Vehicles (EVs) [15]. The same study took into consideration improving consumer comfort when scheduling power utilisation. Another study examined that how power usage was scheduled in both residential and business settings and suggested the PSO algorithm to minimise PAR and electricity costs while maximising user comfort [16]. The peak-to-average ratio (PAR) was improved by combining real-time pricing (RTP) and inclining block rate (IBR) tariffs to control high power usage during periods of low energy cost. Additionally, as explained in [17], artificial intelligence was incorporated into the system design to provide a choice of energy consumption alternatives based on prior experiences. A user input link was added to the system in order to offer customised energy-saving services. Shirazi et.al (18) suggested an enhanced building automation system that would boost the effectiveness of energy utilisation in commercial flats. Customers may track and manage their energy use with the proposed system, as well as find possible opportunities for energy savings.

Although its advantages in the field of load scheduling, mathematical approaches like MILP and MINLP have a high computational complexity [19, 20]. Heuristic algorithms, on the other hand, provide greater flexibility within predetermined restrictions, are simpler to develop, and have a lower computational complexity [21, 22]. In our study, we use the BFOA and BPSO heuristic methods to tackle the load

scheduling issue. We selected these algorithms due to their decentralised control system, self-organization, self-optimization, self-protection, and self-healing capabilities [23, 24]. We evaluated the effectiveness of each method in a Day ahead pricing setting using a simulated HEM system [25].

The structure of this paper can be summarized as follows. Section 2 provides an overview of the system model and formulation and proposed solution. The simulation results are then presented and discussed in detail in Section 3. Finally, Section 4 offers concluding remarks on the study.

Design of the proposed system model

In order to undertake Demand Side Management (DSM) in a home context, we've proposed a Home-Based HBPOA in this study. To provide favourable results, our method incorporates crucial phases from the BPSO and BFO optimisation algorithms. The two stages of the HBPOA algorithm's operation. In order to improve the outcomes of BPSO, the second stage employs bacterial management strategies, such as chemotaxis and reproduction, as shown in Fig. 2. The first stage follows to the BPSO procedures. It has been demonstrated that the algorithm considerably enhances our results. The proposed algorithm is used to optimise the performance of an Energy Management Controller (EMC) in a residential environment. It is a comprehensive solution that combines a load scheduling model, a model of household energy demand, and a model of household energy supply made up of renewable energy sources (RES), energy storage systems, and a power grid. A wireless local area network (WLAN) is used by the EMC to communicate with smart appliances and smart metres, as seen in Fig. 1. Smart metres with EMCs are installed in the residential area to allow for two-way communication between utilities and customers. Utility companies and consumers both share information with the EMC, which is in charge of managing appliance scheduling. Users can modify their energy use habits in response to Demand Response (DR) signals. According to various time-based rate programmes, a dynamic pricing controller gives peak prices during peak demand hours and low rates during average demand hours. In short, the HBPOA algorithm suggested in this research offers a practical method for improving DSM in a home environment. In order to optimise energy consumption patterns, the EMC controls communication between utilities and customers, taking into account demand-based dynamic pricing plans.

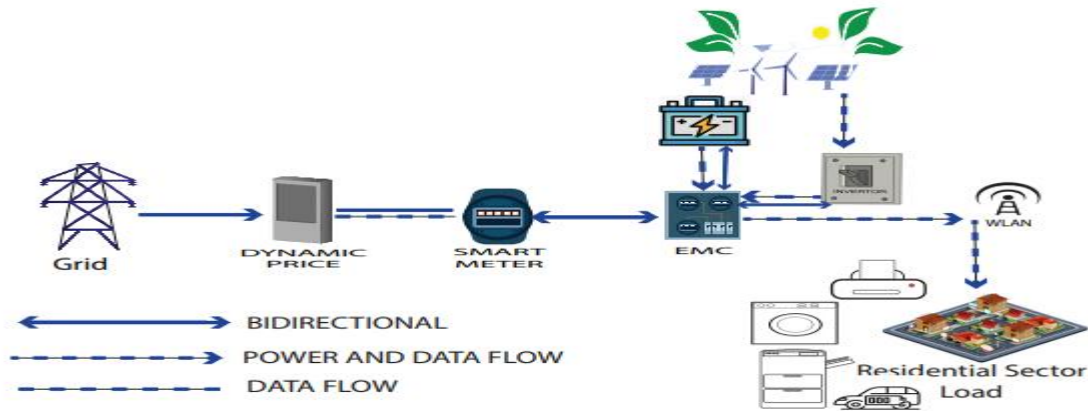


Figure 1: An Intelligent Integrated Framework .

Load Profiling

Based on their involvement in various DR programmes, we have simplified our load categorization procedure in our residential sector into two separate categories. As demonstrated, these groups are referred to as "Time-Adjustable Appliances" and "Baseload Appliances." as shown in Table. 1. Consider the group of appliances A_n , which has two separate subgroups: Let $A_n = A_{ta} \cup A_{bl}$. These subsets depict appliances that, in terms of their energy consumption, are Baseload Appliances and Time-Adjustable Appliances, respectively. Our method of classifying these appliances is based on their unique energy needs over a 24-hour period, marked by the symbol $T = \tau_1, \tau_2, \tau_3, \dots, \tau_{24}$. We can regulate and optimise our overall energy use by looking at the energy consumption trends of each appliance subset inside this time view.

Time-adjustable appliances

It is voluntary to change these devices, such as electric stoves, water pumps, food processors, and microwave ovens, to lower peak hours with lower electricity costs. They belong to the set A_{ta} , with each appliance represented by $a_{ta} \in A_{ta}$, and λ_{ta} is the power rating of each appliance. The net power usage per day ε_{ta} is calculated using Eq. 1.

$$\varepsilon_{ta} = \sum_{a_{ta} \in A_{ta}} [\sum_{\tau=1}^T \lambda_{ta} \times \alpha(\tau)] \quad (1)$$

the total cost per day of all time-adjustable appliances within a time interval T using Eq. 2, which is:

$$\varsigma_{ta}^{total} = \sum_{a_{ta} \in A_{ta}} [\sum_{\tau=1}^T \lambda_{ta} \times \rho(\tau) \times \alpha(\tau)] \quad (2)$$

In Eq. 3, the cost per hour of an adjustable appliance is determined based on the price signal $\rho(\tau)$ and the appliance's ON/OFF state, represented by $\alpha(\tau)$, which is a value between 0 and 1.

$$\sigma_{ta}^{\tau} = \sum_{a_{ta} \in A_{ta}} (\lambda_{ta} \times \rho(\tau) \times \alpha(\tau)) \quad \forall \tau = 1:T \quad (3)$$

We can lower the overall cost of power use by lowering the cost per hour of the adjustable appliances.

Base load appliances

The majority of base load appliances, like refrigerators, internet routers, fans, and lights, run continually on a set schedule. These appliances belong to the set A_{bl} , with each appliance represented by $a_{bl} \in A_{bl}$, and have a power rating of λ_{bl} . The overall power usage per day of base load appliances is ε_{bl} determined by Eq.4.

$$\varepsilon_{bl} = \sum_{a_{bl} \in A_{bl}} [\sum_{\tau=1}^T \lambda_{bl} \times \alpha(\tau)] \quad (4)$$

Base load appliances frequently run for extended periods of time since they are seen to be necessary for daily life. To continue serving customers and provide their basic necessities, their increased consumption is required by Eq.5.

$$\varsigma_{bl}^{total} = \sum_{a_{bl} \in A_{bl}} [\sum_{\tau=1}^T \lambda_{bl} \times \rho(\tau) \times \alpha(\tau)] \quad (5)$$

Using Eq. 6, which takes into factors like the price signal and the power rating of each appliance, it is possible to calculate the cost per hour of consistent appliances. Users can more effectively control their energy use and optimise their usage patterns to reduce their monthly electricity costs by computing the cost per hour.

$$\sigma_b l^T = \sum_{a_{bl} \in A_c} (\lambda_b l \times \rho(\tau) \times \alpha(\tau)) \quad \forall \tau = 1:T \quad (6)$$

Table 1: Description and Categorization of Appliances for the Residential Sector

| Appliance | Power Rating (kw) | Operation (hr) |
|-----------------------------------|-------------------|----------------|
| Time Adjustable Appliances | | |
| Electric stoves | 2 | 2 |
| Water pump | 0.5 | 2 |
| Food processor | 1 | 1 |
| Microwave Oven | 0.6 | 1 |
| Base Load Appliances | | |
| Internet router | 0.015 | 24 |
| Fans | 0.03 | 10 |
| Refrigerator | 0.5 | 24 |
| Lights | 0.015 | 8 |

Residential sector's total load consumption in time interval T is represented by γ Eq.

$$\gamma = \varepsilon_{ta} + \varepsilon_b l \quad (7)$$

Energy Expenses Per Day and Tariff Charges

Based on the price per unit of electricity, the user's cost for power use is calculated. There are many different pricing models, including day-ahead pricing, Critical Peak Pricing (CPP), and Time Of Use (TOU) pricing. In our study, we utilize day-ahead pricing scheme, denoted by $\rho(\tau)$, which represents the price signal for each time interval $\tau \in T$. Eq. 8, illustrates the cost per day for all appliances. To determine the overall cost per day, we add the cost per hour for the entire time period T.

$$\zeta_{total} = \sum_{\tau=1}^T \left(\sum_{a_i \in A_n} (\gamma_{(\tau, a_i)} \times \rho(\tau)) \right) \quad (8)$$

Mathematical Modelling of Solar Power and ESS

Let P_{solar} be the power generated by the solar panels in kW, and P_{load} be the power demand of the load in kW. Then the power balance as following Eq 9:

$$P_{load} = P_{grid} + P_{solar} \quad (9)$$

The excess energy produced by the solar panels during the day can be stored in the electric storage system and released during times of peak demand. The electric storage system is mathematically described in the following manner. Let $E_{storage}$ be the energy stored in the storage system in kWh, P_{charge} be the power used to charge the storage system in kW, and $P_{discharge}$ be the power used to discharge the storage system in kW. Then the energy balance can be written as Eq 10:

$$E_{storage,t} = E_{storage,t-1} + \eta_{charge} \cdot P_{charge,t} \cdot \Delta t - \frac{1}{\eta_{discharge}} \cdot P_{discharge,t} \cdot \Delta t \quad (10)$$

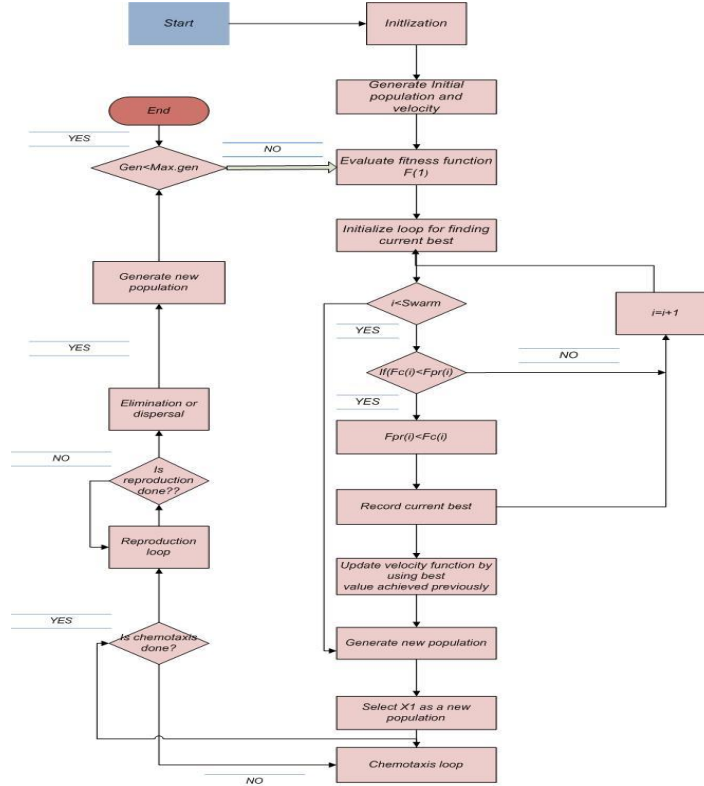


Figure 2: Hybrid BPOA flowchart .

FINDINGS AND ANALYSIS OF SIMULATION RESULTS

Through simulations, the performance of the newly suggested HBPSO-based EMC for DSM in the residential service area is assessed. The newly proposed HBPSO-based EMC is contrasted with previous EMC techniques including BFOA-based EMC and BPSO-based EMC. Cost of power, PAR, and CO₂ emissions—both with and without PV and ESS—are among the evaluating criteria. A residential service area home with two distinct groups of appliances, namely time adjustable and base load appliances, is taken into account during the simulation. The DSM for the residential dwelling is carried out based on the day-ahead pricing scheme shown in Fig 3. Solar irradiation and ambient temperature have a significant impact on a PV system's ability to generate power. We have accounted for 90% of the expected renewable energy (RE) for any given time slot in order to guarantee the dependability and accuracy of our energy scheduling method. In addition, we have set aside 30% of the 90% RE that is accessible during each time slot for the ESS.

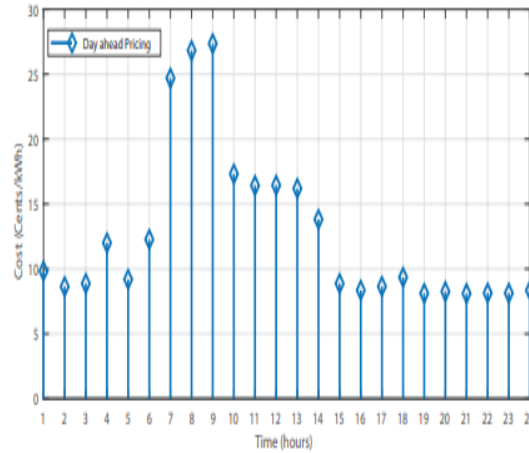


Figure 3: Day-ahead pricing scheme (Cents/kwh)

The amount of energy assigned to charging the ESS, and the unused RE after accounting for a 10% error margin. A thorough understanding of the energy scheduling and storage process is made possible by the presentation of the ESS charging level.

Energy Consumption by Applying HPBOA-Based DSM

Fig 4 shows the power usage patterns for scheduled and unscheduled cases in the residential sector. Unscheduled DSM uses 0.626 kWh of energy in the residential sector. In contrast, DSM based on BPSO has a somewhat lower power consumption, at 0.599 kWh. However, DSM's BFOA-based power consumption rises to 0.654 kWh. Finally, the power usage for DSM based on HPBOA is much lower at only 0.47 kWh. These findings imply that the algorithm employed can affect how effective DSM approaches are. In this situation, HPBOA appears to be the DSM technique with the lowest power consumption.

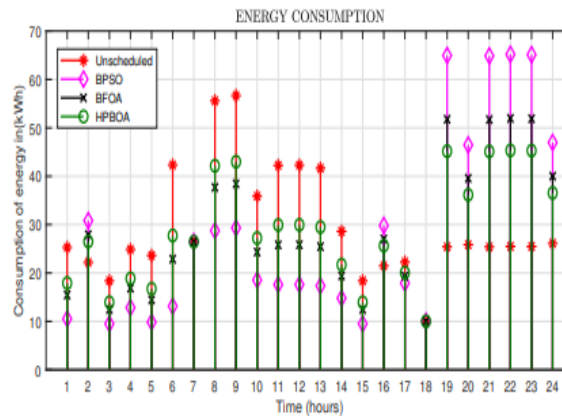


Figure 4: Energy Consumption (kwh)

Scenario 1

In this scenario, the simulation of the residential sector involves analyzing electricity bills 5, PAR 6, user comfort levels, and carbon emissions 7, in the absence of PV source and ESS.

The cost of power per day for unscheduled load, BPSO, BFOA, and HBPOA scheduled load is 7.8\$, 7.04\$, 7.52\$, and 6.64\$, respectively, as shown in Figure 5. These algorithms' respective cost reduction percentages are 9.74%, 3.58%, and 14.87%. The overall cost is reduced for all three algorithms. Notably, compared to both BPSO and BFOA algorithms, our suggested method HBPOA performs much better in terms of cost reduction.

The PAR of scheduled and unscheduled load is shown in Figure 6, with BPSO and BFOA algorithms reducing PAR by 4.1 and 16.6 percent, respectively. These algorithms try to reduce PAR and avoid peak loads, however our suggested HBPOA algorithm outperforms them by evenly distributing loads and moving them to off-peak times. As a consequence, HBPOA efficiently meets the stated target with a significant PAR reduction of 33.33 percent when compared to BPSO and BFOA.

Figure 7, shows the CO₂ emission per hour for each approach. It is clear by comparing the daily CO₂ emission of planned, BPSO, BFOA, and HBPOA loads that HBPOA performs best, with a reduction of 6.21%. The suggested HBPOA algorithm appears to be the most effective in lowering CO₂ emission, with a decrease of 6.21% compared to the other strategies. BFOA and BPSO load exhibit reductions of 1.12% and 4.66%, respectively. In particular, the HBPOA scheduled load had the lowest daily CO₂ emission of all the approaches examined at 664 kg.

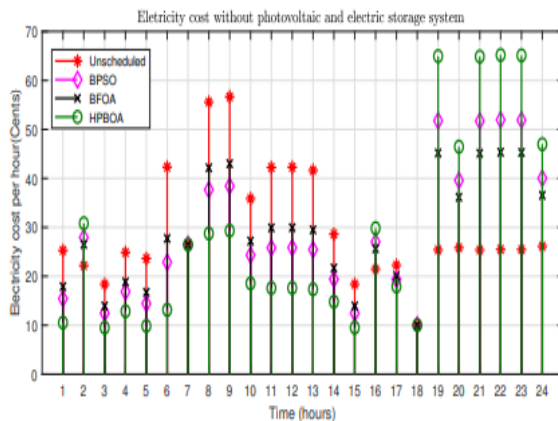


Figure 5: Electricity Cost without PV and ESS

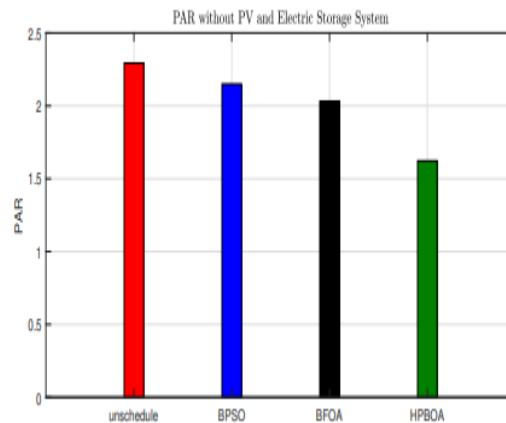


Figure 6: PAR without PV and ESS

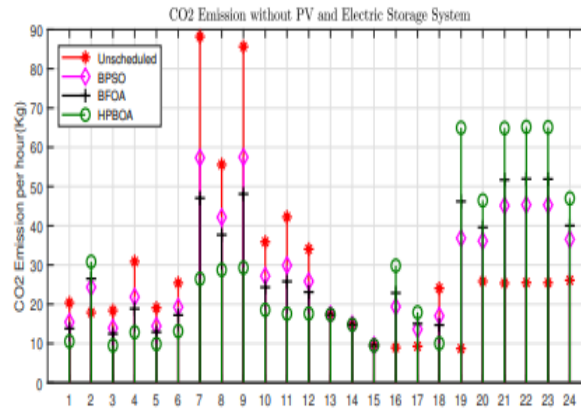


Figure 7: Co₂ Emission without PV and ESS

Scenario 2

In this scenario, the simulation of the residential sector involves analyzing electricity bills 8, PAR 9, user comfort levels, and carbon emissions 10, in the presence of renewable energy sources PV source and ESS.

Figure 8 shows the daily electricity prices for scheduled load, unscheduled load, BPSO, BFOA, and HBPOA. The related expenses are 8.17\$, 6.38\$, 7.22\$, and 5.62\$. Surprisingly, for BPSO, BFOA, and HBPOA, respectively, all three algorithms show cost savings with percentages of 21.90%, 11.62%, and 31.21%. In terms of lowering the overall cost, HBPOA performs much better than BPSO and BFOA. As a result, when compared to the other two algorithms, our suggested algorithm, HBPOA, exhibits greater cost reduction capabilities.

Figure 9 shows the PAR for scheduled and unscheduled load, with BPSO and BFOA algorithms demonstrating reductions of 33.33% and 29.16%, respectively. These methods are designed to reduce peak loads and PAR, but our suggested HBPOA algorithm exceeds them by spreading loads uniformly and moving them to off-peak times. As a result, compared to BPSO and BFOA, HBPOA produces an exceptional PAR decrease of 54.1%, thus completing the desired task. Therefore, compared to the other two algorithms, HBPOA shows higher capabilities in decreasing PAR.

The CO₂ emission per hour for each approach is shown in figure 10. The HBPOA algorithm performs the best, with a reduction of 25.45%, when compared to unscheduled, BPSO, BFOA, and HBPOA planned load in terms of daily CO₂ emission. However, the reductions for the BFOA and BPSO algorithms are 15.54% and 16.64%, respectively. With a reduction in CO₂ emissions of 25.45% when compared to the other strategies, the proposed HBPOA algorithm stands out as the most successful. In particular, the HBPOA scheduled load had the lowest daily CO₂ emission of all the strategies examined at 609 kg. As a result, the HBPOA algorithm outperforms the other two algorithms in terms of lowering CO₂ emissions.

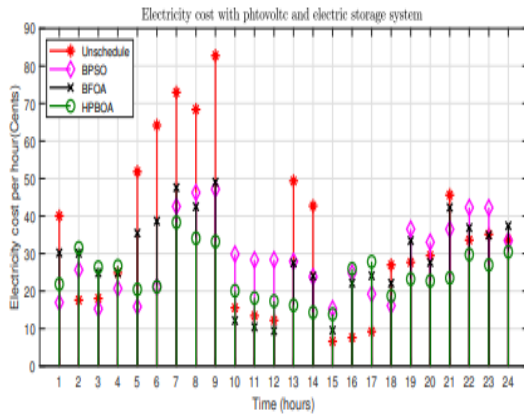


Figure 10: Cost of electricity with PV and ESS

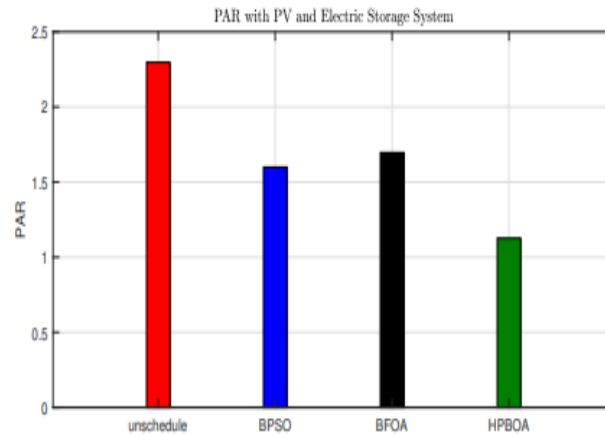


Figure 11: PAR with PV and ESS

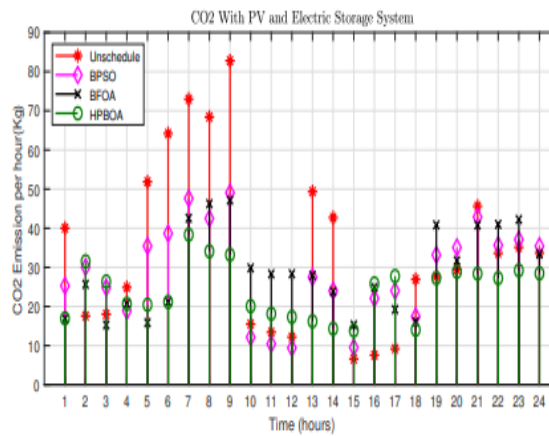


Figure 12: CO₂ Emission with PV and ESS

User Comfort

Table 2 displays the time delay for each kind of load, including time-adjustable and base load appliances. The table's delay timings are correct and haven't been changed in any manner.

Table 2: Delay time user comfort for different load categories in residential sector.

| Scheduling Technique | Time Adjustable Load | Base load |
|----------------------|----------------------|-----------|
| BFOA | 2.34 | 3.11 |
| BPSO | 4.14 | 2.54 |
| HBPOA | 2.1 | 1.32 |

Comparison of Scenario 1 and 2

The scenarios 1 and 2 reflect two distinct DSM situations in SG systems. The 4.2 scenario takes into account the cost of electricity, PAR, and CO₂ emissions in the absence of PV and ESS. The power cost,



PAR, and CO₂ emission under Scenario 3.3 on the other hand are examined in relation to the demand-side management renewable integration of PV and ESS in the smart grid. In order to understand the possible advantages of incorporating PVs and ESS in DSM, it is helpful to compare these two scenarios.

The findings demonstrate that demand-side control can significantly reduce electricity costs, PAR, and CO₂ emissions through the use of PV and electric storage systems. In more precise terms, the cost decrease without PV and ESS is 14.87%, but it increases to 31.21% with PV and an electric storage system. Similar to this, the PAR increases to 54.16% with PV and an energy storage system from 33.33% without either. Without PV and ESS, CO₂ emissions are reduced by 6.21%, but they are reduced by 25.45% with these two technologies.

CONCLUSION

In this article, the proposed HBPOA algorithm outperforms both BPSO and BFOA algorithms, with and without PV and ESS 3.5. The system equitably distributes loads and moves them into off-peak times, which substantially lowers the price of power, PAR, and CO₂ emissions. These results illustrate the efficiency of the proposed HBPOA algorithm in attaining these objectives by reducing electricity cost, PAR and CO₂ emission by 31.21, 54.16, 25.45 percent respectively and show the potential advantages of integrating RE sources and storage systems into demand-side management by that of without PV and ESS which are 14.87, 33.33, 6.21 percent respectively. Future research on the effects of other RE sources and storage technologies, like wind or battery storage, on DSM in SG would be interesting. Investigating how the suggested algorithm affects other performance indicators, such as voltage stability and power quality, as well as how it might be applied to applications other than DSM, would also be helpful.

REFERENCES

- [1] Sattarpour, Tohid, Daryoush Nazarpour, and Sajjad Golshannavaz. "A multi-objective HEM strategy for smart home energy scheduling: A collaborative approach to support microgrid operation." *Sustainable cities and society* 37 (2018): 26-33.
- [2] Agnetis, Alessandro, Gianluca De Pascale, Paolo Detti, and Antonio Vicino. "Load scheduling for household energy consumption optimization." *IEEE Transactions on Smart Grid* 4, no. 4 (2013): 2364-2373.
- [3] Bayraktar, Zikri, Muge Komurcu, Jeremy A. Bossard, and Douglas H. Werner. "The wind driven optimization technique and its application in electromagnetics." *IEEE transactions on antennas and propagation* 61, no. 5 (2013): 2745-2757.
- [4] Beaudin, Marc, and Hamidreza Zareipour. "Home energy management systems: A review of modelling and complexity." *Energy Solutions to Combat Global Warming* (2017): 753-793.
- [5] Zhou, Bin, Wentao Li, Ka Wing Chan, Yijia Cao, Yonghong Kuang, Xi Liu, and Xiong Wang. "Smart home energy management systems: Concept, configurations, and scheduling strategies." *Renewable and Sustainable Energy Reviews* 61 (2016): 30-40.
- [6] Carpinelli, Guido, Gianni Celli, Susanna Mocci, Fabio Mottola, Fabrizio Pilo, and Daniela Proto. "Optimal integration of distributed energy storage devices in smart grids." *IEEE Transactions on smart grid* 4, no. 2 (2013): 985-995.



- [7] Das, Swagatam, Arijit Biswas, Sambarta Dasgupta, and Ajith Abraham. "Bacterial foraging optimization algorithm: theoretical foundations, analysis, and applications." *Foundations of computational intelligence volume 3: global optimization* (2009): 23-55.
- [8] Faria, Pedro, João Soares, Zita Vale, Hugo Morais, and Tiago Sousa. "Modified particle swarm optimization applied to integrated demand response and DG resources scheduling." *IEEE Transactions on smart grid* 4, no. 1 (2013): 606-616.
- [9] Fernandes, Filipe, Tiago Sousa, Marco Silva, Hugo Morais, Zita Vale, and Pedro Faria. "Genetic algorithm methodology applied to intelligent house control." In *2011 IEEE Symposium on Computational Intelligence Applications In Smart Grid (CIASG)*, pp. 1-8. IEEE, 2011.
- [10] Golmohamadi, Hessam, Reza Keypour, Birgitte Bak-Jensen, and Jayakrishnan Radhakrishna Pillai. "Optimization of household energy consumption towards day-ahead retail electricity price in home energy management systems." *Sustainable Cities and Society* 47 (2019): 101468.
- [11] Hubert, Tanguy, and Santiago Grijalva. "Realizing smart grid benefits requires energy optimization algorithms at residential level." In *ISGT 2011*, pp. 1-8. IEEE, 2011.
- [12] Kong, Xiangyu, Bowei Sun, Deqian Kong, and Bin Li. "Home energy management optimization method considering potential risk cost." *Sustainable Cities and Society* 62 (2020): 102378.
- [13] Lim, Kai Zhuo, Kang Hui Lim, Xian Bin Wee, Yinan Li, and Xiaonan Wang. "Optimal allocation of energy storage and solar photovoltaic systems with residential demand scheduling." *Applied Energy* 269 (2020): 115116.
- [14] Cheng, Pei-Hsuan, Tzu-Han Huang, Yi-Wei Chien, Chao-Lin Wu, Chia-Shing Tai, and Li-Chen Fu. "Demand-side management in residential community realizing sharing economy with bidirectional PEV while additionally considering commercial area." *International Journal of Electrical Power & Energy Systems* 116 (2020): 105512.
- [15] Sharifi, Amir Hossein, and Pouria Maghouli. "Energy management of smart homes equipped with energy storage systems considering the PAR index based on real-time pricing." *Sustainable cities and society* 45 (2019): 579-587.
- [16] Aurangzeb, Khursheed, and Musaed Alhussein. "Deep learning framework for short term power load forecasting, a case study of individual household energy customer." In *2019 International Conference on Advances in the Emerging Computing Technologies (AECT)*, pp. 1-5. IEEE, 2020.
- [17] Logenthiran, Thillainathan, Dipti Srinivasan, and Ei Phyu. "Particle swarm optimization for demand side management in smart grid." In *2015 IEEE Innovative Smart Grid Technologies-Asia (ISGT ASIA)*, pp. 1-6. IEEE, 2015.
- [18] Shirazi, Elham, and Shahram Jadid. "Optimal residential appliance scheduling under dynamic pricing scheme via HEMDAS." *Energy and Buildings* 93 (2015): 40-49.
- [19] Soares, João, Tiago Sousa, Hugo Morais, Zita Vale, Bruno Canizes, and António Silva. "Application-Specific Modified Particle Swarm Optimization for energy resource scheduling considering vehicle-to-grid." *Applied Soft Computing* 13, no. 11 (2013): 4264-4280.
- [20] Zhao, Zhuang, Won Cheol Lee, Yoan Shin, and Kyung-Bin Song. "An optimal power scheduling method for demand response in home energy management system." *IEEE transactions on smart grid* 4, no. 3 (2013): 1391-1400.
- [21] Javaid, Nadeem, Sakeena Javaid, Wadood Abdul, Imran Ahmed, Ahmad Almogren, Atif Alamri, and Iftikhar Azim Niaz. "A hybrid genetic wind driven heuristic optimization algorithm for demand side management in smart grid." *Energies* 10, no. 3 (2017): 319.



ICSET-23

*Proceedings of the 5th International Conference on Sustainable
Energy Technologies (ICSET 2023) Peshawar, Pakistan
14-15 December 2023*



UET Peshawar

- [22] Aslam, Sheraz, Adia Khalid, and Nadeem Javaid. "Towards efficient energy management in smart grids considering microgrids with day-ahead energy forecasting." *Electric Power Systems Research* 182 (2020): 106232.
- [23] Aurangzeb, Khursheed, Sheraz Aslam, Herodotos Herodotou, Musaed Alhussein, and Syed Irtaza Haider. "Towards electricity cost alleviation by integrating RERs in a smart community: A case study." In *2019 23rd International Conference Electronics*, pp. 1-6. IEEE, 2019.
- [24] Judge, Malik Ali, Awais Manzoor, Carsten Maple, Joel JPC Rodrigues, and Saif ul Islam. "Price-based demand response for household load management with interval uncertainty." *Energy Reports* 7 (2021): 8493-8504.
- [25] Day ahead pricing for residential customers, MISO daily report archives;2019. [Online]. Available: <http://www.ferc.gov/market-oversight/mkt-electric/midwest/miso-archives.asp>. Accessed on: May 19, 2019

Paper ID: ICSET-2307

Design and Sustainable Fabrication of a PVC Wind Turbine for Clean Energy Generation

Muhammad Shoaib^{1,*}, Abdullah Nawaz¹, Adnan Asghar Khan¹, Muhammad Sulaiman¹, Maira Amjad¹,
Amir Sohail Khan², Habibatallah Saleh³

¹*Energy Management and Sustainability, US-Pakistan Center for Advanced Studies in Energy, University of Engineering and Technology Peshawar, Pakistan*

²*School of Information Engineering, Jiangxi University of Science and Technology, No 86, Hongqi Ave, Ganzhou, Jiangxi, China*

³*Faculty of Energy and Environmental Engineering, the British University in Egypt (BUE), El-Sherouk City 11837, Egypt*

**Corresponding author*

Email: Kabdullahnawaz@gmail.com

ABSTRACT

The generation of electricity from wind power is an exciting development in the field of renewable energy. Availability of energy is crucial to the functioning of today's technological society around the world. Increasing access to electricity is critical to the growth of commerce, agriculture, and transportation. The rising demand for power and the depletion of traditional power supplies used to generate electricity are driving up the price of energy. Therefore, it is of the utmost importance to utilize alternative energy sources such as wind power, solar power, tidal power, geothermal power, etc. Wind is one of the most promising renewable energy sources. It converts the amount of kinetic energy produced by the wind into the rotational power of the shaft, which is then used to create electricity. The goal of this research is to create a low-cost, household wind turbine made of polyvinyl chloride (PVC) that can function in moderate winds. The blades are made out of PVC because it is cheap and widely available. To achieve maximum efficiency, we use solid employment and Computational Fluid Dynamics (CFD) analysis for the blade to optimize the lift force, drag force, and coefficient of lift. We enhance the wind turbine's rotational speed through the implementation of a gearbox ratio, optimizing its performance. The power generation is accomplished using a DC dynamo, a well-known type of generator.

KEYWORDS: PVC, CFD, Wind energy, Fabrication, Sustainability, Generation

INTRODUCTION

Wind refers to a form of solar power. Winds develop as a result of variations in atmospheric pressure and temperature caused by the sun's uneven heating of the atmosphere. This causes the warmer air to expand, resulting in increased pressure in the cooler regions and decreased pressure in the warmer regions. Depending of permanent vegetative coverings and water bodies in a given region, wind-flow patterns will vary. Electricity is generated by wind turbines by harnessing this air movement [1]. Specifically, they use wind's kinetic energy to generate electricity. The wind's cycles and currents are unaffected by the process



of harvesting wind and converting it into energy. Blades, a structure, an internal shaft, and a chamber housing the generator are the basic components of every wind turbine [2].

Wind power, often known as wind energy, is the practise of harnessing wind to create mechanical or chemical energy. To produce electricity, a generator first transforms the kinetic energy into mechanical energy. Mechanical energy can be put to use for tasks such as milling grains or water being circulated. While the electrical variety can be utilised to power appliances like refrigerators and heating systems [3].

Numerous benefits come with wind power, including its limitless and cost-free nature, its clean and eco-friendly features with no greenhouse gas emissions, and its affordability. The fact that turbine blades can injure birds and bats, construction-related noise pollution, and the difficulty of placing wind farms far from populated areas are all drawbacks that are related to wildlife. Both horizontal axis and vertical axis wind turbines have the same basic function of capturing wind energy, but they differ in the efficiency and design of their blades. Horizontal axis turbines are frequently used for large-scale energy production, while vertical axis turbines are better suited for domestic applications due to their lower construction and maintenance costs [4-6]. The efficiency and accuracy of the computational approach to wind analysis of tall structures are suggested by comparisons between experimental data and Computational Fluid Dynamics (CFD) analysis. A case study of aerodynamic mitigation by corner cutting reveals the effectiveness, efficiency, and limitations of minor modification procedures[11]. The presence of a high-rise building reduced the performance of both LES and RANS, showing that forecasting the flow around one is more difficult than forecasting the flow of a straightforward street canyon[12].

There are two different types of wind turbine installations: onshore and offshore. Onshore wind turbines are located on land where, despite being weaker than offshore winds, the wind is still powerful enough to turn the blades and produce electricity [7]. As technology evolved and wind speed data from the oceans became available, offshore installations appeared for more substantial energy production. Initially, these onshore installations signified the development of wind turbine power plants. For onshore installations, location and wind speed are important considerations when deciding between vertical axis wind turbines (VAWTs) and horizontal axis wind turbines (HAWTs). Offshore power facilities, in contrast, take use of the sea's swift winds to produce as much energy as possible. To satisfy the expanding need for offshore technology, research has concentrated on developing offshore technology to meet the growing energy demand, pushing these power plants further from the shore for increased wind exposure [8-10].

Today, everyone wants to create a wind turbine that can be operated continuously and provide the most electricity at low wind speeds. Our PVC-based wind turbine is intended to support the nation's expanding wind power industry by boosting and speeding the rate at which wind energy is used. and developed standard for PVC-based wind power system design, testing, and installation. Our primary objective is to design and perform CFD analysis on blades with the utmost potential for lift, drag, and coefficient of lift.

The structure of this paper can be summarized as follows. Section 2 blade CFD analysis and its specification. The mathematical formulation of design are then presented and discussed in detail in Section 3. Finally, Section 4 offers concluding remarks on the study.

MATERIALS AND METHODS

CFD Analysis

When it comes to comprehending and controlling fluid dynamics, which permeates every aspect of our daily lives, CFD stands out as a crucial instrument. CFD provides a vital link between theory and real-world applications by utilising the computational capacity of computers to tackle challenging fluid dynamic issues. Analytical techniques might be labor-intensive and have a narrow scope, even when they are appropriate for smaller problems. Even though they are extremely accurate, experimental methods necessitate expensive, specialised facilities with exact calibration and painstaking design. Computational approaches, however, present a strong substitute. They offer unrivalled flexibility in simulating and optimising fluid behaviour and can rival the accuracy of experiments at a fraction of the expense, making them an essential tool for addressing the complexities of fluid dynamics in our dynamic world.

Wind Turbine Blade CFD Analysis

Our main goal in our CFD analysis is to maximise the lift force produced by PVC wind turbine blades with a horizontal axis. Our method entails systematically investigating alternative blade configurations to comprehend how they affect lift and drag forces. We iteratively run CFD models by changing important variables including the pipe diameter, blade tip form, curvature, and thickness. We pinpoint the precise blade shape that consistently produces the highest lift force through this rigorous approach. We can adjust the blade geometry using this technique, which will eventually result in the creation of blades that are incredibly effective in capturing wind energy.

CFD Analysis of Blade Having Different Types of Tips Edge and Pipes Diameter

The lift force and coefficient of lift of wind turbine blades were examined in this part using computational fluid dynamics (CFD) analysis to look into the effects of different design parameters. PVC pipe diameter, blade tip edge dimensions, wind speed, static pressure, and air density are some of the factors taken into account. The information below gives a thorough summary of the experimental setup:

Step 1: Analysis of PVC pipe diameter

We examine the impact of adjusting the PVC pipe's diameter on lift force in this stage and keep the following variables constant: the blade specs, static pressure, wind direction, and speed. In this step, we used a CAD model of a small wind turbine with a rotor diameter of 3 metres, blade length of 2.5 metres, tower height of 30 metres, hub height of 4 metres, chord length of 0.2 metres, blade thickness of 0.02 metres, three blades, and a rotor speed of 25 RPM to conduct CFD analysis using the 'CFD Sim' software. We were able to study the effects of changing the PVC pipe diameter while maintaining other factors constant thanks to this technique.

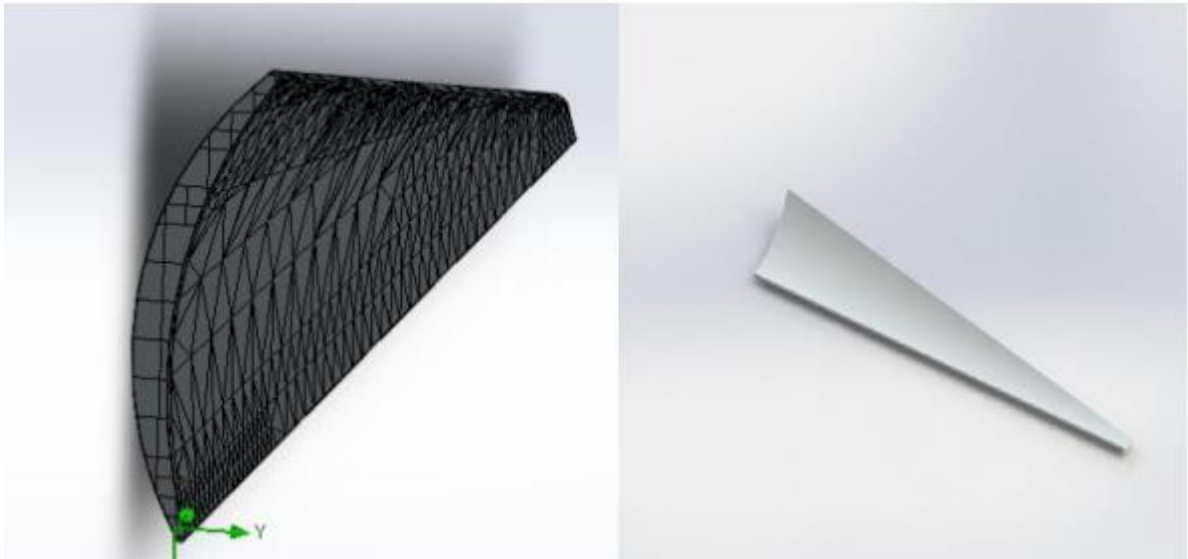


Figure 1: CAD Model of Horizontal Axis Wind Turbine Blade

Step 2: Blade tip edge analysis (1 inch)

In this stage, we reduce the blade's tip edge from two inches to one inch, analyse the effect it has on lift force, and keep the following variables constant: wind speed, direction, static pressure, air density, and PVC pipe diameter. Using the 'CFD Sim' software, a CFD study was performed on a rotor with a diameter of 3 metres, a blade length of 2.5 metres, a tower height of 30 metres, a hub height of 4 metres, a chord length of 0.2 metres, a blade thickness of 0.02 metres, three blades, and a rotor speed of 25 RPM. This method allowed us to evaluate the impact of changing the PVC pipe diameter while keeping other parameters constant.

Step 3: Blade Tip Edge Analysis (3 inch)

In this step, the tip edge of the blade is changed to be 3 inches long, and the wind speed, static pressure, air density, and PVC pipe diameter are kept unchanged while we examine the effects on lift force. Dimension and software is same as step 1 and step 2.

Design of PVC Wind Turbine

Swept area calculation

Determine the wind turbine blades' swept area to make sure there is enough room for them to rotate.

$A = \pi * r^2$ is the formula used to compute the swept area (A) of the blade as shown in Fig 2.

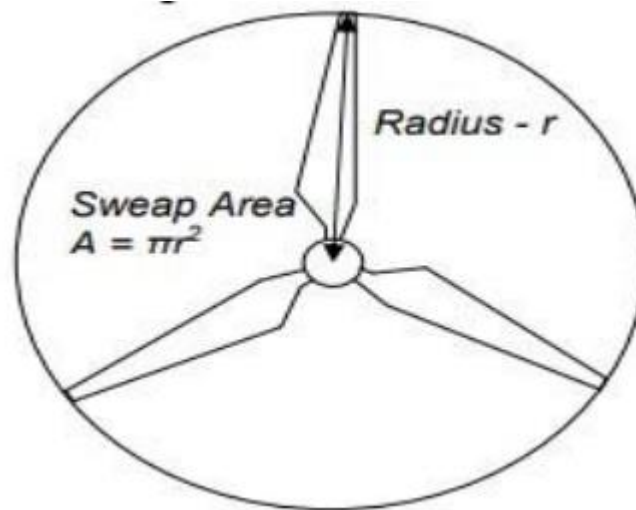


Figure 2: Swept Area

A is the sweep area, and r is the blade's length.

The blade length (r) in this project is specified as 1.52 metres.

$$A = 3.14 * (1.52)^2$$

4.59 square metres per unit Area

As a result, the blades swept area measures 4.59 square metres.

Wind velocity data

- Gather and examine historical wind speed data for the Jalozi neighbourhood in Peshawar, KPK, Pakistan. This information is essential for constructing and erecting the PVC wind turbine.
- **Data Source:** The Peshawar Weather Directorate is the source for the wind speed information.
- **Data Analysis:** Four years of data are gathered to compute the average wind speed, which gives a more thorough picture of the local wind conditions. This is done to make sure the wind turbine is appropriate for the region.
- **Result:** Based on the data gathered, an average wind speed value is derived, and this number will be crucial in establishing the performance and effectiveness of the PVC wind turbine in the Jalozi area as shown in Fig 3.

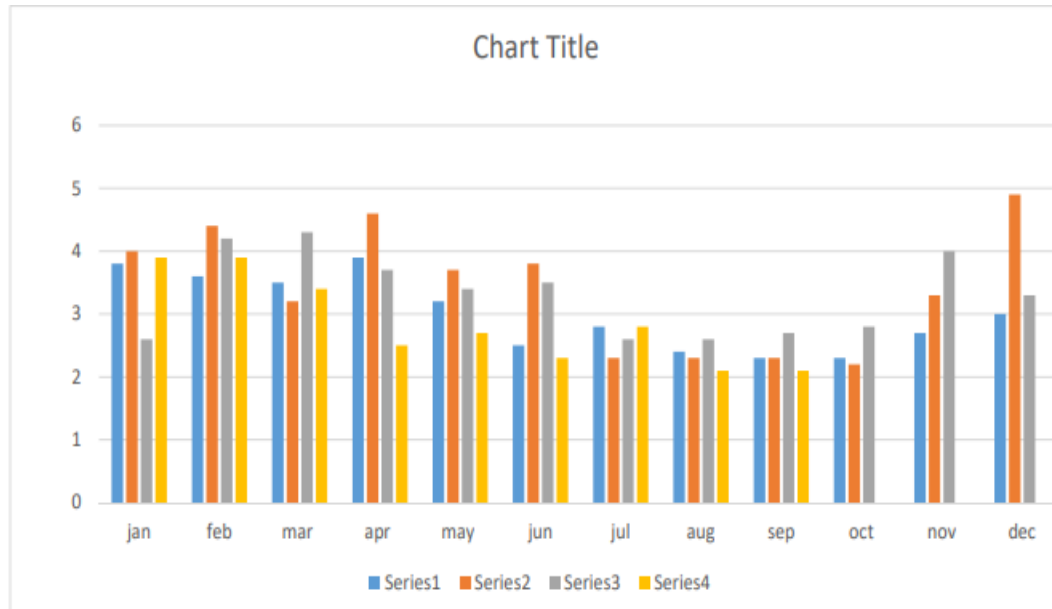


Figure 3: Wind Data of Last Four Years of Jalozai

Power Output Calculation

Data and parameters

- The air density is predicted to be 1.23 kg/m³. Swept Area (A): The blade's swept area is calculated to be 4.59 m².
- The wind turbine's efficiency is indicated by the coefficient of performance, which is reported as 0.40. This is also referred to as the Betz limit, which is the highest efficiency that is conceivably feasible.
- In Jalozai, KPK, Pakistan, the wind speed is reported to be 4.5 m/s at 387 metres above sea level.
- In Cherat, KPK, Pakistan, the wind speed is reported to be 8 m/s at 900 metres above sea level.

Power output calculation at 4.5m/s Wind Speed (Jalozai)

- $P = 0.5 * 1.23 \text{ kg/m}^3 * 4.59 \text{ m}^2 * 0.40 * (4.5 \text{ m/s})^3$, thus output power is $P = 102.89 \text{ W}$.
- As a result, the PVC wind turbine in Jalozai is expected to produce 102.89 watts of power at a wind speed of 4.5 m/s.

Power output calculation at 8m/s Wind Speed (Chirat)

- $P = 0.5 * 1.23 \text{ kg/m}^3 * 4.59 \text{ m}^2 * 0.40 * (8 \text{ m/s})^3$ output power $P = 578 \text{ W}$
- Consequently, Cherat's PVC wind turbine is predicted to produce about 578 watts of power at an average wind speed of 8 metres per second.



Air density, swept area, efficiency as measured by the coefficient of performance (C_p), and the cube of wind speed (V^3) all affect how much power a wind turbine can produce.

To calculate the power output of the PVC wind turbine in various locations and wind conditions, calculations are done for two different wind speeds, one in Jalozai and the other in Cherat.

These estimates offer important insights into the anticipated energy production capacity of the wind turbine at various wind directions and speeds.

RESULTS AND DISCUSSION

According to our investigation, the lift force and coefficient were significantly impacted by the different PVC pipe diameters. The lift force was 1.17 N on average and the lift coefficient was 0.0887 for an 8-inch diameter. It climbed to 1.4732 N and 0.1117 at 10 inches. The greatest impact was 3.1877 N and 0.2416 with a 12-inch diameter. This highlights how crucial pipe diameter is for maximising wind turbine performance.

We kept investigating the impact of PVC pipe diameter on lift force and coefficient in the following stage. We determined an average lift force of 1.4234 N and a lift coefficient of 0.1079 for an 8-inch diameter. With a 12-inch diameter, we saw the highest average lift force of 5.5374 N and a lift coefficient of 0.4198. At 10 inches, this increased to 2.9443 N and 0.2232. These findings confirm the critical position of pipe diameter in optimizing wind turbine performance. A lift coefficient of 0.2173 and an average lift force of 2.8666 N were produced utilizing 8-inch pipe diameter. The average lift force and lift coefficient for a pipe with a 10-inch diameter was 1.6034 N and 0.1215, respectively. The average lift force and lift coefficient for a 12-inch pipe were 1.8185 N and 0.1379, respectively. These results highlight the effect of pipe diameter on lift force and coefficient.

Results shows that each steps involve gradually changing a few parameters while maintaining other factors constant to observe their impact on lift force. A dimensionless measure called the coefficient of lift is used to compare the effectiveness of lift creation in various settings. The findings demonstrate the significance of these design parameters in wind turbine performance optimisation by showing that altering the PVC pipe's diameter and the blade tip edge dimension has a considerable impact on the lift force and its coefficient.

These results offer useful guidance for developing wind turbine blades that can maximise lift force in a variety of scenarios.

Table 1: Shows Combined Results of Different Types of Tips Edge and Pipes Diameter

| Goal Name | Unit | Value | Average Value | Minimum value | Maximum Value | Progress (%) | Use in Convergence | Delta | Criteria |
|---------------|------|-------|---------------|---------------|---------------|--------------|--------------------|-------|----------|
| 8"dial 1"tip | [N] | 1.437 | 1.423 | 1.361 | 1.544 | 100 | Yes | 0.813 | 0.235 |
| 8"dial 2"tip | | 1.161 | 1.178 | 1.157 | 1.213 | 100 | Yes | 0.056 | 0.068 |
| 8"dial 3"tip | | 2.886 | 2.866 | 2.815 | 2.908 | 100 | Yes | 0.024 | 0.026 |
| 10"dial 1"tip | | 2.942 | 2.944 | 2.905 | 3.066 | 100 | Yes | 0.161 | 0.246 |
| 10"dial 2"tip | | 1.481 | 1.473 | 1.420 | 1.482 | 100 | Yes | 0.062 | 1.046 |



ICSET-23



UET Peshawar

| | | | | | | | | | |
|--------------------|--|-------|-------|-------|-------|-----|-----|-------|-------|
| 10" dial 3" tip | | 1.585 | 1.603 | 1.568 | 1.652 | 100 | Yes | 0.083 | 0.226 |
| 12" dial 1" tip | | 5.439 | 5.537 | 5.439 | 5.623 | 100 | Yes | 0.183 | 0.958 |
| 12" dial 2" tip | | 3.256 | 3.187 | 3.079 | 3.450 | 100 | Yes | 0.371 | 0.456 |
| 12" dial 3" tip | | 1.806 | 1.818 | 1.787 | 1.843 | 100 | Yes | 0.055 | 0.080 |

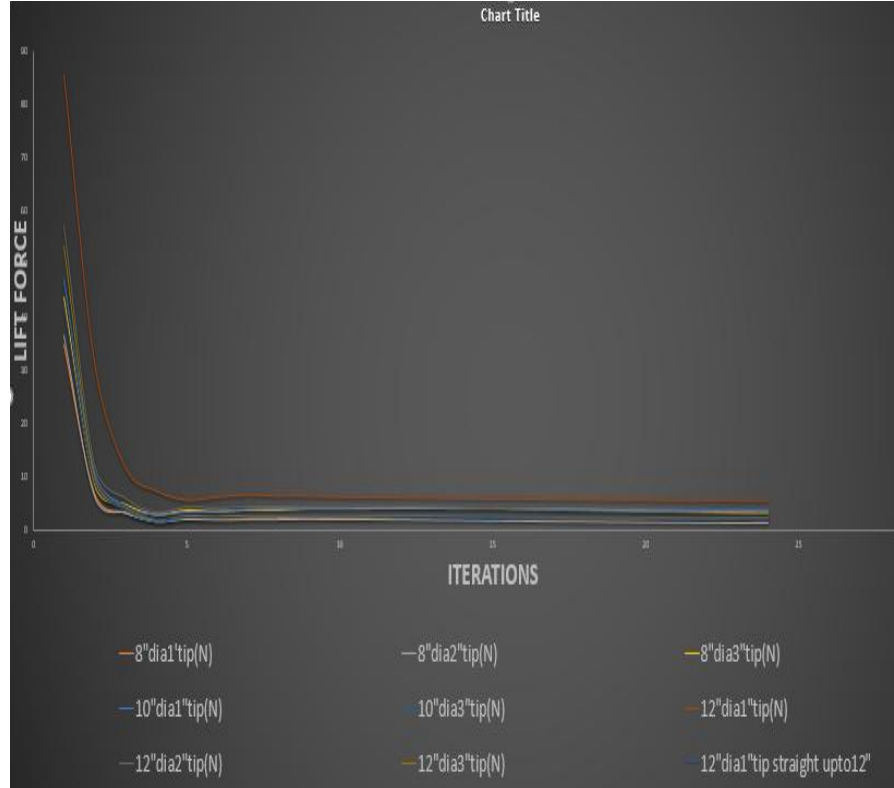


Figure 1: Shows Combined Results of Different Types of Tips Edge and Pipes Diameter

CONCLUSION

The future of wind energy is promising, and by 2030, it is expected to account for 30 percent of the overall generation mix of power. The handmade wind turbine's blades can be constructed in a variety of ways, depending on the mechanical qualities of the materials used. Choosing the materials with great care is of utmost importance. In this scenario, PVC is the most cost-effective and appropriate low-cost material option. The design was created in solid works programme so that exact measurements and curve placement could be achieved. However, it was challenging to have blades that were identical in every way when cutting the PVC pipe. Perhaps greater accuracy could have been achieved with 3D-printed blades, but doing so would have been prohibitively expensive and impractical in most cases. The goal of this work is to simplify



ICSET-23



UET Peshawar

the production of blades for tiny wind turbines. Each and every hardware store ought to stock the stuff easily.

Our goal was to construct a modest wind turbine using just readily available, off-the-shelf components. It's a great option that's not too expensive to implement. It will provide its builders with a free, renewable energy source from the surrounding air currents. There is room for improvement in the material to allow for the construction of larger and more robust DIY small wind turbines suitable for use in residential settings. Aluminium or copper, which are also strong and durable, can be used in place of PVC for this purpose. Increasing the tower's height are going to rise the air's velocity, allowing the blades to spin at a faster rate and producing more energy. In addition, we can construct a robust generator and work on a battery to hold energy.

REFERENCES

- [1] Shankar, R. N., Kumar, L. R., & Ramana, M. V. (2019). Design and fabrication of horizontal axis wind turbine. *International Journal of Research and Analytical Reviews (IJRAR)*, 6(1), 545-549.
- [2] Li, C. T., Ahn, C., Peng, H., & Sun, J. (2012). Synergistic control of plug-in vehicle charging and wind power scheduling. *IEEE Transactions on Power Systems*, 28(2), 1113-1121.
- [3] Jędrzejuk, H. I. (2018). Selection of Renewable Energy Sources for Buildings. In *Design Solutions for nZEB Retrofit Buildings* (pp. 69-97). IGI Global.
- [4] Smith, J. A. (2019). Vertical axis wind turbine design and performance: Assessing the state of the art. *Wind Engineering*, 43(5), 477-489.
- [5] Garcia, M., Martinez, A., & Manwell, J. (2020). Urban wind energy: A review. *Renewable and Sustainable Energy Reviews*, 121, 109673.
- [6] Li, S., Dai, X., Li, P., & Gao, W. (2018). Recent advancements and future prospects of vertical axis wind turbines. *Energy Conversion and Management*, 166, 161-180.
- [7] Smith, A. B., Johnson, C. D., & Wilson, E. F. (2021). Onshore and offshore wind power: A comparative analysis of energy generation and environmental impacts. *Renewable Energy*, 165, 612-625.
- [8] Jones, R. L., & Brown, S. K. (2019). Offshore wind power potential and challenges: A review. *Renewable and Sustainable Energy Reviews*, 109, 372-381.
- [9] Wang, Y., & Zhang, H. (2020). Recent advances in offshore wind turbine technologies: A review. *Renewable Energy*, 157, 895-909.
- [10] Mishnaevsky Jr, L., Branner, K., Petersen, H. N., Beauson, J., McGugan, M., & Sørensen, B. F. (2017). Materials for wind turbine blades: An overview. *Materials*, 10(11), 1285.
- [11] Gaur, N., & Raj, R. (2022). Aerodynamic mitigation by corner modification on square model under wind loads employing CFD and wind tunnel. *Ain Shams Engineering Journal*, 13(1), 101521.



ICSET-23

*Proceedings of the 5th International Conference on Sustainable
Energy Technologies (ICSET 2023) Peshawar, Pakistan
14-15 December 2023*



UET Peshawar

- [12] Shirzadi, M., & Tominaga, Y. (2022). CFD evaluation of mean and turbulent wind characteristics around a high-rise building affected by its surroundings. *Building and Environment*, 225, 109637.

Paper ID: ICSET-2308

A RECONFIGURABLE CIRCULAR PATCH ANTENNA EMBEDDED WITH MAGNETO-STATIC RESPONSIVE STRUCTURES IN MULTI-LAYER SUBSTRATES FOR mmWAVE APPLICATIONS

Wesam Khalil¹, Kiran Nadeem², Muhammad Ayaz^{3,*}

¹Server Security Integration Group, Intel Corporation 2111 NE 25th Ave, Hillsboro, USA

²Department of Electrical and Computer Engineering, COMSATS University Islamabad, Pakistan

³Department of Electrical and Computer Engineering, COMSATS University, Abbottabad Campus, Pakistan

**Corresponding author*

Email: muhammadayaz@uetpeshawar.edu.pk

ABSTRACT

In this paper, a frequency reconfigurable circular patch antenna embedded with Magneto-static Responsive Structures (MRSs) is presented for mmWave applications. To reconfigure the proposed antenna, two lower substrates with thickness of each is 100 μm , tangent loss of 0.002, and permittivity of 3.14 embedded with MRSs structures. The MRS structure consists of a cavity in the substrate filled with silver-coated ferrite particles and is enclosed with top and bottom copper tapes. The noteworthy advantages of using MRSs is that it does not need any additional biasing circuitry for activation. First the antenna is optimized at 38 GHz without any embedded MRSs. Then after extensive simulations and optimization, the antenna is reconfigured at 36.5 GHz, 33.25 GHz and 32 GHz by embedded MRSs at optimum locations beneath of patch. Two lower substrate layers are used to accommodate maximum number of MRSs. It has been explored that if the MRS structures are activated at same position in all layers, the current distribution changed at maximum level. As a result, the proposed designed reconfigured at lower frequency in mmWave band. The achieved gain is 6.65dB, 6.41dB, 5.5dB, 5.3dB at 38GHz, 36.5 GHz, 33.25 GHz, and 32 GHz respectively. Furthermore, the efficiencies achieved are equally impressive, with values of 94.5%, 94.6%, 93.5%, and 92% for the aforementioned frequencies. Moreover, proposed antenna design with reconfigurability feature eliminates the need for additional biasing circuitry, enhances its potential for various mmWave communication applications, making it a highly desirable choice for future wireless communication technologies operating at these high frequencies.

KEYWORDS: mmWave, Reconfigurable antennas, Magneto-static responsive structures.

INTRODUCTION

In today's world of rapid technological advancement, the seamless exchange of information is at the heart of progress across many industries. As the demand for faster data transfer, improved connectivity, and increased bandwidth grows, the role of antennas in enabling efficient communication becomes increasingly important. The use of millimetre-wave (mmWave) antennas is one remarkable innovation that has emerged to meet these needs. These antennas, which operate in the frequency range of 30 GHz to 300 GHz, have piqued the interest of researchers, engineers, and industries alike due to their exceptional applications and a



plethora of benefits. The mmWave frequencies find use in a variety of critical domains, including radar systems that require narrow bandwidths. These frequencies are attractive in wireless energy harvesting initiatives [1-4].

With the rapid advancement of mmWave antennas, researchers' interest in the reconfigurable antennas has increased. The mmWave frequency reconfigurability provides mmWave devices with the adaptability, versatility, and efficiency required for a wide range of Internet of Things (IoT) applications. The reconfigurable antenna can change their operating frequencies, polarization, or main beam direction in real time unlike the traditional antennas, which have fixed frequency features [5]. The researchers face many challenges in designing reconfigurable antennas such as good impedance matching across all operation states of the antenna, proper gain, and stable radiation pattern [5]. Several methods are used in the literature to achieve the frequency reconfigurability.

To achieve the required reconfigurability, PIN diodes are integrated into the radiating surfaces or feeding networks of antennas in [6]. A specific biasing external circuitry is required in this technique to provide stable DC voltage. Various techniques for designing reconfigurable antennas in different frequency bands have been investigated in [7-9]. Similarly, a compact frequency reconfigurable printed antenna for millimetre-wave applications is presented in [10]. To obtain the reconfigurability, two S-PIN diodes are used. Because of technological limitations, PIN diodes face numerous challenges and difficulties: (1) metal dispersive behaviour, (2) diode low efficiency, (3) mismatch between diodes and antennas, and (4) external biasing circuitry requirement [11]. Furthermore, in the mmWaves frequency band, traditional switches are inefficient. Because of the constraints, a suitable replacement should be found in the mmWaves frequency range. The use of Magneto-static Responsive Structures (MRSs) is an important candidate for overcoming these limitations, which has gained increased attention recently. The MRS structure is constructed from a substrate with a cavity filled with Silver Ferrite coated particles. Top and bottom copper tape are used to seal the cavity. These structures can be embedded in the substrate to change the phase of the signal [12–17].

The proposed work in this paper investigates MRS structures for the reconfigurability feature in the mmWaves frequency range. A circular patch antenna with three substrates is designed for 38 GHz. The antenna is built on the upper substrate, while the MRS structures are built on the lower substrate layer 2 and 3. Many significant benefits can be obtained by integrating these MRSs with the antenna. One of the major advantages of the proposed antenna with MRSs is that it does not require any external DC biasing circuitry. Furthermore, it reduces the overall complexity of the system and eliminates the potential failure points associated with biasing circuitry. This paper is structured as follows: Section 2 outlines the intricate design, followed by the presentation of simulation outcomes in Section 3. The final findings of the study are illustrated in Section 4.

Proposed reconfigurable antenna geometry

The proposed antenna in Fig. 1 (a) and (b) is designed at 38 GHz without embedded MRS structure using the CST Microwave Studio Suit 2019. It is made of three substrates with the same thickness of 100 μm , tangent loss of 0.002, and permittivity of 3.14. In the proposed design, the purpose of the two lower substrates is to accommodate the MRSs structures that enable the antenna reconfigurability. In total, 27 MRSs are embedded in each lower substrates directly beneath the patch element, as shown in Fig. 2 (a) & (b). MRSs 1-25 and 26-27 are embedded beneath the patch and the transmission line for both substrate layers respectively. In Fig. 3(a) & (b) shows, the single MRS structure that consists of a cavity in the substrate filled with silver coated ferrite particles. The cavity is closed with top and bottom copper tapes.

These particles can be activated and deactivated using a tiny magnet beneath the cavity. It changes the permittivity of both substrates when activated, which then changes the current distribution on the patch. As a result, the resonant frequency shifts to a different frequency.

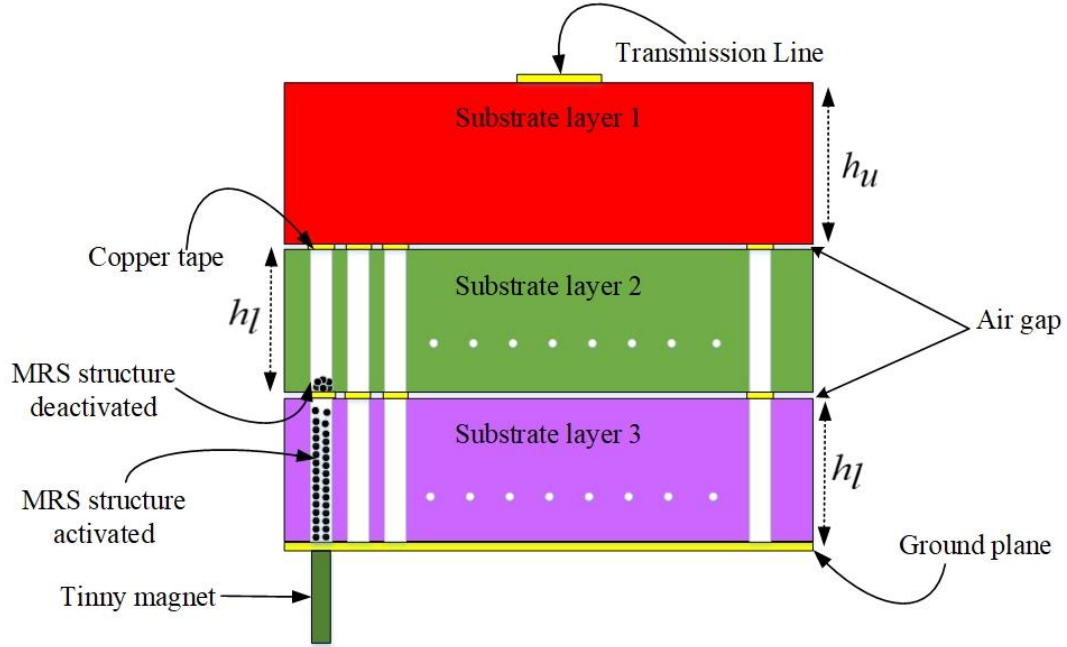


Figure 1(a): Side view of proposed reconfigurable circular patch antenna comprises of three-layer substrates

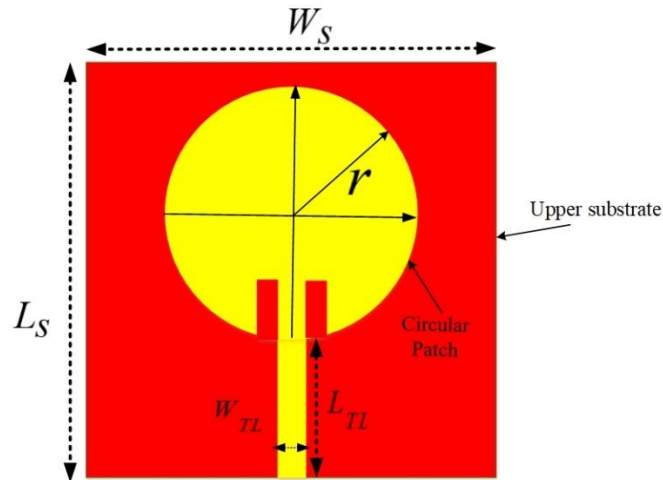


Figure 1(b): Proposed reconfigurable circular patch antenna operating at 38 GHz

Table 1 Proposed Antenna dimensions

| Parameter | Value (μm) | Parameter description |
|-------------|----------------------------|---------------------------------|
| L_S | 4000 | Length of substrate |
| W_S | 3500 | Width of substrate |
| W_{TL} | 200 | Transmission line width |
| L_{TL} | 1400 | Transmission line length |
| d | 550 | Two MRSs centre to centre space |
| dia | 400 | MRS cavity diameter |
| h_u | 100 | Upper substrate thickness |
| h_l | 100 | Lower substrate thickness |
| Copper tape | 400×400 | Copper tape size |

This integrated approach improves the performance of the proposed circular patch antenna with embedded MRS structures while streamlining the overall design. The use of multiple cavities expands the reconfigurability feature, allowing for precise frequency control. Table 1 contains detailed specifications for the substrates, cavities, and other critical parameters. To ensure optimal performance and adherence to the desired mmWave frequency range, these dimensions are determined using simulations, optimisation techniques, and iterative design processes.

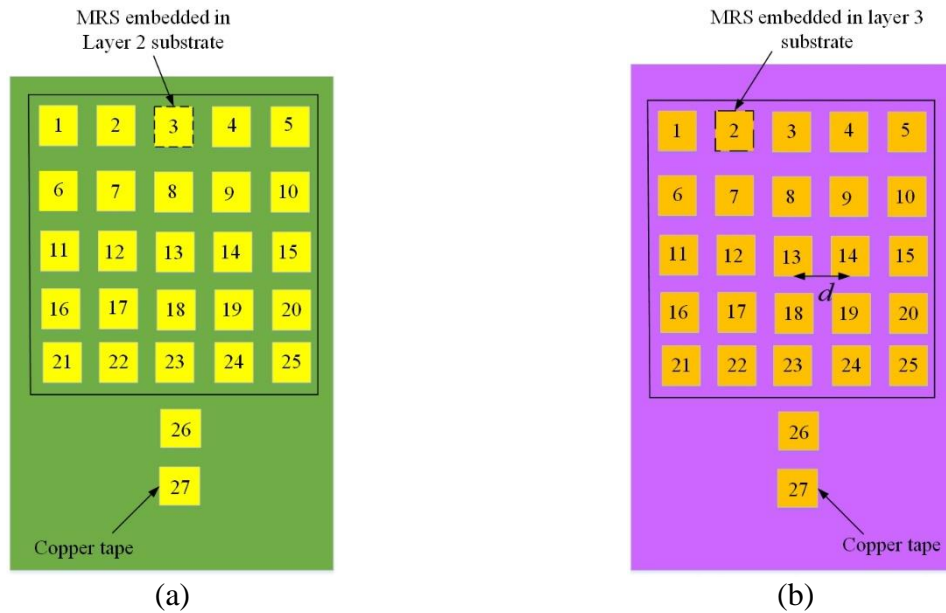


Figure 2: MRSs structures (a) MRSs 1-25 are embedded beneath the patch and MRSs 26-27 are beneath the transmission line in layer 2 (b) MRSs 1-25 are embedded beneath the patch and MRSs 26-27 are beneath the transmission line in layer 3

SIMULATION RESULTS AND DISCUSSION

The mmWave reconfigurable circular patch antenna (depicted in Fig. 1) suggested in this study, along with the inclusion of Magneto-static Responsive Structures (MRSs) as shown in Fig. 2, undergoes comprehensive full-wave simulation. This simulation is conducted using CST Microwave Studio Suite (version 2019) at a frequency of 38GHz. The primary goal of this simulation is to assess the functionality of the proposed antenna, particularly when integrated with numerous MRSs within the two lower substrates. The design is first subjected to full wave simulation without embedding the silver ferrite coated particles in the MRS cavities. In this scenario, the design shows best impedance matching characteristics at 38 GHz, boasting a peak gain of 6.65dB and impressive radiation efficiency of 94.5% shown in Fig. 4, 5 and 6 respectively. After that, multiple MRSs are embedded to reconfigure the antenna at other frequencies. The optimum position for MRS placement is achieved using extensive simulations and design optimization.

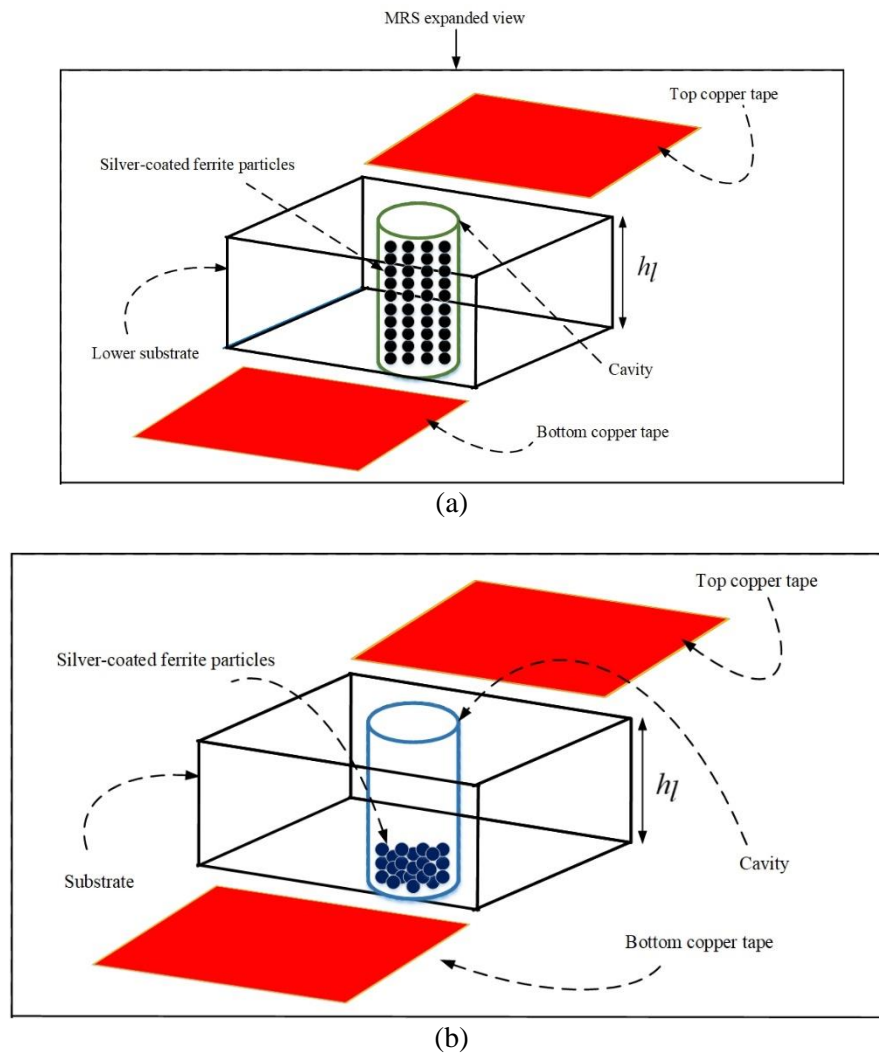


Figure 3: Magneto-static Responsive Structure (MRS) (a) Activated state (b) Deactivated state

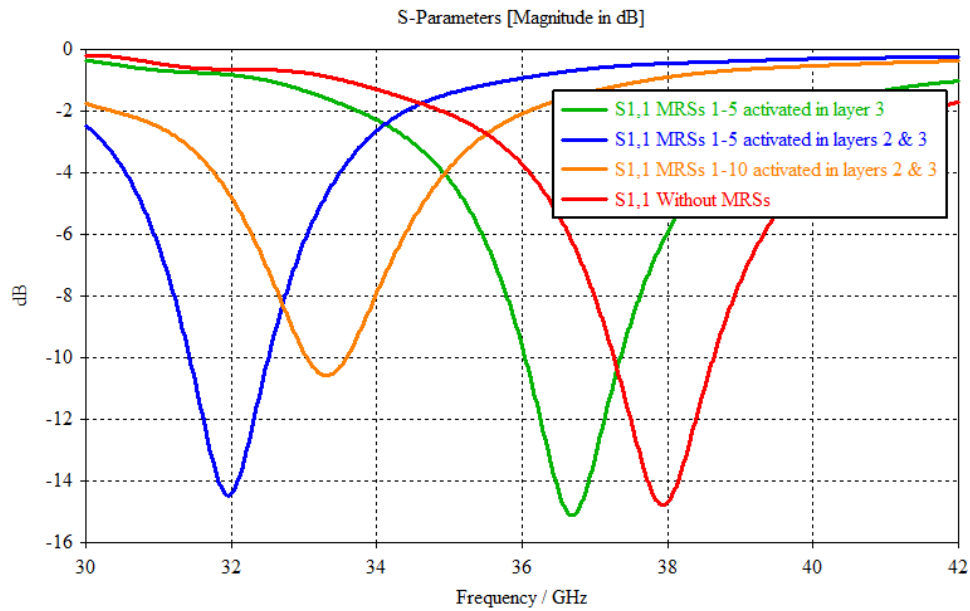


Figure 4: The antenna designed at 38 GHz is reconfigured at 36 GHz, 33.5 GHz and 32 GHz using multiple embedded MRSs in layer 2 and 3

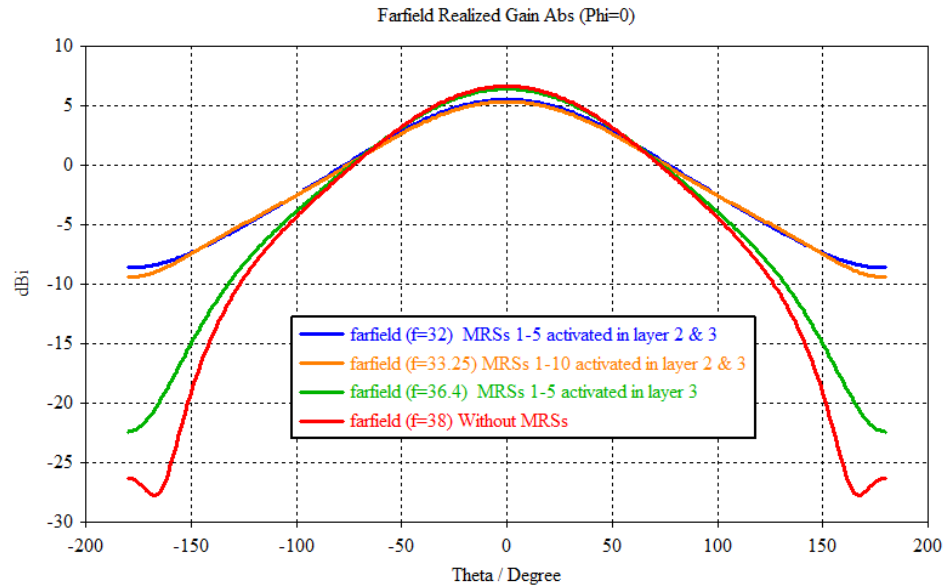


Figure 5: The proposed circular antenna peak gain at 38GHz, 36.4 GHz, 33.25GHz, and 32GHz using multiple embedded MRSs in both layers

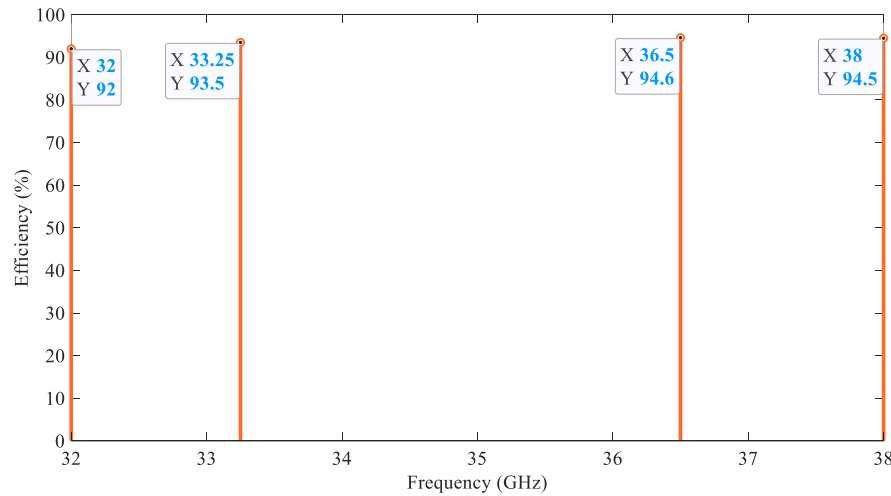


Figure 6: The proposed circular patch antenna radiation efficiencies at 38GHz, 36.5GHz, 33.25GHz, and 32 GHz using multiple embedded MRSs

Activating MRSs 1-5 at their optimum locations within layer 3 results in the optimal configuration. This leads to a reconfigured frequency at 36.5 GHz, accompanied by a gain of 6.41 dB and a radiation efficiency of 94.6%. By activating these MRSs in the specified positions, the effective permittivity of the substrate undergoes alteration, inducing changes in the capacitance and inductance between the patch and the ground. Likewise, the proposed antenna's reconfiguration takes place at various mmWave frequencies, such as 33.25 GHz and 32 GHz. This is achieved by embedding MRSs 1-5 in the layer 2 and layer 3 substrates. Additionally, activating MRSs 1-10 in both substrate layers 2 and 3 at the optimized positions illustrated in Fig. 4 leads to these reconfigurations. In these cases, the measured gain and radiation efficiency values are 5.5 dB, 5.3 dB, and 93.5%, 92%, respectively. Notably, the gain demonstrates a variation of 1.35 dB, while the radiation efficiency experiences a variation of 2.5% due to the presence of multiple embedded MRSs within the two lower substrates.

CONCLUSION

A frequency reconfigurable circular patch antenna embedded with silver particles is proposed for mmWave communication systems. Magneto-static Responsive Structures (MRSs) are incorporated into the two lower substrates to reconfigure the antenna. The design operating frequency is 38GHz, with no MRSs structure. The antenna can be reconfigured at 36.5GHz, 33.25GHz, and 32GHz by embedding multiple MRSs in optimal positions. The proposed design operates at these frequencies with an impressive gain of 6.41 dB and a higher efficiency of 94.6%. It demonstrates that the design with reconfigurability, which eliminates the need for additional DC biasing circuitry, increases its potential for various mmWave communication applications, resulting in a highly beneficial choice for future wireless communication technologies.



ICSET-23



UET Peshawar

REFERENCES

- [1] Rachapudi Madhumitha, Hanumantha, Gurukiran N K, Gagan B, Renuka R Karjur, Ananya Parameswaran, "Frequency Reconfigurable Microstrip Patch Antenna using Different Reconfiguration Techniques for mm wave Applications", 2023 4th International Conference for Emerging Technology (INCET), pp.1-9, 2023.
- [2] V. Muzzupapa, A. Crunteanu, D. Passerieux, C. Borderon, R. Renoud, H. W. Gundel, L. Huitema, "Frequency Reconfigurable Millimeter Wave Antenna Integrating Ferroelectric Interdigitated Capacitors", 2023 17th European Conference on Antennas and Propagation (eucap), pp.1-4, 2023.
- [3] Ayoub Naoui, Bruno Reig, Etienne Perret, Mohamad El-Chaar, Florence Podevin, "Indirect Electrical-Control Through Heating of a gete Phase Change Switch and Its Application to Reflexion Type Phase Shifting", 2023 International Microwave and Antenna Symposium (IMAS), pp.13-16, 2023.
- [4] Daasari Surender, Md. Ahsan Halimi, Taimoor Khan, Fazal A. Talukdar, Nasimuddin, Sembiam R. Rengarajan, "5G/Millimeter-Wave Rectenna Systems for Radio-Frequency Energy Harvesting/Wireless Power Transmission Applications: An overview", IEEE Antennas and Propagation Magazine, vol.65, no.3, pp.57-76, 2023.
- [5] K. Moradi, a. Pourziad, and s. Nikmehr, "a frequency reconfigurable microstrip antenna based on graphene in the terahertz regime," optik, vol. 228, p. 166201, 2021.
- [6] J. Costantine, y. Tawk, s. E. Barbin, and c. G. Christodoulou, "reconfigurable antennas: design and applications," proceedings of the ieee, vol. 103, no. 3, pp. 424-437, 2015.
- [7] M. Borhani, p. Rezaei, and a. Valizade, "design of a reconfigurable miniaturized microstrip antenna for switchable multiband systems," ieee antennas and wireless propagation letters, vol. 15, pp. 822-825, 2015.
- [8] J. Kowalewski, j. Atuegwu, j. Mayer, t. Mahler, and t. Zwick, "a low-profile pattern reconfigurable antenna system for automotive mimo applications," progress in electromagnetics research, vol. 161, pp. 41-55, 2018.
- [9] M. U. Hassan, f. Arshad, s. I. Naqvi, y. Amin, and h. Tenhunen, "a compact flexible and frequency reconfigurable antenna for quintuple applications," radioengineering, vol. 26, no. 3, 2017.
- [10] Awan, w. A., hussain, n., ghaffar, a., naqvi, s., zaidi, a., hussain, m., & li, x. J. (2021, july). A low profile frequency reconfigurable antenna for mmwave applications. In *wits 2020: proceedings of the*



ICSET-23

*Proceedings of the 5th International Conference on Sustainable
Energy Technologies (ICSET 2023) Peshawar, Pakistan
14-15 December 2023*



UET Peshawar

6th international conference on wireless technologies, embedded, and intelligent systems (pp. 1073-1083). Singapore: springer singapore.

- [11] M. Dragoman and m. Aldrigo, "graphene rectenna for efficient energy harvesting at terahertz frequencies," *applied physics letters*, vol. 109, no. 11, 2016.
- [12] M. Ayaz, a. Iftikhar, b. D. Braaten, w. Khalil, and i. Ullah, "a composite right/left-handed phase shifter-based cylindrical phased array with reinforced particles responsive to magneto-static fields," *electronics*, vol. 12, no. 2, p. 306, 2023.
- [13] M. Ayaz and i. Ullah, "a phased array antenna with novel composite right/left-handed (crlh) phase shifters for wi-fi 6 communication systems," *applied sciences*, vol. 13, no. 4, p. 2085, 2023.
- [14] A. Iftikhar, j. Parrow, s. Asif, j. W. Allen, m. S. Allen, and b. D. Braaten, "improving the efficiency of a reconfigurable microstrip patch using magneto-static field responsive structures," *electronics letters*, vol. 52, no. 14, pp. 1194-1196, 2016.
- [15] A. Iftikhar, s. M. Asif, j. M. Parrow, j. W. Allen, m. S. Allen, a. Fida, and b. D. Braaten, "changing the operation of small geometrically complex ebg-based antennas with micron-sized particles that respond to magneto-static fields," *ieee access*, vol. 8, pp. 78956-78964, 2020.
- [16] J. M. Parrow, a. Iftikhar, s. M. Asif, j. W. Allen, m. S. Allen, b. R. Wenner, and b. D. Braaten, "on the bandwidth of a microparticle-based component responsive to magnetostatic fields," *ieee transactions on electromagnetic compatibility*, vol. 59, no. 4, pp. 1053-1059, 2017.
- [17] A. Iftikhar, j. Parrow, s. Asif, b. D. Braaten, j. Allen, m. Allen, and b. Wenner, "on using magneto-static responsive particles as switching elements to reconfigure microwave filters," in *2016 ieee international conference on electro information technology (eit)*, 2016, pp. 192-195.



Paper ID: ICSET-2309

PYROLYSIS REACTOR DESIGN AND PERFORMANCE ASSESSMENT FOR RENEWABLE ENERGY PRODUCTION FROM BAY LEAVES AND BEECH WOOD

Muhammad Osama Aziz^{1,*}, Aqib Nawaz Khan², Muhammad Uzair Khan¹, Yousaf Salim², Muhammad Usman Khan²

¹Department of Mechanical Engineering, University of Engineering and Technology Peshawar, Pakistan

²Department of Energy Systems Engineering, U.S. Pakistan Centre for Advanced Studies in Energy (USPCAS-E),
National University of Sciences & Technology (NUST), Islamabad, Pakistan

**Corresponding author*

Email: osama7aziz@gmail.com

ABSTRACT

People are searching for alternatives to current fossil fuels since they are quickly running out at a time when energy demand is rising day by day. One possible substitute for fossil fuels is pyrolysis. Pyrolysis produces pyrolysis oil, char, and non-condensable synthetic gas by heating the feedstock in an oxygen-free environment. A small-scale fixed bed flow reactor with 2.5 kW powered heating elements is developed, manufactured, and constructed using lessons learned through testing and literature study. To restrict the amount of time that a product spends in the environment and eliminate oxygen, nitrogen gas is utilized as a sweeping gas. The pyrolysis tests are carried out to verify the reactor's functioning. The experiment's feedstock is decided to be beech wood and bay leaves. The difference in mass between the initial feedstock and the final solid product is noted to determine the experiment's yield. The pyrolysis oil and gas product are effectively obtained throughout the experiment.

KEYWORDS: Pyrolysis, Flow Reactor, Nitrogen gas, prototype, Gas Yield

INTRODUCTION

Researchers and scientists are being compelled to find alternatives to fossil fuel resources due to the rising energy demand, the depletion of fossil fuels, and environmental issues like air pollution, deteriorating atmospheric greenhouse gas effects, and climate change [1]. Many sources have been identified up till now, plastics such as Polyethylene terephthalate, Polystyrene, and Polyvinyl Chloride, etc., and biomass such as wood, solid waste, crop residue, dedicated crops such as jatropha, sunflower seeds, and microalgae etc. Plastics are made up of hydrocarbons extracted from fossil fuels thus they cannot be an alternative to fossil fuels, but biomass have the potential to produce equally efficient and cleaner fuels. Many reactors have been designed to process these feedstocks into usable oil. Reactors and their processes amount to the maximum amount of energy usage. Thus, to reduce energy usage and make the process commercially viable, different reactor designs must be tested for small-scale production [2 – 3]. Currently, societies are heavily dependent on very expensive fossil fuels, and most of them are detrimental to our environment with harmful emissions [4].



The laboratory-scale pyrolysis oil yield is hindered by inadequate heating of the biomass, primarily due to the suboptimal reactor design. The existing reactor, a basic cylinder with gas inlets and outlets, leads to a loss of biomass placement, resulting in poor heat transfer efficiency between the biomass and reactor walls. Between the reactor and the furnace, a large amount of heat is also lost. The furnace limits the size of the reactor, which restricts the use of biomass [5 – 6]. To address these issues, suggested reactor improvements include tighter biomass packing, enhanced insulation, and increased reactor size. These enhancements are anticipated to boost pyrolysis oil yield. Furthermore, alternative solutions encompass adopting varied reactor types (fluidized bed or rotary kiln), employing microwave/infrared heating for uniformity, and implementing closed-loop systems to recover lost heat. The choice of solution depends on the application and available resources [7 – 8].

A fixed bed reactor is easier to manufacture due to its non-complex design, but removal of tar and char is one of the main problems of this type of reactor. So, for this purpose, an additional filter must be added to the system. A fluidized bed reactor is a bit harder to manufacture, but it has its advantages which are: extensive surface area contacts between the feedstock and heating medium, and good control of vapor residence time due to varying flow rates of the sweeping medium [9]. In our final decision for design, due to its ease of manufacture fixed bed reactor is selected but with additional benefits of a fluidized bed reactor such as extensive area contact is to be provided between the heating surface and feedstock, and vapor residence time being controlled by using nitrogen as a sweeping gas [10 – 11]. The reactor's shape is tailored to maximize the contact between the feedstock and the heating surface. A square design is chosen to provide the largest possible surface area, facilitating close contact between the feedstock particles and the heating medium [12 – 13].

In this study, novel strategies like pyrolysis have evolved in the search for sustainable energy sources despite dwindling fossil resources and rising energy needs. To reduce heat loss through the air, pyrolysis requires heating feedstock inside of a customized reactor with internal heating devices that make use of metal's greater heat conductivity. By mechanically compacting the feedstock inside the reactor, heat transmission from one particle to another is made easier, and heat losses along the air-medium channel are reduced. Utilizing nitrogen gas to prevent oxygen exposure, a small-scale fixed bed flow reactor with 2.5 kW powered heating elements is used. The reactor's functioning has been confirmed by pyrolysis testing using beech wood and bay leaves as feedstock. Yield is calculated by the mass difference between the starting feedstock and the end solid output. The successful completion of the experiment results in pyrolysis oil and gas products, providing a possible replacement for fossil fuels.

MATERIALS AND METHODS

Design

The furnace's inability to self-heat greatly reduced the reactor's performance. We have created a new design that includes heating components to solve this issue. This change will significantly speed up the heating process and release the volume of the reactor from the confines of the furnace. As the sandwich design from the prior design is essential to improving heat transmission between the biomass and the heating surface, we shall keep it in place. Prior systems used either cylindrical or spherical reactors and furnaces, which made it difficult to distribute heat evenly to the feedstock. The rate of heat transfer was reduced because the sections of the feedstock in direct contact with the reactor walls were adequately heated while those that were not in direct contact did not. This made it more difficult to use the feedstock effectively. We



have made special modifications to the reactor design to guarantee that all feedstock comes into touch with the reactor walls, allowing for uniform heat dispersion, to ensure the process is efficient. There are five primary components to the reactor. the foundation, the body frame, the top cap, the plate (used to force the biomass on the heating surface), and the heating components.

Base

The figures shown, namely Figures 1 and 2, portray the division of the base into two separate pieces. Specifically, Figure 1 visually represents the bottom component, while Figure 2 visually represents the top section. The upper portion of the structure functions as the designated location for the placement of the heating components. It is equipped with perforated apertures that are evenly dispersed on its upper surface, allowing for the efficient dispersion of the gas being transported. Furthermore, a total of four apertures are deliberately created on the lateral surfaces to effectively affix all constituent parts of the reactor by means of threaded fasteners. Conversely, the bottom portion serves as a compartment designed for the introduction of nitrogen gas (N_2) to facilitate the process of sweeping. The design has a N_2 inlet that offers threaded access. In the present design, the introduction of nitrogen gas occurs inside a designated chamber, followed by its uniform distribution into the reaction chamber through a set of closely positioned apertures situated in the top section of the base.

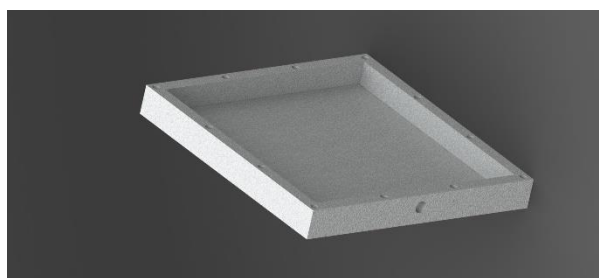


Figure 37: Lower Section

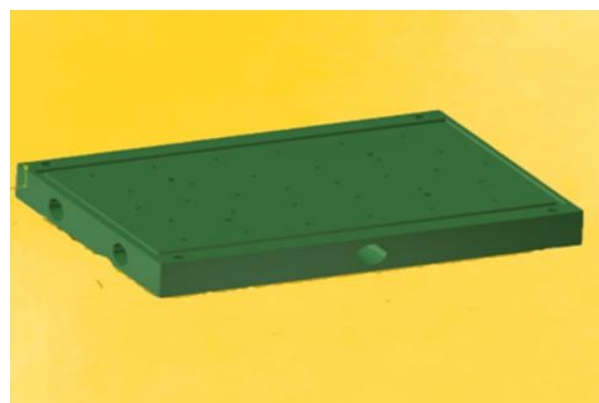


Figure 38: Upper Section

Body Frame

This design has a rectangular frame with a 30 mm thickness (as shown in Figure 3). The area of the frame is designed in such a way that the feedstock will be spread over the top surface of the base to increase the surface contact which will result in uniform distribution of heat to the feedstock. Four holes at the side are drilled to clamp all reactor parts together with the help of nuts and bolts. These 12 holes will reduce the chances of any leakage by tightly sealing the reactor.

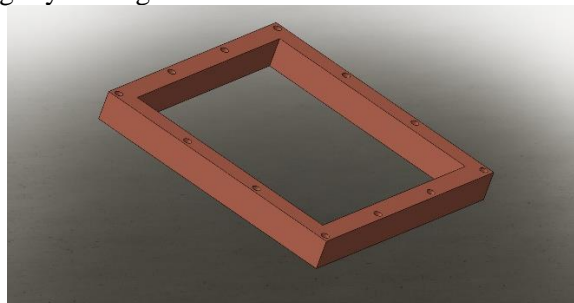


Figure 39: Body Frame

Top Cap

The top cap (as shown in Figure 4) is used to enclose the reactor. It also has a hole that will allow pyrolysis products to pass to the condenser through a valve. A thermocouple will also be installed in this part.

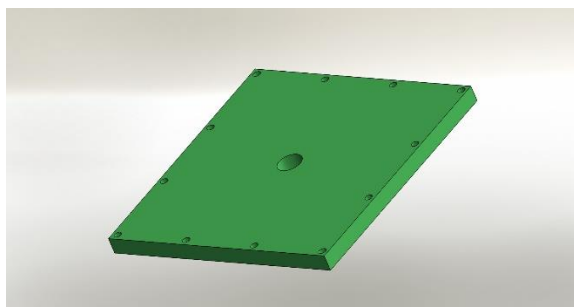


Figure 40: Top Cap

Plate

The reactor design incorporates the use of a perforated plate, as seen in Figure 5, to provide pressure on the biomass, therefore facilitating intimate contact with the heating surface of the reactor. The proximity between objects facilitates an increase in the efficiency of heat transmission. To accomplish this objective, a mechanical mesh is used. A high-quality stainless-steel mesh, characterized by tiny apertures ranging from 0.03mm to 0.1mm, will be strategically placed both above and below the biomass cake. The main objective of this mesh is to effectively impede the passage of chips or solid components derived from the biomass, hence preventing their escape via the apertures where the carrier gas is flowing. Moreover, it functions to inhibit the release of tar and char particles within the resultant gas. The mesh serves as an effective barrier, preventing the chips from descending into the apertures and causing obstruction.

Heating Elements

As shown in Figure 6, the reactor gets its heat via cartridge heating elements. These components resemble industrial heaters with tube shapes that are placed into drilled holes. In a variety of heating processes throughout industries, cartridge heaters are often utilized because of their reputation for delivering localized, accurate heating. They have the capacity to function at a range of watt densities, including low, medium, and high.

The choice of cartridge heaters as the heat source was made because of their small size and high-power output. Four heating components are arranged in this arrangement, and they are all located in the base. Two of them each have a power rating of 750 watts, while the other two have a rating of 500 watts, for a combined heating power of 2500 watts. These heating components are all powered by a 220-volt AC source and have a maximum working temperature of 450 degrees Celsius.

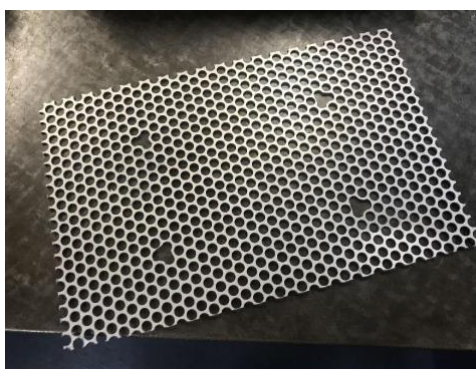


Figure 41: Perforated Plate



Figure 42: Heating Element

Gas Inlet and Outlet (Thermocouples)

A 0.25-inch output diameter compression fitting is used for connecting the sweeping gas source and the sweeping gas inlet. Teflon tape is wound around the threads of the fitting to prevent any leakage. To adjust the thermocouple and to provide an outlet path to the product gas, an outlet is provided at the top cap. At the outlet of the reactor, we employ a tee-shaped fitting. Within this fitting, a thermocouple is positioned at the upper part of the tee, while the product gas exits through the side outlet of this tee-shaped component.



It is crucial for the thermocouple to have direct contact with the base to accurately measure the temperature of the heating surface.

Controller

The PID controller, short for Proportional Integral Derivative controller, is used in many applications owing to its advantageous characteristics. The derivative controller component of the PID controller contributes to a reduction in overshoot, while the proportional controller component facilitates a quicker reaction. Consequently, the inclusion of both components in the PID controller leads to a decrease in both rising time and settling time. The PID controller is used to regulate the temperature of the reactor by modulating the power output based on the thermocouple's feedback. The use of a Proportional-Integral-Derivative (PID) controller may lead to enhanced temperature regulation. Furthermore, the PID controller can regulate the power output of the heaters based on the temperature feedback received from the thermocouples. The controller is equipped with a power output of 220V AC, and a signal input specifically designed for the thermocouple. The temperature detection is performed using a K-type thermocouple. The device has the capability to accurately measure temperatures as high as 1300°C.



Figure 43: The PID controller and K-type thermocouple

Calculation and Experimentation

Calculations

This section includes theoretical calculations for the necessary amount of feedstock and energy use, as well as an assessment of the time needed for the reactor to attain the requisite temperature using a linear model. It should be noted that the exact calculations will be confirmed during real reactor testing.

Equation (1), which connects the mass of the pyrolysis product (m_p), the mass of the reactant (m_r), and the transfer rate (y), is used to calculate the required mass of the feedstock:

$$m_p = y \times m_r \quad \text{Eq. (1)}$$

We set the minimum needed feedstock mass at $m_p = 10$ grams to guarantee an acceptable quantity of pyrolysis oil for analysis.



It is known from the literature that transfer rates on an industrial scale may reach up to 75%. The heating rate at the lab scale is noticeably slower in comparison. As a result, we make a cautious estimate of a 20% yield (Y).

$$Y=20\%$$

$$m_r = 50g$$

When solving the energy equation Eq. (2), the following presumptions were considered. The influence of N₂ carrying gas may be disregarded since its heat capacity is substantially lower than that of metal and feedstock. The real energy usage will thus exceed the estimates. The sum of the heat utilized by the reactor and the feedstock is the total amount of heat energy required.

$$Q_{total} = Q_r + Q_d \quad \text{Eq. (2)}$$

Where the heat produced by the apparatus (reactor) is denoted by, Q_d .

The following equation may be used to calculate the thermal energy:

$$Q = cm\Delta T$$

The heat capacity is c, the mass of the item to be heated is m, and the temperature fluctuation is T.

The average heat capacity of wood is around 1850 J/kg, and m_r is equivalent to 50g.

From 300°C at room temperature to 4500°C, the temperature increases. So $\Delta T=420K$

$$Q_r = 38,850J$$

$$m_d = 11kg$$

Mild steel has a 490 J/kg heat capacity on avg.

$$\Delta T = 420K$$

$$Q_d = 2,263,800J$$

The reactor has received the following total thermal energy:

$$Q_{total} = 38,850 + 2,263,800$$

$$Q_{total} = 2,302,650J$$

When determining the heating rate Eq. (3), the following presumptions were considered:



ICSET-23



UET Peshawar

The heaters run continuously at a power of 2500W. To make the computation easier, the heating is represented as a linear model. Due to various variances in the actual scenario, the changing temperature differential will alter the increasing temperature rate.

If the impact of heat loss is disregarded, it is possible to calculate how long it took to heat the system:

$$t = \frac{Q}{P} \quad \text{Eq. (3)}$$

P stands for the power of the heating components, while Q stands for the heat energy delivered to the system.

As estimated earlier.

$$Q_{total} = 2,302,650J$$

$$\& \quad P = 2500W$$

Consequently, the appropriate time to preheat the system is:

$$t = \frac{2,302,650J}{2500W}$$

$$t = 921.06s = 15.35 \text{ min}$$

Design Conclusion

The heating rate has enhanced remarkably due to the internal heating effect of the reactor. Also, a more accurate temperature control can be attained. For the feedstock cake to be much thinner and the volume of it to be the same the cross-section area of the reactor is increased, consequently the heat can transfer through the feedstock effortlessly. For now, the volume of feedstock can be more flexible. To pass the N₂-carrying gas through the base, the nitrogen gas must pass through holes in the upper part of the base which preheats the nitrogen.

The tar and char particles in the product gas will need to be filtered using a separate filter since a fixed bed reactor is being employed. The reactor's total cost is increased by the electric components, especially the heating elements and the control system.

Fabrication

Material Selection

The pyrolysis process requires a very high temperature, between 450°C and 800°C. Therefore, the process's material should withstand the high temperature. The material should also be inexpensive and simple to process. Since there aren't any significant pressures created within the reactor, the material doesn't need to be especially strong. Mild steel has therefore been chosen as the material for the reactor's construction.

Details about Fabrication of the Parts

To ensure that the SolidWorks-designed components can be manufactured, the personnel at a workshop reviewed the drawings of the parts and showed them to customers. After consideration, it was suggested that welding the parts together, as opposed to subtractive manufacturing, is the preferred option. In other words, the project's various components will be made separately, and then they will be joined together through welding, as opposed to subtractive manufacturing, which creates objects by gradually removing material from a solid block of material. The pieces were suggested for welding since it was less expensive than subtractive production because less material was utilized.

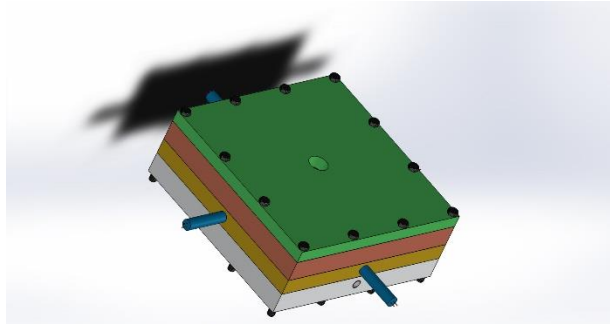


Figure 44: 3D assembly of the reactor

Assembly

To prepare the reactor's sub-assemblies, the various components must first be welded together. Then, 12 countersunk fasteners are used to attach these sub-assemblies together. The reactor's final assembly is created in this manner.



Figure 45: Parts before welding



Figure 46: Parts after welding, drilling, and finishing



Figure 47: Final Assembly

Reactor Testing Methodology

The following two procedures are used to assess the heating of the heating elements and the leak-proofness of the reactor once the components have been assembled.



Figure 48: Heating element



ICSET-23



UET Peshawar

Heater Testing

Because the reactor is very hot during this test, it must be set up on an aluminum block to prevent injuring anything beneath it, such as a table. When the heater is switched ON, the PID control panel will indicate if it is functioning well or not. The temperature is progressively raised to 450°C to prevent overtaxing the heating components. The green light on the controller will also be ON if the heating components are switched ON. And the light on the temperature display will come ON whenever the reactor's temperature reaches the appropriate level.

Gas Leakage Testing

The N₂ gas source is attached, and the flow rate of the N₂ gas should be maintained high, to monitor the reactor's gas leakage. To check for any gas leakage, soap bubbles or suds are dispersed along the contact points between each component.

RESULTS AND DISCUSSION

Experiment Results

Bay Leaves

Two samples of bay leaf powder, weighing 14.8 and 14.5 grams, were pyrolyzed at 480 degrees Celsius using a continuous flow of N₂ carrier gas moving at a rate of 11 Liters per minute in this set of experiments. The whole process took around 20 minutes, including 16 minutes to heat up to 480°C and 4 minutes to hold. Similar results from both studies were obtained:

Around 210°C was the point at which light grey smoke first emerged from the outlet. As the temperature increased, the smoke grew worse. Notably, there was a sharp temperature drop close to the outflow, where 260°C condensed dark-brown oil.

The quantity of smoke generated started to significantly reduce at 390°C, and a minute later, at 480°, solid products were collected at the conclusion of the experiments. Most of these solid objects were black-coloured pellets with pyrophoric properties that caused some of them to spontaneously fire and change colour to white when exposed to air. The major reaction came to an end when the temperature hit 480°C, and it had already begun to significantly drop at 390°C. At the conclusion of the trials, 4.25 grammes and 4.31 grammes of solid products were collected. These solid objects, which were predominantly black pellets, possessed pyrophoric properties that, when exposed to air, caused certain things to spontaneously fire and change colour to white.

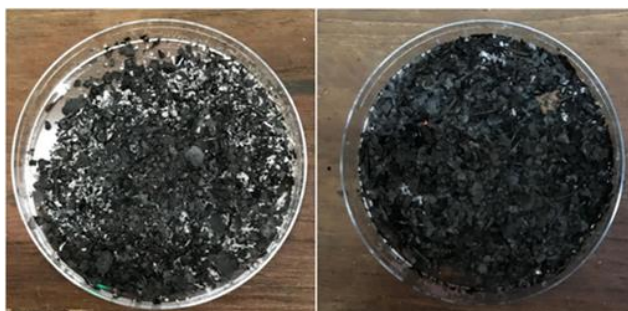


Figure 49: The collected solid product of Bay leaves Sample

Beech Wood

Chip samples of 15.2 grams and 16.5 grams were evaluated in the same manner as bay leaf trials in the beech wood investigations. The results were consistent with the bay leaf test:

Around 225°C, smoke of the same hue started to form; it became denser as the temperature rose. At 270°C, oil condensation started. A significant quantity of oil condensed as it dropped down the outlet in the case of beech wood. At 430°C, smoke production started to dramatically decline, and three minutes later, it completely stopped.

4.03 grams and 4.25 grams of solid goods were gathered at the end of the experiment. The sole difference between these solid residuals and the bay leaves test was the solid residuals' higher particle sizes. These solid products had characteristics comparable to those of the bay leaves test.



Figure 50: Collected solid product for beech wood

Gas Product Yield

Since all reactions follow the law of mass balance and the mass of the solid product generated equals the mass of the gas product generated, the yield of the gas product is determined by the mass change of biomass from the beginning to the end of the experiment, as was previously mentioned. The yield of pyrolysis oil may then be calculated using the literature-based relationship between the vapor and non-



condensable gas after obtaining the yield of the gas product. This equation may be used to get the percentage yield of the gas product:

$$\text{gas yield (\%)} = \frac{m_r - m_p}{m_r} \times 100\%$$

Where m_r is the mass of the biomass (reactant) and m_p is the solid byproduct after pyrolysis. The accompanying histogram and table provide an overview of the gas yield for each experiment based on this equation.

The accompanying histogram and table provide a summary of each experiment's gas production based on this equation.

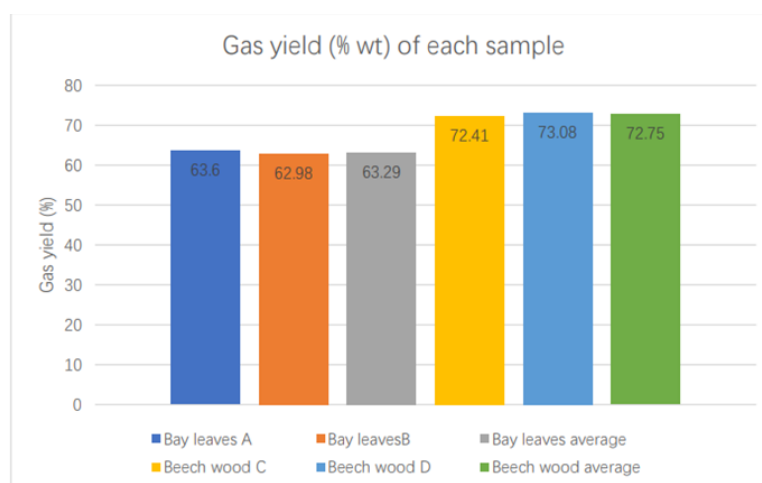


Figure 51: Gas yield for each sample

CONCLUSION

We have successfully developed a small-scale, compact reactor via research and development that is suited for the quick pyrolysis of feedstock. For smaller-scale pyrolysis operations, this novel reactor design that promotes efficiency and compactness is the best option. Furthermore, a flow reactor that we painstakingly planned, made, and put together provides the optimal environment for the thermal degradation of materials. The pyrolysis process may be precisely controlled using this reactor system, improving both the quality and yield of the end products.

Our reactor's ability to pre-heat N₂ gas before it interacts with the fuel is one outstanding characteristic. The reaction conditions are optimized during the preheating process, which helps to increase performance in general. In addition, the design of our reactor puts a high priority on heat efficiency, effectively reducing heat losses while in operation. By doing this, it optimizes energy use and makes sure the pyrolysis process runs as efficiently as possible. To make pyrolysis technology more effective and sustainable for a range of applications, we are working together to progress in this field.

FUTURE WORK

Heat Loss Mitigation

It is essential to think about putting thermal insulation measures in place to prevent the significant heat loss that occurs throughout the procedure. This may include enclosing the reactor in thermal insulation materials or coating the reactor's surface with specialist thermal insulation paints. By maintaining greater temperatures throughout the system, these methods may increase energy effectiveness.

Cyclone Tar Particle Filter

Tar particles may be successfully removed from the gas stream by adding a cyclone filter and positioning it after the product's gas exit. This improves the product gas's quality and purity while lowering the risk of equipment fouling or blockage.

Water-Cooled Condenser

A water-cooled condenser's design is a potential first step toward effectively condensing the gas product. It facilitates the collection and isolation of priceless pyrolysis products, facilitating their further processing and application.

Distillation Units

Consider placing distillation units farther down the chain of processes. Using these machines, pyrolysis oil may be refined into a variety of distillates, including gasoline, diesel, kerosene, and other useful products. The final items become more adaptable and marketable as a result of this process.

Alternative Carrying Gases

It is recommended to do experiments with alternative carrying gases like steam or argon to examine various elements of the reactor's operation. This experiment may provide important information on how the reactor reacts to various operating circumstances.

Using renewable energy in integration

Think about using renewable energy sources like solar electricity to increase the system's sustainability and affordability. Solar panels may be used to provide energy, which may subsequently be used to run the reactor's heaters. This decreases the need for non-renewable energy sources, as well as the effect on the environment and operating expenses.

Suggestions for Techno-Economic Analysis

- 1) **Cost-Benefit Analysis:** To determine if the whole pyrolysis process is economically viable, do a thorough cost-benefit analysis. This should include projected equipment capital expenditures, operational expenses, and sales of pyrolysis products.



ICSET-23



UET Peshawar

- 2) Assess the system's energy efficiency while taking into consideration the prospective incorporation of renewable energy sources. Determine the energy savings and the investment's payback time.
- 3) Analyze the potential for pyrolysis products, such as pyrolysis oil, gas, and distillates, as well as the market demand. Analyze market competitiveness and price patterns.
- 4) To ascertain the environmental advantages of the pyrolysis process, such as decreased greenhouse gas emissions and waste reduction, consider completing an environmental impact assessment.
- 5) Regulatory Compliance: Ensure that all applicable laws, rules, and licenses are obeyed by the pyrolysis plant. Recognize the legal and regulatory environment to steer clear of future problems.
- 6) Perform a scale-up study, if necessary, to ascertain the viability and any possible difficulties associated with moving from a small-scale reactor to a larger industrial-scale operation.
- 7) By taking care of these issues, you may not only maximize the pyrolysis system's performance but also decide on its viability from an economic and environmental standpoint.

REFERENCES

- [1] S. Dey, A. Sreenivasulu, G. T. N. Veerendra, K. V. Rao, and P. S. S. A. Babu, "Renewable energy present status and future potentials in India: An overview," *Innovation and Green Development*, vol. 1, no. 1, p. 100006, Sep. 2022, doi: 10.1016/j.igd.2022.100006.
- [2] A. Trada, A. Chaudhary, D. Patel, and D. S. Upadhyay, "An alternative fuel production from sawdust through batch-type pyrolysis reactor: Fuel properties and thermodynamic analysis," *Process Safety and Environmental Protection*, vol. 167, pp. 332–342, Nov. 2022, doi: 10.1016/J.PSEP.2022.09.023.
- [3] S. V. Vassilev, D. Baxter, L. K. Andersen, and C. G. Vassileva, "An overview of the chemical composition of biomass," *Fuel*, vol. 89, no. 5, pp. 913–933, May 2010, doi: 10.1016/j.fuel.2009.10.022.
- [4] J. Huang, X. Lu, and M. B. McElroy, "Meteorologically defined limits to reduction in the variability of outputs from a coupled wind farm system in the Central US," *Renew Energy*, vol. 62, pp. 331–340, Feb. 2014, doi: 10.1016/J.RENENE.2013.07.022.
- [5] J. S. Tumuluru, B. Ghiasi, N. R. Soelberg, and S. Sokhansanj, "Biomass Torrefaction Process, Product Properties, Reactor Types, and Moving Bed Reactor Design Concepts," *Front Energy Res*, vol. 9, p. 728140, Sep. 2021, doi: 10.3389/FENRG.2021.728140/BIBTEX.
- [6] H. A.-H. Ibrahim and H. A.-H. Ibrahim, "Introductory Chapter: Pyrolysis," *Recent Advances in Pyrolysis*, Jan. 2020, doi: 10.5772/INTECHOPEN.90366.
- [7] S. Gulshan, "Fast Pyrolysis of Biomass in a Fluidized Bed for Production of Bio-oil and Upgradation by Ex-situ Catalytic Bed".
- [8] S. K. Sansaniwal, K. Pal, M. A. Rosen, and S. K. Tyagi, "Recent advances in the development of biomass gasification technology: A comprehensive review," *Renewable and Sustainable Energy Reviews*, vol. 72, pp. 363–384, 2017, doi: 10.1016/j.rser.2017.01.038.



ICSET-23

*Proceedings of the 5th International Conference on Sustainable
Energy Technologies (ICSET 2023) Peshawar, Pakistan
14-15 December 2023*



UET Peshawar

- [9] M. Kaltschmitt, D. Thrän, and K. R. Smith, “Renewable Energy from Biomass,” *Encyclopedia of Physical Science and Technology*, pp. 203–228, 2003, doi: 10.1016/B0-12-227410-5/00059-4.
- [10] P. Biniiaz, N. A. Shirazi, T. Roostaie, and M. R. Rahimpour, “Wastewater treatment,” *Advances in Bioenergy and Microfluidic Applications*, pp. 303–327, Jan. 2021, doi: 10.1016/B978-0-12-821601-9.00012-1.
- [11] F. Author, mgr inż Leszek Stepień Supervisor, and dr hab inż Marek Sciazko, “Introduction to fluidization,” 2015.
- [12] W. H. Chen *et al.*, “Progress in biomass torrefaction: Principles, applications and challenges,” *Prog Energy Combust Sci*, vol. 82, p. 100887, Jan. 2021, doi: 10.1016/J.PECS.2020.100887.
- [13] O. A. Kolenchukov *et al.*, “Numerical and Experimental Study of Heat Transfer in Pyrolysis Reactor Heat Exchange Channels with Different Hemispherical Protrusion Geometries,” *Energies* 2023, Vol. 16, Page 6086, vol. 16, no. 16, p. 6086, Aug. 2023, doi: 10.3390/EN16166086.

Paper ID: ICSET-2310

DESIGNING AND OPTIMIZATION OF ON-GRID HYBRID RENEWABLE ENERGY SYSTEM FOR BOTH IRRIGATION AND ELECTRIFICATION OF VILLAGE IN KHYBER PAKHTUNKHWA

Hasan Ayaz Khan*, Hassan Abdullah Khalid, Syed Ali Abbas Kazmi

Department of Electrical Power Engineering, US-Pakistan Centre for Advanced Studies in Energy, National University of Sciences and Technology, Islamabad, Pakistan

**Corresponding author*

Email: ayazhasan795@gmail.com

ABSTRACT

Integration of remote areas with a national grid system is an unresolved dilemma for developing economies. Additionally, a significant portion of electrical energy produced in Pakistan is through non-renewable imported fossil fuels. Therefore, it results in an elevated cost per kW-hr along with a huge impact on environmental degradation. To address these issues, this study focuses on devising a novel Hybrid Energy System (HEEs) to manage electrical energy consumption for agricultural irrigation and remote locals in the Khyber Pakhtunkhwa (KPK) province having limited electrical supply. The required water volume for the proposed irrigated land is determined by utilizing CROPWAT 8.0 and CLIMWAT 2.0 software tools. On-grid Hybrid Energy System (HES) is presented due to the advantages of high reliability and cost-effectiveness over conventional single-source systems. Using the Hybrid Optimization Model for Electric Renewables (HOMER), the research performs the techno-economic analysis of various HES configurations including Hydro, Solar, Wind, and Grid. The financial feasibility of the proposed system is evaluated using the HOMER software. The findings reveal that HES with the integration of hydro, solar, wind, and grid has an economical Cost of Energy (COE) equal to \$0.006274. In contrast, other combinations, such as solar, wind, and grid possess COE of \$0.0252, and solar, micro hydro, and grid, which result in a COE of \$0.0267 respectively.

KEYWORDS: Hybrid energy, Micro Hydro, Homer, Renewables, Sustainable energies, Solar PV.

INTRODUCTION

Electrification plays an important role in the development of a country. The World Summit on Sustainable Development (WSSD) acknowledges the importance of electricity for the eradication of poverty. Individual Power Producers (IPPs) firms supply a significant portion of the electrical energy consumed by Pakistan as shown in Fig 1. It is well-known that IPPs use imported fossil fuels such as RLNG, RFO, and Coal. Since the imported fuel cost is dynamic and dependent on various socio-political developments. Therefore, it results in an unstable and unpredictable power market. Usually, high-cost electricity is produced in such situations which leads to a shortfall of electricity. Furthermore, a lengthy hour (14 -18) of load shedding is incorporated to adjust the shortfall specifically in rural areas [2]. Pakistan Being an agricultural country, has its economy dependent on agriculture many peoples are linked to the agriculture sector for earning their lives, especially in rural areas where still 70% of the population lives.



ICSET-23



UET Peshawar

Limited electricity supply to the rural areas has brought irrigation and domestic activities to stand still. In many rural areas, conventional sources of diesel or gas generators are being used for providing water for irrigation purposes which is very costly and contributes to carbon emissions and other environmental hazards such as noise. Globally, irrigation purposes are met by five distinct energy sources. These include Solar Photovoltaic Water Pumping Systems (SPWPSs), Solar Thermal Water Pumping Systems (STWPSs), Wind Energy Water Pumping Systems (WEWPSs), Biomass Water Pumping Systems (BWPSs), and Hybrid Renewable Energy Water Pumping Systems (HREWPSs) [3]. While these energy sources offer cost-effective and environmentally friendly options, their intermittent nature poses a challenge, as they cannot be consistently relied upon. This research focuses on the development of a hybrid system combining different renewable energy sources like Solar, wind, and hydro. The system is designed to meet two types of loads: irrigation load and residential load. Due to the intermittent nature of these renewable energy sources, the hybrid system connected to the grid will provide electricity in the absence of these sources. The logic behind using a grid is that the excess energy can be sold back to the grid which results in a decreased energy rate. HOMER software has been used for the techno-economic feasibility of the project. Different combinations of these renewable energies have been considered and the simulation results dictate that the most economical combination is that of Solar PV, Wind, Micro-hydro, and grid.

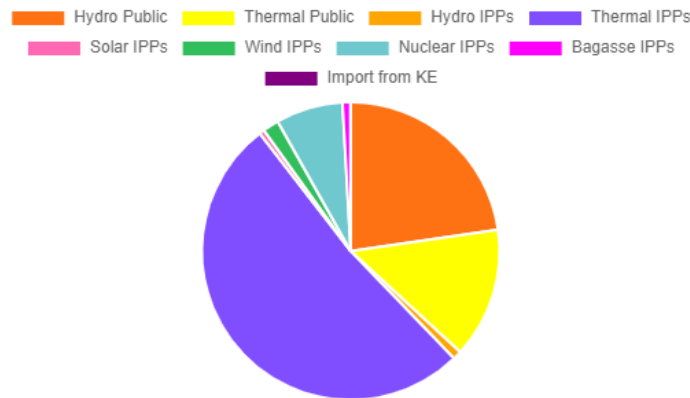


Figure.1: Energy generation of Pakistan in GWh (FY 2017-18) [1]

METHODOLOGY

This hybrid project was simulated by Homer. The simulation outcomes serve as the foundation for the project's feasibility analysis. HOMER software relies on specific input data, including area coordinates and load profiles [4]. Additionally, resource-related data, such as solar irradiance, wind speed, and water flow for micro hydropower plants, are required for effective simulations. providing these input parameters, HOMER generates simulation results that help in the identification of the most viable and optimized solution.

Site Selection for the project

The first step of this grid-connected hybrid renewable energy project is selection of a suitable location [5]. The core objective of the undertaken research revolves around the generation of cost-effective electricity through renewable sources, intended for both irrigation purposes and supply electricity to a village of 30



houses. Following a comprehensive survey, Madad Khan Banda has been identified as the optimal site for this project. This village is in Khyber Pakhtunkhwa province of Pakistan with coordinates 34.4449° N, 72.0129° E. The reason for the selection of Madad Khan Banda as the project site stems from its abundant reservoir of renewable energy resources, including wind, solar, and a minor water canal. Furthermore, this decision is justified by the reason that approximately 20 acres of land that can be used for irrigation is untapped due to the scarcity of water for irrigation—where agriculture is only done upon rainwater and a limited supply of electricity from the utility.

Load Assessment

The load was primarily divided into two distinct classifications: residential load and water pump load. The residential load was assessed through on-site visits and comprehensive surveys to ascertain the quantity, type, wattage, and operational hours of electrical appliances within each household is shown in Table 1 and the total residential energy consumption for winter and summer is summarized in Table 2. The load category pertains to the water pump, intended for both irrigation and water needed for household activities. To determine the load demand of the water pump, an initial step involves calculating the water requisites for both irrigation and household application usage. The assessment for drinking water was established based on an individual's daily requirement of 70 liters, resulting in a cumulative demand of 8,400 liters (equivalent to 8.4m³) per day for a community comprising 30 households, each accommodating 4 individuals. For irrigation, two distinct software tools, namely CROPWAT 8.0 and CLIMWAT 2.0, were employed. These applications need input data such as temperature, average rainfall, and other relevant parameters specific to the proposed site. By inputting this data for two types of crops such as wheat and maize the results show a water requirement of 96.25m³/day for wheat and 120m³/day for maize resulting in an average value of 108.12m³/day.

Table 1: Residential Load Calculation

| No of houses | Light load in Wh | TV load in Wh | Refrigerator load in Wh | Fan load in Wh | Electric iron load in Wh | Mobile charger load in Wh | Summer Load in Wh | Winter Load in Wh |
|--------------|------------------|---------------|-------------------------|----------------|--------------------------|---------------------------|-------------------|-------------------|
| 1 | 4*15*14=840 | 1*80*4=320 | 1*250*15=3750 | 3*80*10=2400 | 1*1200*30=3600 | 1*6*2=12 | 5.536 | 2.768 |
| 2 | 4*15*12=720 | NA | 1*250*14=3500 | 2*80*12=1920 | 1*1200*30=3600 | 2*6*5=60 | 5.852 | 2.666 |
| 3 | 4*15*12=720 | 2*80*4=640 | 1*250*15=3750 | 4*80*10=3200 | 1*1200*30=3600 | 2*6*5=60 | 6.832 | 3.412 |
| 4 | 4*15*14=840 | 1*80*2=160 | 1*250*16=400 | 3*80*10=2400 | 1*1200*30=3600 | 2*6*3=36 | 5.853 | 2.58 |
| 5 | 4*15*8=480 | 1*80*4=320 | NA | 2*80*12=1920 | NA | 1*6*4=24 | 3.2 | 1.55 |
| 6 | 5*15*8=600 | 1*80*2=160 | 1*250*15=3750 | 2*80*12=1920 | NA | 1*6*4=24 | 3.94 | 1.53 |
| 7 | 6*15*6=540 | 1*80*4=320 | NA | 2*80*8=1296 | NA | 1*6*2=12 | 2.992 | 1.56 |
| 8 | 5*15*6=450 | NA | NA | 2*80*8=1296 | NA | 2*6*3=36 | 2.0167 | 1.03 |
| 9 | 4*15*8=480 | NA | NA | 2*80*8=1296 | NA | 2*6*3=36 | 1.576 | 0.716 |
| 10 | 4*15*12=720 | 1*80*2=160 | 1*250*14=3500 | 3*80*10=2400 | 1*1200*30=3600 | 1*6*4=24 | 3.94 | 1.57 |
| 11 | 2*15*8=240 | NA | NA | 2*80*12=1920 | 1*1200*30=3600 | 1*6*4=24 | 1.4 | 0.75 |
| 12 | 4*15*8=480 | NA | NA | 2*80*12=1920 | NA | 1*6*4=24 | 2.152 | 1.75 |



ICSET-23

*Proceedings of the 5th International Conference on Sustainable
Energy Technologies (ICSET 2023) Peshawar, Pakistan
14-15 December 2023*



UET Peshawar

| | | | | | | | | |
|----|--------------|------------|---------------|--------------|----------------|----------|-------|-------|
| 13 | 24*15*5=1200 | 2*80*4=640 | 2*250*14=7000 | 2*80*14=2240 | 1*1200*30=3600 | 3*6*4=72 | 6.567 | 3.48 |
| 14 | 24*15*9=3240 | 2*80*4=640 | 2*250*14=7000 | 5*80*14=9600 | 1*1200*30=3600 | 3*6*4=72 | 6.832 | 3.423 |
| 15 | 4*15*10=600 | 1*80*2=160 | 1*250*14=3500 | 2*80*14=2240 | 1*1200*30=3600 | 1*6*4=24 | 3.94 | 1.98 |

Table 2: Total Summer and Winter Energy Consumption

| Total summer load in kWh | | Total winter load in kWh |
|--------------------------|-------|--------------------------|
| for 15 houses | 158 | 81 |
| Per house | 10.55 | 5.4 |
| For 30 houses | 316 | 162 |

$$P_{\text{pump}} = (\rho g H Q) / \eta \quad (1)$$

Equation 1 is used to calculate the load demand of water pump in kW.

Where ρ is the density of water (1000kg/m³)

g is the gravitational acceleration (9.8m/s²)

H , height in meter (55m in our case)

Q , water flow in m³/hr (19.4m³/hr in our case, considering 6 sunny hours).

Using equation 2 the power turns out to be 6.05Kw.

On average, residential energy consumption stood at 239 KWhr, while the water pump exhibited an average energy consumption of 145.37 KWhr.

Evaluation of Energy Sources

Solar irradiance:

Solar-related information, including irradiation measurements, was obtained through Homer, which imports data from the NASA Surface Meteorology and Solar Energy database. This data was collected by inputting the geographical coordinates of the designated site. Notably, the highest solar irradiation recorded within the chosen area was observed in the month of June, having a magnitude of 7.880 kWh/m²/day. Additionally, an average solar irradiation value of 5.31 kWh/m²/day was computed. Daily radiations in kWh/m²/day are shown in Figure 2.



Figure 2: Daily radiations in kWh/m²/day

Wind Resource

The wind velocity in meters per second (m/s) was determined by the HOMER software, which relies on data from the NASA Surface Meteorology and Solar Energy Database. This data was measured at an elevation of 50 meters. The wind speed within the chosen area is shown in Figure 3, indicating a maximum speed of 8.260 m/s and an average speed of 6.58 m/s. HOMER utilizes the power law formula to calculate wind speeds at the turbine hub height [6].

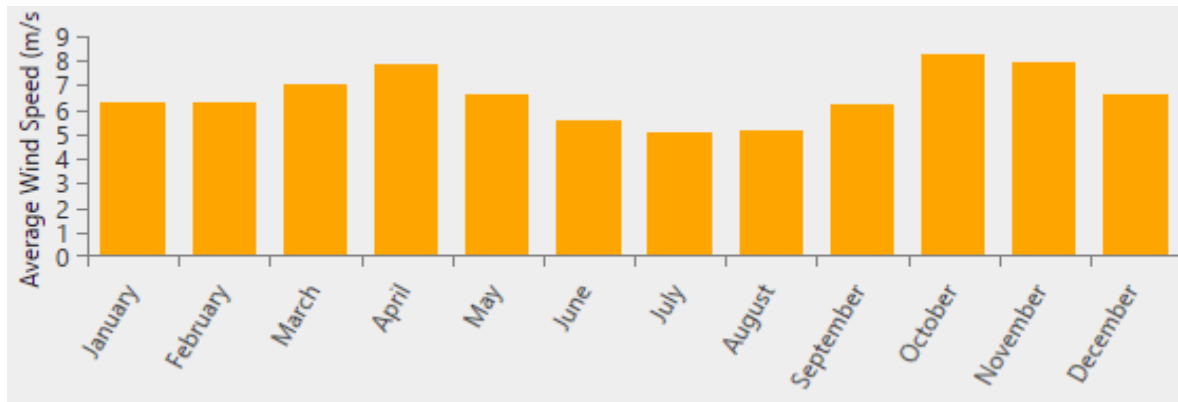


Figure 3: Average wind speed in m/s

Micro Hydro

Hydropower harnesses the energy inherent in water situated at elevated points, channelling it through the turbine, which in turn drives an electrical generator, thereby generating electrical energy. Within the designated area, a flow of water is consistently present in the canal, excluding the months spanning from December through February as shown in Figure 4. The fundamental principle of hydropower is based on the concept that the potential energy of water at height can be used to move the turbine which subsequently runs an electric generator.

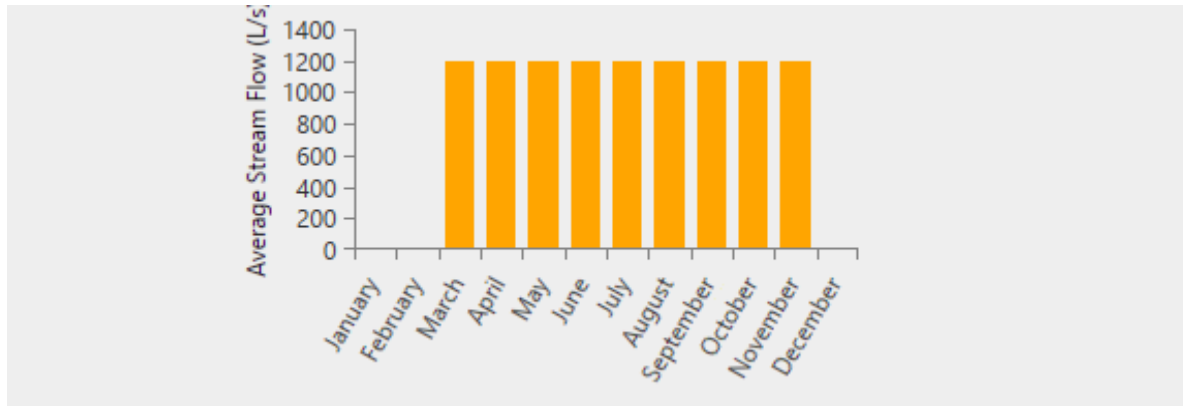


Figure 4: Average stream flow in litres/sec

System Designing

This hybrid project mainly consists of four different energy sources i.e., Solar system, micro-hydro, wind, and grid. The logic behind using the grid is that the excess energy produced by this hybrid system be fed back to the grid through green meters which will have two main advantages i.e., getting rid of costly batteries and it will also result in reduced energy prices in some cases it may earn from the WAPDA.

The famous equation used for calculating electrical power for hydropower plants is:

$$P_{hydro} = \eta \rho g Q H \quad (2)$$

Where

η is the efficiency of the hydropower plant (75%)

ρ is the density of water (1000 kg/m³)

Q is the water flow in m/s (1.2m/s)

H is the height of the water fall in m (2m)

Using equation 2 and Considering percent efficiency of the Mini hydro power plant as 75% the Power that can be obtained from the plant is 16KW.

Solar PV System:

For this project, polycrystalline PV panels were employed. Utilizing Homer, a thorough evaluation of varying solar panel capacities was conducted, facilitating the identification of the most cost-effective configuration. As the output of the solar panels is notably contingent upon solar irradiance and temperature [7] conditions, the integration of MPPT (Maximum Power Tracking Point) technology has been proposed. This innovation continuously monitors and adjusts the operational point on the PV curve, ensuring the panels operate at their optimum capacity, referred to as the Maximum Power Point (MPP). This approach ensures the optimal utilization of the available solar resource. Cot Summary of Solar PV is shown in table 3.

Table 3: Different parameters of Solar PV

| S. No | Parameter | value | unit |
|-------|-----------------------|-------|---------|
| 1 | Capital cost | 660 | \$/kw |
| 2 | Replacement cost | 660 | \$/Kw |
| 3 | O&M cost | 10 | \$/year |
| 4 | Lifetime | 25 | year |
| 5 | Derating factor | 80 | % |
| 6 | Rated power | 250 | W |
| 7 | Short circuit current | 8.76 | A |
| 8 | Open circuit voltage | 37.5 | V |

WIND TURBINE:

Power output from the wind is in direct proportion with the cube of the wind speed [8]. The wind turbine selected for the proposed system is 3kw with model number FT-3000 and a rotor diameter of 3380mm. different parameters of the proposed wind power plant are mentioned in Table 4.

Table 4: Different Parameters of Wind Turbine

| S. No | Parameter | Value | SI Unit |
|-------|------------------|----------|---------|
| 1 | Capital Cost | 890 | \$ |
| 2 | Replacement Cost | 600 | \$ |
| 3 | O&M Cost | 100 | \$/year |
| 4 | Lifetime | 20 | years |
| 5 | Model | FT-3000L | - |
| 6 | Cut in speed | 2.5 | m/s |
| 7 | Rated wind speed | 11 | m/s |
| 8 | Rated voltage | 48 | v |
| 9 | Rated Power | 3000 | W |
| 10 | Rotor diameter | 3380 | mm |
| 11 | Number of blades | 3 | |
| 12 | Approx. weight | 70 | kg |

PV Converter:

Within the framework of the HOMER software, the converter component serves a dual role, functioning both as a rectifier and an inverter [9]. Its primary purpose is to transform the direct current (DC) power derived from the solar panels into alternating current (AC) for utilization by the load. The operational lifespan of this converter module has been designated as 15 years, with an associated efficiency rating of 90 percent. The table provided contains essential details encompassing the cost and pertinent technical specifications of this converter unit.

RESULTS AND DISCUSSIONS

Three alternative combinations of the available resources for the project were simulated in order to find the most cost-effective combination with the lowest NPC (net present cost) and energy cost.

CASE 1:

In this case, the available resources considered are micro hydro, Solar PV panels, and grid. Homer used the available resources to meet the load demand. After simulation of the project for the mentioned available sources results for the hybrid system were obtained which includes 30.9 KW of Solar panels, and 17.7 KW of hydro. The net present cost of the project comes out to be \$62767 and the cost of units produced is \$0.0267 with a payback period of 9.20 years. In this case, a major portion of the load was served by Hydro then followed by Solar PV panels. In case of electricity shortage, the load is to be fed by the grid. The excess energy produced by this hybrid system is only 2.34% which can be sold back to the grid.

CASE 2:

In the second case Solar PV, wind, and grid are being taken into consideration. To meet the load Homer will consider these sources and will select the one which has the least net present cost and cost of energy. This combination results in 42.0KW of Solar PV panels and 50kW of wind power plant. The total energy contributed by the PV system is 75415kWh which is 22.7% of the total energy needed. Similarly, the energy produced by the wind power plant is 208998kWh which corresponds to 62.8% of the total energy requirement of the load. Again, this hybrid system is grid-connected which will supply electricity in the absence of renewable energy sources, in this case, the energy that is being drawn from the grid is 4844kWh which is just 14.6% of the total energy requirement. Furthermore, this combination results in a cheap electricity rate as compared to case 1. In this case, the net present cost of the project is \$105413, and the cost of energy is \$0.0252 with a payback period of 6.20 years.

CASE 3:

In the third case Solar PV, wind, micro-hydro, and grid are being taken into consideration. In this case, all the renewable energy sources have been considered to meet the load. The resources and load specifications have been provided to Homer and the project was simulated which resulted in 16.1Kw of solar PV panels, 50kW of wind power, and 17.7kW of hydro power plant. In this case, the net present cost of the project is \$28514 which is quite a lesser amount as compared to that in case 1 and case 2, and the cost of energy is \$0.006274 with a payback period of 7.02 years. The reason for its economical cheapness is that in this case 27.8% of energy was supplied by micro which is cheaper than both wind and Solar PV. A schematic diagram for case 3 is shown in Figure 5 and annual energy production is depicted in Table 5 and is visualized in Figure 6.

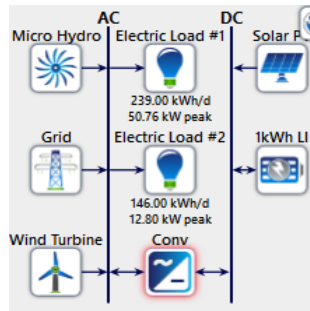


Figure 5: Schematic Diagram for case 3

Table 5: Annual Electricity Production in Case 3

| Electricity Production | | | Electricity consumption | | | Quantity | | |
|------------------------|----------|-----------|-------------------------|----------|-----------|--------------------|----------|-----------|
| Source | kWh/year | Percent % | Load type | kWh/year | Percent % | Quantity | kWh/year | Percent % |
| Solar | 28850 | 8.13 | Ac | 140525 | 43.5 | Excess electricity | 2031 | 0.572 |
| Wind power | 208998 | 58.9 | Dc | 0 | | Unmet load | 0 | 0 |
| Micro hydro | 98611 | 27.8 | | | | | | |
| Grid | 18502 | 5.21 | Grid sale | 211064 | 60 | | | |
| Total | 332857 | 100 | Total | 351589 | 100 | Total | 2031 | 0.572 |

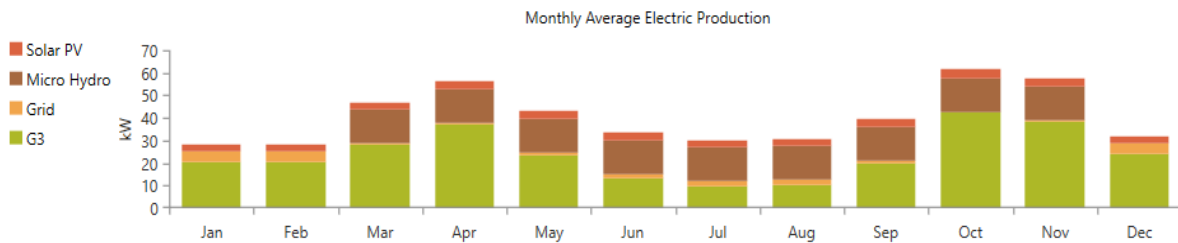


Figure 6: Monthly Average Electricity Generation in case 3

Cost Comparison of Three Cases:

Cost comparison of all the three cases is summarized in table 8. The results dictate that the cheaper case is case number 3 with NPC \$28514 and COE as \$0.006274. This least cost of energy can be justified by the cheapest power source that is micro hydro power plant.

Table 8: Cost comparison of the above three cases

| | Cost of energy in \$ | NPC in \$ | Operating Cost in \$/year | Payback Period in years |
|--------|----------------------|-----------|---------------------------|-------------------------|
| Case 1 | 0.0267 | 62767 | 31471 | 9.20 |
| Case 2 | 0.0252 | 105413 | 25097 | 6.02 |
| Case 3 | 0.006274 | 28514 | 40318 | 7.02 |

CONCLUSION

This paper presents a hybrid energy system that primarily includes Solar PV, Wind power plant, Micro-hydro, and grid. The research is intended to produce cheap electricity which will feed two types of load residential load comprising of a small village of 30 houses and a water pump which is used for irrigation purposes. Three Different combinations of the available resources were considered and simulated by HOMER. Results were obtained for each case, and it was found that the most economical combination was a mix of solar PV, Wind power plant, micro hydropower plant, and a grid with an NPC (net present value) of \$28514 and COE (Cost of energy) as \$.006274 with a payback period of 7.02 years.

REFERENCES

- [1] <https://ntdc.gov.pk/energy>
- [2] M. P. Bakht, Z. Salam, A. R. Bhatti, U. U. Sheikh, N. Khan, and W. Anjum, "Techno-economic modelling of hybrid energy system to overcome the load shedding problem: A case study of Pakistan," *PLoS One*, vol. 17, no. 4 April, Apr. 2022, doi: 10.1371/journal.pone.0266660.
- [3] C. Gopal, M. Mohanraj, P. Chandramohan, and P. Chandrasekar, "Renewable energy source water pumping systems - A literature review," *Renewable and Sustainable Energy Reviews*, vol. 25, pp. 351–370, 2013. doi: 10.1016/j.rser.2013.04.012.
- [4] S. Mishra, G. Saini, A. Chauhan, S. Upadhyay, and D. Balakrishnan, "Optimal sizing and assessment of grid-tied hybrid renewable energy system for electrification of rural site," *Renewable Energy Focus*, vol. 44, pp. 259–276, Mar. 2023, doi: 10.1016/j.ref.2022.12.009.
- [5] J. O. Oladigbolu, M. A. M. Ramli, and Y. A. Al-Turki, "Feasibility study and comparative analysis of hybrid renewable power system for off-grid rural electrification in a typical remote village located in Nigeria," *IEEE Access*, vol. 8, pp. 171643–171663, 2020, doi: 10.1109/ACCESS.2020.3024676.
- [6] P. Roy, J. He, T. Zhao, and Y. V. Singh, "Recent Advances of Wind-Solar Hybrid Renewable Energy Systems for Power Generation: A Review," *IEEE Open Journal of the Industrial Electronics Society*, vol. 3, Institute of Electrical and Electronics Engineers Inc., pp. 81–104, 2022. doi: 10.1109/OJIES.2022.3144093.
- [7] X. Li, Q. Wang, H. Wen, and W. Xiao, "Comprehensive Studies on Operational Principles for Maximum Power Point Tracking in Photovoltaic Systems," *IEEE Access*, vol. 7, pp. 121407–121420, 2019, doi: 10.1109/ACCESS.2019.2937100.
- [8] M. Mallek, M. A. Elleuch, J. Euch, and Y. Jerbi, "Optimal design of a hybrid photovoltaic-wind power system with the national grid using HOMER: A case study in Kerkennah,



ICSET-23

*Proceedings of the 5th International Conference on Sustainable
Energy Technologies (ICSET 2023) Peshawar, Pakistan
14-15 December 2023*



UET Peshawar

- Tunisia,” in *2022 International Conference on Decision Aid Sciences and Applications, DASA 2022*, Institute of Electrical and Electronics Engineers Inc., 2022, pp. 725–729. doi: 10.1109/DASA54658.2022.9765310.
- [9] G. Ali, H. H. Aly, and T. Little, “Using HOMER software to investigate, size and apply renewable energy sources in a convention center in Sabratha, Libya,” in *3rd International Conference on Electrical, Communication and Computer Engineering, ICECCE 2021*, Institute of Electrical and Electronics Engineers Inc., Jun. 2021. doi: 10.1109/ICECCE52056.2021.9514156.

Paper ID: ICSET-2311

DESIGN OF METAMATERIAL BROADBAND SOLAR ABSORBER FABRICATED BY A MULTILAYER HOLLOW FLOWER-SHAPED STRUCTURE

Hamza Farooq*, Ahsan Sarwar Rana

Department of Electrical and Computer Engineering, Air University, Islamabad, Pakistan

**Corresponding author*

Email: hamzafarooq587@yahoo.com

ABSTRACT

A class of artificial materials with unique structures is referred to as metamaterials. So we introduce a wide-spectrum absorber consisting of two Metal-Dielectric-Metal (MDM) layers. The bottom MDM layer is composed of three multi-layered Tungsten-Hafnia-Tungsten materials while the top cross structure is also composed of three layered Tungsten-Hafnia-Tungsten hollow flowered-shaped structures with a cavity in the center. Tungsten, known for its high melting point (3422 °C) and excellent conductivity, is employed as the metal layer, while hafnia, due to its low refractive index and high melting point (2800 °C), is used as the dielectric layers. This combination enables efficient light absorption across a wide range of frequencies. Based on our proposed absorber, we have discovered that the Bandwidth of absorption becomes 90% when it reaches the range (300–1547 nm), with an incredible average absorption of 95.66137%. At the same time, 615 nm is the thickness of the complete structure. Additionally, the characterization of an MDM-based broadband solar absorber is thoroughly examined in this study. The absorber's distinct electromagnetic features are used to effectively collect solar energy over a broad range. The design is upgraded for improved energy harvesting, solar thermal systems, photovoltaics, and thermal photonic devices.

KEYWORDS: Metamaterial, Broad band absorber, MDM, Tungsten, Hafnia.

INTRODUCTION

The world's need for energy has skyrocketed, and using fossil fuels has resulted in numerous environmental issues [1]. Solar energy stands out as an exceptional, cost-effective renewable energy source. One efficient method for achieving broad-spectrum light absorption is through the use of blackbody paint. While this technique is both quick and affordable, it's important to note that premium infrared calibration blackbody sources still come at a relatively high cost. In recent years, there has been a surge in demand for compact and effective electromagnetic absorbers. This increased interest is a direct result of the growing popularity of solar thermal systems and photothermal conversion technologies. Among various types of absorbers, Broadband Metal-Dielectric-Metal (MDM) absorbers have gained significant attention for their remarkable absorption performance across a wide frequency range. Recently, Metamaterials have attracted scientists because of their tremendous optical and thermal features like spectral filtering, sensing, thermal absorption, utilization, etc. [2,3]. Since Landy et al. originally suggested the concept of Metal-Dielectric-Metal (MDM) structure in 2008, broadband absorbers have been the subject of thorough investigation [4].



Wideband absorbers with complete broadband absorption offer a lot of applications as mentioned above. The application potential of materials made with noble metals was however constrained by their expensive cost and low heat resistance, leading people to start thinking about metals with high melting points such as tungsten, hafnia, and others. Broadband absorbers are made to have strong absorption characteristics throughout a broad variety of wavelengths, generally including the infrared (IR) spectrum [5]. Carbon-based materials like carbon nanotubes as well as other metal oxides and composites, are frequently employed for broadband absorbers [6]. To obtain high absorption across a broad frequency range, broadband absorbers must optimize their material composition, thickness, and surface structure [7]. Different manufacturing methods for MDM absorbers are described, taking into account things like scalability, affordability, and compatibility with incorporation into energy-harvesting devices. Refractory metals also have high melting points. Another promising combination of refractory materials for broadband MDM absorbers is Tungsten (W) and Hafnium dioxide (HfO_2) [8,9]. Tungsten, a transition metal known for its capability to withstand high temperatures, offers remarkable absorptivity and low reflectivity across a wide frequency range. On the other hand, hafnia, a dielectric material composed of hafnium and oxygen, possesses a high refractive index, enabling enhanced impedance matching and increased absorption capabilities [10,11]. The integration of tungsten and hafnia in MDM absorbers holds great potential for achieving efficient absorption across a wide range of frequencies. Simulated results show that the materials' intrinsic optical and thermal characteristics and superb structure produced over 95% ultra-wideband absorption at wavelengths between (300-2500 nm). These absorbers are essential for applications because they can successfully reduce reflection and transmission while maximizing absorption by varying the configuration and characteristics of subwavelength structures. Broadband metamaterial absorbers have become effective, adaptable solutions for electromagnetic wave absorption across an extensive frequency range. This research focuses on improving metamaterial broadband absorber designs to improve absorption efficiency while preserving structural simplicity. We can obtain improved absorption properties by systematic parameter adjustment and analysis.

MATERIALS & METHODS

Proposed Design

Figure 1 shows details of an ultra-broadband Solar Absorber. W (Tungsten) and HfO_2 (hafnium dioxide) make up the six-layer structure's whole material composition. Periodically, the W- HfO_2 -W substrate displays a three-layer hollow, floral array with a cavity in the center. The ellipse's X and Y axes have radii of "R" and "r," respectively, while the cavity's radii are "a" respectively. 'T1', 'T2', 'T3', 'T4', 'T5', and 'T6' are the thicknesses of the structure consisting of HfO_2 and W materials from top to bottom. The simulation's precise parameters for the suggested absorber are T1=220 nm, T2=85 nm, T3=60 nm, and T4=50 nm, T5=150 nm, T6=50 nm for metal W and HfO_2 . By employing periodic boundary restrictions in the x-y dimensions, the entire arrays may be condensed into a single unit cell.

Optimization of Design

The transmission and reflection effects are reduced by a flawlessly coordinated layer boundary in the z-direction. When transverse magnetic mode plane waves are affected vertically from above the arrays. The simulations are performed through freeware software available online such as Meep & Optiwave, as they utilize FDTD (finite difference time domain) algorithms. The thickness of each layer is achieved after applying sweep configuration at various values of heights and that points were selected where the highest value of absorption was achieved. Sweep configuration when applied on the thickness of the bottom and



spacer layer we saw that absorption in the visible regime increased as we increased height so we selected those values of heights where maximum absorption was achieved. The same method was followed when we dealt with cross-layer thickness [11]. A metamaterial broadband absorber's design may be made more effective by adjusting the shape and material characteristics to effectively absorb a wide range of frequencies. The absorber may be tailored to absorb electromagnetic waves across a wide spectrum by incrementally changing variables such as unit cell size, layout, and material composition.

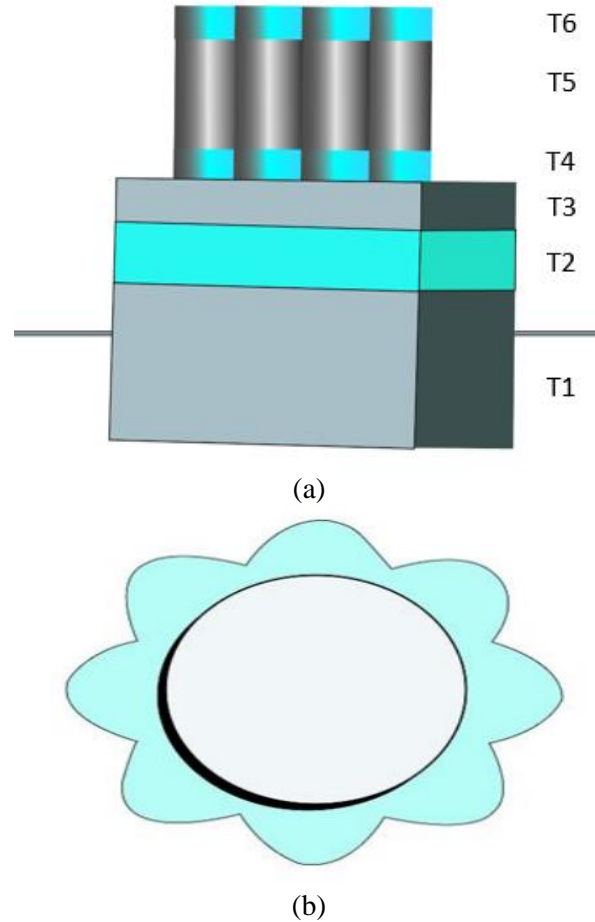


Figure 1: (a) 3-Dimensional outlook of the cell (b) Topmost outlook of the cell

Equations

The total absorption may be calculated using Equation 1 given below. According to the equation, absorption is effectively the difference between 1 (total energy) and reflection and transmission coefficients. Low reflection and transmission coefficients in an MDM broadband absorber will lead to greater absorption levels. This equation provides a precise metric for assessing the efficacy of the absorber design by



ICSET-23



UET Peshawar

quantifying the absorption performance of the MDM broadband absorber while taking into account the decrease in reflected and transmitted energy. These absorbers may efficiently modify the input radiation, allowing for absorption across a variety of frequencies, by utilizing complex structural arrangements on a subwavelength scale.

$$A = 1 - T - R \quad (1)$$

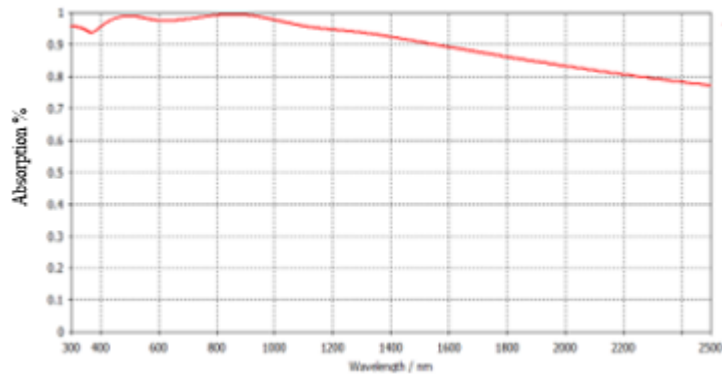
RESULT & DISCUSSION

Broadband Absorption & Efficiency

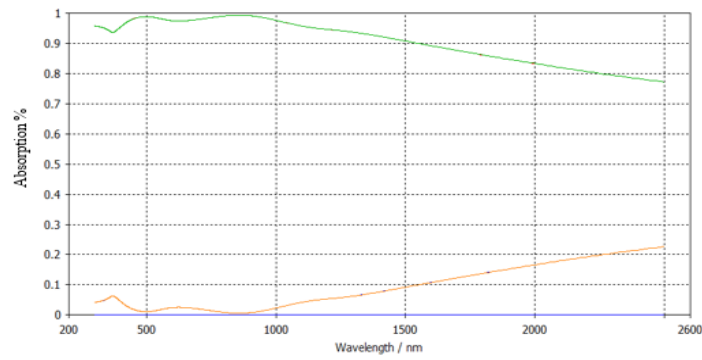
Figure 2 displays the simulation results for the suggested absorber, the x-axis characterizes wavelength in nm whereas the y-axis denotes absorption of the absorber. The suggested absorber has exceptionally high absorptivity (>80%) at wavelengths between 300 to 2252 nm. The bandwidth at which absorptivity exceeds 90% is 1247 nm (300-1547 nm), which is well matched to the spectrum of solar energy. The average absorptivity in the (300-1590 nm) nm wavelength range is 96.6%. There is still a strong absorptivity of 95.7% over the entire solar radiation range (300-2500 nm). At 783.45nm and 925.4632nm, strong absorption of greater than 99% is attained. The above-mentioned data is obtained through various calculations on MS Excel software, the absorption graphs mentioned below from Figure 2 are inserted in MS Excel software via Notepad software, and after doing this average absorption is calculated via various commands on MS Excel. When average absorption is achieved things become clear and we can find out different values of wavelength where average absorption is highest or lowest and we see that average absorption is greater than 90% from 300 to 1547 nm.

Electric Field Intensity Distribution

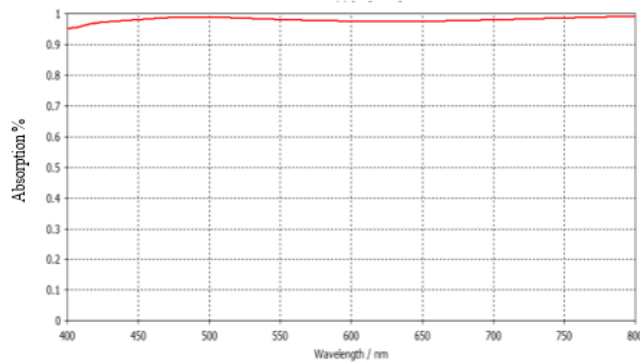
The proposed absorber exhibits broadband absorptance, and field intensity distribution profiles that are looked at two distinct wavelengths. The suggested structure's electric field distribution is examined. In this case, we simulate wavelengths of 428 nm (shorter waves) and 634 nm (visible domain) while maintaining the source's normal to the z-axis. In the below-mentioned figures, we perceive the scattering of an electric field, it becomes evident that its primary concentration occurs around the peripheries and extends towards corners for the shorter wavelengths at 400nm. These patterns mimic the dispersion of the electric field, whereas larger wavelengths cause the field strength to diminish from the corners of the unit structure. However, most of the magnetic field is concentrated near the unit structure's edge [11]. The majority of the power loss at 400 nm happens near the unit structure's border. It features many polarity orientations for incident natural light at once. The absorbent's spectrum is present when the incident light transitions from TM (Transverse Magnetic Wave) to TE (Transverse Electric Wave) polarization. Excited expression Plasmon is often easily impacted by polarization angle changes, but because the planned absorber's surface structure is symmetrical, it is not, in this case. When electromagnetic waves are incident through a certain angle, it is also important to take this into account. There are instances where the high-absorption band's breadth steadily shrinks as the incidence angle rises. When the incoming light angle is less than 50 degrees, the absorber has an optimum influence on the absorption spectrum, which can generally fulfill the demands.



(a)

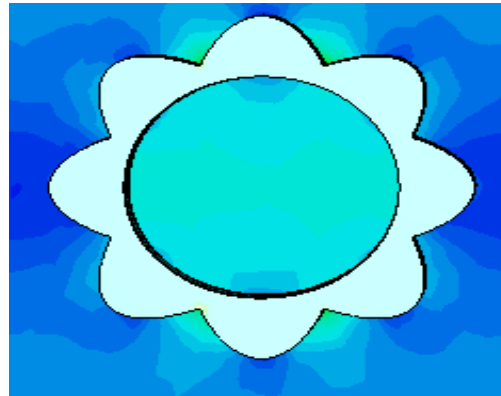


(b)

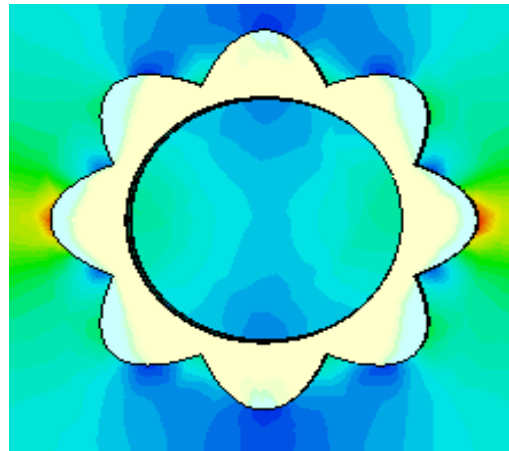


(c)

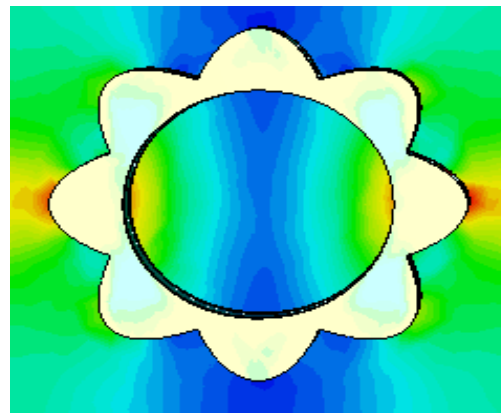
Figure 2: (a), (b) Broadband Absorption spectrum for higher wavelength, (c) for visible regime



(a)



(b)



(c)

Figure 3: (a) Electric Field at 428nm, (b) at 634nm, (c) 1400 nm



CONCLUSION

The suggested MDM-based broadband solar absorber can effectively catch solar radiation and provide novel approaches for gathering sustainable energy. Our work shows that Metal Dielectric Metal (MDM) absorbers may reach amazing absorption performance via careful design and engineering, making them interesting candidates for a variety of applications. In this paper, we presented a hollow flowered shaped structure for a metamaterial solar absorber. It is observed the presence of a cavity significantly enhances the absorption, with a broadband working array of 300-2500 nm, the suggested absorber achieves 95.65% absorption. The suggested absorber is also independent of polarization and is just 615 nm thick.

ACKNOWLEDGMENTS

We would like to express our sincere gratitude for the generous support provided for this research. This work was made possible through the support of Ahsan Sarwar Rana, who played a pivotal role in advancing our study.

REFERENCES

- [1] Zheng, Z.P., Luo, Y., Yang, H., Yi, Z., Zhang, J.G., Song, Q.J., Yang, W.X., Liu, C., Wu, X.W., & Wu, P.H. (2022). Thermal tuning of terahertz metamaterial properties based on phase change material vanadium dioxide. *Physical Chemistry Chemical Physics*, 24, 8846–8853.
- [2] Jiang, L., Yi, Y., Tang, Y., Li, Z., Yi, Z., Liu, L., Chen, X., Jian, R., Wu, P., & Yan, P. (2022). A high-quality factor ultra-narrow band-perfect metamaterial absorber for monolayer molybdenum disulfide. *Chinese Physics B*, 31, 038101
- [3] Al-badri, K.S.L., Abdul Karim, Y.L., & Alkurt, F.Ö. (2021). Simulated and experimental verification of the microwave dual-band metamaterial perfect absorber based on a square patch with a 45-degree diagonal slot structure. *Journal of Electromagnetic Waves and Applications*, 35, 1541–1552.
- [4] Abdul Karim, Y.I., Muhammad Sharif, F.F., Bakır, M., & Awl, H.N. (2021). Hyper sensitized Metamaterials Based on a Corona-Shaped Resonator for Efficient Detection of Glucose. *Applied Sciences*, 11, 103.
- [5] Ijaz, S., Rana, A.S., Ahmad, Z., Rehman, B., Zubair, M., & Mehmood, M.Q. (2021). Exploiting zirconium nitride for an efficient heat-resistant absorber and emitter pair for solar thermophotovoltaic systems. *Optics Express*, 29(20), 31537.
- [6] Zhou, Y., Qin, Z., Liang, Z., Meng, D., Xu, H., Smith, D.R., Liu, Y. (2021). Ultra-broadband metamaterial absorbers from long to very long infrared regimes. *Light-Sci. Appl.* 10, 138.
- [7] Zhao, F., Lin, J., Lei, Z., Yi, Z., Qin, F., Zhang, J., Liu, L., Wu, X., Yang, W., Wu, P. (2022). Realization of 18.97% theoretical efficiency of 0.9 μ m thick c-Si/ZnO heterojunction ultrathin-film solar cells via surface plasmon resonance enhancement. *Phys. Chem. Chem. Phys.* 24, 4871–4880.
- [8] Zhu, W.L., Yi, Y.T., Yi, Z., Bian, L., Yang, H., Zhang, J.G., Yu, Y., Liu, C., Li, G.F., Wu, X.W. (2023). High-confidence plasmonic sensor based on photonic crystal fiber with a U-shaped detection channel. *Phys. Chem. Chem. Phys.*
- [9] Zheng, Z., Luo, Y., Yang, H., Yi, Z., Zhang, J., Song, Q., Yang, W., Liu, C., Wu, X., Wu, P. (2022). Thermal tuning of terahertz metamaterial properties based on phase change material vanadium dioxide. *Phys. Chem. Chem. Phys.* 24, 8846–8853.



ICSET-23

*Proceedings of the 5th International Conference on Sustainable
Energy Technologies (ICSET 2023) Peshawar, Pakistan
14-15 December 2023*



UET Peshawar

- [10] Liu, F., Qi, L. (2021). A simple two-layer broadband metamaterial absorber for solar cells. Mod. Phys. Lett. B 17, 2150291.
- [11] Li, L., Gao, H., Yi, Z., Wang, S., Wu, X., Li, R., Yang, H. (2022). Comparative investigation on synthesis, morphological tailoring, and photocatalytic activities of Bi₂O₂CO₃ nanostructures. Colloids Surfaces a Physicochem. Eng. Asp. 644, 128758.

Paper ID: ICSET-2312

**CASE STUDY: ANALYSING ENERGY USE INTENSITY (EUI) FOR ENERGY
EFFICIENCY AND OPTIMIZATION IN AN EDUCATIONAL BUILDING**

Inam Ullah^{1,*}, Kaleem Afzal Khan², Muhammad Amar Zaib Khan¹, Dr. Mohammad Adil¹

¹Department of Civil Engineering, UET Peshawar, Pakistan

²Department of Civil Engineering, GIK Institute, Topi, Swabi, Pakistan

**Corresponding author*

Email: engginam22@gmail.com

ABSTRACT

This research paper offers an exhaustive examination of Energy Use Intensity (EUI) within an educational facility, emphasizing energy efficiency and optimization strategies and their implications for sustainability. The investigation integrates billing data, Autodesk Insight simulations, and on-site evaluations to pinpoint opportunities for enhancing sustainable energy utilization. The outcomes are presented focusing on a comprehensive perspective on EUI trends. The results indicated that actual Energy use Intensity (EUI) from the billing data of the educational facility is (100 kWh/m² per year) but the EUI calculated from Autodesk Insight simulations is (152 kWh/m² per year). This discrepancy suggests that the building may not be operating as efficiently as its design may intended. However, to enhance sustainability, we proposed optimization strategies such as Heating, Ventilation, and Air Conditioning (HVAC) upgrades, renewable energy integration (solar panels), lighting improvements, and occupant engagement, with the aim of reducing EUI and fostering energy conservation. These energy conservation strategies resulted in a remarkable decrease in EUI from the initial 152 kWh/m² per year to a significantly improved -23.25 kWh/m² per year, representing a reduction in energy usage of almost 115%. This study contributes valuable insights into the advancement of energy-efficient practices in educational buildings, supporting the broader goal of sustainability in the built environment.

KEYWORDS: Energy Use Intensity (EUI), Energy Efficiency, Energy Optimization, Educational Building, Sustainability, Autodesk Insight.

INTRODUCTION

Efficiently managing energy consumption in educational buildings holds immense importance in our contemporary world, where sustainability is at the forefront of global concerns (Economidou et al., 2020). With this perspective in mind, this scientific research paper is dedicated to a thorough investigation of Energy Use Intensity (EUI) (Mahiwal et al., 2021) within an educational facility. The research places a strong emphasis on resolving the complex dynamics of energy efficiency and optimization strategies and how they play a pivotal role in advancing the broader concept of sustainability (Toli and Murtagh, 2020). The study integrates an array of elements, weaving together empirical billing data, innovative insights derived from Autodesk Insight 360 (Maglad et al., 2023) simulations, and scrutiny facilitated by on-site assessments. The study aims to precisely explore, critically examine, and unlock the latent potential for creating an appropriate interaction between sustainable energy practices and the rigorous demands posed by



ICSET-23



UET Peshawar

educational infrastructure. The study is based on an educational building known as the Department of Civil Engineering (CED), University of Engineering and Technology (UET) which is located along the main university road in Peshawar, within the province of Khyber Pakhtunkhwa (KPK) as shown in Figure 1. The study will not only illustrate the path toward sustainable energy practices within educational institutions but also set a pioneering standard for a more energy-efficient future that extends to other buildings.

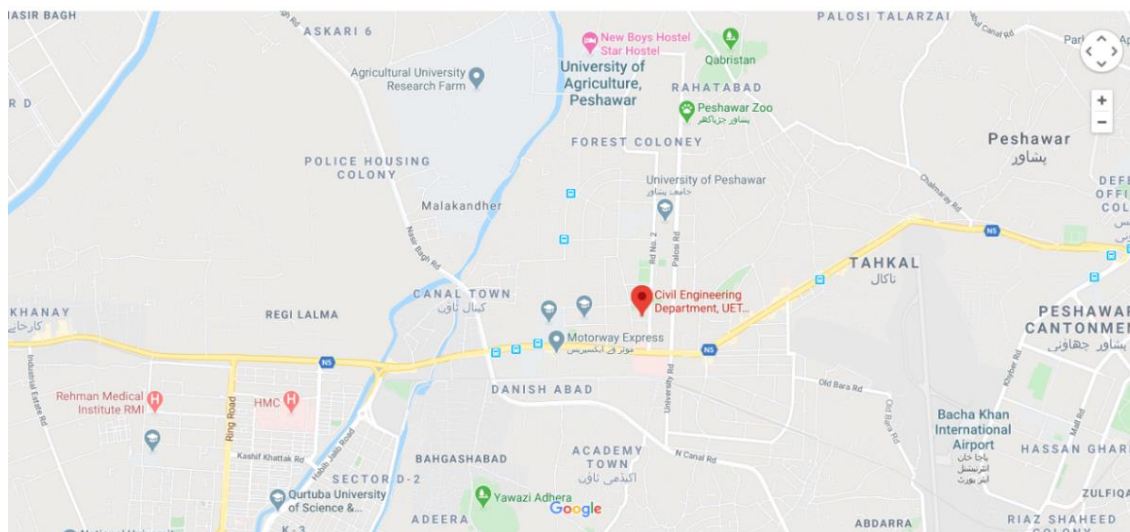


Figure 52: Location of the analyzed educational building (CED, UET Peshawar)

In the context of energy efficiency and optimization in educational buildings, the extant literature underscores the critical role that Energy Use Intensity (EUI) analysis plays in shaping sustainable practices (Olawumi and Chan, 2019). Previous research has illuminated the multifaceted aspects of EUI, demonstrating its significance as a pivotal metric for evaluating and enhancing energy performance in educational facilities (Harputlugil and de Wilde, 2021). Studies have revealed that the judicious application of EUI assessments, coupled with empirical data collection, can unveil the intricate dynamics of energy utilization within such buildings (Hsien-te and Chia-ju, 2021). Additionally, the literature highlights the importance of employing cutting-edge tools like Autodesk Insight simulations to identify potential areas for energy improvement and to bridge the gap between theoretical design and real-world operational outcomes (de Queiróz et al., 2019). This body of work collectively underscores the urgency of fostering energy conservation, sustainability, and reduced EUI in educational buildings while providing a foundation for the optimization strategies discussed in this case study (Mansor and Sheau-Tingi, 2019).

METHODOLOGY

The methodology section of this research encompasses a structured approach that encompasses essential facets of our investigations. It encompasses the gathering of the data required for our comprehensive analysis, the EUI analysis and its subsequent calculations, the simulations conducted using Autodesk Insight, and the invaluable insights derived from thorough on-site assessments. Together, these components form the methodology of our investigative process.

Data Collection

The data collection summarized in Figure 2 required for the analysis involved:

- Monthly energy consumption data was collected from billing records for the educational building.
- The total floor area was measured and converted to square meters.

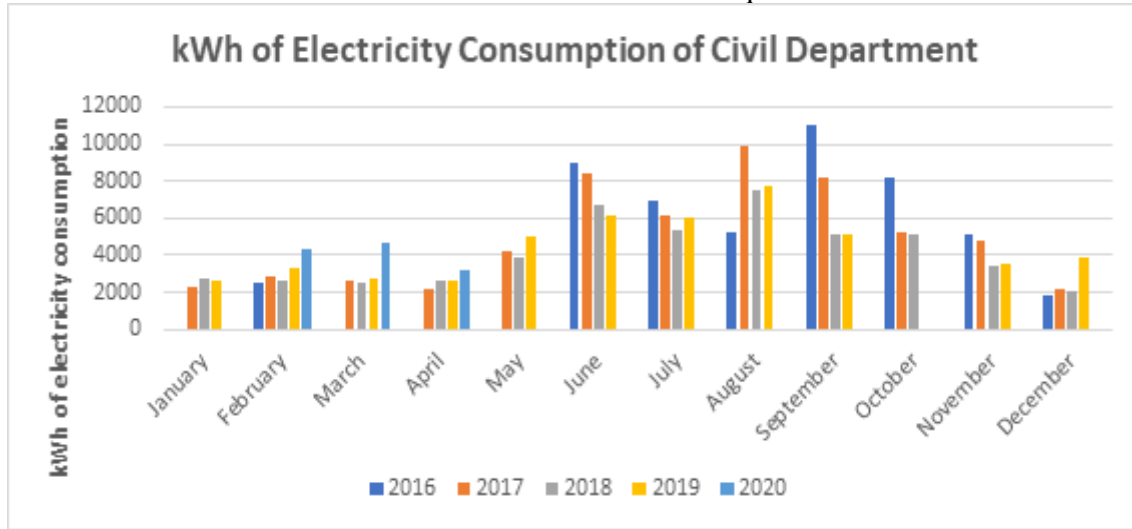


Figure 53: Electricity Consumption of the educational building (CED, UET Peshawar) in kWh

EUI Calculation:

For the EUI calculation, the monthly energy consumption was converted to kWh and the floor area to square meters followed by using Equation 1:

$$EUI = \frac{\text{Total Energy Consumption in kWh}}{\text{Total Floor Area in m}^2} \quad \text{Equation 1}$$

Autodesk Insight Simulation:

First, a detailed Building Information Modelling (BIM) model of the building was created, existing conditions were modelled as per real conditions. Then the model was transferred to Autodesk Insight, a building performance analysis tool, which was used to simulate the energy performance of the building. The key parameters, including Plug load, HVAC systems, lighting, infiltration control, window glazing, renewable energy integration (solar panels) and occupant behaviour, were adjusted to explore optimization scenarios. The Autodesk Revit model of the educational building is presented in Figure 3.



Figure 54: The Autodesk Revit Model of CED, UET Peshawar building

On-Site Assessment:

A thorough on-site assessment was carried out to collect pertinent data regarding occupant behaviour, area measurements and equipment utilization as illustrated in Table 7

Table 7 Measured data of the educational building

| S.No. | Name | Condition Type | Area (ft ²) | Volume (ft ³) |
|-------|-------------|-------------------|-------------------------|---------------------------|
| 1 | CLASSROOM 1 | Heated and cooled | 468 | 6786 |
| 2 | CLASSROOM 1 | Heated and cooled | 468 | 6786 |
| 3 | CLASSROOM 1 | Heated and cooled | 468 | 6786 |
| 4 | CLASSROOM 1 | Heated and cooled | 468 | 6786 |
| 5 | CLASSROOM 1 | Heated and cooled | 750 | 10875 |
| 6 | CLASSROOM 1 | Heated and cooled | 600 | 8700 |
| 7 | CLASSROOM 1 | Heated and cooled | 600 | 8700 |
| 8 | CLASSROOM 1 | Heated and cooled | 600 | 8700 |
| 9 | OFFICE 1 | Heated and cooled | 180 | 2610 |
| 10 | OFFICE 1 | Heated and cooled | 171 | 2479.50 |
| 11 | OFFICE 1 | Heated and cooled | 99 | 1435 |
| 12 | OFFICE 1 | Heated and cooled | 110 | 1595 |
| 13 | OFFICE 1 | Heated and cooled | 113 | 1634.8 |
| 14 | CLASSROOM 2 | Heated and cooled | 468 | 6786 |
| 15 | CLASSROOM 2 | Heated and cooled | 468 | 6786 |
| 16 | CLASSROOM 2 | Heated and cooled | 468 | 6786 |



ICSET-23



UET Peshawar

| S.No. | Name | Condition Type | Area (ft ²) | Volume (ft ³) |
|-------|-------------|-------------------|-------------------------|---------------------------|
| 17 | CLASSROOM 2 | Heated and cooled | 468 | 6786 |
| 18 | CLASSROOM 2 | Heated and cooled | 750 | 10875 |
| 19 | CLASSROOM 2 | Heated and cooled | 600 | 8700 |
| 20 | CLASSROOM 2 | Heated and cooled | 600 | 8700 |
| 21 | CLASSROOM 2 | Heated and cooled | 600 | 8700 |
| 22 | OFFICE 2 | Heated and cooled | 180 | 2610 |
| 23 | OFFICE 2 | Heated and cooled | 171 | 2479.50 |
| 24 | OFFICE 2 | Heated and cooled | 99 | 1435 |
| 25 | OFFICE 2 | Heated and cooled | 110 | 1595 |
| 26 | OFFICE 2 | Heated and cooled | 113 | 1634.8 |
| Total | | | 10,190 ft ² | 147,746.6 ft ³ |



Figure 55: On-site assessment of CED, UET Peshawar

RESULTS AND DISCUSSION

The research yields a notable contrast in EUI values from two distinct sources, which are Autodesk Insight simulations and billing data. The results are presented in the next sections.

Autodesk Insight Simulated (EUI):

Autodesk Insight simulations projected an EUI of approximately 152 kWh/m² per year. These simulations considered various factors, including building envelope, HVAC systems, lighting, and occupant behavior as shown in Figure 56. This value reflects the theoretical energy consumption based on the building's design and operation.

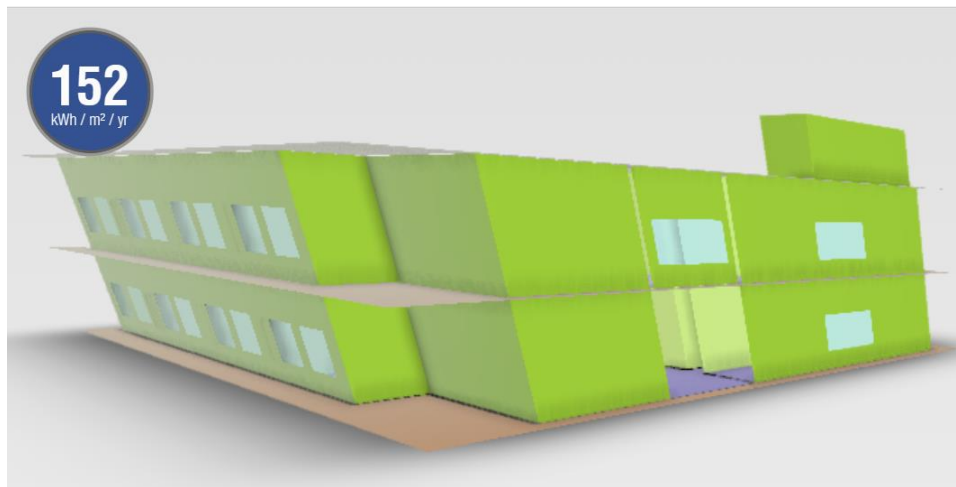


Figure 56: Autodesk Insight Simulation of the CED, UET Peshawar

EUI calculated from actual billing data:

The EUI calculated from actual billing data indicates an average energy consumption of approximately 100 kWh/m² per year over the studied period. This value represents real-world energy usage, accounting for fluctuations in occupant behavior, weather conditions, and system performance.

Comparing both EUI values

The EUI calculated through Autodesk Insight simulations (152 kWh/m² per year) is notably higher than the billing data's EUI (100 kWh/m² per year). This discrepancy suggests that the building may not be operating as efficiently as its design intended. Factors like suboptimal equipment performance or occupant behaviours may contribute to this difference.

Optimization strategies for energy efficiency:

The following optimization strategies were identified based on the EUI analysis, aimed at impacting energy conservation, sustainability, and reducing EUI:

HVAC System Upgrade:

One of the optimization strategies is the upgradation of the HVAC system to a more energy-efficient model. Implement a programmable thermostat (Tamas et al., 2021) to optimize heating and cooling schedules while regularly maintaining and cleaning HVAC equipment to ensure optimal performance.

Lighting Efficiency:

Replacing the traditional incandescent bulbs with high energy-efficient LED lighting can help in the attainment of efficiency. Implementing occupancy sensors and daylight harvesting systems like solar panels and batteries to control lighting based on occupancy and natural light levels can also optimize energy and ultimately the EUI values.

Infiltration Control:

Infiltration control has transformed buildings, enhancing energy efficiency, reducing costs, and improving indoor comfort. It's a key element of sustainable and resilient construction.

Energy-Efficient Appliances and Equipment:

Replacement of outdated appliances and equipment with ENERGY STAR-rated models (Bhavsar and Wazirani, 2023) and high-efficiency equipment can help improve EUI and reduce overall energy consumption along with the implementation of power management systems to reduce standby power consumption.

Occupant Engagement:

Conducting energy awareness campaigns and involving building occupants in energy-saving practices, such as encouraging the shutting of the lights and equipment when not in use, plays a pivotal role in optimizing energy utilization and fostering sustainability.

Renewable Energy Integration:

Exploring the potential for incorporating renewable energy sources, such as solar panels or wind turbines, to offset energy consumption forms a strategic approach towards sustainability.

Building Automation and Controls:

Installing building automation systems (BAS) (Quinn et al., 2020) for real-time monitoring and control of energy usage represents a proactive measure to enhance energy efficiency. Simultaneously, implementing smart controls for lighting, HVAC, and other systems serves as a strategic step toward optimizing energy utilization and achieving sustainable practices.

Optimization impact on energy conservation and sustainability:

The implementation of these optimization strategies is poised to exert a substantial influence on energy conservation, bolster sustainability efforts, and facilitate a noteworthy reduction in Energy Use Intensity (EUI) within the educational building as evident by Figure 57. Preliminary results reveal promising outcomes, including:

- A remarkable reduction in energy consumption by approximately 115%.



ICSET-23



UET Peshawar

- A substantial decrease in EUI from the initial 152 kWh/m² per year to a significantly improved - 23.25 kWh/m² per year.

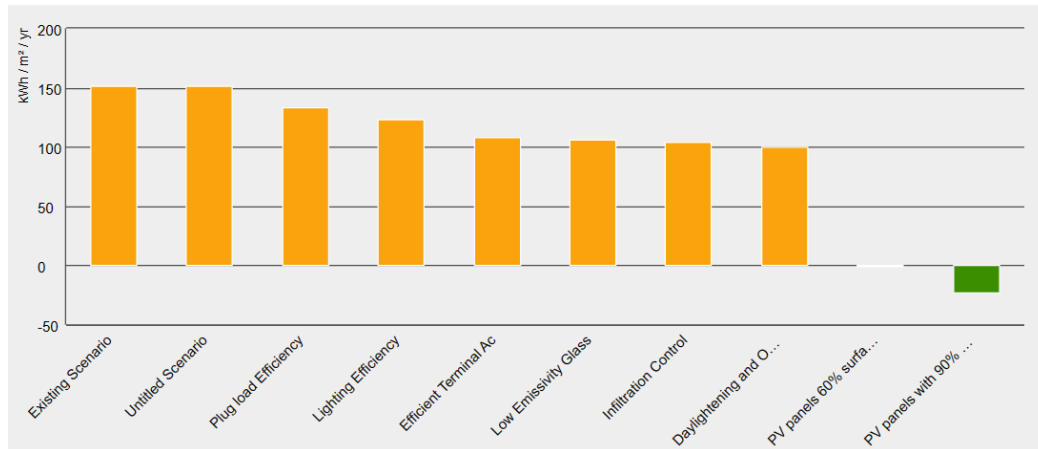


Figure 57: Comparison of the energy optimizations in Autodesk Insight 360

CONCLUSION

The comparison between the two aforementioned EUI values and energy conservation strategies underscores the imperative of ongoing monitoring and the persistent pursuit of energy performance optimization within educational buildings. Here are the main conclusions:

- The contrasting EUI values underscore the imperative of bridging the gap between theoretical design and real-world operation to achieve energy efficiency.
- The energy conservation strategies resulted in a remarkable decrease in EUI from the initial 152 kWh/m² per year to a significantly improved -23.25 kWh/m² per year, representing a reduction in energy usage of almost 115%
- This reaffirms the need for persistent monitoring and optimization to ensure alignment with sustainability goals.

ACKNOWLEDGEMENTS

The authors extend their gratitude to the Department of Civil Engineering, UET Peshawar for supporting this research.

REFERENCES

- [1]. Bhavsar, A., Wazirani, N., 2023. Building Energy Modelling with eQUEST Model and Energy Conservation Measures at Narayana Hrudayalaya Hospital, Bangalore. School of Technology GSFC University.



ICSET-23

*Proceedings of the 5th International Conference on Sustainable
Energy Technologies (ICSET 2023) Peshawar, Pakistan
14-15 December 2023*



UET Peshawar

- [2]. de Queiróz, G.R., de Campos Grigoletti, G., dos Santos, J.C.P., 2019. Interoperability between Autodesk Revit and EnergyPlus for thermal simulations of buildings. *PARC Pesquisa em Arquitetura e Construção* 10, e019005–e019005.
- [3]. Economidou, M., Todeschi, V., Bertoldi, P., D’Agostino, D., Zangheri, P., Castellazzi, L., 2020. Review of 50 years of EU energy efficiency policies for buildings. *Energy and Buildings* 225, 110322.
- [4]. Harputlugil, T., de Wilde, P., 2021. The interaction between humans and buildings for energy efficiency: A critical review. *Energy Research & Social Science* 71, 101828.
- [5]. Hsien-te, L., Chia-ju, Y., 2021. Hotel energy rating system using dynamic zone EUI method in Taiwan. *Energy and Buildings* 244, 111023.
- [6]. Maglad, A.M., Houda, M., Alrowais, R., Khan, A.M., Jameel, M., Rehman, S.K.U., Khan, H., Javed, M.F., Rehman, M.F., 2023. Bim-based energy analysis and optimization using insight 360 (case study). *Case Studies in Construction Materials* 18, e01755.
- [7]. Mahiwal, S.G., Bhoi, M.K., Bhatt, N., 2021. Evaluation of energy use intensity (EUI) and energy cost of commercial building in India using BIM technology. *Asian Journal of Civil Engineering* 22, 877–894.
- [8]. Mansor, R., Sheau-Tingi, L., 2019. The psychological determinants of energy saving behavior. Presented at the IOP Conference Series: Materials Science and Engineering, IOP Publishing, p. 012006.
- [9]. Olawumi, T.O., Chan, D.W., 2019. An empirical survey of the perceived benefits of executing BIM and sustainability practices in the built environment. *Construction Innovation* 19, 321–342.
- [10]. Quinn, C., Shabestari, A.Z., Misic, T., Gilani, S., Litoiu, M., McArthur, J., 2020. Building automation system-BIM integration using a linked data structure. *Automation in Construction* 118, 103257.
- [11]. Tamas, R., O’Brien, W., Quintero, M.S., 2021. Residential thermostat usability: Comparing manual, programmable, and smart devices. *Building and Environment* 203, 108104.
- [12]. Toli, A.M., Murtagh, N., 2020. The concept of sustainability in smart city definitions. *Frontiers in Built Environment* 6, 77.

Paper ID: ICSET-2313

PHYSICS-INFORMED NEURAL NETWORKS FOR NUMERICAL SOLUTION OF 1D HYPERBOLIC PDEs

Siraj-ul-Islam, Fatima Javed*, Masood Ahmad

Department of Basic Sciences, University of Engineering and Technology, Peshawar, Pakistan

**Corresponding author*

Email: fatimajaved3215@gmail.com

ABSTRACT

This article using the feed forward neural network to design an automatic numerical solver by proposing physics-informed neural networks (PINNs)—neural networks that incorporate model equations like partial differential equations (PDEs) as an integral part of the neural network architecture. The primary objectives of this paper are to demonstrate the utilization of PINNs model for one-dimensional hyperbolic PDEs and to conduct a comparative analysis with analytical solutions. This model is able to solve various hyperbolic problems, and has shown promising numerical result even in the data deficient scenario. Jupyter Notebook is used for programming.

KEYWORDS: Machine learning, physics-informed neural network, feed forward neural network, hyperbolic PDEs.

INTRODUCTION

Hyperbolic PDEs have a substantial impact in numerous dimensions of the energy industry. An illustration of their application is in modelling flow of fluid (e.g. using the conservation of momentum equation) in underground oil and gas reservoirs. These simulations are important for optimizing production strategies and managing reservoirs. The conservation of energy equation is used to model the temperature and heat transfer within the reservoir. It accounts for heat conduction and convection within the reservoir. Additionally, hyperbolic PDEs can be used to model the transport of ions and electrons within energy storage materials (e.g. using the continuity equation), thereby improving the efficiency and performance of energy storage devices. These equations provide valuable insights into wave-like phenomena, heat transfer, fluid dynamics, and other crucial processes within the energy sector.

In numerous scientific and industrial scenarios, solving partial differential equations becomes essential for describing physical phenomena. Fast and accurate prediction of numerical solutions to PDEs is an extensively researched problem in the domain of numerical analysis. After decade of research, numerous numerical methods exist today to solve PDEs. They include finite volume, finite element, finite difference and so on. All these techniques have common difficulty such as curse of dimensionality in high dimensions, also depend upon tailoring to the specifics of a particular PDE e.g. shocks or convection dominance, strong nonlinearities. In this work we aim to explore the particular Deep Learning (DL) nature of PINNs [1-3], which enables us to tackle such task and overcome the challenges of the existing numerical methodologies.



The excessive applicability of machine learning methods in the fields like natural speech processing [4], image recognition [5], and medical diagnosis [6], among others, has been both the reason and significance of the heightened interest in this field over the last ten years. Machine learning methods are also finding applications to solve problems in the domain of scientific computation, including numerical analysis. In their latest exploration of Physics-Informed Deep Learning [3], the authors presented the approach of PINNs to infer solution to non-linear PDEs. In this context, the problems can be addressed directly, without the need for making prior assumptions, local time-stepping, or linearization. Our analysis suggests that these neural networks are certainly capable of detecting the specified dynamics and overcome numerical challenges associated with discontinuity and stability.

In section 2, our objective is to present an informative overview on PINNs. In section 3 we establish the PINNs framework for solving 1D hyperbolic PDE, including initial and boundary conditions. For better numerical results we compare the output with the exact solution. Finally, in section 4, we provide the conclusion of the work.

PHYSICS-INFORMED NEURAL NETWORKS

PINNs is a machine learning approach that combines neural networks with physical principles for function approximation, such as PDEs or other physics-based problems

Neural Networks; PINNs used neural networks as function approximators. The type of neural network under consideration in this context is the multilayer feed-forward neural network [7, 8]. Feed forward neural networks, or FFNNs are neural networks (NNs) characterized by multiple hidden layers where information flows in a unidirectional manner without any feedback loops.

Physics constraints; PINNs incorporate the physical information (which is called residual in this case) and constraints as a component of the loss function by applying Automatic Differentiation [9].

- **Loss function;** The loss function contains on the initial and boundary conditions, as well as the residual of the PDE at interior points within the domain (called collocation points). This term we needed to find the optimal parameters of the network and assist the network to learn the physics of the problem.
- **Automatic Differentiation (AD);** AD is one of the most frequently used technique in scientific computation to automatically and accurately compute the gradients of neural network outputs with respect to the model parameters and input variables.

Figure 1 shows a structure of Physics-Informed neural network, PINNs is made up of PDE residual (2) with the boundary and initial conditions. The network processes its input variables to generate output ' U_θ '. The output is employed to compute derivatives based on the provided equation. The network behaviour is determined by the parameter set ' θ '. The final step is to minimize the loss function (3), using an optimizer (Adam), in order to obtain neural network parameters ' θ '

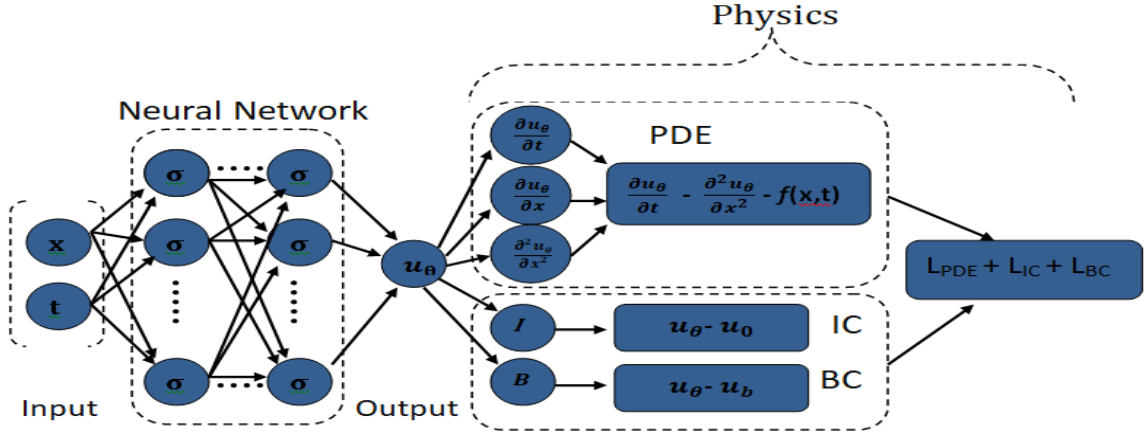


Figure 1: PINN structure

PINNS method for 1d hyperbolic pde

We present the PINNs approach to estimate the solution, $U : [0, T] \times \Gamma \rightarrow \mathbb{R}$ of 1D hyperbolic PDE where general equation is

$$\partial_{tt} U(t, x) + \mathcal{L}[U](t, x) = 0, \quad (t, x) \in [0, T] \times \Gamma, \quad (1a)$$

with the boundary and initial conditions,

$$U(0, x) = U_0(x), \quad \partial_t U(t, x)|_{t=0} = U_1(x), \quad x \in \Gamma, \quad (1b)$$

$$U(t, x) = U_b(x), \quad (t, x) \in [0, T] \times \partial\Gamma, \quad (1c)$$

where \mathcal{L} is linear differential operator that acts upon U , Γ a bounded domain in \mathbb{R}^d , with $\partial\Gamma$ representing its boundary and T is the final time. The technique constructs a neural network output $U_\theta(t, x)$, which approximates the solution $U(t, x)$ of equation (1). Here $U_\theta(t, x)$ represents an approximated solution generated by a feed forward neural network with the parameters θ .

PINNs approach and loss function

The PINNs approach based on the residual of PDE (1a) defined as;

$$r_\theta(t, x) = \partial_{tt} U_\theta(t, x) + \mathcal{L}[U_\theta](t, x), \quad (2)$$

PINNs take the underlying PDE (1) into account. By Automatic Differentiation capabilities in Tensorflow library [10], we find the derivatives of the approximated solution U_θ with respect to their spatial and temporal variables to evaluate the residual (2) at collocation points. The initial and boundary conditions will be approximated at initial and boundary points. Then the physics embedded in the differential equation

is made accessible for the loss function. The PINNs strategy for the solution of equation (1) proceeds by minimization of loss function;

$$\varphi_{\theta}(X) = \varphi_{\theta}^r(X^r) + \varphi_{\theta}^0(X^0) + \varphi_{\theta}^b(X^b), \quad (3)$$

where X represents a set of training data and φ_{θ} consists of the following components;

- The mean square value at collocation points $X^r = \{(t_i^r, x_i^r)\}_{i=1}^{N_r} \subset [0, T] \times \Gamma$

$$\varphi_{\theta}^r(X^r) = \frac{1}{N_r} \sum_{i=1}^{N_r} |r_{\theta}(t_i^r, x_i^r)|^2,$$

- The mean square discrepancy at initial $X^0 = \{(t_i^0, x_i^0)\}_{i=1}^{N_0} \subset \{0\} \times \Gamma$ and boundary points $X^b = \{(t_i^b, x_i^b)\}_{i=1}^{N_b} \subset (0, T] \times \partial\Gamma$

$$\varphi_{\theta}^0(X^0) = \frac{1}{N_0} \sum_{i=1}^{N_0} |U_{\theta}(t_i^0, x_i^0) - U_0(x_i^0)|^2, \text{ and } \varphi_{\theta}^b(X^b) = \frac{1}{N_b} \sum_{i=1}^{N_b} |\partial_t U_{\theta}(t_i^b, x_i^b) - U_1(x_i^b)|^2,$$

$$\varphi_{\theta}^b(X^b) = \frac{1}{N_b} \sum_{i=1}^{N_b} |U_{\theta}(t_i^b, x_i^b) - U_b(t_i^b, x_i^b)|^2,$$

where $U_{\theta}(t, x)$ is the network estimation of the solution $U(x, t)$. To optimize the loss function, we employ the Adam optimizer to attain the optimal parameters θ of neural network.

PINN Solver

We will adhere to the PINN framework outlined in [11, 12].

Table 1: Network layout to solve example problem

| Parameters | Value | Statement |
|------------|-------|---|
| N_0, N_b | 50 | Number of initial and boundary points |
| N_r | 200 | Number of collocation points |
| L | 4 | Number of Hidden layers |
| n | 50 | Neurons per layer |
| σ | Tanh | Non linear activation function |
| Optimizer | Adam | To obtain the optimal parameters θ |
| $\Phi(X)$ | MSE | Loss function on training data X |

Numerical Outcomes

In this section, we will show various numerical outcomes access by solving 1D hyperbolic equation using PINNs approach. We compare the results with analytical solution. We show the errors and execution time of PINNs solution at different number of iteration (also known as epochs). The accuracy of the method is computed using the expressions;

$$\begin{cases} \text{MSE} = \frac{1}{N} \sum_{i=1}^N |U_{\theta}^i - U^i|^2 \\ l_{\infty} = \max |U_{\theta}^i - U^i| \end{cases}$$

where N is the number of points in $[0, T] \times \Gamma$.

Example of 1D hyperbolic PDE

Test problem 1: As an example, let us consider a hyperbolic partial differential equation. In a single spatial dimension, the hyperbolic PDE in [13], subject to Dirichlet boundary conditions, is expressed as follows;

$$2 \partial_{tt} U(t, x) + x^2 \partial_{xx} U(t, x) - 2x \partial_x U(t, x) + \pi^2 x^2 U(t, x) = 0, \quad x \in [0, 1], \quad t \in [0, 1] \quad (4)$$

with initial and boundary conditions

$$U(0, x) = x \sin(\pi x), \quad \partial_t U(t, x)|_{t=0} = -x \sin(\pi x), \quad (4b)$$

$$U(t, 0) = U(t, 1) = 0. \quad (4c)$$

The exact solution for $U(t, x)$ is given by

$$U(t, x) = e^{-t} x \sin(\pi x). \quad (5)$$

Let us define residual of underlying PDE (4) to be given by

$$r_{\theta} = 2 \partial_{tt} U_{\theta} + x^2 \partial_{xx} U_{\theta} - 2x \partial_x U_{\theta} + \pi^2 x^2 U_{\theta}. \quad (6)$$

Subsequently, we proceed to estimate $U(t, x)$ using a feed forward neural network. The parameters θ can be trained by minimizing the loss function (3).

When trying to solve this problem (4) with PINNs by using the configuration, see Tab. 1. The boundary and initial data points, X^b and X^0 as well as collocation point X^r , are generated randomly from a uniform distribution, see Fig. 2. We observe that the predicted solution is much more coincide with the exact solution presented in Fig. 3. The difference between the exact and approximated solution by PINNs presented in Fig. 4. The loss is considerably small i.e. $\phi(X) = 4.2 \times 10^{-5}$, see Fig. 5. The errors at different number of iteration (also known as number of epochs) and execution time of above example illustrated in Tab. 2. As we increased the number of epochs, the accuracy improved.

Numerical realization and solution plotting

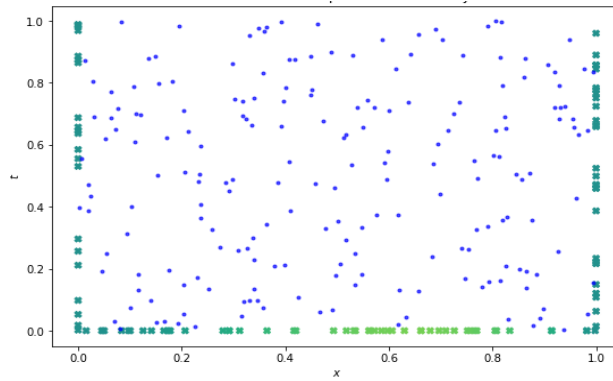


Figure 2: Positions of collocation points and boundary data

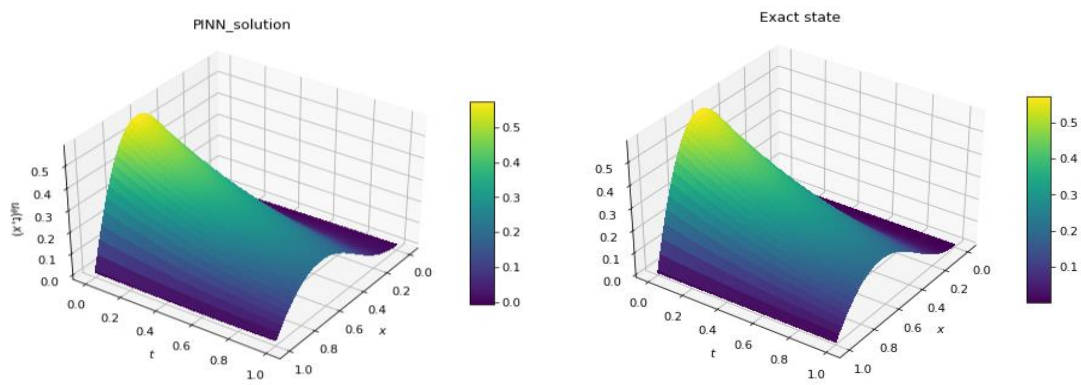


Figure 3: PINN and Exact solution

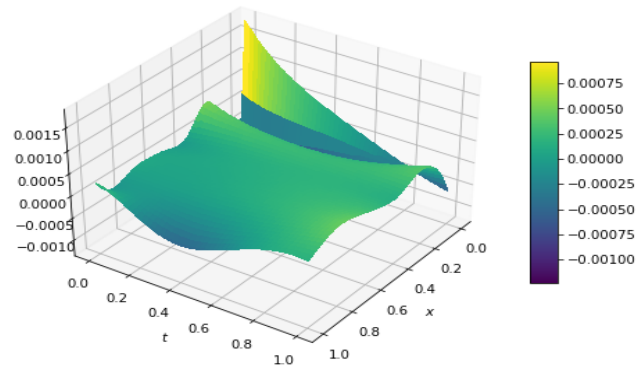


Figure 4: Difference between PINN approximation and exact solution

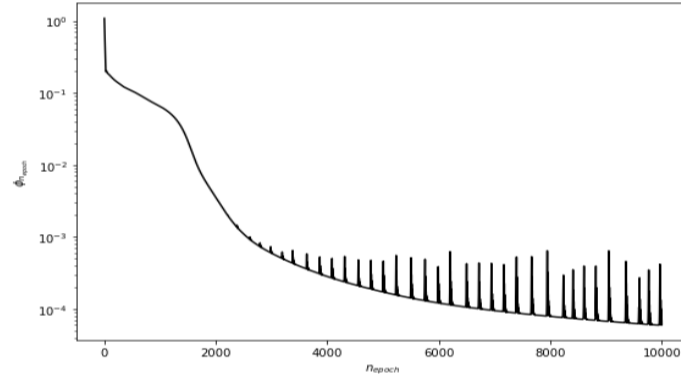


Figure 5: Loss function (by Adam optimization)

Table 2: Errors and execution time

| η_{epoch} | l_{∞} | MSE | Time(s) |
|-----------------------|----------------------|----------------------|---------|
| 5 000 | 1.7×10^{-2} | 4.3×10^{-5} | 42 |
| 10 000 | 3.8×10^{-3} | 5.9×10^{-6} | 71 |
| 15 000 | 3.0×10^{-3} | 1.8×10^{-6} | 103 |
| 20 000 | 1.8×10^{-3} | 9.2×10^{-7} | 133 |

CONCLUSION

PINNs approach provide an accurate solution, which is derivable and continuous in the entire domain without any prior assumptions, local time-stepping, or linearization. The suggested approach provides a good estimation, even with small dataset. The PINNs solver implementation is not concerned about stability and oscillations, in contrast to conventional numerical methods. The suggested approach provides a good estimation with small dataset for 1D hyperbolic problems.

REFERENCES

- [1] M. Raissi, P. Perdikaris, and G. E. Karniadakis. (2017). *Physics informed deep learning (part i): Data-driven solutions of nonlinear partial differential equations*. arXiv preprint arXiv:1711.10561.
- [2] M. Raissi, P. Perdikaris, and G. E. Karniadakis. (2017). *Physics informed deep learning (part ii): Data-driven discovery of nonlinear partial differential equations*. arXiv preprint arXiv:1711.10566.
- [3] M. Raissi, P. Perdikaris, and G. E. Karniadakis. (2019). *Physics-informed neural networks: A deep learning framework for solving forward and inverse problems involving nonlinear partial differential equations*. Journal of Computational physics, **378**: p. 686-707.
- [4] LeCun, Y. Bengio, Y. Hinton, Geoffrey. (2015). *Deep learning*. nature, **521**(7553): p. 436-444.
- [5] A. Krizhevsky, I. Sutskever, and G. E. Hinton. (2017). *ImageNet classification with deep convolutional neural networks*. Communications of the ACM, **60**(6): p. 84-90.
- [6] I. Kononenko. (2001). *Machine learning for medical diagnosis: history, state of the art and perspective*. Artificial Intelligence in medicine, **23**(1): p. 89-109.



ICSET-23

*Proceedings of the 5th International Conference on Sustainable
Energy Technologies (ICSET 2023) Peshawar, Pakistan
14-15 December 2023*



UET Peshawar

- [7] K. Hornik, M. Stinchcombe, and H. White. (1989). *Multilayer feedforward networks are universal approximators*. Neural networks, **2**(5): p. 359-366.
- [8] S. Cuomo, et al. (2022). *Scientific machine learning through physics-informed neural networks: Where we are and what's next*. Journal of Scientific Computing, **92**(3): p. 88.
- [9] A. G. Baydin, P. A. Pearlmutter, A. A. Radul. (2018). *Automatic differentiation in machine learning: a survey*. Journal of Machine Learning Research, **18**: p. 1-43.
- [10] E. Haghighat, and R. Juanes. (2021). *A Keras/TensorFlow wrapper for scientific computations and physics-informed deep learning using artificial neural networks*. Computer Methods in Applied Mechanics and Engineering, **373**: p. 113552.
- [11] J. Blechschmidt, O. G. Ernst. (2021). *Three ways to solve partial differential equations with neural networks—A review*. GAMM-Mitteilungen, **44**(2): p. e202100006.
- [12] J. Mack. (2021). *Physics informed machine learning of nonlinear partial differential equations*.
- [13] J. Flores, et al. (2023) *A spatio-temporal fully meshless method for hyperbolic PDEs*. Journal of Computational and Applied Mathematics, **430**: p. 115194.

Paper ID: ICSET-2314

IDENTIFICATION AND EVALUATION OF RISK ASSESSMENT IN STEEL MANUFACTURING INDUSTRY

Sajid Ahmad^{1,*}, Rehman Akhtar², Ishtiaq Ahmad³, Khizar Azam³, Amad Ullah Khan⁴, Tayeed Wahab¹

¹Department of Industrial Engineering, University of Engineering and Technology Peshawar, Pakistan

²Department of Management Sciences, Brains Institute Peshawar, Pakistan

³Department of Mechanical Engineering, University of Engineering and Technology Peshawar, Pakistan

⁴Department of Chemical Engineering, University of Engineering and Technology Peshawar, Pakistan

**Corresponding author*

Email: sajidahmad@uetpeshawar.edu.pk

ABSTRACT

The concept of risk encompasses both probability and implications. The primary objective of this study is to identify the inherent risks of steel industries of Pakistan. The steel manufacturing industry, pivotal to Pakistan's infrastructure and development, is fraught with inherent risks that can impact both operations and safety. This study delves deep into these risks, employing a multi-faceted approach to identify and assess them. The research conducted in this study comprises two distinct phases. Primarily, the HAZOP (Hazard and Operability) technique is utilized, a qualitative method that systematically detects deviations from standard operations and gauges the efficacy of preventative measures. Complementing this, the research introduces the Preliminary Hazard Analysis (PHA), a quantitative tool that evaluates the frequency and severity of each identified risk, culminating in a comprehensive risk matrix. This dual-methodology approach has successfully spotlighted 39 distinct risks, each meticulously categorized based on risk scores, causative factors, and potential impacts. Furthermore, these findings propose suitable solutions for risk control or mitigation. The Preliminary Hazard Analysis (PHA) employs a risk framework to prioritize risks for comprehensive operational planning, while the Hazard and Operability (HAZOP) approach is capable of identifying likely deviations from the intended design parameters. The findings not only shed light on these risks but also proffer viable solutions for risk control and mitigation. Furthermore, the study underscores the adaptability and expansiveness of the HAZOP technique, originally conceived for chemical handling facilities but now applicable across diverse sectors. The study conducted at a steel bar manufacturing facility in Peshawar, Pakistan, and the insights gleaned from this research hold the potential to be a cornerstone for similar industries aiming to bolster their operational safety and efficiency.

While numerous studies have explored risk assessment in the steel industry, there remains a gap in the comprehensive identification and evaluation of inherent risks specific to Pakistan's steel industries. This study bridges this gap by employing the HAZOP technique combined with Preliminary Hazard Analysis, offering a localized perspective on risk assessment in the steel bar manufacturing sector.

KEYWORDS: HAZOP, PHA, Semi Quantitative Risk Analysis, Risk Matrix.



ICSET-23



UET Peshawar

INTRODUCTION

The steel bar manufacturing industry plays a crucial role in multiple sectors of the economy, establishing direct connections with industries such as construction, automotive, machinery and equipment industry. Additionally, this industry indirectly influences manufacturing, mining, infrastructure, public works, oil and gas, and various other sectors. Nonetheless, this sector presents substantial hazards that have the potential to adversely affect the well-being of employees, the natural surroundings, and the quality of Products. In order to maintain the long-term viability of the sector, it is essential to identify and assess potential risks, as well as formulate efficient techniques for risk management. The primary objective of this study is to determine and assess potential hazards within the steel bar manufacturing process through the utilization of a complete risk analysis methodology. The study will examine the potential dangers connected with the production process, evaluate the environmental effect, assess occupational health and safety concerns, and analyse product quality. The findings of this study will contribute valuable insights into the risks involved in the production of steel bars and establish a basis for developing an effective risk mitigation strategy. This study aims to provide a substantial contribution to the existing body of knowledge regarding risk management in the manufacturing business, with a specific focus on the steel bar manufacturing sector. The findings of this study will ultimately contribute to the long-term viability of the steel bar manufacturing sector through risk reduction and enhancements in product safety and quality.

The steel manufacturing industry, being a cornerstone for various sectors, is not devoid of significant hazards. While international research has delved into risk assessments for steel production, there is a noticeable research gap in the context of Pakistan's steel industries. This study aims to address this lacuna, providing a comprehensive risk analysis tailored to the local industry's nuances and challenges.

LITERATURE REVIEW

Risk management encompasses a series of protocols and frameworks designed to identify prospective opportunities and address negative consequences.

The successful implementation of management strategies, activities, and protocols is evident from its clear definition. Risk management encompasses a range of activities, including the identification, assessment, evaluation, monitoring, and review of risks. The actions of identification, investigation, and evaluation discussed here are classified as components of risk assessment. The design of the workplace has a significant impact on the occurrence of hazardous circumstances in contemporary times, posing possible risks to individuals, assets, and the environment. This harm has the potential to occur both during routine operations and in the aftermath of unforeseen catastrophes, which are progressively escalating in their catastrophic nature. The understanding and mitigation of risk are contingent upon the specific objectives and viewpoints of the discourse. (Dewi, Bastori et al. 2020) suggest different ideas, opinions, methods and techniques related to risks, the uncertainty and the efficiency for risk evaluation in steel industry. They also suggest the importance of proper approach for risk management taking into account both qualitative and quantitative methods. (Cheraghi, Baladeh et al. 2022) Developed a hybrid decision making approach to filter the best suitable and viable solution proposed by HAZOP methodology. HAZOP provides a compressive and multiple solution for every risk, it's not feasible to implement every proposed solution for mitigation of risks. (Kim, Lee et al. 2018) introduces a model to identify the potential risk and their priority, focusing the importance of a systematic approach for risk assessment. The model introduced helps decision makers in risk mitigation and assessment of overseas steel-plant projects. (Depczyński, Secka et al. 2023) introduced a model for identification of potential risks and their priority, focusing the importance of a systematic approach to risk assessment. (Nordlöf, Wiitavaara et al. 2015) emphasis on safety culture in large steel manufacturing companies. This article focuses on risk from the worker perspective focusing on the importance of safe working procedures in the industry exposed



to risks. (Mousavian, Mansouri et al. 2017) focuses on health risk associated with heavy metal exposure in steel industry. The main goal of the research is to assess long term exposure risk of workers particularly in smelting unit of an alloy steel factory highlighting the implications of such exposure to health. (Marhavilas, Filippidis et al. 2022) Proposed a hybrid methodology by combining Analytical-Hierarchy-Process(AHP) with HAZOP for identification of critical issues and ranking risk for workplace of petrochemical industry. (Mokhtarname, Safavi et al. 2022) Applied multivariable process monitoring algorithm and HAZOP to perform a holistic and accurate analysis for effective evaluation of process and to provide and optimal safeguarding strategy for various risks. As stated by the source cited as (Kaplan and Garrick 1981), risks are defined as weaknesses that are linked to potential injury or accidents. they propose that uncertainty alone does not inherently represent a risk. However, when uncertainty coexists with the potential for adverse outcomes or losses, it can be classified as a risk. According to (Khan and Zsidsin 2012) the conventional definition of risk implies an unfavorable state. However, it is worth noting that certain authors hold contrasting viewpoints on this matter. Risk encompasses both the potential for financial loss and the opportunity for financial gain. (Kaplan and Garrick 1981). It is necessary to recognize the potential presence of a hazard in order to assess its impact. Comprehending the extent of risk entails the examination of both the possible escalation and reduction in its likelihood, rendering it a subjective and comparative concept. The HAZOP technique was initially devised to identify potential dangers in facilities engaged in the handling of hazardous chemicals, with the primary aim of minimizing significant incidents such as explosions, fires, and the discharge of hazardous compounds into the environment. Nevertheless, the identification of dangers and operational concerns that have proven to be successful has resulted in the expansion of the Hazard and Operability (HAZOP) technique to encompass other types of facilities throughout the years. (Lyons, Adams et al. 2004) used HAZOP in medical field for diagnosis purposes, while (Jagtman, Hale et al. 2005) utilized the concept for road safety measures and (Fthenakis and Trammell 2003) used HAZOP to analyze risk in photovoltaic facility among others. The HAZOP technique has its origins in the Critical Analysis Procedure developed by the Imperial Chemical Industries in the mid-1960s. It was subsequently published as a formalized strategy for spotting deviations from design objectives around a decade later. (Lawley 1974) recognized and provided a clear definition of the challenge posed by the growing complexity of contemporary processes. They argued that traditional methodologies, which rely on equipment-focused approaches, are insufficient for accurately evaluating this complexity. Consequently, the researchers proposed a set of fundamental principles to guide the implementation of operability studies and hazard analyses in order to address this issue. (Galante, Bordalo et al. 2014), numerous methods are examined and classified into two overarching categories, distinguished by the approach and methodology employed in recording and analyzing outcomes: tree analysis and spreadsheet analysis. The utilization of the tree analysis approach is employed to find a sequential series of risks across all operations. (McCoy, Wakeman et al. 2000), the TNO Red Book provides a comprehensive overview of the fault tree analysis method, which is considered a prominent example of the "analysis in trees" approach. By utilizing a statistical methodology to ascertain the mean and standard deviation of individual probabilities during the computation process, fault trees might exhibit a heightened degree of intricacy. (Khaviya, Kavitha et al. 2017) and (Hwang, Jo et al. 2010) employed qualitative approach to identify and assess risks. (Agrawal, Jain et al. 2014) and (Kotek and Tabas 2012) categorized risks based on probability and consequences as high, medium and low. In quantitative risk analysis, the aim is to assess the occurrence and potential impacts of the identified risks. (KARAHAN and AKOSMAN 2018) and (Kumar and Mishra 2019) assigned values to occurrence of risk in order to identify the risk level. In this study, we proposed qualitative and semi quantitative risk analysis approach to identify and prioritize risks in steel bar manufacturing industry. To measure the subjective methodology, a hazard structure and parameters of frequency and severity will be utilized. Semi-quantitative analysis is a more predictable and comprehensive approach to assess and comparing hazards. To perform semi quantities' risk analysis, an equivalent amount of data is necessary as that needed for subjective analysis. This research combines Risk Matrix and HAZOP to propose a detail risk management method,



taking quantitative and qualitative analysis of hazards into consideration. The ultimate goal of the study is to measure the severity and consequences of hazards and propose appropriate mitigation actions.

PROBLEM STATMENT

Every manufacturing industry has numerous operations and tasks that are carried out on a daily, and every one of these operations and activities has its own inherent risk that needs to be identified and evaluated. The failure to detect these risks can lead to substantial challenges and expenses for the industry, thereby exerting a detrimental impact on competitiveness, employee trust, and overall operational effectiveness. The objective of this research is to conduct a comprehensive assessment and mitigation of risks associated with the various operations and activities involved in the steel production process.

RESEARCH METHODOLOGY

The successful completion of this investigation is dependent upon the robustness of the research approach employed. A research approach was devised to identify and assess risk assessment practices within the steel bar manufacturing sector. For data collection, a questionnaire was designed to identify and categorize various types of hazards. The study inquiries and goals were effectively tackled utilizing this approach, which entailed conducting interviews with industry management personnel to confirm the accuracy of the data. Additionally, the study involved the observation of the physical context and work environment in which personnel carry out their tasks, with the aim of obtaining significant insights to address the highlighted concerns.

Data Collection

The process of data collection involved conducting interviews and making observations of both workers and management personnel within the sector. The interviews were done in a non-systematic manner on several days, based on the individual work schedules of each participant. The study employed qualitative research methodologies to collect data from the specific group, while also conducting observations to evaluate the behaviours exhibited by both employees and employers with relation to worker safety inside the manufacturing process. Currently the industry is adopting a reactive methodology to any hazard or accident that can occur which cost a lot to the industry in terms of time, resources and finances. Having a specific risk mitigation methodology can lead to not only save time but also resources including man, machine, material. This research will help the industry in adopting a proactive approach to risk management. This study not only identifies the various risk but also categorize the based on their severity, likelihood of occurrence and impact. Having such insights can help the industry to adopt a proactive approach to any unforeseen event.

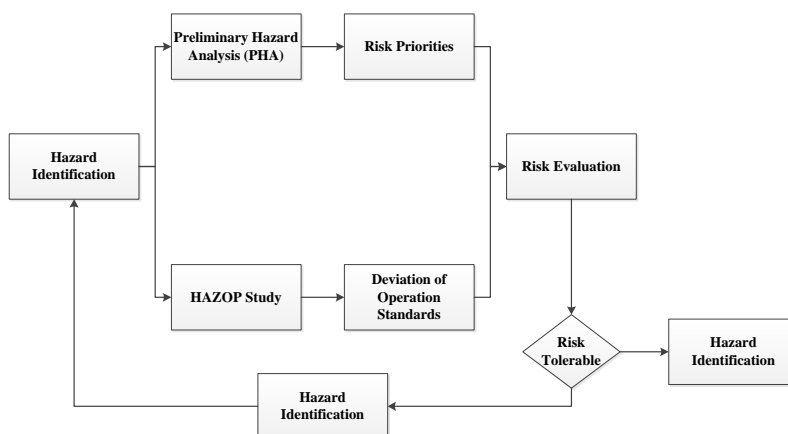


Figure 58: Research Methodology

Data Analysis

The obtained data was analysed utilizing Microsoft Excel software in order to distinguish and categorize the diverse array of hazards inherent in the steel manufacturing process, spanning from the procurement of raw materials through the final stages of producing finished goods. Every individual process within the business has a distinct array of hazards that have the ability to risk the safety of both personnel and the company.

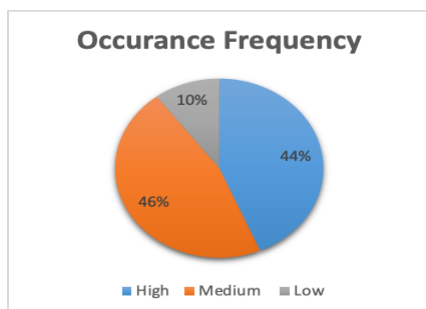


Figure 2: Occurrence Frequency

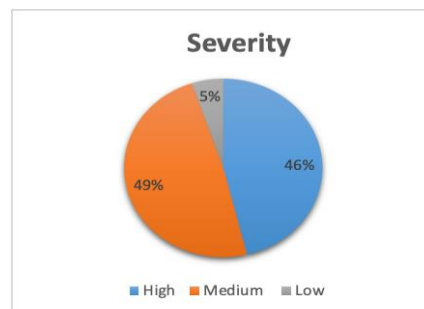


Figure 3: Severity of Risks

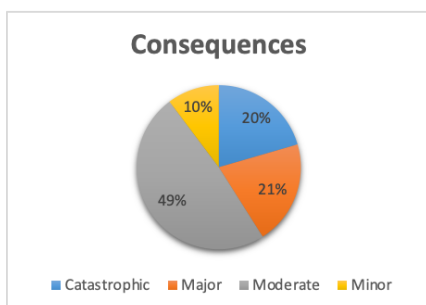


Figure 4: Consequences



Figure 5: Nature of Risks



Utilizing HAZOP specific point of the production process termed as “study nodes” are the main focus. These nodes are specific to steel production like smelting, shaping, refining, where HAZOP technique is implemented to assess the specific risks in each step. HAZOP predict relevant accidental scenarios. Various literature supports the HAZOP in foreseeing potential hazards in steel manufacturing process. A crucial aspect of HAZOP is to identify design features that are susceptible to deviation from the design intent which may lead to undesirable states. In steel production process this could be related to the design of the furnaces, moulds, and other equipment where deviation can lead to inefficiencies or hazards.

Hazard Identification

The identification of hazards was initially conducted through the utilization of preliminary hazard analysis, which was subsequently followed by a comprehensive hazard analysis employing the Hazard and Operability Study (HAZOP) methodology. Hazards can be categorized into two distinct groups: controllable and uncontrollable. Controllable hazards provide the potential for effective management, whereas uncontrolled hazards, such as natural disasters, lack the capacity for management. The objective is to effectively manage controlled hazards and reduce their frequency in order to offset substantial losses within the industry. This study aims to identify and analyse the controllable hazards that arise throughout the production process of steel bars, with the objective of developing effective strategies to mitigate and control these hazards. Several risks have been found in some units of the steel bar manufacturing process.

Preliminary Hazard Analysis

Primary stage of hazard control in the steel bar manufacturing industry involves conducting a preliminary hazard analysis (PHA) to identify all possible hazards that may occur in the system. Through PHA, potential hazards are identified in the system, and risks are assessed during the initial stage to determine the severity and frequency of the hazards. The assessment utilizes comprehensive data regarding the target system's capacity and configuration, as well as the interactions among individuals and other systems. The outcomes of the risk analysis aid in identifying areas that may require further measurement and analysis in the future. The PHA also provides information on the frequency and severity of the identified hazards. During the PHA, each hazard or risk is assigned a code based on its severity, such as C represents Critical, L represents negligible or low, M represents Minor, S represents Serious, and V represents Very serious. All these codes are not absolute and may be modified based on the specific circumstances.

Table 8: Different Risk Observed

| | | | |
|---|---|----|---|
| 1 | Fire outbreak in the production area | 20 | Inadequate communication between workers and management |
| 2 | Machine malfunction due to poor maintenance | 21 | Insufficient staffing levels |
| 3 | Electrical hazards due to faulty wiring | 22 | Overloading of equipment |
| 4 | Chemical spills from the storage containers | 23 | Improper installation of equipment |
| 5 | Corrosion and rust formation on equipment | 24 | Improper calibration of equipment |
| 6 | Falling objects from the storage racks | 25 | Improper machine guarding |



| | | | |
|----|--|----|--|
| 7 | Worker falls from elevated areas | 26 | Failure of safety devices such as emergency stop buttons |
| 8 | Exposure to harmful gases | 27 | Lack of proper lighting in the production area |
| 9 | Explosion due to gas leakages | 28 | Inadequate storage space for finished goods |
| 10 | Equipment breakdown | 29 | Environmental pollution caused by waste discharge |
| 11 | Failure of computer control systems | 30 | Inadequate waste disposal systems |
| 12 | Failure of emergency shutdown systems | 31 | Inadequate fire suppression systems |
| 13 | Mechanical failure of equipment | 32 | Improper handling of hazardous waste |
| 14 | Improper handling of raw materials | 33 | Unauthorized access to production areas |
| 15 | Exposure to excessive heat | 34 | Damaging of production equipment |
| 16 | Insufficient ventilation in the production area | 35 | Theft of raw materials or finished goods |
| 17 | Inadequate personal protective equipment (PPE) usage | 36 | Improper handling of confidential information |
| 18 | Inadequate training of workers | 37 | Contractual and legal disputes with customers |
| 19 | Lack of safety policies and procedures | 38 | Supply chain disruptions due to logistical problems |
| | | 39 | Economic downturns affecting demand for steel products |

Table 2: Probability of Risks

| Score | Likelihood | Occurrence Probability |
|-------|------------|---|
| 12 | Routine | Highest probability of occurrence |
| 9 | Weekly | Occurs on weekly basis |
| 6 | Bi-Weekly | Occurs on bi-weekly basis |
| 3 | Quarterly | Will occur on multipole occasions throughout lifespan |
| 1 | Odd Hours | Although improbable, there is a potential of occurrence |

Based on the above given risk assessment matrix and the subsequent classification of hazards into varying levels of risk, a Process Hazard Analysis (PHA) sheet was produced. The provided Public Health Assessment (PHA) document offers comprehensive data pertaining to multiple parameters, including frequency and severity rates. The risk scores in the table were computed using equation 1. The PHA sheet encompasses columns that comprehensively delineate each hazard, encompassing its origin, resultant impact, likelihood of occurrence, and magnitude of severity. A comprehensive Process Hazard Analysis (PHA) sheet can be found in Appendix A, located inside the appendix part of this document.

$$\text{Risk Score} = \text{Likelihood} * \text{Severity}. \quad (1)$$

Table 3: Risks Severity

| Score | Probability | Occurrence of likelihood |
|-------|--------------|--|
| 12 | Critical | Loss of life or significant health risks |
| 9 | Very Serious | Potentially life-threatening injuries or multiple injuries requiring hospitalization |
| 6 | Serious | Significant injuries that involve hospitalization or numerous medical treatments. |
| 3 | Minor | Minor injuries requiring basic first aid. |
| 1 | Negligible | Injuries that do not require medicinal action |

Table 4: Risk Assessment Table for Different Risks

| Risk Score | Risk Level | Action Taken |
|------------|----------------------|--|
| 1 | Negligible | Precaution measures are required. |
| 3,6,9,12 | Minor (Controllable) | No immediate emergency actions are necessary, but existing preventive measure should be maintained |
| 12,27,36 | Moderate | Moderate necessary protective measures should be implemented to reduce risk level. |
| 57,72,81 | Critical | Critical, immediate action is needed, ongoing measure should be conducted under supervision and control if the risk has not reached a hazardous state. |
| 108,144 | Uncontrollable | The process should not be operated until the risk is mitigated to a tolerable level. Individual actions should be suspended and activities should be halted if hazard cannot be prevented. |

After conducting a Process Hazard Analysis (PHA), the subsequent phase entails the identification of any operability issues within the system. The HAZOP methodology is widely recognized as a leading approach for identifying potential process vulnerabilities. Nevertheless, it is crucial to possess a comprehensive understanding of specific prerequisites prior to undertaking a Hazard and Operability Study (HAZOP).

- Process flow diagrams (PFD)
- Layout drawings
- Operational instructions.
- Equipment Start-up and shut-down measure.
- HAZOP Methodology

To implement the Hazard and Operability (HAZOP) method in practice, bellow steps are typically taken:

- I. Clearly define the objectives, aims research objectives
- II. Create a team for the study
- III. Prepare a study plan
- IV. Perform a team review
- V. Document the outcomes.



ICSET-23



UET Peshawar

Hazop Team

In order to carry out a Hazard and Operability study (HAZOP), it is imperative to establish a team of a minimum of four and a maximum of ten persons. It is imperative to choose a HAZOP team leader and ensure that all team members receive suitable training and are allocated distinct roles. In order to define the extent of the research project for the entire team, the leader of the HAZOP analysis will assign specific tasks to each team member.

Risk Evaluation

By employing the HAZOP methodology, one can effectively detect and evaluate diverse risks by scrutinizing the prospective origins and ramifications linked to each peril. In order to assess the risks that have been identified, a HAZOP worksheet is utilized in accordance with the HAZOP process flow diagram. In order to effectively execute a risk analysis, the procedure is segmented into distinct nodes based on the Process and Instrumentation Diagram (P&ID). Subsequently, a suitable guide word is selected for each node to accurately represent the pertinent process parameter. The guiding word serves to identify any deviation that may occur throughout the process. Thorough analysis is conducted to investigate all possible factors contributing to the deviation, as well as its potential outcomes. Subsequently, appropriate actions for control are suggested, taking into account a comprehensive comprehension of the deviation.

Table 5: HAZOP Work Sheet

| HAZOP Work Sheet | | | | | | | |
|---|-----------------|------------|-----------|--|--|---|---|
| Study Title: Steel Manufacturing Industry | | | | | Page of: XYZ | | |
| HAZOP Team: Taimoor | | | | | Dated: | | |
| Parts Consider: Production | | | | | | | |
| No. | Risk Name | Guide Word | Deviation | Possible Causes | Consequences | Safeguards | Mitigation Plan |
| 1 | Production area | More | High | Electrical faults, flammable materials mishandling | Property damage, injuries, production disruption | Fire detection systems, fire extinguishers, emergency protocols | Implement fire prevention measures, conduct regular fire drills |

Risk Reduction

After the identification of all potential risks, encompassing their origins, impact, severity, and occurrence frequency, the subsequent step involves the implementation of measures to control or mitigate them. The preliminary hazard analysis serves the purpose of identifying risks, assessing their severity and likelihood of occurrence. On the other hand, the Hazard and Operability research is conducted to identify hazards and operability issues, and afterwards classify them based on their severity, which can range from critical to negligible. The application of a risk decision matrix is employed to classify hazards according to their risk score, which incorporates considerations of both their probability and magnitude. The risk assessment table delineates the necessary course of action for each identified hazard in the event that it



materializes. Manageable hazards are effectively mitigated through either their complete removal or the implementation of measures to lessen their impact.

Hazards have been recognized throughout the entire process of steel bar manufacture, and a range of risk assessment methodologies are employed to manage and mitigate risks in regions of heightened risk. In order to mitigate deviations and prevent undesirable events, it is imperative to enact the prescribed measures. The Preliminary Hazard Analysis (PHA) is employed for the purpose of hazard identification, whereas the Hazard and Operability (HAZOP) technique is utilized to address both operability concerns and hazard identification inside the process. This study proposes that the integration of Process Hazard Analysis (PHA) with Hazard and Operability Study (HAZOP) can yield significant enhancements in process efficiency, mitigation of unintentional hazards, and resolution of operability concerns. Hence, this research endeavour has the potential to aid individuals in discerning the most effective risk management strategies for their respective endeavours.

Table 6: Hybrid Spread Sheet

| Hybrid Spread Sheet | | | | | | | |
|---------------------|-----------|--|--|---------------------|----------|----------------|---|
| Guide Word | Deviation | Causes | Consequence | Frequency | Severity | Risk Level | Mitigation |
| HAZOP Portion | | | | From PHA Tool | | | |
| More | High | Electrical faults, flammable materials mishandling | Property damage, injuries, production disruption | Routine | Critical | Uncontrollable | Implement fire prevention measures, conduct regular fire drills |
| HAZOP Portion | | | | Portion of PHA Tool | | | |

FUTURE RECOMMENDATIONS

The mitigation of hazards in manufacturing processes is distinct for each individual process and necessitates the implementation of specific strategies to guarantee safety. One methodology that can be employed is Hazard and Operability Study (HAZOP), which is a widely recognized and efficient approach for the identification and analysis of hazards within a given process. This method involves the utilization of predetermined guide words to systematically examine process parameters and pinpoint potential risks. The implementation of HAZOP and PHA techniques can enhance worker confidence and efficiency by effectively safeguarding the system's safety. This study emphasizes the importance of implementing effective approaches to minimize or eliminate risks in the production process. Furthermore, the findings of this research can be applied to other steel manufacturing sectors as well. This study employs PHA and HAZOP as risk management methodologies, while it is worth noting that alternative techniques such as HAZOP combined with Fault tree analysis can also be utilized. From the available literature it is clear that advance methods like Analytic Hierarchy Process, Fuzzy Inference System, and the different available frameworks like RIDM, STAMP, SPTA, FRAM should be integrated. These methodologies and frameworks can be considered for future research in risk assessment in steel manufacturing industry. This

project has the potential to serve as a foundational paradigm for future research in comparable industries globally, regardless of whether it pertains to new or established installations.

REFERENCES

- [1] Agrawal, N., et al. (2014). "Evaluation of Hazards in Crusher and Material handling of Cement Industry." *International Journal on Emerging Technologies* 5(1): 17.
- [2] Cheraghi, M., et al. (2022). "Optimal selection of safety recommendations: a hybrid fuzzy multi-criteria decision-making approach to HAZOP." *Journal of Loss Prevention in the Process Industries* 74: 104654.
- [3] Depczyński, R., et al. (2023). "Decision-Making Approach in Sustainability Assessment in Steel Manufacturing Companies—Systematic Literature Review." *Sustainability* 15(15): 11614.
- [4] Dewi, D., et al. (2020). *Manufacturing Risk Identification in the Steel Industry*. E3S Web of Conferences, EDP Sciences.
- [5] Fthenakis, V. and S. Trammell (2003). "Reference guide for hazard analysis in PV facilities." Brookhaven National Laboratory draft report.
- [6] Galante, E., et al. (2014). "Risk assessment methodology: quantitative HazOp." *Journal of Safety Engineering* 3(2): 31-36.
- [7] Hwang, J.-G., et al. (2010). Hazard analysis of train control system using HAZOP-KR methods. 2010 International Conference on Electrical Machines and Systems, IEEE.
- [8] Jagtman, H., et al. (2005). "A support tool for identifying evaluation issues of road safety measures." *Reliability Engineering & System Safety* 90(2-3): 206-216.
- [9] Kaplan, S. and B. J. Garrick (1981). "On the quantitative definition of risk." *Risk analysis* 1(1): 11-27.
- [10] KARAHAN, V. and C. AKOSMAN (2018). "Occupational health risk analysis and assessment in cement production processes." *Turkish Journal of Science and Technology* 13(2): 29-37.
- [11] Khan, O. and G. A. Zsidsin (2012). *Handbook for supply chain risk management: Case studies, effective practices, and emerging trends*, J. Ross publishing.
- [12] Khaviya, S., et al. (2017). "A risk assessment study on occupational hazards in cement industry." *Int Res J Eng Technol* 4: 12.
- [13] Kim, M.-S., et al. (2018). "Risk assessment and mitigation model for overseas steel-plant project investment with analytic hierarchy process—Fuzzy inference system." *Sustainability* 10(12): 4780.
- [14] Kotek, L. and M. Tabas (2012). "HAZOP study with qualitative risk analysis for prioritization of corrective and preventive actions." *Procedia Engineering* 42: 808-815.
- [15] Kumar, M. and M. K. Mishra (2019). "Risk Assessment in Cement Manufacturing Process." *International Journal of Engineering Research & Technology* 8(4): 147-150.

- [16] Lawley, H. (1974). "Operability studies and hazard analysis." *Chem. Eng. Prog.* 70(4): 45-56.
- [17] Lyons, M., et al. (2004). "Human reliability analysis in healthcare: a review of techniques." *International Journal of Risk & Safety in Medicine* 16(4): 223-237.
- [19] Marhavidas, P. K., et al. (2022). "Safety-assessment by hybridizing the MCDM/AHP & HAZOP-DMRA techniques through safety's level colored maps: Implementation in a petrochemical industry." *Alexandria Engineering Journal* 61(9): 6959-6977.
- [20] McCoy, S., et al. (2000). "HAZID, a computer aid for hazard identification: 4. Learning set, main study system, output quality and validation trials." *Process Safety and Environmental Protection* 78(2): 91-119.
- [21] Mokhtarname, R., et al. (2022). "Application of multivariable process monitoring techniques to HAZOP studies of complex processes." *Journal of Loss Prevention in the Process Industries* 74: 104674.
- [22] Mousavian, N. A., et al. (2017). "Estimation of heavy metal exposure in workplace and health risk exposure assessment in steel industries in Iran." *Measurement* 102: 286-290.
- [23] Nordlöf, H., et al. (2015). "Safety culture and reasons for risk-taking at a large steel-manufacturing company: Investigating the worker perspective." *Safety science* 73: 126-135.

Paper ID: ICSET-2315

DC MICRO-GRID WITH THE SLIDING MODE CONTROL: APPLICATION OF BI-DIRECTIONAL BUCK/BOOST CONVERTER

Jamal Javed*, Mubassir Ali Shah, Fawad Khan

Electrical Energy System Engineering, Center for Advanced Studies in Energy, University of Engineering and Technology Peshawar, Pakistan

**Corresponding author*

Email: jameswebyouth@gmail.com

ABSTRACT

Renewable energy sources exist in abundance in the world, generally and in Pakistan, especially. Such sources are environment friendly and are most reliable and effective for power generation usage. This makes us to side-line the thermal power sources for generation, in most of the generation scenarios, owing to their ill-effects on the environment. Such sources include wind, solar, hydro, biomass etc. Sun is considered the ultimate source of energy owing to the reason that it is indestructible and occurs almost 9 hours in various countries during day time. Today, apart from the AC sources of electric power, DC sources are gaining much importance due to the rapid growth in the DC operated technologies. The ever-rising scope of the employment of the DC sources, the associated energy storage devices and the associated loads run by such power system, require direct current (DC) micro-grids and this is the reason such micro-grids have assumed much importance in the eyes of the global stakeholder. For the reliable running of the micro-grid, a control strategy is required. The aim of the use of such a control system or technique which is the core study of this research work is to make the DC bus voltage to remain within its limits and with no variations in its value so as to maintain a power balance in the system. This proposed control mechanism will be used in the BES unit. The nonstop charging and discharging of the DC power both to and from the BES would allow for the achievement of the control objectives. Thus, SMC method of control is preferred and worth to be implemented due to the gains that it offers such as its robustness when it comes for the sudden changes in the input power and for the load.

The SMC control method has been employed in the Battery Energy Storage (BES) component model in this paper. The control of the system is achieved through the charge and discharge from the BES. For observation of the performance of SMC, three case studies have been carried out. For simulation results, DC micro-grid model has been created. The micro-grid model is then run in the Simulink environment of the MATLAB software for acquiring the required performance results vis-à-vis PI control. Finally, the comparison work is carried out in order to validate that SMC performs better than PI control method in case when the intermittency and load changes affect the output voltage of the PV system and thus affects the smooth and reliable running of the system for power production. Main key findings in the work have been identified such that the SMC has reduced the oscillations during transients, has offered a faster settling time with respect to the bus voltage and also SMC has provided better results during the load changes and changes in the solar irradiance. The three case studies have shown the robust performance of the SMC control when utilized with the PV system. Thus, SMC has been proved to give a response which proves to be fast.



ICSET-23



UET Peshawar

KEYWORDS: Sliding mode control (SMC), BES, Photovoltaic (PV), PI, SC.

INTRODUCTION

Semiconductors are extensively utilized in the today's technologically developed world and are basically DC components that will, undoubtedly, dominate the entire field of electrical and electronic devices. They have been discovered in the 1960s. Thus, most of the electrical loads will now be considered to be compatible to the DC power sources. The carbon free sources of energy including mainly the photovoltaic (PV) arrays, hydrogen fuel cells and, more importantly, the energy storage devices/units have seen an unprecedented rise in their numbers and interestingly are all compatible with the DC power sources. The penetration frequency of components which are compatible with the DC sources and loads is going upward in the graph and so their widening scope is imminent. The components used in the sources and loads in the power system, that are compatible with DC, have been seeing their demand increasing day by day, hence their penetration in the power system area is inevitable. About 30% of the power generated, today, passes through some kind of power electronic converters before being used. Today it is widely accepted as a fact that the percentage will increase to 80% within the next decade. However, the process in the conversion of power is associated with the losses of power in the power system [1]. So, it would prove to be better and suitable option if the steps in the power conversion process are reduced.

Because of the above-mentioned implications, time has come that we consider the advantages of DC sources over the AC ones in the electrical power system [2]. No doubt, the DC micro-grid, alone, used in the power system for use has some constraints associated with it such as the protection of the DC system, its safety, the standards and the associated equipment used in such system. Thus, a DC grid system is put in operation so as to increase the overall performance and efficiency of the system rather than replacing the conventional AC based system.

The major aim to conduct such a research work is to sort out the issues arising in the stability of the DC based micro-grids which usually are caused by the intermittent behavior of the Res and the sudden changes in the load. The main component of the DC system namely the BES would function by regulating the voltage in the bus through charge and discharge from the BES, so to regulate and keep the power balance in the DC system. The conventionally used PI control system would have been used but since the converter used is a non-linear one, so in order for the control system to be simplified, a control system based on the non-linear characteristics is used. The control system with non-linear characteristics used in the research study is the SMC [3]. SMC is an effective control strategy which is used to design such controllers which would prove to be robust for even higher order complex non-linear power sources which would be operating in uncertain scenarios. SMC offers the major advantage that it guarantees the stability of the system and also would prove to be robust when it comes to considering the parameters and the uncertain conditions occurring in the line and the load [4].

SOLAR DC POWER SYSTEM

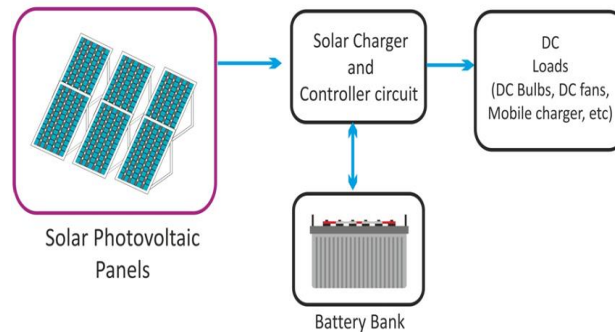


Figure 59: Schematic View of Solar DC Power System

The major purpose of conducting this research work is to deal with the issue of the stability of the power system that arises in the DC based micro-grid system. Such issue of stability occurs due to the intermittent nature of the renewable power sources and also partly due to the fluctuations occurring at the load side. The Battery Energy Storage system, also known in short as the BES, is a component of the power system which helps to regulate the voltage in the bus by the charge and discharge operation. This operation helps in maintaining the balance of power in the micro-grid system. PI is a commonly used control technique for the controlling of the power converters in the DC system. The PI control is linear method of control of the DC-to-DC converter which helps in reducing the error by the adjustment of the input to the control system by performing a control action. However, major disadvantage of the PI regulator is the inability of handling uncertainty in the system including parameter variations and external disturbances. As the converter used is a non-linear one, so for simplification of the process, a non-linear control method is employed for use in the proposed power system.

The aim and objective of the research thesis, under consideration, is to use a method which would control the DC-to-DC power conversion thereby converting DC power to a regulated DC power with little to no attenuation and properly in line with the requirements of the load. Therefore, the foremost objective is finding a control method which will meet the expectations without any difficulty in its operation. The system is also expected to cope with the requirements of power and size limits, so that the whole control system may not be a cause of disturbance in case it has to be repaired or replaced [5][6].

RESEARCH METHODOLOGY

DC micro-grids play an important role in interconnecting local or islanded units of power producers, energy storage systems and loads that generate, store and consume electrical power respectively. The power is DC in nature. DC micro-grid can work while grid connected or in isolation. As compared to the AC micro-grids, DC micro-grids offer several advantages such as they are easy to control, have higher efficiency, have higher quality, have higher reliability in operation mode and offer reduced greenhouse effect. The outline layout of the DC micro-grid is shown below. [7][8]

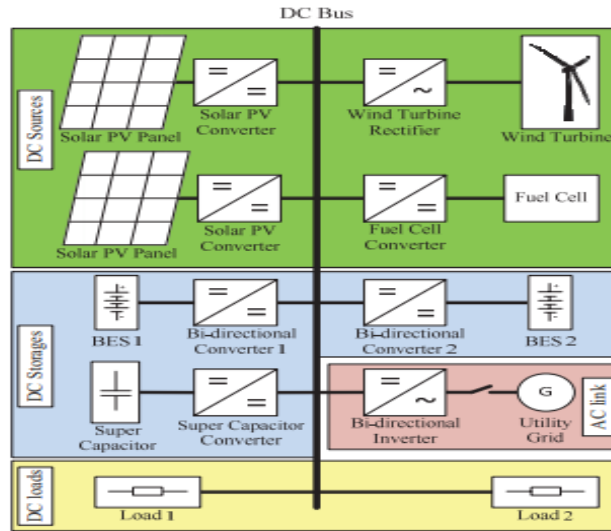


Figure. 60 Schematic Layout of DC micro-grid

A general layout of the DC based micro-grid system contains the following components:

DC power sources: DC power sources may include the PV panels or any other renewable source of electric power like the turbines run with the help of wind energy and hydrogen fuel cells.

DC power storage system: The DC power storage system includes the components like the Battery Energy Storage Systems and super capacitors.

DC loads: DC loads consist of those loads which are compatible with the DC power system.

PV panel modeling

The PV panel model is considered as a current source driven by the radiant energy of the sun [9]. This current source is in parallel with the diode. Also, shunt and series resistances are connected to the output. Figure.3 shows the equivalent circuit of a solar cell [10].

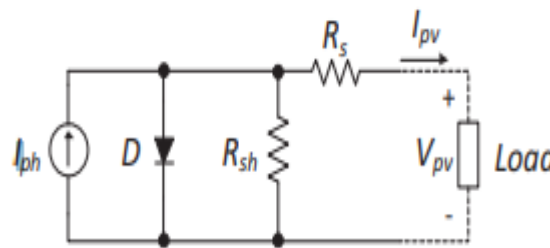


Figure 61 Equivalent Circuit Diagram of Solar PV Cell

The PV cell model is represented by the following equation:

$$I_{pv} = n_p I_{ph} - n_p I_{sat} \left[\exp \left(\left(\frac{q}{AKT} \right) \left(\frac{V_{pv}}{n_s} + I_{pv} R_s \right) \right) - 1 \right]$$

$$I_{ph} = \left(I_{ss0} + k_i(T - T_r) \times \frac{S}{1000} \right)$$

$$I_{sat} = I_{rr} \left(\frac{T}{T_r} \right)^3 \exp \left(\left(\frac{qE_{gap}}{kA} \right) \times \left(\frac{1}{T_r} - \frac{1}{T} \right) \right) \quad (1)$$

Here: V_{oc} = Rated open circuit voltage

I_{ph} = Photon current

I_{sat} = Module reverse saturation current

q = Charge on electron (1.602×10^{-19} C)

A = Ideality factor

k = Boltzman constant (1.38×10^{-23} J/K)

R_s = Series resistance of a PV cell

R_{sh} = Shunt/parallel resistance of a PV cell

I_{ss0} = Short circuit current

K_i = Short circuit current temperature coefficient

T_r = Reference temperature (300 K)

I_{rr} = Reverse saturation current at T_r

E_{gap} = Energy of the band gap for silicon (1.12 eV)

N_p = Number of cells in parallel

N_s = Number of cells in series

S = Solar irradiation level

T = Surface temperature of the PV

PV array modeling

The number of PV panels can be determined for a selected site by using the formula given as under

$$\text{Number of Panels} = \frac{\text{Installed Capacity}}{\text{Output Power of Solar Panel}} \quad (2)$$

Moreover, to find the total land areas that would be needed for installing PV panels can be calculated from the following expression:

$$\text{Total Area Required} = \text{Number of Panels} \times \text{Length} \times \text{Breath} \quad (3)$$

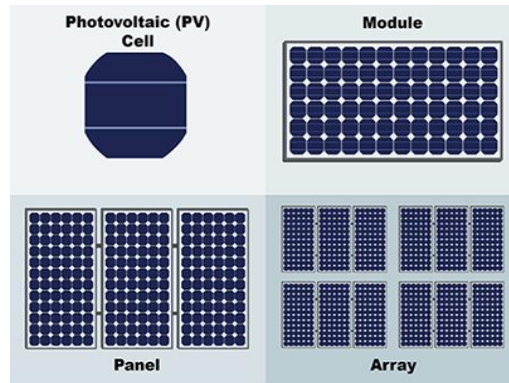


Figure 62: PV Panel Module and Array

Solar Energy Resource

The clearness index can be calculated by using the following formula.

$$k_T = \frac{H_{ave}}{H_{o,ave}} \quad (4)$$

Here, H_{ave} shown the average radiation per month that falls on the surface of the earth horizontally in kWh/m²/day.

$H_{o,ave}$ shows the radiation that falls on the straight surface at the peak point of the earth's atmosphere in kWh/m²/day. It is also referred to as the extraterrestrial horizontal radiation.

The intensity of the solar radiation at the top of earth's atmosphere can be calculated by using the following formula:

$$G_{on} = G_{sc}(1 + 0.033 \cdot \cos \frac{360n}{365}) \quad (5)$$

Here, G_{sc} shows the solar constant having a value of 1.367 kW/m² and 'n' shows the days from 1 to 365 for the whole year. The extraterrestrial radiations coming from the sun which are normal to the horizontal surface can be calculated from the following formula:

$$G_o = G_{on} \cos \theta_z \quad (6)$$

Here θ_z shows us the zenith angle in degrees

Battery modeling

While modeling the battery as one of the important components for the DC micro-grid system, two parameters are important which should be taken into consideration. One is the battery terminal voltage V_b and the other is the state of charge (SOC). Such parameters determine the status of the battery and are represented by the equations as under:

$$V_b = V_o - K \frac{Q}{Q - \int i_b dt} + A \cdot \exp(-B \int i_b dt) - R_b \cdot i_b \quad (7)$$

$$SOC = 100 \left(1 - \frac{\int i_b dt}{Q} \right) \quad (8)$$

Here: R_b is the internal resistance of the battery, V_o is the open circuit voltage, i_b is the battery current, Q is the battery capacity, K is the polarization voltage, A is the exponential voltage and B is the exponential capacity. The battery model is already being provided in the MATLAB/Simulink tool. The equivalent circuit of the battery is shown in the Fig. 5 and the parameters of the lead acid battery are given in the table 1.

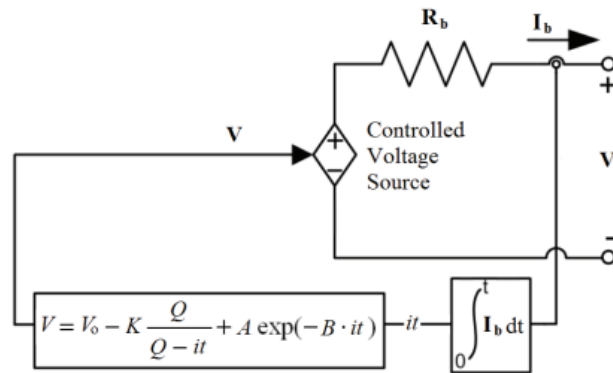


Figure 5: Equivalent Circuit

Table 9: BES Model Parameters

| Symbol | Description | Value | Units |
|--------|-------------------------|-------|-------|
| V | Nominal Voltage | 196 | V |
| Q | Rated Batter Capacity | 150 | Ah |
| SOC | Initial State-of-Charge | 50 | % |

Sliding mode control (SMC) implementation

At this critical stage, Sliding Mode Control (SMC) method is implemented in DC-DC power transfer control via a bidirectional boost converter. The battery converter is scheduled to operate in voltage regulation (VR) mode to maintain the power balance of the system. The sliding mode control used in this system is equipped with a washout filter. The washout filter plays a role in controlling the power balance.

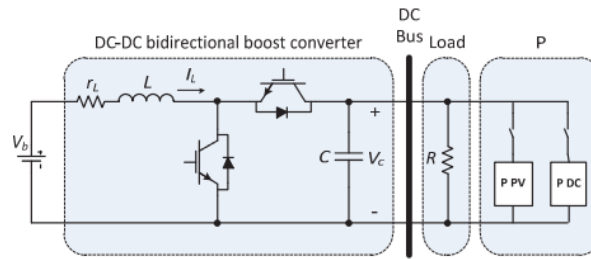


Figure 6: Simplified DC micro-grid Model

RESULTS

Test System and Parameters

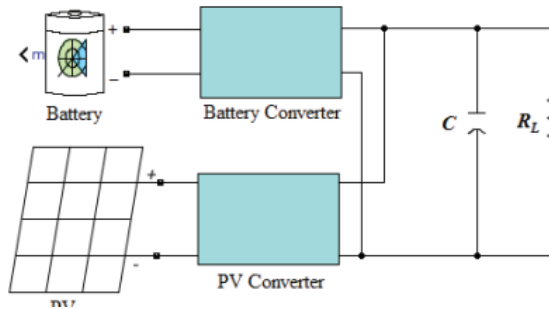


Figure 63: General Test System Layout

MATLAB / Simulink simulations are performed to show the validity of the SMC method for the DC based micro-grid system.

The simulation is run on a DC micro-grid model that includes photovoltaic panel, a battery typically a lead acid one and some DC loads. Table 2 shows the important parameters upon which the battery energy storage, PV panel, their associated converters and the loads depend during the simulation. A schematic layout of a typical case study test unit has been shown in the Figure 7 and its associated control block diagram has been shown in Figure 7.

Table 10: Simulation Case Studies Parameters

| Symbol | Description | Value | Units |
|-----------|---------------------------|--------|------------------|
| C | Capacitance | 50 | μF |
| L | Inductance | 2.5 | Mh |
| RL | Inductor resistance | 5 | $\text{m}\Omega$ |
| f_s | Switching frequency | 100 | KHz |
| 2δ | Hysteresis band | 0.3796 | A |
| V_b | Battery Voltage | 196 | V |
| $V_c(0)$ | Initial capacitor voltage | 196 | V |
| ω | Cuff-off frequency | 283 | Rad/sec |
| k | Scalar control parameter | 10 | - |
| Q | Battery capacity | 150 | Ah |
| P | Solar PV Power | 1.2 | KW |

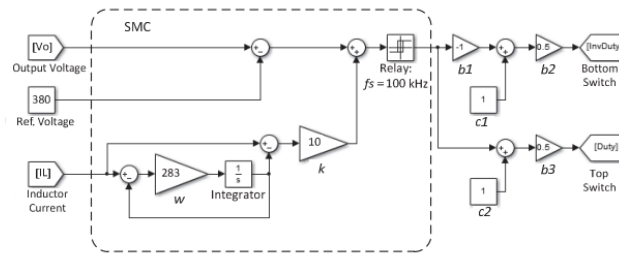


Figure 64: Block Diagram of SMC Based on the Washout Filter

Case Study

In this research paper, we have carried out three case studies. Also, the classical PI control system has been put under implementation to get its results for the purpose of comparison of the results with that of the SMC in each case study [11] [12].

Case 1: Regulation of the Bus Voltage

The value of the DC load in this particular case study is set at 160Ω and the total simulation time is set at 0.05 seconds. The results obtained from the simulation in this case study have been shown in the Fig. 8 and Fig. 9. The results from the simulation while using the SMC method have shown us the rising time to be of 1.7 ms, the settling time to be of 4.4 ms and have shown no overshoot. The results of the simulation in this case study with the SMC method of control has been compared with the PI method of control. The graph showing the solid blue line is the result obtained using the SMC method and dashed red line shows the result obtained from the PI control method. The capacitor output shows a voltage level with no overshoot in the SMC method as compared to the PI control method which has shown an overshoot of 2.45 %. It can infer from the comparison of the results of both the control methods that the PI has a settling time (6.9 ms in this case) slower than that of the SMC. Main block model for Case 1 is given as follows:



Incremental Conduction MPPT controller

The diagram illustrates the Incremental Conduction MPPT controller. It starts with two input voltages, V_{pv} and V_{ref} , which are processed through blocks 1 and 2. The output of block 2 is fed into block 3, which calculates the derivative dI/dV . This derivative is then multiplied by the output of block 2 to produce $V(dI/dV)$. This value is added to the output of block 2 to produce $I+V(dI/dV)$. This sum is then compared with zero in block 8. If the result is greater than zero, the duty cycle D is decreased (block 9). If the result is less than zero, the duty cycle D is increased (block 10). The duty cycle D is then limited by block 4 to ensure it is between 0 and 1. The limited duty cycle is then used to generate the switching function g in block 5. The switching function g is then multiplied by the output of block 2 to produce the final PWM signal.

157

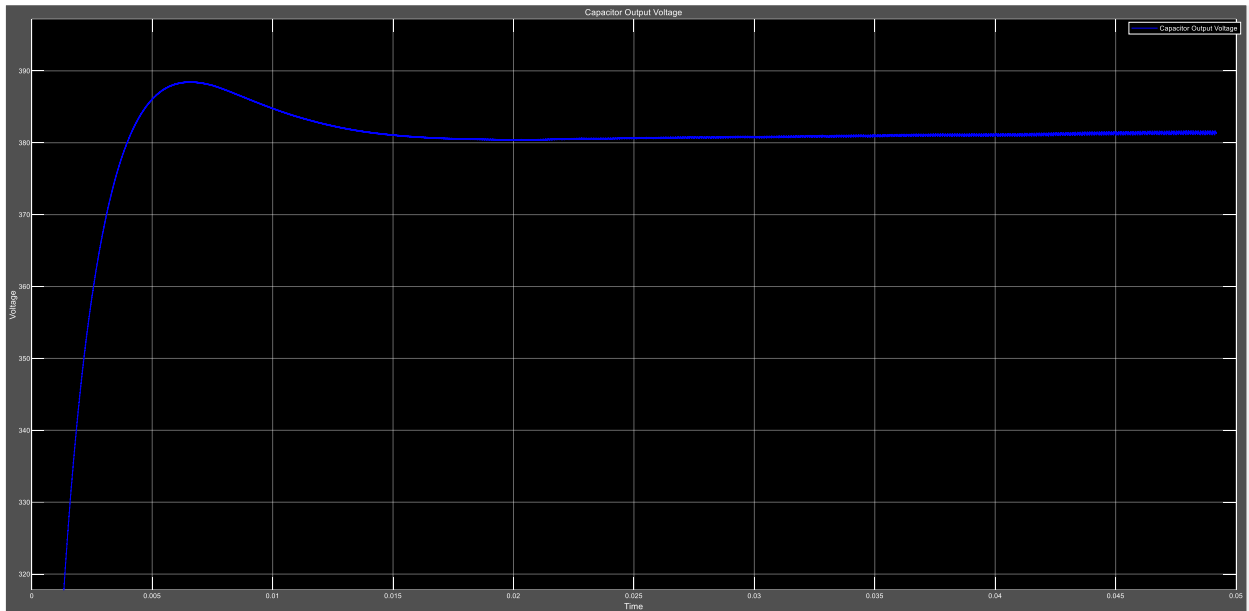


Figure 67: Capacitor Output Voltage Simulation Result Case 1

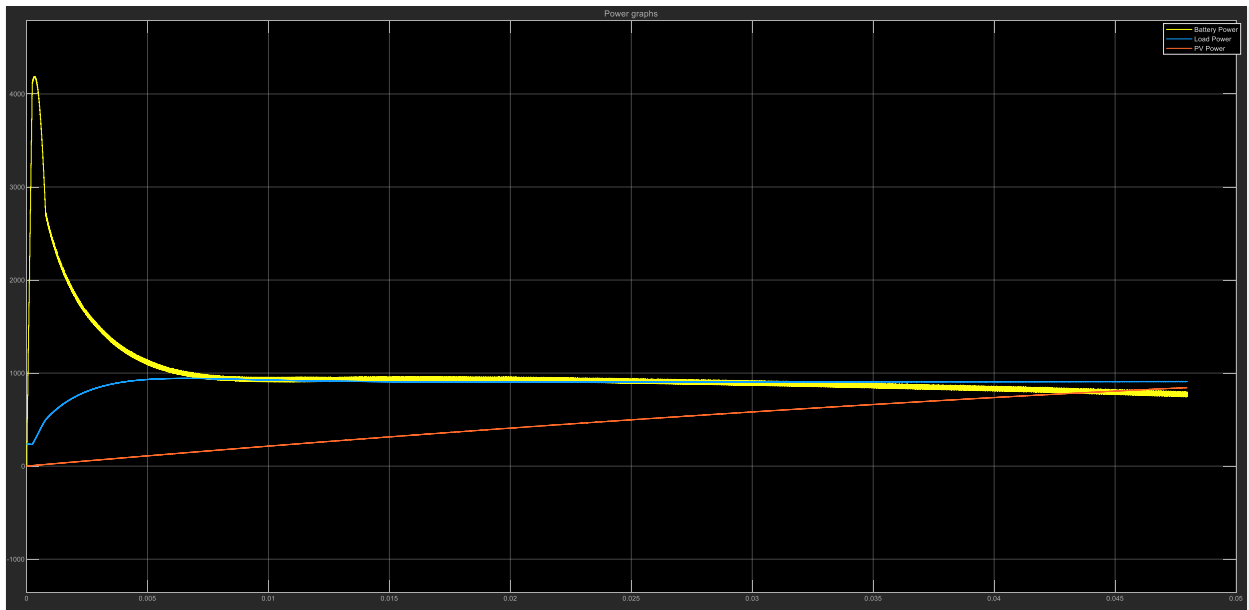


Figure 68: Powers in DC micro-grid (Battery, Load, PV power) Case 1

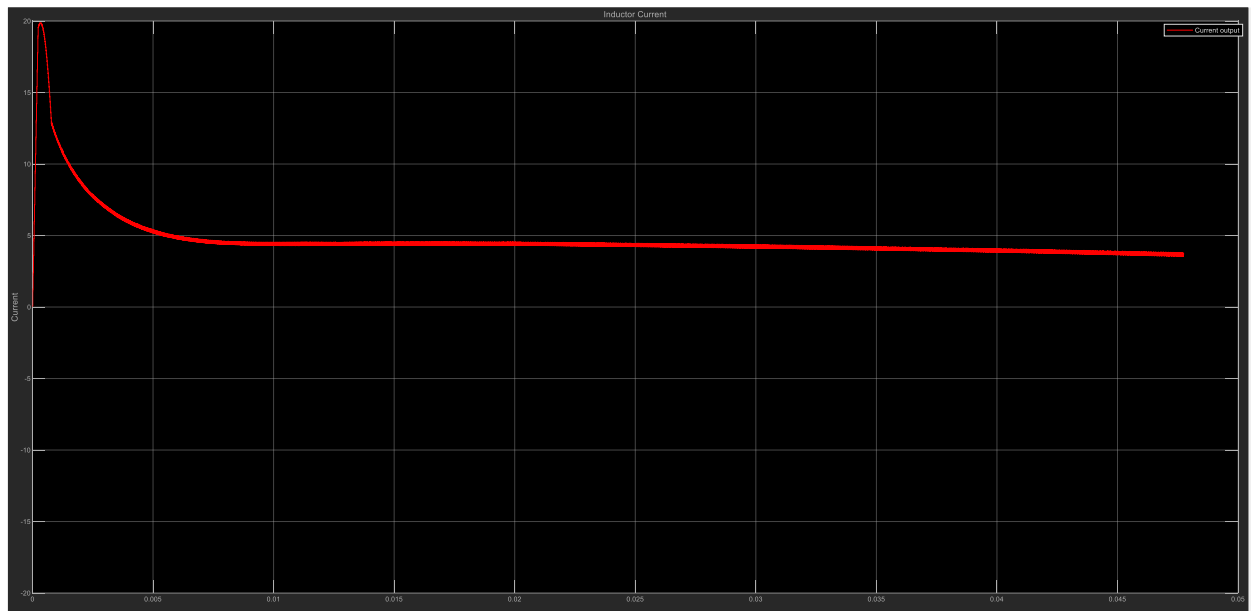


Figure 69 Inductor Current Output Simulation Result Case 1

Case 2: Variation in the Solar Power

The solar power, generated from the sunlight by the PV panel, changes over time due to the variation in the amount of solar radiation, absorbed by the panels. The PV panel in this simulation case study has been provided with different inputs, so that the effect of the variations in the solar irradiance on the output power can be studied both with the SMC and the PI control methods. This case study has been carried out with sole purpose of examining the ability of the SMC in tracking the variations occurred in the output by the fluctuating PV input. The load used here is of $220\ \Omega$ and the simulation time has been set at 0.35 seconds. The results of the simulation of this case study have been shown in the Figures 15,16,17 and 18.

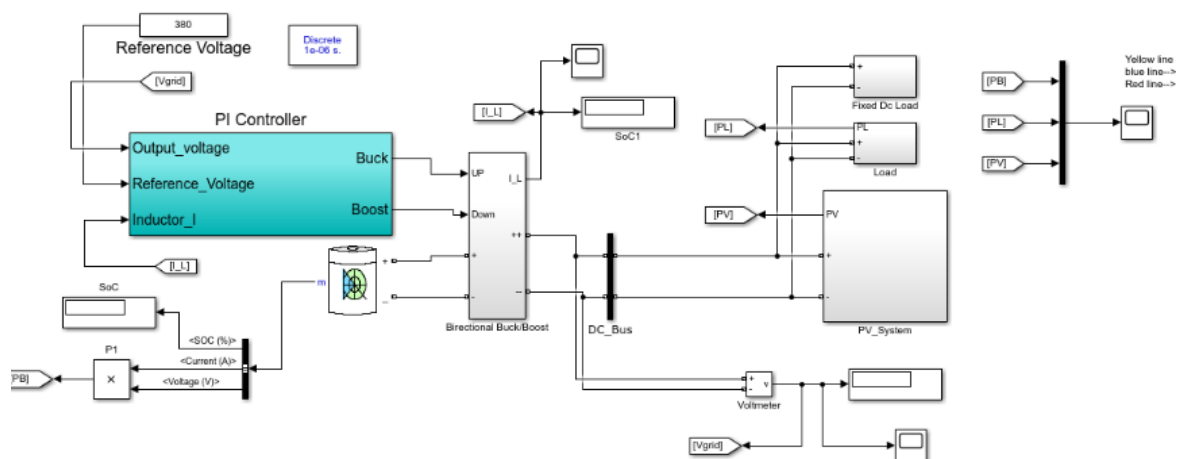


Figure 70: Main Block Case 2

The figure given above shows the main block for the case study for the solar variation effect on the output of the system

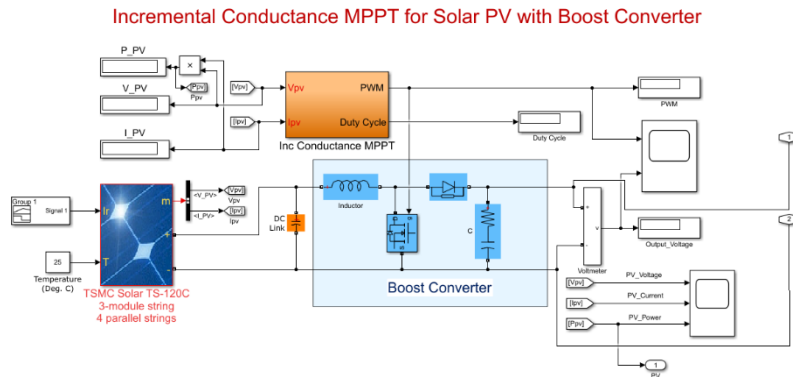


Figure 71: PV System with Incremental Conductance MPPT and Boost Converter Case 2

The figure given above shows the block diagram for the boost converter with the MPPT system. The MPPT maintains the maximum power obtained from the PV system in case of variations in the solar irradiance

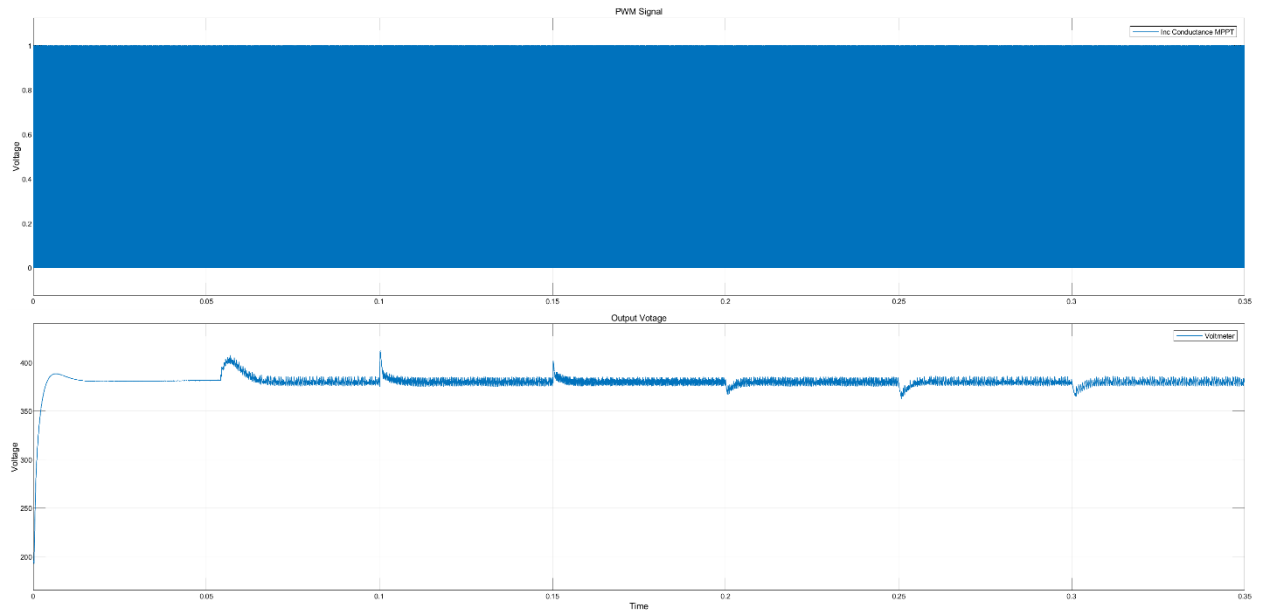


Figure 72: PWM and Voltmeter graph

The PWM graph has been shown above. The MPPT system operates by running the boost converter with the help of the PWM controller. This helps in maintaining the voltage at the output which has also been given along with the graph for PWM.

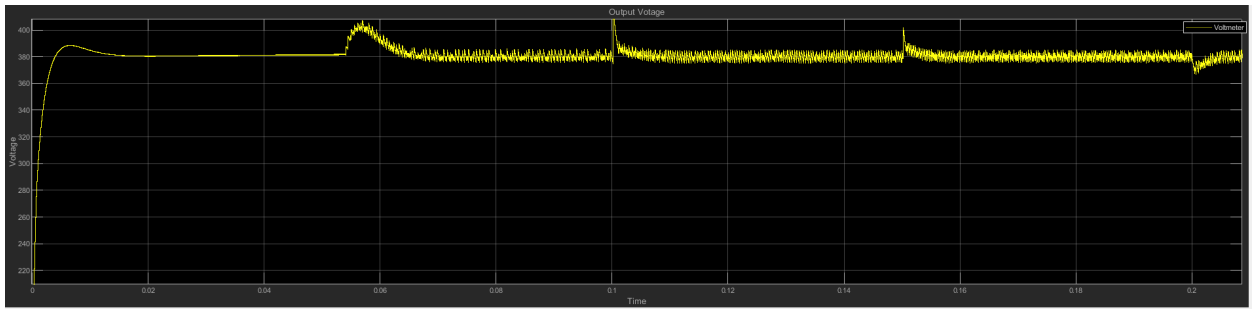


Figure 73: Capacitor Output Voltage Simulation Result Case 2

The above given graph is for the output voltage which shows that with the variations in the solar power available, the voltage swells and dips occur. The SMC reduces the fluctuations at the output. Moreover, compared to other control systems like PI, SMC induces fewer oscillations during the transient states – when changes occur in the input.

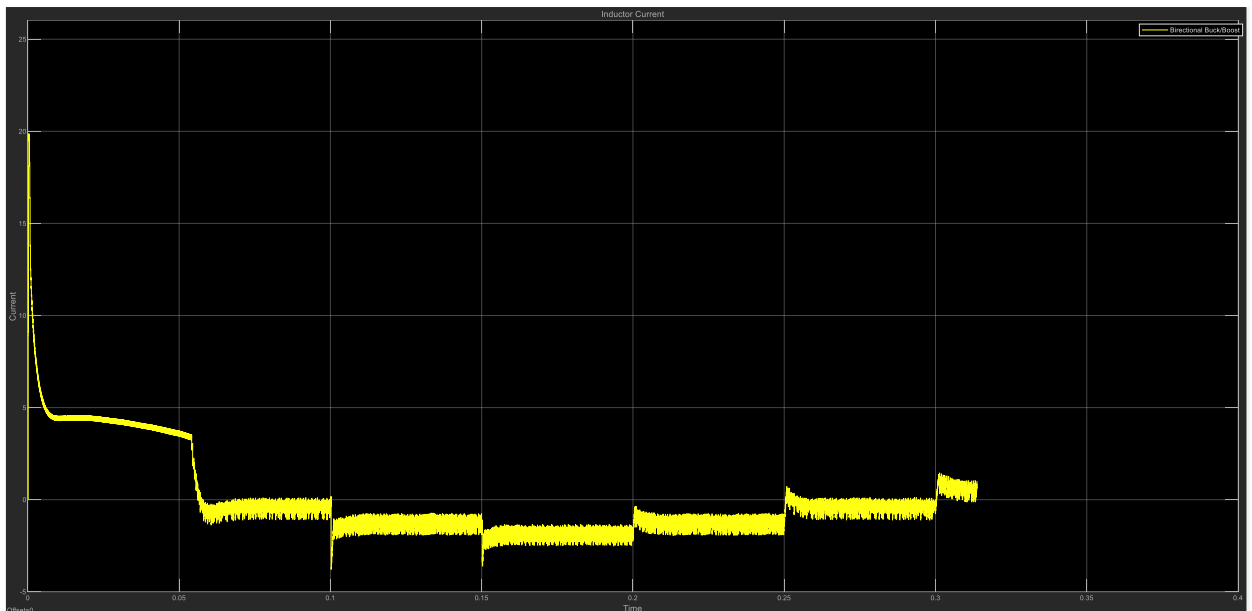


Figure 74: Inductor Current Output Simulation Result Case 2

The output current through the inductor is shown in the above graph. It shows the gradual variation in the current with each transient in the system input that is the solar power input. This also shows the current increases with each decrease in the value of the input. The current increase is caused by the BES, which tracks the changes at the output, thus tries to maintain the power available to the loads.



162

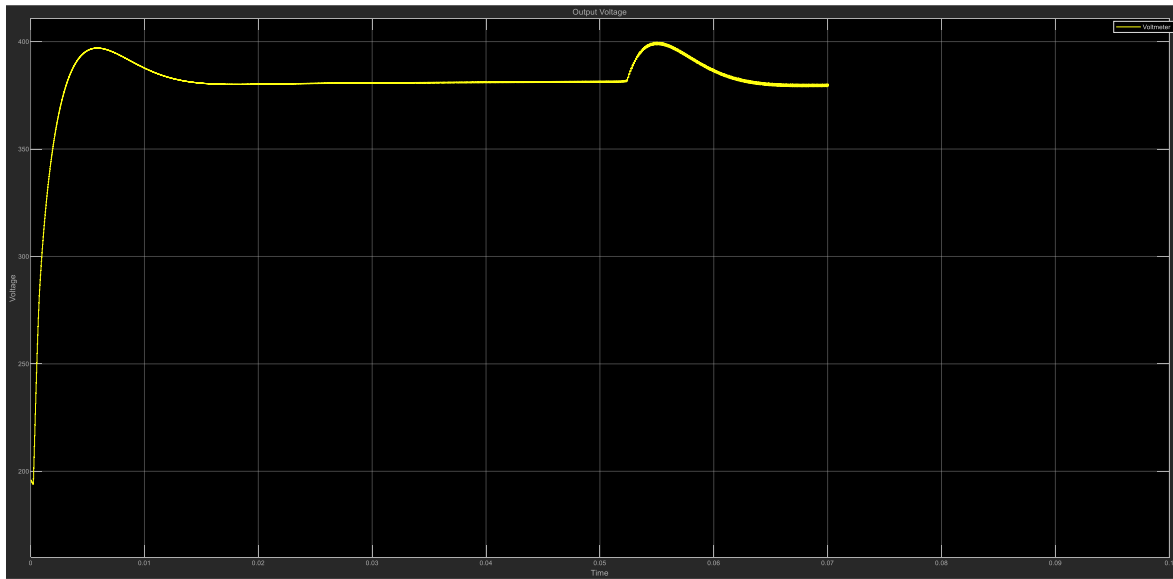


Figure 77: Output Voltage Simulation Result Case 3

The output voltage graph given above shows the voltage dip that occurs when the load is increased one by one, connected through the CBs. After every 0.1 sec, the CB associated with each one of the DC loads gets short-circuited, thus connecting the required load to the system according to the demand of the simulation case study. Similarly, at 0.3 sec in the graph, when the load is suddenly reduced for every further 0.1 sec, the voltage swell is observed. This verifies the statement that the SMC doesn't allow high overshoots or undershoots in the voltage.

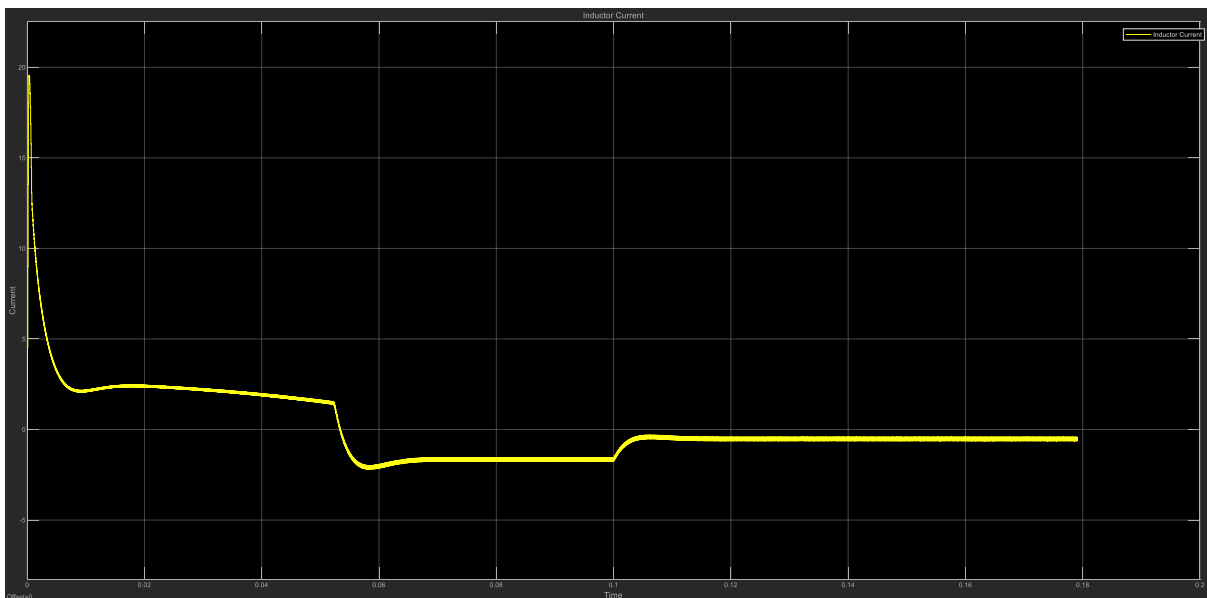


Figure 78: Inductor Current Output Simulation Result Case 3



ICSET-23



UET Peshawar

The above graph for the output current, through the inductor, shows that as the load is increased systematically one by one, current at the output increases after every 0.1 sec. Similarly, when the load is again reduced through the CBs, the output inductor current again falls in magnitude/value.

CONCLUSION

The sliding mode control method is a good choice of the converter designers. This method has been used in the converter of the PV system for maintaining a stable working of the DC based micro-grid. A MATLAB is run in order to check the performance of the sliding mode control method. The simulation results have shown that the SMC method can effectively keep the voltage stable and maintain a power balance in the DC micro-grid system through the charge and discharge operation of the BES in the events of changes in the solar radiation or the load power consumption. The sliding mode control method has been found to provide a good response to the transients as compared to the conventional control method of PI. During encounter of transients, SMC outperforms PI control by an average of 0.387% in voltage overshoot / undershoot. In today's ever developing and technologically advanced world, the use of intelligent machines like computer has increased manifold. Now the development of advanced control algorithms is possible with the help of sophisticated computer programs/soft-wares. One of the advanced control algorithms is the sliding mode control that has garnered the attention of the control engineers and converter designers due to the merits and ease of implementation it offers. It is so chosen because it is equally suited for use in linear as well as non-linear systems. Major configurations of the SMC method have been discussed in the paper and major areas of the application of SMC have been elaborated too. Second order sliding mode controllers, super twisting controllers, arbitrary order sliding mode controllers have been discussed with an application point of view. Also, the integration of different algorithms with the SMC and the progress made in this aspect has been the subject of this research study along with the merits and de-merits of the earlier configurations of SMC. An adaptive and intelligent technique-based SMC algorithm which has recently been developed by researchers has been discussed. Such algorithms are considered effective in the event of uncertain conditions in the system.

REFERENCES

- [1] J. Xiao and W. Peng, "Multiple modes control of household DC microgrid with integration of various renewable energy sources," IECON Proc. (Industrial Electron. Conf.), pp.1773–1778, 2013.
- [2] X. Liu, P. Wang, and P. C. Loh, "A hybrid AC/DC microgrid and its coordination control," IEEE Trans. Smart Grid, vol. 2, no. 2, pp. 278–286, 2011.
- [3] E. Fossas and A. Ras, "Second order sliding mode control of a buck converter," Proc. IEEE Conf. Decis. Control, vol. 1, no. December, pp. 346–347, 2002.
- [4] M. Furat, "Experimental Evaluation of Sliding-Mode Control Techniques," Çukurova Üniversitesi Mühendislik-Mimarlık Fakültesi Derg., vol. 27, no. 1, pp. 23–37, 2012.
- [5] M. Kumar, S. N. Singh, and S. C. Srivastava, "Design and control of smart DC microgrid for integration of renewable energy sources," IEEE Power Energy Soc. Gen. Meet., pp. 1–7, 2012.
- [6] M. E. Ropp and S. Gonzalez, "Development of a MATLAB/simulink model of a single-phase grid-connected photovoltaic system," IEEE Trans. Energy Convers., vol. 24, no. 1, pp. 195–202, 2009.
- [7] O. Tremblay, L. A. Dessaint, and A. I. Dekkiche, "A generic battery model for the dynamic simulation of hybrid electric vehicles," VPPC 2007 - Proc. 2007 IEEE Veh. Power Propuls. Conf., no. V, pp. 284–289, 2007.



ICSET-23

*Proceedings of the 5th International Conference on Sustainable
Energy Technologies (ICSET 2023) Peshawar, Pakistan
14-15 December 2023*



UET Peshawar

- [8] A. P. N. Tahim, D. J. Pagano, and E. Ponce, “Nonlinear control of dc-dc bidirectional converters in stand-alone dc Microgrids,” *Proc. IEEE Conf. Decis. Control*, pp. 3068–3073, 2012.
- [9] D. J. Pagano and E. Ponce, “On the robustness of the DC-DC boost converter under washout SMC,” *2009 Brazilian Power Electron. Conf. COBEP2009*, pp. 110–115, 2009.
- [10] Y. Chaibi, M. Salhi, and A. El-Jouni, “Sliding mode controllers for standalone PV systems: Modeling and approach of control,” *Int. J. Photoenergy*, vol. 2019, no. 1c, 2019.
- [11] A. Etxeberria, I. Vechiu, H. Camblong, and J. M. Vinassa, “Comparison of sliding mode and PI control of a hybrid energy storage system in a microgrid application,” *Energy Procedia*, vol. 12, pp. 966–974, 2011.
- [12] C. Morel, “Zl 2 4,” pp. 1824–1829, 1824.

Paper ID: ICSET-2316

PORTABLE ECO-FRIENDLY SEED GERMINATION SYSTEM

Syed Faakhir Abid*, Hassan Raza, Faiq Sharif, Faheem Ul Haq
Robotics Team, Hadaf Group of Colleges, Peshawar, Pakistan

**Corresponding author*

Email: syedfaakhirabid@gmail.com

ABSTRACT

As the world confronts pressing ecological challenges and the need for sustainable food production, there is a growing demand for innovative solutions that harmonize technological advancements with environmental consciousness. In response to this global urgency, we present our pioneering research on the "Portable Eco-Friendly Seed Germination System using Arduino." This cutting-edge system amalgamates the power of Arduino microcontrollers with eco-friendly materials, ushering in a new era of smart and sustainable seed germination practices. Our research showcases how this versatile and portable system can revolutionize agricultural practices, promoting resource efficiency, adaptability, and greener outcomes for a more sustainable future.

KEYWORDS: Confronts, Ecological, Versatile, Revolutionize, Efficiency, Adaptability.

INTRODUCTION

The current era demands a holistic approach to agricultural practices that not only bolster food production but also respect and protect the delicate balance of our ecosystems. Sustainable agriculture, therefore, holds the key to addressing the pressing challenges of environmental degradation, climate change, and resource scarcity. Seed germination, being the foundational stage of plant growth, assumes paramount importance in this quest for sustainable farming.

Traditional seed germination methods have been characterized by inherent limitations, including excessive resource consumption, lack of precision control, and minimal adaptability to diverse environmental conditions. The advent of microcontroller technology, particularly the Arduino platform, provides a promising avenue for revolutionizing seed germination practices by combining automation, data-driven insights, and eco-friendly principles.

Our research introduces a groundbreaking solution - the "Portable Eco-Friendly Seed Germination System using Arduino." This innovative system capitalizes on the power of Arduino microcontrollers to enable smart, efficient, and eco-conscious seed germination, driving agricultural practices towards a more sustainable and greener future. Researchers and hobbyists can customize the control algorithms to suit specific plant species and growth requirements, allowing for more efficient and cost-effective germination [1].

The use of a portable seed germination system using Arduino can be a key factor in its successful adoption and implementation in sustainable agriculture practices. Several features contribute to the ease of use of such a system:

Intuitive Interface:

A user-friendly graphical interface that allows growers to easily interact with the system, set germination parameters, and monitor the progress of seeds is essential. The interface should be straightforward, well-organized, and visually informative.

Automation and Smart Control:

The automation capabilities of an Arduino-based seed germination system streamline the process and reduce the need for constant manual adjustments. Smart control algorithms ensure that the system maintains optimal conditions for seed germination without constant supervision.

Plug-and-Play Setup:

A user-friendly plug-and-play setup simplifies the installation and initial configuration of the system. Growers should be able to set up the hardware and connect the Arduino components with ease, even with minimal technical expertise.

Precise Sensor Readings:

Accurate and reliable sensor readings for temperature, humidity, and light intensity are crucial for successful seed germination. The system should provide real-time feedback on environmental conditions to enable timely adjustments if needed.

Customizable Germination Parameters:

The ability to customize germination parameters such as temperature, humidity levels, and light cycles allows growers to cater to the specific needs of different plant species.

Remote Monitoring and Control:

An Arduino-based system with remote monitoring and control capabilities enables growers to check and adjust germination conditions from anywhere, enhancing convenience and flexibility.

Error and Alert Notifications:

The system should be equipped with error detection and alert notifications to promptly notify growers of any issues or deviations from optimal conditions, allowing them to take corrective actions.

Energy Efficiency:

Arduino-based seed germination systems can be designed to be energy-efficient, utilizing low-power components and renewable energy sources such as solar panels. This approach contributes to sustainable and eco-friendly agricultural practices [2].

COMPONENTS

Arudiono Nano:

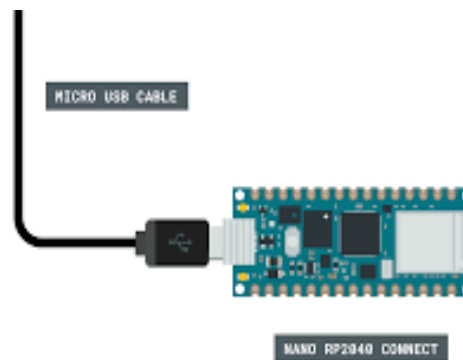


Figure 1: Arduino Nano



ICSET-23



UET Peshawar

As shown in Fig. 1., Arduino Nano, a compact and versatile microcontroller board, emerges as a potent tool in advancing seed germination practices. Its small form factor and powerful capabilities make it an ideal choice for automating and controlling key parameters during the germination process. Equipped with various input and output pins, the Arduino Nano seamlessly interfaces with sensors, actuators, and displays, enabling real-time monitoring and precise adjustments of essential factors like temperature, humidity, and light intensity.

With its low power consumption and compatibility with renewable energy sources, the Arduino Nano fosters eco-friendly seed germination systems, aligning with sustainability objectives. Its ease of use and extensive community support empower growers to customize germination parameters to suit diverse plant species, fostering adaptability and scalability in agricultural settings.

The Arduino Nano's incorporation in seed germination projects accelerates research and facilitates knowledge exchange among growers, researchers, and enthusiasts. From small-scale urban farms to large agricultural operations, its cost-effectiveness and effectiveness have the potential to revolutionize seed germination practices, ultimately contributing to a greener and more resilient future for sustainable agriculture.

Digital humidity and temperature sensor (DHT-11):



Figure 2: Digital Humidity And Temperature Sensor

As shown in Fig. 2., The DHT11 sensor, a popular and cost-effective humidity and temperature sensor, plays a pivotal role in optimizing seed germination processes. With its compact size and simple interface, the DHT11 provides growers with valuable insights into critical environmental conditions within germination chambers or seedling trays.

Accurate humidity measurements from the DHT11 enable growers to maintain optimal moisture levels, a vital factor in promoting successful seed germination. By preventing under or over-watering, the sensor ensures that seeds receive the ideal moisture content required for germination.

Furthermore, the DHT11's precise temperature readings aid in creating an ideal climate for seedlings. With temperature being a crucial parameter for germination success, the sensor helps growers maintain consistent warmth during the initial stages of growth.



The sensor's real-time data is invaluable in monitoring the progress of seed germination and making timely adjustments to ensure an optimal environment. Its ease of integration with Arduino and other microcontrollers enables seamless automation and precise control of germination conditions.

Overall, the DHT11 sensor proves to be a valuable tool for growers in their pursuit of eco-friendly and efficient seed germination practices. By facilitating data-driven decision-making and providing critical insights into environmental parameters, the DHT11 sensor supports growers in their efforts towards sustainable and successful agricultural outcomes.

Soil Moisture Sensor (Fc-28):

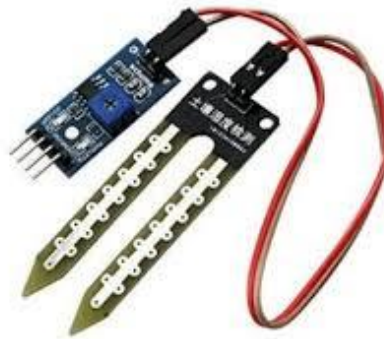


Figure 3: Soil Moisture Sensor

The FC-28 sensor as shown in Fig. 3., commonly known as a soil moisture sensor, plays a vital role in optimizing seed germination processes by providing essential information about the moisture content in the growing medium. This sensor is specifically designed to measure the volumetric water content of the soil or substrate, making it a valuable tool for growers to ensure proper hydration during the germination phase.

When used in seed germination systems, the FC-28 sensor as shown in Fig. 3. continuously monitors the moisture level in the growing medium, allowing growers to maintain an ideal balance between hydration and aeration for the seeds. By avoiding excessive moisture that could lead to waterlogging or inadequate hydration that may hinder germination, the sensor assists in creating an optimal growing environment.

With its simple interface and compatibility with microcontrollers like Arduino, the FC-28 sensor enables seamless integration into automated seed germination systems. By connecting it to the controller, growers can receive real-time data on soil moisture levels, empowering them to make timely adjustments to the irrigation schedule.

The FC-28 sensor's affordability and reliability make it a popular choice for growers seeking cost-effective solutions to ensure successful seed germination. Whether used in small-scale urban farming or large-scale agricultural operations, the sensor serves as an essential tool in promoting eco-friendly and resource-efficient practices.

In conclusion, the FC-28 sensor's ability to monitor soil moisture levels accurately contributes significantly to the success of seed germination. By facilitating precise irrigation control and reducing water



ICSET-23



UET Peshawar

wastage, the sensor aids growers in their pursuit of sustainable agriculture while fostering healthier and more robust seedling growth.

Heating Element:



Figure 4: Heating Element

As shown in Fig. 4., Heating elements are crucial components used in seed germination systems to maintain optimal temperatures for successful seed germination. These elements play a vital role in creating a warm and controlled environment, especially in regions with colder climates or during the colder seasons when natural heat may not be sufficient.

Heating elements, such as resistive heating coils or heating mats, generate controlled amounts of heat that can be directed towards the germination chamber or seedling trays. By providing a consistent and regulated heat source, the elements ensure that seeds receive the warmth they need to stimulate germination and promote healthy seedling growth.

In seed germination systems using Arduino or other microcontrollers, the heating elements can be easily integrated and controlled through digital temperature sensors. This automation allows growers to maintain precise and stable temperatures, reducing the risk of temperature fluctuations that could adversely impact germination success.

Furthermore, heating elements can be designed to be energy-efficient, helping growers adopt more sustainable practices. By using low power heating elements or incorporating renewable energy sources, such as solar panels, the seed germination system can reduce its environmental impact while ensuring optimal conditions for seeds.

Overall, heating elements play a crucial role in fostering successful seed germination by creating an ideal environment for the seeds to thrive. With their controllability, automation capabilities, and potential for energy efficiency, these elements contribute to eco-friendly and resource-efficient seed germination practices.

Ultra Violet Light (UV):



Figure 5: Ultra Violet LED

As shown in Fig. 5., UV (Ultraviolet) light, though not commonly used as the primary light source for seed germination, can play a beneficial role in certain germination scenarios. UV light falls outside the visible light spectrum and is typically divided into three types: UV-A, UV-B, and UV-C. Each type has distinct effects on plants and seed germination.

- **UV-A Light:** UV-A light, which has the longest wavelength among UV lights, can promote seed germination indirectly. It stimulates photoreceptors in plants, triggering specific growth responses, such as stomatal opening and photo-morphogenesis. These responses, in turn, can improve seedling vigor and resilience.
- **UV-B Light:** UV-B light, with a shorter wavelength, is known to have both positive and negative effects on seed germination. In moderate doses, it can trigger stress responses, stimulating the production of protective compounds like secondary metabolites. These compounds can aid in seed defense against pathogens and pests, potentially improving overall germination success. However, excessive UV-B exposure can be harmful and inhibit germination.
- **UV-C Light:** UV-C light, with the shortest wavelength, is germicidal and has potent disinfectant properties. It can be used to sterilize seeds or growing media, reducing the risk of contamination from pathogens or harmful microorganisms. By ensuring a clean and pathogen-free environment, UV-C light indirectly supports germination success.

It is essential to note that prolonged exposure to UV light, especially UV-B and UV-C, can be harmful to plants and seeds. Careful consideration should be given to the dosage and duration of UV light exposure during seed germination. Many plant species do not require UV light for germination, and excessive exposure can be detrimental to seedlings' health and development.

In conclusion, while UV light can have positive effects on seed germination under controlled conditions and in moderation, it is not a common or primary light source used for this purpose. UV light's potential benefits lie in its ability to stimulate specific growth responses and aid in seed sterilization. Growers should exercise caution and ensure proper dosage and exposure times to maximize any potential benefits while avoiding harmful effects.

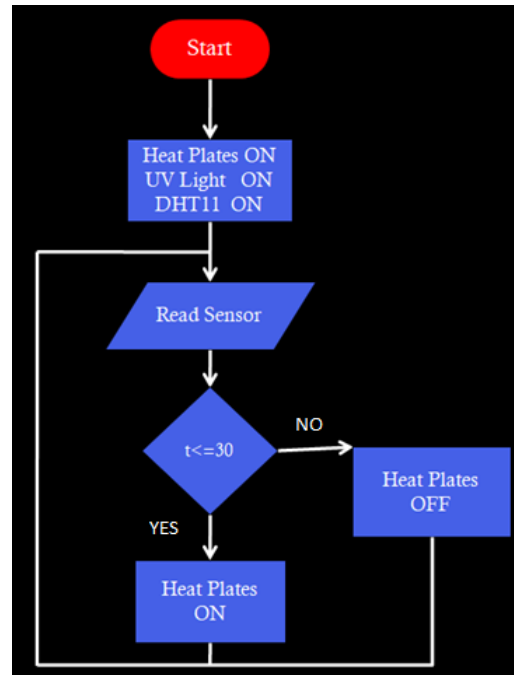


Figure 6: Flow Chart

Technical Aspects

a. Abbreviations and Acronyms:

- **Arduino:** Advanced Research and Development Organization.
- **PWM:** Pulse Width Modulation.
- **LED:** Light Emitting Diode.
- **RH:** Relative Humidity.
- **DHT:** Digital Humidity and Temperature.
- **USB:** Universal Serial Bus.

b. Units:

- **Temperature:** Unit: Celsius (°C) Description: Temperature is a critical factor in seed germination, influencing the rate and success of the process. In Arduino-based systems, temperature sensors provide readings in degrees Celsius, representing the heat levels within the germination chamber or environment.
- **Soil Moisture:** Unit: Percentage (%) Description: Soil moisture denotes the amount of water present in the soil. Arduino-controlled soil moisture sensors provide readings in percentage, indicating the relative moisture inside the germination chamber's soil.
- **Humidity:** Unit: Percentage (%) Description: Humidity denotes the amount of water vapor present in the air. Arduino-controlled humidity sensors provide readings in percentage, indicating the relative humidity inside the germination chamber or the surrounding environment.

Some Common Mistakes:

- Using inappropriate or low-quality sensors, or placing them incorrectly within the germination chamber, can lead to inaccurate data readings.
- Failing to implement data logging and analysis features can result in a missed opportunity for continuous improvement.
- A common oversight is neglecting the system's adaptability to varying seed types or environmental conditions.
- Choosing non-biodegradable or chemically harmful materials for construction can undermine the eco-friendly essence of the system.
- While automation is a significant advantage of Arduino-based systems, over-reliance without human oversight can be detrimental. Failure to monitor sensor accuracy, calibrate actuators, or detect system malfunctions may result in undesirable conditions for seed germination, leading to reduced yields and wasted resources.
- Neglecting energy efficiency considerations can lead to unnecessary power consumption, especially in off-grid or remote setups. Failing to implement low-power components, energy-saving algorithms, or alternative energy sources can hamper the system's eco-friendly attributes.

RESULTS AND DISCUSSION

Using Arduino technology, the stages of corn seed germination can be effectively monitored and controlled to optimize growth conditions. Here are the key stages and how Arduino can be utilized in each phase:

Preparation Stage:

As shown in Fig. 7, the corn seeds are selected, cleaned, and prepared for germination. The Arduino system can be utilized to set up the germination environment, including the selection of appropriate substrates and containers. The system can also be programmed to sterilize the seeds and the growing medium to reduce the risk of contamination.



Figure 7: Preparing the environment and Seed

Imbibition Stage:



Figure 8: Imbibition Stage

In the imbibition stage, Fig. 8, the corn seeds absorb water, initiating the germination process. Arduino sensors, such as moisture sensors (e.g., FC-28 sensor, as shown in Fig. 3.), can be integrated into the system to monitor and maintain the optimal moisture levels in the growing medium. The system can be programmed to trigger automated irrigation based on preset moisture.

During the imbibition stage, corn seeds absorb water, initiating the germination process. The Arduino system maintained optimal moisture levels (around 30-40%) by triggering automated irrigation when moisture thresholds were reached.

Germination Stage:

In this stage, as shown in Fig. 9, the seeds start to sprout, and roots and shoots begin to develop. The Arduino system can monitor and regulate the temperature through temperature sensors (e.g., DHT11, as shown in Fig. 2.) and heating elements to maintain the ideal germination temperature. The germination stage saw the emergence of the radicle and shoot from the seed. The controlled heating elements system maintained a stable temperature of 25-30°C, promoting rapid and uniform germination. Researchers can program Arduino controllers to create customized growth profiles for different plant species. This adaptability is particularly valuable for experiments and research [3].



Figure 9: Germination Stage

Monitoring and Data Collection:

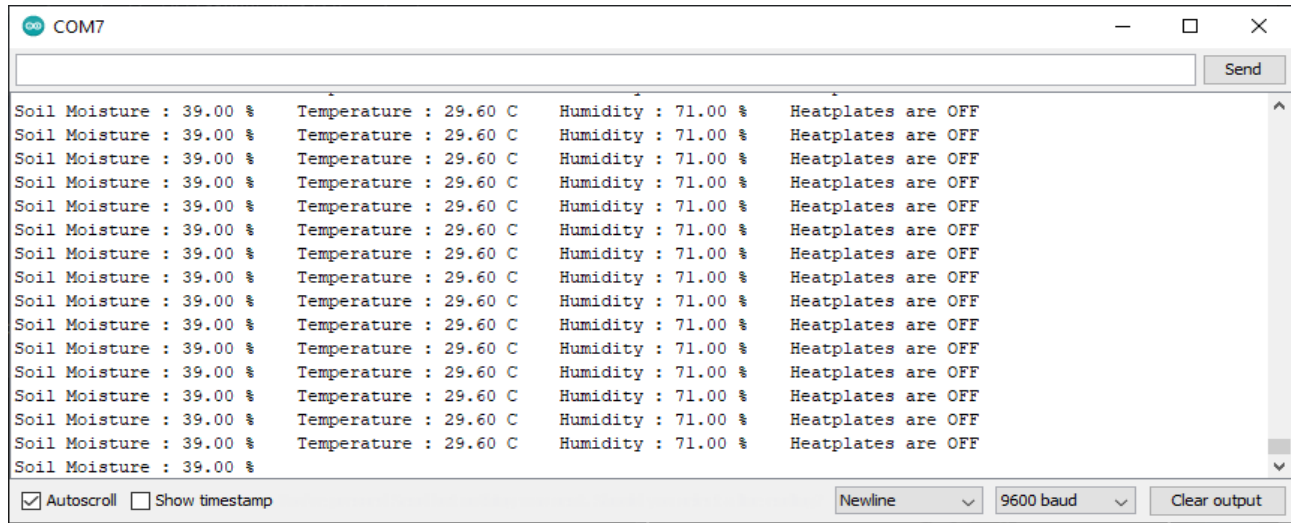


Figure 10: Serial Monitor displaying the live data

Table I. Data of the sensors

| S.no | Readings | | | |
|------|---------------|-------------|----------|------------|
| | Soil Moisture | Temperature | Humidity | Heatplates |
| 1 | 39 % | 29.6° C | 71.7% | OFF |
| 2 | 40 % | 29.5° C | 71.6% | OFF |
| 3 | 48 % | 23.5° C | 64.8% | ON |
| 4 | 49 % | 23.6° C | 64.7% | ON |

Throughout all stages of corn seed germination, Arduino-based data logging can be implemented to continuously record environmental parameters, such as temperature, humidity, and moisture levels. Table. 1 shows the environment which was required for the seed to germinate. Arduino-based systems can continuously monitor soil moisture levels, temperature, and light intensity, adjusting these parameters in real-time to create an optimal germination environment. This level of automation ensures higher germination rates and improved crop yields [4].

Seedling Growth Stage:



Figure 11: Seedling Growth

During the seedling growth stage, as shown in Fig. 11, the Arduino-controlled light source provided appropriate light intensity, mimicking natural daylight conditions. Light exposure was adjusted based on seedling growth requirements at different stages.

Table II. Temperature, Humidity and Soil Moisture Required for Different Seeds

| Seed Name | Seed Requirements | | |
|-----------|-------------------|----------------|------------|
| | Soil Moisture | Temperature | Humidity |
| Corn | 30% to 40% | 25° C to 30° C | 70% to 75% |
| Bean | 30% to 40% | 25° C to 30° C | 60% to 70% |
| Lettuce | 40% to 50% | 15° C to 25° C | 70% to 75% |
| Carrot | 20% to 30% | 15° C to 25° C | 70% to 80% |

Table. II shows the requirements of some seeds which can be used in the portable eco-friendly seed germination system.

Results:

Fig. 12 shows the final preview portable eco-friendly seed germination after the germination of seed. The Arduino-controlled portable seed germination system exhibited significant improvements in germination efficiency and seedling growth compared to uncontrolled conditions. The system achieved an average germination rate of 90% within 3-4 days, whereas uncontrolled conditions showed a germination rate of 70% within the same period. Seedlings grown under controlled conditions exhibited more robust growth, evident from increased shoot and root lengths and higher biomass accumulation.



Figure 12: Final preview of portable eco-friendly seed germination system after the germination of seed

Portable design of seed germination system

Fig 12. Shows a unique design of the portable eco-friendly seed germination system. As the word “portable” speaks of something which is light and small enough to be easily carried or moved. The portable Seed germination is the revolution to old seed germination models as it brings the feature to be easily carried anytime, anywhere without the getting worried about the seed.



Figure 13: Unique design allowing the system to change position in any direction

Fig. 13 shows a system that can be moved in any direction making it a portable eco-friendly seed germination system. The channels in the system allows the two environments to be moved, replaced and even withstand each other by its smart locking mechanism.



Fig 14. Unique design allowing the system to be kept on each other for carrying around

Fig. 14 shows the True feature of the portable eco-friendly seed germination system. The unique design allows the system to be transformed into its vertical form; bringing the center of mass in the middle, making it easy to carry around and to be locked while carrying to ensure the safety of the system.

CONCLUSION

This portable eco-friendly seed germination system using Arduino represents a promising and transformative advancement in sustainable agriculture. By leveraging the power of Arduino microcontrollers and intelligent automation, this system empowered growers with precise control over critical germination parameters, such as temperature, humidity, and soil moisture. The corn seed used in the system achieved an average germination rate of 90% where the system maintained a stable temperature of 25-30°C, 30-40% soil moisture, and 70-75% humidity whereas uncontrolled conditions showed a germination rate of 70% within the same period. The portable eco-friendly aspects of the seed germination system using Arduino are equally noteworthy. Incorporating low-power components and renewable energy sources aligns with sustainable practices, reducing the environmental impact while fostering resource-efficient seed germination.

REFERENCES

- [1] Biswas, A., et al. (2020). Arduino-based IoT platform for smart farming. In Proceedings of the 2020 International Conference on Smart Electronics and Communication (ICOSEC) (pp. 261-266). IEEE
- [2] Rahman, M. S., et al. (2020). Design and development of an energy-efficient IoT-based smart irrigation system. Sustainable Energy Technologies and Assessments, 41, 100819)



ICSET-23

*Proceedings of the 5th International Conference on Sustainable
Energy Technologies (ICSET 2023) Peshawar, Pakistan
14-15 December 2023*



UET Peshawar

- [3] Gomes, T. M., et al. (2019). An IoT-based agricultural decision support system: A comprehensive review. *Computers and Electronics in Agriculture*, 157, 436-453
- [4] Kadhim, A. A., et al. (2021). Design and Implementation of Arduino-Based Smart Irrigation System. *International Journal of Engineering Research & Technology*, 10(1), 79-82

Paper ID: ICSET-2317

ESTIMATING LITHIUM-ION BATTERY INTERNAL CIRCUIT PARAMETERS, OPEN CIRCUIT VOLTAGE AND AMPERE-HOUR CAPACITY AT DIFFERENT TEMPERATURES

Ejaz Ahmed^{1,2,*}, Babar Sattar Khan¹, Ihtesham Jadoon¹, Shahbaz Khan², Abdul Wadood²

¹Department of Electrical and Computer Engineering, COMSATS University Islamabad Attock Campus, Pakistan

²Electrical Engineering Department, Aerospace & Aviation Campus Kamra, Air University, Pakistan.

**Corresponding author*

Email: 225258@aack.au.edu.pk

ABSTRACT

Lithium ion battery internal resistance and Open Circuit Voltage (OCV) are important factors to be considered while design of (BMS) Battery Management systems for practical usage. There variations in different temperature conditions must be studied. This study uses polarisation capacitance and polarisation resistance within a Thevenin equivalent circuit model of a lithium battery and estimating those parameters through charge discharge test. Additionally, the paper explores the underlying factors contributing to the disparity in the RC time constant and provides a comprehensive characterization of the accurate determination of the RC time constant. Subsequently, the precise mathematical representation of the operational features of the circuit in two distinct states was derived. This study examines how temperature changes affect lithium-ion battery performance. Due to increased impedance, lower temperatures limit high-current applications. In contrast, higher temperatures accelerate capacity loss due to accelerated chemical reactions. Thermal cycling also degrades capacity. Battery longevity and performance depend on maintaining the right temperature. Results gained through experimentation and is useful in understanding behaviour of batteries From the results the main findings of paper are below freezing temperature battery is just 75% efficient and loses its 25% power due to losses.

KEYWORDS: BMS: Battery-management system; OCV: Open-Circuit Voltage; R_c: Series Resistance; SOC: State of Charge; R_p: Parallel Resistance; C_p: Branch Capacitance.

INTRODUCTION

Lithium-ion batteries are widely used in latest electronics equipment and are heart of modern electronics there is a need to design high energy and low cost batteries. Thus, the precise consideration and effect of internal resistance must be considered for reliable design. For accurate design of BMS as these factors are used for SOC (State of charge) estimation. Directly measuring the tiny physical properties of lithium batteries poses challenges for sensors and measurement methodologies [1]. The identification of parameters in analogous models of lithium batteries is a crucial concern within the field of battery management. [2]. the battery model can be categorised into three distinct models based on its various constituent mechanisms: the electrochemical model, the black box model, and the equivalent circuit model

[3]. The electrochemical model is founded upon the examination of chemical reactions occurring within the battery, and a partial differential equation is formulated to depict the dynamics of the electrodes and electrolyte [4]. This technology is well-suited for achieving optimal design and conducting safety analyses of batteries. The black-box model refers to a mathematical representation, which can be either linear or non-linear, that is utilised to describe the voltage response characteristics exhibited by batteries [5]. However, in order to provide adequate support, a data-driven algorithm is typically required. This may involve the utilisation of methods such as the neural network approach, support vector regression method, and particle filter method. [6]. The authors of reference [7] have suggested and validated a first-order equivalent Thevenin circuit model that incorporates self-healing features; this model was tested on an experimental platform. Lithium ion batteries structure is quite complex chemistry and variation between SOC and terminal voltage are not same open circuit voltage equals to terminal voltage, if we wait for 3 hours to allows charges to become stabilize so we have to test and applying charge and discharge current and finding the relation between both in form of higher order equations. Also with temperature variations we cannot fully charge and discharge battery to its full capacity due to complex interdependence in rate of chemical reactions with temperature changes. In this paper First portion includes the estimation of internal parameters secondly experimental results of OCV at both charge and discharge cycle and averaged plotted at four different temperatures 0, 10, 25 and 45⁰ Celsius. Third portion includes Charge and discharge capacity also includes the variations of internal resistance in full charge and discharge cycle at 25⁰ Celsius.

Battery modelling

In Figure 1 shows single branch RC model of Battery, the symbol Y_k denotes the terminal voltage of the battery, while R_i is battery series resistance. These parameters are used to describe the variation in voltage response during battery charging and discharging. The symbols R_1 and C_1 are used to denote the polarization resistance and polarization capacitance within the battery, respectively. The circuit comprising of resistor R_{tc} and capacitor C_{dl} is capable of accurately representing the gradual fluctuations in battery voltage that occur throughout the processes of charging and discharging. This standard model for lithium ion batteries used in latest algorithms for SOC and SOH estimation.

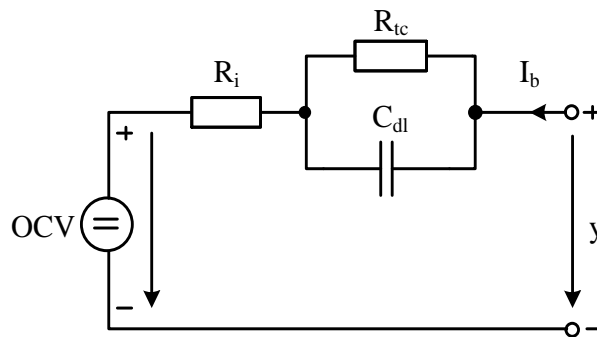


Figure 1: Model of Li-ion battery

The open circuit internal generated voltage and terminal voltage become nonlinear with inclusion of RC parallel equation is related as,

$$Y_k = OCV(Z_K, a_K) - V_{CdlK} - R_i I_K \quad (1)$$



Where $OCV(Z_k, a_k)$ is open circuit voltage, and is function of Impedance changes through cycle.

V_{Cdl} is voltage loss across parallel RC branch due to diffusion.

R_{tc} is Charge transfer loss across parallel RC which is resistive in nature.

R_i is ohmic loss due to heating.

Y_k is output terminal Voltage at K instant at battery terminal.

For test common lithium ion cell used in laptops is used having mAh rating of 3200 and 4.2 V this battery has been connected with sensing circuit to monitor current and voltages also for charging and discharging purpose battery tester is used for acquisition purpose lab-view software compatible with NI-Cyrio controller.

Table 1: Nominal Battery Rating

| No | Item | Specification |
|----|--------------------------|---------------|
| 1 | Type | NCR 18650-B |
| 2 | Ccapacity of Battery | 3200 mAh |
| 3 | Maximum voltage | 4.2 V |
| 4 | Charging Cut off Current | 0.31 A |
| 5 | Rated voltage | 3.6 V |
| 6 | Cut off voltage | 2.5 V |

METHODOLOGY

The process of determining the battery equivalent circuit model and its parameters involves two significant phases. The initial task is determining the pulse sequence to charge and discharge of the battery. In order to assert in the time constant of R-C branches below is flow diagram of whole process.

It is necessary to analyze the data collected during the relaxation period. The transitory response of the circuit is determined by the R_0 and R-C branches of the equivalent circuit once the pulse current is no longer present. The subsequent significant stage involves the estimation of model parameters through the curve manipulation process. The first step involves conducting a pulse discharge or charge test in order to get data that captures the dynamic behavior of the battery. In the context of pulse discharge testing, the rest curve behavior exhibits characteristics like the charge dynamics of an RC circuit. In this scenario, equation 2 is employed as the fitting function to analyze and interpret the results. The behavior of the rest curve in a pulse charge test exhibits dynamics similar to the discharge dynamics of an RC circuit can be modelled by equation 3.

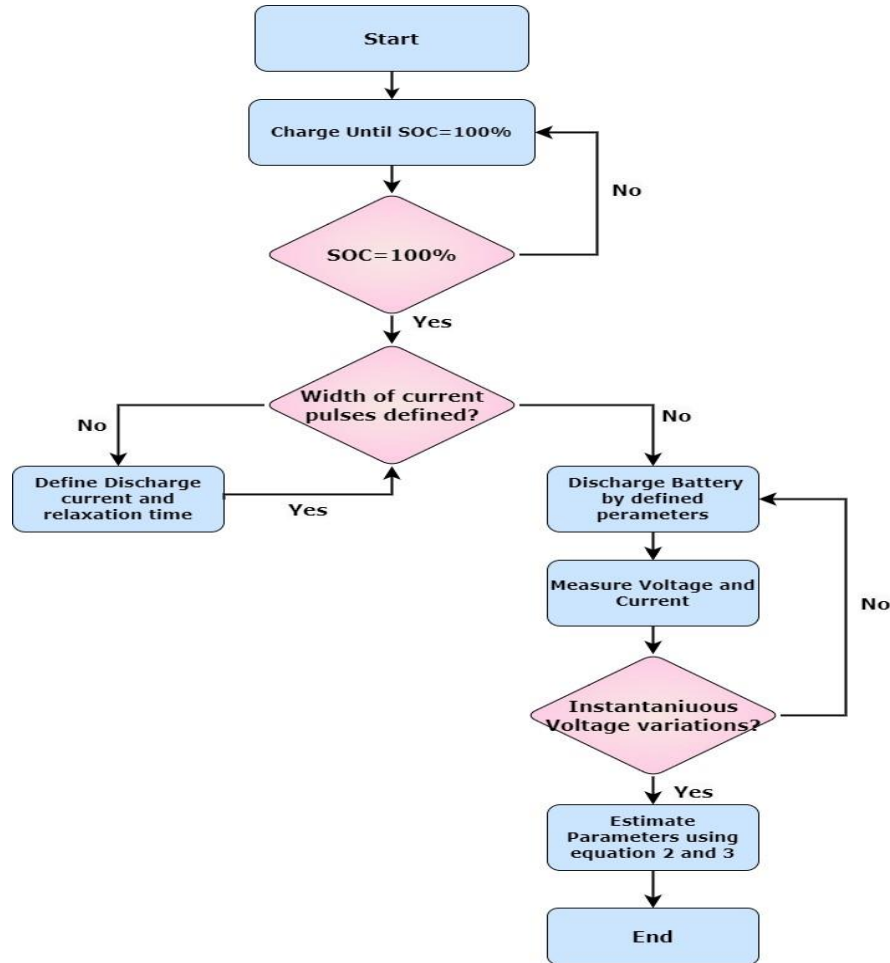


Figure 2: Process Flow Chart

$$V(t) = V(f) + V_1 (1 - \exp(-\frac{t}{T})) \quad (2)$$

$$V(t) = V(f) + V_1 (\exp(-\frac{t}{T})) \quad (3)$$

Step 2: Individually allocate the remaining curves to accommodate each of them independently. Figure 3 depicts the behavior of battery dynamics, specifically highlighting the pulse that offers significant insights into the (OCV) and circuit dynamics at the specified (SOC). Understanding the specific contributions of each constituent to the dynamic behavior of a system is of utmost significance. The resistance component, denoted as R_0 , is accountable for the immediate change in voltage, whether it be a drop or increase. On the other hand, the resistance-capacitance (R-C) branches are responsible for the occurrence of transients. One notable observation is to the prolonged settling period.[8] uses same time constant approach for different models.

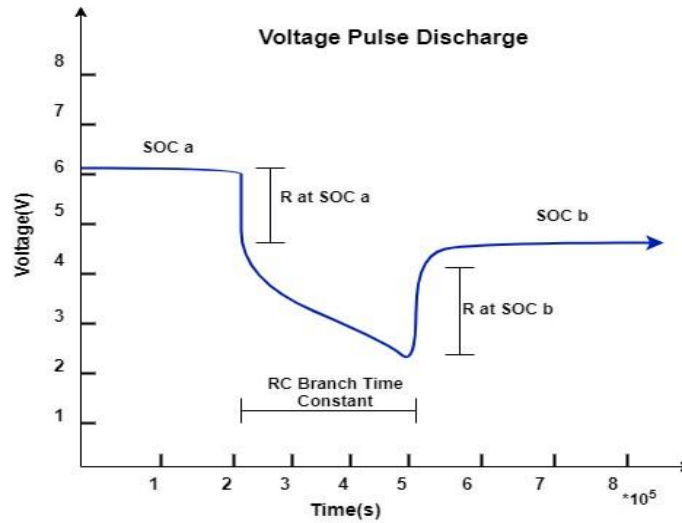


Figure 3: Voltage change at Discharge cycle

The value of series resistance is computed from ratio of change in voltage at SOC a and SOC b to change in value of discharging current average value at both instants is considered series resistance whereas branch resistance is computed from difference formula of change in voltage to change in current from region of (2 to 5) $\times 10^5$ seconds as shown in above figure 3 and value of capacitance of branch is computed by dividing time constant value with resistance i.e. $C_p = \tau/R_p$.

RESULT AND DISCUSSION

The internal resistance one series resistor and parallel RC branch is computed at full charge and discharge cycle by applying 16 pulses each 159 mAh for 15 minutes having gap of 3 hours in between then 4 pulses then 2 and last CV pulse as shown in Figure.4 is applied from these pulses voltage response is plotted and using current and voltage pulse shape resistance is calculated.

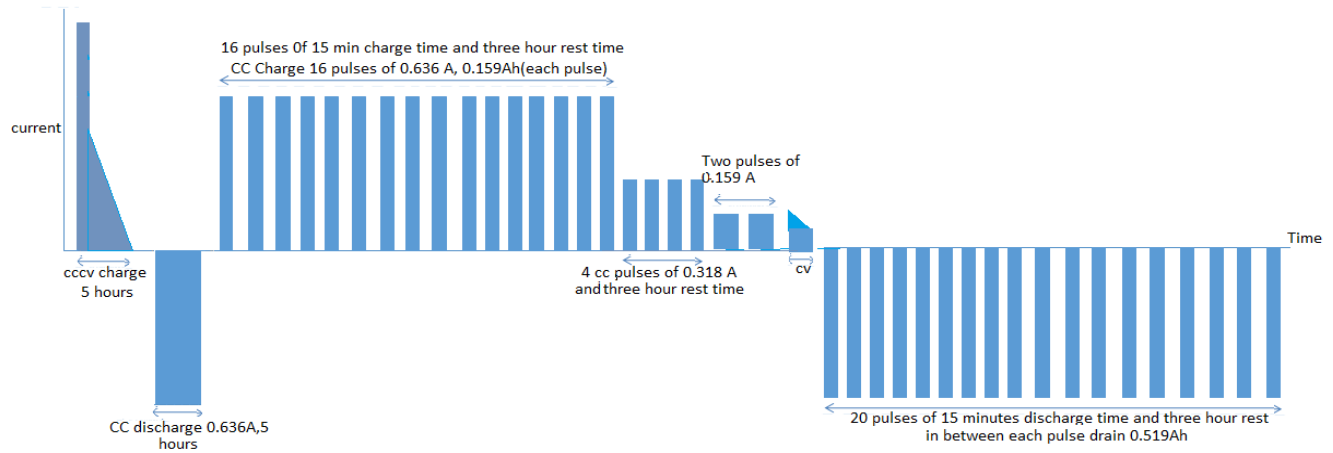


Figure 4: Current pulses for Charging and Discharging

Shows full charge and discharge voltage up and below is the current pulses with temperature monitoring with thermal camera results.

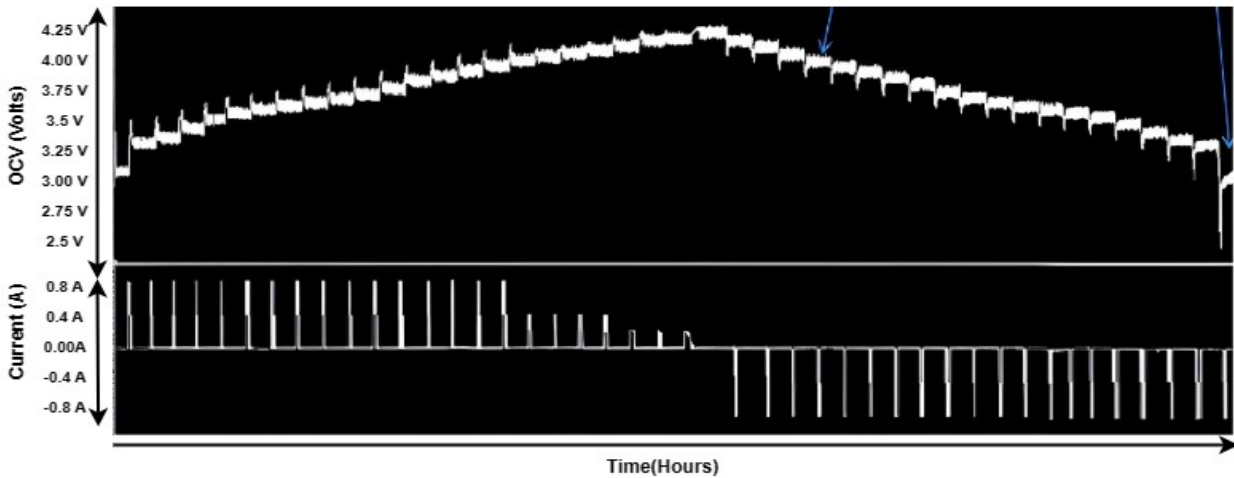


Figure 5: Temperature of battery at various time

Fundamental physical processes influence the circuit parameters of lithium-ion batteries during charge and discharge cycles at varying temperatures. Due to decreased ion mobility, lower temperatures increase internal resistance, whereas higher temperatures decrease resistance. Temperature-induced alterations in the double-layer capacitance at electrode-electrolyte interfaces have an effect on capacitance. Temperature also impacts voltage response times, resulting in voltage hysteresis at low temperatures. In addition, elevated temperatures can hasten capacity degradation due to increased side reactions and material degradation.



These series and parallel elements are very important and used in as model parameters during design of Charge convertors simulations. As the battery ages the value of series resistor become higher so this parameter can be used to find the useful life left in battery. These parameters are used in accurate SOC estimation Algorithms such as Kalman Filter these parameters can also be estimated using Recursive Least Square for that we need online parameter estimation and full profile data. These parameters are also computed with EIS (Electro Chemical Impedance) Spectroscope which plots the Neiquist plot from SOC data.

Table 2: Equivalent circuit parameters

| Soc | Charging | | | Soc | Discharging | | |
|-----|----------------|----------------|------|-----|----------------|----------------|-------|
| | Rs(Ω) | Rp(Ω) | Cp | | Rs(Ω) | Rp(Ω) | Cp |
| 5 | 0.169 | 0.076 | 7365 | 95 | 0.169 | 0.016 | 13828 |
| 10 | 0.3078 | 0.0307 | 9622 | 90 | 0.17 | 0.016 | 78075 |
| 15 | 0.15 | 0.041 | 4136 | 85 | 0.14 | 0.04 | 14620 |
| 20 | 0.22 | 0.03 | 8706 | 80 | 0.11 | 0.016 | 13737 |
| 25 | 0.153 | 0.0153 | 1893 | 75 | 0.177 | 0.016 | 26550 |
| 30 | 0.14 | 0.074 | 2875 | 70 | 0.161 | 0.048 | 16727 |
| 35 | 0.153 | 0.0303 | 1160 | 65 | 0.161 | 0.048 | 5550 |
| 40 | 0.178 | 0.01 | 2392 | 60 | 0.193 | 0.032 | 8225 |
| 45 | 0.167 | 0.046 | 5143 | 55 | 0.161 | 0.016 | 18248 |
| 50 | 0.169 | 0.061 | 7524 | 50 | 0.161 | 0.016 | 20559 |
| 55 | 0.12 | 0.046 | 6530 | 45 | 0.161 | 0.012 | 22266 |
| 60 | 0.152 | 0.015 | 1504 | 40 | 0.161 | 0.032 | 7875 |
| 65 | 0.17 | 0.03 | 7652 | 35 | 0.13 | 0.048 | 1916 |
| 70 | 0.13 | 0.03 | 8126 | 30 | 0.14 | 0.064 | 5800 |
| 75 | 0.147 | 0.04 | 7125 | 25 | 0.161 | 0.064 | 6787 |
| 80 | 0.164 | 0.03 | 8046 | 20 | 0.161 | 0.048 | 13390 |
| 85 | 0.15 | 0.024 | 6766 | 15 | 0.161 | 0.048 | 975 |
| 90 | 0.146 | 0.03 | 4163 | 10 | 0.187 | 0.048 | 1300 |
| 95 | 0.33 | 0.06 | 1478 | 5 | 0.31 | 0.11 | 2387 |
| 100 | 0.06 | 0.04 | 6000 | 0 | 0.58 | 0.35 | 3813 |

Above **Table 2** shows the values of resistances and capacitances It includes data from both charging and discharging cycle From the computations it is seen that series resistance remains fairly constant after 10% SOC i.e. 0.2 Ohms as shown in Table 2

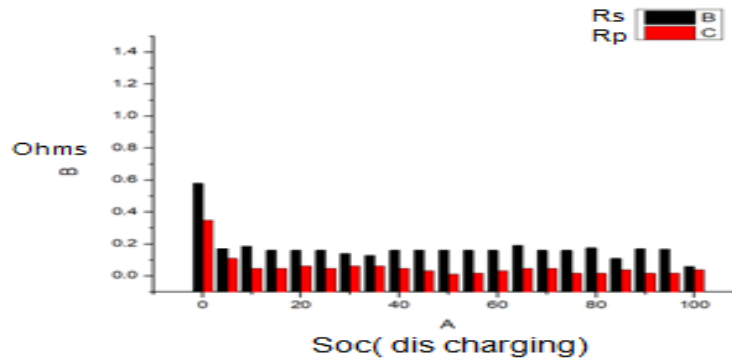


Figure 6: Series and Parallel resistance

The black bars represent series resistance and red bars represents parallel branch resistance each are plotted against SOC. The variation of parallel capacitor responsible for transient response is order of thousands of farads which is also plotted against SOC.

The variation of open circuit voltage from fully discharge SOC 0 to 100% can be seen that at every temperature initially open circuit voltage rises sharply up to 20% then fairly remains constant it is due to fact that initial series resistance is maximum and remain constant it can be seen that open circuit is 3.11V at 45^o C and with decreasing temperature increases to 3.3V it can be seen that with increase in temperature OCV decreases the relation between temperature and OCV. From Figure. 7 it can be seen that OCV curve shifts upwards with reduction in temperature and have inverse relation.

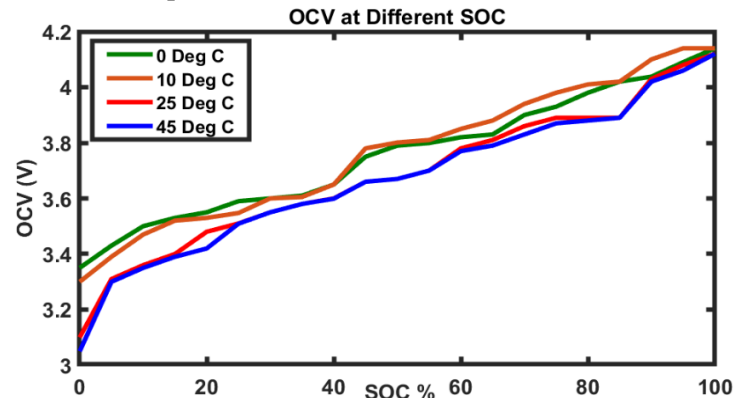


Figure 7: Open Circuit Voltage at different Temperatures

For capacity measurement battery is firstly charge in CCCV mode with values of current 0.2C up to maximum voltage there will remain some capacity which will be charged by applying CV mode 4.2V till charging current becomes approximate zero. Then through ampere hour counter using lab-view code we can compute capacity for discharge use 0.2C in CC mode and note capacity. Same procedure was applied at 5 different temperatures and following are observations in Figure. 8, shows capacity reduction with temperature effect.

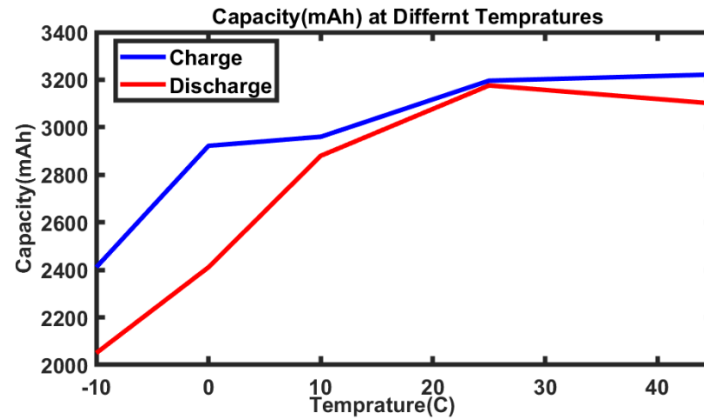


Figure 8: Open Circuit Voltage at different Temperatures

From the results it can be seen that below freezing temperature battery is just 75% efficient and at room temperature and above almost rated value ie 3200mAh is obtained. also from curve as seen in Figure. 8 it is seen that usefull energy loss during charge and discharge is almost same at room temperature and is considerable value below freezing. and parallel resistance has also same response.

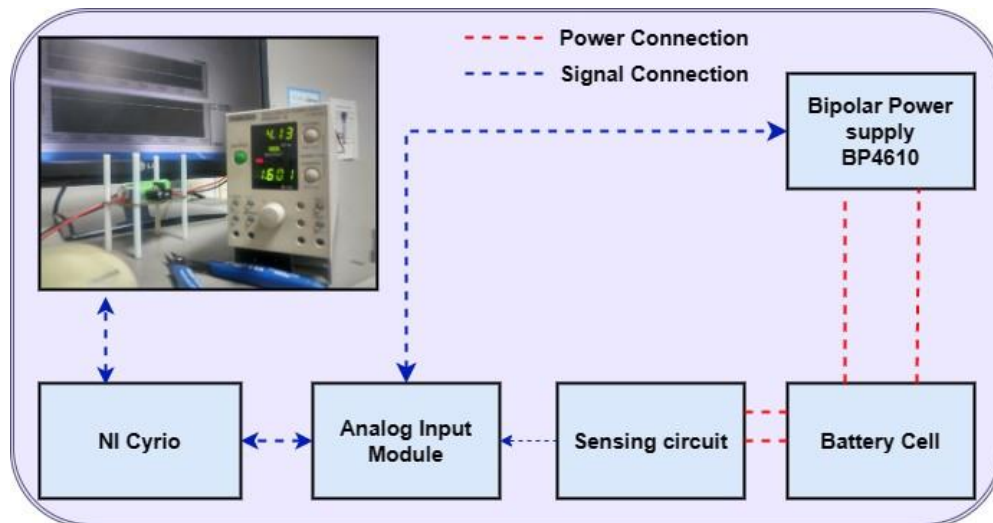


Figure 9: Experimental Setup

In accordance with the plan shown in Figure 9, laboratory experiments were conducted at the stand. It consists of tested battery NCR 18650-B, programmable electric power supply BP4610, a National Instruments Ni Cyrio, analog Input Chase for measuring device, and current sensor.

CONCLUSION

From the experimental data it is concluded that with the increase in temperature the open circuit voltage is decreased capacity also decreases while lowering temperature. And internal resistance becomes fairly constant after 10% SOC the experimental setup is shown in Figure. 8 with power supply battery setup and Lab-view for data acquisition. The analysis of accurate perimeter can help to find useful life of device further temperature variation analysis help manufacturer to take possible steps in material design to compensate temperature factor by packaging or changing material. Further future work can be done by include online parameter estimation with temperature effects, and can increase the reliability of BMS systems.

REFERENCES

- [1] Peng, J., Jia, S., Yang, S., Kang, X., Yu, H. and Yang, Y., 2022. State estimation of lithium-ion batteries based on strain parameter monitored by fiber Bragg grating sensors. *Journal of Energy Storage*, 52, p.104950.
- [2] Cheng, K.W.E., Divakar, B.P., Wu, H., Ding, K. and Ho, H.F., 2010. Battery-management system (BMS) and SOC development for electrical vehicles. *IEEE transactions on vehicular technology*, 60(1), pp.76-88.
- [3] Vermeer, W., Mouli, G.R.C. and Bauer, P., 2021. A comprehensive review on the characteristics and modeling of lithium-ion battery aging. *IEEE Transactions on Transportation Electrification*, 8(2), pp.2205-2232.
- [4] Pramanik, S. and Anwar, S., 2016. Electrochemical model based charge optimization for lithium-ion batteries. *Journal of Power Sources*, 313, pp.164-177.
- [5] Khalfi, J., Boumaaz, N., Soulmani, A. and Laadissi, E.M., 2021. Box–Jenkins black-box modeling of a lithium-ion battery cell based on automotive drive cycle data. *World Electric Vehicle Journal*, 12(3), p.102.
- [6] Dong, G., Zhang, X., Zhang, C. and Chen, Z., 2015. A method for state of energy estimation of lithium-ion batteries based on neural network model. *Energy*, 90, pp.879-888.
- [7] Pei, Z., Zhao, X., Yuan, H., Peng, Z. and Wu, L., 2018. An equivalent circuit model for lithium battery of electric vehicle considering self-healing characteristic. *Journal of Control Science and Engineering*, 2018.
- [8] Rajanna, B.V. and Kumar, M.K., 2020. Comparison of one and two time constant models for lithium ion battery. *International Journal of Electrical & Computer Engineering (2088-8708)*, 10(1).



ICSET-23



UET Peshawar

Paper ID: ICSET-2318

CLIMATE CHANGE IMPACTS ON SUSTAINABLE BIOENERGY GENERATION IN PAKISTAN

Aqib Nawaz Khan^{1,*}, Muhammad Osama Aziz², Yousaf Salim¹, Muhammad Usman Khan¹, Muhammad Uzair Khan²

¹Department of Energy Systems Engineering, U.S. Pakistan Centre for Advanced Studies in Energy (USPCAS-E),
National University of Sciences & Technology (NUST), Islamabad, Pakistan

³Department of Mechanical Engineering, University of Engineering and Technology Peshawar, Pakistan

**Corresponding author*

Email: aqbikhan@yahoo.com

ABSTRACT

Climate change poses a significant existential risk to contemporary society, since it jeopardizes critical infrastructure and causes disruptions in many energy subsectors, particularly in emerging nations. The importance of strategic climate predictions cannot be overstated in the effective management of future bioenergy resources, particularly in nations with abundant agricultural resources. This research investigates the complex relationship between temperature, precipitation, and agricultural productivity, with a specific emphasis on Pakistan as a case study. Drawing upon data derived from the fifth phase of the Coupled Model Intercomparison Project (CMIP5) with a spatial resolution of 25 km, our study uses a predictive approach to estimate the potential yields of wheat, maize, rice, and sugarcane. This estimation is contingent upon the consideration of optimal growth circumstances, as well as the influence of temperature and precipitation. The study reveals significant disparities in agricultural productivity among urban areas in Pakistan. Muzaffarabad and Quetta have been identified as prominent centres for wheat production, with yields of 3083.3 and 3319.28 Kgs/Hec., respectively, during the time periods of 2081-2099 and 2061-2080. Peshawar and Sibi demonstrate promising prospects for maize cultivation, with yields ranging from 6717 to 6801 Kgs/Hec. It is projected that Bannu will yield a quantity of rice ranging from 2576.25 to 2616.84 Kgs/Hec. between the years 2041 and 2060. Similarly, Muzaffarabad is expected to produce a rice yield ranging from 2640 to 2681 Kgs/Hec. Islamabad exhibits considerable potential with a yield of 69422 Kgs/Hec. in the period of 2041-2060, and 70101 Kgs/Hec. in the period of 2081-2099, subject to variations in precipitation. The impact on planting seasons is of significance, as it has the ability to elicit beneficial outcomes in multiple urban areas, hence facilitating enhanced agricultural yield. The present study investigates key aspects, namely agricultural residue ratios and characteristics associated to biofuels. Significantly, this study finds cities that are highly suitable for the establishment of future bioenergy facilities, using a thorough set of criteria. This research highlights the importance of implementing bioenergy policies that consider the implications of climate change. By comprehensively examining the complex interplay between climate variables and crop productivity, this study provides valuable insights that can guide evidence-based policy formulation. The results of our study provide essential guidance for the development of sustainable bioenergy production in Pakistan. These findings offer useful insights into effectively addressing the difficulties presented by climate change, while simultaneously promoting economic growth and environmental conservation.



ICSET-23



UET Peshawar

KEYWORDS: Climate Change Impacts, Bioenergy Generation, Temperature and Precipitation, Representative Concentration Pathways (RCPs) 4.5 & 8.5, Crops

INTRODUCTION

It's important to remember that numerous subsystems work together to determine Earth's climate and weather. Human activity has dominated global climate since the middle of the 20th century. The Intergovernmental Panel on Climate Change forecasts a 0.5 °C increase in world average temperature over the 20th century. Mccarl et. Al. [1] predicting a rise of up to 1.4 °C by the end of the twenty-first century. Greenhouse effect emissions, osmotic stress, and poor air quality are all related with the use of fossil energy, which is currently the largest energy source in the world and a major contributor to climate change [2], [3]. Many scientists anticipate that climate change would alter river hydrological cycles in the Himalayas, affecting hundreds of millions of people [4], [5].

Bioenergy is most affected by climate change, but it also has the greatest chance for scientific and financial innovation to combat global warming. Widespread usage of land-intensive bioenergy feedstocks may harm the ecology, economy, and climate [6]. Production, use, and regulation stakeholders are seeking to quantify sustainability as bioenergy output rises. Since sustainability is a set of evolving goals rather than a fixed state, assessments must weigh the pros and downsides of different approaches. Sustainability is affected by the environment, economics, and society, which can be measured in many ways [7], [8]. Future climate change projections help manage bioenergy resources such catastrophic flooding, droughts, and sustainable farming in areas with high bioenergy production potential [9]. Climatic change studies also depend on general circulation model (GCM) climate projections [10]. Due to climate data ambiguity, high-altitude studies with limited data can be trusted less [11].

Global warming would affect crop productivity in several nations by changing temperature and precipitation. The country's latitude, terrain, and other factors determine the damage. Climate change may alter topsoil pH, soil humidity, and temperature, which affect crop development [12]. Climate change may affect agricultural productivity directly and indirectly. Changes in soil composition, insect infestations, diseases, and weeds are indirect effects of temperature and precipitation fluctuations [13]. McBride et al. created a 19-characteristic framework with 6 categories to evaluate bioenergy systems' environmental impact (soil condition, water quality and extent, greenhouse gases, biodiversity, air quality, and productivity). The suite is designed to capture bioenergy's main environmental impacts across diverse channels, locales, and management measures [14]. An optimization-assessment strategy for sustainable bioenergy production was created to generate cost-effective and ecologically friendly strategies and policies by altering livestock and crop patterns, distributing water and energy resources, and considering system uncertainties [5]. Kung et al. used a stochastic programme with recourse integrated model to examine how water rivalry between sectors may affect agronomic practices and bioenergy growth. This model optimises bioenergy generation while considering future water usage equilibria [15]. Detrended Quantile Delta Mapping Quantile Mapping and other statistical downscaling/bias-correction strategies can help Pakistanis comprehend past, present, and future severe events (1996–2095). From 1976 to 2095, QDM was the only way to maintain long-term climate change signals [16].

All of these recent bioenergy studies, as well as most of others before them, provided thorough data on various countries or regions that were especially sensitive to climate change during the century. No



ICSET-23



UET Peshawar

Pakistani studies have compared climate change-induced temperature and precipitation. This research does not evaluate CMIP5, bias correction, etc. This research quantifies climate factors (temperature and precipitation), forecasts Pakistan's most significant crops, and determines which city will be most adaptable to climate change in terms of crops and bioenergy in the coming century.

MATERIALS AND METHODS

Study Area

The South Asian area has been identified as a "Hub" for changing climate, and the melting of snow and glaciers is expected to have far-reaching consequences for the region's bioenergy capacity [4], [5]. Islamic Republic of Pakistan (Pakistan) is a country in South Asia at 30.3753° N, 69.3451° E. Pakistan's varied landscape and weather patterns reflect the country's rich cultural history. Tropical to temperate, with drier southern coastal areas. Due to heavy rain during monsoon season, flooding is common. Pakistan has four seasons: a cool, dry winter (December–February), a warm, dry spring (March–May), a wet summer (June–September), and a windy fall (October–November). Extreme variations in annual rainfall are common, as are stretches of both drought and flooding [17].

This article examines cities from many Pakistani provinces, each with its distinct climatic and physical characteristics (Figure 79). Each of the provinces of Balochistan and Khyber Pakhtunkhwa has two cities, while the provinces of Gilgit Baltistan, Punjab, Azad Kashmir, and the Islamabad Capital Territory only have one.

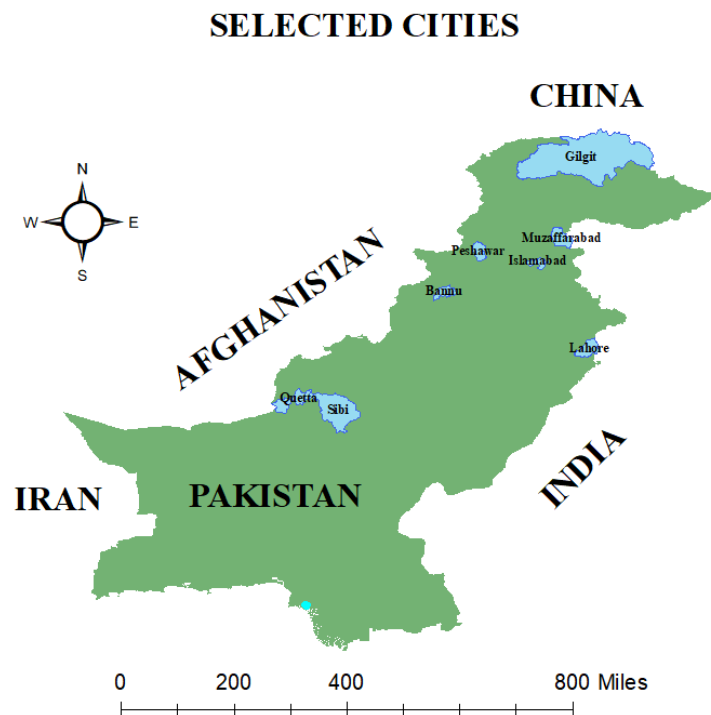


Figure 79: Geographical location of Pakistan and the cities under observation (study area)

Datasets

Table S1 displays monthly data from the Pakistan Meteorological Department (PMD), Research and Development wing, for key ecological indicators of agricultural waste or bioenergy, including mean temperature, mean dry bulb temperature at 0300 UTC, precipitation, and mean relative humidity at 0300 UTC, from 2000 to 2020 at eight different sites. These locations include Gilgit, Quetta, Muzaffarabad, Islamabad, Peshawar, Bannu, Lahore, and Sibi.

The rate of increase in each city's mean temperature over time was then used to rank them. Independent estimates for mean temperature and precipitation are shown in ArcGIS's Table 11 and Figure 80. Experts from the Research and Development (R&D) division of the Pakistan Meteorological Department (PMD) have previously reviewed the accuracy and usefulness of this dataset, but it has been validated over the past decade by comparison to data obtained from the meteorological station at the National University of Science and Technology (NUST).

Table 11: Profiles of study area between time period 2000-20 (a) Temperature (°C) (b) Precipitation (mm)

| CITIES | Average Temperature (°C) | Average Precipitation (mm) |
|--------------|--------------------------|----------------------------|
| Gilgit | 16.10417 | 145.1625 |
| Quetta | 17.4425 | 233.5992 |
| Muzaffarabad | 20.47417 | 1417.56 |
| Islamabad | 21.52917 | 1283.833 |
| Peshawar | 23.20417 | 577.6283 |
| Bannu | 23.3425 | 354.0867 |
| Lahore | 24.90833 | 670.805 |
| Sibi | 27.0575 | 205.6092 |

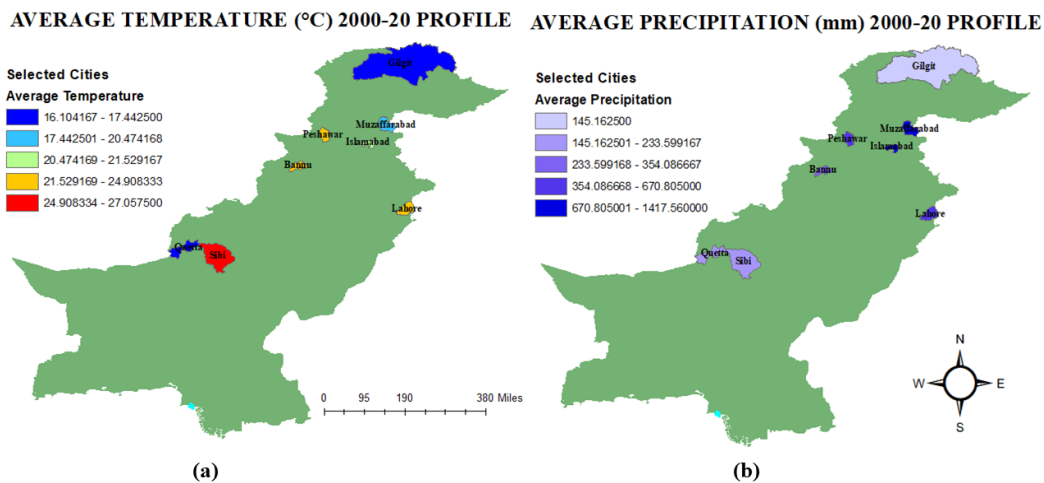


Figure 80: Profiles of study area between time period 2000-20 (a) Temperature (°C) (b) Precipitation (mm)



ICSET-23



UET Peshawar

Using the CMIP5 repository's publicly available representative concentration pathways (RCPs) from March 2013, we modelled future climate change [18]. The results of the Climate Explorer KNMI programme were compared to the PMD's expected mean temperature and precipitation data at a 25km resolution, and the results of the simulation were also checked against historical data. This research extrapolated the yield of many crops into the future of 2100 using data for the year 2020 gathered from the database of the Pakistan Bureau of Statistics. To better understand the trend changes of these crops presented in Table S2, data from the database of the Pakistan Bureau of Statistics was analyzed for the time period 2016-17 to 2020-21 (P) [19].

This research examined Pakistan's major crops—wheat, maize, rice, and sugarcane. The Pakistan Bureau of Statistics estimates agricultural yields. Pakistan's food security depends on wheat, its main crop. Table S2 shows the contribution of these crops to GDP [19].

Experimental Design

We selected eight cities, collected their data, and predicted the climate using two RCPs (4.5 and 8.5) for 2100. We calibrated them against the PMD database and Climate Explorer KNMI programme. Target crop production was studied. The future situation was divided into four 20-year periods (2021-40, 2041-60, 2061-80, and 2081-99) then extrapolated using a model across the century to eliminate uncertainty. Pakistani target crops were considered.

MODEL

Stage-I

We calibrated climate model evaluations using PMD and Climate Explorer KNMI. This section details strategies. Climate models are not perfect, therefore simulated and observed climatology will differ. As the projection develops, the expected climate shift will confuse the model state's climate approach. Short-term climate estimates are bias-corrected [20].

Pakistan grows two seasons. "Kharif" is the first planting season. Rice, sugarcane, cotton, maize, moong, mash, bajra, and jowar dominate this season's agriculture. "Rabi," is the second season. Mostly wheat, gramme, lentil (masoor), tobacco, rapeseed, barley, and mustard. The agriculture industry performed well in 2020–21, rising 2.77% instead of 2.8%. Wheat, rice, sugarcane, maize, and cotton grow 4.65% annually [19] Table 12 shows the approved crop calendar for Pakistan.

Table 12: Approved crop calendar for Pakistan

| DATES OF RELEASE OF CROP ESTIMATES | | | |
|------------------------------------|-----------|-----------|------------|
| CROPS | First | Second | Final |
| Wheat (Rabbi) | 1st Feb. | 1st April | 1st August |
| Maize (Kharif and Rabbi) | - | - | - |
| Rice (Kharif) | 1st Sept. | 1st Dec. | 1st Feb. |
| Sugarcane (Kharif) | 1st July | 1st Nov. | 1st April |



ICSET-23



UET Peshawar

The yield information for the intended crops as analyzed in section 2.2 follows. We look at how they've changed over the past few years and what percentage of a shift there has been. Following that, the perfect conditions are examined. Wheat grows best between 19 and 22 °C [21], maize between 28 and 34 °C [22], rice between 25 and 35 °C [23], and sugarcane between 27 and 38 °C, according to the literature. Variable yield losses occur across crops for every degree Celsius as the temperature rises. Wheat yields fall by 6% for every 1°C rise in temperature [21], [24]–[26], maize yields by 7.4% for every 1°C increase in temperature [22], [25], [27], rice yields by 3.2% for every 1°C increase in temperature [23], [25], and sugarcane yields by 10% for every 1°C increase in temperature. Wheat requires between 500 and 750 mm [28]–[30], maize between 500 and 1000 mm [25], [31], [32], rice between 1000 and 2520 mm [25], [32], [33], and sugarcane between 1000 and 1500 mm [32], [34]–[37] for maximum development.

Stage-II

Then, in the stage-II, we employed the extrapolation method [38]. We then compared how much different crops might suffer from temperature or precipitation drops. Next, we assessed how far off each city's anticipated temperature or precipitation was. If the weather was good, the projected harvest was assessed. The study uses independent estimates because agricultural yield depends on several parameters, including temperature, precipitation, humidity, water availability, land, etc.

Stage-III

Bioenergy generation depends mostly on RCR, the ratio of agricultural residual to crop output. Environmental indicators may be needed throughout biofuel manufacturing. The supply chain includes raw material manufacturing, management, processing, and application. Most of these classes apply to the first two stages of the supply chain (feedstock generation and harvesting), whereas only a few apply to the third and fourth stages. In the beginning, when there are more categories to choose from and they are more diversified, it is harder to prioritise and assess indicators. Consider the context while selecting and interpreting biodiversity indicators. Indicators can be used for site-specific recovery programmes and regionally vulnerable species habitat requirements. Bioenergy generation depends mostly on RCR, the ratio of agricultural residual to crop output. Environmental indicators may be needed throughout biofuel manufacturing. The supply chain includes raw material manufacturing, management, processing, and application. Most of these classes apply to the first two stages of the supply chain (feedstock generation and harvesting), whereas only a few apply to the third and fourth stages. In the beginning, when there are more categories to choose from and they are more diversified, it is harder to prioritise and assess indicators. Consider the context while selecting and interpreting biodiversity indicators. Indicators can be used for site-specific recovery programmes and regionally vulnerable species habitat requirements [39]. Figure 81 summarizes the whole methodology performed in this research.

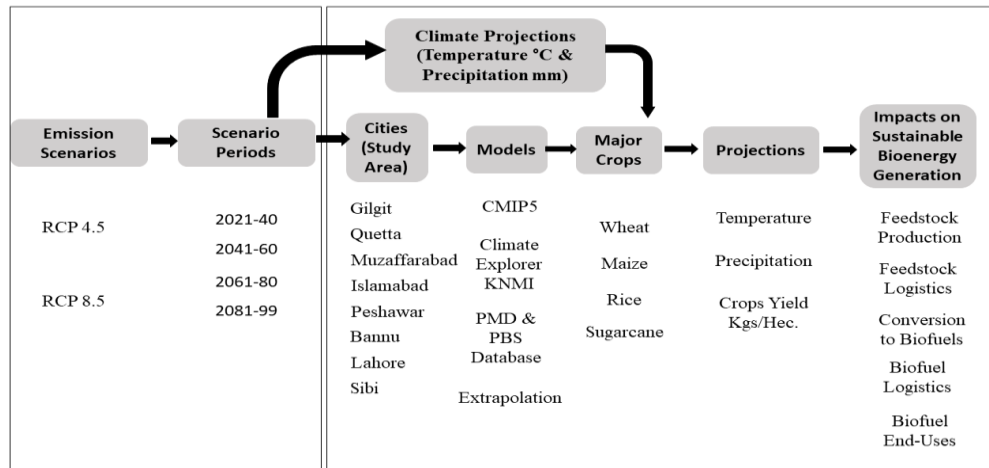


Figure 81: Methodology flowchart adopted in this study

Figure 81 explains that we conducted an in-depth analysis of gathered data using two prominent climate models, namely RCPs 4.5 and 8.5, and incorporated four different models: CMIP5, Climate Explorer KNMI, PMD, and PBS Database and Extrapolation, as illustrated in Figure 2. Calibration and validation processes were rigorously applied to all four models across eight diverse cities, namely Gilgit, Quetta, Muzaffarabad, Islamabad, Peshawar, Bannu, Lahore, and Sibi. Our study focused on estimating the projected changes in temperature and precipitation for these selected cities. To enhance the accuracy of our modeling, we divided the future scenario, spanning from 2021 to 2099, into four distinct sub-scenarios, each covering 20-year periods (e.g., 2021–40, 2041–60, 2061–80, and 2081–99). This approach was adopted to minimize potential uncertainties inherent in the modeling process. In essence, our proposed factorial design method comprehensively addresses the risks associated with sample artifacts by exploring a wide range of simulation combinations.

RESULTS AND DISCUSSION

Climate Projections (Stage-I)

Bioenergy is reliant on several variables, because climate change affects the producing business, we focus on how temperature and precipitation effect bioenergy. Since their analysis has never been done in the context of climate change implications on sustainable bioenergy generation, we used CMIP5, PMD database, and Climate Explorer KNMI software for RCPs to analyse temperature and precipitation variations in eight cities with different climates across the nation. Each city's estimates using Pakistan Meteorological Department data. The IPCC Fifth Assessment Report (AR5) downscaled climate change scenarios to 25km. Climate affects behaviour. Two concentration paths illustrate the findings.

Temperature Projections

Forecasts of future temperatures are made using the RCP 4.5 and RCP 8.5 scenarios. A minimum of two cities are selected from each province in Pakistan. The following cities are being considered: Gilgit, Quetta, Muzaffarabad, Islamabad, Peshawar, Bannu, Lahore, and Sibi. They're listed in ascending order of

temperature. The entire century is divided into four sections: 2021–2040, 2041–2060, 2061–2080, and 2081–1999. Table 13 and Figure 82 display the average increases in temperature for the sections of the country under consideration.

Table 13: Average temperatures(°C) for each city across the century under RCP 4.5 and 8.5

| CITIES | RCP 4.5 | | | | RCP 8.5 | | | |
|--------------|---------|---------|---------|----------|---------|---------|---------|---------|
| | 2021-40 | 2041-60 | 2061-80 | 2081-99 | 2021-40 | 2041-60 | 2061-80 | 2081-99 |
| Gilgit | 11.566 | 12.8555 | 13.1777 | 13.62526 | 11.7793 | 13.4910 | 16.2788 | 18.7745 |
| Quetta | 18.1145 | 19.7055 | 20.4447 | 20.92995 | 18.5467 | 20.3785 | 22.9350 | 25.8364 |
| Muzaffarabad | 19.3629 | 20.4600 | 21.2174 | 21.61281 | 19.0518 | 20.5941 | 23.1045 | 25.4498 |
| Islamabad | 22.8213 | 23.8332 | 24.5381 | 25.29853 | 23.279 | 24.4904 | 26.7160 | 29.0832 |
| Peshawar | 24.3427 | 25.4571 | 25.9916 | 26.57703 | 24.5552 | 25.9730 | 28.3971 | 30.8219 |
| Bannu | 25.6726 | 26.6468 | 27.2680 | 27.63595 | 25.9101 | 27.1123 | 29.3060 | 31.5267 |
| Lahore | 25.4959 | 26.3356 | 27.3674 | 28.11789 | 26.0385 | 27.0970 | 29.4722 | 31.8423 |
| Sibi | 29.1083 | 30.2859 | 30.9331 | 31.31096 | 29.4302 | 30.8814 | 32.9023 | 35.2287 |

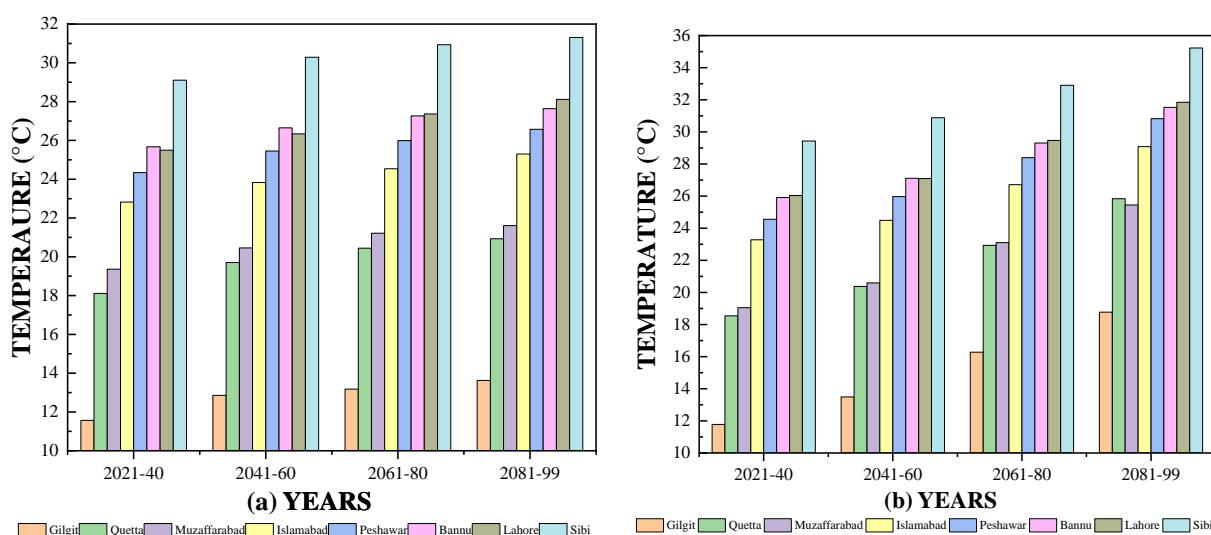


Figure 82: Average temperatures(°C) for each city across the century under RCP (a) 4.5 (b) 8.5

Table 13 and Figure 82 shows that the climate-related temperature rise under the intermediate RCP 4.5 scenario follows a rather constant trend over the time periods anticipated for the whole century. As expected [40], our findings reveal that the selected locations would see a temperature increase of around 1°C to 1.5°C between the years 2021–40 and 2041–60 as a result of the CO₂ that is trapped in the earth's atmosphere [41]. The decades 2061–2080 and 2081–2099, however, show a declining trend. The RCP 4.5 emissions scenario, a stabilization scenario that uses a variety of technologies and techniques to reduce greenhouse gas emissions, predicts that emissions will begin to decline after 2045–55, and that the rate of temperature increase would level off by the end of the century as the radiative forcing level

stabilizes at 4.5 W/m^2 before 2100 [40], [41]. With regards to agricultural output and bioenergy generation in the context of climate change, this scenario is somewhat positive.

Because to government-initiated steps and the shift to solar energy generation at the household level due to load shedding, Bannu has the lowest temperature rise (1.96327°C) throughout the century [42], with the highest growth of 3.8% between 2021-2040 and 2041-2060, followed by a fall after [40], [41]. Gilgit has the second-lowest temperature increase (2.05926°C), but its location and climate give it a unique pattern from Bannu [43].

Quetta, situated as it is on the Baluchistan plateau, experiences extremes of both hot summers and cold winters [44]. An increase of 2.81536°C in temperature is the most extreme effect of climate change on the city. Rapid population growth, polluting industries, cars, and chlorofluorocarbon-emitting refrigerators are the main contributors to this problem [45], [46]. The interconnected factors of industrialization, a large number of automobiles, and urbanization have led to the second- and third-highest temperature rises throughout the whole century in Lahore and Islamabad, respectively [47].

Table 13 and Figure 82 shows that under RCP 8.5, the temperature will increase by 7.2897°C (Quetta) by the end of the century, which is 39.34% more during the period of 2021–2099 [45], [46]. Bannu experiences the smallest relative temperature increase of any site (2.168 %, or 5.61661°C) between the years 2021 and 2099 under RCP 8.5 [42]. The average temperature rises in the country's selected areas due to climate change by the end of the century is projected to be 27.98%. Projections for the selected region based on RCPs are shown for the whole century in Figure 83.

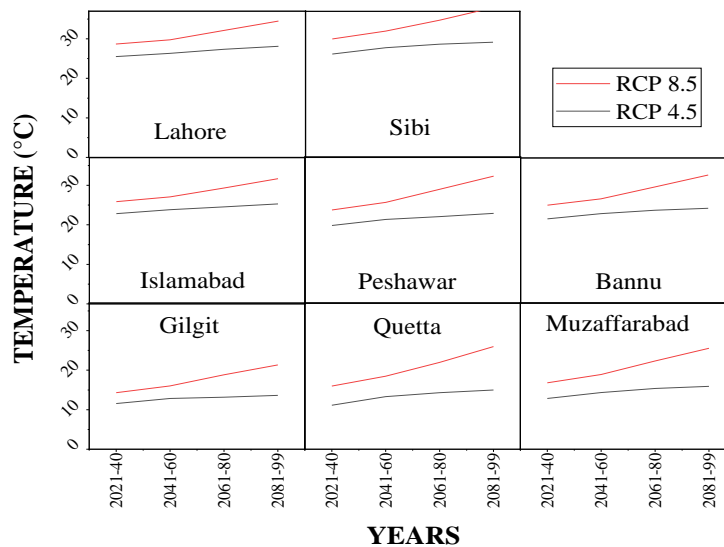


Figure 83: Average temperatures($^{\circ}\text{C}$) for each city across the century under RCP 4.5 and RCP 8.5

Precipitation Projections

Precipitation is predicted under the RCP 4.5 and RCP 8.5 scenarios. Each province in Pakistan has at least two of its major cities included. Gilgit, Quetta, Muzaffarabad, Islamabad, Peshawar, Bannu, Lahore, and Sibi are among the proposed host cities. They're scattered about at random in terms of precipitation. The entire century is broken up into four sections: 2021–40, 2041–60, 2061–80, and 2081–1999. Table 14 and Figure 84 show average increases in precipitation across the examined areas.

Table 14: Average precipitations(mm) for each city across the century under RCP 4.5 and 8.5

| CITIES | RCP 4.5 | | | | RCP 8.5 | | | |
|---------------------|---------|---------|---------|----------|---------|---------|---------|---------|
| | 2021-40 | 2041-60 | 2061-80 | 2081-99 | 2021-40 | 2041-60 | 2061-80 | 2081-99 |
| Gilgit | 135.2 | 127.196 | 134.789 | 142.8367 | 158.954 | 162.737 | 175.658 | 189.605 |
| Quetta | 275.6 | 259.284 | 274.763 | 291.1672 | 299.58 | 306.71 | 331.062 | 357.349 |
| Muzaffarabad | 1751.9 | 1648.18 | 1746.58 | 1850.855 | 1803 | 1845.91 | 1992.47 | 2150.67 |
| Islamabad | 1627 | 1530.68 | 1622.06 | 1718.9 | 1659.32 | 1698.81 | 1833.69 | 1979.29 |
| Peshawar | 501.22 | 471.547 | 499.699 | 529.5312 | 527 | 539.542 | 582.382 | 628.623 |
| Bannu | 412.4 | 387.985 | 411.148 | 435.6943 | 436.587 | 446.977 | 482.467 | 520.775 |
| Lahore | 920.6 | 866.100 | 917.806 | 972.5997 | 939.54 | 961.901 | 1038.27 | 1120.71 |
| Sibi | 429 | 403.603 | 427.698 | 453.2319 | 451.456 | 462.200 | 498.899 | 538.512 |

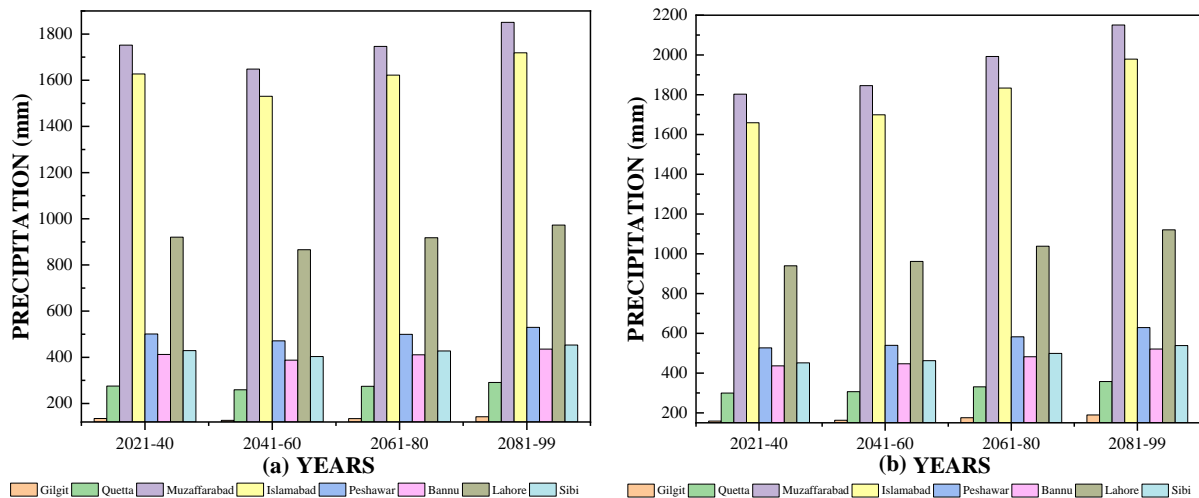


Figure 84: Average precipitations(mm) for each city across the century under RCP (a) 4.5 (b) 8.5

Changes in precipitation due to climate change are shown to follow a rather steady pattern throughout the whole century (as seen in Table 14 and Figure 84) under the intermediate RCP 4.5 scenario. Our findings confirm the expected decrease of 7-8% [48], [49] for the selected regions between 2021-40

and 2041-60 due to the CO₂ trapped in the earth's atmosphere and the subsequent rise in temperature [41]. However, the decades 2061–2080 and 2081–2099 saw a resumption of the trend toward growth. Radiative forcing is expected to stabilize at 4.5 W/m² by the turn of the century, as predicted by the RCP 4.5 emissions scenario, and the rate of precipitation drop is forecast to level out by the end of the century. The RCP 4.5 scenario is a stabilization scenario that uses a wide range of emission-reducing technologies and strategies to stabilize global warming [41], [48], [49]. With regards to agricultural output and bioenergy generation, this scenario is slightly optimistic in light of climate change.

Gilgit, because of its position and climatic zone, has had the greatest rise in precipitation (6.7% or 7.6367 mm) throughout the length of the century studied [43]. Between 2020 and 2021-40, there was the largest rise (21.1 mm), then a fall of 8.0038 mm between 2021-40 and 2041-60, and then a rise thereafter [41], [48], [49]. Quetta and Gilgit share the same weather conditions, therefore they both see an increase in precipitation of 6.43 %, or 15.5672 mm.

Islamabad has the smallest rise in precipitation (5.82%) of any city because of the moisture in the air, which causes rain to fall in the hills' woodlands and so reduces the temperature there throughout the summer [50]. Lahore has the second lowest precipitation increases of any area throughout the past century due to the interconnected effects of industrialization, a high number of vehicles, and urbanization [47].

For RCP 8.5, Table 14 and Figure 84 shows that precipitation will rise faster than under RCP 4.5 throughout the course of the century, reaching a high of 26.87% at Gilgit (during the period of 2021-2099) [43]. Islamabad shows the smallest percentage increase in precipitation (20.243%, or 319.973 mm) from 2021 to 2099 under RCP 8.5 compared to other locations [47], [50]. Due to climate change, certain parts of the country may expect an average increase in precipitation of 22.15% by the turn of the century. Figure 85 provides a century-long summary of the projections for the chosen region based on two RCPs.

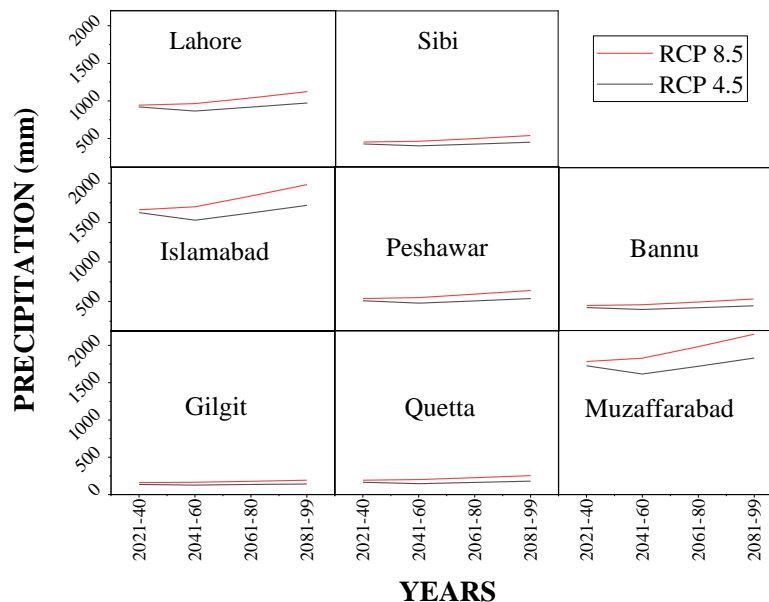


Figure 85: Average precipitation(mm) for each city across the century under RCP 4.5 and RCP 8.5

Effect of Temperature on Crops (Independent Estimate) (Stage-II)

Critical crops in Pakistan are impacted by both high and low heat extremes. Temperature, precipitation, humidity, water supply, land availability, etc. are only a few of the many critical elements that affect crop yields. In this part, temperature is the only independent estimate that matters since it will be used to test how the selected crops react to higher or lower temperatures.

RCP 4.5

The temperature shift under RCP 4.5 is shown for many time intervals, beginning in the base year 2020 and extending into the intervals chosen to split the whole century. The historical temperature shifts are shown in Table 15.

Table 15: Change in temperatures(°C) under RCP 4.5

| CHANGE IN TEMPERATURE (°C) | | | | | | | | |
|----------------------------|--------|---------|--------|--------|----------|--------|--------|--------|
| YEARS | Gilgit | Quetta | Muzaf. | Isl. | Peshawar | Bannu | Lahore | Sibi |
| 2021-40 | 1.196 | -3.7554 | 0.603 | 0.5213 | 0.18271 | 0.3827 | 1.156 | 0.6683 |
| 2041-60 | 1.2895 | 1.59093 | 1.0971 | 1.012 | 1.11443 | 0.9742 | 0.8397 | 1.1777 |
| 2061-80 | 0.3223 | 0.73919 | 0.7574 | 0.7048 | 0.53451 | 0.6211 | 1.0318 | 0.6472 |
| 2081-99 | 0.4475 | 0.48524 | 0.3954 | 0.7604 | 0.58538 | 0.3679 | 0.7504 | 0.3778 |

Since RCP 4.5 is a stabilization scenario, all the temperatures by the end of the century are optimistic and all fall under the 2°C tolerance set by the Paris Agreement [51]. Table 15 shows that between 2021 to 2040, daily horizontal radiation and other variables would produce an average reduction in temperature of 3.75541 °C for the city of Quetta [44]–[46].

Wheat output over the century is presented in Table 16, with temperature fluctuations by RCP 4.5. Wheat production is 2974 Kgs/Hec at the present. Muzaffarabad only produced more wheat in 2061–80 and 2081–99. Results show that Peshawar, Quetta, Islamabad, and Muzaffarabad are also favorable.

Table 17 shows RCP 4.5's projected changes in century-long maize output as a result of rising temperatures. This year's expected maize harvest is estimated at 5,970 Kgs/Hec. The research shows that in all four horizons (2021–40, 2041–60, 2061–80, and 2081–99), only Sibi will produce more maize than is done at present. Gilgit is the worst city in which to grow corn. There is a middle ground of maize production in Bannu and Lahore.

Table 16: Wheat Production (Kgs/Hec) w.r.t temperature 4.5

| WHEAT PRODUCTION (Kgs/Hec) | | | | |
|----------------------------|---------|---------|---------|---------|
| CITIES | 2021-40 | 2041-60 | 2061-80 | 2081-99 |
| Gilgit | 1328.66 | 1520.7 | 1578.2 | 1658.1 |
| Quetta | 2536.25 | 2743.01 | 2874.91 | 2961.5 |
| Muzaffarabad | 2626.37 | 2877.64 | 3012.8 | 3083.3 |
| Islamabad | 2745.78 | 2646.87 | 2521.1 | 2385.4 |
| Peshawar | 2518.04 | 2357.11 | 2261.73 | 2157.3 |
| Bannu | 2276.28 | 2144.81 | 2033.98 | 1968.3 |
| Lahore | 2253.36 | 2200.34 | 2016.23 | 1882.3 |
| Sibi | 1648.15 | 1495.45 | 1379.97 | 1312.6 |

Table 17: Maize Production (Kgs/Hec) w.r.t temperature 4.5

| MAIZE PRODUCTION (Kgs/Hec) | | | | |
|----------------------------|---------|---------|---------|---------|
| CITIES | 2021-40 | 2041-60 | 2061-80 | 2081-99 |
| Gilgit | 0 | 0 | 0 | 0 |
| Quetta | 1351.98 | 1863.88 | 2190.44 | 2404.81 |
| Muzaffarabad | 1575.1 | 2197.2 | 2531.83 | 2706.49 |
| Islamabad | 3442.58 | 3687.45 | 3998.82 | 4334.76 |
| Peshawar | 4006.41 | 4404.84 | 4640.97 | 4899.58 |
| Bannu | 4604.96 | 4930.44 | 5204.84 | 5367.39 |
| Lahore | 4661.69 | 4792.95 | 5248.78 | 5580.3 |
| Sibi | 6160.06 | 6538.11 | 6824.01 | 6990.94 |

Literature displays annual rice yields under RCP 4.5 temperature projections. Rice yields presently stand at 2524 Kgs/Hec. The results suggest that in 2021–40 and 2041–60, Lahore would produce more maize than Pakistan now does, while in 2041–60, Bannu would produce more and in 2081–99, Peshawar would produce more. Lahore, Bannu, Peshawar, and Islamabad are highly sought-after locations for rice farming.

Table 19 shows RCP 4.5's projected temperature changes alongside sugarcane production throughout the course of the century. The current yearly sugarcane yield is 69536 Kgs/Hec. The results imply that in 2061–80 and 2081–99, Lahore and Bannu would produce more sugarcane than Pakistan already produces. Lahore, Bannu, Peshawar, and Sibi would be cities of importance for sugarcane farming.

Table 18: Rice Production (Kgs/Hec) w.r.t temperature 4.5

| RICE PRODUCTION (Kgs/Hec) | | | | |
|----------------------------------|----------------|----------------|----------------|----------------|
| CITIES | 2021-40 | 2041-60 | 2061-80 | 2081-99 |
| Gilgit | 1375.42 | 1462.35 | 1488.37 | 1524.52 |
| Quetta | 1922.02 | 2015.61 | 2075.31 | 2114.5 |
| Muzaffarabad | 1962.81 | 2076.55 | 2137.72 | 2169.66 |
| Islamabad | 2304.23 | 2349 | 2405.93 | 2467.34 |
| Peshawar | 2407.31 | 2480.15 | 2523.33 | 2570.61 |
| Bannu | 2516.74 | 2576.25 | 2502.36 | 2472.64 |
| Lahore | 2527.11 | 2551.11 | 2494.32 | 2433.71 |
| Sibi | 2327.72 | 2258.6 | 2206.33 | 2175.81 |

Table 19: Sugarcane Production (Kgs/Hec) w.r.t temperature 4.5

| SUGARCANE PRODUCTION (Kgs/Hec) | | | | |
|---------------------------------------|----------------|----------------|----------------|----------------|
| CITIES | 2021-40 | 2041-60 | 2061-80 | 2081-99 |
| Gilgit | 0 | 0 | 0 | 0 |
| Quetta | 10755.7 | 18813.1 | 23953.1 | 27327.3 |
| Muzaffarabad | 14267.6 | 24059.5 | 29326.5 | 32075.6 |
| Islamabad | 43661.7 | 47516 | 52416.9 | 57704.7 |
| Peshawar | 52536.3 | 58807.6 | 62524.3 | 66594.8 |
| Bannu | 61957.5 | 67080.6 | 71399.6 | 73958.1 |
| Lahore | 62850.5 | 64916.5 | 72091.2 | 77309.4 |
| Sibi | 66544.5 | 60593.9 | 56093.9 | 53466.5 |

Figure 86 shows radar plots of RCP 4.5 wheat, maize, rice, and sugarcane yields vs temperature at the indicated times and places.

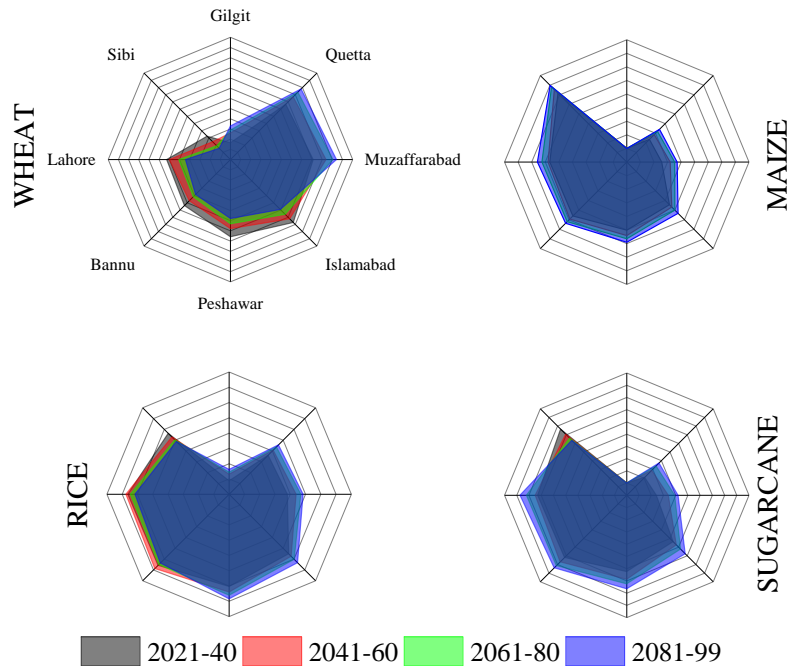


Figure 86: Wheat, Maize, Rice and Sugarcane Production (Kgs/Hec) w.r.t temperature 4.5

RCP 8.5

The temperature shift under RCP 8.5 is shown for many time intervals, beginning in the base year 2020 and extending to the intervals chosen to split the whole century. Table 20 shows the historical temperature shifts that have taken occurred.

Table 20: Change in temperatures under RCP 8.5

| CHANGE IN TEMPERATURE (°C) | | | | | | | | |
|----------------------------|---------|---------|---------|---------|----------|---------|---------|---------|
| YEARS | Gilgit | Quetta | Muzaf. | Isl. | Peshawar | Bannu | Lahore | Sibi |
| 2021-40 | 1.40932 | -3.3232 | 0.29183 | 0.979 | 0.39527 | 0.62013 | 1.69855 | 0.99021 |
| 2041-60 | 1.71172 | 1.83179 | 1.54235 | 1.2114 | 1.41781 | 1.2022 | 1.05848 | 1.41121 |
| 2061-80 | 2.78784 | 2.55645 | 2.51036 | 2.22567 | 2.42405 | 2.19368 | 2.37525 | 2.02097 |
| 2081-99 | 2.49563 | 2.90146 | 2.3453 | 2.36715 | 2.42484 | 2.22073 | 2.37011 | 2.32634 |

Since RCP 8.5 is a worst-case scenario, it predicts that global warming will be no more than 5–7 °C by the end of the century [52]. In Table 20, we can observe that daily horizontal radiation and other variables will lead Quetta to cool by 3.3232 °C between 2021 and 2040 [44]–[46].

In Table 21 we can see the RCP 8.5 projected temperature increase with the century-long wheat yield. The current annual wheat production is 2974 Kgs/Hec. The results suggest that within the selected time periods, no city's wheat output will exceed that of the present century save for Quetta in 2061-80. Major sugarcane-growing centers in Pakistan will include Quetta, Muzaffarabad, and Islamabad.

Table 21: Wheat Production (Kgs/Hec) w.r.t temperature 8.5

| WHEAT PRODUCTION (Kgs/Hec) | | | | |
|----------------------------|---------|---------|---------|---------|
| CITIES | 2021-40 | 2041-60 | 2061-80 | 2081-99 |
| Gilgit | 1328.66 | 1634.1 | 2131.56 | 2576.88 |
| Quetta | 2536.25 | 2863.11 | 3319.28 | 2289.42 |
| Muzaffarabad | 2626.37 | 2901.59 | 2776.91 | 2358.41 |
| Islamabad | 2745.78 | 2529.61 | 2132.46 | 1710.07 |
| Peshawar | 2518.04 | 2265.04 | 1832.5 | 1399.81 |
| Bannu | 2276.28 | 2061.04 | 1670.32 | 1274.05 |
| Lahore | 2253.36 | 2064.49 | 1640.65 | 1217.72 |
| Sibi | 1648.15 | 1389.2 | 1028.58 | 613.465 |

Table 22 shows maize production and RCP 8.5 temperature projections for the century. Current annual maize production is 5970 Kgs/Hec. Some cities, such as Islamabad and Peshawar between 2081 and 2099, Bannu and Lahore between 2061 and 2080, and Sibi between 2021 and 2040, are predicted to produce more maize than the country's present lot. It's likely that the aforementioned municipalities would have a sizable corn harvest.

Table 22: Maize Production (Kgs/Hec) w.r.t temperature 8.5

| MAIZE PRODUCTION (Kgs/Hec) | | | | |
|----------------------------|---------|---------|---------|---------|
| CITIES | 2021-40 | 2041-60 | 2061-80 | 2081-99 |
| Gilgit | 0 | 0 | 350.064 | 1452.58 |
| Quetta | 1351.98 | 2161.22 | 3290.61 | 4572.42 |
| Muzaffarabad | 1575.1 | 2256.48 | 3365.5 | 4401.61 |
| Islamabad | 3442.58 | 3977.75 | 4961.01 | 6006.76 |
| Peshawar | 4006.41 | 4632.77 | 5703.66 | 6774.91 |
| Bannu | 4604.96 | 5136.07 | 6105.19 | 5295.2 |
| Lahore | 4661.69 | 5129.31 | 6178.64 | 5156.07 |
| Sibi | 6160.06 | 5580.61 | 4687.78 | 3660.05 |

Table 23 displays the expected temperature rise under RCP 8.5 with the century-long rice yield. As of right now, annual rice production averages 2524 Kgs/Hec. According to the results, in the years 2061–2080,



Islamabad, Bannu, and Lahore would all produce more rice than the present production of country. Sibi and Peshawar, in addition to the aforementioned cities, would also contribute significantly to the nation's rice supply.

Table 23: Rice Production (Kgs/Hec) w.r.t temperature 8.5

| RICE PRODUCTION (Kgs/Hec) | | | | |
|---------------------------|---------|---------|---------|---------|
| CITIES | 2021-40 | 2041-60 | 2061-80 | 2081-99 |
| Gilgit | 1375.42 | 1513.68 | 1738.84 | 1940.41 |
| Quetta | 1922.02 | 2069.97 | 2276.45 | 2510.79 |
| Muzaffarabad | 1962.81 | 2087.38 | 2290.14 | 2479.56 |
| Islamabad | 2304.23 | 2404.07 | 2581.84 | 2436.51 |
| Peshawar | 2407.31 | 2521.83 | 2491.92 | 2296.08 |
| Bannu | 2516.74 | 2616.84 | 2418.52 | 2239.15 |
| Lahore | 2527.11 | 2612.6 | 2405.09 | 2213.66 |
| Sibi | 2408.48 | 2291.27 | 2128.04 | 1940.15 |

Table 24 shows RCP 8.5's expected temperature change alongside the sugarcane production throughout the course of the century. At the present rate of production, sugarcane yields are 69536 Kgs/Hec. Based on the findings, by the years 2061–2080, 2041–2060, and 2021–2040, cities like Peshawar, Bannu, and Lahore would be responsible for more sugarcane production than the entire country. Along with the aforementioned cities, Sibi and Islamabad would also produce a sizable amount of sugarcane.

Table 24: Sugarcane Production (Kgs/Hec) w.r.t temperature 8.5

| SUGARCANE PRODUCTION (Kgs/Hec) | | | | |
|--------------------------------|---------|---------|---------|---------|
| CITIES | 2021-40 | 2041-60 | 2061-80 | 2081-99 |
| Gilgit | 0 | 0 | 0 | 12339.2 |
| Quetta | 10755.7 | 23493.2 | 41269.8 | 61445.3 |
| Muzaffarabad | 14267.6 | 24992.5 | 42448.5 | 58576.8 |
| Islamabad | 43661.7 | 52085.2 | 67561.7 | 68957.3 |
| Peshawar | 52536.3 | 62395.2 | 73728.1 | 56866.7 |
| Bannu | 61957.5 | 70317.1 | 67408.1 | 51966.1 |
| Lahore | 62850.5 | 70210.7 | 66252 | 49771.2 |
| Sibi | 66544.5 | 56453.4 | 42400.3 | 26223.9 |

The radar graphs in Figure 87 demonstrate the relationship between temperature and RCP 8.5 rice, wheat, maize, and sugarcane yield at the selected sites across the defined time periods.

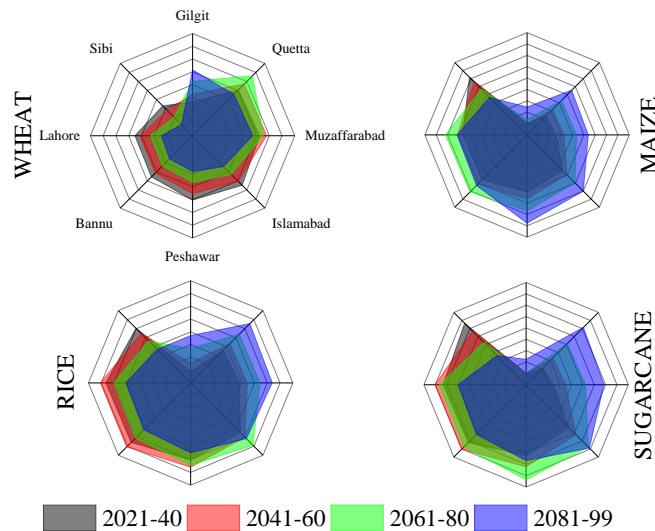


Figure 87: Wheat, Maize, Rice and Sugarcane Production (Kgs/Hec) w.r.t temperature 8.5

Effect of Precipitation on Crops (Independent Estimate) (Stage-II)

Extremely high or low rainfall quantities, in comparison to the ideal amount of precipitation for such crops, can have a negative effect on important crops in Pakistan. Factors such as climate, precipitation, humidity, water, and land availability, and so on all have profound effects on crop production. When considering independent estimations, the single variable in this section's essential indicators is precipitation, which is there to see how it affects the crops that have been chosen.

RCP 4.5

Precipitation shifts under RCP 4.5 are displayed in Table 25 for various time intervals, beginning with the base year 2020 and going on through the intervals chosen to split the whole century.

Table 25: Change in precipitation(mm) under RCP 4.5

| CHANGE IN TEMPERATURE (°C) | | | | | | | | |
|----------------------------|--------|---------|---------|--------|----------|---------|--------|---------|
| YEARS | Gilgit | Quetta | Muzaf. | Isl. | Peshawar | Bannu | Lahore | Sibi |
| 2021-40 | 21.1 | 33.6 | 112.6 | 46.4 | 24.22 | 28 | 40 | 19 |
| 2041-60 | -8.004 | -16.315 | -103.71 | -96.32 | -29.6722 | -24.414 | -54.5 | -25.397 |
| 2061-80 | 7.9536 | 15.4793 | 98.396 | 91.381 | 28.1514 | 23.1629 | 51.706 | 24.0951 |
| 2081-99 | 8.0469 | 16.4034 | 104.271 | 96.837 | 29.832 | 24.5456 | 54.793 | 25.5336 |

Offered that RCP 4.5 is a stabilization scenario, all projected precipitation by the century's end is optimistic and falls within the 7-8% margin given [48], [49].



Table 26 shows RCP 4.5-calculated precipitation changes and century-long wheat output. Wheat yields at now are at 2974 Kgs/Hec. It is only in the decades 2021–40 and 2081–99 that Peshawar's wheat output will be higher than it is right now.

Table 26: Wheat Production (Kgs/Hec) w.r.t precipitation 4.5

| WHEAT PRODUCTION (Kgs/Hec) | | | | |
|-----------------------------------|----------------|----------------|----------------|----------------|
| CITIES | 2021-40 | 2041-60 | 2061-80 | 2081-99 |
| Gilgit | 0 | 0 | 0 | 0 |
| Quetta | 0 | 0 | 0 | 0 |
| Muzaffarabad | 0 | 0 | 0 | 0 |
| Islamabad | 0 | 0 | 0 | 0 |
| Peshawar | 3191.7 | 2403.01 | 2973 | 3432 |
| Bannu | 2081 | 1703.18 | 2077 | 2111.56 |
| Lahore | 2153.36 | 2104 | 2149.65 | 2129 |
| Sibi | 2103.4 | 2039.54 | 2100.01 | 2210 |

Table 27 shows RCP 4.5's projections for maize output over the course of the century, adjusted for changes in average annual precipitation. This year's average yield for maize is 5970 Kgs/Hec. Only in Peshawar will more maize be produced than at now throughout all four time periods (2021–40, 2041–60, 2061–80, and 2081–99). Growing maize is another viable option in Lahore. Bannu and Sibi have average yields of maize.

Table 27: Maize Production (Kgs/Hec) w.r.t precipitation 4.5

| MAIZE PRODUCTION (Kgs/Hec) | | | | |
|-----------------------------------|----------------|----------------|----------------|----------------|
| CITIES | 2021-40 | 2041-60 | 2061-80 | 2081-99 |
| Gilgit | 0 | 0 | 0 | 0 |
| Quetta | 0 | 0 | 0 | 0 |
| Muzaffarabad | 0 | 0 | 0 | 0 |
| Islamabad | 0 | 0 | 0 | 0 |
| Peshawar | 6530 | 6121 | 6412 | 6717 |
| Bannu | 4980 | 4210 | 4968 | 5367.39 |
| Lahore | 5848 | 5713 | 5839.12 | 5901 |
| Sibi | 5130 | 4871 | 5121.56 | 5641 |

Table 28 shows RCP 4.5's projected changes in precipitation over the course of the century and how they'll affect rice production. The current yearly rice yield is 2524 Kgs/Hec. In light of these findings, Muzaffarabad and Islamabad might contribute more to Pakistan's maize output in the future than they do now. For those interested in cultivating rice, the cities of Muzaffarabad, Islamabad, and Lahore are the most desirable locations.

Table 28: Rice Production (Kgs/Hec) w.r.t precipitation 4.5

| RICE PRODUCTION (Kgs/Hec) | | | | |
|---------------------------|---------|---------|---------|---------|
| CITIES | 2021-40 | 2041-60 | 2061-80 | 2081-99 |
| Gilgit | 0 | 0 | 0 | 0 |
| Quetta | 0 | 0 | 0 | 0 |
| Muzaffarabad | 2627 | 2612 | 2621 | 2640 |
| Islamabad | 2610 | 2599 | 2601 | 2629 |
| Peshawar | 0 | 0 | 0 | 0 |
| Bannu | 0 | 0 | 0 | 0 |
| Lahore | 2103 | 2003 | 2099 | 2356 |
| Sibi | 0 | 0 | 0 | 0 |

Table 29 displays the sugarcane yield in relation to the change in precipitation expected under RCP 4.5 over the course of the century. Sugarcane yield has increased to 69536 Kgs/Hec each year. Findings suggest that no municipality will increase sugarcane production beyond current levels. Cities like Muzaffarabad, Islamabad, and Lahore will be crucial for sugarcane growing.

Table 29: Sugarcane Production (Kgs/Hec) w.r.t precipitation 4.5

| SUGARCANE PRODUCTION (Kgs/Hec) | | | | |
|--------------------------------|---------|---------|---------|---------|
| CITIES | 2021-40 | 2041-60 | 2061-80 | 2081-99 |
| Gilgit | 0 | 0 | 0 | 0 |
| Quetta | 0 | 0 | 0 | 0 |
| Muzaffarabad | 64530 | 64555 | 64511 | 63415 |
| Islamabad | 65231 | 69422 | 65220 | 64330 |
| Peshawar | 0 | 0 | 0 | 0 |
| Bannu | 0 | 0 | 0 | 0 |
| Lahore | 68631 | 67115 | 68610 | 68789 |
| Sibi | 0 | 0 | 0 | 0 |

In Figure 88, we see radar graphs for the chosen sites that depict rice, wheat, maize, and sugarcane production for RCP 4.5 in relation to precipitation during the specified time periods.

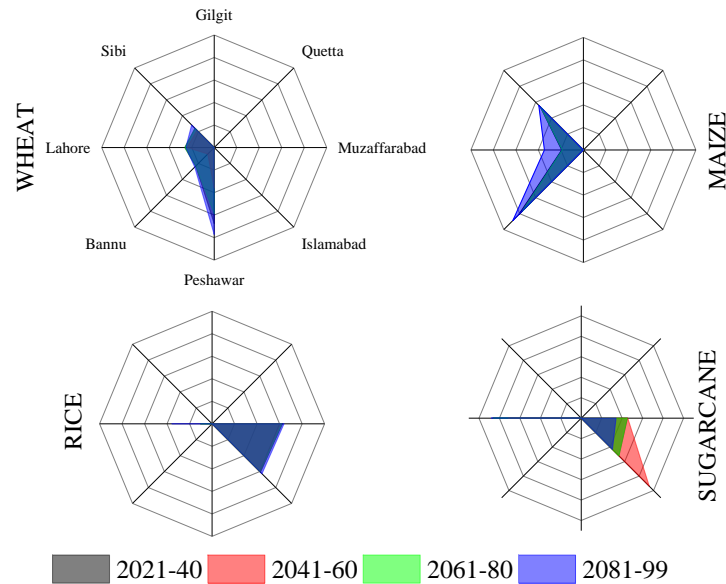


Figure 88: Wheat, Maize, Rice and Sugarcane Production (Kgs/Hec) w.r.t precipitation 4.5

RCP 8.5

Precipitation shifts under RCP 8.5 are displayed in Table 30 for many time intervals, from the base year 2020 through the intervals selected to split the whole century.

Table 30: Change in precipitation(mm) under RCP 8.5

| CHANGE IN TEMPERATURE (°C) | | | | | | | | |
|----------------------------|---------|---------|---------|---------|----------|---------|---------|---------|
| YEARS | Gilgit | Quetta | Muzaf. | Isl. | Peshawar | Bannu | Lahore | Sibi |
| 2021-40 | 44.584 | 57.58 | 163.7 | 78.721 | 50 | 52.187 | 58.94 | 41.456 |
| 2041-60 | 3.7831 | 7.13 | 42.911 | 39.492 | 12.5426 | 10.3908 | 22.3611 | 10.7447 |
| 2061-80 | 12.9213 | 24.3528 | 146.566 | 134.886 | 42.8397 | 35.49 | 76.3749 | 36.6987 |
| 2081-99 | 13.9473 | 26.2864 | 158.202 | 145.595 | 46.2411 | 38.3079 | 82.439 | 39.6126 |

As the worst-case scenario, RCP 8.5 forecasts that by the end of the century, precipitation would increase only in some regions while decreasing everywhere else [43].

Table 31 shows RCP 8.5's expected precipitation change in relation to wheat yield over the course of the century. The current yearly wheat yield is 2974 Kgs/Hec. The results show that, with the exception of Peshawar for the whole century and Sibi in 2081–2099, the wheat output of no city would exceed that of the 20th century across the selected time periods.

Table 31: Wheat Production (Kgs/Hec) w.r.t precipitation 8.5

| WHEAT PRODUCTION (Kgs/Hec) | | | | |
|----------------------------|---------|---------|---------|---------|
| CITIES | 2021-40 | 2041-60 | 2061-80 | 2081-99 |
| Gilgit | 0 | 0 | 0 | 0 |
| Quetta | 0 | 0 | 0 | 0 |
| Muzaffarabad | 0 | 0 | 0 | 0 |
| Islamabad | 0 | 0 | 0 | 0 |
| Peshawar | 3440 | 3480 | 3603.1 | 3815.6 |
| Bannu | 2118 | 2201 | 2440 | 2700 |
| Lahore | 2135 | 1615.4 | 1411.4 | 1210 |
| Sibi | 2215 | 2310 | 2478 | 3478 |

Table 32 shows maize output during the course of the century in line with the precipitation change expected by RCP 8.5. Current annual maize production is 5970 Kgs/Hec. The research shows that several cities, particularly Peshawar throughout the century, Lahore in the years 2061-80, and Bannu and Sibi in the years 2081-99, would produce more maize than the country at the time. Greater quantities of maize would be produced in the aforementioned urban centers.

Table 32: Maize Production (Kgs/Hec) w.r.t precipitation 8.5

| MAIZE PRODUCTION (Kgs/Hec) | | | | |
|----------------------------|---------|---------|---------|---------|
| CITIES | 2021-40 | 2041-60 | 2061-80 | 2081-99 |
| Gilgit | 0 | 0 | 0 | 0 |
| Quetta | 0 | 0 | 0 | 0 |
| Muzaffarabad | 0 | 0 | 0 | 0 |
| Islamabad | 0 | 0 | 0 | 0 |
| Peshawar | 6721 | 6748 | 6779 | 6801 |
| Bannu | 5410 | 5541 | 5912 | 5979 |
| Lahore | 5874 | 5901 | 5972 | 5899 |
| Sibi | 5655 | 5699 | 5899 | 5974 |

Table 33 shows the century-long rice yield in response to RCP 8.5's projected shift in precipitation. The average yearly yield of rice is now 2524 Kgs/Hec. In the years 2061–80 and 2081–99, Lahore would produce more rice than the rest of the country, followed by Muzaffarabad and Islamabad, which consistently outperform.

The present annual sugarcane output rate is 69536 Kgs/Hec, and

Table 34 shows how that rate would vary over the course of the century with the expected change in precipitation based on RCP 8.5. As the results show, in the years 2081–199 alone Lahore will produce more sugarcane than the country's present yield.

Table 33: Rice Production (Kgs/Hec) w.r.t precipitation 8.5

| RICE PRODUCTION (Kgs/Hec) | | | | |
|---------------------------|---------|---------|---------|---------|
| CITIES | 2021-40 | 2041-60 | 2061-80 | 2081-99 |
| Gilgit | 0 | 0 | 0 | 0 |
| Quetta | 0 | 0 | 0 | 0 |
| Muzaffarabad | 2655 | 2668 | 2674 | 2681 |
| Islamabad | 2619 | 2628 | 2662 | 2670 |
| Peshawar | 0 | 0 | 0 | 0 |
| Bannu | 0 | 0 | 0 | 0 |
| Lahore | 2348 | 2352 | 2529 | 2560 |
| Sibi | 0 | 0 | 0 | 0 |

Table 34: Sugarcane Production (Kgs/Hec) w.r.t precipitation 8.5

| SUGARCANE PRODUCTION (Kgs/Hec) | | | | |
|--------------------------------|---------|---------|---------|---------|
| CITIES | 2021-40 | 2041-60 | 2061-80 | 2081-99 |
| Gilgit | 0 | 0 | 0 | 0 |
| Quetta | 0 | 0 | 0 | 0 |
| Muzaffarabad | 63445 | 62001 | 60032 | 54030 |
| Islamabad | 64666 | 64364 | 61951 | 56213 |
| Peshawar | 0 | 0 | 0 | 0 |
| Bannu | 0 | 0 | 0 | 0 |
| Lahore | 68401 | 69501 | 69450 | 70101 |
| Sibi | 0 | 0 | 0 | 0 |

Site-specific radar plots of rice, wheat, maize, and sugarcane yields vs precipitation under RCP 8.5 are shown in Figure 89 for the selected locations and time periods.

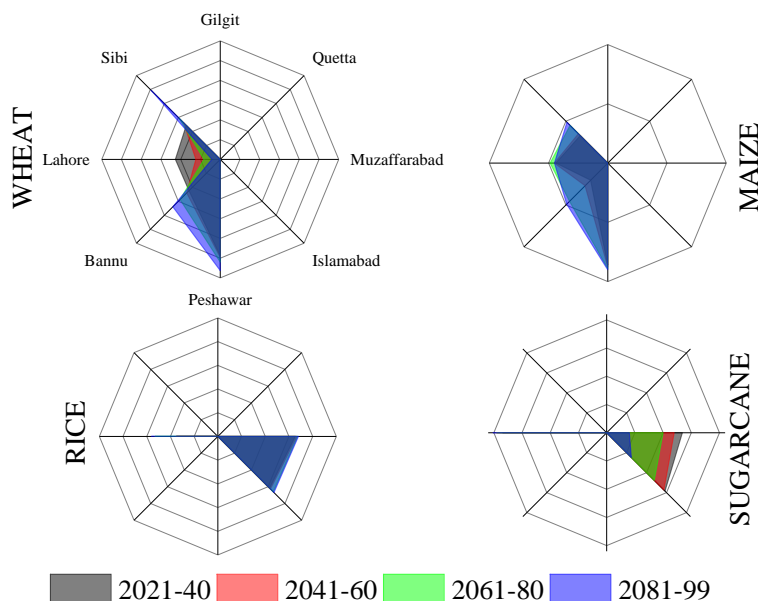


Figure 89: Wheat, Maize, Rice and Sugarcane Production (Kgs/Hec) w.r.t precipitation 8.5

Impact on Sustainable Bioenergy Generation (Stage-III)

Bioenergy potential was calculated by first projecting future crop yields based on two different scenarios for the coming century (RCP 4.5 and RCP 8.5). Due to the importance of agricultural biomass as a feedstock for the creation of bioenergy, the strategy required doing a study on each of the selected cities and selecting the most appropriate location based on the data. This study aims to put a number on how much waste will result from farming [53], [54]. Figure 90 displays the ratio of residue to crop.

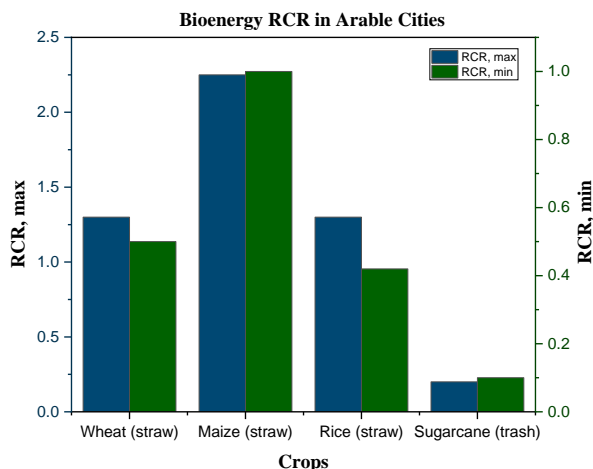


Figure 90: Residue to crop ratios (RCR) (World Bank and AEDB, 2016)

As said, the RCR is crucial to bioenergy generation. Figure 91 lists the other main parameters affecting bioenergy generation's sustainability. Environmental indicators may be needed at various biofuel supply chain phases. The supply chain includes feedstock production, management, conversion, and use. Figure 91 shows several indicators. Most of these categories apply to feedstock production and harvesting, whereas fewer apply to later stages. Early on, there are more categories, and they are more diversified, making it harder to select and quantify data. Biodiversity indicators should be selected and interpreted according to their locality. Indicators might indicate site-specific recovery programmes and habitat needs for regionally threatened species [39]. Smeets and Faaij (2010) emphasise that expert judgement and global ecosystem analysis may estimate the spatial areas needed to conserve biodiversity, but site-specific circumstances and biodiversity goals yield the most effective protected areas. Thus, biodiversity goals create effective protected areas. However, common ecological metrics like total vegetative cover, species richness, and presence, density, or cover of indicator species have region- and scale-specific meanings and should represent the evaluation purpose [55]. The biofuel supply chain presented in Figure 91 may employ greenhouse gas indicators throughout all steps.

In light of everything that has been said, it is possible that we will conclude: The progress toward a more sustainable bioenergy system is directly affected by RCR and the other criteria. The data we've collected will be analyzed to identify which towns have the most potential to maximize output from the biofuel system depicted in Figure 91.

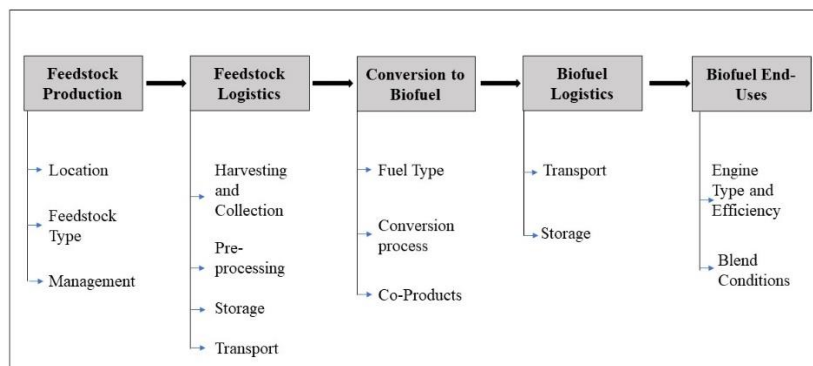


Figure 91: Biofuel System

Muzaffarabad, Quetta, and Peshawar improved wheat production the most, whereas Peshawar improved overall. Maize, which has bioenergy potential, has performed well in Sibi and Peshawar. Bannu and Muzaffarabad will produce the most rice due to the shifting climate. Lahore, Peshawar, and Islamabad sugarcane tiled figures are encouraging. You just read about all these tests' results. Thus, these locations should have feedstock logistics units to strengthen the environment. These power plants will also boost biodiversity. They will create jobs and lower biomass transport costs, helping the entire community in the previously named cities reach sustainability goals [8].

Summary

According to wheat forecast, Peshawar (2081-99) would have the highest output in terms of precipitation (RCP 4.5 & 8.5), whereas Muzaffarabad (2081-99) and Quetta (2061-80) will have the highest



production in terms of temperature (RCP 4.5 & 8.5). In terms of temperature (RCP 4.5 & 8.5), Sibi (2081-99) and Peshawar (2081-99) will produce the most maize, whereas Peshawar (2081-99) will produce the most maize in terms of precipitation (RCP 4.5 & 8.5). Bannu (2041-60) will yield the most rice based on temperature (RCP 4.5 & 8.5), whereas Muzaffarabad (2081-99) would produce the most rice based on precipitation (RCP 4.5 & 8.5). Based on temperature (RCP 4.5 & 8.5), Lahore (2081-99) and Peshawar (2061-80) would produce the most sugarcane, whereas Islamabad (2041-60) and Lahore (2081-99) will do so based on precipitation (RCP 4.5 & 8.5).

CONCLUSION

Climate change challenges bioenergy and lifestyle. Pakistan's designated cities' bioenergy systems will suffer in extreme climate change. This study examined how climate change affects sustainable bioenergy production in Gilgit, Quetta, Muzaffarabad, Islamabad, Peshawar, Bannu, Lahore, and Sibi in Pakistan. Temperature and precipitation variations and their consequences on city wheat, maize, rice, and sugarcane output were calculated in Kgs/Hec using datasets and other models to predict RCP 4.5 and 8.5 under various future scenario-periods. Without ideal circumstances, crops would suffer. Both impacts will work together to fulfil bioenergy clients' rising needs. This positive feedback effect will hurt Pakistan, a developing nation with a weak economy. According to the RCP 4.5 scenario, agricultural production in some cities may be ideal for temperature and precipitation by 2050 if emissions start to fall. Only Quetta's temperature dropped during RCP 4.5 and 8.5, then rose till the end of the century. Muzaffarabad, Sibi, Bannu, and Lahore would produce the most wheat, maize, rice, and sugarcane in the late century at temperature RCP 4.5. Quetta and Peshawar will produce most wheat, rice, maize, and sugarcane (RCP 8.5). Peshawar, Muzaffarabad, Islamabad, and Lahore may grow wheat, maize, rice, and sugarcane with RCP 4.5 and 8.5 precipitation. Canal systems, energy- and temperature-resistant devices, and water efficiency can reduce the consequences. The fact that crops production in places like Lahore, which have a high population density and significant seasonal temperature variations, is not as severely impacted by temperature as in some smaller districts in the nation suggests that this region is more dependent on other, more important factors. The entirety of this study's findings are depicted in Figure 92.

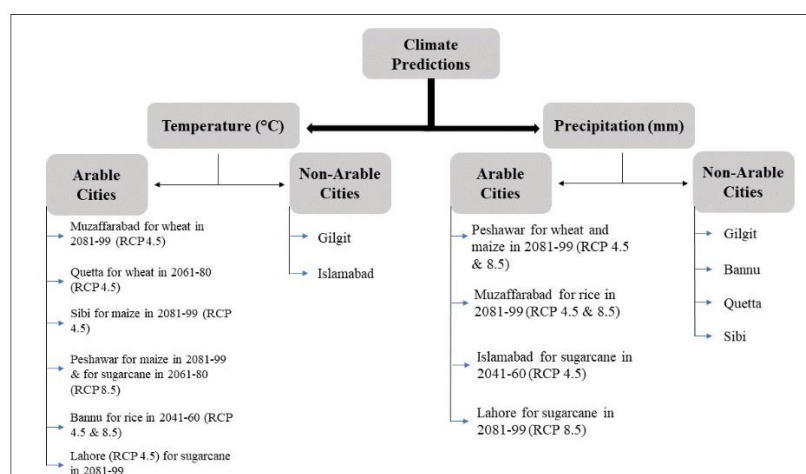


Figure 92: Summarized Results



ICSET-23



UET Peshawar

This research recommends crop protection and renewable energy. After Pakistan's recent floods, it would take 60 days for the water to drain and 30 days for the soil to be suitable for agriculture. Climate change and rising temperatures in colder locations melt glaciers, causing the deluge. The first and most significant idea is to build more dams and canals to store and channel water in challenging conditions. Given Pakistan's two disastrous floods in the past decade, it's vital. This study suggests planting crops in climate-resilient locations. Finally, renewable energy should be prioritized at the national and domestic levels by offering incentives. It is the finest climate change plan.

ACKNOWLEDGEMENTS

The authors are thankful to the Pakistan Meteorological Department, Pakistan Bureau of Statistics' and National University of Sciences and Technology (NUST), Islamabad assistance and are gratefully acknowledged. No funding taken for the subject study.

CONFLICT OF INTERESTS

The authors affirm that they do not have any competing interests.

CREDIT AUTHORSHIP CONTRIBUTION STATEMENT

Aqib Nawaz Khan: Conceptualization, Data Correction, Methodology, Formal Analysis, Investigation, Validation, Writing. **Muhammad Osama Aziz:** Conceptualization, Methodology. **Yousaf Salim:** Investigation, Visualization. **Muhammad Usman Khan:** Review and editing, Project Administration. **Muhammad Uzair Khan:** Review and editing.

FUNDING

No funding information for the subject study

REFERENCES

- [1] B. a Mccarl, "Adaptation Options for Agriculture, Forestry and Fisheries. A report to the UNFCCC Financial and Technical Support Division," 2007.
- [2] A. Raheem, P. Prinsen, A. K. Vuppalladadiyam, M. Zhao, and R. Luque, "A review on sustainable microalgae based biofuel and bioenergy production: Recent developments," *J. Clean. Prod.*, vol. 181, pp. 42–59, 2018, doi: 10.1016/j.jclepro.2018.01.125.
- [3] Z. Jiang *et al.*, "Assessment of bioenergy development potential and its environmental impact for rural household energy consumption: A case study in Shandong, China," *Renew. Sustain. Energy Rev.*, vol. 67, pp. 1153–1161, 2017, doi: 10.1016/j.rser.2016.09.085.
- [4] A. R. Bajracharya, S. R. Bajracharya, A. B. Shrestha, and S. B. Maharjan, "Climate change impact assessment on the hydrological regime of the Kaligandaki Basin, Nepal," *Sci. Total Environ.*, vol. 625, pp. 837–848, 2018, doi: 10.1016/j.scitotenv.2017.12.332.
- [5] A. F. Lutz, W. W. Immerzeel, P. D. A. Kraaijenbrink, A. B. Shrestha, and M. F. P. Bierkens, "Climate change impacts on the upper indus hydrology: Sources, shifts and extremes," *PLoS ONE*, vol. 11, no. 11. 2016. doi: 10.1371/journal.pone.0165630.



- [6] F. Creutzig *et al.*, “Bioenergy and climate change mitigation: An assessment,” *GCB Bioenergy*, vol. 7, no. 5, pp. 916–944, 2015, doi: 10.1111/gcbb.12205.
- [7] A. D. Hecht, D. Shaw, R. Bruins, V. Dale, K. Kline, and A. Chen, “Good policy follows good science: Using criteria and indicators for assessing sustainable biofuel production,” *Ecotoxicology*, vol. 18, no. 1, pp. 1–4, 2009, doi: 10.1007/s10646-008-0293-y.
- [8] R. A. Efroymsen *et al.*, “Environmental indicators of biofuel sustainability: What about context?,” *Environ. Manage.*, vol. 51, no. 2, pp. 291–306, 2013, doi: 10.1007/s00267-012-9907-5.
- [9] M. Azmat, M. U. Qamar, C. Huggel, and E. Hussain, “Future climate and cryosphere impacts on the hydrology of a scarcely gauged catchment on the Jhelum river basin, Northern Pakistan,” *Sci. Total Environ.*, vol. 639, pp. 961–976, 2018, doi: 10.1016/j.scitotenv.2018.05.206.
- [10] A. F. Lutz, H. W. ter Maat, H. Biemans, A. B. Shrestha, P. Wester, and W. W. Immerzeel, “Selecting representative climate models for climate change impact studies: an advanced envelope-based selection approach,” *Int. J. Climatol.*, vol. 36, no. 12, pp. 3988–4005, 2016, doi: 10.1002/joc.4608.
- [11] N. Forsythe *et al.*, “Application of a stochastic weather generator to assess climate change impacts in a semi-arid climate: The Upper Indus Basin,” *J. Hydrol.*, vol. 517, pp. 1019–1034, 2014, doi: 10.1016/j.jhydrol.2014.06.031.
- [12] H. L. Lee, “The impact of climate change on global food supply and demand, food prices, and land use,” *Paddy Water Environ.*, vol. 7, no. 4, pp. 321–331, 2009, doi: 10.1007/s10333-009-0181-y.
- [13] R. Biswas, B. Chandra, and K. Viswavidyalaya, “Chapter -5 Climate Change Impact on Agriculture Chapter -5 Climate Change Impact on Agriculture Chapter - 5 Climate Change Impact on Agriculture Author Guest Faculty , Department of Agricultural Statistics , Seacom,” no. July, 2021, doi: 10.22271/ed.book.1184.
- [14] A. C. McBride *et al.*, “Indicators to support environmental sustainability of bioenergy systems,” *Ecol. Indic.*, vol. 11, no. 5, pp. 1277–1289, 2011, doi: 10.1016/j.ecolind.2011.01.010.
- [15] C. C. Kung and T. Wu, “Influence of water allocation on bioenergy production under climate change: A stochastic mathematical programming approach,” *Energy*, vol. 231, p. 120955, 2021, doi: 10.1016/j.energy.2021.120955.
- [16] S. Ali *et al.*, “Assessment of climate extremes in future projections downscaled by multiple statistical downscaling methods over Pakistan,” *Atmos. Res.*, vol. 222, no. January, pp. 114–133, 2019, doi: 10.1016/j.atmosres.2019.02.009.
- [17] “Pakistan Climate,” Encyclopedia of the Nations.
- [18] K. E. Taylor, R. J. Stouffer, and G. A. Meehl, “An overview of CMIP5 and the experiment design,” *Bull. Am. Meteorol. Soc.*, vol. 93, no. 4, pp. 485–498, 2012, doi: 10.1175/BAMS-D-11-00094.1.
- [19] Government of Pakistan, “02-Agriculture Economic survey 2021,” 2021.
- [20] . International CLIVAR Project Office, “Data and bias correction for decadal climate predictions,” *CLIVAR Publ. Ser.*, vol. No. 150, no. 150, p. 6 pp, 2011.
- [21] K. Venkatesh, K. M. Senthilkumar, H. M. Mamrutha, G. Singh, and G. P. Singh, *High-temperature stress in wheat under climate change scenario, effects and mitigation strategies*. INC, 2022. doi: 10.1016/b978-0-12-816091-6.00014-6.
- [22] J. I. Lizaso *et al.*, “Impact of high temperatures in maize: Phenology and yield components,” *F. Crop. Res.*, vol. 216, no. October 2017, pp. 129–140, 2018, doi: 10.1016/j.fcr.2017.11.013.
- [23] H. A. H. S. H. A. K. B. A. T. Q. S. Hussain, *Temperature Extremes: Impact on Rice Growth and Development*. Springer Link, 2019.
- [24] A. M. S. Kheir *et al.*, “Impacts of rising temperature, carbon dioxide concentration and sea level on wheat production in North Nile delta,” *Sci. Total Environ.*, vol. 651, pp. 3161–3173, 2019, doi:



- 10.1016/j.scitotenv.2018.10.209.
- [25] C. Zhao *et al.*, “Temperature increase reduces global yields of major crops in four independent estimates,” *Proc. Natl. Acad. Sci. U. S. A.*, vol. 114, no. 35, pp. 9326–9331, 2017, doi: 10.1073/pnas.1701762114.
- [26] H. Ji *et al.*, “Effects of jointing and booting low temperature stresses on grain yield and yield components in wheat,” *Agric. For. Meteorol.*, vol. 243, no. April, pp. 33–42, 2017, doi: 10.1016/j.agrformet.2017.04.016.
- [27] J. du Plessiss, “Maize Production,” *Dir. Agric. Inf. Serv. Dep. Agric. South Africa*, 2003.
- [28] “Major Crops and their Distribution (Basic).”
- [29] G. Naheed and A. Mahmood, “Water Requirement of Wheat Crop in Pakistan,” *Pakistan J. Meteorol.*, vol. 6, no. 11, pp. 89–97, 2009.
- [30] N. Mazhar, M. Sultan, and D. Amjad, “Impacts of Rainfall and Temperature Variability on Wheat Production in District Bahawalnagar, Pakistan From 1983-2016,” *Pak. J. Sci.*, vol. 72, no. 4, p. 348, 2020.
- [31] “Important Food Crops (Rice, Wheat, Maize, Millets, Pulses and Barley) and Horticultural Crops.”
- [32] G. Fan, A. Sarabandi, and M. Yaghoobzadeh, “Evaluating the climate change effects on temperature, precipitation and evapotranspiration in eastern Iran using CMPI5,” *Water Supply*, vol. 21, no. 8, pp. 4316–4327, 2021, doi: 10.2166/ws.2021.179.
- [33] “Rice production in India,” 2022.
- [34] M. Chandiposha, “Potential impact of climate change in sugarcane and mitigation strategies in Zimbabwe,” *African J. Agric. Res.*, vol. 8, no. 23, pp. 2814–2818, 2013, doi: 10.5897/AJAR2013.7083.
- [35] S. Afghan and M. Jamil, “Climate change impact on sugar Industry of Pakistan-An overview,” no. September 2013, 2014.
- [36] S. Pipitpukdee, W. Attavanich, and S. Bejranonda, “Climate change impacts on sugarcane production in Thailand,” *Atmosphere (Basel)*, vol. 11, no. 4, pp. 1–15, 2020, doi: 10.3390/ATMOS11040408.
- [37] H. Guo *et al.*, “Crop resilience to climate change: A study of spatio-temporal variability of sugarcane yield in a subtropical region, China,” *Smart Agric. Technol.*, vol. 1, no. June, p. 100014, 2021, doi: 10.1016/j.atech.2021.100014.
- [38] M. Z. C Brezinski, *Extrapolation methods: theory and practice*. Elsevier, 2013.
- [39] P. M. K. Gary M. Fellers, “California Red-legged Frog (*Rana Draytonii*) Movement and Habitat Use: Implications for Conservation,” *J. Herpetol.*, vol. 41:276–286, 2007.
- [40] D. Herring, “Climate Change: Global Temperature Projections,” 2012.
- [41] “Climate Model: Temperature Change (RCP 4.5) - 2006 - 2100,” 2013.
- [42] A. Khan, S. Ali, S. A. Shah, and M. Fayaz, “Impact of temperature and precipitation on net revenue of maize growers in Khyber Pakhtunkhwa, Pakistan,” *Sarhad J. Agric.*, vol. 34, no. 4, pp. 729–739, 2018, doi: 10.17582/journal.sja/2018/34.4.729.739.
- [43] A. Nizami, J. Ali, and M. Zulfqar, “Climate change is real and relevant for sustainable development, an empirical evidence on scenarios from north-west Pakistan,” *Sarhad J. Agric.*, vol. 36, no. 1, pp. 42–69, 2020, doi: 10.17582/journal.sja/2020/36.1.42.69.
- [44] S. Baloch, “Climate change: Balochistan hit by abnormal weather.”
- [45] A. Khan, “Climate Change and Quetta,” 2020.
- [46] W. Ahmed, J. A. Sheikh, A. Z. Kouzani, and M. A. Parvez Mahmud, “The role of single end-users and producers on ghg mitigation in Pakistan—A case study,” *Sustain.*, vol. 12, no. 20, pp. 1–12,



- 2020, doi: 10.3390/su12208351.
- [47] F. J. E. Tearle, "Industrial development in Pakistan," *J. R. Cent. Asian Soc.*, vol. Volume 52, no. 3–4, 2011, doi: <https://doi.org/10.1080/03068376508731912>.
- [48] H. N. Annisa and B. D. A. Nugroho, "Analysis and Projections of Rainfall using representative concentration pathways (RCPs) Scenarios in Sleman Yogyakarta," *IOP Conf. Ser. Earth Environ. Sci.*, vol. 653, no. 1, 2021, doi: 10.1088/1755-1315/653/1/012099.
- [49] R. Dahal, Vaskar & Shakya, Narendra Man & Bhattarai, "Estimating the Impact of Climate Change on Water Availability in Bagmati Basin, Nepal," *Environ. Process.*, vol. 3. 10.1007, 2016.
- [50] S. Salma, S. Rehman, and M. a Shah, "Rainfall Trends in Different Climate Zones of Pakistan," *Pakistan J. Meteorol.*, vol. 9, no. 17, pp. 37–47, 2012.
- [51] H. Selin and A. Najam, "Paris Agreement on climate change: the good, the bad, and the ugly," 2015.
- [52] K. Riahi *et al.*, "RCP 8.5-A scenario of comparatively high greenhouse gas emissions," *Clim. Change*, vol. 109, no. 1, pp. 33–57, 2011, doi: 10.1007/s10584-011-0149-y.
- [53] M. Hiloidhari, D. Das, and D. C. Baruah, "Bioenergy potential from crop residue biomass in India," *Renew. Sustain. Energy Rev.*, vol. 32, pp. 504–512, 2014, doi: 10.1016/j.rser.2014.01.025.
- [54] World Bank and AEDB, "Biomass Atlas for Pakistan," no. April, 2016.
- [55] E. M. W. Smeets and A. P. C. Faaij, "The impact of sustainability criteria on the costs and potentials of bioenergy production - Applied for case studies in Brazil and Ukraine," *Biomass and Bioenergy*, vol. 34, no. 3, pp. 319–333, 2010, doi: 10.1016/j.biombioe.2009.11.003.

APPENDIX A. SUPPLEMENTARY DATA

Table S1: Dataset from PMD

| CITIES | 2000-04 | 2005-08 | 2009-12 | 2013-16 | 2017-20 |
|----------------------------------|---------|---------|---------|---------|---------|
| TEMPERATURE (°C) | | | | | |
| Gilgit | 16 | 16.2 | 16.025 | 16.225 | 16.05 |
| Quetta | 17.62 | 17.25 | 17.2 | 17.675 | 17.425 |
| Muzaffarabad | 21.36 | 20.725 | 20.9 | 20.075 | 19.25 |
| Islamabad | 21.86 | 21.45 | 21.8 | 21.425 | 21.075 |
| Peshawar | 23.48 | 23.175 | 23.25 | 23.1 | 22.975 |
| Bannu | 24.04 | 23.925 | 23.575 | 22.55 | 22.6 |
| Lahore | 25.24 | 25.05 | 25.05 | 24.325 | 24.85 |
| Sibi | 27.8 | 27.325 | 26.525 | 26.6 | 27 |
| DRY BULB TEMPERATURE (°C) | | | | | |
| Gilgit | 12.46 | 11.625 | 11.4 | 11.975 | 12.175 |
| Quetta | 12.56 | 12.625 | 12.825 | 13.425 | 13.525 |
| Muzaffarabad | 15.76 | 15.175 | 15.3 | 15.2 | 14.375 |



ICSET-23

Proceedings of the 5th International Conference on Sustainable
Energy Technologies (ICSET 2023) Peshawar, Pakistan
14-15 December 2023



UET Peshawar

| | | | | | |
|------------------------------|---------|---------|----------|----------|----------|
| Islamabad | 17.38 | 17.2 | 17.475 | 17.35 | 17.4 |
| Peshawar | 19.26 | 19.05 | 19.05 | 19.5 | 19.3 |
| Bannu | 22.18 | 20.95 | 20.35 | 20.125 | 19.825 |
| Lahore | 21.98 | 21.9 | 21.95 | 21.85 | 21.525 |
| Sibi | 23.38 | 23.075 | 23.075 | 24.36667 | 24.15 |
| PRECIPITATION (mm) | | | | | |
| Gilgit | 134.06 | 134.35 | 178.675 | 146.725 | 132.7 |
| Quetta | 161.72 | 237.125 | 298.5 | 209.375 | 267.475 |
| Muzaffarabad | 1299.7 | 1598.5 | 1376.875 | 1365.425 | 1449.425 |
| Islamabad | 1189.56 | 1418 | 962.5 | 1476.075 | 1374.2 |
| Peshawar | 453.68 | 646.625 | 622.875 | 535.6 | 480.25 |
| Bannu | 207.26 | 398.35 | 382 | 435.125 | 360.825 |
| Lahore | 509.88 | 669.325 | 588.175 | 838.1 | 754.3 |
| Sibi | 113.5 | 255.625 | 252.175 | 181.4 | 232.05 |
| RELATIVE HUMIDITY (%) | | | | | |
| Gilgit | 65.6 | 71.625 | 72.425 | 71.5 | 69.625 |
| Quetta | 54.1 | 63.425 | 60.775 | 51.7 | 46.45 |
| Muzaffarabad | 75.08 | 79.1 | 77.725 | 80.275 | 77.875 |
| Islamabad | 77.42 | 80.8 | 77.075 | 81.15 | 79.5 |
| Peshawar | 69.52 | 71.275 | 69.725 | 67.275 | 66.5 |
| Bannu | 54.96 | 60.1 | 58.95 | 65.45 | 64.1 |
| Lahore | 68.04 | 70.025 | 68.075 | 71.8 | 71.475 |
| Sibi | 54.82 | 65.475 | 66.45 | 55.1 | 57.8 |

Table S2: Dataset from PBS

| YEARS | WHEAT YIELD | | MAIZE YIELD | | RICE YIELD | | SUGARCANE YIELD | |
|---------------------|-------------|----------|-------------|----------|-------------|----------|-----------------|----------|
| | (Kgs /Hec.) | % Change | (Kgs /Hec.) | % Change | (Kgs /Hec.) | % Change | (Kgs /Hec.) | % Change |
| Gilgit | 2974 | - | 4550 | - | 2514 | - | 61972 | - |
| Quetta | 2851 | -4.1 | 4718 | 3.7 | 2568 | 2.1 | 62096 | 0.2 |
| Muzaffarabad | 2806 | -1.6 | 4968 | 5.3 | 2563 | 0 | 60956 | -1.8 |



ICSET-23

*Proceedings of the 5th International Conference on Sustainable
Energy Technologies (ICSET 2023) Peshawar, Pakistan
14-15 December 2023*



UET Peshawar

| | | | | | | | | |
|------------------|------|------|------|-----|------|-----|-------|------|
| Islamabad | 2867 | 2.2 | 5615 | 13 | 2444 | -5 | 63827 | 4.7 |
| Peshawar | 2974 | 3.7 | 5970 | 6.3 | 2524 | 3.3 | 69536 | 8.9 |
| Bannu | 2974 | - | 4550 | - | 2514 | - | 61972 | - |
| Lahore | 2851 | -4.1 | 4718 | 3.7 | 2568 | 2.1 | 62096 | 0.2 |
| Sibi | 2806 | -1.6 | 4968 | 5.3 | 2563 | 0 | 60956 | -1.8 |

Paper ID: ICSET-2319

ANFIS BASED EVALUATION OF THE MICROGRID RESILIENCE UNDER MULTIPLE FACTORS

Muhammad Zeshan Afzal^{1,*}, Muhammad Aurangzeb¹, Sheeraz Iqbal², Irfan Jamil¹, Abdul Rehman¹,
Muhammad Aqeel Anjum³

¹Department of Electrical Engineering, Southeast University, Nanjing, PR China

²Department of Electrical Engineering, University of Azad Jammu and Kashmir, Muzaffarabad, AJK, Pakistan

³Department of Energy and Environment, Southeast University, Nanjing, PR China

**Corresponding author*

Email: zeshanafzal423@yahoo.com

ABSTRACT

In order to effectively handle system resilience in both synchronised and islanded grid modes, this study proposes the implementation of a bidirectional Adaptive Neuro-Fuzzy Inference System (ANFIS) with Fuzzy Logic Control (FLC). The aim is to solve the challenges posed by catastrophic disaster scenarios as well as ordinary operational settings. The system integrates many components, including solar panels, wind turbines, batteries, and load management, to optimise energy use. The control of power distribution among the solar, wind, and supercapacitor components of the battery system is facilitated by an Adaptive Neuro-Fuzzy Inference System (ANFIS). Firstly, we proceeded with the formulation of a control algorithm that is appropriate for the present condition of the system. Subsequently, a relevant Adaptive Neuro-Fuzzy Inference System (ANFIS) component is used to assume control in accordance with the designated operational mode, therefore enhancing resilience in emergency situations, promoting energy conservation, and ensuring the maintenance of normal operations. A bidirectional converter is employed to interface with the battery in order to maintain a consistent value of the DC connection and facilitate energy distribution in accordance with generation and demand. In order to prevent excessive depletion or overcharging of the battery, the ANFIS algorithm adeptly manages the power extraction from the photovoltaic (PV) source by taking into account the current load. The utilisation of islanding circumstances within wind systems serves to enhance the overall efficiency of the system and prolong the lifespan of the battery. The utilisation of synchronous reference frame transformation for control enhances the operational effectiveness of the inverter. The ANFIS system, which is built on fuzzy rule design, is utilised to coordinate control methodologies based on the prevailing conditions of solar and wind power, as well as the state of charge (SOC) of the battery. The evaluation of synchronised grid operation with Adaptive Neuro-Fuzzy Inference System (ANFIS) is conducted in conjunction with Particle Swarm Optimisation (PSO). The robustness of the system is demonstrated using Matlab/Simulink, encompassing both typical and extreme events. The present study focuses on the application of Fuzzy Logic Control (FLC) in optimising the State of Charge (SoC) of a microgrid system. Additionally, Particle Swarm Optimisation (PSO) is employed as a means to enhance the performance of the FLC algorithm.

KEYWORDS: ANFIS, Microgrids, Particle Swarm Optimization, Resilience Operation

INTRODUCTION

The subject of microgrid (MG) resilience in the face of significant disruptive events is becoming increasingly important to researchers and engineers in the power and energy sector. Events of significant magnitude and profound implications are commonly classified as "low probability, high impact" due to their infrequent occurrence. The occurrence of such disasters has shown a notable increase in recent decades as a consequence of climate change [1].

The magnitude and intensity of weather-related incidents, along with other global occurrences, have experienced substantial growth throughout the course of time [2]. In the past ten years, a significant number of the ten most substantial hurricanes throughout the preceding forty years have resulted in damages amounting to no less than \$1 billion [3]. In the year 2017, a total of eight significant weather-related calamities impacted both the United States and other regions across the globe [4]. A cumulative count of eight incidents has been recorded, with five of these incidents impacting a subscriber base over one million, while the least impactful event affected approximately 0.3 million members.

Under both normal and abnormal circumstances, the existing electric power systems are designed to maintain operational stability. Nevertheless, the issue of maintaining consistent operation in the face of unplanned and high-risk accidents continues to be a significant problem (Reference 5). Therefore, these systems lack resilience but possess reliability.

A system is considered resilient when it is capable of restoring its normal operation and minimising power supply disruptions during significant outages [6]. The authors in reference [7] have conducted a comprehensive examination of many viewpoints regarding the resilience of the system and have formed the concept of system resilience. The resilient system, as defined in reference [7], is characterised by its capacity to effectively handle the most crucial load during significant periods of service disruption.

In the field of power systems, there is a tendency to conflate dependability and resilience, however this is an inaccurate assumption. Significant disparities can be observed between the two entities, as illustrated in Figure I. The probability and predictability of events are generally low in a resilience system, but they tend to be high in a dependable system.

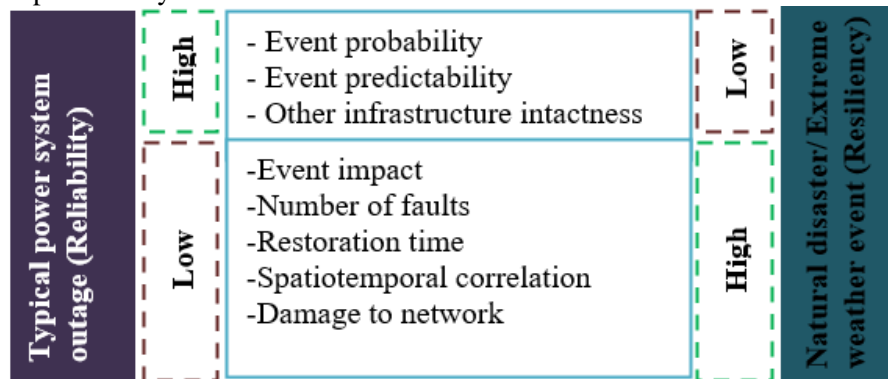


Figure 1: Reliability vs Resilience

Some regions are more likely to suffer various forms of natural disasters. As a result, different regions have adopted actions to boost their local resilience [8, 9] and analyses of the effects of previous events [10–15]. The MGs operation can be divided into normal, resilient, and resynchronization as shown in Figure II. The major operation switching between different modes is prone to uncertainties in systems. Uncertainty refers to the factors that cannot be predicted with certainty but have a major influence on MGs operation. These

uncertainties exist because the time of interruption major disruption and the restoration period of MG is not known. Other uncertain factors that may affect the MGs operation are forecasting errors and MGs load.

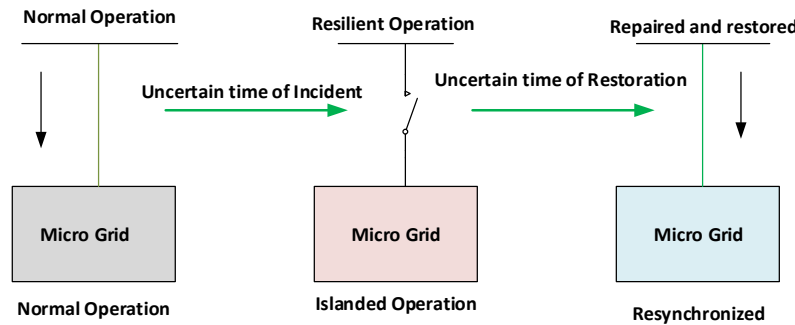


Figure 2: Microgrid operation states

The use of MGs to improve resilience has grown popular among the most common solutions identified in previous studies. This is due to the ability of MGs to maintain penetration of renewable and the capability of islanding.

MGs are used to improve the resilience of power plants during major disruption events. In such cases, tie switches are used to disconnect the affected area from the main grid and divide it into separate MGs. MGs can be useful for black businesses, black communities, and local MGs. In the event that one MG is unable to carry its own weight, the others can help out to ensure that the job is done. In black start resource, the supporting renewable (Generator) is started which has been interrupted due to some disaster.

Strategies used by MGs to boost resilience are another area of interest for researchers. From a resilience perspective, different strategies are used by MGs in the event of a major interruption. The effective scheduling of essential loads in emergency and resource scheduling is necessary to ensure proper islanding and load management of MG. To enhance the resilience of MGs, various studies have been carried out including proactive scheduling [16-18], advance operation schemes, and outage management [19-20]. In proactive schemes, the scheduling is done before any major outage. In advance operation, multi-agent system (MAS) or other artificial based techniques are employed. In outage management, the emergency load is identified and fed via local resources to avoid any uncertain situation.

Because of their islanding capability and potential to facilitate the adoption of renewable energy, MGs are being researched as a method to deal with major power interruption situations. To better describe the function that MGs play in making power systems more dependable, we apply an FLC-based bidirectional analytic approach in this study.

In recent literature review, the resilience is addressed by using various methods that shift from one mode control to the other based on various factors, such as weather [21-24], wind speed [22,26], solar power [29], SOC [25], operational cost and load shedding [26]. However, these methods use state of the art algorithms but mode shifting from one state to other state is done on crisp values. On the other hand, it is pertinent that different modes changes include several parameters that must be taken care off before shifting from one mode of operation to the other to make system resilient. For example, a bad weather condition or rainy day may reduce the available DG power but during this operation if the temperature is low and SOC is high but load consumption is also low then system may work in normal operation after that changing to emergency conditions for longer periods. It has been observed that mode changing is done on crisp values while not considering multiple factors. In our presented model, a Bidirectional control with ANFIS logic controller is designed to increase the resiliency while taking multiple factors into account during modes of operation selection.

A bi-directional mode of analysis with ANFIS and PSO is carried out in this model.

In this step entails modelling the broad contexts of power system resilience, which incorporates regional attempts to improve resilience, for photovoltaics (Power management by ANFIS), wind power (Power management by Fuzzy), and batteries (Power management by Super capacitor).

In the second step, the strategies utilized by microgrid for enhancing their resilience during major outage events such as Rainy Weather, Load Shedding and Extreme Weather Events are analyzed.

Our designed model work on Multiple factors simultaneously and not work on Crisp value. Each element is given a degree of membership in the set.

MATERIALS AND METHODS

Due to their islanding capabilities and adaptability to renewable energy integration, microgrids (MGs) are seen as a practical solution for handling major power interruptions. This research uses a Fuzzy Logic Control (FLC)-based two-way analytical approach to better understand the role that MGs play in improving power system resilience.

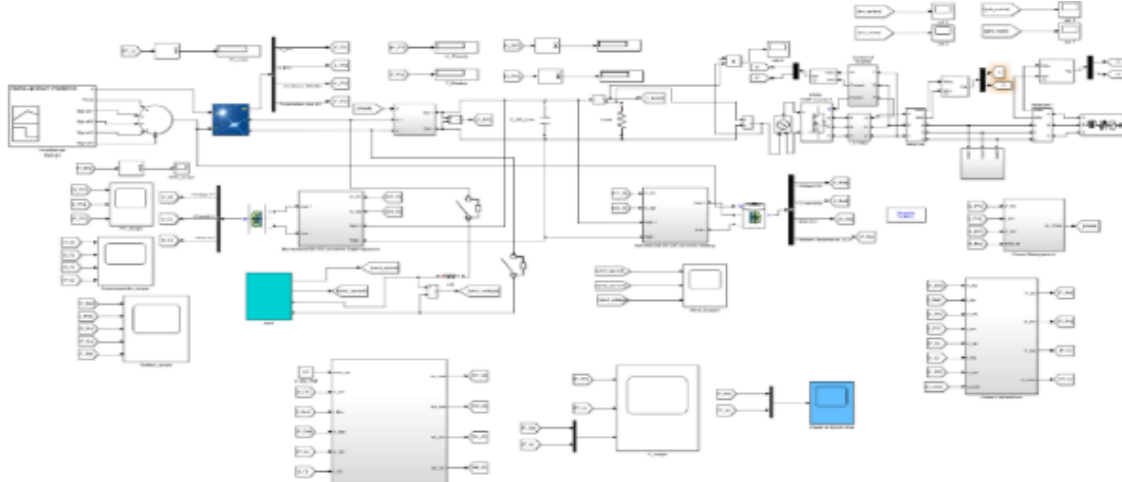


Figure 3: Presented model in matlab

In this study, above stated parameters are considered while using fuzzy values instead of using fixed crisp values for the decision of operation mode of MGs. The fuzzy values allow a better decision to switch between the modes of operation based upon various parameters as input membership functions. Then, based on the defined rule base for ANFIS (FLC), control actions be made to switch between emergency, normal, and energy conservation mode as given in Table 01 and Table 02.

Table 1: Available Percentage, Energy Mode & Corresponding Membership Function

| Solar & Wind Percentage Available | Solar & Wind Percentage Available | Solar & Wind Percentage Available |
|--------------------------------------|--------------------------------------|--------------------------------------|
| 0-30% | 0-30% | 0-30% |
| 30-60% | 30-60% | 30-60% |
| 60-100% | 60-100% | 60-100% |

Table 2: FLC Output to Switch b/w Modes

| Solar/Wind | NL | M | PL |
|------------|----|----|----|
| NL | NL | NL | M |
| M | NL | M | PL |
| PL | M | PL | PL |

To demonstrate the efficacy of bidirectional mode analysis with FLC, Matlab/Simulink software used. Figure 4 shows the proposed strategy to get expected results for a resilient system. Moreover, a comparative study between the presented strategy and Proportional Integral (PI) controller realized. The main aim is to compare the MGs load modes status in the normal as well as disrupted event for both controllers.

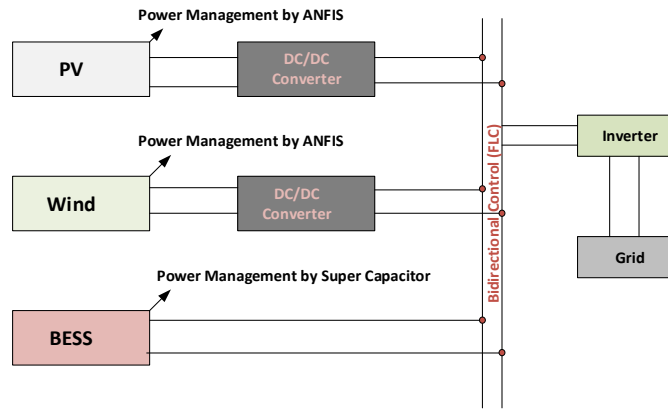


Figure 4: Schematic diagram proposed topology

RESULT AND DISCUSSION

The above figure no 5 represents the variable conditions of temperature variations. The all variance was taken in sequence. Starting and ending time of the signals can be clearly seen.

The voltage, current and power of PV module is shown figure 6 in this fig. At 0.05 the MPPT starts to work. Then the voltage, current and power shows the uniformity in nature under variable temperature conditions.

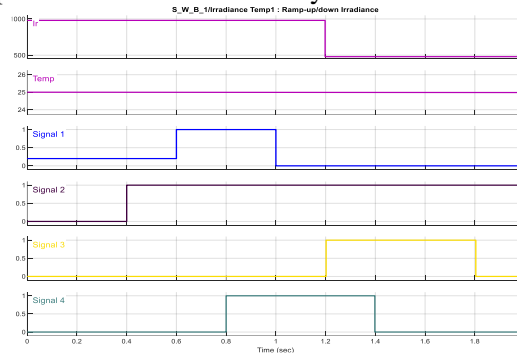


Figure 5: Temperature variation signals

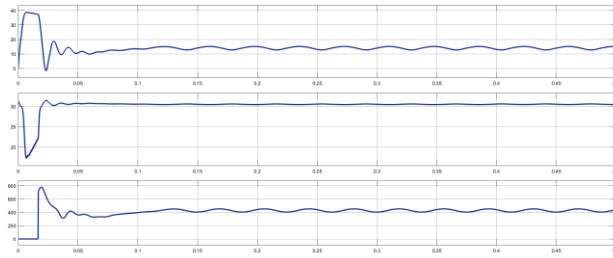


Figure 6: PV output

The voltage, current, SOC and power of super capacitor was shown in the fig 7. When it performs as charging condition, then the voltage is gradually reduced but current increases and then saturate at fixed position. The SOC were changes continuously. But when the super-capacitor works under no loaded condition the operation reverse.

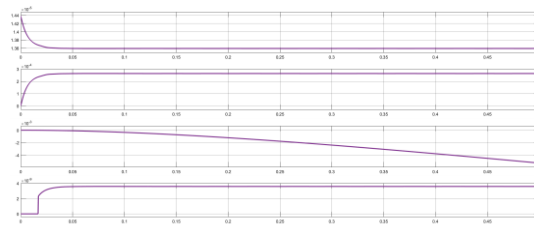


Figure 7: Super capacitor scope

The voltage, current, SOC and power were shown in the Fig8. The all waveform response can be shown, at the start decrease in voltage and then in the stable form but SOC is different, due to the initial condition of 30%. when the switching operation change from 30 to 60% then SOC show the different behavior. The last one shows the temperature of the battery.

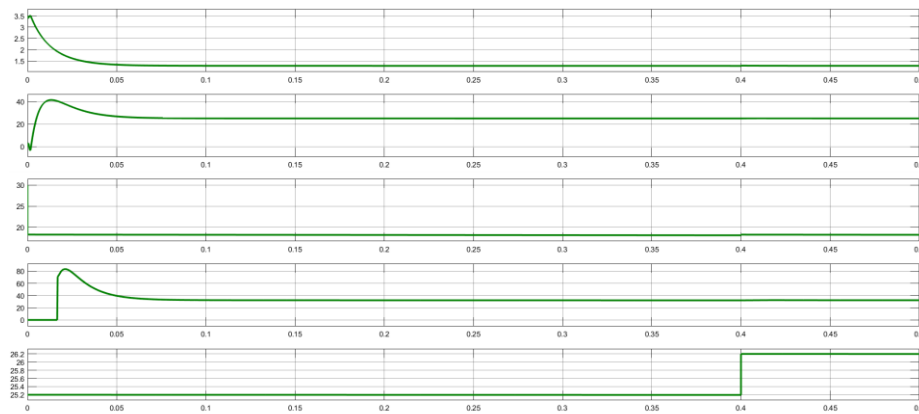


Figure 8: Battery scope

The figure 9 shows the response of the Power of PV, power of Load and battery power with supercapacitor.

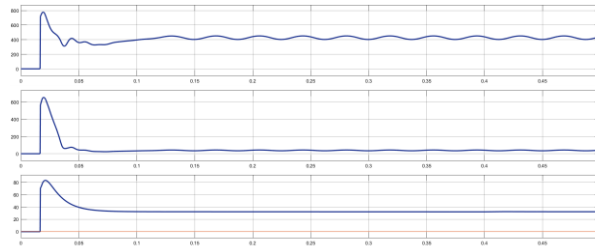


Figure 9: PV Power, Load Power, Batter and super-capacitor Power

The wind speed, Voltage and power were shown in the fig10. The variable wind condition can be seen from the fig. Simultaneously the voltage and power were not change at variable conditions. The response of the system is stable.

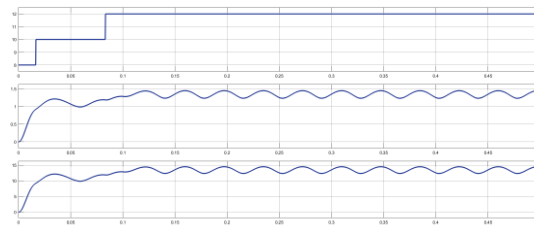


Figure 10: Wind speed voltage and power

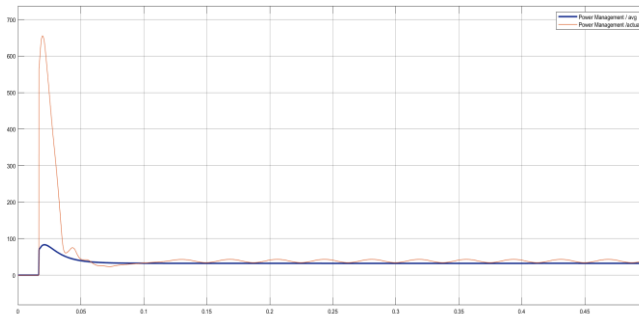


Figure 11: Power management with ANFIS

The power management by proposed technique shows in figure 11 its effectiveness. Initially a high surge was shown in the fig, but under proposed technique the nature of the curve shows the smooth variation with very low spike. It also shows that when it is synchronized with the grid the fluctuations are less with low harmonics. After synchronization the system response is very smooth.

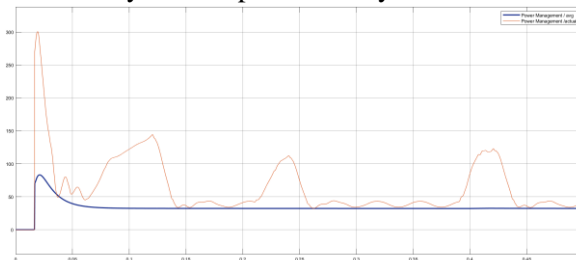


Figure 12: Power management with PSO



The power management by PSO (Particle Swarm Optimization) is presented in the above figure. Initially a high surge was shown in the fig 12, but under PSO technique the nature of the curve shows the variation with High spike. It also shows that the when it synchronized with the grid the fluctuations still present in the system with low harmonics. After synchronization the system response is not very smooth.

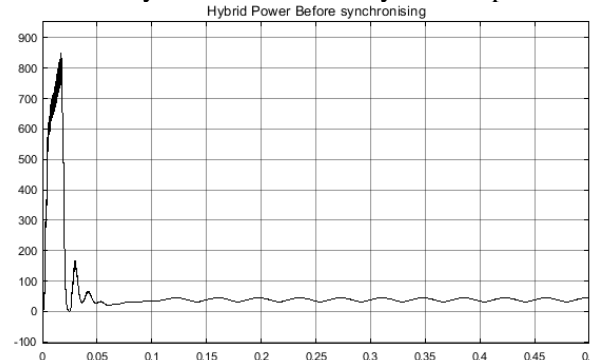


Figure 13: Hybrid power in islanding condition with ANFIS

The Hybrid Power by proposed technique shows its effectiveness. Initially a high surge was shown in the fig, but under proposed technique the nature of the curve shows the smooth variation. After 0.05 second, the system response is smooth and no fluctuations in the system. FLC applied to make the system stable.

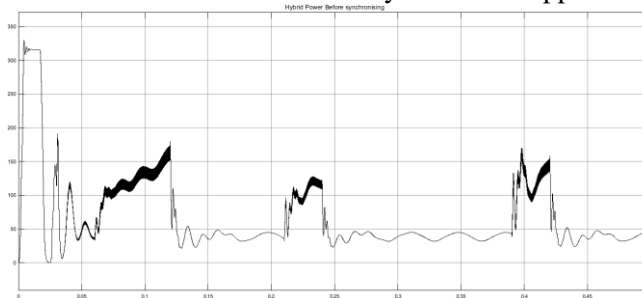


Figure 14: Hybrid power in islanding condition with PSO

The response of the system in Islanding condition with is not effective. Up and down in the fluctuations shows the instability of the system with Particle Swarm Optimization.

Figure 15 shows the active and reactive power of the Inverter under ANFIS rules applied to the system. Inverter output in active and reactive power is smooth and after synchronization, the inverter is working in smooth condition.

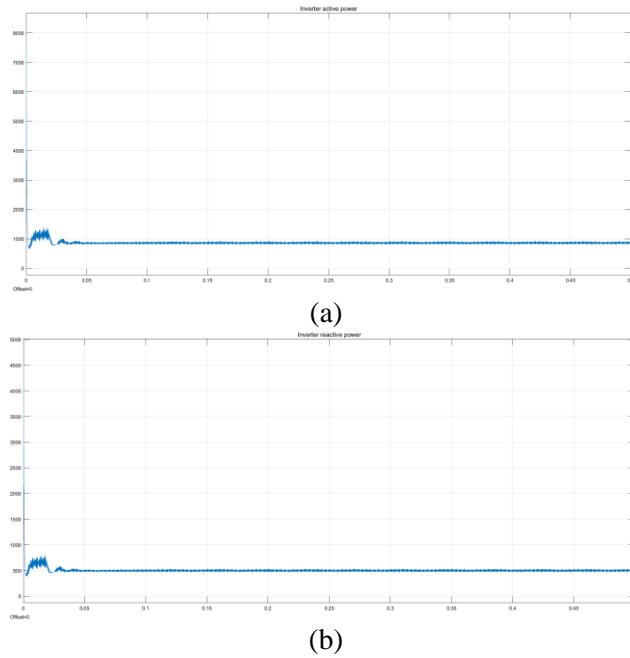


Figure 15: (a) Inverter Active Power (b) Inverter Reactive Power

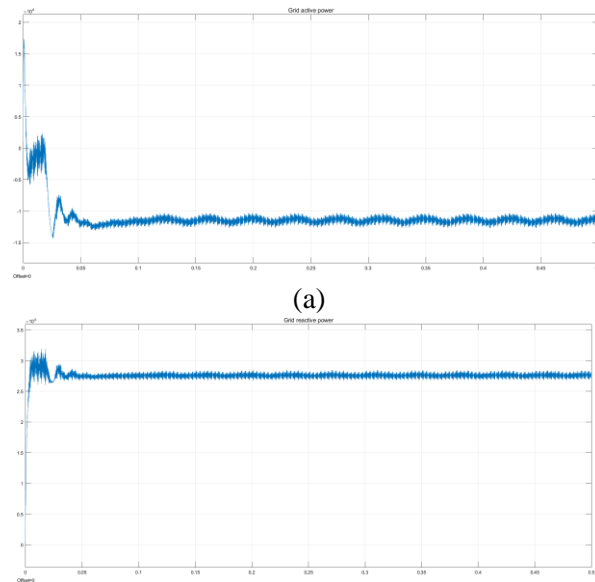


Figure 16: (a) Grid Active Power (b) Grid Reactive Power

From the above figure we can see the Grid power (active and reactive). The system shows the smooth response. Output shows no harmonics in the system.

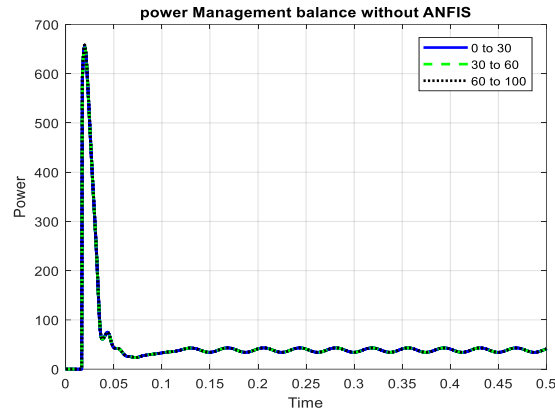


Figure 17: Power Management Balance Response under the conditions of 30%,60% and 100% without ANFIS

The above figure shows the response of power Management balance under different Load conditions. Without ANFIS response of the system is overlap and power management is not working properly to fulfill the criteria of 30%, 60% and 100%

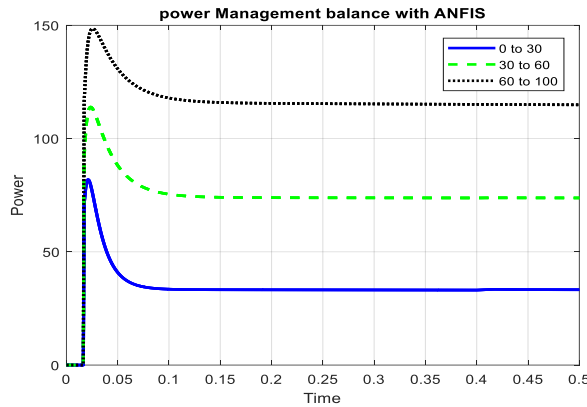


Fig 18: Power Management Balance Response under the conditions of 30%,60% and 100% with ANFIS

The above figure shows the response of power Management balance under different Load conditions. With ANFIS response of the system is stable and power management is not working properly to fulfill the criteria of 30%, 60% and 100%. All the operation modes are working Properly. 3 different regions of operation are clearly managed with AFNIS technique.

The SOC condition of battery is 30%, 60% and 100%. To keep such condition relational operator was used. This condition is same for both the techniques. And then it was operated with the ideal switch on-off switch. The conditions of operation compared with output of PSO and ANFIS with battery and ref voltage source. If battery condition full fills 30% then relay switch change the position automatically.

Islanding Detection Performance

One critical aspect of microgrid resilience is the ability to detect and respond to islanding conditions promptly. Islanding occurs when a portion of the microgrid becomes disconnected from the main utility grid but continues to operate autonomously. The developed control system incorporates an islanding detection mechanism to ensure the safety and stability of the microgrid during such events.

The islanding detection system relies on monitoring various parameters and assessing their behavior to identify potential islanding situations. In our simulation, we tested the islanding detection performance under various scenarios, including sudden grid disconnection, load changes, and renewable energy fluctuations.

Figure 19 illustrates the response of the islanding detection mechanism during a simulated islanding event. As shown, the system successfully detects the islanding condition within a short timeframe and triggers appropriate actions to maintain the microgrid's stability. The detection mechanism considers factors such as frequency deviation, voltage deviations, and rate of change of frequency (ROCOF), among others, to make accurate decisions.

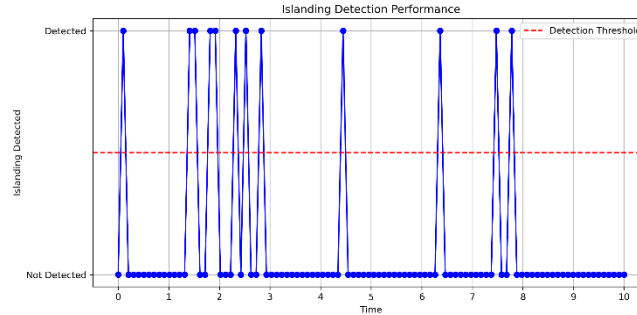


Figure 19. Islanding detection performance during a simulated event

Moreover, the islanding detection system proved effective in distinguishing between actual islanding events and transient disturbances. This capability prevents unnecessary disconnection of the microgrid from the utility grid during momentary disturbances, ensuring seamless operation while maintaining grid stability.

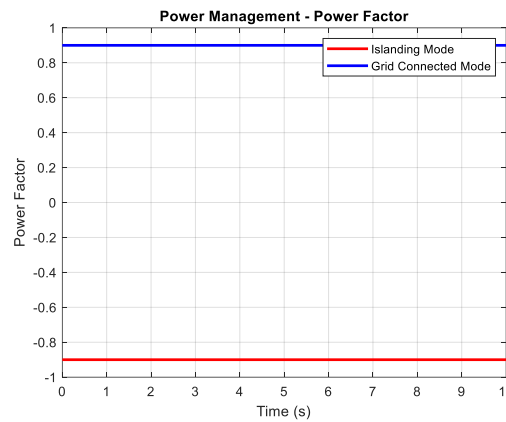


Figure 93 Power Management Power Factor

Commonly used to identify islanding is the Rate of Change in Frequency (ROCOF) technique. The theory stems from the observation that the system's frequency undergoes fast fluctuations upon islanding. One definition of the ROCOF is:

$$ROCOF = \frac{df}{dt}$$

where f is the system's frequency and t is the elapsed time.

System parameters and desired detection sensitivity inform the ROCOF threshold value. The typical ROCOF threshold is between 0.5 and 1 Hz/s.



It's worth noting that the ANFIS-based control approach enhances the islanding detection system's accuracy by providing real-time inputs based on the microgrid's actual operating conditions. This dynamic input helps the detection mechanism adapt to changing scenarios and improve its overall performance.

CONCLUSION

The isolated three-phase applications, control of a solar PV-wind hybrid system is presented. Solar and wind energy are combined in a DC connection with a backup battery. The load is fed by an inverter. PV is connected to the DC interface through a boost converter that performs MPPT (Demand Power Control) and boosts the output voltage as needed. A rectifier and boost converter incorporate the wind energy conversion PMSG into MPPT's DC connection. For battery integration, a bidirectional converter maintains the DC link at a predetermined level to distribute energy according to energy generation and load demand. By matching current load needs, the ANFIS algorithm precisely pulls electricity from the photovoltaic (PV) source to prevent battery exhaustion or overcharging. Islanding boosts wind system efficiency and battery life. A synchronous reference frame transition boosts inverter performance. Optimisation adjusts AC output voltage, obtains accurate load active power data, and simplifies operation. The inverter is carefully adjusted for output voltage and frequency. The PV Boost, bidirectional converter, and inverter perform efficiently with inner current and outer voltage control modes.

REFERENCES

- [1] M. Panteli, D. Trakas, P. Mancarella, and N. Hatziaargyriou, "Boosting the power grid resilience to extreme weather events using defensive islanding," *IEEE Trans Smart Grid*, vol. 7, no. 6, pp. 2913–2922, 2016.
- [2] A. Hussain, V. H. Bui, and H.-M. Kim, "A resilient and privacy-preserving energy management strategy for networked microgrids," *IEEE Trans Smart Grid*, vol. 9, no. 3, pp. 2127–2139, 2018.
- [3] Z. Liang, Q. Alsafasfeh, and W. Su, "Proactive Resilient Scheduling for Networked Microgrids With Extreme Events," *IEEE Access*, vol. 7, pp. 112639–112652, 2019.
- [4] S. Iqbal, A. Xin, M. U. Jan, H. Rehman, S. Salman, and S. A. Abbas Rizvi, "Improvement in the Efficiency of Inverter Involved in Microgrid," in *2018 2nd IEEE Conference on Energy Internet and Energy System Integration (EI2)*, Beijing, 2018, pp. 1-5.
- [5] M. H. Amirioun, F. Aminifar, and H. Lesani, "Resilience-oriented proactive management of microgrids against windstorms," *IEEE Transactions on Power Systems*, vol. 33, no. 4, pp. 4275-4284, 2017.
- [6] M. Panteli, C. Pickering, S. Wilkinson, R. Dawson, and P. Mancarella, "Power system resilience to extreme weather: fragility modeling, probabilistic impact assessment, and adaptation measures," *IEEE Transactions on Power Systems*, vol. 32, no. 5, pp. 3747-3757, 2016.
- [7] S. Iqbal et al., "Feasibility Study and Deployment of Solar Photovoltaic System to Enhance Energy Economics of King Abdullah Campus, University of Azad Jammu and Kashmir Muzaffarabad, AJK Pakistan," in *IEEE Access*, vol. 10, pp. 5440-5455, 2022, doi: 10.1109/ACCESS.2022.3140723.



- [8] A. Gholami, T. Shekari, and S. Grijalva, "Proactive management of microgrids for resiliency enhancement: An adaptive robust approach," *IEEE Transactions on Sustainable Energy*, vol. 10, no. 1, pp. 470-480, 2017.
- [9] R. M. Elavarasan et al., "A Comprehensive Review on Renewable Energy Development, Challenges, and Policies of Leading Indian States with an International Perspective," *IEEE Access*, vol. 8, pp. 74432–74457, 2020, doi: 10.1109/ACCESS.2020.2988011.
- [10] S. Iqbal, A. Xin, M. U. Jan, and M. A. Abdelbaky, "Improvement of Power Converters Performance by an Efficient Use of Dead Time Compensation Technique," *Appl. Sci.*
- [11] X. Dong, H. Lin, R. Tan, R. K. Iyer, and Z. Kalbarczyk, "Software-defined networking for smart grid resilience: Opportunities and challenges," in *Proceedings of the 1st ACM Workshop on Cyber-Physical System Security*, 2015, pp. 61-68.
- [12] F. H. Jufri, V. Widiputra, and J. Jung, "State-of-the-art review on power grid resilience to extreme weather events: Definitions, frameworks, quantitative assessment methodologies, and enhancement strategies," *Applied Energy*, vol. 239, pp. 1049-1065, 2019.
- [13] S. Iqbal, S. Habib, N.H. Khan, M. Ali, M. Aurangzeb, and E.M. Ahmed, "Electric Vehicles Aggregation for Frequency Control of Microgrid under Various Operation Conditions Using an Optimal Coordinated Strategy," *Sustainability*, vol. 14, no. 5, p. 3108, 2022.
- [14] S. Iqbal et al., "Role of Power Electronics in Primary Frequency Control and Power Quality in an Industrial Micro-grid Considering V2G Technology," *2019 IEEE 3rd Conference on Energy Internet and Energy System Integration (EI2)*, 2019, pp. 1188-1193, doi: 10.1109/EI247390.2019.9062071.
- [15] M. Aurangzeb, A. Xin, S. Iqbal and M. U. Jan, "An Evaluation of Flux-Coupling Type SFCL Placement in Hybrid Grid System Based on Power Quality Risk Index," in *IEEE Access*, vol. 8, pp. 98800-98809, 2020, doi: 10.1109/ACCESS.2020.2996583.
- [16] H. Ur Rehman, X. Yan, M. A. Abdelbaky, M. Ullah Jan, and S. Iqbal, "An advanced virtual synchronous generator control technique for frequency regulation of grid-connected PV system," *Int. J. Electr. Power Energy Syst.*, vol. 125, no. June 2020, p. 106440, 2021, doi: 10.1016/j.ijepes.2020.106440.
- [17] Z. Wang, et al., "Risk-limiting load restoration for resilience enhancement with intermittent energy resources," *IEEE Transactions on Smart Grid*, vol. 10, no. 3, pp. 2507-2522.
- [18] S. Iqbal et al., "Aggregation of EVs for Primary Frequency Control of an Industrial Microgrid by Implementing Grid Regulation Charger Controller," *IEEE Access*, vol. 8, pp. 141977–141989, 2020, doi: 10.1109/ACCESS.2020.3013762.
- [19] A. Hussain, V. H. Bui, and H.-M. Kim, "Resilience-oriented optimal operation of networked hybrid microgrids," *IEEE Transactions on Smart Grid*, vol. 10, no. 1, pp. 204-215, 2017.
- [20] N.-M. Zografou-Barredo, et al., "Micro Grid Resilience-Oriented Scheduling: A Robust MISOCP Model," *IEEE Transactions on Smart Grid*, 2020.
- [21] M. Aurangzeb, X. Ai, M. Hanan, M. U. Jan, H. Ur Rehman and S. Iqbal, "Single Algorithm Mpsso Depend Solar And Wind Mppt Control And Integrated With Fuzzy Controller For Grid Integration," *2019 IEEE 3rd Conference on Energy*



ICSET-23

*Proceedings of the 5th International Conference on Sustainable
Energy Technologies (ICSET 2023) Peshawar, Pakistan
14-15 December 2023*



UET Peshawar

- [22] C. Wang et al., "Resilience enhancement with sequentially proactive operation strategies," *IEEE Transactions on Power Systems*, vol. 32, no. 4, pp. 2847-2857, 2016.
- [23] M. U. Jan, A. Xin, H. U. Rehman, M. A. Abdelbaky, S. Iqbal, and M. Aurangzeb, "Frequency Regulation of an Isolated Microgrid With Electric Vehicles and Energy Storage System Integration Using Adaptive and Model Predictive Controllers," *IEEE Access*, vol. 9, pp. 14958-14970, 2021, doi: 10.1109/ACCESS.2021.3052797.
- [24] Z. Bie, Y. Lin, G. Li, and F. Li, "Battling the extreme: A study on the power system resilience," *Proceedings of the IEEE*, vol. 105, no. 7, pp. 1253-1266, 2017.
- [25] M. U. Jan, A. Xin, M. A. Abdelbaky, H. U. Rehman, and S. Iqbal, "Adaptive and Fuzzy PI Controllers Design for Frequency Regulation of Isolated Microgrid Integrated with Electric Vehicles," *IEEE Access*, vol. 8, pp. 87621-87632, 2020, doi: 10.1109/ACCESS.2020.2993178.
- [26] M. Panteli et al., "Boosting the power grid resilience to extreme weather events using defensive islanding," *IEEE Transactions on Smart Grid*, vol. 7, no. 6, pp. 2913-2922, 2016.

Paper ID: ICSET-2320

NATURAL GAS FLOW OPTIMIZATION IN GAS TRANSMISSION NETWORK USING PRESSURE PROFILING & ISOLATION TECHNIQUES

Syed Tahir Shah¹, Fazal Muhammad^{2,*}, Syed Kashif Shah³, Maleeha Gul⁴

^{1,2}Department of Electrical Engineering, UET Mardan, Pakistan

³Dassu Hydro Project WAPDA, Dassu, District Kohistan, Pakistan

⁴Bio-Chemistry Department, NMC Nowshera, Khyber Pakhtunkhwa, Pakistan

**Corresponding author*

Email: fazal.muhammad@uetmardan.edu.pk

ABSTRACT

In recent days, natural gas relatively clean and quality source of energy which is recovered from deep wells by expensive drilling activities. The recovered substance is purified by processing in multiple stages to remove the unwanted/contaminants like dust, dirt, crude oil and other particles. Mostly, gas utilities are concerned regarding essential objectives of quantity / quality of natural gas delivery, financial outcome and safe natural gas volumetric inventory in the transmission gas pipeline. Gas quantity and quality are primarily related to standards / advance metering procedures in processing units / transmission system and the financial outcome is defined by purchasing and selling gas, also operational cost of transmission pipeline. Natural gas transmission Network having different range of diameters of pipelines used for transportation of natural gas from gas producing sources to Gas control stations/end users. This research results answer few of the issues in accuracy / metering procedures via multiple advanced gadgets for gas flow attributes after being utilized to the transmission system and research. The effects of good pressure management in transmission gas pipeline network in contemplation to boost the gas volume deposited in the existing network and finally curbing gas losses Unaccounted for gas (UFG) for financial benefits. Furthermore, depend on the results and their observation, it is directed to enhance the maximum allowable working/operating pressure (MAOP) of the system to 1235 PSIG from the currently round about 900 PSIG, such that the capacity of the network could be entirely utilized. In gross, the results depict that the current model is very efficient and provided excellent result in a minimum possible time.

KEYWORDS: Natural Gas, Pipeline Network, AGA, UFG, Transmission Pack

INTRODUCTION

The energy efficiency and conservation is an integral part of most of the businesses, and essential to an organizational success and client satisfaction of any natural gas transportation company. The Natural gas provides good energy which boosts a client service, reduces the operational costs, and improves the monetary position of the organization [1]. Although, the company's operations differ in nature thus do their energy efficiency, the partners have the same role and importance in any supply chain. In the past, businesses operated as separate units with no or minimum dependence on other organizations; but in recent times, businesses is operating as energy efficiently and success of a business is linked with the success of energy conservation. Today, the competition is between efficient energy supply rather than the single business units



which have some kind of energy losses [2]. Similarly, in other parts of the globe, the reliance of Pakistan on natural gas elevates over the last few decades and, a continuous and proper supply of natural gas has become mandatory for the businesses and also daily activities in all spectrum of society. The Natural gas from indigenous gas sources was supplied to consumer to meet demands till 2016. But, owing to the declining current reserves and no alternative for the same, the import of LNG was initiated to bridge the gap between supply and demand. From that moment on, the quantum of the RLNG in the natural gas mixture is on upward trend [3]. The supply chain of natural gas has become intricate and confusing after the injection of imported LNG both in basis of supply continuity and the economics of natural gas [4]. Hence, to optimize supply chain of natural gas is the answer to provide a low cost and continuous energy resource. Consequently, the size and complication of the NG pipeline network will also rise exponentially.

There are two publicly owned companies in Pakistan, that are involved in the business of gas transmission and distribution i.e., Sui Northern Gas Pipelines Ltd. (SNGPL) and Sui Southern Gas Company (SSGC); with the former operating in Punjab, KPK, AJK and parts of Sindh and, the latter in Sindh and Baluchistan. Our research is focused on the optimization of the transmission network of SNGPL with minimum losses (UFG). Sui Northern Gas Pipelines Ltd [7]. (SNGPL) is the largest integrated natural gas provider in the country with an area of operation expanding over Punjab, KPK, AJK, and some parts of Sindh. SNGPL is involved in the construction of gas pipeline networks and, the transmission and distribution of natural gas [8]. The transmission network of SNGPL has a pipeline length of more than 9100 km, which is increasing with each passing year [9].

Pakistan Energy supplies by Source 2021-22

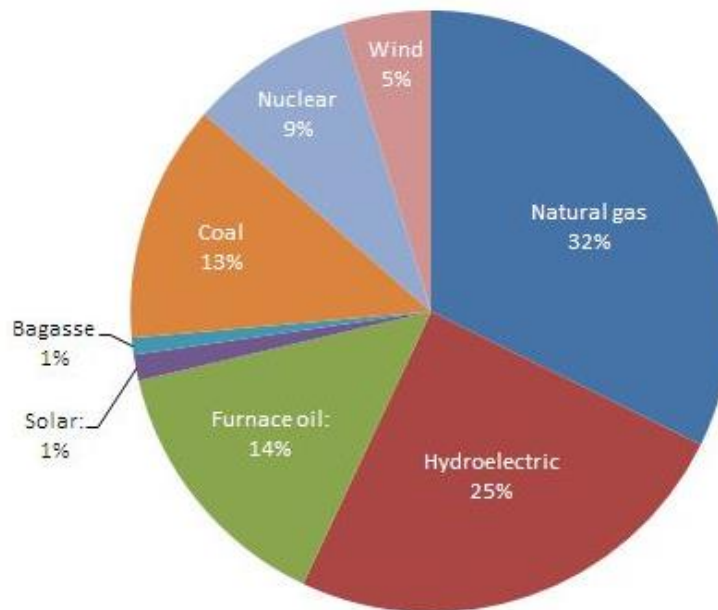


Figure 1. The Energy Mix of Pakistan as of 2021-22

The agreement between Russia and Pakistan overlaying the North-South gas pipeline, which will transport natural gas from Karachi to Lahore, is the most recent example. The transmission network is a



ICSET-23



UET Peshawar

high-pressure system of natural gas, which transports natural gas from its different sources including indigenous gas fields and Regasified Liquefied Natural Gas (RLNG) terminals to the border of different cities, towns, and industrial hubs [10]. Therefore, the safe and uninterrupted operation of the transmission network has strategic importance, whereas, optimal expansion and operation are very important in terms of cost [11]-[12].

The natural gas flow dynamics in transmission pipeline network are complex due to the relation between the gas stream pressure and gas flow [5]. Further, the demand and supply gap of gas makes our system to save the gas through pressure profiling and gas isolation technique during off peak and night hours. The data retrieval of measurement gadgets is compulsory to study the daily/hourly load trends which further needs to the adjustment of Pressure Control Valves installed at all 10 nodes for the control of gas flow. In literature, the uni-directional gas flow is considered in the sample network model using software applications with installed measurement gadgets in this sample network. Orifice Meter Runs with Flow Computers using software of American Gas Association standard (AGA-3) i.e. Roclink with modbus protocol for SCADA communication, Bristol, Field tools and Kelton Gas flow software programs. Similarly, American Gas Association (AGA-8)'s complaint software programs are utilized for the gas turbine meters installed at nodes along with Electronic Volume Correctors (EVCs) i.e. Telves and Cordal. In this research work, it is assumed that sample network model can operate in single direction to fully utilize maximum capacity of the transmission network and the nodes. The objective of this study is to develop a sample model for the network considering flow, pressure, demand supply ratio limits and other constraints. The same has been validated by applying it to a small network as case study and to develop different scenarios for the existing and future flows on the network [6]. The considerable gas losses UFG can be reduced by even small pressure reduction or flow restriction in off peak times in the existing Network design and operation conditions. The desirable UFG target has been studied in three different case studies considering measurement gadgets data analysis which has minimized the gas flow by optimizing system gas pressure and flow variables.

SYSTEM MODEL

The complex pipeline network includes three types of pipelines along the transportation route

Gathering Pipeline System

The gathering system consists of low/high-pressure pipelines, depending upon the wellhead pressures, which transport the raw gas from wellheads to the gas processing plants[2]. Like pressures, diameters also depend on the flow of natural gas through the pipelines [13]. In the gathering system, the raw gas can be multiphase that contains the oil, gas, and water all in the gaseous form, depending on the nature of the reservoir. The gathering pipelines are carefully designed keeping in view the composition of natural gas if it contains sulfur compounds, which may deteriorate the pipeline and result in potential hazards. A typical gathering pipeline system is shown in Figure 2.

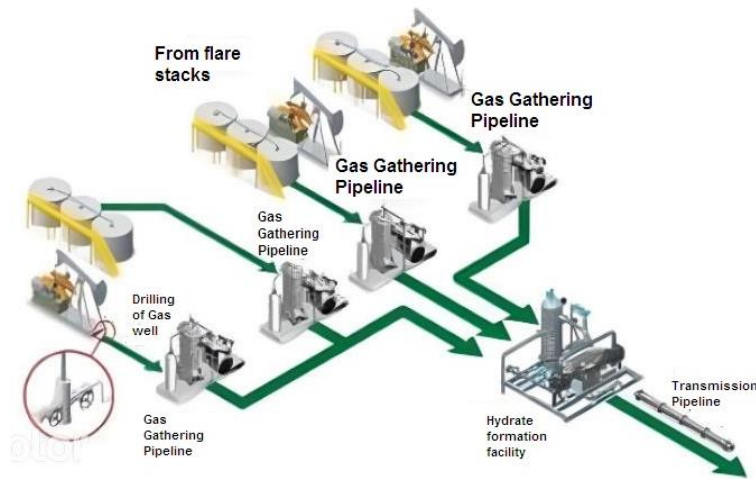


Figure 2. Gathering Pipeline System

Transmission Pipeline System

The natural gas transmission pipeline systems are comprised of high-pressure pipelines, pressure ranging typically 200-1500 psi, with a diameter range between 6-48 inches. These systems carry natural gas from the production facilities and deliver it over large distances to the consumption hubs. The natural gas transmission networks form the middle part of the natural gas transportation system [14]. They act as a bridge between production facilities and the gas distribution networks. A hypothetical transmission network is shown in Figure 3.

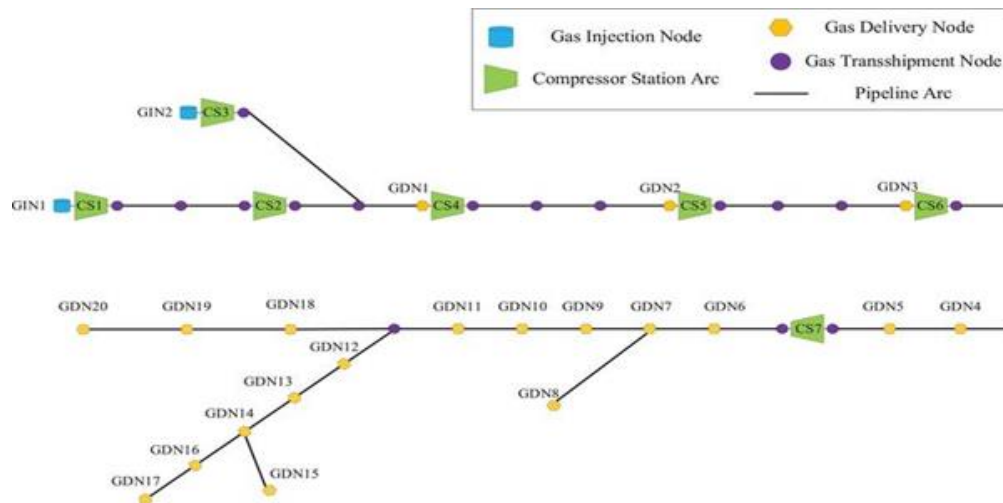


Figure 3. A Typical Gas Transmission Network

Distribution Pipeline Systems

The gas distribution systems are low-pressure pipeline networks with diameters ranging from 2 to more than 24 inches. These networks deliver natural gas from the city gate station to the end consumers. The smaller diameter pipelines can be made of mild steel (MS) or high-density polyethylene (HDPE) [15]. A typical Gas Distribution is shown in Figure 4.

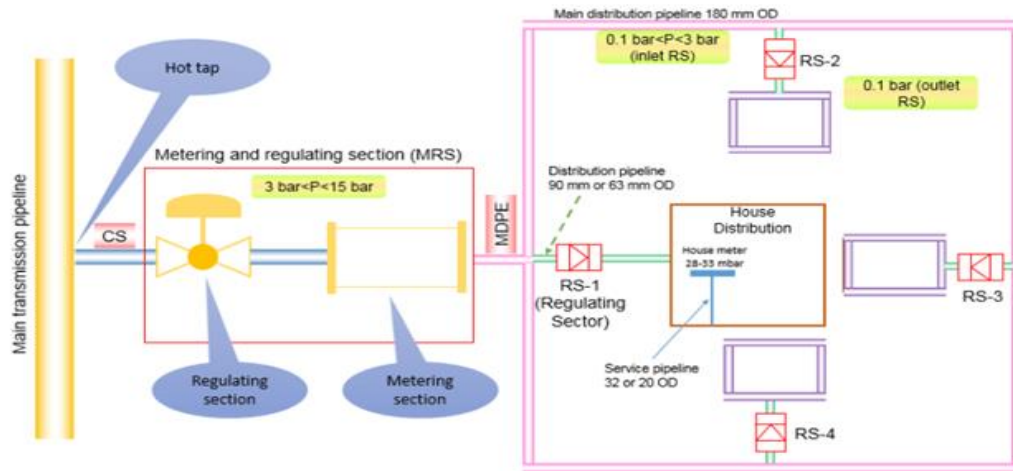


Figure 4. A typical Gas Distribution

RESULTS AND ANALYSIS

The generalized gas network of 10 Gas Control Stations/Nodes have been taken for the experimental workup as a case study. Each node has different flow capacity and different load requirement due to population of villages at the downstream of nodes where gas supply network is available. All the nodes must have advance measurement gadgets with healthy conditions to record pressure/flow logs with correct time. For the cross checking of measurement gadgets, check meter (source) must be available to ensure the health of downstream network gadgets for accuracy in measurement in the installed gadgets on nodes. The network is operated by different pressure settings by using pressure control regulators.

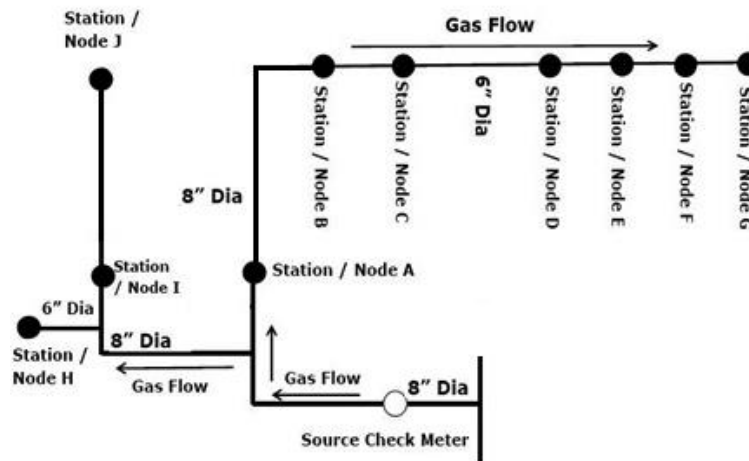


Figure 5. Schematic diagram of Transmission Gas Pipeline Network with Gas Control Stations.



A.

From the analysis of flow computers/EVC's retrieved data logs of gas pressure /flow at all ten nodes, it is clearly derivative from below table and graph that due to smart pressure profiling at Gas Control Stations (Nodes) almost 52.04% Gas flow reduced due to pressure reduction in off peak hours (day time) while 37.25% gas saving observed during night time by further reducing the gas pressure as the consumers have very less demand of gas usage for 8 hours during night. The average daily load observed as approximately 22.75 Million Cubic feet Per Day (MMCFD) at this sample Network. But the gas leakage / losses (UFG) is needed to be further minimized at defective points at the downstream of Distribution network while the transmission pack has improved up-to some extent in the night saving of gas.

Table 1: Average flows during peak, off peak and night shift gas flow thru Sales Meter Stations

| Sr. No. | Nodes | Classification with Capacity (MMCFD) | Peak Flow | | Off Peak Flow | | Night | |
|---------|-------|--------------------------------------|-----------------|----------------|-----------------|----------------|-----------------|----------------|
| | | | Pressure (PSIG) | Volume (MMCFD) | Pressure (PSIG) | Volume (MMCFD) | Pressure (PSIG) | Volume (MMCFD) |
| 1 | A | 1 | 19.65 | 0.89 | 9.36 | 0.42 | 3.45 | 0.01 |
| 2 | B | 8 | 33.93 | 5.78 | 15.42 | 2.63 | 3.98 | 0.55 |
| 3 | C | 2.5 | 29.85 | 2.93 | 12.98 | 1.33 | 7.20 | 0.88 |
| 4 | D | 2.5 | 8.15 | 0.25 | 3.40 | 0.10 | 3.30 | 0.09 |
| 5 | E | 2.5 | 15.22 | 1.44 | 6.09 | 0.58 | 4.45 | 0.52 |
| 6 | F | 1.5 | 18.75 | 1.09 | 9.38 | 0.55 | 5.25 | 0.40 |
| 7 | G | 1.5 | 14.95 | 1.22 | 7.48 | 0.61 | 3.56 | 0.44 |
| 8 | H | 2.5 | 20.35 | 1.29 | 10.18 | 0.65 | 5.98 | 0.47 |
| 9 | I | 2.5 | 15.1 | 1.7 | 7.55 | 0.85 | 4.33 | 0.62 |
| 10 | J | 30 | 28.73 | 11.97 | 14.36 | 5.99 | 6.59 | 4.61 |
| Total | | | | 28.56 | | 13.71 | | 8.59 |

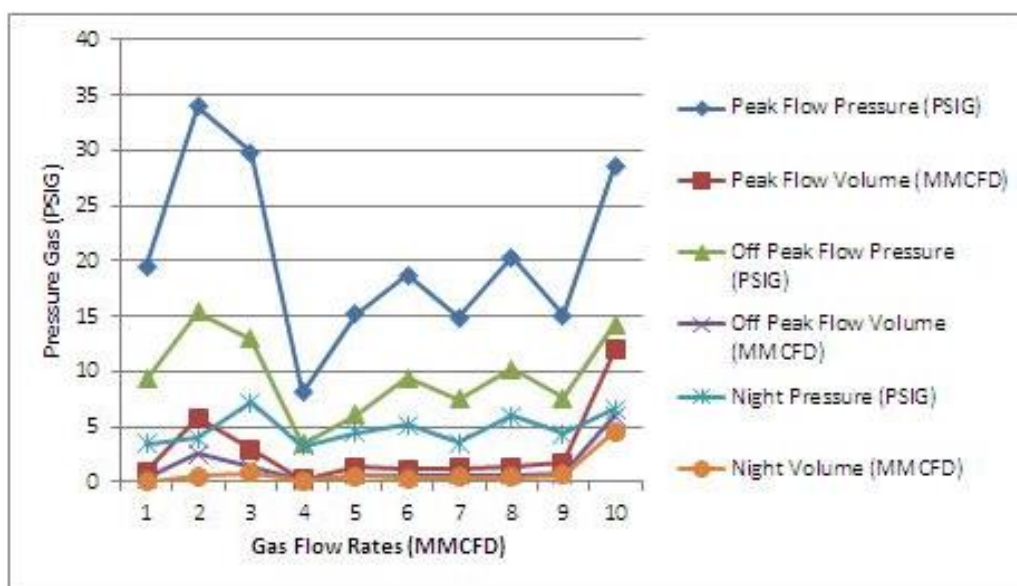


Figure 6. Pressure/Flow rate diagram of Smart Pressure Profiling through Pressure Control Valves



B.

From the analysis of flow computers/EVC's retrieved data logs of gas pressure /flow at all ten nodes in Case Study-II, it is clearly derivative from below table and graph that due to further pressure reduction / profiling up-to 50% at Gas Control Stations (Nodes) almost 51.78% Gas flow reduced due to pressure reduction in off peak hours (day time) while 29.44% gas saving observed during night time by further reducing the gas pressure. The average daily load observed as approximately 18.65 Million Cubic feet Per Day (MMCFD) at this sample Network, due to this pressure reduction approximately 4.10 MMCFD gas saved as compare to Case Study-I and this will further increase the pack by this volume of gas. Also the gas leakage / losses (UFG) is minimized at defective points at the downstream of Distribution network while the transmission pack has improved as compared to case Study-I saving of gas.

Table 2: Average flows during peak, off peak and night shift gas flow thru Sales Meter Stations

| Sr. No. | Nodes | Classification with Capacity (MMCFD) | Peak Flow | | Off Peak Flow | | Night | |
|---------|-------|--------------------------------------|-----------------|----------------|-----------------|----------------|-----------------|----------------|
| | | | Pressure (PSIG) | Volume (MMCFD) | Pressure (PSIG) | Volume (MMCFD) | Pressure (PSIG) | Volume (MMCFD) |
| 1 | A | 1 | 13.755 | 0.58 | 6.55 | 0.27 | 3.45 | 0.17 |
| 2 | B | 8 | 23.751 | 3.50 | 10.80 | 1.59 | 3.98 | 0.75 |
| 3 | C | 2.5 | 20.895 | 1.55 | 9.08 | 0.70 | 7.20 | 0.46 |
| 4 | D | 2.5 | 5.705 | 0.19 | 2.38 | 0.08 | 3.30 | 0.16 |
| 5 | E | 2.5 | 10.654 | 1.11 | 4.26 | 0.44 | 4.45 | 0.33 |
| 6 | F | 1.5 | 13.125 | 0.84 | 6.56 | 0.42 | 5.25 | 0.25 |
| 7 | G | 1.5 | 10.465 | 0.94 | 5.23 | 0.47 | 3.56 | 0.28 |
| 8 | H | 2.5 | 14.245 | 0.99 | 7.12 | 0.50 | 5.98 | 0.29 |
| 9 | I | 2.5 | 10.57 | 1.31 | 5.29 | 0.65 | 4.33 | 0.49 |
| 10 | J | 30 | 20.11 | 9.43 | 10.05 | 4.71 | 6.59 | 3.78 |
| Total | | | | 20.44 | | 9.83 | | 6.96 |

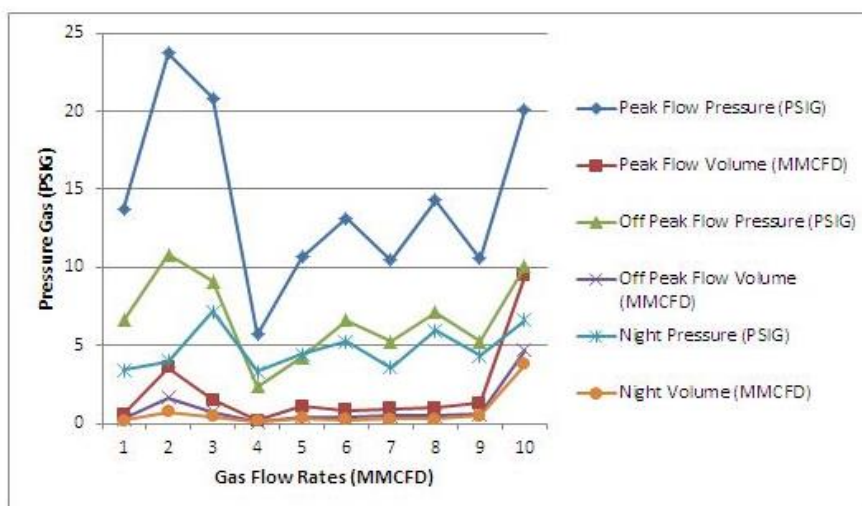


Figure 7. Pressure/Flow rate diagram of Smart Pressure Profiling through Pressure Control Valves

C.

From the analysis of flow computers/EVC's retrieved data logs of gas pressure /flow at all ten nodes in Case Study-III, it is clearly derivative from below table and graph that due to minimum pressure reduction / profiling up-to 55% at Gas Control Stations (Nodes) almost 57.932% Gas flow reduced due to pressure reduction in off peak hours (day time) while 60.34% gas saving observed during night time by implementing shutdown (Zero Gas flow at 6 nodes) and further minimizing the remaining nodes gas pressure at night. The average daily load observed as approximately 15.50 Million Cubic feet Per Day (MMCFD) at this sample Network, due to this pressure reduction approximately 7.25 MMCFD gas saved as compare to Case Study-I and 3.15 MMCFD gas is saved as compare to Case Study-II. The best analysis is observed in this sample model as almost 7.25 MMCFD gas increased the pack by this volume of gas. Also the gas leakage / losses (UFG) is highly minimized at defective points at the downstream of Distribution network while the transmission pack has improved as compared to both case Study-I & case study-II saving of gas.

Table 3: Average flows during peak, off peak and night shift gas flow thru Sales Meter Stations

| Sr. No. | Nodes | Classification with Capacity (MMCFD) | Peak Flow | | Off Peak Flow | | Night | |
|---------|-------|--------------------------------------|-----------------|----------------|-----------------|----------------|-----------------|----------------|
| | | | Pressure (PSIG) | Volume (MMCFD) | Pressure (PSIG) | Volume (MMCFD) | Pressure (PSIG) | Volume (MMCFD) |
| 1 | A | 1 | 11.79 | 0.71 | 5.61 | 0.25 | 3.45 | 0.01 |
| 2 | B | 8 | 20.36 | 2.62 | 9.25 | 1.58 | 3.98 | 0.55 |
| 3 | C | 2.5 | 17.91 | 1.84 | 7.79 | 0.80 | 0.00 | 0.00 |
| 4 | D | 2.5 | 4.89 | 0.2 | 2.04 | 0.06 | 3.30 | 0.09 |
| 5 | E | 2.5 | 9.132 | 1.152 | 3.65 | 0.35 | 0.00 | 0.00 |
| 6 | F | 1.5 | 11.25 | 0.872 | 5.63 | 0.33 | 0.00 | 0.00 |
| 7 | G | 1.5 | 8.97 | 0.976 | 4.49 | 0.37 | 0.00 | 0.00 |
| 8 | H | 2.5 | 12.21 | 1.032 | 6.11 | 0.39 | 0.00 | 0.00 |
| 9 | I | 2.5 | 9.06 | 1.36 | 4.53 | 0.51 | 0.00 | 0.00 |
| 10 | J | 30 | 15.24 | 8.78 | 7.62 | 3.59 | 3.59 | 2.61 |
| Total | | | | 19.54 | | 8.23 | | 3.26 |

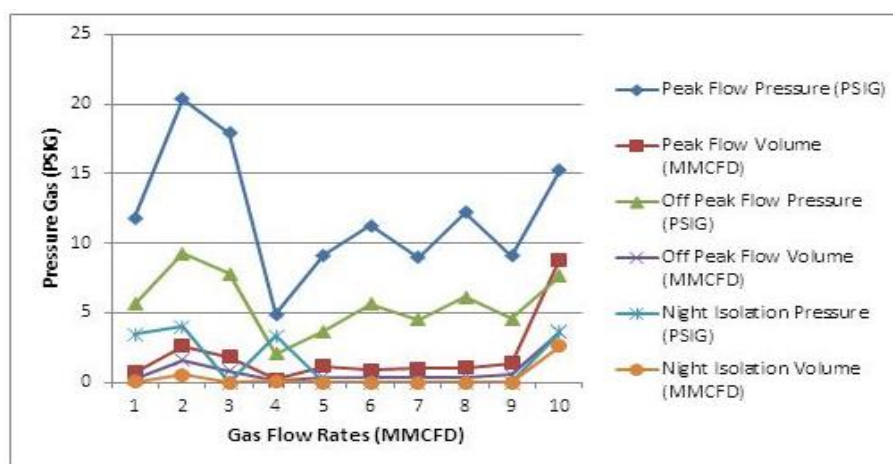


Figure 8. Pressure/Flow rate diagram of Smart Pressure Profiling through Pressure Control Valves



CONCLUSION AND FUTURE WORK

The financial loss faced by the Natural Gas Company is one of the prime issues in respect of UFG (Gas losses). To address this issue, reconciliation of gas volume and network load balancing techniques have been considered to identify UFG and the associated factors in considered case studies in one of sample Network. Leakage is one of the main factors of UFG following measurement error, however, reconciliation of gas volume is assumed one of the techniques to eliminate the gas metering errors while for minimizing the leakages UFG gas losses the smart pressure profiling is considered to be the best tool till the rehabilitation of old network. The remedial actions have also been taken as part of this study which results in reduction of UFG at downstream network as discussed in case study-III i.e. savings of 7.25 MMCFD gas per day and ultimately adding to the transmission pack instead of gas loss.

The implementation of sample network model to the any organization doing the business of gas transportation using transmission pipeline network cannot only result into savings of gas means reduced gas losses (UFG) thus increasing financial impact of the Natural Gas Company. The research study is restricted to an area comprising known consumers which resulted a decrease of UFG figure from 18.09% to 14.6% in the year 2022-23.

Since, the privilege to this method in the gas transmission network must be segregated for the reconciliation of gas volume data and correcting the measurement errors using advance measurement techniques specially installations of gas meters on TBSs (Town Border Stations) and ensuring weekly reconciliation of gas volume which not only helps in leakage rectification but reducing UFG, therefore, initiatives required to be taken by the gas utilities companies to make profitable the organization.

REFERENCES

- [1] Bianchini, A., Sacconi, C., Guzzini, A., & Pellegrini, M. (2018). Gas Smart Metering in Italy: State of the Art and Analysis of Potentials and Technical Issues,” in Proceedings of 23rd Summer School “"Francesco Turco"” - Industrial Systems Engineering 2018; Grand Hotel et des PalmesPalermo; Italy; 12 September 2018.
- [2] B. Company, “BP Statistical Review of World Energy 2021”, University of Bradford.
- [3] Jun Zhou, Jinghong Peng, Guangchuan Liang and Tao Deng, “Layout optimization of tree-tree gas pipeline network”, Journal of Petroleum Science and Engineering, volume 173, pages 666-680.
- [4] <https://www.sngpl.com.pk>
- [5] Sircar, A., Yadav, K. Optimization of city gas network: a case study from Gujarat, India. SN Appl. Sci. 1, 769 (2019).
- [6] Report on Smart Gas Metering. (2010). [online].[accessed 8 June 2020].
- [7] Liu, K., Biegler, L. T., Zhang, B., and Chen, Q. (2020). Dynamic Optimization of Natural Gas Pipeline Networks with Demand and Composition Uncertainty. Chem. Eng. Sci. 215, 115449.
- [8] Rey, J. R. C., Pio, D. T., and Tarelho, L. A. C. (2021). Biomass Direct Gasification for Electricity Generation and Natural Gas Replacement in the Lime Kilns of the Pulp and Paper Industry: A Techno-Economic Analysis. Energy 237, 121562.
- [9] Statistical Review of World Energy (2021). Statistical Review of World Energy. London:



ICSET-23

*Proceedings of the 5th International Conference on Sustainable
Energy Technologies (ICSET 2023) Peshawar, Pakistan
14-15 December 2023*



UET Peshawar

- [10] Su, H., Chi, L., Zio, E., Li, Z., Fan, L., Yang, Z., et al. (2021). An Integrated, Systematic Data-Driven Supply-Demand Side Management Method for Smart Integrated Energy Systems. *Energy* 235, 121416. doi:10.1016/j.energy.2021.121416.
- [11] Wood, D. A. (2020). The Natural Gas Sector Needs to Be Mindful of its Sustainability Credentials. *Adv. Geo-energy Res.* 43, 229–232. doi:10.46690/ager.2020.03.01
- [12] Zhang, T., Bai, H., and Sun, S. (2021). A Self-Adaptive Deep Learning Algorithm for Intelligent Natural Gas Pipeline Control. *Energ. Rep.* 7, 3488–3496.
- [13] Li, Z., Zhang, H., Meng, J., Long, Y., Yan, Y., Li, M., et al. (2020). Reducing Carbon Footprint of Deep-Sea Oil and Gas Field Exploitation by Optimization for Floating Production Storage and Offloading. *Appl. Energ.* 261, 114398.
- [14] Andre J, Bonnans F, Cornibert L (2009) Optimization of capacity expansion planning for gas transportation networks. *Eur J Oper Res* 197(3):1019–1027.
- [15] Babu BV, Angira R, Chakole PG, Syed Mubeen JH (2003) Optimal design of gas transmission network using differential evolution. In: *Proceedings of the second international conference on computational intelligence, robotics, and autonomous systems (CIRAS-2003)*, Singapore, December 15–18, PS0402, pp 01–07.

Paper ID: ICSET-2321

Energy Efficient HVAC System Selection for an Educational Building

Adnan Daud Khan, Muhammad Riazul Islam*

Renewable Energy Engineering, US-Pakistan Center for Advanced Studies in Energy, University of Engineering and Technology Peshawar, Pakistan

**Corresponding author*

Email: mriazulislam.uspcase@uetpeshawar.edu.pk

ABSTRACT

One of the current rising challenges in technical and engineering research is energy efficiency. Globally, the demand for energy conservation rises along with the construction of especially tall structures. As the air conditioning system consumes the most energy in buildings. The kind of technology employed has a considerable impact on both its energy usage and energy efficiency. As the conditioned air for a space can be achieved through different HVAC systems which mainly includes Variable Refrigerant Flow system, Package type Air Handling Units, DX- Air Handling Units and Chiller type HVAC system. Chiller is further categorise in water cooled chiller and air cooled Chiller system. This study compares different types of HVAC system for operation in an educational building to get the most suitable and energy efficient cooling system. Technically, this study was performed using the Hourly Analysis Program software to determine the thermal load of the building and the electrical load was calculated from the catalogues of different manufacturers against that thermal loads of the respective systems and the electrical consumptions of each system has been calculated on annual basis. Depending upon the available conditions and the nature of the building and temperature requirements, most suitable HVAC system has been proposed for the selected building of University of Engineering and Technology Peshawar, Pakistan. This paper will contribute in selecting the appropriate HVAC system for any educational building with similar conditions.

KEYWORDS: HVAC, VRF, Chiller, EER, COP

INTRODUCTION

As long as the human comfort is important, the more energy efficient system that provides the comfort level is also important. As we look around in educational buildings, along with quality education, good quality of indoor air is also a basic requirement. HVAC system pays most important role in providing human comfort and a quality indoor air. To provide the best indoor air with an energy efficient system, proper design and HVAC system must be selected during the design phase. The HVAC system's primary goal is to ensure the thermal comfort of its users. This comfort level can be achieved through different HVAC systems. Depending upon the nature of building, owner budge and the plan of the designer different HVAC system may be proposed. Variable refrigerant flow (VRF), Direct Expansion Air Handling Units (DX-AHU) and Chillers are the most common HVAC systems.

Now a day almost all sort of buildings including commercial building, residential buildings, educational building and hospitals require HVAC system to treat the unconditioned air and to get comfortable and best indoor air quality. In HVAC system the HVAC equipment brings outdoor air and treat as per design



condition and then distributed throughout the space with needs to be centralized. These processes can be achieved through different types of HVAC systems. Depending upon the architectural plan of the building, the building owner requirements and the HVAC designer, different HVAC system may be selected.

The heating, cooling, and ventilation systems are among the necessary procedures. Humidification and dehumidification techniques can be implemented as additional processes. These procedures may be carried out by utilizing the appropriate HVAC equipment, such as heaters, air conditioners, ventilation fans, and dehumidifiers. Depending upon the type of the building, different HVAC systems may be proposed. These HVAC systems include variable refrigerant flow (VRF System), Direct Expansion Air Handling Units (DX-AHU) and Chiller System which may be Air Cooled and Water Cooled Type Chillers. All of the mentioned HVAC system has its advantages and limitations. In this study we have taken the department of Mechatronic Engineering, University of Engineering and Technology Peshawar, Pakistan, as a reference building.

Moreover, in this study we have calculated the actual cooling and heating load of the building and then we have proposed different HVAC systems, depending upon the given conditions and as per design requirements it has been noted that a chiller uses less electrical energy as compare to other VRF systems and a chiller is recommended for such type of educational buildings.

METHODOLOGY

In this study the total cooling load of the building has been calculated by using the HAP software as mentioned below.

Load Calculation Details And Results

The Ashrae outdoor design conditions for Peshawar station are given as follows:

Table I: Ashrae weather conditions for Peshawar station [1]

| Station | Peshawar, Pakistan |
|----------------------|--------------------|
| Latitude | 24 degree |
| Longitude | 72.5 degree |
| Summer Dry Bulb (°C) | 41.8 |
| Winter Wet Bulb (°C) | 29.4 |
| Winter Dry Bulb (°C) | 3.2 |

The load calculations for the reference building under the above mentioned designed conditions has been performed with the “Hourly Analysis Programmed” HAP 4.9. Based on the following input parameters i-e the thickness of the wall has been considers as 9 inches, the wattage of light has been consider as 1.5 watt per square feet, The average ceiling height has been taken as 10 feet and the value of outdoor air circulation rate in offices and class room has been taken as 5 CFM and 10 CFM respectively.

Total cooling and heating load and the total required flow of design air has been calculated and presented in Table 2. As clearly seen from Table 2. The total cooling load of the building is 166.5 Tons. if we consider 10% factor of safety, the total cooling load will be 180 tons.

Table 2: HAP report for Department of Mechatronics Engineering, UET

| Description | Values |
|--------------------------------|--------|
| Total coil Cooling load (Tons) | 166.5 |
| Sensible coil load (MBH) | 1244 |
| Coil CFM at Jun 1600 (CFM) | 42805 |
| ft ² /Ton | 136.9 |
| Resulting RH % | 49 |
| Max Coil Heating Load (MBH) | 841.1 |
| Coil CFM at Des Htg (CFM) | 24780 |

System Selection

As per the calculated load, different HVAC systems have been proposed and the advantages and disadvantages of these systems in order so select the appropriate HVAC system under the same conditions have been shown below. As it is clear from the above calculations and Table 2, that the total cooling load of the building is round about 180 tons. We have different options for selecting the HVAC system, which are listed below in table 3 and table 4.

Table 3: Option 1 VRF system

| VRF System | |
|--------------------------------------|--------|
| Description | values |
| | 180 |
| No. of Unit Outdoor Condensing Units | 05 |
| Cooling Capacity of Each Unit (Tons) | 37 |
| No. of Modules | 03 |
| Capacity /No. of Indoor Units | |
| 3 Ton | 20 |
| 2 Ton | 30 |
| 1.5 Ton | 40 |

Table 4: Option 2 Air Cooled Chiller system

| Air Cooled Chiller | |
|-------------------------------------|--------|
| Description | values |
| Total Cooling load (Tons) | 180 |
| No. of Chillers | 01 |
| Capacity /No. of Air Handling Units | |
| 40 Ton | 02 |
| 30 Ton | 02 |
| 20 Ton | 02 |

We have choices either to go for VRF system or we can also select an air-cooled chiller of 180 tons cooling capacity at the design conditions. The breakdown of load for VRF system includes 05 outdoor units each of 36 tons and each unit shall be consisting of 03 modules having both cooling and heating option while the breakdown of load for chiller system includes an air cooled chiller of 180 ton cooling capacity at the design conditions. The aim of this paper is to study and compare both the VRF system and Chiller system



applications, merits and demerits of both the systems and select the most suitable and an optimized HVAC system on the basis of above-mentioned conditions.

Variable Refrigerant Flow (Vrf) System

A refrigerant system known as a variable refrigerant flow (VRF) system typically consists of an outdoor unit that supplies a network of indoor units. The variable refrigerant flow (VRF) systems were first developed in Japan over 20 years ago and have since gained popularity throughout the world. However, they are still mostly uncommon in the United States. Since 1987, when it first entered European markets, the technology has progressively increased its market share all over the world. Around 50% of medium-sized commercial buildings (up to 70,000 ft² [6500 m²]) and one-third of big commercial buildings in Japan use VRF systems (more than 70,000 ft² [6500 m²])[2]. VRF systems are more sophisticated, higher capacity ductless multi split systems with the enhanced ability to link ducted fan coil units. With multiple compressors, multiple evaporators, and extensive management and control systems for oil and refrigerant, they are fundamentally more advanced than multiplies. Since they don't offer ventilation, a different ventilation system is required. The heat pump type and the heat recovery type are the two popular VRF types. On the other hand, Heat recovery VRF system can provide both cooling and heating on same unit. the heat pump type VRF system only provides only cooling or heating at a time.

Advantages of VRF System

The variable Refrigerant flow VRF system is almost 20 years old technology which has so many advantages. Some of the main applications and advantages of the VRF system are listed below:

1. *Easy Installation:* Unlike Chiller which are very heavy in weight and need crane for movement and installation, a VRF outdoor is comparatively lightweight and each module of the VRF system can be installed and fitted, without the use of any heavy machinery. The comparatively reduced weight may also reduce the requirements for the structural reinforcement of roof. Multiple indoor systems are connected to the one or more outdoor unit to achieve the desired cooling or heating but the system can be controlled by a common control system.
2. *User Friendly:* The variable refrigerant Flow systems are very easy to operate and maintain. As chillers requires an expert for operation and highly experienced technician for solving the technical issues.
3. *Testing and Commissioning:* With its standardized setups and advanced electronic controls, VRF systems strive for commissioning that is almost plug-and-play. The maintenance expenses for a VRF should be lower than for water-cooled chillers because they are DX systems; therefore problems with water treatment are avoided. Similar to any DX system, a VRF's maintenance primarily include changing filters and cleaning coils.
4. *Energy Efficiency Ratio (EER):* VRF systems' energy efficiency is influenced by a number of variables. Duct losses, which are frequently estimated to account for 10% to 20% of the total airflow in a ducted system, are essentially eliminated by the VRF. Each condensing unit in VRF systems typically contains two to three compressors, one of which is a variable speed compressor, allowing for extensive capacity modulation.

Below mentioned Table 3 have values from the Catalogue of Mitsubishi Electronics showing the nominal capacities of different models under same design conditions. In this catalogue the EER values of VRF system at different load valves has been taken noted:

Table 5: VRF catalogue of Mitsubishi Electronics [3]



| Model | | FDC1 200 | FDC1 250 | FDC130 0 |
|---|-----|-------------|-------------|-------------|
| Nominal Cooling Capacity | kw | 120 | 125 | 130 |
| Cooling Power Consumption | kw | 32.88 | 35.9 | 38.92 |
| Rated Energy Efficiency Coefficient in Cool | EER | 3.65 | 3.48 | 3.34 |
| Rated Energy Efficiency Coefficient in Heat | COP | 4.21 | 4.13 | 4.04 |
| Rated Current in Cool | AMP | 52.50 | 57.40 | 62.30 |

This method produces high part-load efficiency, which translates to significant seasonal energy efficiency as HVAC systems typically operate between 40% and 80% of their maximum capacity for the majority of the time [4].

Chiller Type Hvac System

Compressor, condenser, evaporator, and expansion device make up a chiller, a device that uses a vapor-compression or absorption refrigeration cycle to cool a fluid by extracting heat from it. As AHU system and Chillers system are categorized into Variable Air Volume (VAV). Based on national guidelines and standards, a VAV system provides a minimal amount of outdoor air to satisfy the occupants' need for indoor air quality (IAQ) [5].

A chiller has many advantages as shown by 'Nur, Sukri and their fellows in their study regarding the Optimal Operation of Chiller Plant in an Academic building. They have shown in their study that the electrical cost of chiller can be reduced up to 23% by making the system optimal as per their study [6].

Advantages of Chiller Type System

1. *Longer Life.* The life of the chiller unit is analyzed, as indicated in table 4, taking into account the equipment's ageing and degradation, condition evaluation, failure risk assessment, feedback experience, design life, and other factors.

Table 6: Life Assessment of Chillers [7]

| Condenser Type | Design Life (Year) | Aging Life (Years) | Feedback Experience Life (Year) | Comprehensive Life (Year) |
|---|--------------------|--------------------|---------------------------------|---------------------------|
| Water-Cooled | 40/50 | 40/25 | 25 | 25 |
| Water-Cooled (with outdoor water tower) | 25 | 20 | NA | 20 |
| Air-Cooled | 20 | 15 | 16 | 15 |

As clear from above-mentioned table the both the water cooled chillers and Air cooled Chillers have tremendous lifespan as compare to the VRF system.

2. *Indoor Plant Room.* Water cooled chiller has the advantage for businesses that don't have enough access to outdoor space, water-cooled chillers stay inside buildings while these chillers are non-noisy during the operation hours.



3. *Safety*. As the water cooled chillers used water as a primary refrigerant which is nontoxic and nonflammable like other chemicals, this make them safer for people who operates them.
4. *Energy Efficiency Ratio*. Both the water cooled and air cooled chillers have better energy efficiency ratio values on higher loads and water cooled chillers have better heat transfer ratio.
5. The EER values of chiller for the specific load and design conditions has been taken from manufacturer catalogue.

TABLE 7: Chillers Catalogue [8]

| Technical Specification | | | | |
|----------------------------|-----------|-------|-------|-------|
| Model | | 140S | 170S | 200S |
| Capacity Control | Step-less | | | |
| Cooling Capacity (Nominal) | KW | 503 | 578 | 659 |
| Power Input (Cooling) | KW | 154.6 | 176.1 | 199.8 |
| EER | | 1.080 | 1.072 | 1.066 |
| COP | | 3.255 | 3.280 | 3.29 |

Electrical Consumption

As the reference building is an educational building, we assume the total working hours from 9:00AM to 2:00PM which means 6 hours per day and 30 hours per week assuming Saturday and Sunday as off. So total working hours are 130 hours per month.

Table 8: VRF Data

| ELECTRICAL CONSUMPTION OF VRF SYSTEM | | | | |
|--------------------------------------|-----------------|------------|-------|------------------------|
| MODEL | CAPACITY KW | EFFICIENCY | HOURS | ELECTRICAL CONSUMPTION |
| FDC1200 | 120 | 4.21 | 130 | 65676 |
| FDC1250 | 125 | 4.13 | 130 | 67113 |
| FDC1300 | 130 | 4.04 | 130 | 68276 |
| total | 68276 X 5 units | | | 341380 |

Table 9: Air Cooled Chiller Data

| ELECTRICAL CONSUMPTION OF CHILLER SYSTEM | | | | |
|--|----------|------------|-------|------------------------|
| MODEL | CAPACITY | EFFICIENCY | HOURS | ELECTRICAL CONSUMPTION |
| 140S | 503 | 3.25 | 130 | 212518 |
| 170S | 578 | 3.28 | 130 | 246459 |
| 200S | 659 | 3.29 | 130 | 281854 |

It shall be remember that the above calculation are made on full load condition while as per site, it is not necessary to occur full load for all the time, so the consumption will reduce accordingly

RESULTS AND DISCUSSION

As from the HAP software, the total cooling load of the building is 180 tons including 13% of factor of safety. Similarly, total design air flow rate is 42805 CFM and design relative humidity is 49 %. Based on the above mentioned findings from HAP software, it is clear that both the VRF and Chiller systems have its own advantages and applications. It is abundantly obvious from the preceding discussion that, while keeping in mind the design parameters and the available resources, both variable refrigerant flow (VRF) type systems and Chiller type systems offer enormous benefits. Some of the results from the aforementioned study has been added as following:

- While chillers are more efficient at peak load (i-e 170 tons to 180 tons), VRF type systems are more efficient at part load (115 tons to 125 tons).
- VRF systems are designed for smaller loads, whereas chillers are more efficient for greater loads.
- In contrast to chillers, which are a more sophisticated system and require a specialist to operate and maintain, VRF systems are simple to install, operate, and maintain.
- While a VRF system does not allow for the addition of fresh air, it will be necessary to establish a separate ventilation system, a chiller system has the provision for adding fresh air to deliver the clean air as required by Ashrae conditions.
- A separate plant room is not necessary for a VRF system, although a chiller system will need one.
- Chillers outlast VRF systems in terms of longevity.
- VRF systems are more affordable than chillers in comparison.
- Compared to chillers, VRF systems require less maintenance.

CONCLUSION

As per the above discussion and manufacture catalogues which show the nominal energy efficiency and seasonal energy efficiency, it obviously understood that Chillers have greater EER and COP values at peak loads but it is also known to us that the reference building is an educational building which consists of Class-rooms, student's library, multi-functional halls and faculty offices, all of which suggests that only class-rooms and student's library will remain occupied throughout the working hours and the other spaces will be occupied in break times. This makes it easy to design and select the most suitable HVAC system.

If we select chiller system for this building, it will give high energy efficiency rating compare to VRF. Also VRF system is good choice to select for part load conditions as VRF gives higher EER ratings on part load as compare to Chillers. But one of the limitations of VRF system will be the lack of provision of Fresh air inside the conditioned space. And for that we will required a separate DXFA- AHU (Direct Expansion Fresh Air AHU) to exhaust the recirculated air to outside and to add fresh air as per ASHRAE conditions for an educational building.

Therefore, it is concluded that chiller uses only 82.5% of electricity that is required for VRF system at same load condition which means chiller is best option to select and based on this study we recommend to select the chill water HVAC system for this educational building.



ICSET-23



UET Peshawar

ACKNOWLEDGEMENTS

My sincere thanks are due to my supervisor and adviser Dr. Adnan Daud Khan. His consistent supervision, direction, and inspiration made it possible for me to complete this research study. I'm honoured to have the chance to complete this paper with his guidance.

REFERENCES

- [1] I. Edition, *2021 ASHRAE HANDBOOK*.
- [2] A. Layeni, C. Nwaokocha, G. Solomon, M. Sulaiman, A. Kasali, and A. Olanrewaju, "Design and Engineering Economic Analysis of a Variable Refrigerant Flow (VRF) and Mini-Split Air Conditioning System," *Curr. J. Appl. Sci. Technol.*, vol. 15, pp. 1–25, Mar. 2019, doi: 10.9734/cjast/2019/v34i130111.
- [3] H. Pump, H. Recovery, and W. Cooled, "CATALOGUE VRF SYSTEMS HEAT PUMP HEAT RECOVERY".
- [4] B. W. Goetzler and M. Ashrae, "Variable Refrigerant Flow Systems," no. April 2007, 2016.
- [5] X. Yu, D. Yan, K. Sun, T. Hong, and D. Zhu, "Comparative study of the cooling energy performance of variable refrigerant flow systems and variable air volume systems in office buildings," *Appl. Energy*, vol. 183, pp. 725–736, 2016, doi: 10.1016/j.apenergy.2016.09.033.
- [6] N. I. Zulkafli, M. F. Sukri, M. M. Tahir, A. Muhajir, and D. P. Hanak, "Optimal Operation of Chillers Plant in Academic Building by using Linear Programming Approach," *Chem. Eng. Trans.*, vol. 97, no. September, pp. 91–96, 2022, doi: 10.3303/CET2297016.
- [7] F. P. An, X. Qian, and J. Peng, "Study on life cycle management system for chillers in nuclear power plant Study on life cycle management system for chillers in nuclear power plant," 2018.
- [8] A. Systems, "Technical Data".

Paper ID: ICSET-2322

Gap Analysis between Academic Research and Policy Making in Energy Sector of Pakistan

Junaid Alamgir

US-Pakistan Center for Advanced Studies in Energy, University of Engineering and Technology Peshawar, Pakistan

**Corresponding author*

Email: junikhan104@gmail.com

ABSTRACT

This research is focused upon the evaluation of area of overlapping between energy academia and energy policy making. Evaluation of developed hypothesis suggest that interaction between energy academia and policy making is not strong enough, neither the research produced by academia is significantly utilized in policy making nor significantly taken into account for policy understanding or guidance. Barriers in the uptake of academic research in policy matters depends upon one's position in energy sector i.e people associated with academia students and faculty members have greater access and information of relevant research articles about policy matters but bureaucratic/ administrative formalities in government procedures refrain them in the uptake of research in policy matters. Energy professionals have less access & knowledge about research articles relevant to policy matters but ignorance of budget practicalities in research recommendation and time constraints associated to achieving policy goals refrain them from uptake of academic research.

KEYWORDS: Hypothesis

INTRODUCTION

The vague concept of fundamental differences between academic's researchers and policymakers in terms of their values, Motivation, Obligations, and their area of interest has proven persuasively. These Differences hinder the process of informing and influencing the policy in different fields including energy directly by academic research. Usually the aim and motivation of academic research of energy sector is to increase the Knowledge and to discover efficient ways and sources of energy utilization while some research are carried out to provide efficient solutions to the existing problems facing by energy sectors, and to produce experts human resource to tackle the operational matters of energy sectors. While on the other hand if we closely observe the policy practices in sector of energy the motivations and objectives are concretely attached to the operational issues like developing policy for sustainable energy development, for satisfying energy shortage, and for operational matters or governing different energy institutes [1].

Scholar of Research utilization earlier presents the notion of difference between academic research and policy making process this difference is because they are poorly connected and operated under different rules and regulations, the language these both use is different from each other their motivation by reward is different from each other [2][3]. The academic researchers do them researches for increasing knowledge, while the goals of policymakers are concretely attached to the operational issues [4]. The existence of



ICSET-23

*Proceedings of the 5th International Conference on Sustainable
Energy Technologies (ICSET 2023) Peshawar, Pakistan
14-15 December 2023*



UET Peshawar

difference between policymakers and academic researchers is hindering the process of influencing the policy directly by research of academia. Researchers cannot understand the reason behind the resistance towards change in policy beside there is present clear and convincing evidence. While on the hand the policymakers express their feeling of discontent that many researchers are unable to understand, access and digest their findings for policy related decisions in time [5].

A study conducted in United States in which 155 officials from mental health department were interviewed the study found that instrumental use of academic research is very rare specially in a condition when the issues are more complex and having uncertain consequences and multiple persons are involved in the decision making process [6]. In November 2011 and March 2013 a team of researchers in queen land university Australia conducted a survey of 2084 public servants at different provincial and federal levels in which they were asked about their use of academic research in their policy related works this survey targeted policy relevant government officials in 21 different departments at state (Queen land, Victoria and New South wales) and federal level. The survey results show that among the respondent's majority of them (58%) were using electronic databases including Google for downloading academic research and only 30% of respondent were facing difficulties in accessing full text versions of academic researches on policy. More ever using of academic research in their policy related matters among all respondents most of them (60%) told that they use or get help from academic research for their policy related works and for use in their written policy documents. On a question ranging from 1 (Frequently) to 5 (Never) about use of academic research in past for policy understanding the means value of the results was 2.062 which is very close to occasionally. In Three different questions ranging from 1 (Always) to 5 (Never) respondents were asked that how many times they received relevant academic research, how many times they cite directly relevant academic research and how many times they adopt relevant academic research in their policy works or writing policy documents the mean of all responses were 3 which shows an average which is showing no special inclination for use of relevant academic research in policy matters. The final output of the studies shows that Australian public servants related to policy matters suggests that the concept of two communities i.e. large difference between academia and policy related officials is not appropriate and this concept is misleading and that much more suitable and appropriate account of relationship is necessary between the two [7]. Another study which was conducted in United states where 113 servants of policy departments were interviewed about the use of Academic research, the study results shows that people who are involved in policy practices are reluctant for drawing policy advice from the academic researchers [8]. In Canada A study was conducted in which 833 officials from federal and provincial level were interviewed using by using like art-scale questions for interview about the use of academic research by them in the process of policy making and practices the answer options ranges from 1(for never) to 5(for always) The results of the study shows that the overall responses from the officials about the adoption of academic research for policy making was average 2.15 and the score for the influence of academic research in the process of policy making was 2.25 [9]. In Canada another was conducted to explore the relationship between policy making process and academic research in this study 1512 policy workers from policy departments in their nine provincial governments were asked questions by interview the results of this study shows that the Canadian policy workers may not have the capacity to practice a high level evidence based policy making [10]. In united kingdom of Britain a study was conducted in which 340 senior level civil servants from different policy areas and departments were interviewed the results of the study shows that there is a major difference that what senior level civil servants seen as important discipline and what academic institute seen as important [11]. In united states another study was carried out in which 204 upper level executives involve in policy making process in the united states government were interviewed regarding the use of social science in the process of policy making. These executives were questioned

carefully to determine whether they are in contact with influential academic researchers relevant to their area of policy the results of the study was that no such liaison exist and contact whether formal or informal exist between academic researchers and upper level policy making executives is very rare [12] .

To meet increasing energy demand in cost effective manners and to address certain issues related to energy sector Pakistan formulated and implemented different energy policies in different times. Over all aim of all the policies was to ensure reliable and continuous energy supply with effective cost in order to enhance the lifestyle of citizens and increase the economic activities. In case of power policies Pakistan ministry of power play the major role in policy formulation and implementation while coordination on policies formulation its legislation and regulation is done by energy wing of Pakistan planning commission. Up to yet now Pakistan have formulated and implemented total of 5 policies in power sector which are briefly discussed as under [13]. This study primarily examine the area of overlapping between energy academia and energy policy making, utilization of energy research produced by academia in policy practices, causes of hindrance in research uptake in policy matters and what type of barriers both face on their side in the uptake of academic research in policy practices.

METHODOLOGY

Hypothesis has been developed after detailed literature review on this topic, which has been tested by using technique of multivariate regression analysis. Survey tool has been used to collect variables for hypothesis testing by regression analysis. Figure 3.1 shows the flow chart of methodology employed.

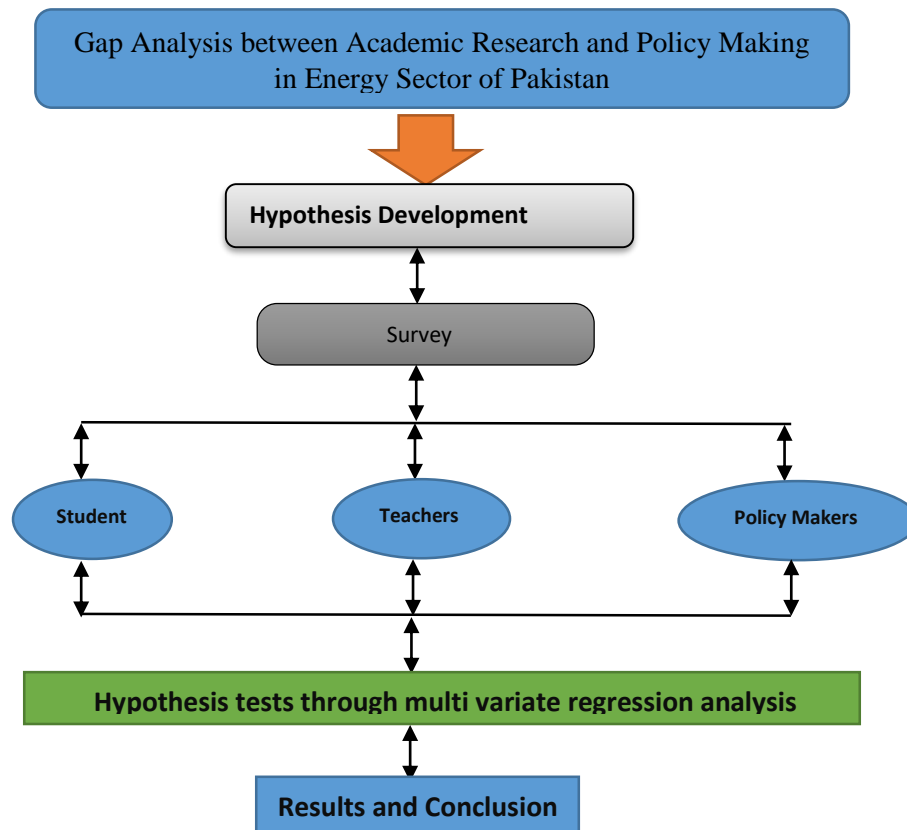


Figure 1: Flow Chart of Approach

Hypothesis

1. Academic research is neglected in Pakistan energy policy making

For evaluation of the aforementioned hypothesis the impact of three variable: percent use of academic research citation in policy/academic documents in last 5 years, number of times academic research studied for understanding policy/academic matters in last 5 years, and number of policy/academic document(s) written in last five years drawn on academic research, will be observed, on the description of job in energy sector.

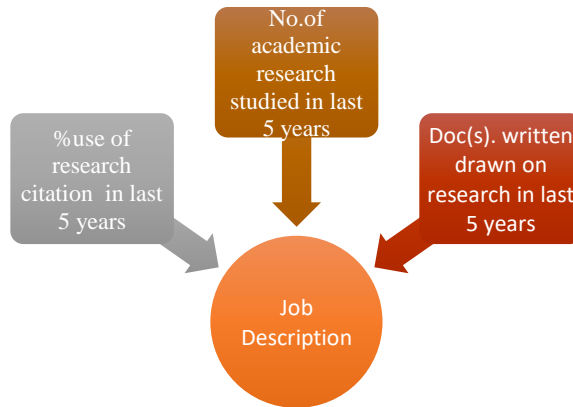


Figure 2: Theoretical model of hypothesis

2. There are barriers in the uptake of academic research in energy policy matters.

For the evaluation of aforementioned hypothesis the impact of four variables: percentage of access to full text academic research, percentage information about relevant research publication forums i.e. websites, journals, articles, online documents etc, No. of times communicated during last five years for research uptake, and causes of hindrance in research uptake, have been observed on Job description

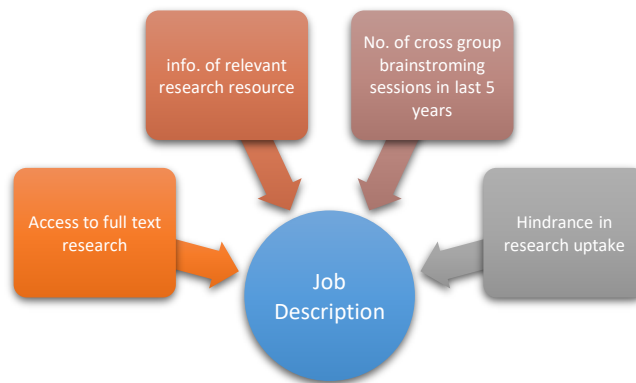


Figure 3: Theoretical model of hypothesis

Survey

To collect variables a survey has been devised which consist of questions relevant to hypothesis variables, responses have been collected from energy students, Academic faculty and Energy policymakers and energy consultants from both public and private sector and energy department officials. A questioner consists of 12 different questions in which first four question are about data genesis and remaining 8 question are about energy policymakers or practitioners and academia perception about energy sector. The survey distributed among 400 participant online and physically, among whom 226 responded. The breakdown of participant and targeted energy departments and organizations are as follow.

- I. Students of different energy discipline from different universities have been approached 76 responded.
- II. Faculty member of different energy disciplines affiliated with different universities across the country have been approached 43 responded.
- III. Policy practitioners (Policy makers, consultants and energy department officials) have been approached 103 responded. The survey has been sent to Pakistan Planning Commission Energy Wing, Ministry of water and power (Power division) government of Pakistan, Ministry of energy government of Pakistan, Water and Power developing authority WAPDA (power Wing), NTDC, PESCO, IESCO, FESCO, QESCO, MEPCO, TESCO, HESCO, Nation energy conservation authority NEECA, Pukhtunkhwa energy developing organization PEDO, Khyber Pukhtunkhwa oil and gas limited KPOGCL, Ministry of energy Government of KPK, Private power infrastructure board PPIB, Alternate energy development board AEDB, Oil and gas regulatory authority OGRA, National electric power regulatory authority NEPRA

Regression Analysis

Regression analysis is the method employed for measuring the degree at which one or more than one predictor (independent variable, IV) and one or more than one response (Dependent variable, DV) are linearly related to each other. The dependent variables DVs are plotted on Y-axis and independent variables IVs are plotted on X-axis the regression is performed to check the correlation of variables i.e. whether they have strong correlation or not and if they have then what is the direction of correlation, positive for direct proportionality and negative for inverse proportionality, after regression scatter plot with regression fitted line is obtained for dependent variable DV against Independent variable IV and values of y intercept (where fitted line intercept on Y axis) and slope of line are put into straight line equation.

$$Y = m(X) + C \quad (1)$$

Where,

Y= Dependent Variable DV,

X= Independent Variable IV,

m= Slope of the fitted line

C= y intercept

RESULTS

- I. For the evaluation of hypothesis “Academic Research is neglected in Pakistan Energy Policy Making” “Job description” has been plotted on Y-axis as dependent variable (DV) while percentage of citation of academic research in policy/professional/academic in last five years, no. of times research studied for understanding policy or academic matters in last five years, document(s) written drawn on research in last five years have been plotted on X-axis as independent variable (IV).

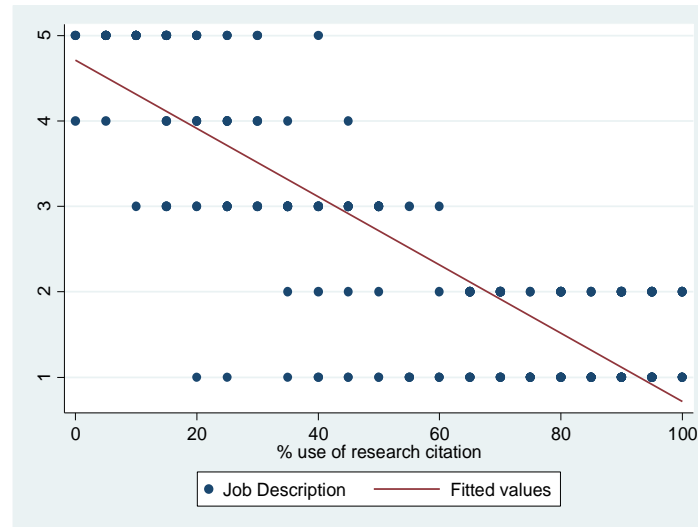


Figure 4: Scattered & regression fitted plot for DV and IV

$$Y = m(X) + C$$

$$Y = 4.7 - 0.04X$$

Based on the perception of the survey participants, a negative correlation between the job description and percentage use of research citation in energy sector has been observed with a five percent step increase in percentage of academic research citation. As job description move upward from student to energy department official, the percentage use of citation of academic research in policy/professional/ academic documents decreases, showing that citation of academic research is less used in policy documents and professional reports by energy professionals than academic documents and professional reports by affiliates of academia.

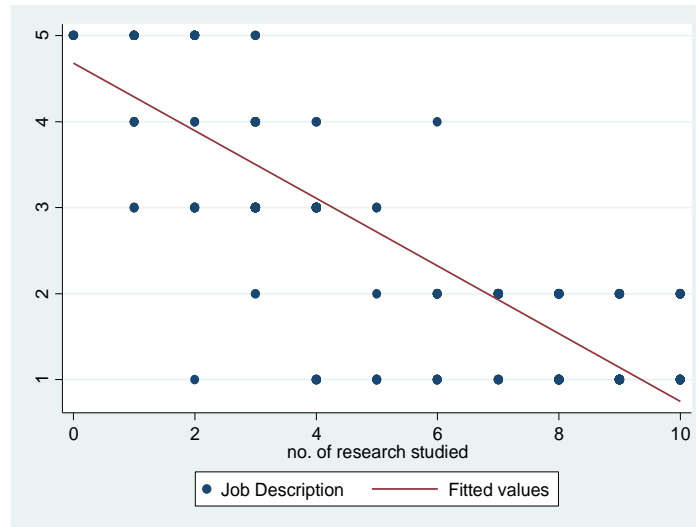


Figure 5: Scattered & regression fitted plot for DV and IV

$$Y = m(X) + C$$

$$Y = 4.7 - 0.4X$$

Based on the perception of the survey participants, a negative correlation between the job description and no. of times research studied for understanding policy in energy sector has been observed with a unit step increase in no. of times research studied for understanding policy. As job description move upward from student to energy department official, no. of times research studied in last five years for understanding policy matters decreases, showing that academic research is less studied in last five years by by energy professionals than affiliates of academia.

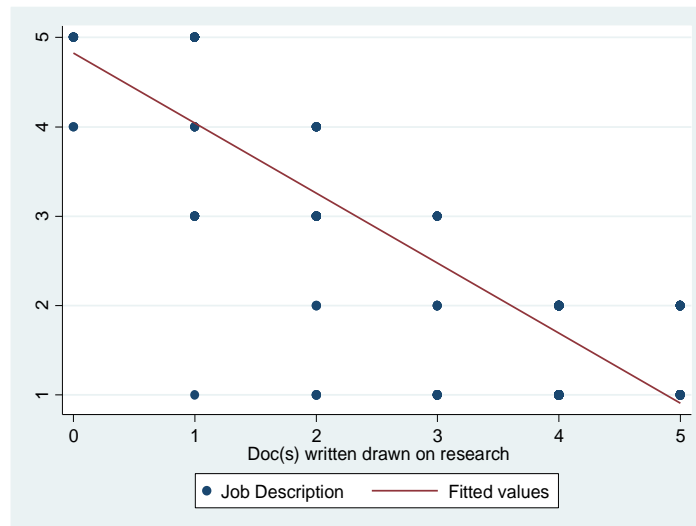


Figure 6: Scattered & regression fitted plot for DV and IV

$$Y = m(X) + C$$

$$Y = 4.8 - 0.79X$$

Based on the perception of the survey participants, a negative correlation between the job description No. of times documents written by energy professionals has been observed with a unit step increase in No. of times documents written in last five years drawn on academic research. As job description move upward from student to energy department official, No. of times documents written in last five years drawn on academic research decreases, showing that professional documents drawn on academic research is less written by energy professionals than affiliates of academia.

- II. For the evaluation of hypothesis “there are barriers in the uptake of academic research in energy policy matters” Job description” has been plotted on Y-axis as dependent variable (DV) and percentage access to full text research, information about relevant publication resources, cross-group brain storming sessions in last 5 years and hindrance in research uptake in policy matters have been plotted on X-axis as independent variable (IV).

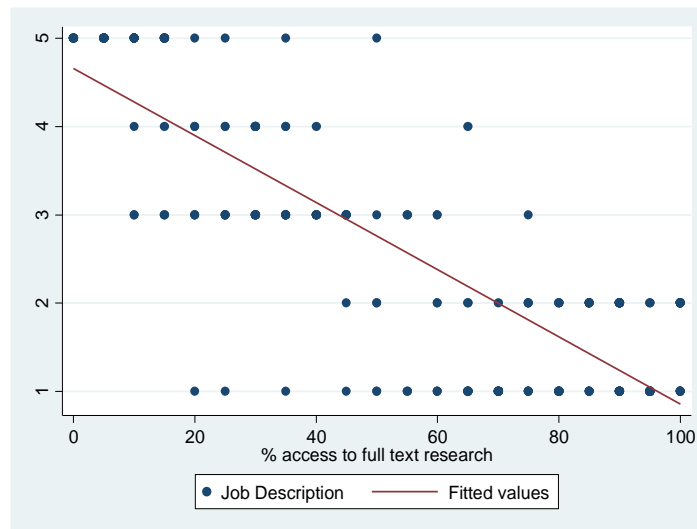


Figure 7: Scattered & regression fitted plot for DV and IV

$$Y = m(X) + C$$

$$Y = 4.6 - 0.03X$$

Based on the perception of the survey participants, a negative correlation between the job description and access to full text research in energy sector has been observed with a five percent step increase in access to full text research. As job description move upward from student to energy department official, the percentage access to full text research decreases, showing that energy policymakers and professionals have less access to full text research than affiliates of academia.

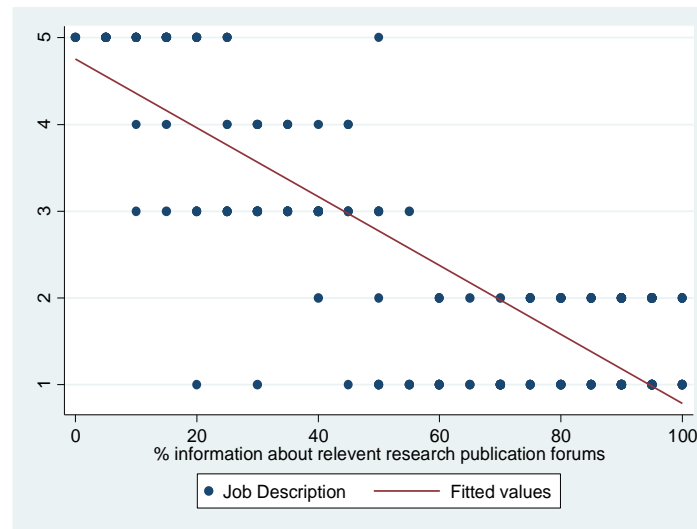


Figure 8: Scattered & regression fitted plot for DV and IV

$$Y = m(X) + C$$

$$Y = 4.7 - 0.04X$$

Based on the perception of the survey participants, a negative correlation between the job description and information about relevant publication resources with energy policymakers has been observed with a five percent step increase in access to full text research. As job description move upward from student to energy department official, the information about relevant publication resources decreases, showing that energy policymakers and professionals have less information about relevant publication resource than affiliates of academia.

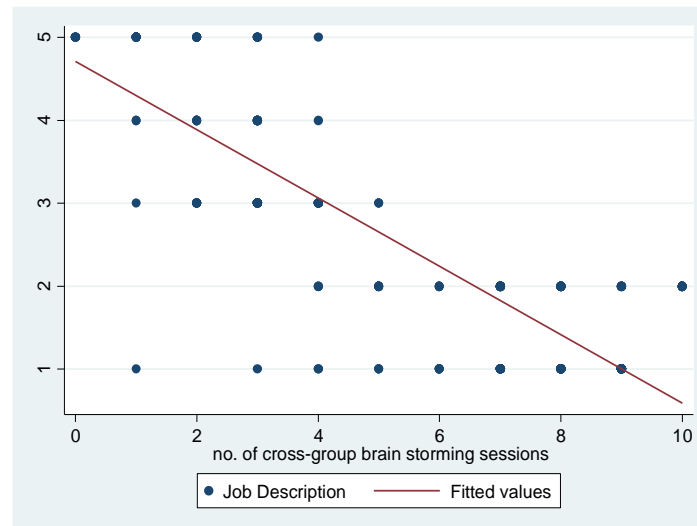


Figure 9: Scattered & regression fitted plot for DV and IV

$$Y = m(X) + C$$

$$Y = 4.7 - 0.41X$$

Based on the perception of the survey participants, a negative correlation between the job description and no. of cross-group brainstorming sessions in energy sector has been observed with a unit step increase in no. of cross-group brainstorming sessions. As job description move upward from student to energy department official, no. of cross-group brainstorming sessions decreases, showing that energy professionals have less interacted with academia for brainstorming sessions with academia on policy matters than affiliates of academia.

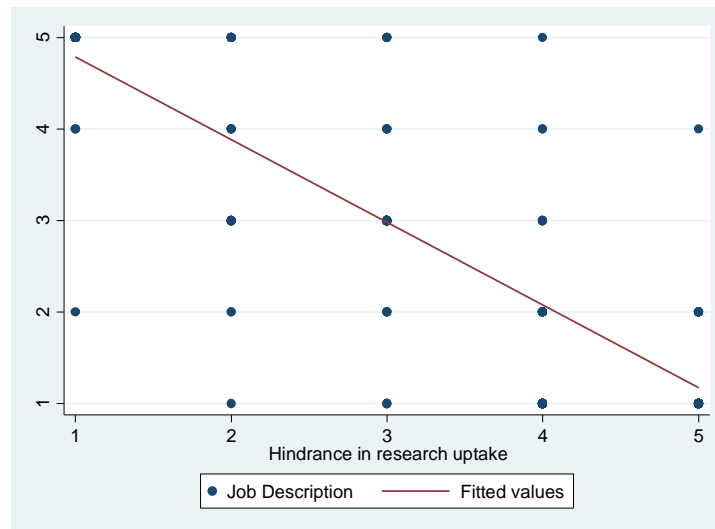


Figure 10: Scattered & regression fitted plot for DV and IV

$$Y = m(X) + C$$

$$Y = 5.7 - 0.9X$$

Based on the perception of the survey participants, a negative correlation between the job description and hindrance has been observed with a unit step increase in hindrance. As job description move upward from student to energy department official, the hindrance changes from bureaucratic/ administrative formalities to time constrains, showing that hindrance faced by affiliates of academia is mostly bureaucratic/ administrative formalities while the other hand hindrance faced by energy professionals in research uptake are the time constrains and ignorance of budget practicalities in research recommendations.

CONCLUSION

The outcomes of the survey responses for the developed hypothesis, after regression analysis shows that the interaction between academia and energy policy making is not strong enough, neither the research produced by academia is significantly utilized in policy making nor significantly taken into account for policy



ICSET-23



UET Peshawar

understanding or guidance, trends suggest utilization of academic research is mostly among academicians but on the hand policy practitioners rely less on academia produced research.

Trends shows barriers exists among energy academia and policy practitioners, uptake of academic research in policy matters depends upon one's position in energy sector, affiliates of academia have greater access and information about research publication resources relevant to policy matters, but they face bureaucratic/ administrative formalities in government procedures as a major cause of hindrance in research uptake in policy matters, on the other hands energy professionals have less access & knowledge about research publication resources relevant to energy policies but the causes which hinder the research uptake in policy matters on their side are the ignorance of budget practicalities by in research recommendation and time constraints associated to achieving policy goals.

ACKNOWLEDGEMENTS

The completion of this research article was not possible without help of so many people, who assists me. I am thankful to all of them. Specifically parents, my teachers, my friends and class mates for their constant encouragement and support. I am also grateful to US Pakistan Center for Advanced Studies in Energy at University of Engineering and Technology Peshawar and United States Agency for International Development (USAID) for providing chance to get scholarship for master's studies and completes my research work.

REFERENCES

- [1] Caplan N. (1979) The Two-Communities Theory and Knowledge Utilization. *American Behavioral Scientist*.;22(3):459-470.
- [2] Caplan N., Morrison, A., & Stambaugh, R. J. (1975). *The use of social science knowledge in policy decisions at the national level: a report to respondents*. Ann Arbor, Institute for Social Research, University of Michigan.
- [3] John Young.(2005). Research, Policy and practice: Why developing Countries are different 727–734
- [4] Hemsley-Brwon W., Jane. (2004). Facilitating Research Utilization: Cross –Sector Review of Research Evidence. *International Journal of Public Sector Management* 17(6):534-53
- [5] Poppen. P, (1978) “Social Scientist Attempt to Influence Public Policy,” *SPSSI News-Letter* 148:10-12
- [6] Dunn, William. (1980). The Two-Communities Metaphor and Models of Knowledge Use: An Exploratory Case Survey. *Science Communication - SCI COMMUN.* 1. 515-536. 10.1177/107554708000100403.
- [7] Edwards, Meredith. (2005). Social Science Research and Public Policy: Narrowing the Divide1. *Australian Journal of Public Administration*. 64. 68 - 74. 10.1111/j.1467-8500.2005.00417.x.



ICSET-23

*Proceedings of the 5th International Conference on Sustainable
Energy Technologies (ICSET 2023) Peshawar, Pakistan
14-15 December 2023*



UET Peshawar

- [8] Frenk, Julio (1992) .Balancing Relevance and Excellence: Organizational Responses to Link Research with Decision Making: Social Science and Medicine 35(11):1397-1404
- [9] Mark G. School of policy studies Queens university (2017) “Reconnecting the “two solitude” of academia and policy world”.
- [10] Hewlett, Michael, and Joshua Newman. (2010).Policy Analysis and Policy Works in Federal System. Policy Advice and its Contribution to Evidence Based Policy Making in Multilevel Governance System. Policy and Society 29(2):123-36.
- [11] Raadschelders, Jos C.N.(2011) .Public Administration.The Interdisciplinary Study of Government.Oxford,UK:Oxford University Press.
- [11] Talbot, Colin and Carole Talbot. (2014) .Sir Humphrey and the Professor: What Does White hall want from Academics? Manchester UK: University of Manchester.
- [12] Arum k, Muhammad. M, Aron K, (2016) Lope Holes in Public Policy Making: A Case Study of Pakistan: Journal of Political Studies, Vol, 23, Issue-2,,373:396.
- [13] Ali A. (2012) Pakistan issues in energy policy. Create Space Independent Publishing Platform;
http://www.academia.edu/34180037/Issues_in_Energy_Policy_Pakistan_Edition

Paper ID: ICSET-2323

COMPARATIVE STUDY OF RENEWABLE ENERGY RESOURCES IN RURAL AREAS OF KHYBER PAKHTUNKHWA

Sohail Ahmad, Haseeb Ahmad Khan*, Jalil Ahmad

Department of Electrical Engineering, UET Mardan, Mardan, Khyber Pakhtunkhwa, Pakistan

**Corresponding author*

Email: haseebkhan@uetmardan.edu.pk

ABSTRACT

As global electricity demand continues to rise, the need for innovative renewable energy systems becomes increasingly vital, reducing reliance on conventional energy sources. In response, we have optimized different renewable Energy resources to design a Renewable system in Rural Areas of Khyber Pakhtunkhwa, Pakistan consisting of grid design, wind and solar installations, converter implementation and Batteries configuration. This innovative approach aims to curtail payments to the grid. To assess the viability of this system, HOMER Pro software is utilized, enabling the analysis of diverse scenarios and the subsequent evaluation of power generation, pollutant emissions, net present costs, and average electrical roduction expenses, the energy sold to or purchased from the grid. HOMER Pro, a Software used for Optimization of Different Renewable Energies (RE), represents a software tool crafted to aid in the creation of different Renewable Energy power plants configurations. The software furnishes four distinct categories of optimized results, presented in both graphical and tabulated formats to enhance visualization. Notably, the proposed systems design ranks as the most economical option when considering operating costs, net present costs, and emissions of gases. Additionally, there is a need for more studies that consider the long-term environmental and sustainability implications of optimized renewable energy solutions. Furthermore, exploring optimization strategies for integrating renewable energy sources into existing infrastructure and addressing grid stability issues remains a significant research challenge. As we can see that the world is going to Renewable Energy resources therefore it is very crucial to design and optimized different renewable energy sources to overcome our needs. In the proposed Paper we have selected three different areas of Khyber Pakhtunkhwa i.e District Mardan, Chitral and Muhmand, and for all the three location we have design On-grid systems to compare them that in which location the On-grid system is the most economical. Therefore, as we can see that in all three locations the On-grid system in location 1 gives us the best optimized results.

KEYWORDS: Renewable Energy, Optimization, HOMER Pro, On-grid System, Net Present Cost.

INTRODUCTION

Over 1.5 billion individuals across the globe continue to lack access to electricity, a critical factor contributing to the economic development of regions and entire countries. The expansion of electrification significantly enhances living standards and creates a multitude of opportunities, thanks to the availability of electric power. The provision of sustainable and clean energy sources, including electricity, remains an ongoing global development challenge. Rural electrification stands out as a pressing concern in numerous



ICSET-23



UET Peshawar

developing nations, particularly in Africa and Asia, where a substantial portion of the population resides in remote areas far removed from the primary electrical grid.[1]. For instance, consider Pakistan, the home country of the author of this study, where 62.56% of the population resides in rural regions, while the remainder resides in urban areas [2].

Renewable energy or Renewable power originate from natural resources or natural processes which will eventually be replenished with time. Renewable energy is available in many forms; it may be either from the sun directly or it may be due to the heat which is generated deep in the earth surface. This mean that power and Energy from the sun, wind, sea, hydro, biomass, geothermal, biofuels and hydrogen make the RE sources [3].

In the last decade, Renewable electricity grew approximately 10% of world supply. There is a significance decreased in Fossil fuel that is around 6% and in nuclear up to 2% decrease. the proportion of hydropower decreased by 1%, at the same time the renewable energy sources that is Sun & Wind increased by 8%. Biomass and geothermal also increase by only 1%. 3,146 gigawatts are mounted in one 135 international locations, at the same time as 156 nations have legal guidelines regulating the renewable energy sector [4].

The sun stands as the most abundant and sustainable energy source, with approximately 108,101,4 MWh of solar energy reaching the Earth's surface every year. This amount is roughly 10,000 times greater than the global demand for primary energy[4]. Consequently, it is imperative to explore suitable technologies for harnessing this abundant energy resource.

Wind power, also known as wind energy, primarily involves the utilization of wind turbines to produce electricity. It stands as a widely embraced, sustainable, and renewable energy source with a considerably lesser environmental footprint compared to the combustion of fossil fuels. Throughout history, wind power has been harnessed through sails, windmills, and windpumps. However, in contemporary times, its predominant application lies in the generation of electricity [5].

In the previous year, around 60% of total electricity of the U.S is generating from renewable energy sources that is, solar and wind (46% from solar, 17% from wind) [6]. In a recent Report from the World Wind Energy Association (WWEA), the latest figures for global wind energy capacity are presented. As of the conclusion of 2018, the worldwide installed wind energy capacity stood at nearly 600 gigawatts (GW), as illustrated in Figure 1. This represents a notable increase of 50 GW compared to the preceding year. Notably, this cumulative wind energy capacity now fulfils approximately 6% of the world's electricity demand, solidifying wind energy as the leading non-hydro provider of renewable energy [7].

In 2006, wind turbines in the United States produced a total of 26.6 billion kWh of electricity annually, sufficient to supply over 2.4 million households with power. While this quantity could energize a city larger than Los Angeles, it represents only a modest portion of the nation's overall electricity production, approximately 0.4 percent. However, it's important to note that wind-generated electricity has been experiencing rapid growth in recent years. In 2006, it surpassed wind generation levels in 2002 by two and a half times [8].

The study on the "Comparative study of Renewable Energy Resources" contributes significantly to the field by offering innovative strategies to maximize the utilization of renewable energy sources like solar, wind, and hydro. It provides practical insights for designing and operating renewable energy systems with greater efficiency and reduced environmental impact. Furthermore, the research contributes to the transition toward sustainable energy solutions by addressing technical, economic, and environmental aspects. By optimizing resource allocation and integration into existing grids, this study contributes to more resilient and reliable energy systems. Ultimately, it fosters a deeper understanding of renewable energy optimization, benefiting both academia and industry.

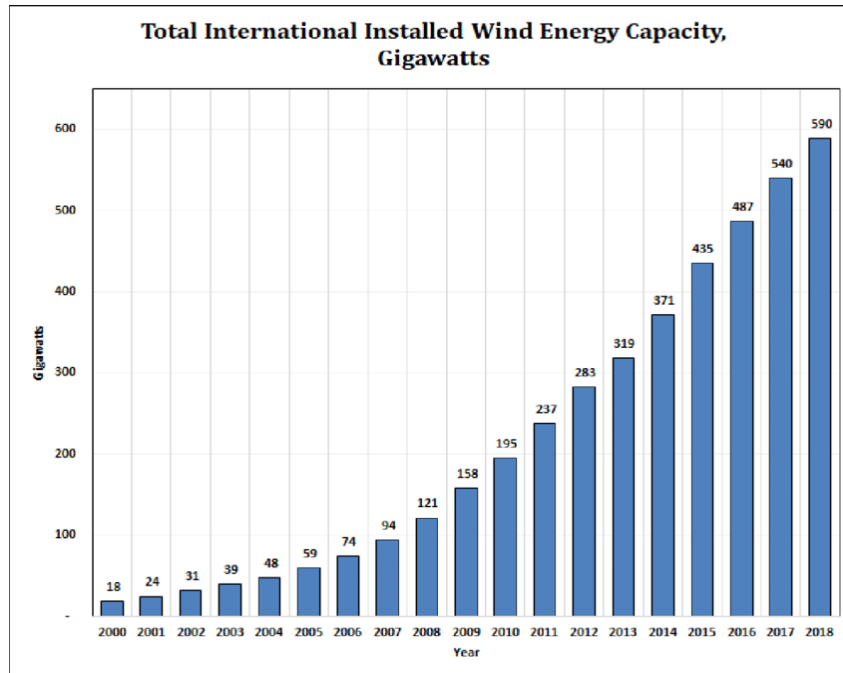


Figure 1: Global wind energy capacity growth [7]

Types of Power System

When contemplating the numerous advantages of solar energy, it becomes crucial to familiarize yourself with the currently available types of solar systems. This knowledge will empower you to select the most appropriate one for your home. There are three primary types of solar power systems: grid-tied (on-grid), off-grid, and hybrid. Each of these systems provides a distinct power generation and storage solution, catering to various needs and preferences [9]. These Systems are explained one by one.

On-grid Power System

On-grid system is a type of system in which the complete system is connected to the grid [10]. This system comprises solar panels, a wind turbine, an inverter, and the necessary equipment for connecting to the grid. Grid-connected systems are suitable for a range of applications, including residential, commercial, and larger-scale setups. They differ from off-grid solar power systems in several ways. Typically, grid-connected systems do not require a battery backup since any excess energy generated beyond the immediate load automatically feeds into the connected utility grid.

An On-grid solar system operates without the need for a battery storage system and is directly connected to the National Grid via an inverter, as depicted in Figure 2. As solar panels convert sunlight into energy or wind turbines generate power, your home efficiently utilizes this green energy source to operate your appliances. Any surplus energy you generate is seamlessly fed back into the Grid, and you may receive compensation through the Feed-in-Tariff or SEG programs, providing an additional benefit. One notable advantage of an on-grid system is the assurance that your energy supply will consistently have the backing of the National Grid, ensuring uninterrupted power availability.

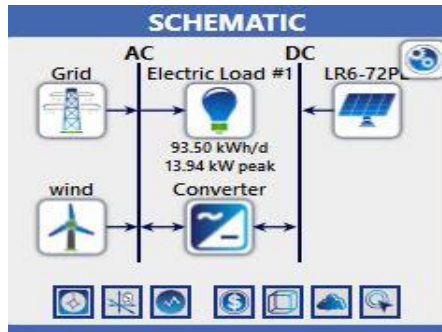


Figure 2: On-grid power system taken from the HOMER software

Off-Grid Power System

An Off-grid system is the one in which the main Grid is not connected to the system and batteries are used for backup is term as Off-grid power system [11] as shown in figure 3. An off-grid system, also known as a standalone system or mini-grid, is self-sufficient in generating power and operating appliances independently. These systems are particularly well-suited for providing electricity to small communities. Off-grid electrification systems prove to be practical solutions for remote regions in countries where access to electricity is limited or non-existent due to dispersed populations and challenging living conditions. The term "off-grid system" signifies the ability to sustain a living without relying on the conventional power grid or other centralized systems. In these systems, electrical energy generated through solar photovoltaic panels needs to be stored or reserved since the energy requirements of the load can vary from the output of the solar panels. Typically, a battery bank is employed for this purpose.

A primary category within solar power systems is the off-grid system, also recognized as a standalone power system (SAPS). This system operates by harnessing electricity from solar panels and wind turbines, directing it towards charging a solar battery through a charger controller. Subsequently, this stored electricity is converted using an inverter, enabling it to power the appliances within a home or business. This approach of storing electricity in a solar battery ensures the capacity to sustain a residence with solar energy, even during nighttime or periods of reduced sunlight exposure. An Off-grid system consist of Renewable sources, Batteries, Inverter and load [12].

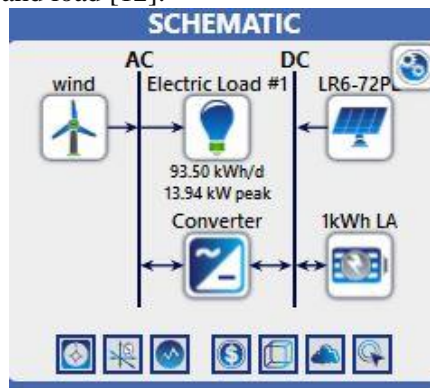


Figure 3: Off-grid Power system taken from the HOMER software

Hybrid Power System

Hybrid solar systems amalgamate solar panel technology, wind turbines, and solar batteries to craft an eco-friendly energy solution that incorporates a backup energy reserve. While a hybrid PV system



maintains its connection to the National Grid, any solar energy generated is initially stored within a home battery solution, as illustrated in Figure 4.

The primary advantage of a hybrid solar system lies in the ability to store excess energy in a battery, enabling you to utilize your solar power for household needs during nighttime hours and reduce the export of surplus energy to the Grid. Furthermore, unlike an on-grid system, in the event of a national grid outage, you can rely on your battery supply for energy. This capability, known as "islanding," proves particularly beneficial for property owners residing in regions prone to power interruptions [12].

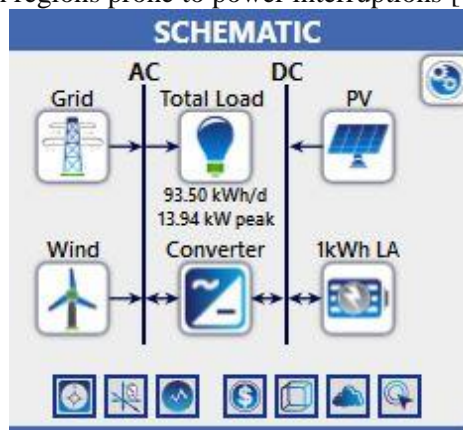


Figure 4: Hybrid system taken from the HOMER software

HOMER Pro or Hybrid Optimization of Multiple Electric Renewables, stands as a microgrid software solution adept at addressing the challenges associated with crafting cost-efficient microgrid system designs, suitable for both off-grid and grid-connected configurations. Developed by the National Renewable Energy Laboratory in the United States, this computer simulation software employs various renewable resources and components in the system design process. The software encompasses three core functions: [13].

1. simulation
2. Optimization
3. Analysis

During the Optimization, the HOMER evaluates both the lifecycle cost and the viability of the envisioned power system. HOMER has the capacity to simulate diverse power setups, encompassing combinations of PV arrays, generators, wind turbines, run-off-river hydro turbines, battery banks, and more. It can model both off-grid and grid-connected systems capable of supplying electrical and thermal loads [14]. During the optimization procedure, HOMER identifies the most economical approach for fulfilling the electricity demand. Additionally, HOMER offers a sensitivity analysis feature, which evaluates the impact of uncertainties or alterations in variables. This analysis involves reiterating the optimization process for each sensitivity variable, allowing for a comprehensive assessment of potential changes and their effects [15].

The complexity arising from various technical setups, component variations, fuel expenses, and resource availability can make it challenging to determine the most efficient and practical system. However, HOMER's optimization and sensitivity analysis algorithms streamline the process, facilitating the discovery and assessment of the optimal system configuration. It's worth noting that simulation outcomes can differ significantly based on the sizing of components, such as generator capacity, PV panel dimensions, wind turbine size, and more [15].

Homer Pro is a widely used software tool for the analysis of renewable energy projects, particularly in the field of microgrid and distributed energy system design. It offers several advantages that make it a preferred choice compared to other software options:

1. **User-Friendly Interface:** Homer Pro provides a user-friendly interface that allows users with varying levels of expertise to model and analyze complex energy systems. Its intuitive design and graphical user interface make it accessible to both beginners and experts.
2. **Comprehensive Optimization:** Homer Pro offers powerful optimization capabilities, allowing users to find the most cost-effective energy system configuration for a given set of inputs and constraints. It considers factors such as equipment costs, energy generation, load profiles, and fuel prices to optimize system design.
3. **Detailed Financial Analysis:** The software provides detailed financial analysis tools that help users assess the economic feasibility of their projects. It calculates key financial metrics such as the net present Cost (NPC), internal rate of return (IRR), and payback period.
4. **Integration of Weather Data:** Homer Pro can integrate historical weather data, which is essential for accurately modelling the performance of renewable energy sources like solar and wind.
5. **Industry Standard:** Homer Pro has been used in numerous research studies, industry projects, and academic institutions, establishing itself as an industry standard for microgrid and renewable energy system analysis.

RESULTS AND ANALYSIS

HOMER Pro software optimize a system depending on Energy demand and supply in each hourly time step for 365days [16]. At every time step, the HOMER scrutinizes the energy requirements and availability, conducting energy flow calculations for every system setup. HOMER conducts these meticulous energy balance assessments for each system configuration, determining their feasibility. This process is reiterated to optimize the results across various sensitivity variables.

On-grid System cost analysis of Location 1

For location 1 we have selected district Mardan. In an on-grid connected system, the setup is integrated with the grid to provide backup power. The cost analysis of the grid-connected system is illustrated in Figure 5. In the component architecture section for PV, we have a capacity of 32.3 kW, with an accompanying 18 kW converter. In the cost section, the overall system cost over a 25 -year period is computed, yielding a cost of energy (COE) at \$0.0261, a Net Present Cost (NPC) of \$19,221, and an initial system cost of \$16,100.

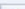
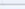
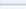


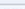

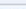







| Export... | Optimization Results | | | | | | | | | | | | | | | | | | | | |
|---|---|---|---------|---|-----------|---|----------------|---|----------|---|----------|---|----------|---|------------------------|---|----------------------|---|--------------|---|-------------------|
| | Left Double Click on a particular system to see its detailed Simulation Results. | | | | | | | | | | | | | | | | | | | | |
| Architecture | | | | | | | Cost | | | | System | | | | | | | | | | |
|  |  |  | PV (kW) |  | Grid (kW) |  | Converter (kW) |  | Dispatch |  | COE (\$) |  | NPC (\$) |  | Operating cost (\$/yr) |  | Initial capital (\$) |  | Ren Frac (%) |  | Total Fuel (L/yr) |
| |  |  | 32.3 | | 999,999 | | 18.0 | | CC | | \$0.0261 | | \$19,221 | | \$241.48 | | \$16,100 | | 85.0 | | 0 |
| | |  | | | 999,999 | | | | CC | | \$0.100 | | \$44,118 | | \$3,413 | | \$0.00 | | 0 | | 0 |

Figure 5: Optimization result for location 1

Figure 6 displays the electricity generation from the PV system, which amounts to 64,130 kWh per year. The consumption, on the other hand, is 56,911 kWh per year. The surplus energy serves as a buffer to address any load variations, ensuring the system's adaptability. Alternatively, any excess electricity can be sold back to the grid.

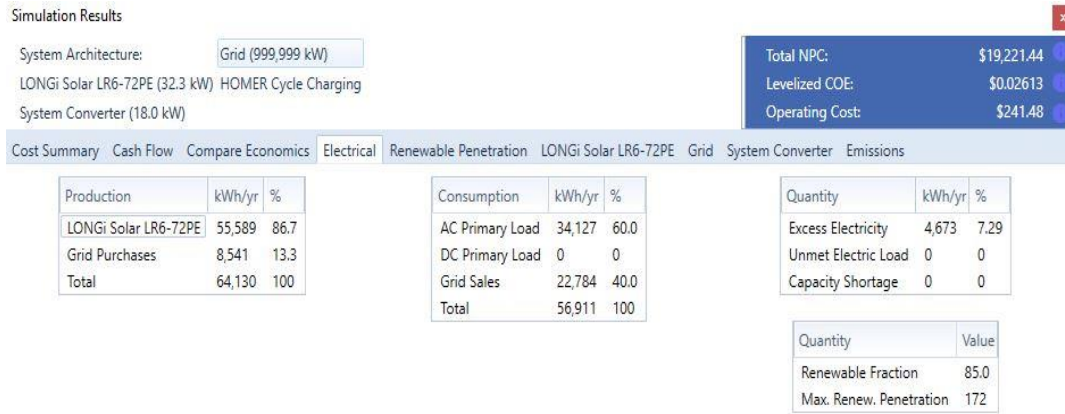


Figure 6: Complete electrical parameter of location 1

The average monthly electricity Production is given in the figure 7 as we can see that there are two sources of power i.e PV the Orange and the Grid the Green one.

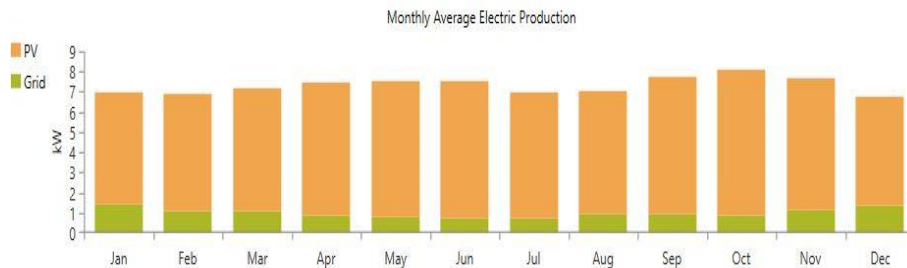


Figure 7: Monthly average electric production chart

In Figure 8 there are basically two graphical representations the one above shows the total AC Primary load that is the blue color while the orange color shows the total PV power production on hourly basis in the month of June in which the solar power production is maximum in Khyber Pakhtunkhwa. While the graph below shows the power or energy sold to and purchased from the Grid, the blue one shows the energy which is sold while the Red one shows the energy purchased from the Grid.

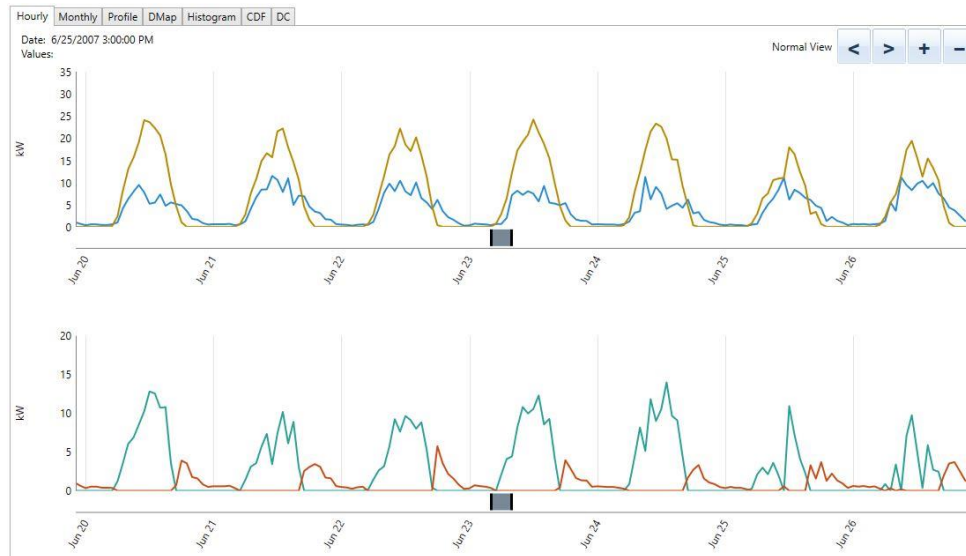


Figure 8: Graphical representation of location 1

On-grid System cost analysis of Location 2

We have selected District Chitral for location 2. The optimization results of On-grid power system for location 2 is given in the figure 9 where we have a total of 32.3KW PV is required and 18kW inverter is required for the system. As it is in district Chitral so we will select the Optimized result which have Wind Power so here we have on Generic 3kw wind Turbine. In cost section the cost of the whole system for 25 years is calculated, where COE (cost of energy) is \$0.0351, NPC (Net Present Cost) is \$25,195 and the initial cost for the system is \$20,100 and the Operating cost per years is \$294.

| Optimization Results | | | | | | | | | | |
|--|---------------|------|-----------|----------------|----------|----------|----------|------------------------|----------------------|---------------|
| Left Double Click on a particular system to see its detailed Simulation Results. | | | | | | | | | | |
| Architecture | | | | Cost | | | | System | | |
| Warning | LR6-72PE (kW) | Wind | Grid (kW) | Converter (kW) | Dispatch | COE (\$) | NPC (\$) | Operating cost (\$/yr) | Initial capital (\$) | Ren. Frac (%) |
| | 32.8 | | 999,999 | 18.0 | CC | \$0.0344 | \$23,740 | \$575.67 | \$16,298 | 81.2 |
| | 32.3 | 1 | 999,999 | 18.0 | CC | \$0.0351 | \$25,195 | \$394.15 | \$20,100 | 85.3 |
| | | | 999,999 | | CC | \$0.100 | \$44,118 | \$3,413 | \$0.00 | 0 |
| | | 1 | 999,999 | | CC | \$0.0990 | \$44,257 | \$3,114 | \$4,000 | 12.8 |
| | | | | | | | | | | 0 |

Figure 9: Optimization Results for location 2

In figure 10 the total electricity produced by the system is given as 61,562 kWh/year in which 48,980kwh/y is from solar, 4,424kwh/y is from wind and 8,158kwh/y is purchased from the Grid and the total electricity used is 55,523kWh/year and the remaining electricity which is excess electricity we can use it if there is a change in load or we can send it to the grid and buy some free Units of electricity for the backup.



ICSET-23

Proceedings of the 5th International Conference on Sustainable
Energy Technologies (ICSET 2023) Peshawar, Pakistan
14-15 December 2023



UET Peshawar

| Cost Summary | | | Cash Flow | | | Compare Economics | | | Electrical | | | Renewable Penetration | | | LONGi Solar LR6-72PE | | | Generic 3 kW | | | Grid | | | System Converter | | | Emissions | | |
|----------------------|--|--|-----------|--|--|-------------------|--|--|-----------------|--|--|-----------------------|--|--|----------------------|--|--|-------------------------|--|--|--------|--|--|------------------|--|--|-----------|--|--|
| Production | | | kWh/yr | | | % | | | Consumption | | | kWh/yr | | | % | | | Quantity | | | kWh/yr | | | % | | | | | |
| LONGi Solar LR6-72PE | | | 48,980 | | | 79.6 | | | AC Primary Load | | | 34,127 | | | 61.5 | | | Excess Electricity | | | 3,779 | | | 6.14 | | | | | |
| Generic 3 kW | | | 4,424 | | | 7.19 | | | DC Primary Load | | | 0 | | | 0 | | | Unmet Electric Load | | | 0 | | | 0 | | | | | |
| Grid Purchases | | | 8,158 | | | 13.3 | | | Grid Sales | | | 21,396 | | | 38.5 | | | Capacity Shortage | | | 0 | | | 0 | | | | | |
| Total | | | 61,562 | | | 100 | | | Total | | | 55,523 | | | 100 | | | | | | | | | | | | | | |
| | | | | | | | | | | | | | | | | | | Quantity | | | Value | | | | | | | | |
| | | | | | | | | | | | | | | | | | | Renewable Fraction | | | 85.3 | | | | | | | | |
| | | | | | | | | | | | | | | | | | | Max. Renew. Penetration | | | 175 | | | | | | | | |

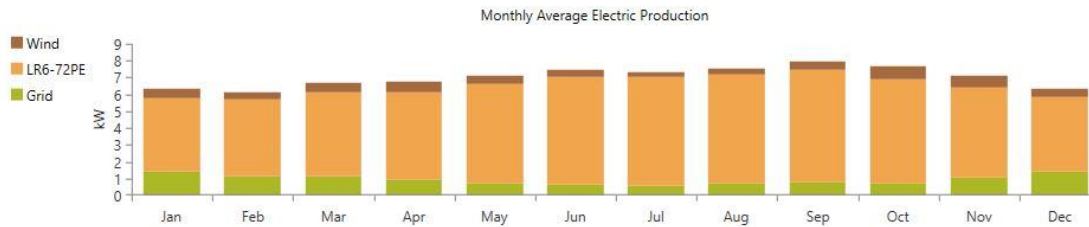


Figure 10: Electrical Parameter for location 2

In Figure 11 there are basically two graphical representations the one above shows the total AC Primary load that is the pink colour while the orange colour shows the total PV power production on hourly basis in the month of June in which the solar power production is maximum in Khyber Pakhtunkhwa. While the graph below shows the Wind speed (green), wind power output (blue) and power or energy sold to and purchased from the Grid, the red one shows the energy which is sold while the brown one shows the energy purchased from the Grid.

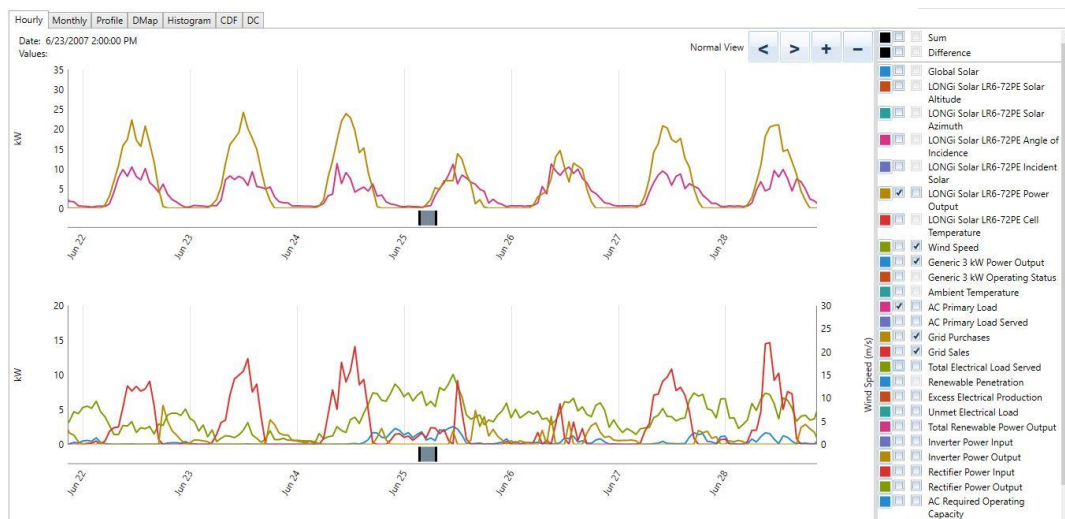


Figure 11: Graphical representation for location 2



On-grid System cost analysis of Location 3

We've chosen Mohmand district as our third location. In Figure 12, you can find the cost analysis for this particular location. In the architecture of components section for photovoltaics (PV), we've opted for a 33.3 kW setup, complemented by an 18kW converter. The cost analysis covers a 25-year timeframe, and here are the key financial metrics: the Cost of Energy (COE) amounts to \$0.0270, the annual Operating Cost is \$256.39, the Net Present Cost (NPC) stands at \$19,811, and the initial system cost is \$16,497.

Export...

Optimization Results

Left Double Click on a particular system to see its detailed Simulation Results.

| Architecture | | | | | | | | Cost | | | | System | |
|---|---|---|---|---|---|--|--|--|--|--|--|--|---|
|  |  |  |  | LR6-72PE (kW)  | Grid (kW)  | Converter (kW)  | Dispatch  | COE (\$)   | NPC (\$)   | Operating cost (\$/yr)   | Initial capital (\$)  | Ren Frac (%)   | Total Fuel (L/yr)  |
| |  |  |  | 33.3 | 999,999 | 18.0 | CC | \$0.0270 | \$19,811 | \$256.39 | \$16,497 | 85.0 | 0 |
| | |  | | | 999,999 | | CC | \$0.100 | \$44,118 | \$3,413 | \$0.00 | 0 | 0 |

Figure 12: On-grid Optimization result for location 3

Figure 13 illustrates the electricity output from the PV system, amounting to 64,558 kWh per year, while the consumption stands at 56,834 kWh per year. The surplus energy serves as a cushion to accommodate any fluctuations in the load, ensuring system resilience. Alternatively, any surplus electricity can be supplied to the grid. The monthly electricity production is depicted in Figure 13, highlighting two power sources: PV in orange and the grid in green.



Figure 13: Electrical Parameter of location 3

In Figure 14 there are basically two graphical representations the one above shows the total AC Primary load that is the blue colour while the orange colour shows the total PV power production on hourly

basis in the month of June in which the solar power production is maximum in Khyber Pakhtunkhwa. While the graph below shows the power or energy sold to and purchased from the Grid, the blue one shows the energy which is sold while the Red one shows the energy purchased from the Grid. Brown colour shows Excess of electricity production.

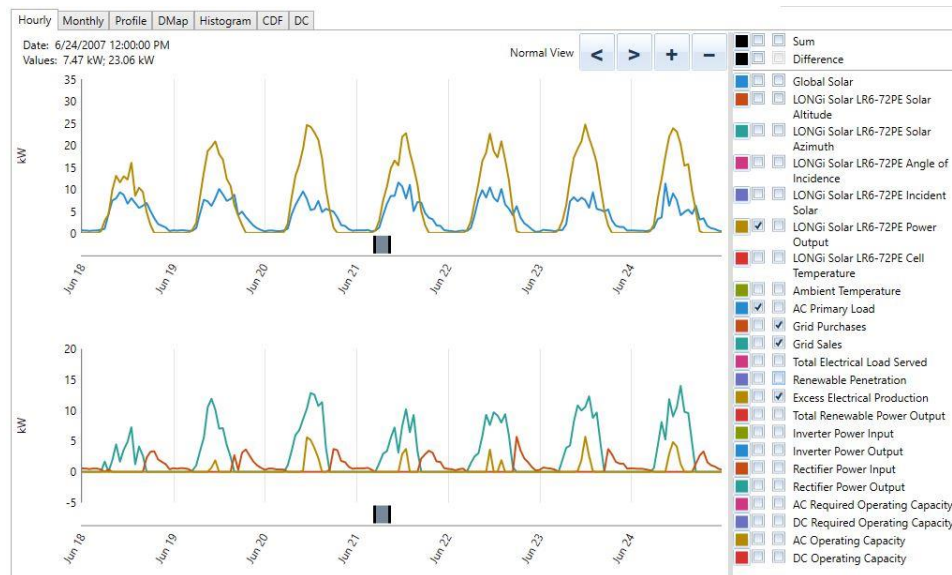


Figure 14: Graphical representation of location 3

CONCLUSION

The given paper shows the Optimization of Grid connected systems for three different rural Areas in the province Khyber Pakhtunkhwa of Pakistan. In the given locations we have taken the same load but different locations i.e District Mardan, District Chitral and district Mohmand and the renewable energy sources are for this study are the Solar and Wind Energy. In the two locations of the given areas, we will use solar as renewable energy source while in district Chitral located in the north of Pakistan in KPK (Khyber Pakhtunkhwa) province where the wind speed is faster as compared to the other two locations therefore will use Wind energy as renewable energy source. The optimization results shows that the grid connected system is more economically and if we compare it with one another the results shows that the On-grid system for the Location 1 is more economical as compared to the other two location because the NPC (net present cost), the operation cost and the initial cost is less than the other two locations. Therefore, it is proposed that grid connect system in location 1 is more economical as compared with other locations.

Future trends in renewable energy will likely focus on:



Hybrid Energy Systems: Emphasizing the integration of multiple renewable sources, future research could utilize advanced simulation modelling and optimization algorithms to design and control hybrid energy systems for increased reliability.

Energy Storage Optimization: Given the importance of energy storage, methodologies employing machine learning and predictive analytics can optimize the operation and sizing of energy storage solutions in renewable energy grids.

Decentralization and Microgrids: As microgrids gain popularity, studies might employ agent-based modelling and distributed control strategies to optimize decentralized renewable energy systems, enhancing local energy resilience.

These methodologies will help navigate the evolving landscape of renewable energy optimization while addressing challenges like intermittency, grid integration, and environmental impact.

ACKNOWLEDGEMENTS

I express my gratitude to everyone I've had the privilege of collaborating with on this and other related projects. All the members of my department have generously Imparted invaluable personal and professional guidance, enhancing my understanding of scientific research and life as a whole.

REFERENCES

- [1] Crousillat, E., R. Hamilton, and P.J.W.B. Antmann, *Addressing the electricity access gap*. 2010.
- [2] *Pakistan - Rural Population(Trading Economics)*. 2023: World Bank.
- [3] Ellabban, O., et al., *Renewable energy resources: Current status, future prospects and their enabling technology*. 2014. **39**: p. 748-764.
- [4] Quaschnig, V., *Understanding Renewable Energy Systems*. Vol. 2. April 11, 2016. 424.
- [5] Wikipedia. *Wind Power*. Available from: https://en.wikipedia.org/wiki/Wind_power.
- [6] *Office of Energy Efficiency & Renewable Energy -Renewable Energy*. [cited 2023; Available from: <https://www.energy.gov/eere/renewable-energy>.
- [7] Dorrell, J. and K.J.E. Lee, *The cost of wind: Negative economic effects of global wind energy development*. 2020. **13**(14): p. 3667.
- [8] Center, M.a.S.A., *U.S. Department of Energy, Office of Energy Efficiency and Renewable Energy*. 2007.
- [9] Solution, I.S. *The 3 Types of Residential & Commercial Solar Power Systems*. [cited 2023 september]; Available from: <https://ilumsolar.com/the-3-types-of-residential-commercial-solar-power-systems/#:~:text=The%20three%20types%20of%20solar,generation%20and%20power%20storage%20experience>.
- [10] Mondal, M.A.H. and A.S.J.R.e. Islam, *Potential and viability of grid-connected solar PV system in Bangladesh*. 2011. **36**(6): p. 1869-1874.
- [11] Xu, L., et al., *Off-Grid Solar PV Power Generation System in Sindh, Pakistan: A Techno-Economic Feasibility Analysis*. 2019. **7**(5): p. 308.
- [12] Solar, D., *The different types of solar PV systems*, in *deege solar 2022*, Deege solar



ICSET-23

*Proceedings of the 5th International Conference on Sustainable
Energy Technologies (ICSET 2023) Peshawar, Pakistan
14-15 December 2023*



UET Peshawar

- [13] Lameck, N., *Design and Optimisation of PV-Biogas Hybrid system for rural electrification in Rwanda*. 2018.
- [14] Ghafoor, A., et al., *Current status and overview of renewable energy potential in Pakistan for continuous energy sustainability*. 2016. **60**: p. 1332-1342.
- [15] *HOMER Pro User Manual*.
- [16] Udayakanthi, G., *Design of a Wind-Solar Hybrid Power Generation System in Sri Lanka*. 2015.

Paper ID: ICSET-2324

INTEGRATED EVACUATED TUBE COLLECTOR AND HEAT STORAGE TO IMPROVE HEATING EFFICIENCY

Abdullah Khan*, Adnan Daud Khan

Renewable Energy Engineering, US-Pakistan Center for Advanced Studies in Energy, University of Engineering and
Technology Peshawar, Pakistan

**Corresponding author*

Email: abdullahkhan.ree@uetpeshawar.edu.pk

ABSTRACT

This research looks on the integration of paraffin in an evacuated tube collector system (ETSC) for effective solar thermal energy heating. Lower operating temperatures are achieved while retaining suitable mean heating medium temperatures. Because paraffin allows for greater temperatures, it is perfect for enterprises that require hot water at high temperatures. The ETSC system lowers heat losses, increases heat collecting efficiency, and emphasis the value of thermal energy storage. Overall, paraffin integration improves the performance and durability of solar thermal systems, increasing their efficiency and sustainability for a wide range of applications. The results showed that using paraffin as thermal storage material can largely improve the heating efficiency of the storage system and can work more efficiently than the collector alone itself.

KEYWORDS: Phase Change Mediums; Heat Storage; Evacuated Tube Collector; Paraffin wax

INTRODUCTION

Solar energy is in the limelight in the current period, which is characterized by a rising worldwide need for renewable energy sources. It stands out as the model for green and clean energy solutions. In the complex web of our present energy mix, solar energy plays a key role. It not only improves the environment but also offers promise for a more sustainable future [1].

Solar thermal and solar chemical processes are the two main methods used to harvest solar energy. These methods reflect the fusion of cutting-edge engineering and science to harness and use the sun's plentiful energy. The temperature thresholds at which energy is best used are used to create a complex categorization scheme for solar thermal activities [2]. The solar thermal technology's many different uses may be distinguished by this triangle of low, medium, and high temperatures. For instance, as the name implies, low temperatures have a place in residential heating systems, which are used to warm and comfort homes. On the other hand, a range of industrial activities, from manufacturing processes to water heating in commercial organizations, are powered by medium temperatures. In a sense, solar thermal technology shines most brilliantly at the high-temperature end of the temperature range. Here, the extreme heat produced acts as the foundation for the production of electricity, enabling the conversion of sunlight into a potent source of power [2].

Solar energy has many benefits, but, it also have certain drawbacks, such as limited sun-shine hours during the day. To address this issue, researchers incorporate heat storage technology into solar energy to



overcome limited sun hours, allowing nighttime power generation. Reduced temperature swings, high storage density, and appropriateness for solar-assisted plants are some of the advantages of latent energy-based storage systems. The research focuses on phase-changing materials and heat exchanger design for effective latent heat utilisation, as well as methods for accelerating melting/freezing. [3]. However, a trade-off arises when a porous solid matrix is included in phase-changing material systems [4]. By easing heat absorption and release, it improves heat storage efficiency, but it also decreases the volume of phase-changing material that is readily available. To maximize energy storage without compromising efficiency, the design and quantity of the porous insert must be balanced correctly. Moreover, temporal mismatches between ETSC energy supply and end-user demand might occur [4]. This study's primary objective is to examine the effects of paraffin integration on a number of significant solar thermal system parameters. We focus on its effects on heat losses, heating medium temperatures, and boiler longevity specifically. This work greatly adds to the amount of knowledge already known in the subject through careful testing and analysis.

Our research clarifies the viability of adding paraffin into solar thermal systems as well as its potential benefits by giving quantitative data and doing in-depth studies. Future developments in solar thermal technology will be significantly influenced by these ideas. Our efforts pave the way for the creation of solar thermal systems that are more effective on both an energy and environmental level. Essentially, we want to leverage paraffin integration strategically to move the sector toward more environmentally friendly and sustainable energy sources.

MATERIALS AND METHODS

The experimental design includes a solar thermal system with a phase change material (PCM) incorporated into an evacuated tube collector (ETC/S) for thermal energy storage. The PCM is used in the ETC/S system to improve heat transmission and control system temperatures while utilizing solar radiation to power the system. Paraffin is chosen as the PCM for integration because of its favorable thermal characteristics. The melting and freezing points of the paraffin substance were [36 degrees melting temp] and [25 degrees or lower freezing temperature], respectively. The paraffin is encapsulated inside an heat storage facility.

The thermocouples are connected to an Arduino microcontroller to make data collection and real-time monitoring easier. The thermocouples' voltage outputs are read by the Arduino microcontroller, which is programmed to translate them into matching temperature readings by using the proper calibration formulae. Temperature readings at regular intervals can likewise be recorded and stored using an Arduino

Table 1: Test parameters and permissible deviations of certain parameters during measurement periods [4]

| Parameters | Values | Deviation |
|---|--------|-----------------------|
| Intensity of Solar radiation G, W/m ² | 900 | ± 50 W/m ² |
| Difference between Initial temperature of heating medium and ambient air, $t_m - t_a$, K | 0 | ± 3 W/m ² |

These above mentioned measurement periods are conducted under specific test conditions, with certain permissible deviations for various parameters. These test conditions ensure standardised and controlled experimentation.

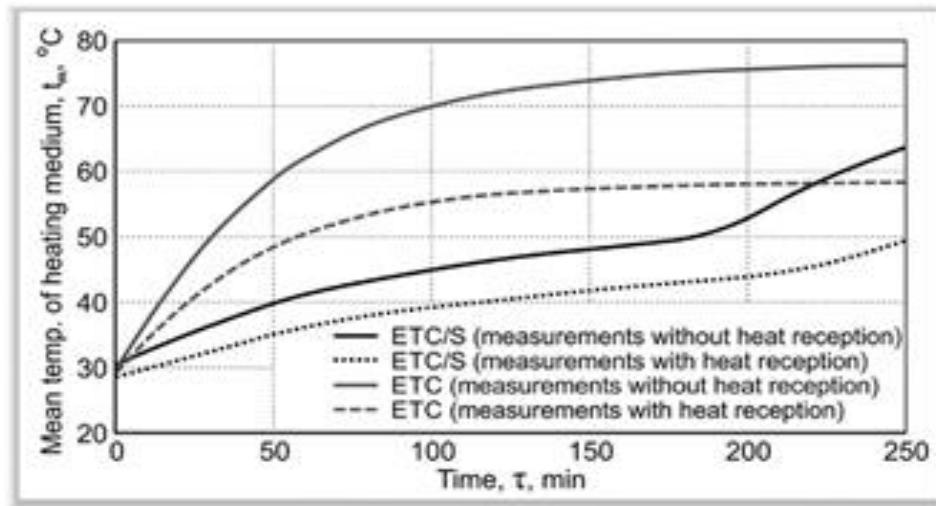


Figure 1: Heating medium mean temperature distribution as a function of time [5]

RESULT AND DISCUSSION

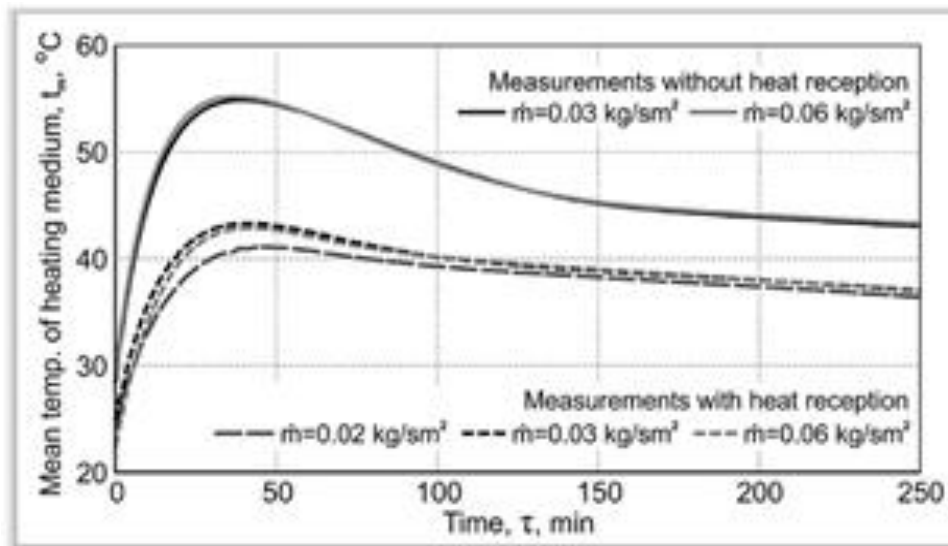


Fig 2. Heating medium mean temperature distribution as a function of time during the ETC/S discharge cycle [5]

The behaviour of the heating medium temperature in our investigation is well-illustrated in Figure 2. We found that the temperature was held constant at 56°C throughout the data measurement series though in the absence of heat reception. The temperature did, however, noticeably increase when heat receiving was added, rising to about 43.5°C. This temperature was notable since it was just 1.5°C below the projected operating temperature of 45°C for domestic hot water (DHW) and space heating (SH) systems, demonstrating the applicability of our strategy.

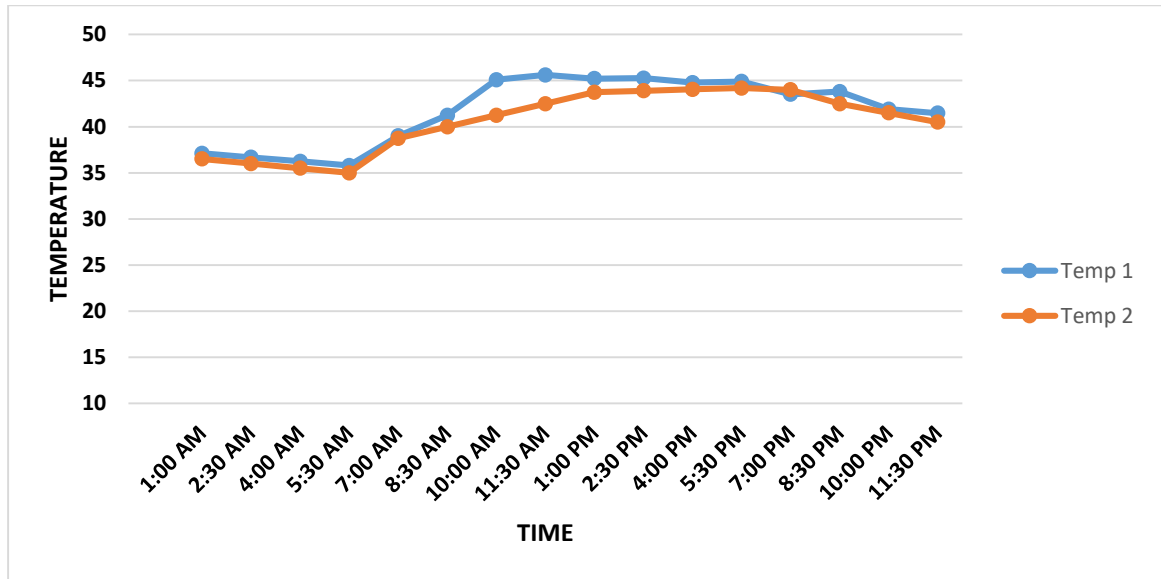


Figure 3: Real Time Data of Solar Collector for 24 Hours

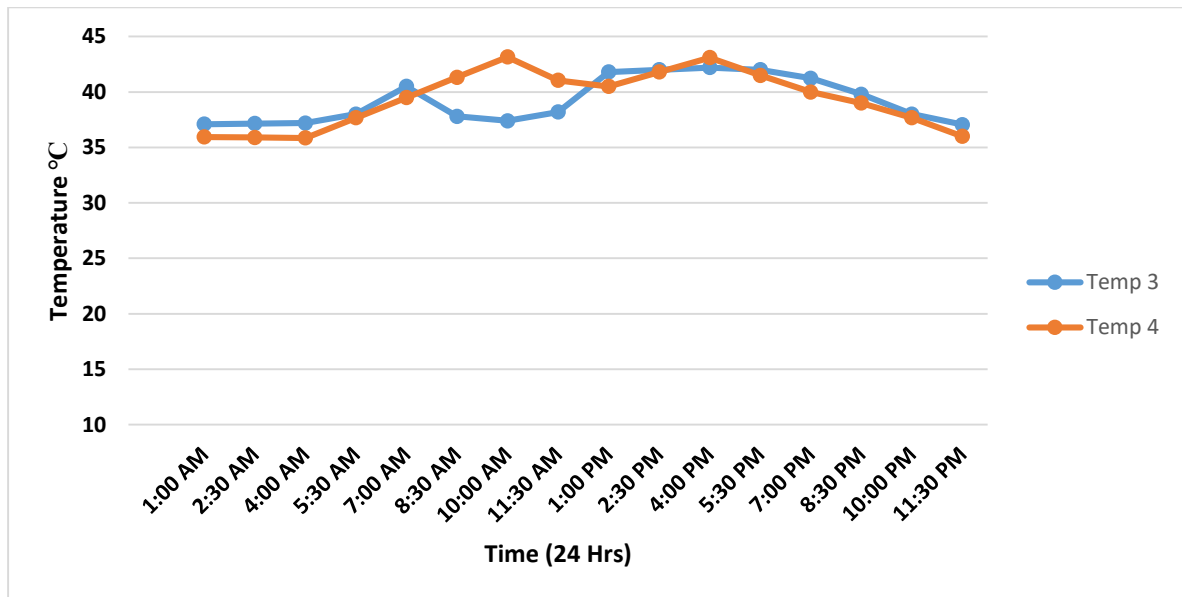


Figure 4: Real Time Data of Heat Storage Tank for 24Hrs

Above mentioned figures 3 & 4, clearly show us that heat is transferred from the heat storage to the collector. That show that the system is capable of storing and then releasing the heat energy for the heating purposes.

Regardless of the mass flow rate, our observations showed that the heating medium's maximum temperature was always reached within the first 40 to 50 minutes of the discharge cycle. This

temporal pattern provides insightful information about the dynamics of the system and identifies possible directions for improving heat transfer and utilization effectiveness in real-world settings.

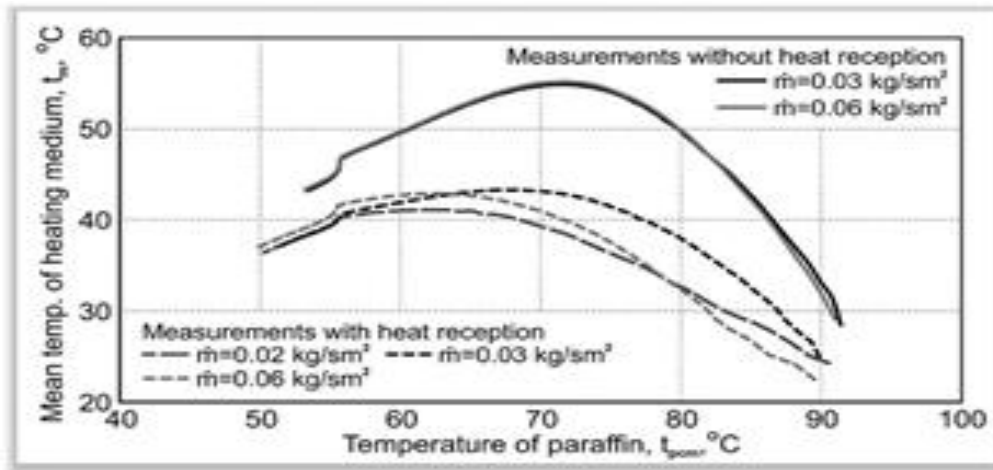


Figure 5: Heating medium mean temperature dependence on the paraffin temperature during the discharge cycle [5]

Figure 3 shows that the mean heating medium temperature remained mostly steady, averaging approximately 72°C and 68°C, respectively, both with and without heat reception. But when we carefully look at the without heat reception's measurement series, we see a very slight drop in the temperature of the heating medium. The system's paraffin phase-changing material's lowering temperature can be blamed for this drop. Surprisingly, the change in the heating medium's temperature itself was barely noticeable compared to how much the paraffin temperature dropped.

However, the paraffin temperature in the heat reception measurement series continued to decrease, and this time it was nearly twice as substantial as the decrease in the heating medium temperature. This disparity is due to increased internal heat losses that hastened the measurement series' decline in the absence of heat reception.

These findings illuminate the intricate dynamics of the system under various conditions by highlighting the complicated interplay between the heating medium and the paraffin phase-changing material. They also offer relevant data on the factors influencing temperature changes, which is important for enhancing the efficiency and performance of solar thermal systems.

CONCLUSION

A basic problem for solar thermal systems is finding a harmonic balance between the amount of solar energy available and the actual need for heat. In this situation, thermal energy storage stands up as a key answer. Within this context, adding paraffin to an Energy Thermal Storage and Conversion (ETC/S) system offers a number of remarkable benefits. While ensuring that mean heating medium temperatures stay at sufficient levels, it is able to lower operational temperatures. Additionally, strategic actions like increasing the number of evacuated tubes or connecting numerous ETC/S devices in series can be taken to improve the performance of such systems. These modifications have the ability to significantly raise heating medium temperatures, making them appropriate for use in situations where high-temperature hot water is required in businesses.



ICSET-23



UET Peshawar

Notably, the inclusion of paraffin to the ETC/S system produces exceptional performance when compared to traditional ETC systems. It results in a significant decrease in heat losses and more effective heat absorption all day long. Depending on the mass flow rate of the heating medium, the ETC/S system with paraffin showed a considerable increase in useable heat production during the discharge cycle, ranging from 45% to 79%.

In conclusion, adding paraffin to solar thermal systems offers a variety of benefits. In addition to increasing heat production, it also reduces heat losses, extending the boiler's useful life. Collectively, our results highlight how paraffin integration may significantly improve the efficacy and efficiency of solar thermal systems.

ACKNOWLEDGEMENTS

My profound gratitude goes out to Prof. Adnan Daud for his unwavering leadership, CAS-E UET Peshawar for their essential support, and our families for their unending love and support ways. Once again thanks to all of them.

REFERENCES

- [1] Zalba, B., et al., *Review on thermal energy storage with phase change: materials, heat transfer analysis and applications*. Applied thermal engineering, 2003. **23**(3): p. 251-283.
- [2] Mao, C., et al., *Mathematical model development and optimal design of the horizontal all-glass evacuated tube solar collectors integrated with bottom mirror reflectors for solar energy harvesting*. Applied Energy, 2019. **238**: p. 54-68.
- [3] Shirinbakhsh, M., N. Mirkhani, and B. Sajadi, *A comprehensive study on the effect of hot water demand and PCM integration on the performance of SDHW system*. Solar Energy, 2018. **159**: p. 405-414.
- [4] Sharafeldin, M. and G. Gróf, *Experimental investigation of flat plate solar collector using CeO₂-water nanofluid*. Energy conversion and management, 2018. **155**: p. 32-41.
- [5] Feliński, P. and R. Sekret, *Experimental study of evacuated tube collector/storage system containing paraffin as a PCM*. Energy, 2016. **114**: p. 1063-1072.

Paper ID: ICSET-2325

PASCAL POLYNOMIAL COLLOCATION METHOD FOR INVERSE HEAT PROBLEM

Siraj-ul-Islam, Muhammad Sattar*, Masood Ahmad
Department of Basic Sciences and Islamiyat, UET Peshawar, Peshawar, Pakistan

**Corresponding author*
Email: sattarmuhammad835@gmail.com

ABSTRACT

This paper introduces a new approach for solving partial differential equations (PDEs) in the context of inverse heat problems. The proposed technique utilizes a collocation scheme with Pascal's polynomial. The results demonstrate accuracy and practicality of the suggested approach, as well as the favourable condition number of the coefficient matrix in the discretized algebraic system.

KEYWORDS: Inverse heat problems, Collocation methods, Pascal polynomial, Well-conditioned system matrices.

INTRODUCTION

Solving time-dependent inverse heat problems (IHPs) can pose significant challenges, particularly when dealing with partial differential equations (PDEs). However, the ability to solve these PDEs is crucial for various practical applications in fields such as aerospace engineering, nuclear physics, metallurgy, non-destructive testing, heat conduction, optics, communication theory, oceanography, computer vision, cardiology, and medical imaging.

The IHPs addressed in this paper follow a general form represented by Equation.

$$\omega_{\tau} = F(\omega_{xx}, \omega_{yy}, \omega_x, \omega_y, H(\tau)), \quad a < x, y < b, \quad \tau < 0 \quad (1)$$

where ω denotes a physical phenomenon, $H(\tau)$ represents a heat or material source, and F captures the underlying physical law governing the system.

Unfortunately, finding a solution to this equation is not always guaranteed due to the presence of unknown terms. Moreover, these problems often suffer from ill-posedness, making the numerical results highly susceptible to noise in the input data. Numerous solution techniques exist for tackling such inverse problems, but the main challenge lies in dealing with the ill-conditioned system matrix resulting from discretizing the linear system.

To address this issue, this study proposes a simple numerical approach based on Pascal polynomials.



This method offers a good numerical solution and yields a relatively well-conditioned system matrix, which significantly enhances the accuracy of the approach. By employing this proposed technique, the challenges associated with solving IHPs can be mitigated, leading to more reliable results.

Numerous numerical techniques are covered in the literature on numerical solutions for IHPs (see [1] and [2]). Due to their effectiveness, implicit schemes are frequently used to solve IHPs, whereas explicit methods are typically thought to be less effective [3]. In earlier publications, the method of basic solution was put forth as a numerical strategy for IHPs ([4]-[5]). Other pertinent numerical techniques that concentrate on resolving IHPs include the boundary element method (BEM) [6], the iterative BEM ([7], [8]), the Tikhonov regularization technique (TRT), the operator-splitting method [9], the lattice-free high-order finite-difference method [[10] In [[11], a recent study tackling time-dependent inverse heat problems is described. Mallat's book also has the citation [12].

In light of the difficulties encountered in numerically solving inverse heat problems (IHPs), this paper presents a straightforward and precise numerical approach based on Pascal polynomials. The proposed method offers a stable numerical solution and overcomes some of the challenges faced by other IHP-specific techniques. Notably, the system matrix of the proposed approach exhibits favourable conditioning, which significantly contributes to the accuracy of the method.

Pascal Polynomial

Pascal's polynomial, which can be arranged in the so, called Pascal's triangle, is a triangular array of numbers that was discovered by the French mathematician Blaise Pascal in the 17th century. The numbers in the triangle are arranged such that each number is the sum of the two numbers immediately above it, and the rows are numbered starting from 0.

The numerical solution of partial differential equations (PDEs) can be obtained easily by adapting the polynomial expansion method. By using collocation points in the spatial domain, the numerical solution can be obtained straightforwardly. However, directly applying the polynomial expansion method may pose risks due to the highly ill-conditioned coefficient matrix formed by the algebraic equations' outcomes, especially when dealing with high-order polynomials. To mitigate the ill-conditioned behaviour of the coefficient matrix, certain remedies might be necessary. The polynomials used in the numerical solution $\omega(x, y)$ of the considered PDEs are the elements of the following matrix:

$$\begin{bmatrix} 1 & y & y^2 & \dots & y^{n-1} & y^n \\ x & xy & xy^2 & \dots & xy^{n-1} & xy^n \\ x^2 & x^2y & x^2y^2 & \dots & x^2y^{n-1} & x^2y^n \\ \vdots & \vdots & \vdots & \dots & \vdots & \vdots \\ x^n & x^ny & x^ny^2 & \dots & x^ny^{n-1} & x^ny^n \end{bmatrix}.$$

This matrix considers the elements limited to the left-upper triangle, which is also known as Pascal's triangle expansion.

Hence, $\omega(x, y)$ is sought of the form:

$$\omega(x, y) = \sum_{j=1}^m \sum_{k=1}^j c_{jk} x^{j-k} y^{k-1}. \quad (2)$$

In Eq. (2), the highest degree of the polynomial is $m-1$, c_{jk} represents the coefficients that need to be determined, and $n = m(m+1)/2$ corresponds to the total number of coefficients. Using Eqn. (2), we can write:

$$\omega_x(x, y) = \sum_{j=1}^m \sum_{k=1}^j c_{jk} [(j-k)x^{j-k-1}y^{k-1}] \quad (3)$$

$$\omega_y(x, y) = \sum_{j=1}^m \sum_{k=1}^j c_{jk} [(k-1)x^{j-k}y^{k-2}]. \quad (4)$$

Where $\omega_x(x, y)$ and $\omega_y(x, y)$ are the partial derivatives of $\omega(x, y)$ with respect to x and y , which will be used to solve the PDE.

Pascal Polynomial Scheme For One-Dimensional Inverse Heat Problem

Consider the following form of one-dimensional inverse heat problem (IHP): $\{[11]\}$:

$$\omega_\tau(x, \tau) = \omega_{xx}(x, \tau) + H(\tau), \quad a < x, y < b, \quad \tau < 0 \quad (5)$$

subject to the initial and boundary conditions:

$$\omega(x, 0) = g(x),$$

$$\omega(a, \tau) = \omega_o(\tau),$$

$$\omega_x(a, \tau) = \omega_l(\tau),$$

where ω and $H(\tau)$ represent the unknown solution and the unknown heat source, respectively. To determine these unknowns, additional information is provided in the form of:

$$\omega_x(b, \tau) = q_o(\tau).$$

METHODOLOGY

To numerically solve the IHP, we begin by taking the partial derivative of Eq. (5) with respect to x and employing the transformation $\omega_x(x, \tau) = \mu(x, \tau)$ resulting in the following equation:

$$\mu_\tau(x, \tau) = \mu_{xx}(x, \tau), \quad a \leq x \leq b, \quad \tau > 0. \quad (6)$$

The transformed boundary conditions are as follows:

$$\mu(x, 0) = g'(x),$$

$$\mu(a, \tau) = \omega_l(\tau),$$

$$\mu_x(b, \tau) = q_o(\tau).$$

To construct the Pascal polynomial approximation scheme, we initiate the approximation as follows:

$$\mu(x, \tau) = \sum_{i=0}^n \lambda_i x^i \quad (7)$$

Differentiating Eq. (7) with respect to x , we obtain:

$$\mu_x(x, \tau) = \sum_{i=0}^n i \lambda_i x^{i-1} \quad (8)$$

Similarly, the 2nd derivative can be expressed as:

$$\mu_{xx}(x, \tau) = \sum_{i=0}^n i(i-1) \lambda_i x^{i-2} \quad (9)$$

Assume that τ_o represents the present time level and $\tau = \tau_o + \Delta\tau$ represents the following time level. We obtain the time derivative in Eq. (6) by using the implicit technique:

$$\frac{\mu(x, \tau) - \mu(x, \tau_o)}{\Delta\tau} = \mu_{xx}(x, \tau).$$

By rearranging, we get:

$$\mu(x, \tau) = \mu(x, \tau_0) - \Delta\tau \mu_{xx}(x, \tau) \quad (10)$$

Substituting Eq. (7) and Eq. (9) into Eq. (10) and subsequent discretization at the collocation points leads to the following system of algebraic equation

$$\sum_{i=0}^n \lambda_i \left[x^i - \Delta\tau \sum_{i=0}^n i(i-1)x^{i-2} \right] = \mu(x, \tau_0) \quad (11)$$

Similarly, Eq. (11) can be written in matrix form as:

$$Ac = b$$

where

$$A = \left[x^i - \Delta\tau \sum_{i=0}^n i(i-1)x^{i-2} \right]$$

and

$$b = \mu(x, \tau_0).$$

NUMERICAL RESULTS

In this section, we tackle one-dimensional inverse heat problems (IHPs) using the Pascal polynomial approach and assess the numerical outcomes for a test situation. We also discuss the ideas of absolute and relative boundary noise. The representation of the absolute noise is $\widehat{q}_0(\tau) = q_0(\tau) + \sigma$, where $\widehat{q}_0(\tau)$ is the original quantity and σ denotes the noise level.

To quantify the accuracy of our method, we employ the maximum absolute error, denoted as E_{ab} . This error metric is defined as follows:

$$E_{\infty} = \max(E_{ab})$$

The absolute difference between the exact representation of the heat source, $H(\tau)$, and its numerical representation, $\widehat{H}(\tau)$, is shown above as

$$E_{ab} = |H(\tau) - \widehat{H}(\tau)|$$

One Dimensional IHP Example

Problem 1

Consider the following example having an exact solution for the IHP and presented in [13]. The solution of the problem is given by:

$$\omega(x, \tau) = e^{-\tau} \sin x + 3x^2\tau + \frac{1}{4}x^4, \quad 0 \leq x \leq 1, \quad \tau \leq 2.1,$$

$$H(\tau) = -6\tau$$

We selected $m=10$, $n=20$ with various noise levels for this test problem, as shown in **Tab. 1**. These tables make it obvious that the results produced, are accurate in the absence of noise in the data, as seen in **Tab. 1**. However the accuracy decrease when noise is added. The accuracy also improves by decreasing the value of $\Delta\tau$, as illustrated in **Tab. 2**.

The condition number of the coefficient matrix is also calculated and compared with the method [13]. The comparison results are presented in Tab. 3. The table clearly indicates that the condition number of the Pascal polynomial is smaller than the condition number of the method [13].

Graphs of the solution are also plotted with and without adding noise in the data, as shown in **Fig. 1, 1(a)** and **1(b)**. In these graphs, the heat dependent source $H(\tau)$ is plotted against $\Delta\tau$. It can be seen that the results with and without noise in the data are not same i.e by adding 1% and 5% noise, the errors in the solution increase. In **Fig. 1(c)**, a magnified image of 1% noise in the data of problem 1 is shown.

Table 1: Comparison of errors at $\Delta\tau = 0.00001$

| m, n | 0% noise | 1% noise | 10% noise |
|---------|-------------------------|-------------------------|-------------------------|
| 10, 20 | 1.7865×10^{-5} | 1.8410×10^{-2} | 1.8410×10^{-1} |
| 10, 30 | 1.7865×10^{-5} | 2.7400×10^{-2} | 2.7430×10^{-1} |
| 10, 50 | 1.7865×10^{-5} | 4.0300×10^{-2} | 4.0280×10^{-1} |
| 10, 80 | 1.7865×10^{-5} | 4.9900×10^{-2} | 4.9910×10^{-1} |
| 10, 100 | 1.7865×10^{-5} | 5.2700×10^{-2} | 5.2730×10^{-1} |

Table 2: Comparison of absolute error on $m, n = 20, 10$

| $\Delta\tau$ | E_{ab} |
|--------------|-------------------------|
| 0.1 | 1.6700×10^{-2} |
| 0.01 | 1.8000×10^{-3} |
| 0.001 | 1.7851×10^{-4} |
| 0.0001 | 1.7865×10^{-5} |
| 0.00001 | 1.7867×10^{-6} |

Table 3: Comparison of condition number of Pascal polynomial and [13]

| m, n | Pascal polynomial | [13] |
|----------|--------------------------|--------------------------|
| 20, 20 | $1.6847 \times 10^{+14}$ | $5.0716 \times 10^{+19}$ |
| 30, 30 | $1.9260 \times 10^{+14}$ | $9.4524 \times 10^{+20}$ |
| 50, 50 | $6.4033 \times 10^{+18}$ | $8.3471 \times 10^{+20}$ |
| 80, 80 | $8.4092 \times 10^{+18}$ | $8.6991 \times 10^{+21}$ |
| 100, 100 | $1.1809 \times 10^{+19}$ | $2.8315 \times 10^{+21}$ |

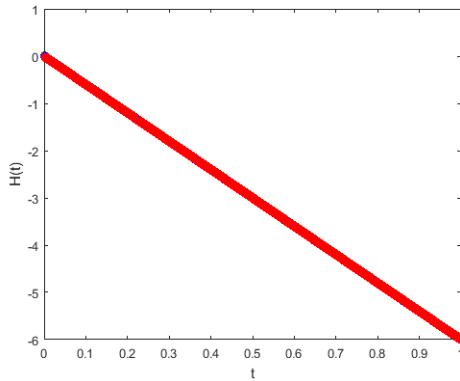


Figure 1: Pascals Polynomial

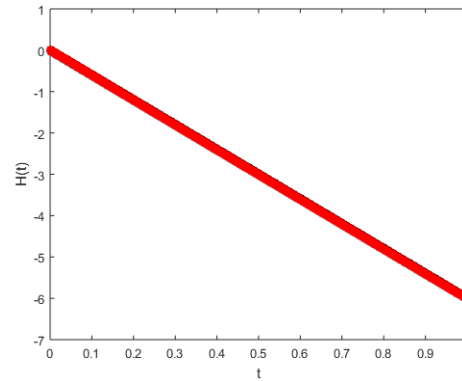


Figure 1(a): 1% noise in the data

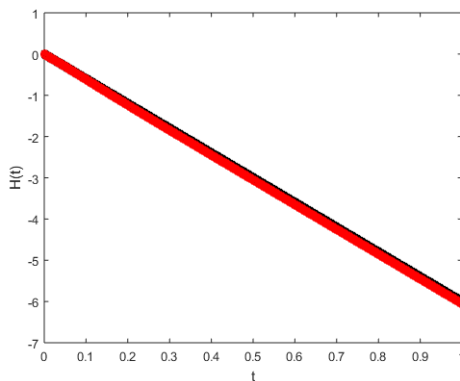


Figure 1(b): 5% noise in the data

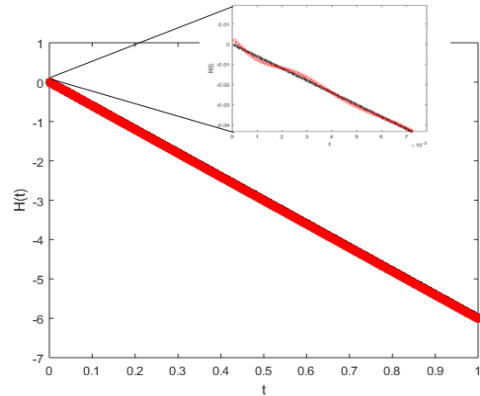


Figure 1(c): Magnified image of 1% noise

CONCLUSION

This paper introduces a novel collocation procedure aimed at accurately evaluating the unknown time-dependent heat source in one-dimensional IHPs. Through the utilization of Pascal polynomials, a well-conditioned linear system is derived for the challenging ill-posed differential equation, enabling precise approximations of both the solution and the heat source. The proposed method exhibits robustness against realistic noise interference in the measured data for one-dimensional problems.

REFERENCES

- [1] G. Stolz, "Numerical solutions to an inverse problem of heat conduction for simple shapes", *J Heat Transfer*, vol. 82, n^o 1, p. 20–25, 1960.
- [2] D. V. Widder, *The Heat Equation*, vol. 67. Academic Press, 1976.
- [3] C.-S. Liu, C.-L. Kuo, e W.-S. Jhao, "The multiple-scale polynomial Trefftz method for solving inverse heat conduction problems", *Int J Heat Mass Transf*, vol. 95, p. 936–943, 2016.



ICSET-23

Proceedings of the 5th International Conference on Sustainable
Energy Technologies (ICSET 2023) Peshawar, Pakistan
14-15 December 2023



UET Peshawar

- [4] N. S. Mera, “The method of fundamental solutions for the backward heat conduction problem”, *Inverse Probl Sci Eng*, vol. 13, n° 1, p. 65–78, 2005.
- [5] C. H. Tsai, D. L. Young, e J. Kolibal, “An analysis of backward heat conduction problems using the time evolution method of fundamental solutions”, *Comput Model Eng Sci*, vol. 66, n° 1, p. 53, 2010.
- [6] H. Han, D. B. Ingham, e Y. Yuan, “The boundary element method for the solution of the backward heat conduction equation”, *J Comput Phys*, vol. 116, n° 2, p. 292–299, 1995.
- [7] N. S. Mera, L. Elliott, D. B. Ingham, e D. Lesnic, “An iterative boundary element method for solving the one-dimensional backward heat conduction problem”, *Int J Heat Mass Transf*, vol. 44, n° 10, p. 1937–1946, 2001.
- [8] N. S. Mera, L. Elliott, e D. B. Ingham, “An inversion method with decreasing regularization for the backward heat conduction problem”, *Numerical Heat Transfer: Part B: Fundamentals*, vol. 42, n° 3, p. 215–230, 2002.
- [9] S. M. Kirkup e M. Wadsworth, “Solution of inverse diffusion problems by operator-splitting methods”, *Appl Math Model*, vol. 26, n° 10, p. 1003–1018, 2002.
- [10] K. Iijima, “Numerical solution of backward heat conduction problems by a high order lattice-free finite difference method”, *Journal of the Chinese Institute of Engineers*, vol. 27, n° 4, p. 611–620, 2004.
- [11] Siraj-ul-Islam e S. Ismail, “Meshless collocation procedures for time-dependent inverse heat problems”, *Int J Heat Mass Transf*, vol. 113, p. 1152–1167, 2017.
- [12] S. Mallat, *A wavelet tour of signal processing: the sparse way*. Academic press, 2008.
- [13] M. Amirfakhrian, M. Arghand, e E. J. Kansa, “A new approximate method for an inverse time-dependent heat source problem using fundamental solutions and RBFs”, *Eng Anal Bound Elem*, vol. 64, p. 278–289, 2016.

Paper ID: ICSET-2326

TECHNO-ECONOMIC ANALYSIS OF ALUMINIUM BUSBAR IN LOW VOLTAGE ELECTRICAL DISTRIBUTION PANEL

Faisal Najam^{1,*}, Nayyar Hussain Mirjat¹, Shoaib Ahmed Khatri¹, Lala Rukh²

¹Electrical Engineering, Mehran UET Jamshoro, Jamshoro 76062, Pakistan

²School of Engineering, University of Galway, H91, Ireland

**Corresponding author*

Email: faisal.najam.ranipur@gmail.com

ABSTRACT

This research explores Aluminium as a viable alternative to copper for bus bars in low-voltage distribution panels, an appropriate investigation among increasing global energy demands and reducing copper reserves. Guided by DIN-43670 and IEC 61439-1-2020 standards, the study conducts a detailed techno-economic and thermal analysis of aluminium and copper bus bars, involving temperature variations, cost-efficiency, and weight advantages. An innovative approach leveraging real-time data collection reveals the thermal behaviour of the materials, supported by a practical case study involving a 150 KW load and fiber-reinforced material enclosure to assess Aluminium's performance. The weights of Copper and Aluminum bus bars per meter are 1.33 kg/m and 1.08 kg/m, respectively. A single copper bus bar with a width of 30 mm and a thickness of 5 mm weighs 1.064 kg for an 8mm length. Meanwhile, an Aluminum bus bar with a width of 40 mm and a thickness of 10 mm weighs 0.864 kg for the same length. The findings highlight Aluminium's potential not only to meet but exceed the efficiency of copper, presenting a sustainable solution that promises reduced costs and enhanced power delivery efficiency. By shedding light on Aluminium's untapped potential, this study indicates a model shift in the industry, encouraging stakeholders to reconsider the conventional reliance on copper. It stands as a keystone for future research to raise sustainable and economically prudent innovations in power distribution systems.

KEYWORDS: Aluminium Busbar, Copper, Cost Analysis, DIN Standards, IEC Standard, Sustainable Energy, Technoeconomic Analysis, Thermal Behaviour.

INTRODUCTION

The demand for energy is escalating, and growing interest and capacity in renewable energy thereby augments the necessity for efficient electrical distribution systems. Historically, Copper has been the preferred conductor, revered for its superior conductivity properties. However, the diminishing reserves of copper among other earth minerals and the accompanying environmental repercussions compel us to explore alternative solutions. This research investigates Aluminium (Al) as a potential substitute in power systems, aiming to assess its viability, economic efficiency, and environmental sustainability. It is appropriate to conceptualise bus bars as the vital conduits in the electricity distribution network.

Al offers a cheaper alternative to Copper for use in Large Busbar Box (LBB) in electrical distribution systems. This study provides a result of a techno-economic analysis of Al busbar in low voltage electrical distribution panel based on research review and experimental work. To achieve the research



objectives, we propose to conduct a rigorous thermal analysis through current injection experiments and a techno-economic evaluation encompassing various parameters such as weight, resistance, transportation logistics, and cost-efficiency. Furthermore, we aim to design bus bars that would facilitate a reduction in power loss. Alves et al. [1] have proposed a simulating mathematical model for the control gear in which heat is generated internally, which is the necessary equipment in electricity distribution. The model uses methods of algebra and uses concept design of a software program and compare the behaviour at different points and the parameter's detailed analysis is provided by simulation and permits prediction at critical points and real-time monitoring. Szulborski et al. [2] conducted a study on achieving uniform heat distribution in low-voltage switchgear-connected bus bars at rated current. They used simulation tools like Maxwell 3D, Transient Thermal, and Fluent CFD to streamline cost-effective product development. These simulation outcomes endorse dependable, LV switchgear design for construction applications. Guided by DIN-43670 and IEC 61439-1-2020 standards [3]. Plesca et al. [4] introduced a mathematical model for analysing bus bar thermal behaviour, considering various factors such as current levels, cross-sections, lengths, and contact resistance values. This model holds value in optimising and designing bus bars within power distribution systems, contributing to efficient system planning and design. Furthermore, a study on electrical joint ageing by Al and Cu contact members has emphasised the importance of connection design and maintenance in ensuring consistent and stable networks in electrical power systems [5]. Another research effort proposed a thermal simulation model for switchgear, revealing that an increase in input current leads to higher temperatures and mechanical stress on the switchgear [6]. Additionally, a 3D electromagnetic multi-physics model was presented, considering factors such as radiation, contact resistance, skin effect, and gas flow distribution to investigate contact spacing, contact position's impact on power loss, and the effect of contact number through simulation [7]. In an analysis of medium-voltage panel board bus bars, both Copper and Al experienced significant temperature increases under high loads. Copper exhibited slightly lower temperatures, while Al emerged as a cost-effective and lightweight material choice based on considerations of thermal performance, cost, and weight [8]. Lastly, a practical thermal design technique for bolted connections between copper busbars in switchgear was explored, including a parametric analysis of contact resistance. This research also delved into silver-plated connections of the bus bar, utilising thermal simulation data to inform cooling system design for the switchgear [9].

Sampaio et al. [10] have examined hybrid busbars made of aluminium and copper, specifically assessing how temperature affects their electrical performance at the joints. Various joint types, including fastened, friction stir spot welded, sheet-bulk compressed, and injection lap riveted, were tested using a specialized lab apparatus and numerical simulations. The findings reveal that the electrical resistance of these hybrid busbars can increase by over 30% at temperatures reaching the upper limit set by the IEEE standard for metal-clad switchgear.

Bolted busbar connections, commonly using copper, are prevalent in battery systems. This study explores the potential benefits of Aluminum as a lighter, cost-effective alternative, specifically focusing on its reliability and resistance to corrosion. Testing was conducted on four bolted Aluminum configurations, considering both operational and environmental conditions relevant to battery systems. Nickel-plated Aluminum demonstrated the most stable resistance, enduring over 6,000 cycles across varied temperatures and remaining unaffected in corrosive conditions. In contrast, brushed Aluminum connections showed more resistance variation, emphasizing the need for a joint performance factor below 1.5 for long-term reliability. As the battery industry grows more interested in Aluminum, this research highlights the importance of developing standardized testing environments for Aluminum contacts and offers a methodology for



ICSET-23



UET Peshawar

evaluating new contact configurations [11]. Due to the Rising cost of copper, aluminum is the most competitive conductor to replace copper in electrical distribution system by undertaking techno-economic analysis of competitive conductor.

The prevalent use of Copper in power systems, as seen in Pakistan and globally, presents challenges related to cost, weight, corrosion, and copper reserve depletion. These challenges align with findings in the literature that underscore Copper's limitations. To address these issues, this research explores the substitution of Copper with Al, known for its cost-effectiveness, lower weight, and corrosion resistance. By conducting Thermal Analysis (IEC Standard 61439-1-2020) and Techno-Economic analysis on 150 kW load scenarios, we compare Copper (30*5 mm DIN standard) and Al (40*10 mm DIN standard) bus bars. The research aims to recommend specific Al sizes that outperform Copper, reducing costs, resistance, power loss, and weight in power distribution systems, contributing to the ongoing discourse on sustainable material choices. To achieve this aim, the following research objectives are achieved.

- To develop an experimental model of a single-phase low-voltage bus bar system.
- To conduct Thermal and Techno-economic analysis of Aluminium and Copper bus bars
- To analyse the results and devising study recommendations.

The following sections describe the methodology of techno-economic analysis, and results (broken into three parts) i) thermal analysis, ii) cost analysis, iii) power loss analysis of Al vs Cu, followed by the study's conclusion.

RESEARCH METHODOLOGY

Figure 1 depicts the copper bus bar assembly vs the Al bus bar assembly, both enclosed within boxes.

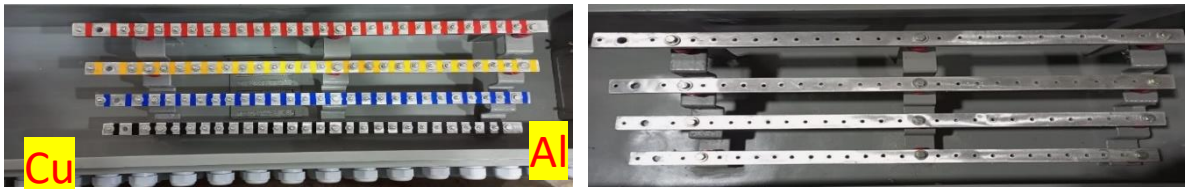


Figure 1: Copper and Al Busbar boxes

The flow chart of the Research methodology is given below in Figure 2.

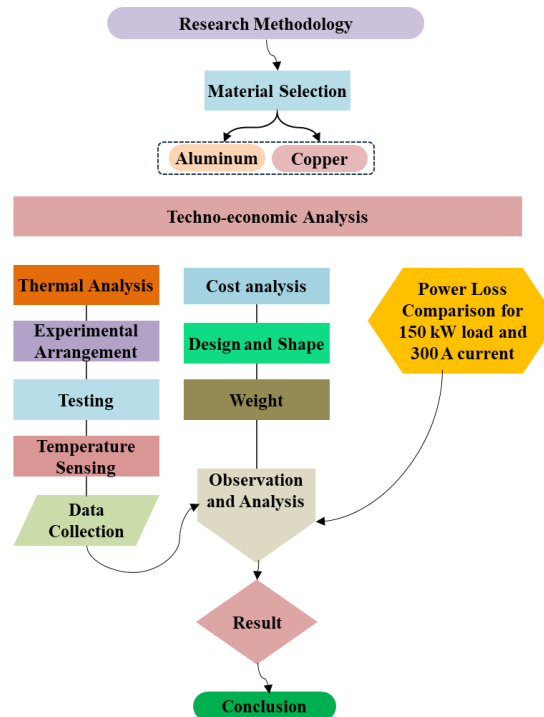


Figure 2: Research Methodology

This study primarily focuses on conducting a comprehensive investigation and comparative analysis of the thermal and operational characteristics of Copper and Al utilised as bus bars within low-voltage distribution panels. The research's Techno-Economic Analysis scrutinises both Al and Copper, encompassing critical aspects such as weight considerations, cost implications, efficiency losses, size parameters, and compliance with DIN Standards. Furthermore, the study incorporates thermal testing procedures aligned with the guidelines set forth by the International Electrotechnical Commission (IEC). The findings derived from this research endeavour are comprehensively detailed within the confines of this paper. Notably, these bus bars share a common length of 800mm; however, the copper bus bar has a width and thickness of 30mm and 5mm, respectively, per DIN Standard 63671. Conversely, the Al bus bar maintains the same length but features a width of 40mm and a thickness of 10mm, aligning with DIN Standard 63670 specifications.

Our thermal analysis aimed to assess the thermal characteristics of both Al and copper bus bars under various load conditions. This assessment was conducted through practical experimentation, eschewing the use of simulation software, and centred on empirical observations and measurements.

Experimental Configuration and Arrangement

A 300A-rated alternating current was applied to assess the temperature rise at the busbar's incoming point. Subsequently, thermal behaviour was observed at various positions along the bus bars. The evaluation followed the guidelines specified in the IEC standard IEC-61439-1 (IEC, 2020) which facilitated the measurement of temperature rise for copper and Al bus bars. Thermocouples were strategically placed on the bus bars, and their positions are visually represented in Figure 3.



In the distribution panel, we deployed 14 thermocouples to measure temperatures at specific locations within the box precisely. These thermocouples were of the K-type variety, composed of Nickel-chromium and Nickel-aluminium elements, and had an average length of 2.5 meters. They were strategically positioned to connect observation points on the bus bars to a temperature meter.

Our experiment focused on various key points within the bus bar box, including the incoming bus bar terminal, areas near joints, midpoints along the bus bars, and the outgoing terminal of a 150-kW large bus bar box. We affixed specialised sensors to these locations using Al tape. These sensors recorded temperature readings at hourly intervals.

Our primary objective was to ensure that the temperature did not exceed a predefined limit when subjected to a 300A current. The test continued until a one-degree Celsius temperature increase per hour was observed at all measuring points. We then compared these data points to the room temperature to determine the extent of temperature rise. Additionally, we paid close attention to how we securely attached the temperature sensors to the bus bars. Finally, we conducted a comparative analysis of the results for both copper and Al bus bars. This comparison encompassed factors such as energy losses, cost considerations, and ensuring that the metal components did not experience excessive heating, ensuring the metal structures' safety when used in electrical applications. K-type temperature sensors were intentionally located along the bus bars to arrest temperature variations at definite points.

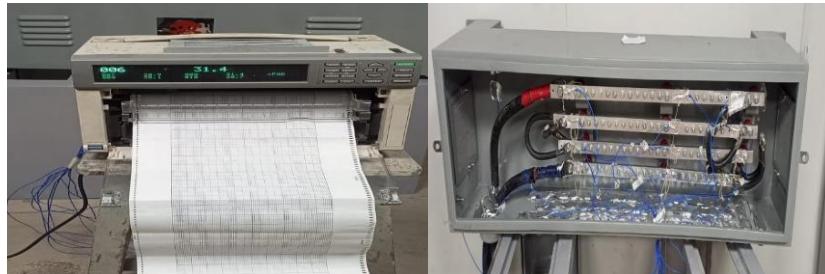


Figure 3: Sensors from logger machine on bus bars

Load Scenarios and Data Collection:

Our thermal experiments encompassed a range of load scenarios, employing injected currents to match distinct operating conditions. Temperature data was gathered using K-type sensors that interfaced with a data logger device. Over the course of approximately 8 hours, the data logger recorded temperature readings at 30-minute intervals, ceasing its operation when the bus bars reached a saturation point characterised by a one-degree Celsius temperature rise, in compliance with the IEC 61439 Standard. Our focus during the experiment was determining temperature changes and designs in Al and copper bus bars. Results from the logger machine's recorded data illuminated the responses of these materials to varying current concentrations and load conditions. The temperature analysis table is given in the Table.1

A meticulous cost examination revealed a significant cost differential between Al and Copper. Specifically, Al exhibited a cost advantage, approximately one-third of the expense associated with Copper. Weight considerations held paramount importance in our evaluation. It is noteworthy that Al possesses a lower weight profile than Copper. This weight reduction facilitates ease of transportation and handling. A comprehensive weight comparison and corresponding data are provided in Table 2 within the Results section.



Table 1: Position of Sensors on the busbar during testing (Temperature rise test of large bus bar box 25/07/23)

| Sensors | Location | Sensors | Location |
|---------|--------------------------|---------|------------------------------|
| T1/U1 | Red left (Main outgoing) | T8/U8 | Blue mid |
| T2/U2 | Red mid | T9/U9 | Blue right (Joint) |
| T3/U3 | Red right (Joint) | T10/U10 | Neutral left (Main incoming) |
| T4/U4 | Yellow left (Joint) | T11/U11 | Neutral mid |
| T5/U5 | Yellow mid | T12/U12 | Neutral right (Joint) |
| T6/U6 | Yellow right (Joint) | T13/U13 | Ambient 1 |
| T7/U7 | Blue left (Joint) | T14/U14 | Ambient 2 |
| | | * | Average of T13/U13 & T14/U14 |

The reduced weight of Al translated into heightened transportation efficiency, effectively mitigating the logistical complexities and associated costs that arise when dealing with bulkier copper components. Our assessment of losses considered adherence to DIN standards, ensuring rigorous precision in our analysis. Notably, our observations indicated that Al bus bars, when conforming to DIN standards, exhibited diminished losses when juxtaposed with copper counterparts. Furthermore, the augmentation of the Al bus bar's cross-sectional area notably improved its resistance characteristics.

To amalgamate our findings effectively, we directed our attention towards a detailed scenario involving a 3-Phase load with a power rating of 150KW. This targeted approach allowed us to meticulously discern the performance disparities between Al and Copper under controlled conditions, culminating in developing distinct insights, with a pronounced emphasis on the economic aspects elucidated through cost analysis.

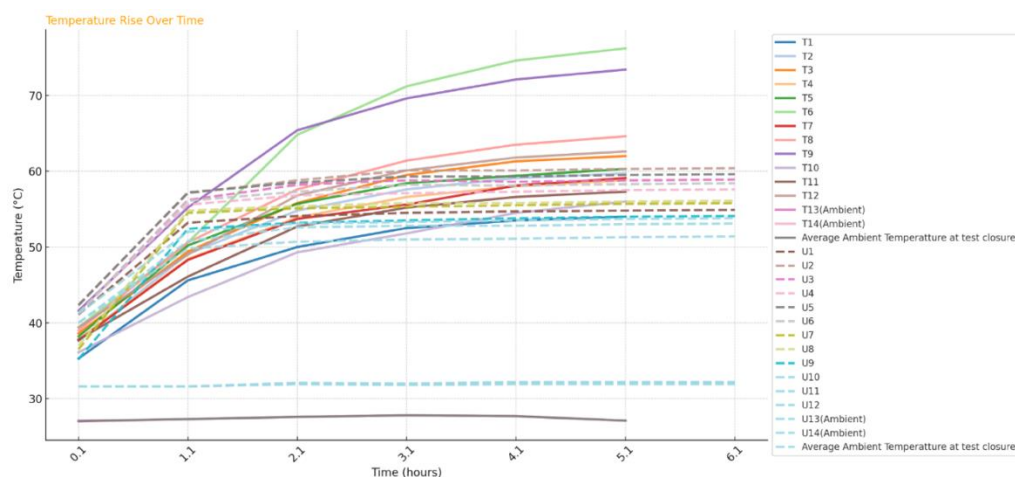


Figure 4 Thermal Analysis of Al (T sensors) and Cu (U sensors) Busbar boxes

RESULTS AND DISCUSSION

Thermal Testing

We conducted a comprehensive Thermal Analysis of Al and Copper Busbars, adhering to the rigorous standards in IEC guidelines. During testing, Al and Copper initially exhibited temperature increases at joint positions due to issues related to tightness and finishing. However, after addressing these specific



challenges, the subsequent tests yielded successful results. Notably, these results supported the viability of replacing Copper bus bars of size 30*5 with Al counterparts sized at 40*10 within the context of a 150-kW large bus bar box. Figure 4 shows results from thermal analysis for both Al and Cu.

Over 6 hours, all sensors from groups T (T1 to T14) for Al and U (U1 to U14) for Cu demonstrated a general upward trend in temperature, suggesting a consistent rise over time, although with distinct patterns within and between groups. In group T, sensors T1 and T2 have showcased a relatively steady increase, indicating a consistent heating environment, while T3, T4, and T5 exhibited pronounced fluctuations, with T4 starting at a notably higher temperature. Comparatively, U1 and U2 from group U portrayed a steeper rise initially, moderating over time, with U1 consistently registering higher temperatures.

Meanwhile, U3 to U5 showed more varied fluctuations, with U5 experiencing a significant dip and subsequent rise between the 2nd and 3rd hours, hinting at a dynamic thermal environment. Across both groups, the initial temperatures were highest for T4 and U1, and by the end of the 6-hour period, T1 and U1 registered the highest temperatures, suggesting the greatest overall heating effect.

The results derived from our thermal analysis distinctly affirmed Al's compliance with the IEC 61439 - 2022 standards. This validation underscores Al's capacity to replace Copper in the 150-kW load scenario, offering a range of advantages such as reduced losses, lower weight, enhanced corrosion resistance, and cost-efficiency. Notably, both Copper and Al bus bars exhibited comparable heat dissipation capabilities. Compliance with DIN standards necessitated an increase in width and depth for the Al bus bar, which subsequently passed the thermal testing regimen.

Cost Analysis

The cost analysis shows that Al bus bars have lower material costs and reduced production expenses associated to Copper. This price benefit makes Al a preferable choice for to use in the field, while maintaining condition and operation. For weight comparison, aluminium's weight is less than Copper's weight when carrying the same current. Weight is an essential factor to consider in the techno-economic analysis of aluminium compared to Copper, as it can impact a system's cost, efficiency, and performance. Here is a comparison of the weight of aluminium and Copper.

Table 2 Cost comparison of AL and Copper

| Name | Length in m square | Area in mm square | Bus No | According to din standard Weight kg/m | Single bus bar weight | Total weight | cost per kg/m | Total Cost |
|------|--------------------|-------------------|--------|---------------------------------------|-----------------------|--------------|---------------|------------|
| CU | 0.8 | 0.00015 | 4 | 1.33 | 1.064 | 4.256 | 4300 | 18300.8 |
| AL | 0.8 | 0.0004 | 4 | 1.08 | 0.864 | 3.456 | 1400 | 4838.4 |

The inherent cost-effectiveness, lighter weight, and enhanced ease of transportation and installation associated with Al render it a favourable choice throughout the system's entire lifecycle. Moreover, the significant size difference between Al and Copper bus bars further underscores the economic viability of adopting Al as a preferred material in this context.

Power Losses Comparison of Aluminium & Copper

In the context of power losses, we evaluated Al bus bar designs and their associated costs when compared to Copper. We found that the 30*5 Al bus bar performed worse than Copper regarding losses and current-carrying capacity. However, a 40*5 Al bus bar outperformed Copper for 8-10 years, its losses increased. Finally, a 40*10 Al bus bar proved better than Copper for a 150 kW load over an extended period. All bus bars were designed according to DIN standards. Refer to Table 3 and Figure 5 for detailed data.

Table 3 Power loss calculations according to size

| Name | Power loss | KW/H loss | 24 hours loss | 1 year loss | 50 years loss | 100 years loss |
|----------|------------|-----------|---------------|-------------|---------------|----------------|
| Al 40*10 | 4.734 | 0.004734 | 0.113616 | 41.46984 | 2073.492 | 4146.984 |
| AL 30*10 | 6.312 | 0.006312 | 0.151488 | 55.29312 | 2764.656 | 5529.312 |
| Cu 30*5 | 7.776 | 0.007776 | 0.186624 | 68.11776 | 3405.888 | 6811.776 |
| Al 40*5 | 9.468 | 0.009468 | 0.227232 | 82.93968 | 4146.984 | 8293.968 |
| AL 30*5 | 12.624 | 0.012624 | 0.302976 | 110.58624 | 5529.312 | 11058.624 |

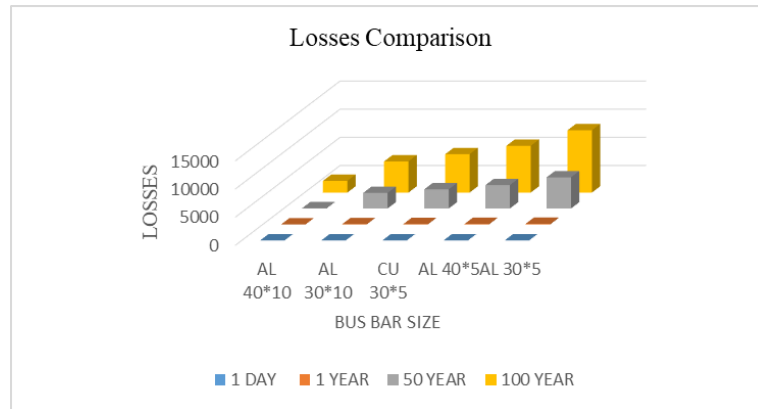


Figure 5: Power loss comparison of AL and CU bus bar

To demonstrate aluminium's viability, a practical case study involving a 150-KW load and fibre-reinforced material was conducted. This study confirms aluminium's ability to meet load and material requirements, reinforcing its suitability for the amalgamation of aluminium's thermal performance, cost-effectiveness, and weight advantages positions it as an appealing choice for real-world applications.

CONCLUSION

The present study embarked on a thorough journey to resolve the comparative merits and demerits of utilising Al and Copper as materials for bus bars, leveraging a robust experimental model grounded in real-time data collection and analysis. Through a series of thermal and techno-economic analyses, we have shed light on these materials' pivotal role in influencing the efficiency, cost-effectiveness, and sustainability of low-voltage bus bar systems. Our findings underscore the potential of Al as a viable alternative to Copper, demonstrating notable advantages in terms of reduced weight, lower costs, and favourable thermal performance characteristics. The techno-economic analysis further substantiated the economic viability of Al, highlighting its capacity to diminish power delivery charges and thereby alleviate the financial burden on consumers. Moreover, the research fills a significant gap in the existing literature by being one of the pioneering studies conducted in Pakistan, offering a fresh perspective in a region where such analyses are scant. The adherence to DIN standards and IEC standard 61439-1-2020 in the design and thermal analysis phases ensured a rigorous approach to the research, paving the way for reliable and replicable results. As we navigate a world grappling with the pressing demands of energy efficiency and sustainable development, the insights garnered from this study stand as a testament to the untapped potential of Al in revolutionising bus bar systems. It beckons a paradigm shift in the industry, urging stakeholders to reconsider the conventional preference for Copper in light of the compelling advantages presented by Al. Looking forward,



ICSET-23



UET Peshawar

we advocate for further research to delve deeper into this promising avenue, exploring the full benefits of Al bus bars. We aspire that this study serves as a springboard for future investigations, fostering innovations grounded in sustainability and economic prudence.

ACKNOWLEDGEMENTS

The authors are grateful to Electric Gears Corporations (Pvt.) Ltd. Karachi Pakistan for providing the testing facility for thermal, cost, and power loss analysis.

REFERENCES

- [1] A. Alves, M. de Campos, P. S. Sausen, J. M. Lenz, and A. T. Z. R. Sausen, "Thermal Model for Copper Busbar and Electrical Connections for Controlgear Design," *J. Control. Autom. Electr. Syst.*, vol. 33, no. 2, pp. 710–717, 2022, doi: 10.1007/s40313-021-00851-5.
- [2] M. Szulborski, S. Łapczyński, and Ł. Kolimas, "Thermal analysis of heat distribution in busbars during rated current flow in low-voltage industrial switchgear," *Energies*, vol. 14, no. 9, 2021, doi: 10.3390/en14092427.
- [3] IEC, *INTERNATIONAL STANDARD*. 2020.
- [4] A. Plesca, "Thermal analysis of busbars from a high current power supply system," *Energies*, vol. 12, no. 12, 2019, doi: 10.3390/en12122288.
- [5] M. Oberst, S. Schlegel, and S. Großmann, "On the Aging of Electrical Joints with a Copper and an Aluminum Contact Member," *Electr. Contacts, Proc. Annu. Holm Conf. Electr. Contacts*, vol. 2019-September, pp. 27–35, 2019, doi: 10.1109/HOLM.2019.8923935.
- [6] S. Nur Amalina Mohd Halidi, R. Athirah Rosli, H. Ghafar, N. Suhada Abdullah, and K. Mei Hyie, "Temperature rise effects on busbars used in low voltage switchgear," no. May, pp. 273–274, 2018.
- [7] J. Zhong, B. Zhang, Y. Guo, Y. Yao, Z. Wang, and H. Zhang, "Research on power loss calculation and temperature rise simulation of AC high voltage GIS busbar," *ICEPE-ST 2017 - 4th Int. Conf. Electr. Power Equipment- Switch. Technol.*, vol. 2017-December, pp. 720–725, 2017, doi: 10.1109/ICEPE-ST.2017.8188936.
- [8] S. Valarmathi, M. E. Energy Engineering, and S. Thirumuruga Veerakumar, "Analysis of Temperature Rise and Comparison of Materials of Bus Bar used in the MV Panel Board," *Int. J. Comput. Appl.*, no. Md, pp. 975–8887, 2015.
- [9] C. Viswanatha, G. P. Vittal, and V. M. Babu, "Temperature rise test effect of elevated temperature on 2500 Amps low voltage distribution board," *2014 6th IEEE Power India Int. Conf.*, pp. 1–4, 2015, doi: 10.1109/poweri.2014.7117667.
- [10] R. F. V. Sampaio, J. P. M. Pragana, I. M. F. Bragança, C. M. A. Silva, and P. A. F. Martins, "Thermo-electrical performance of hybrid busbars: An experimental and numerical investigation," *Proc. Inst. Mech. Eng. Part L J. Mater. Des. Appl.*, vol. 237, no. 1, pp. 70–80, 2023, doi: 10.1177/14644207221102514.
- [11] A. Elkjaer, G. Ringen, R. Bjorge, C. H. Musinoi Hagen, S. Laedre, and N. Magnusson, "Reliability of Bolted Aluminum Busbars for Battery Systems: Effect of Nickel Coating and Corrosive Environment," *IEEE Trans. Transp. Electrification*, vol. 9, no. 1, pp. 1060–1071, 2023, doi: 10.1109/TTE.2022.3196309.

Paper ID: ICSET-2327

NUMERICAL SOLUTION OF 1D PARABOLIC PDES WITH INTEGRAL BOUNDARY CONDITION VIA HAAR WAVELETS COLLOCATION METHOD

Masood Ur Rehman*, Masood Ahmad, Siraj Ul Islam
Department of Basic Sciences and Islamiyat, UET Peshawar, Pakistan

**Corresponding author*
Email: masoodkth@gmail.com

ABSTRACT

The Haar wavelets collocation method is a powerful numerical technique used to solve parabolic differential equations with integral boundary conditions. In this thesis, we provide a brief overview of the method and its application. In this method, the highest derivatives involved in the governing equation is approximated using a linear combination of Haar wavelet basis functions.

An expression for the unknown can be obtained by integrating the highest derivative multiple times, enabling us to easily incorporate the integral boundary conditions. The compact support and multiresolution characteristics of the Haar wavelets make them a popular choice for approximating the solution of differential equations.

KEYWORDS: Haar wavelet, Condition number, Poisson equation, Nonlocal boundary condition.

INTRODUCTION

The Haar wavelets collocation method (HWCM) is a mathematical method utilized for tackling differential conditions. This strategy is especially beneficial for solving parabolic PDEs with integral boundary conditions. The technique utilizes Haar wavelets, which are piecewise consistent capabilities that structure an orthonormal reason for the space of square-integrable capabilities. The Haar wavelets collocation strategy includes approximating the arrangement of the differential condition utilizing a direct blend of Haar wavelets. The collocation focuses, which are the hubs where the differential condition is assessed, are picked as the midpoints of the Haar wavelets.

The technique utilizes Haar wavelets, which are piecewise consistent capabilities that structure an orthonormal reason for the space of square-integrable capabilities. The HWCM includes approximating the arrangement of the differential condition utilizing a direct blend of Haar wavelets. The collocation focuses, which are the hubs where the differential condition is assessed, are picked as the midpoints of the Haar wavelets. Integral boundary conditions are a sort of limit condition where the arrangement is connected with a necessary of the arrangement over the space limit. These sorts of boundary conditions frequently emerge in physical science and designing issues, for example, in heat transfer and fluid mechanics. Along these lines, interest in making computational methodology for the numerical arrangement of PDEs with various kinds of nonlocal conditions has been growing speedy.

As the Haar wavelet is characterized in an extremely straightforward manner, their execution of the Haar wavelets collocation method (HWCM) becomes simpler than the finite element method [1] and spectral method [2]. The computational time taken by this strategy is relatively less on the grounds that the Haar matrices and its integrals are determined and put away in the memory once and a similar worth is utilized in every iteration. Aside from this property, the Haar wavelets are minimalistically upheld orthonormal functions. These properties lead to a colossal decrease in the computational expense of the strategy.

In order to solve nonlinear singly modified differential equations with a variety of pairings of boundary conditions, including initial, boundary, two-point, integral, and multi-point integral boundary conditions, the goal of this [3] is to create and enhance a higher-order HWCM. For the numerical solution of a class of Lane-Emden equations with Dirichlet, Neumann, and Neumann-Robin type boundary conditions that arise in diverse physical models, they offer in this [4] a numerically stable technique based on the HWCM. Another technique for solving integral and partial differential equations (PDEs) is wavelets collocation. In [5], [6], Legendre wavelets are used to solve integral equations, and Haar wavelets are used in [7], [8], [9] to solve time-dependent PDEs. Recently, HWCMs have been used to solve one- and two-dimensional linear and nonlinear direct and inverse problems numerically [10], [11], [12].

MATERIALS AND METHODS

The Haar wavelet family for $r \in [0, 1)$ is given by

$$\chi_n(r) = \begin{cases} 1; & \varsigma_1 \leq r < \varsigma_2 \\ -1; & \varsigma_2 \leq r < \varsigma_3 \\ 0; & (\text{otherwise}) \end{cases} \quad n=1,2,3, \dots \quad (1)$$

$$\text{where } \varsigma_1 = \frac{j}{q}, \varsigma_2 = \frac{j+0.5}{q}, \varsigma_3 = \frac{j+1}{q}, \quad (2)$$

$$q = 2^i, i = 0,1,2, \dots, I \text{ and } j = 0,1,2, \dots, q-1.$$

Here the whole number i is the expansion boundary and j is the interpretation boundary. The index of χ_n in Eq. (1) is calculated by $n = q + j + 1$. For the minimum values of $q = 1$ and $j = 0$, we have $n = 2$; the maximum value of n will be $n = 2q = 2^{I+1}$, where I is the maximal level of resolution. It is assumed that for $n = 1$, the scaling function is given as

$$\chi_{-1}(r) = \begin{cases} 1 & 0 \leq r < 1 \\ 0 & \text{otherwise.} \end{cases} \quad (3)$$

We need the following integrals of the Haar wavelets to solve the parabolic partial differential equations given in Eq. (1) to Eq. (1),

$$p_{n,1}(r) = \int_0^{z_1} \chi_{n,1}(\tau) d\tau, \quad (4)$$

$$p_{n,v}(r) = \int_0^{z_1} \chi_{n,v-1}(\tau) d\tau \quad v = 2,3, \dots \quad (5)$$

These integrals can be calculated analytically with the help of Eq. (1), by doing so we get

$$\begin{aligned}
 p_{n,1}(r) &= \begin{cases} z_1 - \varsigma_1 ; & \varsigma_1 \leq r < \varsigma_2, \\ \varsigma_3 - z_1 ; & \varsigma_2 \leq r < \varsigma_3, \\ 0 ; & \text{otherwise.} \end{cases} \\
 p_{n,2}(r) &= \begin{cases} 0 ; & 0 \leq r < \varsigma_1, \\ \frac{1}{2}(z_1 - \varsigma_1)^2 ; & \varsigma_1 \leq r < \varsigma_2, \\ \frac{1}{4m^2} - \frac{1}{2}(\varsigma_1 - z_1)^2 ; & \varsigma_2 \leq r < \varsigma_3, \\ \frac{1}{4m^2} ; & \varsigma_3 \leq r < 1. \end{cases} \\
 p_{n,3}(r) &= \begin{cases} 0 ; & 0 \leq r < \varsigma_1, \\ \frac{1}{6}(z_1 - \varsigma_1)^3 ; & \varsigma_1 \leq r < \varsigma_2, \\ \frac{1}{4m^2}(z_1 - \varsigma_2) + \frac{1}{6}(\varsigma_3 - z_1)^3 ; & \varsigma_2 \leq r < \varsigma_3, \\ \frac{1}{4m^2}(z_1 - \varsigma_2) ; & \varsigma_3 \leq r < 1. \end{cases} \quad (6) \\
 p_{n,4}(r) &= \begin{cases} 0 ; & 0 \leq r < \varsigma_1, \\ \frac{1}{24}(r - \varsigma_1)^4 ; & \varsigma_1 \leq r < \varsigma_2, \\ \frac{1}{8m^2}(r - \varsigma_2)^2 - \frac{1}{24}(\varsigma_3 - r)^4 + \frac{1}{192m^4} ; & \varsigma_2 \leq r < \varsigma_3, \\ \frac{1}{8m^2}(r - \varsigma_2)^2 + \frac{1}{192m^4} ; & \varsigma_3 \leq r < 1. \end{cases}
 \end{aligned}$$

$$\begin{aligned}
 p_{n,2}(1) &= \begin{cases} \frac{1}{2} & \text{if } i = 1 \\ \frac{1}{4m^2} & \text{if } i > 1 \end{cases} \\
 p_{n,3}(1) &= \begin{cases} \frac{1}{6} & \text{if } i = 1 \\ \frac{1}{4m^2}(1 - \varsigma_2)^2 & \text{if } i > 1 \end{cases} \quad (7) \\
 p_{n,4}(1) &= \begin{cases} \frac{1}{24} & \text{if } i = 1 \\ \frac{1}{4m^2}(1 - \varsigma_2)^2 + \frac{1}{182m^4} & \text{if } i > 1, \end{cases}
 \end{aligned}$$

where $\varsigma_1, \varsigma_2, \varsigma_3$ and m are defined in equation (2). We also need to find

$$\int_0^1 \psi(r) p_{n,2}(t) dt, \quad (8)$$

where $\psi(r)$ is given function. The evaluation of the integral given in Eq. (8) is not a difficult task.

Test Problem

The heat equation is a partial differential equation that depicts how heat is conveyed in a given district over time. It is a numerical portrayal of the manner in which heat diffuses through a substance. The equation is regularly communicated as:

$$\frac{\partial s}{\partial \tau} = \alpha \frac{\partial^2 s}{\partial r^2} + f(r, \tau), \quad 0 < r < 1, 0 < \tau < \tau_f, \quad (9)$$

subject to the initial condition,

$$s(r, 0) = p(r), \quad 0 \leq r \leq 1. \quad (10)$$

The association between the heat equation and energy lies in the way that heat is a type of energy, and the heat equation depicts how this energy is moved and disseminated inside a framework. The equation reflects the basic principle of the conservation of energy. In a close system, the total energy stays steady, and the heat equation depicts how this energy is rearranged over the long haul because of the diffusion of heat.

We consider the following two cases of boundary conditions.

- a) Dirichlet boundary condition at $r = 0$

$$s(0, \tau) = g(\tau), \quad 0 \leq \tau \leq \tau_f, \quad (11)$$

- b) Non-local boundary condition at $r = 1$

$$\int_0^1 \eta(r) s(r, \tau) dr = m(\tau), \quad (12)$$

where the functions $f(r, \tau)$, $p(r)$, $g(\tau)$, $\eta(r)$, $m(\tau)$ and the constant α are known.

Consider the following Haar wavelets approximation

$$\frac{\partial^2 s}{\partial r^2} = \sum_{i=1}^{2M} \lambda_i h_i(r) \quad (13)$$

Partially integrating Eq. (13) twice from 0 to r , then replace r by 1 in the obtained expression of s and $\frac{\partial s(0, \tau)}{\partial r}$. Then puts back this value in the expression of s . By doing so and rearranging the terms of s , the following expression for s can be obtained, which is written in matrix form

$$s = (\mathbf{1} - \mathbf{r})s(0, \tau) + \mathbf{r}s(1, \tau) + (\boldsymbol{\rho}_2 - \mathbf{r}\boldsymbol{\rho}^{\tau_f})\boldsymbol{\lambda}, \quad (14)$$

where

$$\mathbf{r} = [r_1, r_2, \dots, r_{2M}]^T,$$

$$\mathbf{1} = [1, 1, \dots, 1]^T,$$

$$\boldsymbol{\lambda} = [\lambda_1, \lambda_2, \dots, \lambda_{2M}]^T,$$

$$\boldsymbol{\rho} = [\rho_{1,2}(1), \rho_{2,2}(1), \dots, \rho_{2M,2}(1)]^T,$$

$$\boldsymbol{\rho}_2 = \begin{bmatrix} \rho_{1,2}(r_1) & \rho_{2,2}(r_1) \dots & \rho_{2M,2}(r_1) \\ \rho_{1,2}(r_2) & \rho_{2,2}(r_2) \dots & \rho_{2M,2}(r_2) \\ \vdots & \vdots & \vdots \\ \rho_{1,2}(r_{2M}) & \rho_{2,2}(r_{2M}) \dots & \rho_{2M,2}(r_{2M}) \end{bmatrix}^T.$$

Multiplying $\eta_-(r)$ to Eq. (14) and integrates from 0 to 1 with respect to r , then using the nonlocal integral boundary condition to find the unknown $s(1, \tau)$. Then substitutes back the worth of $s(1, \tau)$ in Eq. (14) and utilizing the boundary condition Eq. (11), we get the accompanying articulation for s .

$$s = (1 - r)g(\tau) + \left(\frac{r}{c_2}m(\tau)\right) + \left(\frac{rc_1}{c_2}g(\tau)\right) + \left(\boldsymbol{\rho}_2 - \frac{r}{c_2}\boldsymbol{\rho}^{\tau_f}\right)\boldsymbol{\lambda}, \quad (15)$$

where

$$c_1 = \int_0^1 \eta(r) (1 - r) dr,$$

$$c_2 = \int_0^1 \eta(r) (r) dr,$$

$$\rho_\eta = \int_0^1 \eta(r) \rho dr.$$

Allow $\Delta\tau$ to be the time-step size, and $\tau = \tau_0 + d\tau$ be the time discretization, where τ_0 is the beginning season of each time level, and τ alludes to the furthest limit of the time step, For a time span $[\tau_0, \tau]$, the time subsidiary is approximated by Euler's formula

$$\frac{\partial s(r, \tau)}{\partial \tau} \approx \frac{s(r, \tau) - s(r, \tau_0)}{\Delta\tau}. \quad (16)$$

From Eq. (9), Eq. (13) and Eq. (16), we have

$$\frac{s(r, \tau) - s(r, \tau_0)}{\Delta\tau} = \alpha \mathbf{H} \boldsymbol{\lambda} + f(r, \tau) \quad (17)$$

where

$$\mathbf{H} = \begin{bmatrix} h_1(r_1) & h_2(r_1) \dots & h_{2M}(r_1) \\ h_1(r_2) & h_2(r_2) \dots & h_{2M}(r_2) \\ \vdots & \vdots & \vdots \\ h_1(r_{2M}) & h_2(r_{2M}) \dots & h_{2M}(r_{2M}) \end{bmatrix}^T.$$

Using Eq. (15) in Eq. (17) we have

$$\left(\rho_2 - \frac{r}{c_2} \rho^{\tau_f} - \alpha \Delta \tau \mathbf{H}\right) \lambda = s(r, \tau_0) + \Delta \tau f(r, \tau) - \left((1-r)g(\tau) + \left(\frac{r}{c_2} m(\tau)\right) + \left(\frac{rc_1}{c_2} g(\tau)\right)\right). \quad (18)$$

We have to find λ from this system of equations. Then puts λ into the approximate solution Eq. (15), which gives approximate solution for problem Eq. (9).

Example

Let suppose the problem given in Eq. (9) with the known functions as listed below.

$$\begin{aligned} f(r, y) &= -e^{\tau+r} \\ \rho(\tau) &= e^r \\ g(\tau) &= e^\tau \\ m(\tau) &= \eta e^\tau (e^1 - 1) \end{aligned} \quad (19)$$

The problem's analytical solution is shown as

$$s(r, \tau) = e^{r+\tau} \quad (20)$$

For test problem (19), we choose $M = 16$, $d\tau = 0.005$ and $\alpha = -1$. The numerical results are calculated at various points of η as shown in Table (1). It can be seen that accuracy of the problem does not depend on the value of η .

RESULT AND DISCUSSION

Table 1: Haar wavelets with numerical results in 1D for test problem (19), $\eta = -50$, $\tau_f = 1$, $\alpha = 2$ measurement periods

| | $d\tau = 0.05$ | $d\tau = 0.005$ | $d\tau = 0.0005$ |
|-----|-----------------|-----------------|------------------|
| M | L_∞ | L_∞ | L_∞ |
| 4 | $6.4178e^{-03}$ | $3.3093e^{-04}$ | $2.9316e^{-04}$ |
| 8 | $7.9343e^{-03}$ | $7.0953e^{-04}$ | $2.4748e^{-05}$ |
| 16 | $8.6497e^{-03}$ | $8.5200e^{-04}$ | $5.9483e^{-05}$ |
| 32 | $8.9986e^{-03}$ | $9.0652e^{-04}$ | $8.4083e^{-05}$ |
| 64 | $9.1702e^{-03}$ | $9.2804e^{-04}$ | $9.1324e^{-05}$ |

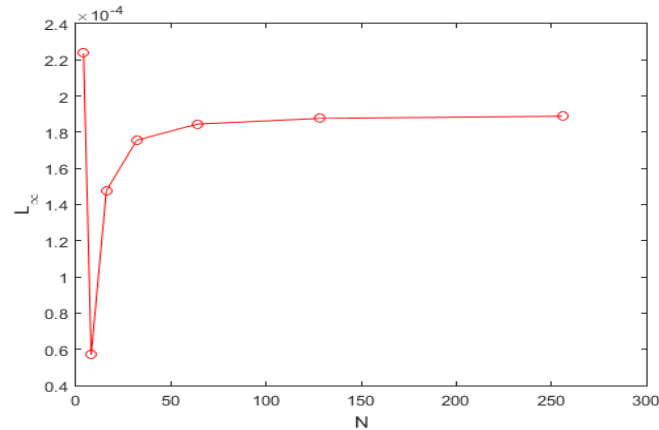


Figure 1: L_∞ error norm versus N of problem (19) via Haar Wavelets Collocation Method

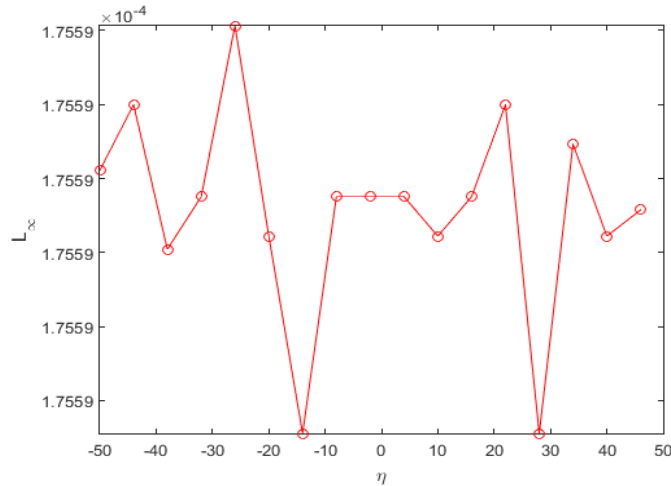


Figure 2: L_∞ error norm versus N of problem (19) via Haar Wavelets Collocation Method

The graph presents the results of a comparison between local meshless methods and numerical results for a test problem (19). However, it can be observed that the local meshless methods perform better for smaller values of η . It is interesting to note that the error for $\eta = 0$ is smaller than the errors for $\eta = \pm 10$. This may suggest that the HWCM perform better when the parameters of the problem are symmetric around zero, which is a characteristic of many physical problems.

CONCLUSION

The major aim of the paper is to find a numerical solution of the partial differential equations with integral boundary conditions via Haar wavelets collocation method. In addition, we also desire to investigate the effectiveness and accuracy of the Haar method on the nonlocal parameter γ_1 and γ_2 .

The numerical section, shows that the proposed Haar wavelets method is reliable and efficient numerical technique for solving parabolic differential equations with integral boundary conditions, when the value of the both nonlocal parameter γ_1 and γ_2 is negative. The Haar wavelets collocation method as



ICSET-23



UET Peshawar

well as the standard finite difference method fails to converge to the exact solution of the PDEs, when the value of both the nonlocal parameter γ_1 and γ_2 is greater than 3.

The numerical section suggests that keeping negative value of γ_1 , while the value of other nonlocal parameter γ_2 is kept positive with same magnitude or keeping the magnitude of γ_1 greater than the γ_2 , the proposed method will provide good accuracy. In reverse scenario, the Haar wavelets will diverge. The collocation approach ensures that the differential equation and integral boundary conditions are satisfied at a set of collocation points, leading to a system of algebraic equations that can be efficiently solved. The Haar wavelets, compact support and orthogonality properties add to the technique's capacity to deal with non-smooth solutions and proficiently catch sharp slopes, making it appropriate for a large number of parabolic problems with integral boundary conditions. Numerical tests have exhibited the technique's viability regarding precision, combination, and computational productivity, displaying its commonsense appropriateness for genuine problems.

In general, the HWCMM offers a promising option for the numerical treatment of PDEs with integral boundary conditions, introducing an integral asset for specialists and experts in different areas of science and engineering.

ACKNOWLEDGEMENTS

I start, for the sake of Allah, The Most Benevolent and The Most Kind to have gave to me great wellbeing, energy, and boldness all through my life, explicitly in my scholastic vocation. All gestures of recognition have a place with Allah, who empowered me to finish this examination work effectively and allow me an opportunity to finish this exploration work in a sound examination climate in the division of Basic Sciences and Islamiyat, UET, Peshawar.

I'm profoundly thankful to my research supervisor Professor Dr. Siraj-ul-Islam and co-supervisor Dr. Masood Ahmad, who made himself accessible consistently to explain my questions, give me helpful ideas, direction, and nonstop support all through my exploration work regardless of his bustling timetable. He checked on a few starting forms of my text, made basic ideas and suggested testing conversation starters. Without his steady motivation, it would have not been imaginable to finish this examination work effectively. His valuable and legitimate help, constant collaboration and consolation will continuously direct me later on research. He is a good example for me since he takes on new difficulties ordinary, deals with them directly with boldness and resolve, and flourishes with succeeding.

I might likewise want to thank my parent for their consistent help, support, and love all through my life. I owe a ton to my sibling Mr. Ijaz Rehman Deputy Director Finance at PEDO, who supported and helped me at each phase of my own and scholarly life and yearned to see this accomplishment materialize. It would be excessively challenging to finish this exploration work effectively without the monetary help of my sibling.

REFERENCES

- [1] C. Bernardi and Y. Maday, "Spectral methods," *Handb. Numer. Anal.*, vol. 5, no. Part 2, pp. 209–485, 1997, doi: 10.1016/S1570-8659(97)80003-8.
- [2] G. Dhatt, E. Lefrançois, and G. Touzot, *Finite element method*. John Wiley & Sons, 2012.
- [3] M. Ahsan, M. Bohner, A. Ullah, A. A. Khan, and S. Ahmad, "A Haar wavelet multi-resolution collocation method for singularly perturbed differential equations with integral boundary conditions," *Math. Comput. Simul.*, vol. 204, pp. 166–180, 2023.
- [4] R. Singh, H. Garg, and V. Guleria, "Haar wavelet collocation method for Lane--Emden equations



ICSET-23

Proceedings of the 5th International Conference on Sustainable
Energy Technologies (ICSET 2023) Peshawar, Pakistan
14-15 December 2023



UET Peshawar

- with Dirichlet, Neumann and Neumann--Robin boundary conditions,” *J. Comput. Appl. Math.*, vol. 346, pp. 150–161, 2019.
- [5] M. K. Kadalbajoo and A. S. Yadaw, “B-Spline collocation method for a two-parameter singularly perturbed convection--diffusion boundary value problems,” *Appl. Math. Comput.*, vol. 201, no. 1–2, pp. 504–513, 2008.
- [6] M. Ahsan, W. Lei, M. Ahmad, M. S. Hussein, and Z. Uddin, “A wavelet-based collocation technique to find the discontinuous heat source in inverse heat conduction problems,” *Phys. Scr.*, vol. 97, no. 12, p. 125208, 2022.
- [7] F. Bulut, Ö. Oruç, and A. Esen, “Higher order Haar wavelet method integrated with strang splitting for solving regularized long wave equation,” *Math. Comput. Simul.*, vol. 197, pp. 277–290, 2022.
- [8] M. K. Kadalbajoo and V. K. Aggarwal, “Fitted mesh B-spline collocation method for solving self-adjoint singularly perturbed boundary value problems,” *Appl. Math. Comput.*, vol. 161, no. 3, pp. 973–987, 2005.
- [9] I. Khan, M. Asif, R. Amin, Q. Al-Mdallal, and F. Jarad, “On a new method for finding numerical solutions to integro-differential equations based on Legendre multi-wavelets collocation,” *Alexandria Eng. J.*, vol. 61, no. 4, pp. 3037–3049, 2022.
- [10] M. Ahsan, I. Ahmad, M. Ahmad, and I. Hussian, “A numerical Haar wavelet-finite difference hybrid method for linear and non-linear Schrödinger equation,” *Math. Comput. Simul.*, vol. 165, pp. 13–25, 2019.
- [11] C. Chen, C. LeBlanc, and R. P. Bobbin, “Differences in the distribution of responses to ATP and acetylcholine between outer hair cells of rat and guinea pig,” *Hear. Res.*, vol. 110, no. 1–2, pp. 87–94, 1997.
- [12] G. Özaltun, A. Konuralp, and S. Gümgüm, “Gegenbauer wavelet solutions of fractional integro-differential equations,” *J. Comput. Appl. Math.*, vol. 420, p. 114830, 2023.

Paper ID: ICSET-2328

INVESTIGATIONS OF DIFFERENT CONFIGURATIONS OF HEAT SINK FOR THERMAL MANAGEMENT OF PHOTOVOLTAIC SYSTEM VIA ACTIVE COOLING

Saqib Khan^{1,2,*}, Muhammad Hanzla Tahir^{2,3}, Asnaf Aziz¹

¹Mechanical Engineering Department Jalozei Campus, UET Peshawar, Pakistan

²Mechanical Engineering Department, UET Lahore, Pakistan

³Mechanical Engineering Department, Balochistan UET Khuzdar, Khuzdar, Pakistan

**Corresponding author*

Email: saqibkhan@uetpeshawar.edu.pk

ABSTRACT

Solar energy among all other resources is primeval and even motives behind wind, biomass, tidal, and wave energy etc. In this research work, major focus is on solar energy production management by means of thermal management of PV module. Therefore, a PV module with 600 W output power is considered because the efficiency of the PV module is declined under actual operating condition and atmospheric impact as well, where the incident solar radiations are assumed to be standard (1000 W/m²). Moreover, the efficiency of the module is dropped by almost 30% of the actual because of the increase in the surface temperature of the module. The PV module is examined by using Computational Fluid Dynamics (CFD) and the model is designed with two different heat sinks arrangement accompanied by velocity inlet laminar flow boundary conditions. The inlet temperature of the working fluid water is considered 25°C. On the next hand, the results declared that double arrangement of heat sinks found to have optimum results as compared to a mono arrangement of heat sinks. One more thing is observed that, with the increase in velocity of the working fluid the temperature of the module decreased dramatically to a value of 36°C at 1.0 m/s velocity using double arrangement of heat sinks. Contrarily, at the same inlet velocity, the temperature of the PV module lowered to a value of 40°C by using a mono arrangement of heat sinks. Hence, it is asserted that with double arrangement of heat sinks, one can optimize the efficiency and power of the module under actual boundary and climatic conditions. Moreover, maximum number of energy units can be saved by implementing these CFD schemes and can be contributed to the energy sustainability of the country.

KEYWORDS: Hybrid photovoltaic system, Heat sink, Efficiency enhancement.

INTRODUCTION

Energy is always a critical component in the development of a country's economy because it is required for all social activities related to education, health care, agroindustry, and employment etc. A nation can't prosper without an appropriate practice of energy [1, 2]. Pakistan is an emerging country and due to current developments in industrial infrastructure, urbanization, and to maintain high population density, the country needs a significant amount of energy to keep things under control. The current proportion of renewable energy in Pakistan's overall energy mix is minimal (~5%). The country's energy demands are met



ICSET-23



UET Peshawar

by using fossil fuels which do not affects the national economy, but also create environmental risks concerning greenhouse gas emissions including CO_{2e}, global warming, and extreme weather events [3]. Furthermore, the usage of fossil fuels depletes natural resources, as a result a new energy economy must be created. Renewable energy resources such as solar, wind, biomass, and hydropower will be used to create energy in this scenario, which will reduce the import bill of fossil fuels and also climate related issues. Geologically, Pakistan is located in the solar belt and has highest solar irradiance values in the universe, with 8-9 hours of daylight and 4.5-7 kWh/m² of solar radiation throughout a day [4]. While most parts of the country received an average of 5.3 kWh/m², which is significantly higher than the global average of 3.6k Wh/m² per day [5]. Hence, Pakistan is a preferred place for the production of solar energy. According to the Energy Ministry of Pakistan, the state can easily produce 2900 GW of solar energy annually [6]. In order to solve existing energy problems, it is imperative to take advantage of present solar energy resources. Meanwhile, investment from both the public and private sectors is required to fully comprehend its potential. PV modules made of silicon semiconductors convert directly incident light into electrical energy. Improving electrical efficiency and reduces its capital cost is a future concern [7]. Environmental variables such as wind speed, ambient temperature, relative humidity, shading impact, dew droplets, dust accumulation, and sun radiations, all contribute to a decrease in efficiency. The material of a solar system also has an effect on its performance [8]. A 0.5% reduction in efficiency occurs when the temperature of a photovoltaic cell rises by 1°C [9]. To improve the efficiency and cost effectiveness of solar power generation, several techniques have been studied and implemented. Concentrators, which are used as a reflector, mirrors, and lenses to focus incoming solar radiation on the PV module, appeared to be a one way to lower the cost of solar energy generation [10-13]. Therefore, the workspace of an expensive semiconductor can be replaced by a less expensive optical management system. In concentrating units, Fresnel lens, Parabolic dish collectors, and Parabolic trough solar collectors are employed [14]. Two possible techniques of removing heat from the surface of the high radiant PV cells are passive and active cooling practices. Passive cooling is more consistent and less costly, because it requires no electrical power, whereas active cooling requires mechanical equipment like pumps and fans etc [15-17]. Passive cooling systems have low heat loss rate compared to active cooling systems because they don't have any moving parts. Active cooling PV systems are more successful in lowering surface temperatures, and heat recovered by the cooling fluid is employed in a variety of thermal applications [18]. For this project, air and water cooling were adopted and in addition, the results elaborated that water offers higher efficiency compared with air.

MATERIALS AND METHODS

Initially, the PV panel is modelled in the SolidWorks, which is found to have under 3D modelling domain of the methodology. After that a standard value of irradiance profile which is 1000 W/m² is considered for this study. The model is comprised of 6 layers, from top to bottom in a sequence that can be seen in the Table 1. *Table* Finally base Aluminium plate containing 20 squared heat sinks per 200 mm of the width of the panel. Furthermore, after finding the temperature and heat flux induction results, the Ansys Fluent domain is considered for the rest of the results regarding thermal management of the entire model including PV layer. Regarding the location of the model, the Lahore Industrial state is agreed. And the whole setup is designed for industrial zone, located in the suburbs of the city Lahore.

Table 1: Hybrid Photovoltaic Panel Properties [19]

| Material Layers | Thickness (mm) | Density (kg/m^3) | Thermal Conductivity ($W/m.K$) | Heat Capacity ($J/Kg.K$) |
|---------------------------------------|----------------|-------------------------|-------------------------------------|-------------------------------|
| Top Glass | 3.2 | 3000 | 0.98 | 820 |
| Font Eva | 0.15 | 960 | 0.31 | 2090 |
| PV Cell | 0.2 | 2330 | 150 | 712 |
| Back Eva | 0.15 | 960 | 0.31 | 2090 |
| Aluminum Absorber | 1 | 2719 | 202.4 | 871 |
| Aluminum Base Including Heat Sinks | 6 | 2719 | 202.4 | 871 |
| Water | - | 0.6 | 2719 | 25 |

The dimensions of the model which are being used in this research study, where it can be observed that the length, width and height of the panel found to have 2172 mm, 1303 mm and 35 mm. whereas I-V curves are available in the figure 1, showing that the maximum values are achieved at 1000 W/m² which is assumed for this study in addition, the lowest relation is found at 200 W/m² flux intensity.

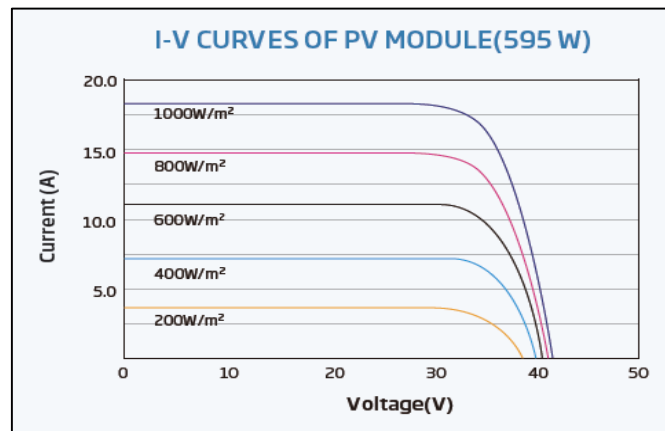


Figure 1: IV Curves of the Proposed Model at Various Irradiances [16]

Indicating that at maximum irradiance values the power and voltage have higher values. Therefore, 1000 W/m² is a good fit for this study, while Mechanical data sheet elaborating the dimensions of the cells, top glass layer, frame, cables, and weight etc. is available in Figure 2.

| MECHANICAL DATA | |
|----------------------|--|
| Solar Cells | Monocrystalline |
| No. of cells | 120 cells |
| Module Dimensions | 2172×1303×35 mm (85.51×51.30×1.38 inches) |
| Weight | 30.6 kg (67.5 lb) |
| Glass | 3.2 mm (0.13 Inches), High Transmission, AR Coated Heat Strengthened Glass |
| Encapsulant material | EVA/POE |
| Backsheet | White |
| Frame | 35mm(1.38 inches) Anodized Aluminium Alloy |
| J-Box | IP 68 rated |
| Cables | Photovoltaic Technology Cable 4.0mm ² (0.006 inches ²), Portrait: 350/280 mm(13.78/11.02 inches) Length can be customized |
| Connector | MC4 EV02 / TS4* |

Figure 2: Mechanical Datasheet of the Model [16]

On the other hand, electrical data points at Standard Test Conditions and Nominal Operating Cell Temperature are given in Figure These values indicate that maximum power, voltage and current consider for this study at 600W, 34.4V and 17.4A at standard test conditions, while at nominal operating cell temperature the values taken to be 454W, 32.0V and 14.18A respectively.

| ELECTRICAL DATA (STC) | | | | | |
|--------------------------------------|--------|-------|-------|-------|-------|
| Peak Power Watts- P_{max} (W)* | 585 | 590 | 595 | 600 | 605 |
| Power Tolerance- P_{max} (W) | 0 ~ +5 | | | | |
| Maximum Power Voltage- V_{MPP} (V) | 33.8 | 34.0 | 34.2 | 34.4 | 34.6 |
| Maximum Power Current- I_{MPP} (A) | 17.31 | 17.35 | 17.40 | 17.44 | 17.49 |
| Open Circuit Voltage- V_{oc} (V) | 40.9 | 41.1 | 41.3 | 41.5 | 41.7 |
| Short Circuit Current- I_{sc} (A) | 18.37 | 18.42 | 18.47 | 18.52 | 18.57 |
| Module Efficiency η_m (%) | 20.7 | 20.8 | 21.0 | 21.2 | 21.4 |

STC: Irradiance 1000W/m², Cell Temperature 25°C, Air Mass AM1.5. *Measuring tolerance: ±3%.

Figure 3: Electrical Datasheet of the Model at Standard Test Conditions [16]

Modelling

Ansys Workbench is being used for this model and meshing of the complete model can be seen, where the number of elements is 394814, number of nodes are 1120655, and the body sizing considered to be 3 mm.

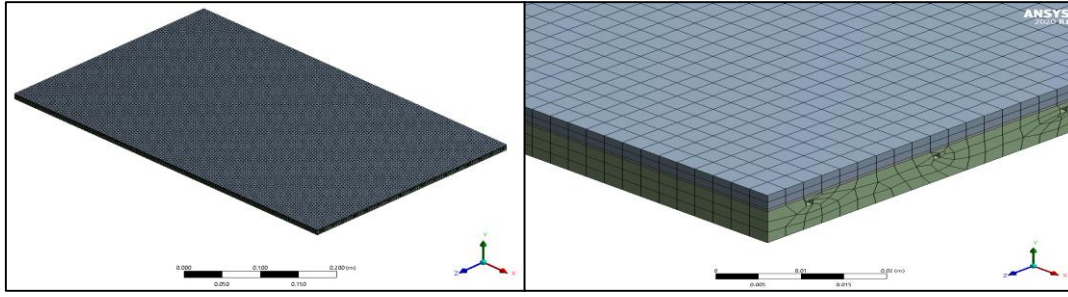


Figure 4: Reference and Proposed Model for Selected Model

Governing Equations

The equations that are being opted for this study is taken from various research articles during literature review, so these equations can be seen in references [20-22].

$$G_{on} = \begin{cases} G_{sc} (1 + 0.033 \cos \frac{360n}{365}) \\ G_{sc} (1.000110 + 0.034221 \cos B + 0.001280 \sin B \\ + 0.000719 \cos 2B + 0.000077 \sin 2B \end{cases} \quad (1)$$

$$B = (n - 1) \frac{360}{365} \quad (2)$$

$$\delta = 23.45 \times \sin \left[360 \frac{n+294}{365} \right] \quad (3)$$

Commencing with Equation (1), G_{on} stands for the extraterrestrial radiation's incident upon a specific plane during the n th day of any given year, whilst G_{sc} symbolizes the solar constant, approximating to approximately 1367 W/m^2 . This decrement, manifesting as a reduction of 0.02% per annum in terms of frequency, is denoted by 'n,' signifying the precise day under scrutiny. Conversely, 'B' designates the slope of the module. The determination of the declination angle, alternatively, can be accomplished by employing Equation (3). In Equation (3), 'δ' signifies the declination angle pertinent to the proposed system, with the incidence angle assuming a pivotal role in shaping the geometrical

$$\cos(\theta) = \sin(\delta) \sin(1) \cos(\beta) + \cos(\delta) \cos(1) \cos(\beta) \cos(\omega) - \sin(\delta) \sin(\beta) \cos(1) \cos(\gamma) + \cos(\delta) \sin(\beta) \sin(\gamma) \sin(\omega) + \cos(\delta) \sin(1) \sin(\beta) \cos(\gamma) \cos(\omega) \quad (4)$$

$$\cos \theta_z = \cos(\delta) \cos(l) \cos(\omega) + \sin(l) \sin(\delta) \quad (5)$$

$$\cos \omega_s = -\frac{\sin(\theta) \sin(\delta)}{\cos(\theta) \cos(\delta)} = -\tan(\theta) \tan(\delta) \quad (6)$$

$$\omega = 15 \times (T_{st} - 12) \quad (7)$$

configuration of the solar arrangement across diverse global locations. Subsequently, the majority of design considerations revolve around the angle of incidence. Illustrated in Equation (4), 'θ' denotes the incidence angle, while 'γ' represents the surface azimuth angle. An incidence angle surpassing 90° indicates that the panel's surface is oriented away from the direct gaze of the sun, positioned on the reverse side. Zenith angle (θ_z), Sunset hour angle (ω_s), and solar hour angle (ω) are then computed employing their respective Equations. Furthermore, the Equations serve as tools for the computation of the ultimate set of values, configuring the specified irradiance profile. The atmosphere exerts a substantial influence on the scattering and absorption of radiation, its interplay subject to periodic fluctuations contingent upon meteorological



ICSET-23



UET Peshawar

vicissitudes and the air mass ratio. Notably, under clear sky conditions, precision in estimation gains prominence. Consequently, within these conditions, the beam irradiance atmospheric transmittance (τ_b) and additional correction factors are evaluated in conformity with Equations (8) through (14), as presented below. Herein, ' K ', ' a_1^* ', ' a_2^* ', ' K^* ', ' a_1^* ', and ' a_2^* ' assume the role of atmospheric constants, whereas ' r_1^* ', ' r_2^* ', and ' r_k ' correspond to correction factors responsive to varying climatic conditions, as encapsulated in Table 2.4. Furthermore, ' A ' signifies the elevation of the specific locale, herein assumed to be 215 meters for Lahore, Pakistan.

$$\tau_b = a_1 + a_2 \exp \left[\frac{-k}{\cos \theta_z} \right] \quad (8)$$

$$a_1^* = 0.4237 - 0.00821(6 - A)^2 \quad (9)$$

$$a_2^* = 0.5055 + 0.00595(6.5 - A)^2 \quad (10)$$

$$K^* = 0.2711 + 0.01858(2.5 - A)^2 \quad (11)$$

$$r_1 = \frac{a_1}{a_1^*} \quad (12)$$

$$r_2 = \frac{a_2}{a_2^*} \quad (13)$$

$$r_k = \frac{K}{K^*} \quad (14)$$

$$G_{cnb} = G_{on} \times \tau_b \quad (15)$$

$$G_{cb} = G_{on} \times \tau_b \times \cos \theta_z \quad (16)$$

$$I_b = I_o \times \tau_b \times \cos \theta_z \quad (17)$$

$$\tau_b = \frac{G_d}{G_o} = 0.271 - 0.294 \tau_b \quad (18)$$

$$G_{cb} = G_{on} \times \tau_d \times \cos \theta_z \quad (19)$$

$$I_{cd} = I_{on} \times \tau_d \times \cos \theta_z \quad (20)$$

These are the complete equations, that are being used in the methodology.

Boundary Conditions

Regarding boundary conditions the following Figure is showing all the possible factors or parameters that are affecting towards the efficiency of the model before cooling. The yellow arrow shows total incident rays of sun white arrow show radiation coming out and black show natural convection. The blue and red arrow show coolant in and out.

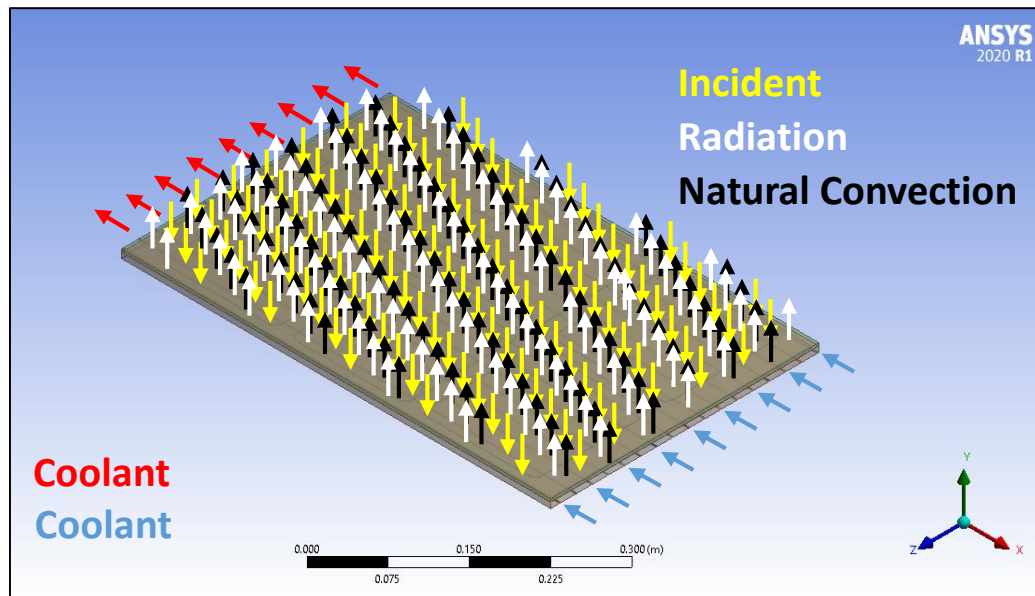


Figure 5: Boundary Conditions for Model.

RESULT AND DISCUSSION

It is important to note that the results from active cooling are also crucial for investigation purposes, as the efficiency at this condition is not ideal. Looking at Figure 694 we can observe the temperature distribution throughout all the layers of PV module including all above and below layers. Showing decreasing trend from top to bottom at 0.01 m/s velocity.

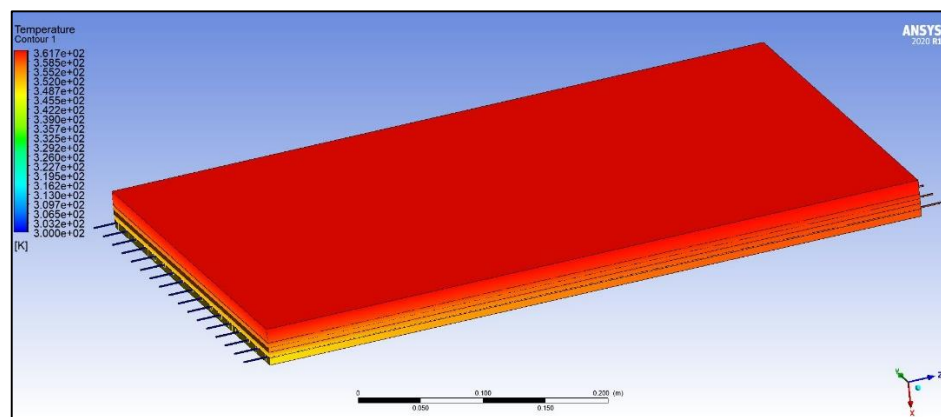


Figure 694: Whole Body Under Analysis During Heat Removal Process at 0.01 m/s of Water Flow

In Figure , the same PV layer is depicted at 0.5 m/s velocity greater than previous ones. This shows that the temperature is decreasing as the simulations are moving towards greater velocity profiles. A same trend of heat removal at different velocities can be observed by varying velocity from 0.1 m/s to 1 m/s and showing that at increasing velocity there is heat removal rate is getting higher as we are going to increase the velocity.

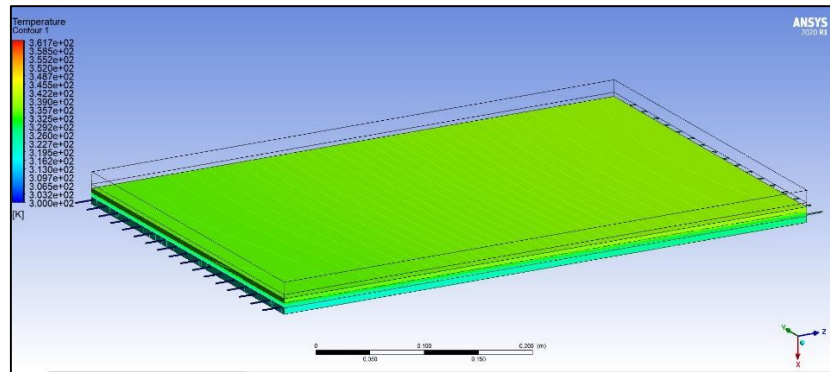


Figure 7: Heat Removing Contour of PV Cells Layer at 1 m/s Velocity

At 0.01 m/s velocity the working fluid at both of the configurations have same temperature of around 60°C whereas, on increasing velocities, the trend declined and the lowest temperature profile achieved. For instance, at final velocity Figure of 1 m/s, the temperature if the working fluid was at 27°C for one layer of heat sink, while for double layer, the inlet and outlet temperature seemed to have equal value that can be easily assessed. Furthermore, as the working fluid's velocity increases, the temperature of the PV module decreases in tandem. The findings demonstrate that a double arrangement of heat sinks yields superior results compared to a mono arrangement. The double heat sink configuration leads to a dramatic temperature reduction, reaching 36°C at a velocity of 1.0 m/s. In contrast, the mono heat sink arrangement results in a module temperature of 40°C under the same inlet velocity.

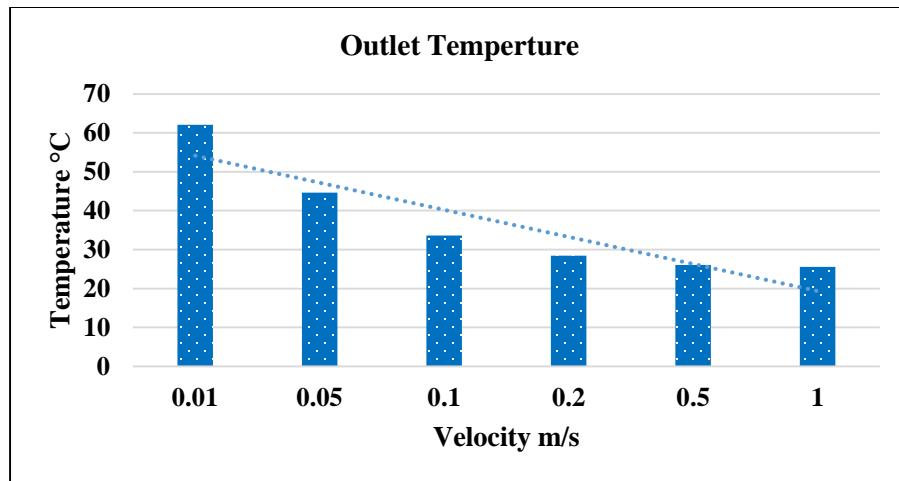


Figure 8: Outlet Temperature of a Coolant Using Single Layer of Heat Sinks w.r.t Velocities

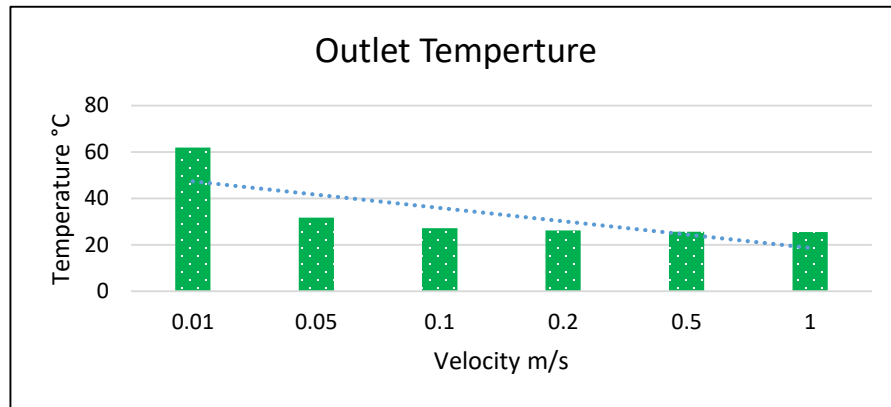


Figure 9: Outlet Temperature of a Coolant Using Double Layer of Heat Sinks w.r.t Velocities

Overall, the double layer arrangement found to have greater impact on decreasing the temperature and increasing the efficiency of the model.

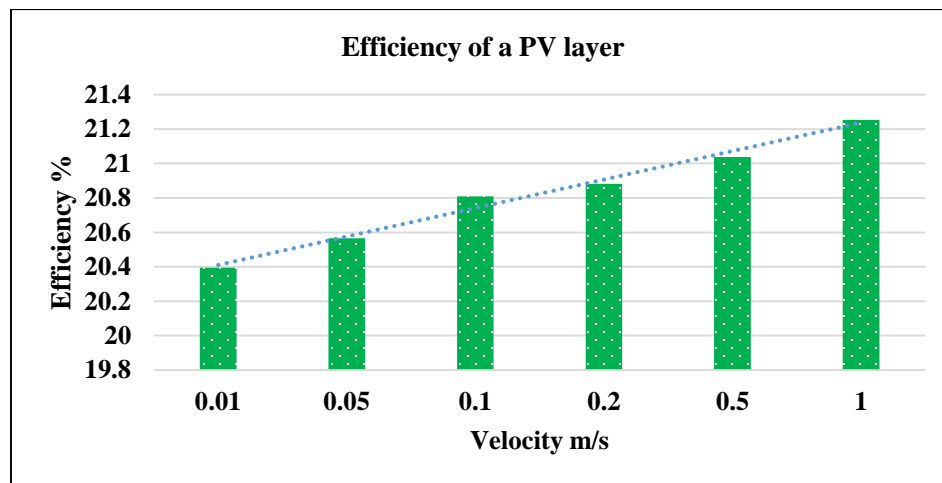


Figure 95: Efficiency of a PV Layer Using Double Layer Of Heat Sinks w.r.t Velocities

Efficiency of the module is dropped by almost 30% of the actual because of the increase in the surface temperature of the module. In addition, the decrease in the temperature of the PV module adjacent to the increase in the temperature of the working fluid is observed at different velocities. On the next hand, the results declared that double arrangement of heat sinks found to have optimum results as compared to a mono arrangement of heat sinks. One more thing is observed that, with the increase in velocity of the working fluid the temperature of the module decreased dramatically to a value of 36°C at 1.0 m/s velocity using double arrangement of heat sinks. Contrarily, at the same inlet velocity, the temperature of the PV module lowered to a value of 40°C by using a mono arrangement of heat sinks. Hence, it is asserted that with double arrangement of heat sinks, one can optimize the efficiency and power of the module under actual boundary



and climatic conditions. Moreover, maximum number of energy units can be saved by implementing these CFD schemes and can be contributed to the energy sustainability of the country.

ACKNOWLEDGEMENTS

I very glad and thankful to almighty Allah who given me courage and strength to complete this research in best possible way under limited resources availability thanks to Dr. Nadeem and Engr. Asnaf Aziz for their support.

REFERENCES

- [1] Abdo, S. and H. Saidani-Scott, *Effect of using saturated hydrogel beads with alumina water-based nanofluid for cooling solar panels: Experimental study with economic analysis*. Solar Energy, 2021. **217**: p. 155-164.
- [2] Ağbulut, Ü., et al., *Performance assessment of a V-trough photovoltaic system and prediction of power output with different machine learning algorithms*. Journal of Cleaner Production, 2020. **268**: p. 122269.
- [3] Ali, F., K.A. Khan, and S. Jahan, *Evaluating Energy Security Performance in Pakistan and India through Aggregated Energy Security Performance Indicators (AESPI)*. European Online Journal of Natural and Social Sciences, 2020. **9**(2): p. pp. 425-442.
- [4] Khosa, A.A., et al., *Performance analysis based on probabilistic modelling of Quaid-e-Azam Solar Park (QASP) Pakistan*. Energy Strategy Reviews, 2020. **29**: p. 100479.
- [5] Lashari, A.A., et al., *The performance prediction and techno-economic analyses of a stand-alone parabolic solar dish/stirling system, for Jamshoro, Pakistan*. Cleaner Engineering and Technology, 2021. **2**: p. 100064.
- [6] Tahir, S., et al., *Techno-economic assessment of concentrated solar thermal power generation and potential barriers in its deployment in Pakistan*. Journal of Cleaner Production, 2021. **293**: p. 126125.
- [7] Zondag, H.A., *Flat-plate PV-Thermal collectors and systems: A review*. Renewable and Sustainable Energy Reviews, 2008. **12**(4): p. 891-959.
- [8] Maleki, A., et al., *A review on the approaches employed for cooling PV cells*. Solar Energy, 2020. **209**: p. 170-185.
- [9] Fouad, M., L.A. Shihata, and E.I. Morgan, *An integrated review of factors influencing the performance of photovoltaic panels*. Renewable and Sustainable Energy Reviews, 2017. **80**: p. 1499-1511.
- [10] Ağbulut, Ü., et al., *Performance assessment of a V-Trough photovoltaic system and prediction of power output with different machine learning algorithms*. Journal of Cleaner Production, 2020: p. 122269.
- [11] Ustaoglu, A., et al., *Experimental and economical performance investigation of V-trough concentrator with different reflectance characteristic in photovoltaic applications*. Journal of Cleaner Production, 2020. **272**: p. 123072.
- [12] Gong, J.-h., et al., *Improving the performance of a 2-stage large aperture parabolic trough solar concentrator using a secondary reflector designed by adaptive method*. Renewable Energy, 2020. **152**: p. 23-33.
- [13] Ustaoglu, A., U. Ozbey, and H. Torlaklı, *Numerical investigation of concentrating photovoltaic/thermal (CPV/T) system using compound hyperbolic-trumpet, V-trough and compound parabolic concentrators*. Renewable Energy, 2020. **152**: p. 1192-1208.
- [14] Renzi, M., L. Egidi, and G. Comodi, *Performance analysis of two 3.5kWp CPV systems under real operating conditions*. Applied Energy, 2015. **160**: p. 687-696.



ICSET-23

*Proceedings of the 5th International Conference on Sustainable
Energy Technologies (ICSET 2023) Peshawar, Pakistan
14-15 December 2023*



UET Peshawar

- [15] Qays, M.O., F. Yasmin, and H.A. Kamal, *A Review on Improved Performance for Solar Photovoltaic Cells by Various Cooling Methods*. Journal of Thermal Energy Systems. **5**(1).
- [16] Hasanuzzaman, M., et al., *Global advancement of cooling technologies for PV systems: A review*. Solar Energy, 2016. **137**: p. 25-45.
- [17] El Kharaz, H., et al., *Performance's improvement methods of PV solar panel by different cooling systems: A Review of Experimental and Numerical studies*. 2020, EasyChair.
- [18] Lebbi, M., et al., *Energy performance improvement of a new hybrid PV/T Bi-fluid system using active cooling and self-cleaning: Experimental study*. Applied Thermal Engineering, 2020: p. 116033.
- [19] Zhou, J., et al., *Temperature distribution of photovoltaic module based on finite element simulation*. Solar Energy, 2015. **111**: p. 97-103.
- [20] Coulson, K.L., *CHAPTER FOUR - Solar Radiation: Diffuse Component*, in *Solar and Terrestrial Radiation*, K.L. Coulson, Editor. 1975, Academic Press. p. 84-141.
- [21] Thekaekara, M.P., *Solar radiation measurement: Techniques and instrumentation*. Solar Energy, 1976. **18**(4): p. 309-325.
- [22] Asim, M., et al., *Investigation of Mono-Crystalline Photovoltaic Active Cooling Thermal System for Hot Climate of Pakistan*. Sustainability, 2022. **14**(16): p. 10228.

Paper ID: ICSET-2329

WIND TURBINE FAILURE RATE AND DOWNTIME SURVEY WITH SPECIAL REFERENCE TO PAKISTAN

Musavir Hussain¹, Nayyar Hussain Mirjat², Faheemullah Shaikh², Lubna Laxmi³

¹Department of Electrical Engineering, Mehran University of Engineering and Technology SZAB Khairpur Mir's,
Khairpur Mir's, Sindh; Pakistan

²Department of Electrical Engineering, Mehran University of Engineering and Technology Jamshoro, Jamshoro,
Sindh; Pakistan

³Department of Electronic and Computer Engineering, University of Limerick, Limerick, V94 T9PX Limerick,
Ireland

**Corresponding author*

Email: enr.musavir@muethkp.edu.pk

ABSTRACT

Scientific Studies pertaining wind turbine system failure frequency rate and downtime provide useful insight to contain various losses. However, rarely studies in the context of Pakistan are reported in the contemporary literature. With the help of SCADA data unexpected failures in wind turbine systems can proactively be detected and diagnosed. This study, as such, presents an analysis of SCADA based disturbance and outage data analyses to investigate the failure rate and downtime of wind turbine systems with focus on the reliability assessment of a 1.5 MW wind turbine system located in Jhampir wind corridor of Pakistan. In addition, careful efforts have been made to identify the most critical faults, events and components that occur most and thus have a significant impact on downtime. This study expands its scope to include the relationship between outages and failure rates of multiple wind turbines in the same wind farm. By correlating these parameters, a comprehensive perspective of the reliability of the wind farm is achieved. It was found that cumulative total failure frequency rate and downtime of the windfarm over one year was 159 and 816 hours respectively. These results further specifically help to identify that pitch system and power converter are the most critical component based on failure frequency and downtime. Findings of this study will be helpful for policy makers and stakeholders for strengthening the resilience of Pakistan's energy infrastructure so that major failure of wind turbines can be prevented in time to reduce production loss and maintenance cost.

KEYWORDS: Failure Rate, Downtime, Permanent Magnet synchronous Generator, Wind Turbine System, reliability.

INTRODUCTION

Wind energy has become the key factor in global energy production as it responds to the growing energy demand and concerns about climate change. The expected wind power generation capacity of 955 GW in 2022 represents significant growth in this sector. The global focus is on expanding the production of renewable energy, especially wind energy, in order to achieve the united nation sustainable goals of reducing carbon dioxide emissions by 2030 and achieving net zero emissions by 2050 [1]. Pakistan, a country



ICSET-23



UET Peshawar

struggling with increasing energy demand and climate change challenges, the pursuit of wind energy is becoming paramount. According to recent data, the cumulative installed capacity of wind power in Pakistan has made significant progress, increasing from just 6 MW initiative 2008 to 1985 MW in 2022 and evolution in Pakistan can be seen in Fig. 1 [2].

The country had several wind farms in operation, and more are under development. The government of Pakistan has also launched policies and incentives to attract investment in renewable energy, including wind power. These policies sought to increase share of renewable energy in country's energy mix to reduce its dependence on the fossil fuels and to address energy shortages government has set the target for 30 percent plus renewable energy resources by 2030 [3].

About 2 decades ago, when wind energy harnessing at larger scale had commenced, the objectives were focused to establish these projects. The operational difficulties at that time were part of the known and unknowns. However, over the years with increased availability requirements, the wind farm shutdown due to faults has become unacceptable as it would result production losses and increased costs.

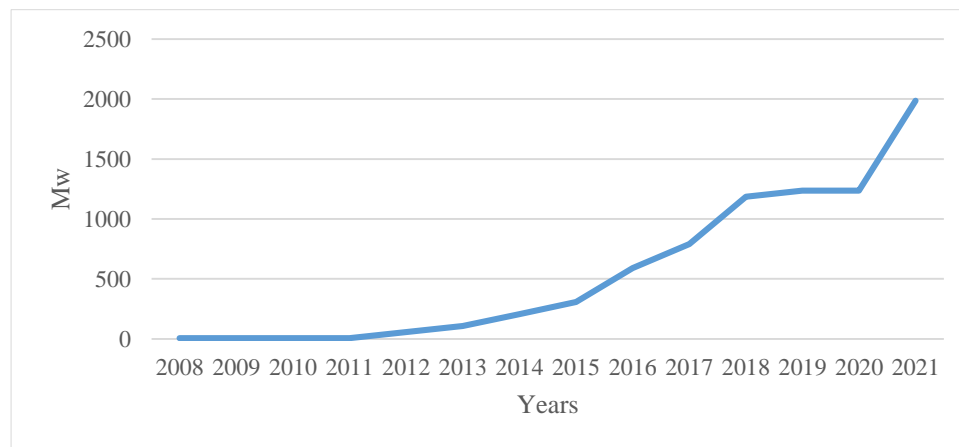


Figure 1: Evaluation of wind industry in Pakistan

As such, reducing the operation and maintenance expenses of wind farms have become a daunting challenge as wind power capacity and challenge pertaining trouble free operation kept growing.

It is estimated that approximately 10-15% and 20–25% of overall cost of electricity generation for onshore and offshore wind farms include alone the operational and maintenance costs respectively. The frequent downtimes at a wind farm would not only reduce production, impact the reliability but also raise the O&M and overall production costs. In order to analyze various fault conditions and failure to avert increased O&M cost and downtime, use and analysis of SCADA data has recently become one of the most promising approaches in Wind Engineering [4].

Considering this, to enhance the reliability and Power availability of Pakistani wind farms it appears crucial step not only to satisfy the country's growing energy needs but also to reduce operational and maintenance cost. Therefore, this research aims to deepen into the complexities of wind energy and discuss the unique challenges, opportunities and strategies to improve system performance.

Condition Monitoring /Health Monitoring of Wind Turbine

Health monitoring is a tool that helps monitor the actual state of an equipment /component to distinguish between when it is behaving strangely and when it is functioning normally. It provides reliable



insight into equipment failures so operations can be planned, and downtime minimized. Most of the research was done using vibration analysis, acoustic emission and strain, torque and various types of individual-sensors based approaches have been developed to measure velocity, acceleration, and displacement. The biggest disadvantage of the aforementioned condition monitoring methods is that they require the installation of special and expensive additional sensors and data collection systems [4], [5], [6], [7]. On the contrary, this study proposes a method that does not require investment in additional equipment but relies exclusively on SCADA (Supervisory Control and Data Acquisition) data, which are already available in all industrial WTs.

A wind turbine is a complex machine with rotating and non-rotating parts that can break. Due to increased wear and tear, wind farm maintenance is critical. Unexpected failure of wind turbine components can increase operational and maintenance costs, ultimately reducing the effective energy consumption of the wind farm. SCADA data is divided into status data and SCADA data. State data tracks all faults and failures over time [4], and this study focuses on event data/state data/failure data and adds value to existing body of literature and would help to improve overall system performance.

Existing Literature Over Failure Rate and Downtime

This literature review summary provides an overview of various research papers related to the failure rate and downtime analysis of wind turbine system. These studies span different years and regions, shedding light on critical aspects of wind turbine performance and maintenance practices. Here's a brief summary of each paper: The study [8] focuses on Turkish onshore wind turbines, emphasizing the importance of reducing the operation and maintenance costs and unplanned downtime. It uses SCADA alarms to estimate failure rates and identifies critical subsystems, particularly "security" and "electrical systems." Scheduled maintenance significantly affects SCADA failures, suggesting the potential of advanced condition monitoring systems. Results clearly show that wind turbines suffer from safety related events causes 40% of total failure and downtime occurrences. This research [9] analyzes the failure and the maintenance data from the various onshore wind farms worldwide, addressing availability, reliability maintainability risk and safety. It introduces a new Reliable Impact Factor (RIF) approach and aims to improve the understanding of wind turbine failure characteristics, maintenance practices, and design improvements. The results of this study showed that 38% of event recorded is of rotor and electrical facilities and gearbox which is 30% and 24% respectively. Focusing on Japan [10], this study examines the failure rate and the downtime and comparison shows that failure rate is similar b/w Europe and Japan. But downtime in Japan is much, longer in comparison to Europe. It was found that wind turbine availability can be improved and levelized cost of energy (LCOE) can be reduced. The research [11] concentrates on the Spanish wind energy sector, highlighting the importance of subassemblies like electrical and control systems and generators in terms of failure frequency rate and downtime. Study critically identified subcomponents and provided insights into wind farm reliability, especially in Spain and it was clarified that most critical subassemblies /subcomponent are Electric and Control in both wind turbine technology i.e. SC and DFIG. This study [12] analyzed the failure rate of a wind farm located in Jiangsu Province, China and highlighted the importance of sub-systems such as hoist/blades, control and electrical systems. The relationship between faults and weather factors is also investigated. Finally, it was concluded that the control system and the electrical system failure are higher, and failure caused by the mechanical component are rare. An article focusing on China [13] discusses the rapid increase in wind turbine capacity and the increase in failures. It identifies the main causes of failure and emphasizes the need for reliable management methods in design, production and maintenance. It was found that frequency converter has the highest failure rate comparison

to another component. This study [14] emphasis to improve the reliability and cost-effectiveness of wind turbines by addressing data processing issues and the possible use of SCADA alarms. It offers a modernized taxonomy for consistent data processing and highlights the potential of SCADA data to improve reliability modeling. It was concluded that Blade and controller failure event occurs frequently. This article [15] examines wind turbine generator failures in China, highlights the impact of cable failures, and suggests ways to improve data security. It quantifies the potential increase in output and power factor if faults are eliminated. Results of this study showed that failure frequency in pitch system was higher in comparison and followed by the control system (CS) and the sensors. On other cable failure caused downtime of downtime 29.29% or 2033 hours followed Pitch System and control system. The Reliawind project [16] aims to improve the reliability of wind turbines through quantitative analysis of data from different turbine manufacturers. It focuses on estimating failure rate, downtime and understanding failure patterns for different maintenance categories. It was found that failure rate of generator is lower in comparison other components, but downtime was higher in comparison. Conversely, pitch system failure rate is higher in comparison to others. This study [17] analyzes the historical reliability of modern wind turbines, especially in Denmark and Germany. It uses reliability analysis methods to analyze the reliability of large wind turbines, while considering the factors such as design, configuration, time, weather and maintenance. Results and analysis show that highest German failure frequency contributor is electric control subassembly rather mechanical such as gearbox.

In this work, a failure rate and downtime survey were carried out, in which 66 wind turbines installed in one windfarm were analyzed over a period of one year. Although wind turbine capacity and number of wind turbines included in this study are smaller than other studies in the region, the specific machine used for reliability analysis in the wind farm are not reported in the current literature. Thus, a study would-be value addition to existing body of literature on the failure rate and downtime of wind turbines.

METHODOLOGY

The Failure frequency rate is determined by dividing number of failures (total) per wind turbine sub assembly / subcomponent by the total years of wind turbines in the entire 66 wind turbine series. Failure frequency rate per subassembly / subcomponent (f_i) was calculated by following relation as follows,

$$f_i = \frac{\sum_{t=1}^T n_{i,t}}{\sum_{t=1}^T N_t \left(\frac{T_t}{8760} \right)} \quad (1)$$

Where as

$n_{i,t}$ = Number of Failures Per Subassembly / Subcomponent in a period (T),

N_t = Total Number of Wind Turbines

T_t = Total Number of Hours in The Period (T)

Correspondingly, downtime for specific subassembly/subcomponent was determine as downtime (total) of subassembly / subcomponent i in a period (T), divided by number of failures of that subassembly in a period (T), as follows [11]:

$$d_i = \frac{\sum_{t=1}^T d_{i,t}}{\sum_{t=1}^T n_{i,t}} \quad (2)$$

f_i and d_i were calculated for subassembly / subcomponent of from compiled data received under non-disclosure agreement b/w MUET NCRA Wind Power Plant Condition Assessment Monitoring Project (MAPCAP) and M/s. Algorithm Consulting. Finally, results were plotted and evaluated.

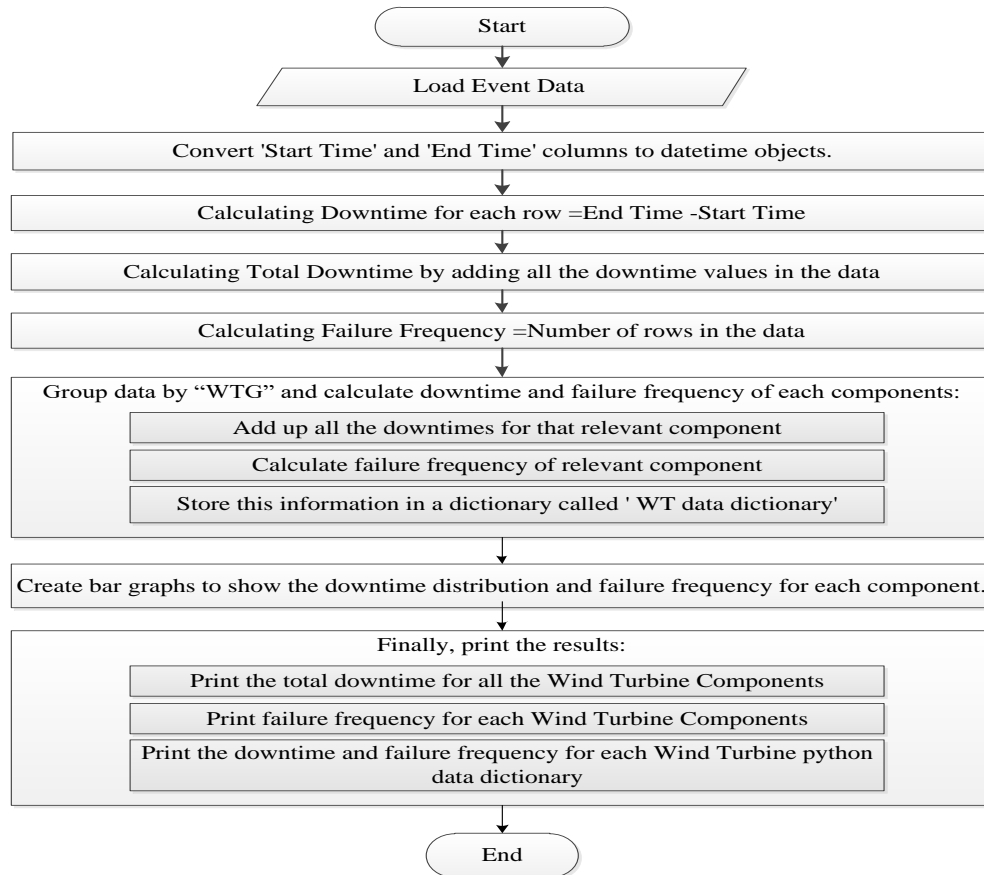


Figure 2: Pseudocode flow chart represent the methodology

Based on these equations code was developed and data was processed in python package and relevant code pseudo labeling is done and presented in flow chart Figure 2.

RESULT AND DISCUSSION

Majority of wind turbines subcomponent / subassemblies contributes to failure frequency rate and downtime. Furthermore, failure frequency rate and downtime survey results are presented by analysing PMSG/ PMDD type wind turbine System as illustrated in Figure 3 and Figure 4, respectively. Power Converter is top in failure frequency rates with the share of (52%) followed by Pitch System (25.7%) and Electric and Control 12.57% and the remaining categories show lower percentages. It was observed that converter is most critical component among all subcomponents / subassemblies having highest failure percentage with average downtime of 5-7 hours. Pitch system which is second most occurring failure causes average downtime of 10 hours to 25 hours.

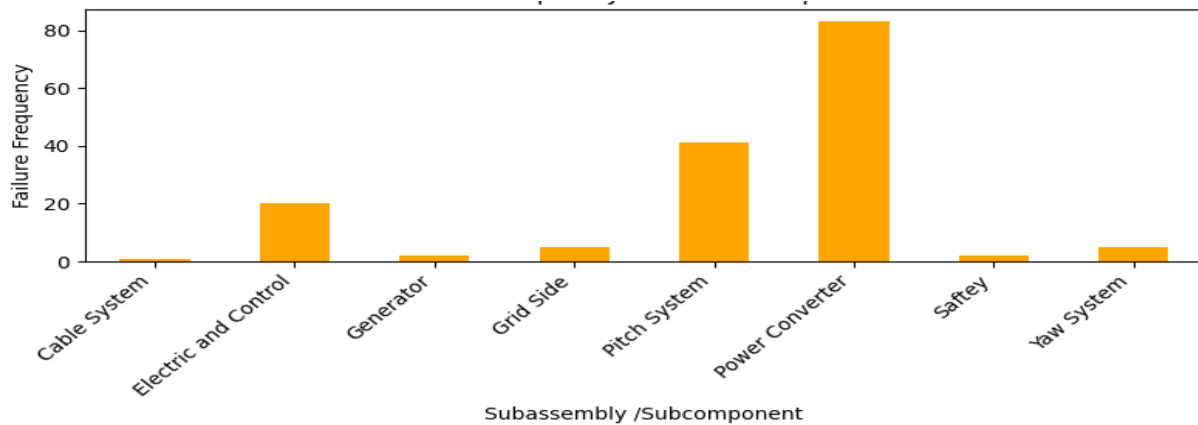


Figure 3: Failure Frequency of Subcomponents/ Sub-Assemblies year 2022

The Power Converter and Pitch System are biggest contributors in downtime ranking, contributing with the (37.8% and 37.2% respectively) of the total followed, in this case, it is also followed by the electric and control subassemblies. The grid side faults are on the fourth position in downtime ranking, with a 4.2% share, followed by yaw system and safety (2.6% and 3.3%, respectively). Remaining categories shows very low percentages.

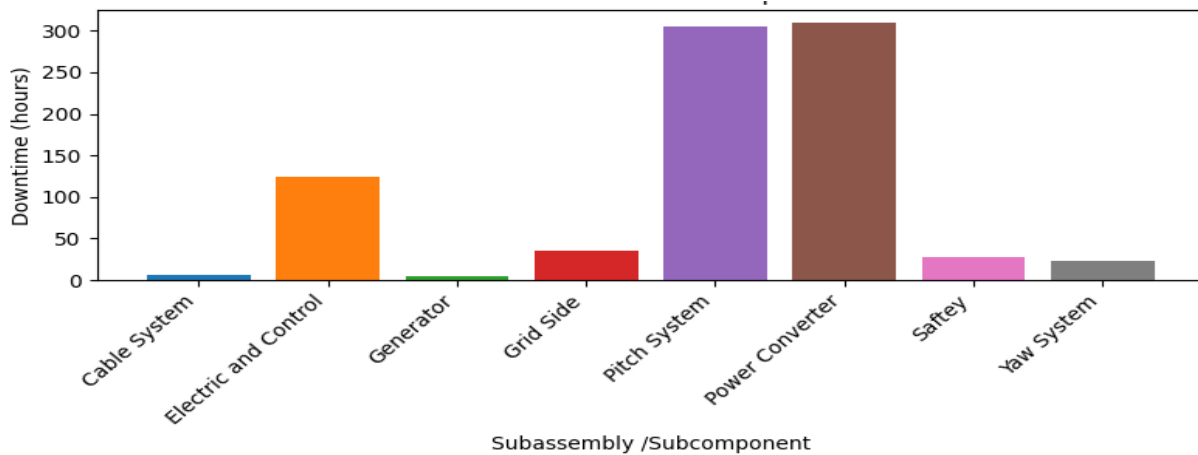


Figure 4: Downtime of Subcomponents/ Subassemblies

Although results for downtime are quite as astonishing power converter as well as pitch system both are identified a critical component based on downtime. As discussed, above power converter causes downtime of few hours but has highest failure occurrence, whereas pitch system causes higher downtime in comparison to other subassemblies. On other hand failure percentage of pitch system is lower in comparison to power converter and that could be the reason for both components to emerged as critical components in this study.



ICSET-23



UET Peshawar

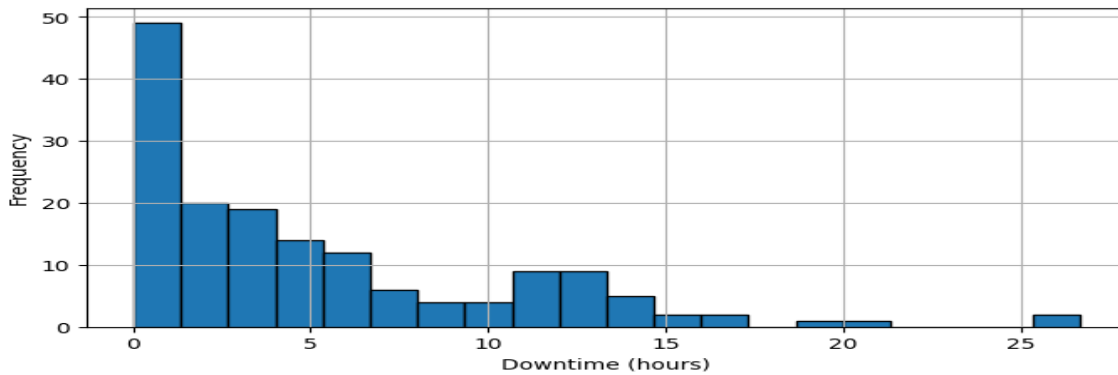


Figure 5: Distribution of Downtime of Windfarm for year 2022

Figure 5 shows distribution of downtime vs failure frequency which clearly depicts that most of failure occurrence caused lower downtime b/w 1- 7 hours. On other hand some events can cause the downtime 25 hours. These indicated that there are two categories of faults in the data set provided one is short term failures and other are long term failures short term failures remains for very short span of time and system is brought back to its operational mode. On other hand long term failures remains large span of time (downtime) for example in the data set provided one failure related Pitch system caused downtime more than 25 hours.

CONCLUSION

Pakistan is new to the wind energy industry but has good wind energy potential and its significance in wind energy sector is clear. Eleven studies were included in the literature review, but none were conducted exclusively in Pakistan. In this scenario, a new study on failure rates and downtime has been conducted for first time in scientific literature in Pakistan. The study was conducted over a period of one year using 66 wind turbines located in a wind farm with permanent magnet direct drive technology. The results showed that the most critical subassemblies are the Pitch system and power converter, followed by electrical and control, while the percentage was lower in other categories. Finally, to integrate this study with existing studies, results of this study were compared with finding of existing relevant studies. The evaluation of results showed that failure rate and downtime values acquired in this survey are within the limits of preceding research for the most of subassemblies. Regarding percentage of failures, exception is the Power Converter, whose percentage clearly exceeds the upper limit. Downtime exceptions can be found in the power converter and the Pitch system.

ACKNOWLEDGEMENTS

This research Acknowledge Higher Education Commission, Pakistan for the research grant with PIN#520-167-0822GE6-69 (50093950) and Mehran University of Engineering and Technology, Jamshoro for providing platform for conducting this research. This research is also supported under “Implementation Agreement” with M/s. Algorithm Consulting on 15th July 2021 to acquire various data from an operational Wind Power Plant (WPP) located at Jhampir wind corridor. This arrangement has been successfully attained under National Electric Power Regulatory Authority’s (NEPRA’s) CSR initiative and named as “MUET NCRA Wind Power Plant Condition Assessment Monitoring Project (MAPCAP)”



REFERENCES

- [1] S. A. Khatri *et al.*, “An Overview of the Current Energy Situation of Pakistan and the Way Forward towards Green Energy Implementation,” *Energies*, vol. 16, no. 1, pp. 1–27, 2023, doi: 10.3390/en16010423.
- [2] D. MOORE, “Chapter 14,” *Pakistan Econ. Surv. Rep.*, pp. 133–150, 2022, doi: 10.2307/j.ctv33www0w.19.
- [3] Z. W. C. R. – P. Ashfaq, “Pakistan to Set 30% plus 30% Renewable Energy Target by 2030,” 2019. <https://wwindea.org/pakistan-to-set-30-plus-30-renewable-energy-target-by-2030/> (accessed Sep. 15, 2022).
- [4] J. Park, C. Kim, M. C. Dinh, and M. Park, “Design of a Condition Monitoring System for Wind Turbines,” *Energies*, vol. 15, no. 2, Jan. 2022, doi: 10.3390/en15020464.
- [5] J. Helsen, “Review of Research on Condition Monitoring for Improved O&M of Offshore Wind Turbine Drivetrains,” *Acoustics Australia*, vol. 49, no. 2. Springer, pp. 251–258, 2021. doi: 10.1007/s40857-021-00237-2.
- [6] W. Qiao and D. Lu, “A Survey on Wind Turbine Condition Monitoring and Fault Diagnosis - Part II: Signals and Signal Processing Methods,” *IEEE Trans. Ind. Electron.*, vol. 62, no. 10, pp. 6546–6557, 2015, doi: 10.1109/TIE.2015.2422394.
- [7] P. Tchakoua, R. Wamkeue, M. Ouhrouche, F. Slaoui-Hasnaoui, T. A. Tameghe, and G. Ekemb, “Wind Turbine Condition Monitoring: State-of-the-Art Review, New Trends, and Future Challenges,” *Wind Resour. Futur. Energy Secur. Environ. Soc. Econ. Issues*, pp. 283–330, 2015, doi: 10.1201/b18529-20.
- [8] N. Sarma, P. M. Tuohy, O. Özgönenel, and S. Djurović, “Early life failure modes and downtime analysis of onshore type-III wind turbines in Turkey,” *Electr. Power Syst. Res.*, vol. 216, no. July 2022, 2023, doi: 10.1016/j.epsr.2022.108956.
- [9] H. Li, W. Peng, C. G. Huang, and C. Guedes Soares, “Failure Rate Assessment for Onshore and Floating Offshore Wind Turbines,” *J. Mar. Sci. Eng.*, vol. 10, no. 12, 2022, doi: 10.3390/jmse10121965.
- [10] Y. Kikuchi and T. Ishihara, “Availability and lcoe analysis considering failure rate and downtime for onshore wind turbines in Japan,” *Energies*, vol. 14, no. 12, 2021, doi: 10.3390/en14123528.
- [11] E. Artigao, S. Martin-Martinez, A. Ceña, A. Honrubia-Escribano, and E. Gomez-Lazaro, “Failure rate and downtime survey of wind turbines located in Spain,” *IET Renew. Power Gener.*, vol. 15, no. 1, pp. 225–236, 2021, doi: 10.1049/rpg2.12019.
- [12] C. Su, Y. Yang, X. Wang, and Z. Hu, “Failures Analysis of Wind Turbines : Case Study of a Chinese Wind Farm,” no. October 2016, 2017, doi: 10.1109/PHM.2016.7819826.
- [13] Y. Lin, L. Tu, H. Liu, and W. Li, “Fault analysis of wind turbines in China,” vol. 55, pp. 482–490, 2016, doi: 10.1016/j.rser.2015.10.149.
- [14] X. Li, G. Huang, and Z. Guo, “Wind Turbine Failures - Tackling current Problems in Failure Data Analysis Wind Turbine Failures - Tackling current Problems in Failure Data Analysis,” 2016, doi: 10.1088/1742-6596/753/7/072027.
- [15] R. Bi, K. Qian, C. Zhou, D. M. Hepburn, and J. Rong, “A survey of failures in wind turbine generator systems with focus on a wind farm in China,” *Int. J. Smart Grid Clean Energy*, pp. 366–373, 2014, doi: 10.12720/sgce.3.4.366-373.
- [16] M. Wilkinson, B. Hendriks, F. Spinato, and T. Van Delft, “Measuring wind turbine reliability, results of the reliawind project,” *Eur. Wind Energy Assoc. Conf.*, pp. 1–8, 2011, [Online]. Available: http://www.gl-garradhassan.com/assets/downloads/Measuring_Wind_Turbine_Reliability_-



ICSET-23

*Proceedings of the 5th International Conference on Sustainable
Energy Technologies (ICSET 2023) Peshawar, Pakistan
14-15 December 2023*



UET Peshawar

- _Results_of_the_Reliawind_Project.pdf
- [17] P. J. Tavner, J. Xiang, and F. Spinato, "Reliability Analysis for Wind Turbines," no. July 2006, pp. 1–18, 2007, doi: 10.1002/we.204.



ICSET-23

Proceedings of the 5th International Conference on Sustainable
Energy Technologies (ICSET 2023) Peshawar, Pakistan
14-15 December 2023



UET Peshawar

Paper ID: ICSET-2330

CHEMICAL TREATMENT OF PHOTOVOLTAIC SILICON SOLAR CELL THROUGH BENZENE - A STEP TOWARDS RECYCLING

Salman Farooq^{1,*}, Abdul Shakoor¹, Muhammad Noman², Sohail Noor³, Fouzia Hussain⁴, Noaman Farooq⁵

¹*Mechanical Engineering, UET Peshawar, Pakistan*

²*US-Pakistan Center for Advanced Studies in Energy, University of Engineering and Technology Peshawar, Pakistan*

³*Material Science Centre, PCSIR Complex Peshawar, Pakistan*

⁵*PCSIR Islamabad, Islamabad, Pakistan*

⁵*Department of Construction Engineering and Management, Military College of Engineering, National University of Sciences & Technology, Risalpur, Pakistan*

**Corresponding author*

Email: salmanfarooq@uetpeshawar.edu.pk

ABSTRACT

The critical issue of end-of-life waste from solar PV modules and the increasing environmental concern is mainly associated with their improper disposal. The projected growth in module waste by the early 2030s and the estimated quantity of 78 million tons by 2050 underscore the urgency of addressing this problem. This study discusses the recycling of PV modules. The primary focus is on the removal of different Si-cell protective layers through Benzene, an organic solvent. To remove EVA from silicon cells, emphasizing safety precautions due to its volatile nature. A successful preliminary test demonstrated EVA dissolution in Benzene, enabling its removal from PV cells within 45 minutes. This study explores the practical aspects of employing Benzene for EVA removal, providing valuable insights for the recycling process.

KEYWORDS:

Recycling of PV panels; Chemical treatment of solar cells; Organic chemicals for recycling; Benzene effects on PV cells.

INTRODUCTION

One of the major components of PV panels is a solar cell to generate electricity in commercial, residential, and industrial setups [1]. A key constraint on planet earth for solar technology sustainability is end-of-life of PV modules. As the modules installation is increasing rapidly, so the modules waste will. It is estimated by The International Renewable Energy Agency that end-of-life waste of modules will appear in substantial quantities by the early 2030's and will be approximately 78 million tons by 2050 [2]. The wafer Si-modules have always been the leading technologies with around 90% market stake as compared to other parallel module technologies [3].



By the end-of-life solar panels will become a threatening waste and may damage the nature if they are not regained or disposed of properly. The recycling was not of interest in the first 25 years of its development [4].

The process of manufacturing PV modules includes laminating individual cells after creating the n-p junction connector layer and securing them within an aluminium frame. When it comes to recycling, the modules need to undergo disassembly. The reclaimed silicon has the tendency to be utilized for different applications such as a raw material for PV production, they can be utilized as an additive in steel production to improve its mechanical properties like hardness, tensile strength, and impact strength. It can also be utilized in the production of non-metal powder in ceramic industry [5].

This study initially explores the utilization of Benzene as an organic solvent for the purpose of removing the EVA layer from the PV cell. It assesses its impact on the silicon cell surface, evaluates its effect on the back-sheet layer, analyzes the removal of bus bars, and investigates the extraction of the silicon cell. The study extends and provides more detail on the simplified approach to employing Benzene and its behavior over time during the removal process.

MATERIALS AND METHODS

The recycling process involves both mechanical and physical processes to eliminate EVA layer which is encapsulated on the solar cells of PV modules according to the flow chart presented in Fig. 1.

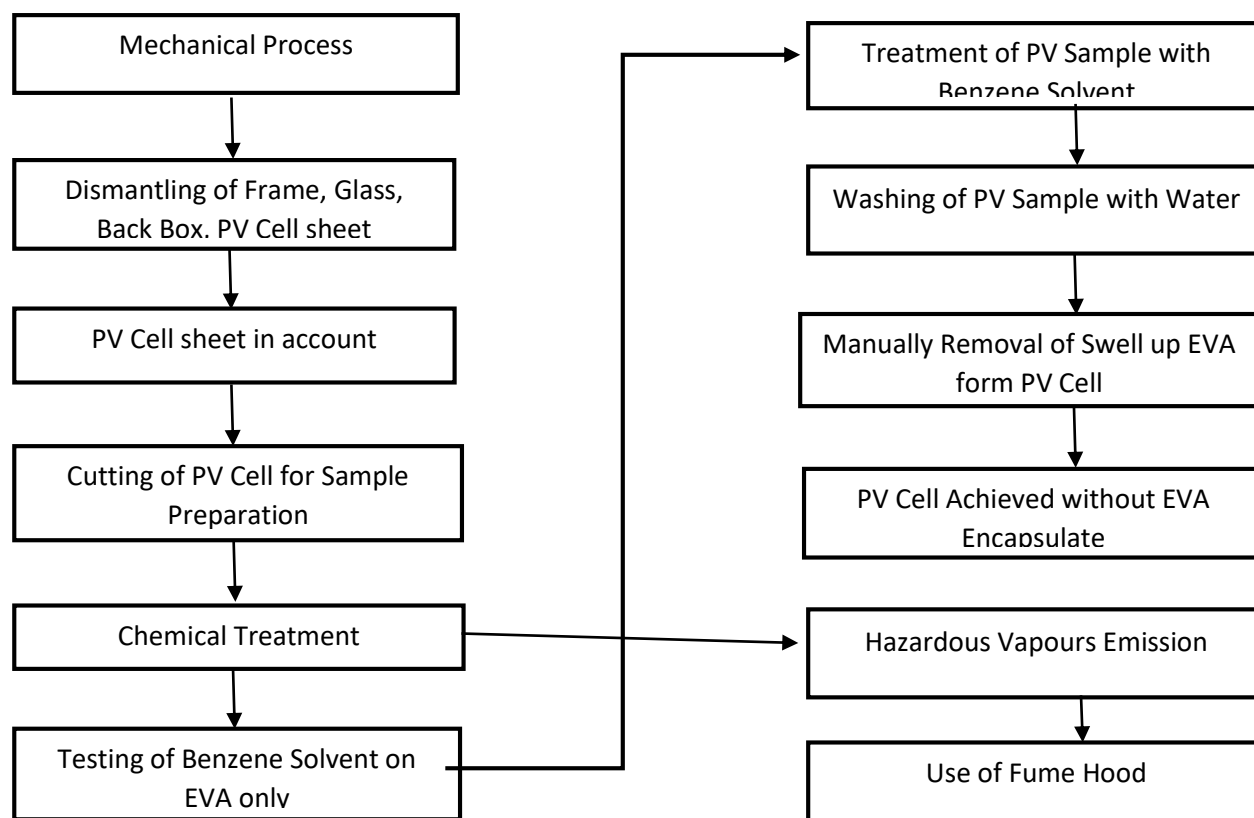


Figure 1: Mechanical and Chemical Processes in PV Module Recycling to Remove EVA Encapsulate

The PV modules production involves laminating process. The laminated module is mounted on aluminium frame. The cells are usually encapsulated with EVA (Ethylene Vinyl Acetate) which is further protected with a glass layer at its front and back-sheet (polyvinyl fluoride). The protection is provided so that the modules can serve for their estimated life of 25 years in the field exposed to weathers and environmental conditions.

The primary process carried out for the removal of EVA from the silicon cell after the removal of glass layer, aluminium frame and the back box was the use of chemical solvent-Benzene.

Benzene (C_6H_6) is an organic solvent having hydrocarbon chain [6] whereas, the EVA is also a hydrocarbon ($C_6H_{10}O_2$) [5].

Primary test was conducted on the EVA layer only to check its dissolution in Benzene. A sample of EVA layer was placed in the beaker containing concentrated Benzene for 5 minutes. Positive results were found in the form of softening and splitting of EVA when checked. The sample of PV cell was immersed in the second stage in the solvent and was observed every after 10 minutes. The EVA layer started swelling and losing its adhesive nature in the beginning. After 45 minutes PV cell sample was removed from the solvent, washed with water and The EVA layer was removed from the cell surface manually. Both primary and secondary stages were performed at room temperature.

The use of Benzene is potentially hazardous due to its volatile nature [7]. Therefore, the process was carried out in an open container and in a fume hood to ensure the safety of the operators.

RESULTS AND DISCUSSIONS

Fig. 2 shows that the PV cell samples are immersed in the Benzene solvent. It indicates that the EVA encapsulate layer has started swelling. Additionally, these illustrations that the swelling area is positively increasing to cover the rest of the area whereas, Fig. 3 shows that the EVA layer after 45 minutes of time has been swollen and lost its adhesive nature considerably and has been removed from both cells manually. Moreover, it explains that the fraction of PV cell got damaged while placed in the Benzene which can be seen as attached to the EVA.



Figure 2: PV cell sample dipped in Benzene



Figure 3: EVA removed from PV cell Sample

Table 1: Observation of EVA removal through benzene for 45 minutes-time interval

| Chemical | Sample Observation Time in Minutes | | | | |
|------------------------------------|------------------------------------|---------------------|--------------------------------------|--------------------------------------|--------------------|
| | 10 | 20 | 30 | 40 | 45 |
| Benzene at room temperature | Swelled corners of EVA | Swelling propagates | swelling and Softening EVA increased | Swelling area increased considerably | Able to be removed |

Table 1 shows that the EVA encapsulate layer has not lost 100% of its adhesive nature consequently it was manually removed. Care must be taken while removing the EVA layer from the PV cell as the thickness of cell is in micrometres and may break if uneven force is applied. Fig 4 shows that the EVA layer in solvent has not lost its complete adhesive nature, some traces of adhesive EVA left over the surface of PV cell were found in the form of droplets while characterized microscopically.

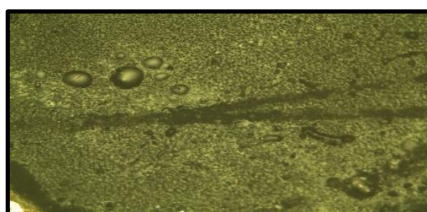


Figure 4: Microscopic image of the PV cell after removal of EVA through Benzene Solvent

As the Benzene solvent is volatile in nature and the process was conducted in an open container placed in a fume hood, the addition of solvent has been required with time interval due to its volatile nature.

As the silicon cell and EVA encapsulate layers have been removed successfully, it is possible to recycle and reuse both PV cell and EVA layer. This can also lead to the potential applications of reclaimed Silicon. By adopting such methodology may produce environmental benefits by recycling of PV modules.

CONCLUSION

In conclusion, PV module production involves a protective encapsulation process that ensures a 25-year lifespan in demanding environmental conditions. To remove EVA from silicon cells during recycling, Benzene, an effective solvent, is employed, as confirmed by a successful initial test. Safety measures, including work in an open container and fume hood, are essential due to Benzene's volatile nature. This approach underscores the commitment to both module durability and operator safety throughout the module's lifecycle.

REFERENCES

- [1] M. F. Azeumo, G. Conte, N. M. Ippolito, F. Medici, L. Piga, and S. Santilli, "Photovoltaic module recycling, a physical and a chemical recovery process," *Solar Energy Materials and Solar Cells*, vol. 193, pp. 314–319, May 2019, doi: 10.1016/j.solmat.2019.01.035.
- [2] "IRENA_IEAPVPS_End-of-Life_Solar_PV_Panels_2016".



ICSET-23

*Proceedings of the 5th International Conference on Sustainable
Energy Technologies (ICSET 2023) Peshawar, Pakistan
14-15 December 2023*



UET Peshawar

- [3] W. Sprenger, H. R. Wilson, and T. E. Kuhn, “Electricity yield simulation for the building-integrated photovoltaic system installed in the main building roof of the Fraunhofer Institute for Solar Energy Systems ISE,” *Solar Energy*, vol. 135, pp. 633–643, Oct. 2016, doi: 10.1016/J.SOLENER.2016.06.037.
- [4] Y. Xu, J. Li, Q. Tan, A. L. Peters, and C. Yang, “Global status of recycling waste solar panels: A review,” *Waste Management*, vol. 75. Elsevier Ltd, pp. 450–458, May 01, 2018. doi: 10.1016/j.wasman.2018.01.036.
- [5] E. Klugmann-Radziemska and P. Ostrowski, “Chemical treatment of crystalline silicon solar cells as a method of recovering pure silicon from photovoltaic modules,” *Renew Energy*, vol. 35, no. 8, pp. 1751–1759, Aug. 2010, doi: 10.1016/j.renene.2009.11.031.
- [6] “Benzene | Definition, Discovery, Structure, Properties, & Uses | Britannica.” Accessed: Sep. 14, 2023. [Online]. Available: <https://www.britannica.com/science/benzene>
- [7] G. F. Kalf, G. B. Post, and R. Snyder, “Solvent Toxicology: Recent Advances in the Toxicology of Benzene, The Glycol Ethers, and Carbon Tetrachloride,” <https://doi.org/10.1146/annurev.pa.27.040187.002151>, vol. Vol. 27, pp. 399–427, Nov. 2003, doi: 10.1146/ANNUREV.PA.27.040187.002151.

Paper ID: ICSET-2331

NUMERICAL SOLUTION OF PDES MODEL USING PHYSICS INFORMED NEURAL NETWORKS

Sabahat Saba*, Siraj-ul-Islam, Masood Ahmad

Department of Basic Sciences, University of Engineering and Technology, Peshawar, Pakistan

**Corresponding author*

Email: saboorkhan742@gmail.com

ABSTRACT

Accurate prediction of numerical solution to Partial Differential Equations (PDEs) is an active research domain in numerical analysis. In this paper an automatic solver for PDEs is constructed by using a Machine Learning (ML) based technique, namely Physics Informed Neural Networks (PINNs). The PINNs is defined as a mean of finding solution to PDEs with capability to tackle problems over various spatio-temporal domains. The accuracy of the method is assessed through one dimensional advection diffusion equation. The influence of increasing number of training epochs upon mean squared loss and computation time is investigated. The accuracy of approximation improves as the number of training epochs increases. Comparison between the computational results of PINNs and the exact solution is carried out, exploiting the meshless nature, accurate and fast prediction and validate use of PINNs in domain of scientific computation.

KEYWORDS: Machine Learning, PINNs, Advection diffusion equation, scientific computation, meshless nature.

INTRODUCTION

The widespread use of deep neural networks in diverse fields of study in science and engineering gives rise to a new prototype of scientific computation namely Physics Informed Neural Networks (PINNs). It is a scientific machine learning technique that embed the real data (Physics of the PDE) into the loss function which is designed to satisfy initial boundary value problems and forcing output of the network to satisfy the governing PDE. Unlike most of data driven approaches that rely on a large volume of training data which is often difficult to obtain for physical experiments, it need small amount of data (PDE problem).

The need for utilizing artificial neural network based techniques instead of well-established numerical method lies in the fact that classical numerical schemes are mesh dependent and yield efficient discrete approximation but fail to provide continuous time solution. Further, PINNs are non-constraint specific and does not incorporate any physical assumptions to the approximations. The flexibility of PINNs lies in the fact that they can be applied equally to both linear and non-linear PDEs.

Background

The ANNs techniques pioneered in early 1990s. Among certain highlights of using ANN as an approximation technique, some notable work is reported in [1-2], the neural networks for the first time was used for solving IBVP. The use of global energy functional for optimization of objective that reduced



memory requirements was a key finding of Gokuzum et al. [3]. Introducing adaptive activation function into DNN, improves the approximation abilities as reported in [15] by Jagtapa et.al. Considerable reform efforts that facilitated research activities was a data efficient approach, explored by Riassi et al. [5-8]. The work was based on using PINNs for nonlinear PDEs in both forward and backward form. In this research we revisit the neural network framework of [7] to solve forward problems.

PHYSICS INFORMED NEURAL NETWORKS

Methodology

The basic neural network architecture and concerned formulations are explained in this section:

The Ann Architecture

The basic structure of NN consist of an input and output layer along with hidden layers which are composed of nodes or neurons and connections between them. The input function to the first layer is processed over multiple hidden layers and is returned as an output of last layer which is NN approximation to PDE. In contrast to typical data driven approaches the training data set of neural network comprise of only initial and boundary data. PINNs utilizes automatic differentiation [9] to compute derivatives of field variables. The network parameters weight and bias are tuned at each epoch in order to minimize loss function during training process. The idea of neural networks models is based on construction of a loss function optimization problem from a directly solving PDE problem.

Problem Formulation

For understanding the nature of PINNs adopted from [7] and its practical application we consider the one dimensional advection diffusion equation. The PDE of this type is used to model many physical phenomena like transfer of water through soil, Pollutant transport in air, transport of heat and humidity in coastal areas.

The general form of 1D Diffusion equation [10] addressed in this paper is given by:

$$\partial_t u + a \nabla u - \mu \Delta u = f \quad \text{in } \Omega \times (0, T) \quad (1.1)$$

$$u = 0 \quad \text{on } \partial \Omega \times (0, T) \quad (1.2)$$

$$u(0) = u_0 \quad \text{on } \Omega \quad (1.3)$$

Where a is the advection velocity field, $\mu > 0$ is the diffusion coefficient, f is the source term and u_0 is the initial data.

The neural network approximation acts as a surrogate of true solution of PDE is given by:

$$u_\theta(t, x) \approx u(t, x)$$

The NN approximation u_θ is differentiated with respect to space and time variables. The residual of PDE is of the form:

$$r_\theta = \partial_t u_\theta + a \cdot \nabla u_\theta - \mu \Delta u_\theta - f$$

Loss Function

Loss function is composed of terms representing mismatch between initial conditions, boundary conditions and residual of PDE at interior points. It is of the form:

$$\mathcal{L}(X) = \mathcal{L}_\theta^r(X^r) + \mathcal{L}_\theta^0(X^0) + \mathcal{L}_\theta^b(X^b), \quad (2)$$

Where $\mathcal{L}_\theta^r(X^r)$, $\mathcal{L}_\theta^0(X^0)$ and $\mathcal{L}_\theta^b(X^b)$ are terms represents loss of residual, initial and boundary conditions and X represents collection of training data consisting of entirely time and space variables. The initial conditions, boundary conditions and physical dynamics of PDE is embedded into loss function which is measure of the extent to which NN based approximation is correct and is defined as a mean squared error . The mean square of residual is:

$$\mathcal{L}_\theta^r(X^r) = \frac{1}{Nr} \sum_{i=1}^{Nr} (r_\theta(t_i^r, x_i^r))^2 \quad (3.1)$$

The initial and boundary mean squared misfit is given by:

$$\mathcal{L}_\theta^0(X^0) = \frac{1}{N0} \sum_{i=1}^{N0} (u_\theta(t_i^0, x_i^0) - u_0(x_i^0))^2 \quad (3.2)$$

$$\mathcal{L}_\theta^b(X^b) = \frac{1}{Nb} \sum_{i=1}^{Nb} (u_\theta(t_i^b, x_i^b) - u_b(t_i^b, x_i^b))^2 \quad (3.3)$$

Where Nr , $N0$ and Nb are sets of collocation, initial and boundary points respectively.

NUMERICAL RESULTS

In this section, we employ the above explained method (1.1) to solve one dimensional Advection- diffusion equation. The purpose is to confirm theoretical result and to quantify accuracy of our method, results are compared with the exact solution of the PDE.

Advection Diffusion Equation

Test Problem 1: Consider the one dimensional advection diffusion equation as given in [10].

$$\partial_t u + a \partial_x u - \mu \partial_{xx} u = 0 \quad \text{in } (0, 1) \times (0, T), \quad (4.1)$$

with initial conditions:

$$u(x, 0) = \exp(x) \quad \text{on } (0, 1), \quad (4.2)$$

And boundary conditions:

$$u(0, t) = \exp((\mu - a) t), \quad (4.3a)$$

$$u(1, t) = \exp(1 + (\mu - a) t) \quad \text{on } (0, T). \quad (4.3b)$$

We selected the velocity field $a = 1$, the diffusion coefficient $\mu = 1$, time $T = 0.1$ and the source term f is considered zero. We apply the PINNs to solve the problem (4.1) with two point Dirichlet boundary condition (4.3a), (4.3b). The exact solution for this problem is given as:

$$\exp(x + (\mu - a)t).$$

We selected the nonlinear activation function *tanh* (hyperbolic tangent function) and gradient descent based optimizer *Adam* [11] which not only provide adaptive learning rate but is also essential to keep momentum.

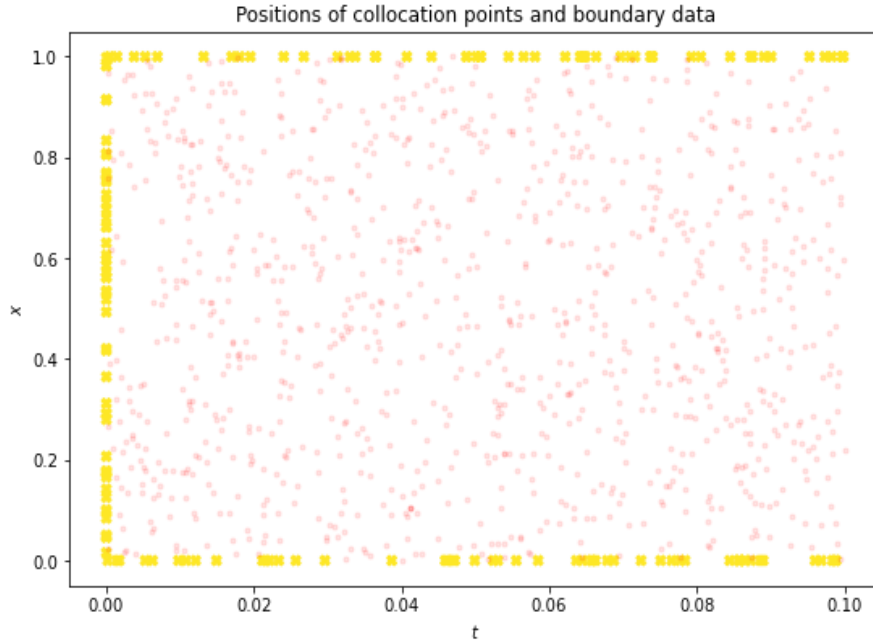


Figure 1: Randomly sampled collocation points (red circles) from interior of domain with initial and boundary data points (cross mark)

The training data for our model is composed of collocation points (interior domain 1000 samples) and boundary points (50 sample) with 50 initial data points as shown in Figure 1. For simplicity the training data points are randomly selected.

To examine the accuracy of predictive solution for our model, we set network structure with 8 hidden layers and 20 neurons (nodes) per hidden layer, a total of 3021 trainable parameters.

The learning rate for our test experiment was set as:

$$\delta(n) = 0.011_{\{a < 1000\}} + 0.0011_{\{1000 \leq a < 3000\}} + 0.00051_{\{3000 \leq n\}} \quad (5)$$

The L_{∞} norm for above test problem is given by:

$$L_{\infty} = \max |U_{approx} - U_{exact}| \quad (6)$$

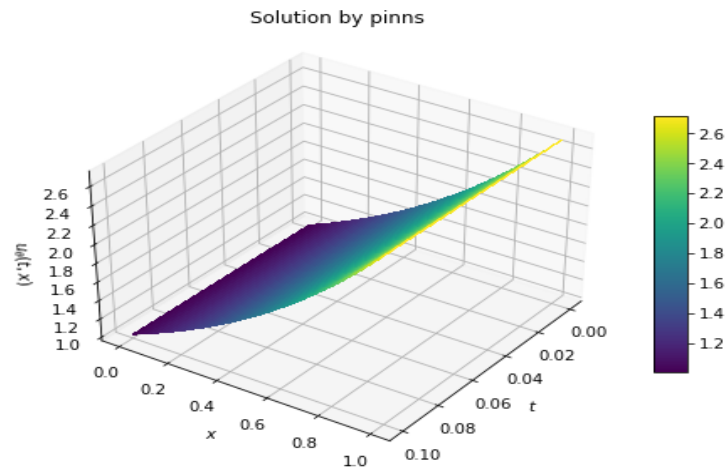


Figure 2 (a): The PINN based approximation of our test problem1 using 5000 training epochs

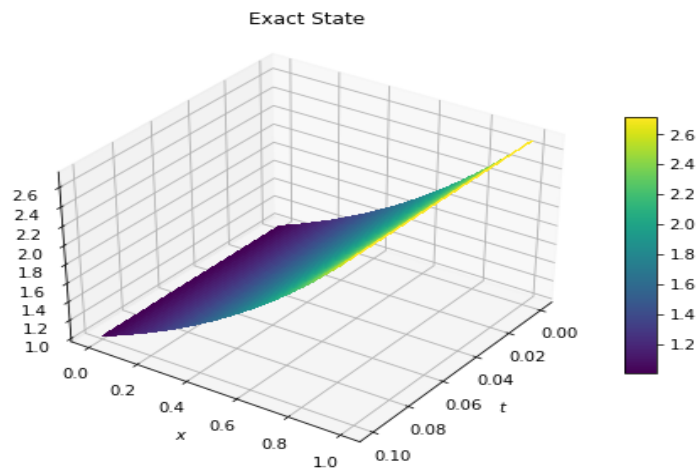


Figure 2 (b): The exact solution of our test problem 1

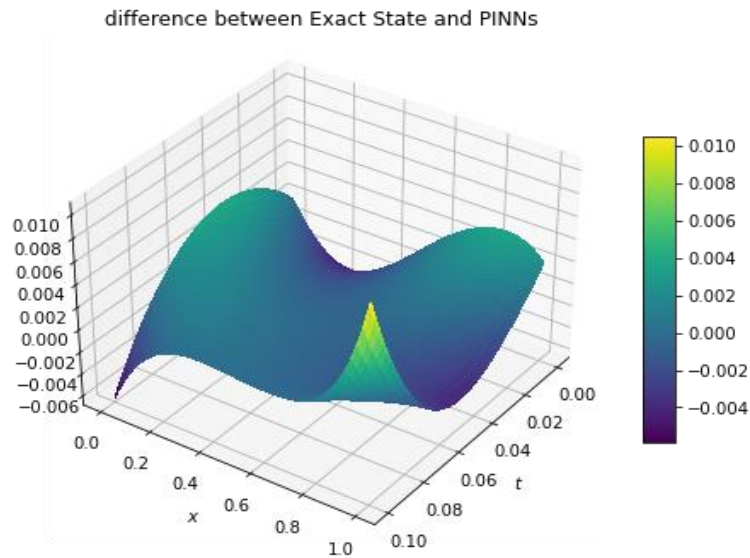


Figure 3 (c): Difference between PINN based approximation and exact solution

It can be seen from above figure 2 (a, b, c) that PINNs approximation is in good agreement with that of exact solution and the difference between PINNs approximation and exact solution lies in interval $[-0.004, 0.004]$ units and in difference plot a negligible region touches the boundary of interval.

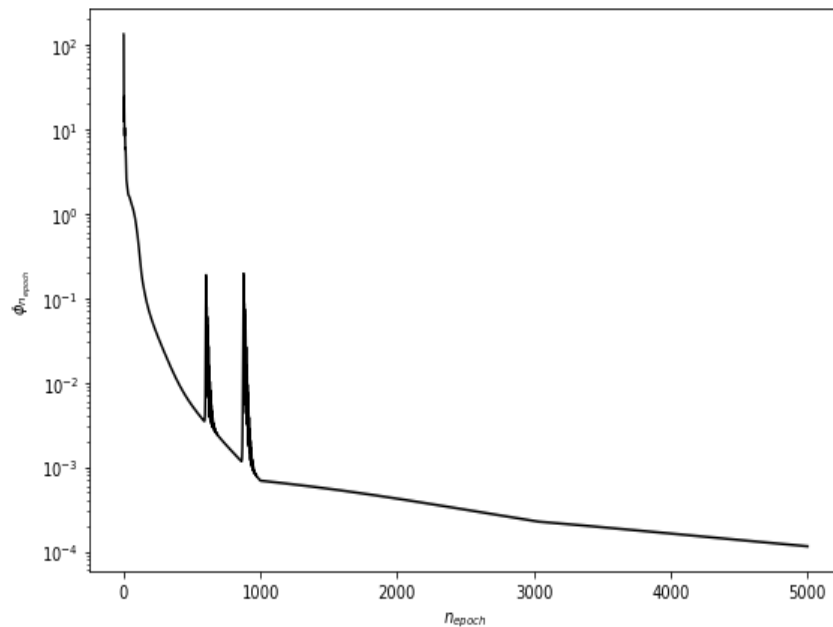


Figure 3 The evolution of loss vs number of training epochs

From figure 3 it can be seen that the values of loss varies with changing the number of iterations. Increasing number of training epochs causes drop in the value of loss function and hence improves the accuracy.

PINNs offer an impressive approximation when number of training epochs increase as it results in small values of loss, also by increasing number of epochs their occur an increase in computational time. For piecewise constant learning rate as defined by equation (5) the results for our test problem 1 can be seen in Table 1.

Table 1: Comparison of loss function, computational time and L_∞ for changing number of training epochs. No. of layers=8, neurons=20.

| No. of epochs | Loss | L_∞ | MSE | Computation time(sec) |
|---------------|-------------|------------|------------|-----------------------|
| 1000 | 2.6932e-03 | 4.92 e-02 | 1.860e-05 | 12.4962 |
| 2000 | 7.2322 e-04 | 2.53 e-02 | 4.726e-06 | 19.8869 |
| 3000 | 3.9774 e-04 | 1.44 e-02 | 3.678 e-06 | 28.5543 |
| 4000 | 1.4285 e-04 | 5.41 e-03 | 2.140 e-06 | 37.1635 |
| 5000 | 9.5040 e-05 | 5.63 e-03 | 2.784 e-07 | 46.2749 |

Changing the neural network structure also have influence on the L_∞ values. The reduced number of neurons and hidden layers reduce computational cost but causes an increase in L_∞ values. For our test problem 1 it can be seen from table2.

Table 2: Comparison of loss function, computational time and L_∞ for No.of layers=6, neurons=12

| No. of epochs | Loss | L_∞ | MSE | Computation time(sec) |
|---------------|-------------|------------|-------------|-----------------------|
| 1000 | 2.4253 e-03 | 4.88 e-02 | 1.6313 e-06 | 7.94477 |
| 2000 | 3.4973 e-04 | 1.41 e-02 | 3.050 e-06 | 11.9069 |
| 3000 | 6.2924 e-04 | 1.67 e-02 | 1.862 e-06 | 16.7502 |
| 4000 | 1.1393 e-04 | 6.10 e-03 | 1.442 e-06 | 19.8612 |
| 5000 | 9.2633 e-05 | 5.63 e-03 | 1.090 e-06 | 24.0271 |

CONCLUSION

A Physics Informed Neural Network model based on Machine learning technique is used for the numerical solution of PDEs. To see practical applications of our model, we considered one dimensional advection diffusion equation with changing neural network structures. Relation between the accuracy of approximation (the mean squared error, and loss function) and number of iterations is established. Results demonstrate that changing the network structure also influences the performance of model up to some

extent. It is investigated that for an appropriate network structure, PINN offers an impressive approximations and predictive performance.

REFERENCES

- [1] Lee H. and. Kang I.S. (1990). Neural algorithm for solving differential equations. J. Comp. Phy, 91, 110-131.
- [2] Lagaris I. E., Likas A., and Fotiadis D.I. (1998). Artificial neural networks for solving ordinary and partial differential equations. .. IEEE Trans. Neur. Net., 9, 987-1000.
- [3] Göküzüm F. S. khiem Nguyen L. T. and Marc-Andre Keip. (2019). An artificial neural network based solution scheme for Periodic computational homogenization of electrostatic problems, 24, 40.
- [4] Jagtapa A. D. Kawaguchib K. and EmKarniadakis G. (2020) Adaptive activation functions accelerate convergence in deep and physics-informed neural networks. J. comput. Phy., 404, 109-136.
- [5] Raissi M. Perdikaris P. and Karniadakis G. E. (2019). Physics-informed neural networks: A deep learning framework for solving forward and inverse problems involving nonlinear partial differential equations. J. Compt. Phy, 378, 686-707.
- [6] Raissi M. Perdikaris P. and Karniadakis G. E. (2018). Numerical Gaussian Processes for Time-dependent and Non-linear Partial Differential Equations. SIAM J. Sci Comput., 40, 172-198. Raissi M. Perdikaris P. and Karniadakis G. E. (2017). Physics Informed Deep Learning (Part I): Data-driven solutions of nonlinear partial differential equations. arXiv: 1711.10561.
- [7] Raissi M. Perdikaris P. and Karniadakis G. E. (2017). Physics Informed Deep Learning (Part II): Data-driven discovery of nonlinear partial differential equations. arXiv: 1711.10566.
- [8] Baydin A. G. et al. (2018) Automatic differentiation in machine learning: A survey. J. Mach Learn. Res., 18, 1-43.
- [9] Chacon Rebollo T. Fernandez-Garcia S. Moreno-Lopez D. and Sanchez Munoz I. (2023). Spectral multi-scale method for parabolic problems: application to 1D transient advection diffusion equations. Comput. Appl. Math, 42, 1-27.
- [10] Kingma D. P. and Adam j. Ba. (2017). A method for stochastic Optimization. arXiv: 1412.6980.

Paper ID: ICSET-2332

FREQUENCY CONTROL OF MICRO GRID THROUGH WIND POWER AND ELECTRIC VEHICLES

Rehmat Hadi^{1,*}, Kaleem Ullah², Sanam Ijaz³ Shayan Khan⁴

¹*Renewable Energy Engineering, US-Pakistan Center for Advanced Studies in Energy, University of Engineering and Technology Peshawar, Pakistan*

²*Electrical Energy System Engineering, US-Pakistan Center for Advanced Studies in Energy, University of Engineering and Technology Peshawar, Pakistan*

³*Electrical Engineering, UET Peshawar, Peshawar, Pakistan*

⁴*Electrical Engineering, CECOS University of IT & Emerging Sciences, Peshawar, Pakistan*

**Corresponding author*

Email: engrrehmathadi@gmail.com

ABSTRACT

In the last decade, traditional fossil fuel power plants have been replaced by micro-scale systems powered by distributed generation units. Micro grids consist of distributed generating units and loads that are located in various locations. Micro grids are capable of operating either connected to the foremost grid or independently. The micro grid's frequency is regulated by the main grid when they are connected, which makes the micro grid resistant to vulnerabilities. Nevertheless, when operating independently, the grid's frequency is not regulated by any external source, making it highly vulnerable to fluctuations caused by the discontinuous nature of renewable energy sources. In the past, traditional methods relied on backup power from sources such as diesel generators to meet energy needs during periods of intermittent supply. The current power system emphasizes the significant rise in wind power and electric vehicle adoption, which is expected to replace traditional power plants and have a positive impact on the environment. The objective of this research is to create a control system for a micro grid that can incorporate backup power from wind turbines and electric vehicles, as well as traditional power sources, in order to manage the frequency of the micro grid when operating independently. When these energy sources are added to a micro grid, it can lead to a mismatch in power between what is available and what is needed. If there are any interruptions, the wind power plant and electric vehicles will step in to help keep the micro grid frequency stable. The integration of wind energy, electric vehicles, and traditional energy sources in micro grids will reduce power imbalances, thereby improving the security and reliability of micro grid operations. Moreover, it will lower the operating expenses of the system by enabling traditional generators to operate at their minimum capacity and requiring less reserve for active power balancing services.

KEYWORDS: Micro grid, Electric Vehicles, Primary Control, Wind Energy, Active Power Balance

INTRODUCTION

The increasing use of renewable energy sources is making it difficult to maintain the steadfastness and retreat of the power grid. The problems exacerbate when the micro grid is operating in stand-alone mode. To ensure a continuous supply of electricity, a micro grid is made up of various energy sources, energy



storage systems, and connected loads. These components are linked to the distribution level of the main power system network at a single point called the point of common coupling (PCC). The dependability and security of the micro grid are directly linked to the frequency, which is unstable because of the variability of renewable energy sources [1]. It is important to pay close attention to the fluctuations in wind and solar production, as they can lead to significant changes in frequency and power [2,3]. These fluctuations are particularly crucial here. Traditional generating units like diesel and gas turbines have reserves installed to make up for any deficit in power and maintain a stable operating frequency. This process increases operating costs and has an adverse impact on the environment. Studies have been conducted in the literature to tackle these challenges.

As the demand for standalone wind technology applications continues to grow, we are conducting a thorough investigation to choose the most suitable generator for a stand-alone wind energy control system (WECS). The article [4] thoroughly compares synchronous and asynchronous generators for their suitability in wind farms. An important advantage of asynchronous machines is their ability to vary their speed, allowing them to maximize wind energy conversion system (WECS) power and minimize torque fluctuations [5]. A wind turbine generator (WTG) is the most practical alternative to an induction generator for off-grid applications because it has a lower unit cost, built-in resilience, and is easy to use [6]. In order for the induction generator to achieve distant excitation, it necessitates capacitor banks. The self-excited induction generator (SEIG) excitation phenomena are addressed in references [7] to [9]. The SEIG requires the irregular wind flow in order to produce power. Wind speed has an impact on the frequency and amplitude of the SEIG voltage. The load end may experience flicker and instability when unpredictable voltage fluctuations are interfaced with the load directly. To maintain a stable load voltage, power electronic converters incorporate the wind energy conversion system (WECS) with the load [10]. Once again, the sporadic nature of wind energy makes it necessary to have an energy storage system in a WECS [11]. References [12] and [13] conducted a study on storage options for wind energy utilization. [14] covers the benefits of using battery energy storage for a standalone Wind Energy Conversion System (WECS). From a technical perspective, there are significant limitations to integrating renewable energy sources into the electric power grid. Solar and wind, the two main sources of renewable energy, are greatly influenced by the weather. The unpredictability of these resources fundamentally changes the way power is generated. Renewable energy sources have two important characteristics: intermittent availability, such as solar generation at night, and volatility, with constant fluctuations in wind generation depending on wind speed and availability, and solar generation changing with cloud cover. In the past, system designers have seen backup generation as a way to reduce generation variability and help integrate renewable energy sources more effectively. Some examples of rapid-response backup generation systems that often provide a swift reaction to changes in generation are hydro units, gas units, demand management, and energy storage systems. In these circumstances, the backup generation installation may not realize its full value because it is often used primarily to coordinate renewable generation. The deployment's economic sustainability is a growing concern as its cost will be added to the already high capital cost of the renewable energy resource. The main point is that due to the variable nature of these supplies, they cannot fully compensate for a disruption in the utility grid's electricity production. The use of a micro grid can serve as a replacement for backup generation, all the while maintaining reliability. When both of these factors are taken into account together, the following statement is accurate [14].

In [12], a comprehensive investigation is conducted on the design and functioning of a stand-alone micro grid that incorporates distributed solar power generation, battery energy storage systems, and a conventional diesel power plant. MPPT techniques have been utilized and a peak detection control scheme has been put in place to regulate energy from the distributed sources. In [11], the discussion focuses on the two-step



process for designing the best hybrid standalone micro grid with renewable energy sources. The initial step involves creating a linear programming model, followed by evaluating the system's reliability in the next step. The book [15] delves into the dynamics of grid-connected and standalone micro grids.

When discussing micro grids, it involves the distribution of power generation and the integration of sustainable sources. The challenges of maintaining standard voltage and frequency arise when managing decentralized generation and integrating renewable resources in a self-sufficient, non-grid-connected scenario. This occurs because the supply and demand fluctuate due to the irregularity of renewable sources. In this scenario, the micro grid takes on the task of controlling the voltage and frequency of the system. Different methods have been explored and implemented to regulate the voltage and frequency at the independent micro grid level. In [16], a study investigates a potential solution for regulating voltage and frequency in micro grids. The research article discusses the implementation of voltage and current feedback loops in the micro grid converter to help stabilize voltage and frequency. A proportional-integral (PI) controller is used in practical application. The article delves into the application of sliding mode non-integral control in the regulation of frequency in modern micro grids. The Sin Cosine algorithm, referred to as SCA, is utilized for the establishment of the controller. The study comes to a close with the completion of experiments. The method introduced in article [8] uses Proton Exchange Membrane (PEM) fuel cells, fuzzy logic control, and adaptive control techniques to regulate voltage and frequency. The objective of the research is to integrate PEM with inverters to transform direct current into alternating current voltage. The examination of regulating frequency to increase the autonomy of the micro grid is discussed in [14-16], specifically focusing on secondary frequency control in the islanded micro grid. This process entails carefully lowering the reference frequency set point of the network by decreasing demand when there is a mismatch between supply and demand. In a standalone micro grid with a high penetration of renewable resources, [10] explores the concept of frequency decoupling. The article details the addition of a control loop for frequency recovery to inertia and droop control loops in order to stabilize the frequency at its nominal value. Reference [11] provides detailed information on how the battery energy storage system (BESS) regulates the frequency of the micro grid. The research paper delves into the incorporation of Battery Energy Storage Compound (BESC) into autonomous micro grids to balance active power and stabilize frequency. Another method for achieving frequency regulation is through demand response (DR), as mentioned in [17]. This paper achieves two primary goals. Initially, it identifies the mode of the micro grid, establishing if it is operating in a connected to the grid or independent mode. After confirming that the micro grid is operating independently, the next step is to implement Demand Response (DR) to ensure that the micro grid maintains its normal frequency.

The extensive discussion in [17] addresses the regulation of frequency by considering communication delays and utilizing virtual inertia. The research article explains that when frequency fluctuations happen in the micro grid, the information is sent to the micro grid control center. However, communication delays prevent the micro grid from restoring the system's frequency to its predefined limits. Ultra-capacitors are installed to incorporate the concept of virtual inertia. The study in [17] investigates the effective control of frequency in a standalone AC/DC micro grid. This article utilizes a control technique based on fuzzy logic.

MODELING OF THE MICRO GRID

MATLAB SIMULINK is used to simulate the MG in question. This design is intended for a community with 1000 residential households as well as industrial and resistive loads. The sources incorporated in the system consist of Solar PV, wind energy, and a gas power plant that operates as a base-load provider. These sources and their load ratings are detailed in Table 1. The renewable resources in this

micro grid are not always available, which can cause fluctuations in the power system's frequency when there is more demand for power than supply.

This study will explore how to incorporate a wind power plant and Electric Vehicles (EVs) into the MG to serve as reserves for meeting increased active power needs. Electric vehicles (EVs) are designed to serve as both a source and a load. They act as a source through the vehicle-to-grid (V2G) topology and as a load through the grid-to-vehicle (G2V) topology. The SIMULINK (MATLAB) model representing the proposed MG is shown in Figure 1.

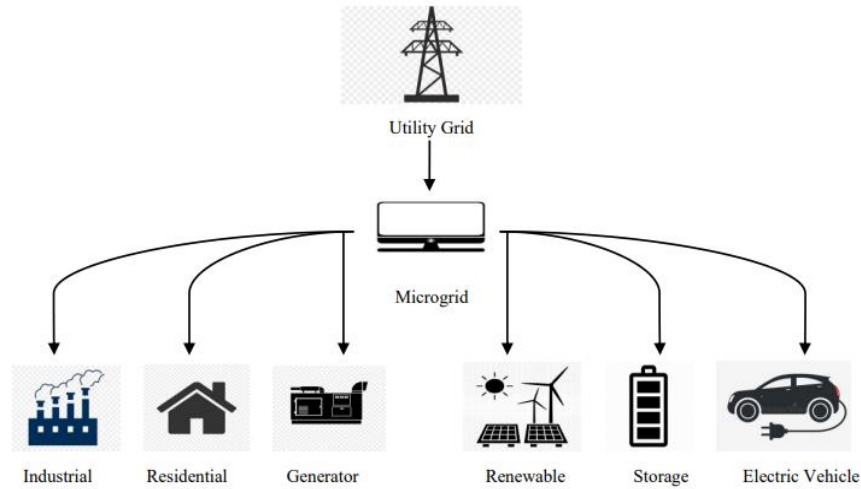


Figure 1: Complete Micro Grid of Proposed Model

Solar Photovoltaic Farm

Due to its abundant availability and easy installation, solar PV is often the top choice among renewable resources. When calculating solar power, important considerations include solar irradiance and temperature. One can use Equation (1) to calculate the solar PV's output power.

$$S_p = \phi \times S \times \xi (1 - 0.005(T_A - 25)) \quad (1)$$

The effectiveness of the solar panel is denoted by ϕ , usually varying between 9% and 12%. S is the effective covered area in square meters, with ξ representing the solar irradiance at 1 Kw/m², and T_A standing for the ambient temperature set at 25 °C. In the proposed framework, solar energy is converted into apparent power according to equation (2). Equation (3) subsequently defines the DC voltages, which are then used to calculate the DC currents based on apparent power. The current-controlled voltage sources receive DC currents in a three-phase setup to directly produce three-phase power for the MG. In Figure 2, the solar irradiance graph is depicted, while Figure 3 shows the 24-hour wind profile.

$$S = \frac{3}{2} (V \times I^*) \quad (2)$$

$$V_1 = \frac{1}{3} (V_{ab} - a^2 \times V_{bc}) \quad (3)$$

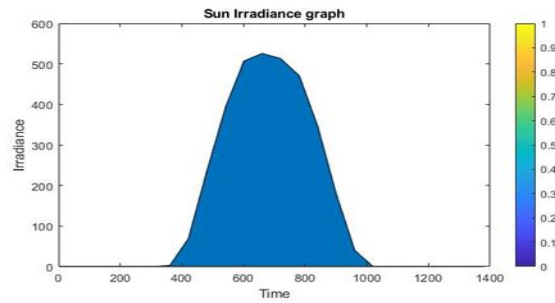


Figure 2: Photovoltaic Irradiance

Gas Generator

In the suggested MG, the Gas generator serves as the primary power provider. It's crucial to maintain some inertia within our power system and not solely depend on renewable resources, which tend to be intermittent. Gas, in contrast to other traditional sources, has a comparatively lower impact on the environment. The SIMULINK model created for this purpose has a power-producing capacity rated at 15MW. As a device generating power according to demand, it plays a role in stabilizing the system frequency when disturbances occur.

Load Across Microgrid

The load linked to the proposed MG comprises residential, industrial, and entirely resistive elements rated at 10MW, 5MW, and 5MW, respectively. Residential demand fluctuates throughout the day, varying with time, as illustrated in Figure 4, displaying the residential load profile over a 24-hour period. Industrial consumption is time-specific, aligned with the industry's designated schedules. A significant portion of our load comprises pure resistance, with a 5MW resistive load integrated into the MG. Industrial equipment demands a substantial amount of reactive power. Residential loads exhibit a mixed nature, involving resistive, capacitive, and inductive elements.

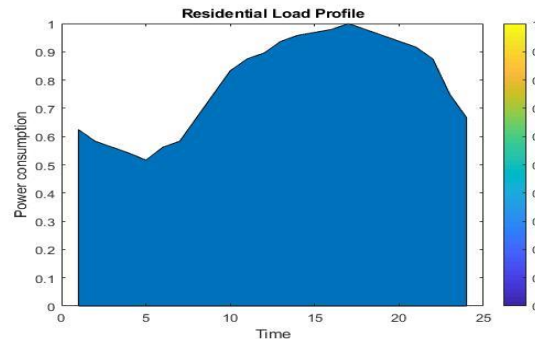


Figure 3: Domestic Load Representation

Wind Power Plant

Wind stands as one of the most viable renewable energy sources, abundantly available in nature. However, its power output from turbines fluctuates due to variations in its nature. Consequently, wind turbines can only generate usable electrical power when wind speed falls within a specific range. Our designed wind turbine boasts a 4MW output power, operating within a wind speed range of 13.5m/s to 15m/s. This wind

power plant serves as both support and reserve, contributing to frequency regulation. The wind profile is depicted in Figure 3, illustrating the power output, which is calculated through equations (4) and (5). Using these equations, power generated by the wind SIMULINK model is integrated into the MG.

$$P_{wind} = P_{mech} \quad (4)$$

$$P_{mech} = \frac{1}{2} (C_p \times (\lambda, \beta) \times A \times \rho_a \times V^3) \quad (5)$$

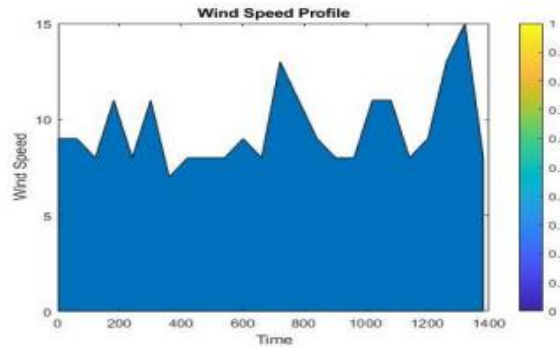


Figure 4: Wind Speed Graphical Representation

Electric Vehicles

Electric vehicles (EVs) are incorporated into the envisioned MG as a versatile load, capable of functioning both as an active power source and a load as per the necessity. When the system frequency drops below the preset nominal value, EVs with ample charge storage switch to a regulatory mode, acting as a source through V2G topology. They cater to the active power demand, thereby restoring the frequency. Conversely, when renewable energy generation exceeds the load, causing the frequency to rise, the EVs are placed on charge mode via the controller. This action, utilizing the G2V topology, consumes the surplus active power, maintaining the rated frequency. 100 EVs into the MG, assuming one EV among every 10 households in a design catering to 1000 households. These 100 EVs are divided into five groups, accounting for the owners' daily routines. Here table 1 displays the EV specifications.

Table 1: Electric Vehicles specification

| ELECTRIC VEHICLES SPECIFICATIONS | |
|---|--------------------|
| Nominal power of single Electric Vehicles | 45 Kilo watt |
| Nominal Power of system | 90 Kilo watt Hours |
| System Efficiency | 92 percent |

Micro Grid Control Algorithm

The control algorithm defines the operational characteristics of any system, responding to real-time system operator requirements and predefined conditions. In the proposed MG, the primary constraints are the system frequency and various generation capacities (solar, wind, V2G, and gas generation). When generation matches demand, the system frequency aligns with the predetermined nominal value. In cases where renewable resources fail to meet load demand due to their intermittent nature, the MG experiences



fluctuations in frequency and voltage. To regulate the frequency, the paper titled "Frequency control of micro grid through wind power and Electric vehicles" introduces a method involving active power balancing between supply and load using Wind power and EVs while Electric vehicles through V2G topology. Conversely, when the system frequency exceeds the nominal value, EVs are linked to the MG to absorb extra power and restore the frequency to its set value through G2V topology. If, during V2G operation, the BESS of EVs lacks reserve power, the MG implements load shedding in certain areas, as determined by ΔP in equation 9. Similarly, in G2V operation, when the BESS of EVs lacks the capacity to draw additional power, the gas generation power plant is adjusted to a lower operating point using governor control. For the proper functioning of the MG, certain conditions must be met

$$P_G = P_L \quad (6)$$

$$P_G - P_L = 0 \quad (7)$$

$$P_G \neq P_L \quad (8)$$

$$P_G - P_L = \pm \Delta P \quad (9)$$

RESULT AND DISCUSSION

Following the 24-hour simulation of the proposed MG in SIMULINK/MATLAB, the results were obtained. To validate these findings, three distinct events were generated within the 24-hour span, coinciding with instances of frequency dropping below its nominal value. These events occurred as follows:

1. Initiation of the industrial load's connection to the MG.
2. Occurrence of partial shading on the solar panels at noon, lasting for 300 seconds.
3. Shutdown of the wind turbine at 10:00 pm due to wind speed surpassing the acceptable range.

During these events, the MG's frequency experienced a decline, prompting the EVs to enact an initial response to regulate the frequency. Figure 5 illustrates the generations and loads over the 24-hour period. Each specific event is detailed in figures 6, 7, and 8, corresponding to event 01, event 02, and event 03, respectively. Furthermore, the combined generation graph in figure 6 reveals that as renewable resource generation increases, the gas generator decreases its output, prioritizing the renewables to supply the load.

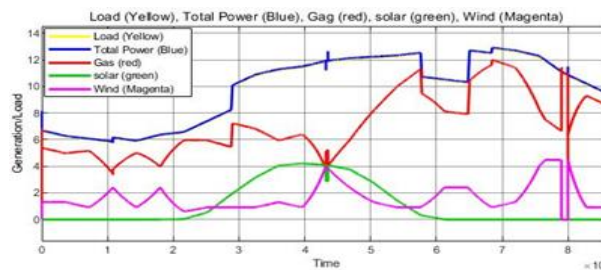


Figure 5: MG Generation/Load profile for 24 hours

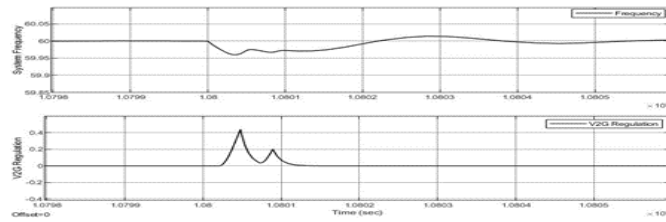


Figure 6: Event 01(The oscillation and control of frequency)

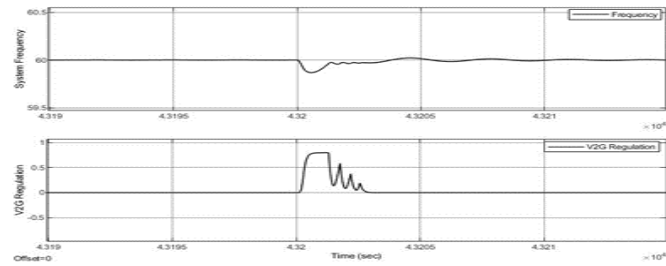


Figure 7: Event 02(The oscillation and control of frequency)

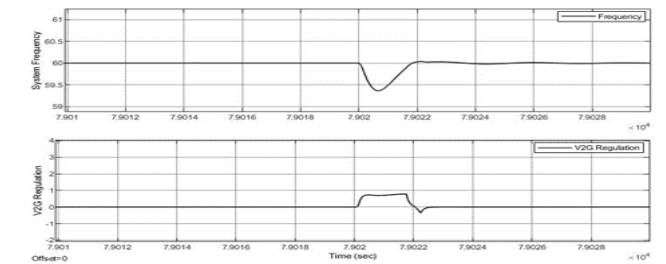


Figure 8: Event 03(The oscillation and control of frequency)

Figures 5 to 8 distinctly illustrate that when frequency fluctuations occur due to heightened demand for active power surpassing generation capacity, EVs play a crucial role in supporting this demand and stabilizing the frequency back to its nominal value. Event 01, event 02, and event 03 are explicitly presented in figures 7, 8, and 9, respectively. In figure 06 above, it's evident that the gas power plant's power generation behaves in contrast to wind power generation, prioritizing renewable sources to supply the load.

CONCLUSION

The study highlights a stand-alone micro grid (MG) that incorporates solar and wind energy sources, in addition to a traditional gas power plant acting as a steady provider with the ability to manage unexpected situations, particularly those stemming from industrial power needs. Solar and wind power, as sustainable sources, align with the demand based on their specific generation patterns. Wind power is especially useful as a backup power source to help keep the frequency stable. When the frequency deviates from its nominal value, it triggers events. The elements can either regulate or charge, depending on the frequency deviations seen in the simulation results. During times of fluctuating frequency, wind power and electric vehicles serve as the primary response mechanism. In the future, improving the EV charge controller with extra data constraints is expected to increase efficiency in integrating EVs with the MG, leading to better overall results.



REFERENCES

- [1] Ullah, K.; Basit, A.; Ullah, Z.; Albogamy, F.R.; Hafeez, G. Automatic Generation Control in Modern Power Systems with Wind Power and Electric Vehicles. *Energies* 2022, 15, 1771. <https://doi.org/10.3390/en15051771>
- [2] R.D. Richardson and G. M. Mcnerney, “Wind energy systems,” *Proc. IEEE*, vol. 81, no. 3, pp. 378–389, Mar. 1993.
- [3] R. Saidur, M.R. Islam, N.A. Rahim, and K.H. Solangi, “A review on global wind energy policy,” *Renewable Sustainable Energy Rev.*, vol. 14, no. 7, pp. 1744–1762, Sep. 2010
- [4] M.T. Ameli, S. Moslehpur, and A. Mirzale, “Feasibility study for replacing asynchronous generators with synchronous generators in wind farm power stations,” *Proc. IAJC – IJME, Int. Conf. Eng. Technol.*, Music City Sheraton, Nashville, TN, US, ENT paper 129Nov. 17–19, 2008.
- [5] G.K. Singh, “Self excited generator research — A survey,” *Electric Power Syst. Res.*, vol. 69, no. 2/3, pp. 107–114, 2004.
- [6] R.C. Bansal, “Three-phase self-excited induction generators: An overview,” *IEEE Trans. Energy Convers.*, vol. 20, no. 2, pp. 292–299, Jun. 2005.
- [7] S.C. Tripathy, M. Kalantar, and N.D. Rao, “Wind turbine driven self-excited induction generator,” *Energy Convers. Manag.*, vol. 34, no. 8, pp. 641–648, 1993.
- [8] A. Chakraborty, “Advancements in power electronics and drives in interface with growing renewable energy resources,” *Renewable Sustainable Energy Rev.*, vol. 15, no. 4, pp. 1816 – 1827, May 2011.
- [9] F. D. Gonz´alez, A. Sumper, O. G. Bellmunt, and R. V. Robles, “A review of energy storage technologies for wind power applications,” *Renewable Sustainable Energy Rev.*, vol. 16, no. 4, pp. 2154–2171, May 2012.
- [10] N.S. Hasan, M.Y. Hassan, M.S. Majid, and H.A. Rahman, “Review of storage schemes for wind energy systems,” *Renewable Sustainable Energy Rev.*, vol. 21, pp. 237–247, May 2013.
- [11] A. M. D. Broe, S. Drouilhet, and V. Gevorgian, “A peak power tracker for small wind turbines in battery charging applications,” *IEEE Trans. Energy Convers.*, vol. 14, no. 4, pp. 1630–1635, Dec. 1999.
- [12] R. Kot, M. Rolak, and M. Malinowski, “Comparison of maximum peak power tracking algorithms for a small wind turbine,” *Math. Comput. Simul.*, vol. 91, pp. 29–40, 2013.
- [13] M. Narayana, G.A. Putrus, M. Jovanovic, P.S. Leung, and S. McDonald, “Generic maximum power point tracking controller for small-scale wind turbines,” *Renewable Energy*, vol. 44, pp. 72–79, Aug. 2012.
- [14] A. Khodaei, “Provisional Microgrid Planning,” *IEEE Transactions on Smart Grid*, vol. 8, no. 3, May 2017, pp. 1096–1104
- [15] H. Bevrani, M. R. Feizi, and S. Ataei, “Robust Frequency Control in an Islanded Microgrid: H_∞ and μ -Synthesis Approaches,” *IEEE Trans. Smart Grid*, vol. 7, no. 2, pp. 706–717, 2016, doi: 10.1109/TSG.2015.2446984.
- [16] S. Vazquez, S. Lukic, E. Galvan, L. G. Franquelo, J. M. Carrasco, and J. I. Leon, “Recent advances on energy storage systems,” *IECON Proc. (Industrial Electron. Conf.)*, pp. 4636–4640, 2011, doi: 10.1109/IECON.2011.6120075.



ICSET-23

*Proceedings of the 5th International Conference on Sustainable
Energy Technologies (ICSET 2023) Peshawar, Pakistan
14-15 December 2023*



UET Peshawar

- [17] D. Xu, J. Liu, X. G. Yan, and W. Yan, "A Novel Adaptive Neural Network Constrained Control for a Multi-Area Interconnected Power System with Hybrid Energy Storage," *IEEE Trans. Ind. Electron.*, vol. 65, no. 8, pp. 6625–6634, 2018, doi: 10.1109/TIE.2017.2767544.

Paper ID: ICSET-2333

SYNTHESIS OF GOLD NANOPARTICLES FOR SOLAR CELL APPLICATIONS

Zulfiqar Ali Ramzan^{1,*}, Adnan Daud Khan¹, Fahad Ullah Zafar¹, Sania Naseer², Qandeel Rehman¹,
Muhammad Saad Rehan¹

¹US-Pakistan Center for Advanced Studies in Energy, University of Engineering and Technology Peshawar,
Pakistan

²Mirpur University of Science and Technology, Mirpur, Azad Kashmir, Pakistan

**Corresponding author*

Email: zulfiqarramzan.ree@uetpeshawar.edu.pk

ABSTRACT

Gold nanoparticles (AuNP) are small gold particles with sizes ranging in nanometers (nm). The introduction of gold nanoparticles in solar cell applications is due to their electrical and optical properties. In this regard, synthesizing gold nanoparticles can be carried out using chemical or biological methods, with most commonly used being the chemical method. To this point, Turkevitch method of using citrate reduction is used to chemically synthesize gold nanoparticles. In this study, precursor solution (HAuCl₄) was synthesized in the laboratory using Turkevitch method with slight modifications. The precursor was characterized using UV-vis spectrophotometer resulting in absorption at 226 nm and 313 nm wavelengths, thus confirming to 0.1 M concentration of HAuCl₄. Secondly, the precursor was then used to synthesize different sizes of gold nanoparticles using citrate reduction method. Two different synthesized solutions were prepared and characterized for their absorption versus wavelength that falls between 520 nm and 580nm. Also, Zeta sizer was used to determine sizes of different prepared gold nanoparticles resulting in sizes ranging from 37 nm to 106 nm. The synthesized gold nanoparticles can be used for different applications including solar cell.

KEYWORDS: AuNP sizes, Gold Nanoparticles, HAuCl₄, UV-Vis, Zetasizer

INTRODUCTION

Gold nanoparticles (AuNPs) are a type of nanomaterial that has been used for decades due to their stability, non-toxicity, and ease of synthesis. They have unique optical and electrical properties that can be controlled by tuning their size and shape [1]. In addition, nanoparticles properties can be tuned due to a change in their size or shape. For instance, the surface area of these nanoparticles to their volume ratio shows an increase when its particle size decreases [2]. This can result in optical characteristics of distinct nature as well as their reactivity is improved.

The synthesis of gold nanoparticles takes place when a precursor for gold nanoparticles is prepared. This precursor can be prepared using wet-chemistry method. Although different techniques have been used for synthesizing gold chloride, chlorine based process [3] has shown best results with no signs of degradation for a couple of months when placed at room temperature. Synthesis of gold nanoparticles has been carried out through different precursors. For instance Au(NO₃)₃ precursor [4] was prepared which



synthesized gold nanoparticles through ultrasonic spray pyrolysis. Moreover, synthesizing gold nanoparticles was also done using gold (I) halides such as gold chloride and gold bromide [5] and due to relatively lower stability of these halides, reducing agent for synthesizing was not used. In this experiment, gold nanoparticles were synthesised using gold (III) chloride, also called as Chloroauric acid.

The use of gold nanoparticles in solar photovoltaic (PV) is a promising area of research, as the properties of Localized Surface Plasmon Resonance (LSPR) of nanoparticles can increase the absorption of light, theoretically improving the photovoltaic performance of solar cells [6]. Gold nanoparticles show Surface Plasmon Resonance (SPR) phenomenon which occurs when light is absorbed and scattered at particular wavelengths due to the collective oscillations of free electrons on the surface of these nanoparticles as shown in **figure 1**. Depending on their shapes and sizes, this results in giving gold nanoparticles different colors from red to purple. Due to such properties, they are used in sensing, photo-thermal therapy, among other applications.

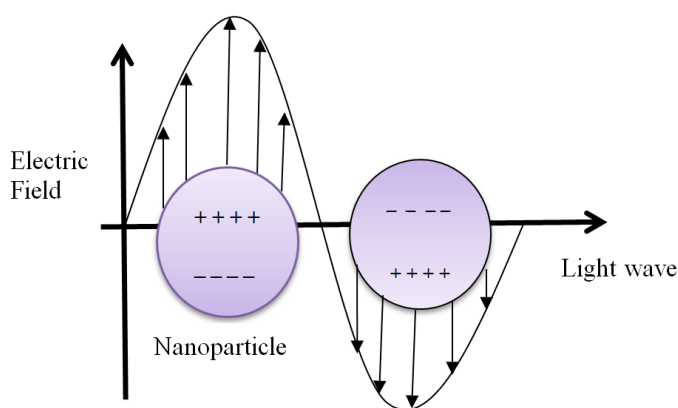


Figure 1: Surface Plasmon Resonance phenomenon in gold nanoparticles

In this research, a precursor solution (HAuCl_4) was prepared in the laboratory and tested using a UV-vis spectrophotometer for its concentration and absorption band. The prepared precursor was then used to synthesize different sizes of AuNPs, which were validated using UV-vis for absorption band and Zeta sizer for determining their sizes. Overall, gold nanoparticles have a wide range of potential applications in bio nanotechnology, medicine, and materials science due to their unique properties and ease of synthesis. The use of gold nanoparticles in solar PV is a promising area of research that could lead to improved efficiency and lower production costs [7].

MATERIALS AND METHODS

Materials

The following chemicals were used in the experiment: Potassium Permanganate (KMnO_4) (Sigma Aldrich, A.C.S, 99.9%), Hydrochloric acid (HCl) (Lab-Scan Analytical Sciences, 37% conc.), Gold foil (Au) (Alfa Aesar, 99.9%), Tri-sodium citrate ($\text{Na}_2\text{C}_6\text{H}_5\text{O}_7 \cdot 2\text{H}_2\text{O}$) (BDH Laboratory Supplies, A.C.S 99.9%), and Chloroauric acid (HAuCl_4) was synthesized at the CASE Material Synthesis Laboratory, UET Peshawar, Pakistan.

Synthesis of Gold Precursor Solution

The given procedure, as described by [8], was followed with slight modifications. To begin, 5.0 g KMnO_4 was added to a conical flask (flask 1). Next, 50 ml of 37% conc. HCl was poured into a burette using a funnel. After 20 ml of HCl was consumed, the temperature of the hotplate under flask 1 was set at 70°C . In a separate, dried conical flask (flask 2), 0.05 g gold foil was cut and placed. Then, 25 ml of 0.1 molar solution of HCl was added to flask 2, which was placed on a hotplate and magnetic stirrer device, with the temperature set at 50°C and stirrer speed at 130 rpm. After the gold dissolved completely and the precursor was formed in flask 2, it was transferred to a small beaker using a filter paper and stored for further use. It is important to filter out the chlorine gas formed during this process using a fume hood to avoid risks of accumulation of it in the laboratory.

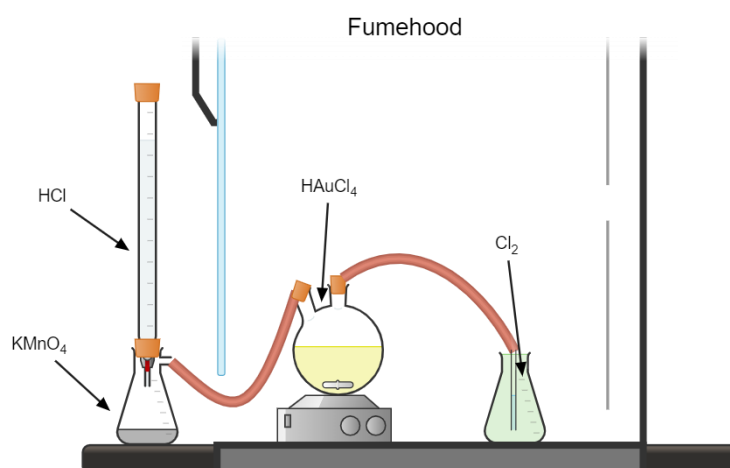


Figure 2: Schematic diagram of synthesis of precursor solution

Synthesis of Different Sizes of Gold Nanoparticles

Sample 1

A 1.28 ml of 0.1M HAuCl_4 is added to 50 ml DI water and placed on magnetic stirrer and hotplate with temperature set at $100-105^\circ\text{C}$ and stirred vigorously until a vortex is formed. Meanwhile, 2 g of Tri-Sodium Citrate is added to 10 ml DI water to make the required solution. After gold solution boils, 1 ml of Tri-Sodium Citrate solution is added. The final solution is purple/ red indicating the formation of gold nanoparticles.

Sample 2

0.5 ml of 0.1M HAuCl_4 is added to 30 ml DI water and placed for boiling with stirring at lower rpm typically 100-120. In addition, 1 g of Tri-Sodium Citrate is added to 5 ml DI water to make the required

solution. As the gold solution starts boiling, 0.5 ml of Tri-Sodium Citrate solution is added. The final color turns purple/ burgundy indicating the formation of gold nanoparticles.

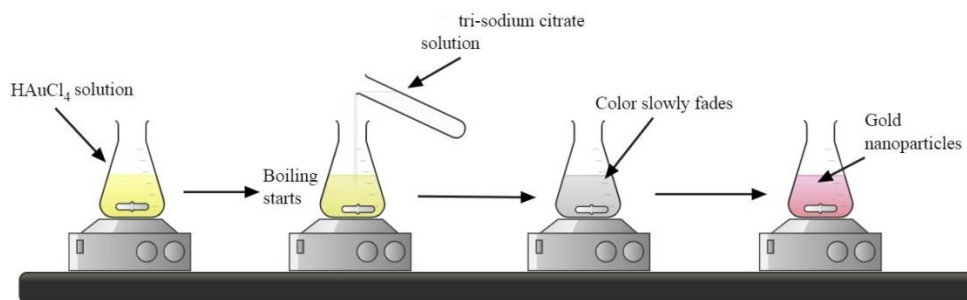


Figure 3: Schematic diagram of synthesis of gold nanoparticles

RESULTS AND DISCUSSION

Characterization was carried out for precursor solution using UV-vis spectrophotometer. Meanwhile, for gold nanoparticles, characterization was carried out using UV-vis for absorption versus wavelength and Zeta sizer Nano ZS was used to determine the size of synthesized gold nanoparticles.

UV-Vis of precursor solution

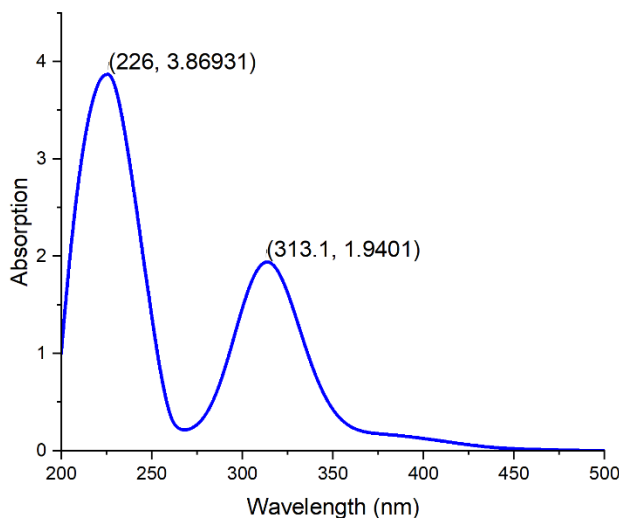


Figure 4: UV-vis of synthesized precursor solution

The sample was analyzed using a UV-vis spectrophotometer, and the wavelengths peaks in Figure 4 were found to be at 313 and 226 nm. These results confirm the tested results to the original results (King et al., 2015), indicating that the concentration is 0.1 M HAuCl_4 . Therefore, it can be concluded that the precursor solution for gold nanoparticles has been successfully synthesized.



UV-Vis of gold nanoparticles samples

UV-Vis spectroscopy was carried out to characterize the synthesized gold nanoparticles, in order to determine their wavelengths versus absorption characteristics. Both the samples were characterized as shown in figure 5 and figure 6.

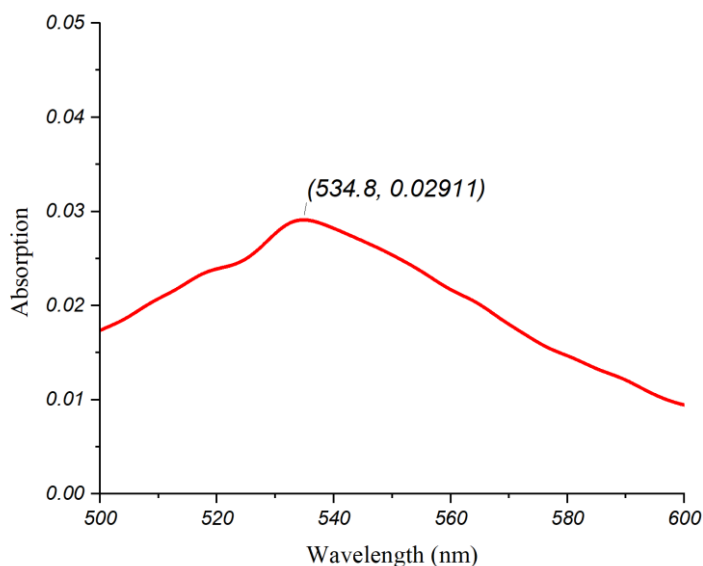


Figure 5: UV-vis of Sample 1 of synthesized AuNP

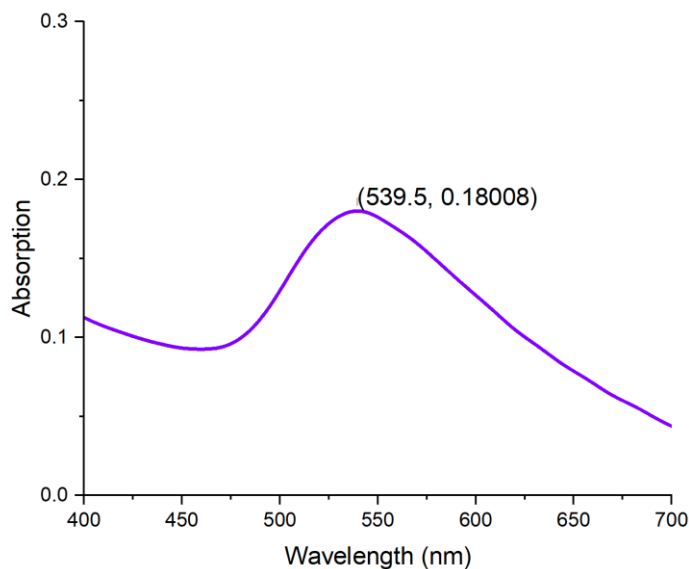


Figure 6: UV-vis of Sample 2 of synthesized AuNP



Both samples are characterized and show their absorption between 520 nm and 580 nm. The Surface Plasmon Resonance (SPR) of gold nanoparticles, such as gold Nano spheres, is visible as a peak between 520 nm and 580 nm, indicating that absorbance values range between these two wavelengths [9]. In contrast, gold Nano rods (AuNR) have absorbance peaks between 600 and 700 nm, and gold nanostars (AuNS) have absorbance peaks between 530 and 550 nm [10].

Sizes of gold nanoparticles

The Zetasizer Nano system, as described by [11], utilizes Dynamic Light Scattering (DLS) to measure the rate of intensity fluctuation and calculate the size of particles. DLS measures Brownian motion and relates it to the size of particles by illuminating them with a laser and analyzing the intensity fluctuations in the scattered light. The Zetasizer Nano system is widely used for colloid, nanoparticle, and protein size and zeta potential measurements. The Zetasizer Nano system is one of the methods used to determine the size of gold nanoparticles.

The samples synthesized were also tested for determining the size of these nanoparticles.

Table 1: Parameters for Zeta Sizer Nano ZS analysis

| Material | Au | Dispersant | DI water |
|------------|-------|----------------|----------|
| RI | 0.20 | RI | 1.340 |
| Absorption | 3.320 | Viscosity (cP) | 1.009 |

The following parameters shown in table 1 are inserted in the Zeta Sizer Nano ZS software, to accurately determine the sizes of synthesized gold nanoparticles. Here, DI water is used as a dispersant as synthesis of gold nanoparticles was carried out using it.

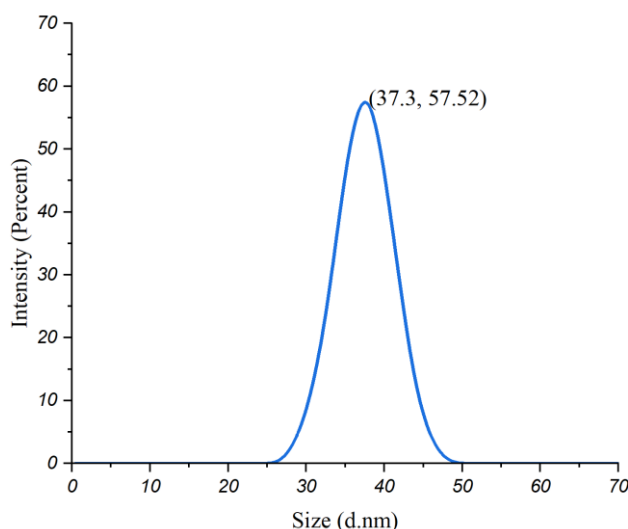


Figure 7: Zetasizer of Sample 1 of synthesized AuNP

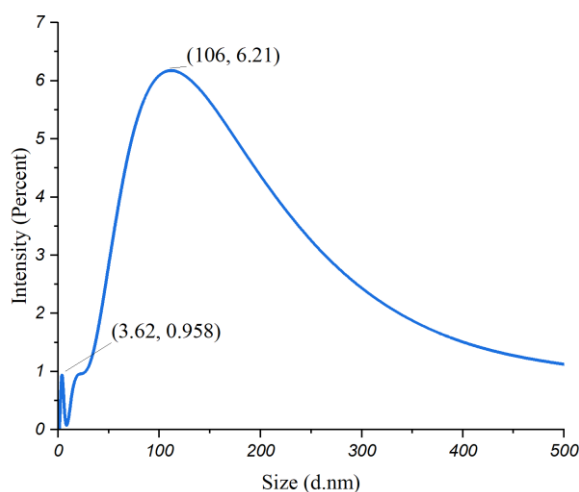


Figure 8: Zetasizer of Sample 2 of synthesized AuNP

Various properties of nanoparticles, such as their shape and agglomeration, can affect their size. Additionally, different methods of particle size characterization measure different properties of particles, such as intensity, volume, and number. As a result, different techniques may produce different results regarding particle size. However, none of the techniques are incorrect; they simply measure different properties of nanoparticles [12].

CONCLUSION

Gold nanoparticles possess unique properties such as localized surface plasmon and total internal reflection, which enable them to capture and scatter light within cells, thereby absorbing maximum light



radiations. Although commercially available, the precursor solution for synthesizing AuNP was synthesized in the laboratory and resulted in a stable solution. This precursor was used to synthesize gold nanoparticles of different sizes, ranging from 37 nm to 106 nm, which were validated using Zetasizer Nano ZS. Future research in synthesizing gold nanoparticles includes making them more stable for a longer shelf period, as they can become unstable due to environmental changes, and exploring other methods besides citrate reduction, such as green synthesis, to synthesize gold nanoparticles.

ACKNOWLEDGEMENTS

The author wants to express his sincere gratitude to Prof. Dr. Adnan Daud Khan for accepting him under his kind supervision and for his ongoing encouragement, valuable suggestions, and constant support, and also to other co-authors for their suggestions and work.

REFERENCES

- [1] M.-C. Daniel and D. Astruc, "Gold Nanoparticles: Assembly, Supramolecular Chemistry, Quantum-Size-Related Properties, and Applications toward Biology, Catalysis, and Nanotechnology," *Chem. Rev.*, vol. 104, no. 1, pp. 293–346, Jan. 2004, doi: 10.1021/cr030698+.
- [2] W. Wang, Q. Chen, C. Jiang, D. Yang, X. Liu, and S. Xu, "One-step synthesis of biocompatible gold nanoparticles using gallic acid in the presence of poly-(N-vinyl-2-pyrrolidone)," *Colloids Surf. Physicochem. Eng. Asp.*, vol. 301, no. 1, pp. 73–79, Jul. 2007, doi: 10.1016/j.colsurfa.2006.12.037.
- [3] J. Turkevich, P. C. Stevenson, and J. Hillier, "A study of the nucleation and growth processes in the synthesis of colloidal gold," *Discuss. Faraday Soc.*, vol. 11, no. 0, pp. 55–75, Jan. 1951, doi: 10.1039/DF9511100055.
- [4] M. Shariq *et al.*, "Successful Synthesis of Gold Nanoparticles through Ultrasonic Spray Pyrolysis from a Gold(III) Nitrate Precursor and Their Interaction with a High Electron Beam," *ChemistryOpen*, vol. 7, no. 7, pp. 533–542, 2018, doi: 10.1002/open.201800101.
- [5] X. Lu, H.-Y. Tuan, B. A. Korgel, and Y. Xia, "Facile synthesis of gold nanoparticles with narrow size distribution by using AuCl or AuBr as the precursor," *Chem. Weinh. Bergstr. Ger.*, vol. 14, no. 5, pp. 1584–1591, 2008, doi: 10.1002/chem.200701570.
- [6] D. Zheng, C. Schwob, Y. Prado, Z. Ouzit, L. Coolen, and T. Pauporté, "How do gold nanoparticles boost the performance of perovskite solar cells?," *Nano Energy*, vol. 94, p. 106934, Apr. 2022, doi: 10.1016/j.nanoen.2022.106934.
- [7] J. Pastuszak and P. Węgierek, "Photovoltaic Cell Generations and Current Research Directions for Their Development," *Materials*, vol. 15, no. 16, Art. no. 16, Jan. 2022, doi: 10.3390/ma15165542.
- [8] S.-R. King, J. Massicot, and A. McDonagh, "A Straightforward Route to Tetrachloroauric Acid from Gold Metal and Molecular Chlorine for Nanoparticle Synthesis," *Metals*, vol. 5, pp. 1454–1461, Aug. 2015, doi: 10.3390/met5031454.
- [9] W. Haiss, N. T. K. Thanh, J. Aveyard, and D. G. Fernig, "Determination of Size and Concentration of Gold Nanoparticles from UV–Vis Spectra," *Anal. Chem.*, vol. 79, no. 11, pp. 4215–4221, Jun. 2007, doi: 10.1021/ac0702084.
- [10] M. Batmunkh *et al.*, "Plasmonic Gold Nanostars Incorporated into High-Efficiency Perovskite Solar Cells," *ChemSusChem*, vol. 10, no. 19, pp. 3750–3753, 2017, doi: 10.1002/cssc.201701056.
- [11] H. Jans, X. Liu, L. Austin, G. Maes, and Q. Huo, "Dynamic light scattering as a powerful tool for gold nanoparticle bioconjugation and biomolecular binding studies," *Anal. Chem.*, vol. 81, no. 22, pp. 9425–9432, Nov. 2009, doi: 10.1021/ac901822w.



ICSET-23

*Proceedings of the 5th International Conference on Sustainable
Energy Technologies (ICSET 2023) Peshawar, Pakistan
14-15 December 2023*



UET Peshawar

- [12] B. Akbari, M. P. Tavandashti, and M. Zandrahimi, "PARTICLE SIZE CHARACTERIZATION OF NANOPARTICLES – A PRACTICAL APPROACH," vol. 8, no. 2, 2011.

Paper ID: ICSET-2334

INVESTIGATING THE EFFECT OF HIGH-TEMPERATURE ANNEALING ON THE OPTICAL PROPERTIES OF SILICON NANO PARTICLES FILM AT REAR SIDE OF SOLAR CELL

Hira Rehman*, Muhammad Noman

US-Pakistan Center for Advanced Studies in Energy, University of Engineering and Technology Peshawar, Pakistan

**Corresponding author*

Email: lutfhira@gmail.com

ABSTRACT

IR current losses are one of the major issues caused by imperfect light trapping in solar cells. Solar cells, electrodes, and reflectors absorb near-band wavelengths parasitically, reducing the cells' efficiency. Parasitic absorption is the undesirable absorption of light or energy by the systems. In optical and electronic systems, the material or different layers absorb undesired light which leads to inefficiency of the systems. By introducing a low refractive index layer between the absorbing layer and the metal reflector, these undesired losses can be reduced. We tested silicon nanoparticle films as a low reflective index layer and created a cell with texture silicon nanoparticles and an aluminum rear reflector. Textured Si wafer with Si nanoparticles /Al aluminum rear reflector achieves an internal reflectance of more than 99%, according to our results. In addition, the effectiveness of these films reduces at high temperatures annealing up to 900°C and 1000°C to below 80%. The achieved reflection from annealed samples drops to 40 %. This means the film does not survive high-temperature annealing.

KEYWORDS: Parasitic absorption, Nano Particle, refractive index

INTRODUCTION

Human society in the 21st century is facing critical challenges of environmental degradation and climate change mainly due to excessive use of fossil fuels. This necessitates the development of alternative technologies that can substitute fossil fuels and provide energy at affordable prices with an acceptable degree of reliability. Solar photovoltaic is one such promising technology, which is monumental in achieving this global agenda. Research is focused on enhancing its efficiency by reducing internal losses for better outcomes.

Existing silicon sun-powered cells have around 1.1 mama/cm² of Infrared current misfortunes or 2.5% of short-out current thickness [1]. These are not the flawed light-catching misfortunes, where light-catching is the peculiarity of way length upgrade in the unlucky retention deficiencies. The finished mono translucent wafer with irregular pyramids has shown equivalent dissipating to as far as possible [2-4]. Rather these are misfortunes brought about by the parasitic retention of pitifully retained frequencies that are 1000nm-1200nm in the meager film contiguous to the silicon wafer (safeguard) as the light connects on different occasions with the front and back surfaces of the cell.



The dispersed infra-red light after two passes in irregular pyramid surfaces, expects a nearby Lambertian conveyance inside the wafer. The light shows up at front and back surfaces with different points of rates within the wafer. [2] the light that compasses at a slanted point to the back surface as for the nearby pyramid front is outside the break cone, it works out assuming a low refractive record dielectric layer is kept on a superficial level. For instance, silicon heterojunction sun-based cells, PERC and TOPCon. The light inside reflects on the off chance that the engrossing layer present is absent within the entrance profundity of coming about a transient wave. In any case, assuming that the fleeting wave faces an engrossing layer the inside reflectance will diminish accordingly taking current from sun oriented cell. Particularly in metal back terminals, including magnificent reflectors like silver, the evanescent wave of a P-enraptured light emphatically coupled to surface Plasmon polarities in metallic back cathodes, makes inward back reflectance fall unexpectedly, for instance, under 90 % and 80% for silver terminal or for no and an extremely fragile dielectric testimony [5].

The way into this issue is to guarantee that sunlight-based cells with high productivity have an infra-red (IR) straightforward dielectric affidavit at their back side which is thicker than the rot length of the transitory wave. Reenactment reveals that this to be 200 nm [5].

Exceptional execution is seen by diminishing refractive records of dielectric testimony as this diminishes the infiltration profundity and field strength of the transitory wave. Inside back reflectance of 99.56% is workable for MgF₂/silver reflector. The di-electric MgF₂ has a reflective file of 1.37 [6].

The single danger of this methodology, nonetheless, is that there are extremely few materials with exceptionally low refractive records to browse, and those are not generally simple and modest to store as layers. For instance, MgF₂ is saved by dissipation which is never effective in the first endeavor as a cycle step in Si sun powered cell making regardless of rehashed endeavors. The cycle drops off the interaction chamber and thickness screen due to interior stress. In expansion to this challenge, the dielectric should imitate such that a metal terminal can make electrical contacts through it to the electron or opening contact.

We as of late shown dielectric/Al back reflectors in silicon sun-oriented cells in which the dielectric was silicon nanoparticles [7]. The silicon Nanoparticles are 5nm in measurement, and the voids between silicon particles and they, when all is said and done, are a lot more modest than the infra-red frequency (IR) that arrives at the back side of the cell, thus the film acts as skilled medium with refractive record tuned by its porosity. The silicon nanoparticles are kept by VSCT (vacuum splash covering procedures). The interaction controllably tunes the film porosity, and in this way controls the refractive record. Moreover, the strategy of splashing is directional for this situation a metal lattice can be utilized for contact development. A correlation of Nano particles-based reflectors to other dielectric films is finished in silicon heterojunction sun-oriented cells.

Similarly, we are in the early stages of using these fluorescent materials in silicon cells with screen-cathodes printed with Al.

This research further investigates the issue at hand by contrasting silicon nanoparticles finished at temperatures above 800°C. We investigate the optical features of the film of the solar cell in the temperature range of 1000 °C.

Nanoparticles Films Deposition

In the first phase of the experimental procedure, the silicon nanoparticle was deposited using the vacuum deposition method onto the thin film. The Si nanoparticle was now formed in the same plate plasma reactor rotated at n 'side by passing the dust-quiet plasma [10]. The continued growth of silane and helium in the base pulls the nucleus out, favoring their growth. The width of these Si nanoparticles was



nearly 5.0 nm and their SD of the band was 15.01% of the width. In the proof chamber, a translation substrate is placed at the bottom of the plasma reactor. The chamber persistently clears the helium (He) streaming the entire framework while the silane is used in particle development. The blend and statement chamber have a cut-molded spout framing a basic tension drop, regularly the plasma pressure is not many Torrs and the testimony chamber pressure is multiple times less with the goal that the gas advances to supersonic speed or close sonic. This gas thusly speeds up nanoparticles through crashes in the spout yet the Nano particles (NPs) can't succeed the gas smoothed out in the downstream chamber, and they experience the substrate to shape a covering. the cycle is more like a Spray affidavit and has a closeness to the "Cold splash process", in any case, the two cycles consume powder as a molecule feedstock and the size of the molecule is considerably bigger. the effect speed of the infringing nanoparticles can be changed by modifying the hole or length between the spout and substrate, the strain proportion across the spout is irrefutably the up or downstream tensions [9]. Modifying the distance thus speed of Nanoparticles thusly directs the adjustment of porosity thus the refractive file of the covering. The thickness of the film or coatings is insignificantly constrained by the speed with which the substrate is swaying under the spout. the device can store film on a substrate up to 5.0" on one side and can create a low refractive record coating of the ideal 200 nm thickness in sun-oriented cells. Generally, a testimony of this sort requires simply 1 moment to be produced. Figure 1 present the image of a silicon nanoparticle covering examining electron microscopy picture of permeable and thick coatings $n=1.09$ and $n=1.53$, individually.

All through this work (n) refractive lists, thickness, and thickness of the movies stored on one side silicon not entirely set in stone through spectroscopic ellipsometry estimations sing model Woollam M 2000. we fit the ellipsometry data (estimated bends) with a Bruggeman viable medium guess just involving silicon and void as a fundamental material [22]. We likewise restricted the frequencies, just above 900nm were fit. This wipes out the apparent and bright light thus staying away from the potential issues brought about by the incorrectness of mass silicon refractive records at more modest frequencies. (connects with frail quantum control in little NPs). the spectrophotometric estimations certify that thick nanoparticle coatings don't retain light with a frequency over 700 nm, in contrast to mass translucent silicon. [7]. This is the explanation as a matter of fact, for what reason to utilize silicon nanoparticles SiNPs rather than a customary straightforward dielectric at the back side of a sun-based cell, without confronting parasitic retention within NPs themselves.

RESULTS OF LOW-TEMPERATURE ANNEALING

Before putting together material for the lab prototype of the solar cell under consideration, we focus on a literature review of optical tests. A typical optical test is shown in Fig 2 below. It is much more like silicon heterojunction cells. the Si nanoparticle layer has the same refractive performance at higher temperatures as the wafer-based. These formless silicon layers don't have infrared parasitic assimilation in the back terminal. The best layer while utilizing silicon heterojunction cell structure [11] with a 150.01nm thick straightforward ITO (indium tin oxide) just 65.015% of 1200nm light isn't caught up in the wafer returns as getaway reflectance. 35% is parasitically retained in ITO/Ag reflector. At the point when the ITO indium titanium oxide is supplanted with silicon nitride SiNx (same refractive list, not absorptive) the reflectance has expansion to 80%, and with SiNps (silicon nanoparticles) or MgF₂. The reflection surpasses to 90%. in surface wafer light cooperates with the back surface ordinarily, this increments back reflection to 99.566% as per past work results. The silicon nano particles SiNps utilized here had a refractive record (n) is roughly 1.401. The more permeable layer, however, has a low refractive file (n) and An adequate number of harsh spaces that lead to undesirable plasmonic retentions in an un-flate silver subsequently bringing

about more regrettable all-out reflectance [7]. To consolidate a nano molecule/metal back reflector in a sun-powered cell, it means a lot to gadget the layers to shape nearby openings where the metal back reflector connects through nanoparticle coatings to electron or opening contact. The sun-oriented cell structure here is made out of an ITO/silicon nanoparticle/silver stack in which ITO transports the charge in nanoparticles to the closest opening. Through metal lattice shadow veil.

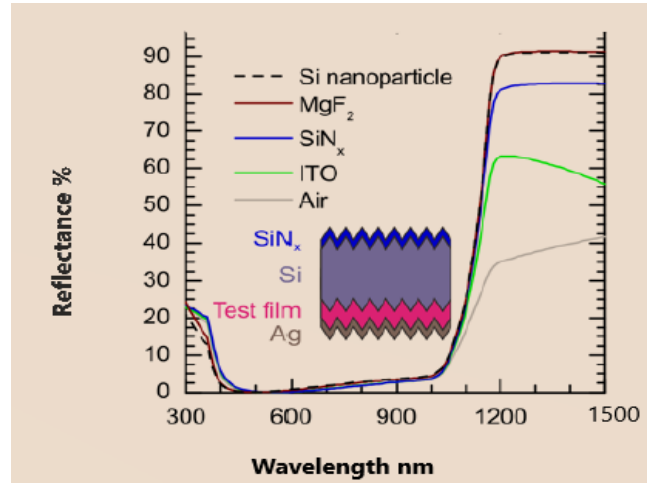


Figure 1: Reflectance spectra with variation in rear dielectrics (200 nm thick) during the optical test Indium zinc oxide, a transparent conductive oxide layer with high mobility of 49.9 cm²/Vs, can be employed without suffering from as much infrared-free carrier absorption as ITO, a layer with lower mobility (TCO) [13].

Figure 3 shows improvement when the best reflector ITO/Ag is replaced by a rear reflector having nanoparticle /Ag in identical heterojunction solar cells.

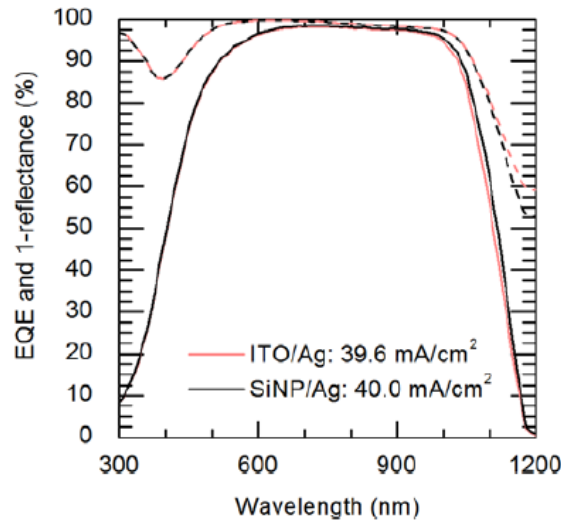


Figure 2: EQE & 1-reflectance of similar silicon heterojunction solar cells having ITO/Ag rear reflector

HIGH-TEMPERATURE ANNEALING OF SILICON NANOPARTICLE COATINGS

Figure 3 delineates a new improvement over the best in class utilizing an extremely speedy and simple statement methodology that requires an unpleasant vacuum. The reserve funds designed at the back of the sunlight-based cell construction would have no TCO and would exploit nanoparticle coatings with additional engrossing back metal terminals, a genuine depiction of an AL-BSF or PERC sun-powered cell, however, the last option structures as of now have dielectric layers at the back, so the addition is negligible much of the time since silver works magnificently as a back reflector with any dielectric and because infrared parasitic retention in the front TCO layer eats into them these cells specifically.

We started by investigating the effectiveness of silicon nanoparticle deposition when annealed at high temperatures of 900 to 950 degrees Celsius. But before this, we analyze previous work, the results of annealing silicon coatings at 800 degrees Celsius. The process of annealing is the same in both cases. we used a furnace with a ratio of 80:20 N: O atmosphere for the annealing test. for low temperatures of less than 200 degrees Celsius, we used a hotplate. In Figure 4 the FTIR spectra of silicon nanoparticles as deposited and following annealing at 180 degrees Celsius for 20 min is shown. the freshly deposited SiNPs have hydride-bonded peaks formed in the silane plasma which after annealing at 180 degrees Celsius diminishes and forms oxides. at high temperatures (800 degrees Celsius) no hydrogen remains as depicted in Figure 4 in the wavelength range of 1100cm⁻¹.

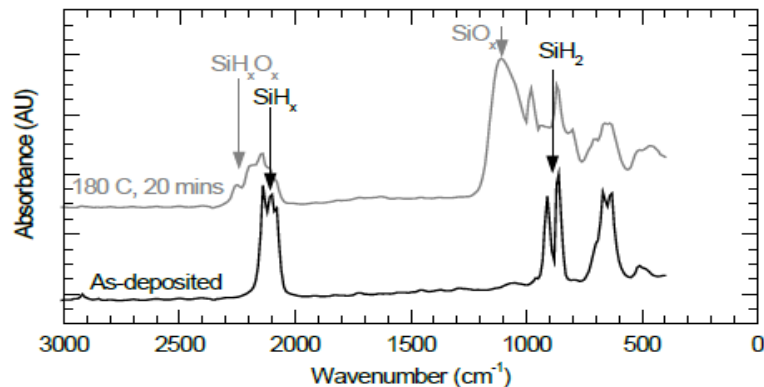


Figure 3: FTIR spectra of SiNPS layers after immediate depositions and following annealing [12]

Only an oxide peak at 1100 cm⁻¹ is recorded after annealing at 500 and 800°C, which isn't displayed, and no hydrogen is left behind. Upon annealing at 800°C, it may be presumed that silicon nanoparticle oxidation is finished, and the silicon layer turns visibly transparent. The ellipsometry data validate the FTIR measurements, which demonstrate that the nanoparticles had undergone oxidation. Temperature is more crucial than annealing time. There must be a process other than compositional change that caused the enhanced absorbance in the visible range.

We propose that following annealing, silicon nanoparticles that are small enough transform into Si cores with oxide shells. The effective optical band gap of the material decreases as a result of the sintering of these cores, which relieves quantum confinement. This theory is supported by enlarged holes after annealing at 800 °C as seen in SEM images (figure 4). Moreover, with annealing silicon nanoparticles coating adhesion to substrate and to each other increases dramatically observed in Taber Abrader tests done in previous studies [12], thus supporting particle sintering. If nanoparticles do not react with aluminum



adversely, these annealed coatings are suitable to use as a transparent infrared dielectric layer in rear reflectors as absorbance does not extend 900 nm [13].

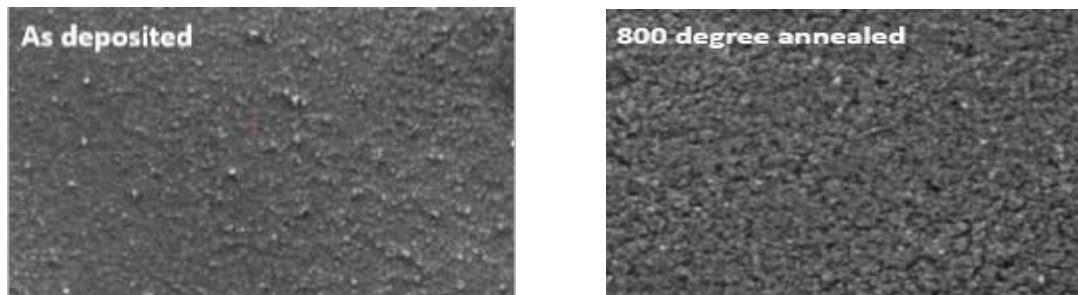


Figure 4: SEM images before and after annealing

Reflection from annealed and unannealed silicon nanoparticle film

The texture wafer with 240nm thick silicon nanoparticle film shows 80 to 90 % reflection for the wavelength range of 1200nm-1400nm. the near-band gap light is reflected with no undesired absorption. The films absorb 99% for 340nm to 700nm for the visible range in a single pass, the reflection is (0-2) %. this shows that the silicon nanoparticle layer can mitigate unintentional absorption for longer wavelengths, which makes the silicon nanoparticles an excellent candidate to be used in silicon solar cells as a reflector. We used the online simulation software SUNSOLVE of PV Light House and simulated the structure of the samples. Both simulation and experimental results showed similarity, as shown in the figure below. (Blue shows Simulation, Red shows Experimental). The software is only used for unannealed sample structures. This shows that silicon nanoparticles can mitigate undesirable absorption by giving high reflection for the near band gap light. From the results, it is concluded that silicon nanoparticles reflect 90% of 1200nm light, with random pyramid texture near Lambertian light trapping achieved. Light interacts several times before escaping the front side the high reflectance of 80-90% indicates the decrease in near band gap light parasitic absorption. The wavelengths with energies lower than the silicon band gap are absorbed in the nanoparticles and the metal reflector. High reflection from samples corresponds to low parasitic absorption. Annealing at high temperatures up to 900°C and above does not show favorable results. The data shows a reduction in the reflection which means an increase in parasitic absorption and so increase in losses.

The high-temperature annealing strongly reduced the sample's reflection and so increased the unwanted plasmonic absorption. The samples later after annealing were metalized with aluminum. Aluminum metallization on annealed samples showed no good effect on reflection as the high temperature enhanced surface roughness. We investigated that greater layer porosity and rougher surface will induce more unwanted plasmonic absorption in the aluminum layer. resulting in worse reflection. Results for the metalized samples are given in the figure.

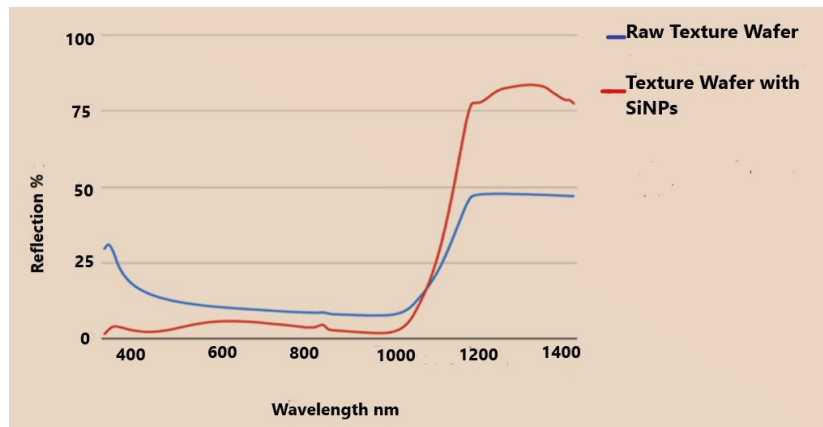


Figure 5: Reflection comparison plot of SiNPs deposited on texture wafer and texture wafer with no SiNPs

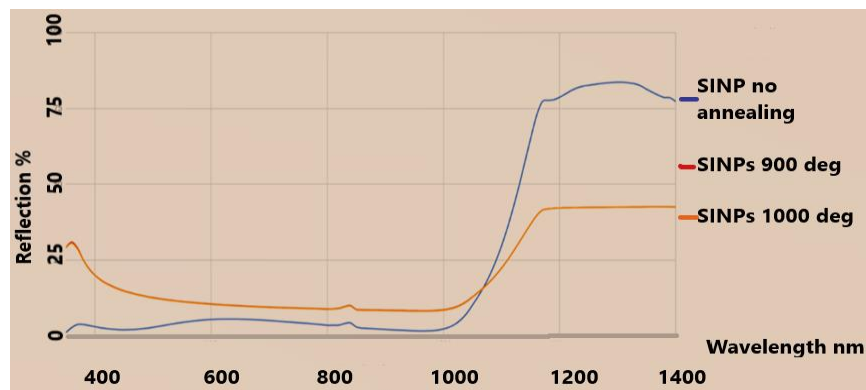


Figure 6: Reflection from annealed silicon nanoparticles

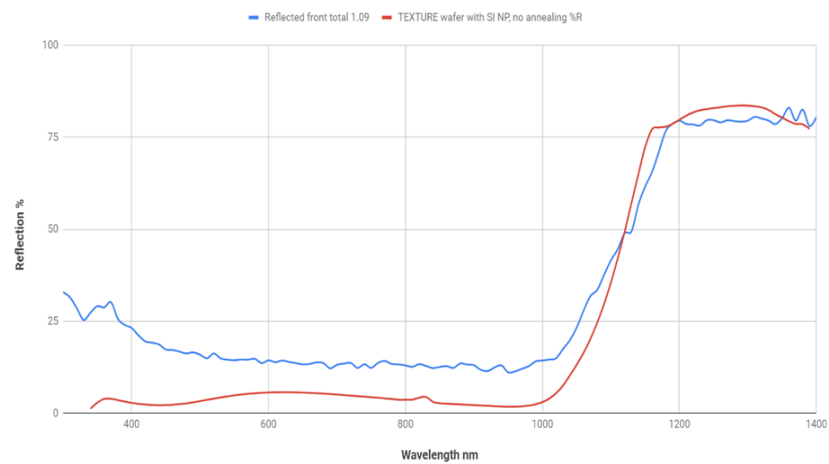


Figure 7: Comparison of experimental and simulation results

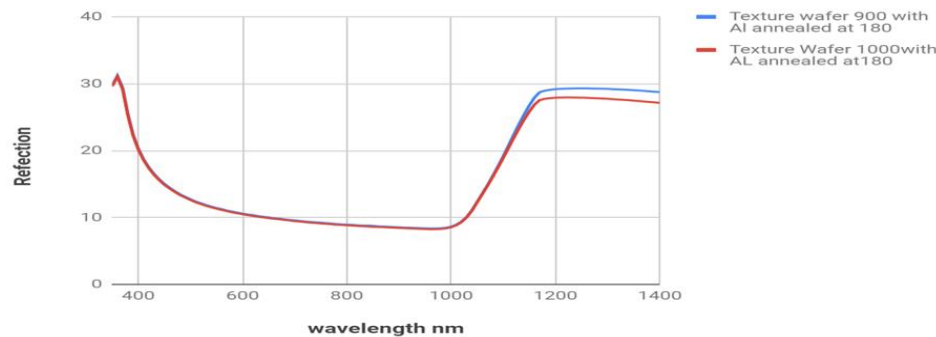


Figure 8: Comparison of reflections of annealed Al metalized samples

CONCLUSION

The plasmonic absorption on the reflective metal surface of the solar cell can be reduced by using a dielectric layer of 200 nm thickness, which is transparent infrared with a low refractive index, can be reduced plasmonic absorption on the reflective metal surface of solar cells by infra-red transparent, low refractive index dielectric layer about 200 nm thick to reduce by inserting s. It is possible that vacuum spraying provides highly controlled silicon nanoparticle coatings and porosity. Particle and pore sizes are much smaller than infrared wavelengths and these layers act as effective media like dielectrics in solar cells with controlled refractive index. We demonstrated that silicon nanoparticle coating sprayed with annealing increases infrared reflectivity and reduces plasmonic undesirable absorption. The coatings can withstand temperatures up to 800 degrees but have been shown to reduce light brightness to IR up to 900 degrees. The pore size of the particles increases at 900 degrees annealing and roughens the layer with poor surface plasmonic absorption resulting in worse than expected total reflection. An important step is to investigate the behavior of aluminum on the silicon coating at a high temperature of 900 degrees. what are the structural changes and how does this temperature change optical and electrical properties, it is expected that as aluminum dope coatings, it should be possible to pass through the dielectric through nanoparticles without inducing any free carrier adsorption without the need for any local modeling.

REFERENCES

- [1] Z. C. Holman, M. Filipič, B. Lipovšek, S. De Wolf, F. Smole, M. Topič, and C. Ballif, "Parasitic absorption in the rear reflector of a silicon solar cell: Simulation and measurement of the sub-bandgap reflectance for common dielectric/metal reflectors," *Sol. Energy Mater. Sol. Cells*, vol. 120, Part A, pp. 426-430, 2014.
- [2] S. Manzoor, M. Filipic, M. Topic, and Z. Holman, "Visualizing light trapping inside textured silicon solar cells," (in preparation).
- [3] A. Ingenito, O. Isabella, and M. Zeman, "Experimental Demonstration of 4n(2) Classical Absorption Limit in Nanotextured Ultrathin Solar Cells with Dielectric Omnidirectional Back Reflector," *Acs Photonics*, vol. 1, pp. 270-278, 2014.
- [4] P. Campbell and M. A. Green, "Light trapping properties of pyramidally textured surfaces," *J. Appl. Phys.*, vol. 62, pp. 243-249, 1987.



- [5] Z. C. Holman, S. De Wolf, and C. Ballif, "Improving metal reflectors by suppressing surface plasmon polaritons: A priori calculation of the internal reflectance of a solar cell," *Light: Science & Applications*, vol. 2, p. e106, 2013.
- [6] Z. C. Holman, A. Descoedres, S. De Wolf, and C. Ballif, "Record infrared internal quantum efficiency in silicon heterojunction solar cells with dielectric/metal rear reflectors," *IEEE Journal of Photovoltaics*, vol. 3, pp. 1243-1249, 2013.
- [7] M. Boccard, P. Firth, Z. J. Yu, K. C. Fisher, M. Leilaoui, S. Manzoor, and Z. C. Holman, "Low-refractive-index nanoparticle interlayers to reduce parasitic absorption in metallic rear reflectors of solar cells," *Physica Status Solidi (a)*, pp. e201700179.
- [8] P. Firth and Z. C. Holman, "Large-area nanoparticle coatings with controllable porosity and 8% non-uniformity formed via aerosol spraying"
- [9] Z. C. Holman and U. R. Kortshagen, "A flexible method for depositing dense nanocrystal thin films: impact of germanium nanocrystals," *Nanotechnology*, vol. 21, p. 335302, 2010.
- [10] L. Mangolini, E. Thimsen, and U. Kortshagen, "High-Yield Plasma Synthesis of Luminescent Silicon Nanocrystals," *Nano Letters*, vol. 5, pp. 655-659, 2005.
- [11] Z. C. Holman, M. Filipic, A. Descoedres, S. De Wolf, F. Smole, M. Topic, and C. Ballif, "Infrared light management in high-efficiency silicon heterojunction and rear-passivated solar cells," *J Appl Phys*, vol. 113, p. 013107, 2013
- [12] M. Tanaka, M. Taguchi, T. Matsuyama, T. Sawada, S. Tsuda, S. Nakano, H. Hanafusa, Y. Kuwano. "Development of new a-Si/c-Si heterojunction solar cells: ACJ-HIT (artificially constructed junction-heterojunction with intrinsic thin-layer)." *Jpn. J. Appl. Phys.* 31(11R), 3518 (1992).
- [13] A. Tomasi, B. Paviet-Salomon, Q. Jeangros, J. Haschke, G. Christmann, L. Barraud, A. Descoedres, J. P. Seif, S. Nicolay, M. Despeisse, S. De Wolf, C. Ballif. "Simple processing of back-contacted silicon heterojunction solar cells using selective-area crystalline growth." *Nature Energy* 2(5), 17062 (2017).
- [14] J. Kegel, H. Angermann, U. Stürzebecher, E. Conrad, M. Mews, L. Korte, B. Stegemann. "Over 20% conversion efficiency on silicon heterojunction solar cells by IPA-free substrate texturization." *Applied Surface Science* 301, 56–62 (2014).
- [15] D. Pysch, A. Mette, S. W. Glunz. "A review and comparison of different methods to determine the series resistance of solar cells." *Sol. Energy Mater Sol. Cells* 91(18), 1698–1706 (2007).

Paper ID: ICSET-2335

THERMAL EFFICIENCY ASSESSMENT, BENCHMARKING AND IMPROVEMENT MEASURES FOR GAS-FIRED CAPTIVE POWER PLANTS IN PAKISTAN

Syed Fawad Hussain Shah^{1,2,*}, Dr. Mohammad A Irfan²

¹Thermal System Engineering, US-Pakistan Center for Advanced Studies in Energy, University of Engineering and
Technology Peshawar, Pakistan

²Center for Industrial and Building Energy Assessments (CIBEA), Pakistan

**Corresponding author*

Email: sfhussain.tse@uetpeshawar.edu.pk

ABSTRACT

Pakistan is on the verge of a massive gas shortage as its production fell by 12.8% since 2017 and this gap is met by importing expensive RLNG. The power sector, being the largest consumer of natural gas, uses about 31.90% of the total natural gas supply. Besides large gas-fired government power plants (GPPs), there are almost 1,211 captive power plants (CPPs) in the country which consume this scarce resource very inefficiently. Halting gas supplies to these individual power plants as happened in 2021, will result in a great economic loss in these post-COVID situations because 610 of these CPPs are of export industries. Transforming the energy mix from depleting natural gas towards indigenous renewable resources could be a long-term solution but energy efficiency is a low-hanging fruit and an inexpensive solution to this problem. An MMBTU of gas saved through inexpensive energy efficiency measures is better than an MMBTU of RLNG imported at a higher cost. According to the integrated energy plan, Pakistan is losing 72.7% of the total input energy to inefficiencies while supplying its primary energy to end consumers and 25% of these losses account for the power generation sector. So, the foremost purpose of this study was to perform a comparative assessment of different gas-fired CPPs, recommend improvement measures, and build an efficiency benchmark for them. Captive power plants of different industries, configurations, and capacities were audited to identify areas of potential energy loss, recommend energy efficiency improvement measures, and quantify energy-saving potential. Whereas the implementation of these ECMs will not only lead to efficient gas utilization and increased plant profitability, GHG emissions will also be reduced which is both a national and an international commitment. Overall fuel savings of 214,157 MMBtu/yr. and emission reduction of 11,350 t-CO₂/yr. were identified in this study.

KEYWORDS: Gas Crises, Captive Power Plants, Energy Auditing, Energy Efficiency, Sustainability

INTRODUCTION

In Pakistan, the demand for affordable and reliable energy is on the rise, increasing by 8 to 10% annually while the energy supply grows at just 7% per year [1]. This situation stems from the country's development, including modernized agriculture, expanding industry, and improved trade and transportation. A major transformation in the energy mix commenced two decades ago to reduce the reliance on expensive



imported oil. Key developments, such as the China-Pakistan Economic Corridor (CPEC) project, installation of RLNG power plants, and Independent Power Plants (IPPs), have increased installed capacity from 22,812 MW in 2013 to 37,261 MW in 2021 [2]. The State of the Industry Report 2019-20 highlights a significant increase in Pakistan's primary energy consumption, rising from 70.3 million metric tons of oil equivalent (MMTOE) to 86.3 MMTOE from 2014 to 2018. Nearly half of these primary energy requirements are met by imported fuels, imposing a hefty financial burden of 17.75 billion USD on the economy. A substantial 72.7% of the input energy is lost due to inefficiencies, with the power generation sector accounting for 25% of these losses. This implies that only 59.1 MMTOE of the total primary energy (86.3 MMTOE) is converted into useful energy [3].

Natural gas plays a significant role, contributing 45.6% to the country's primary energy supply, with local production meeting 35% of this demand. However, local natural gas production fell by 12.8% in May 2021 from its peak in February 2017, leading to a severe gas shortage. The import of expensive RLNG has risen from 0 MMCFD in 2014 to 950 MMCFD in 2021 [2]. RLNG now accounts for 10.6% of the primary energy supply, causing economic setbacks and public unrest due to prolonged natural gas shortages. The power sector, the largest consumer of natural gas, consumes approximately 31.90% of the total natural gas supply (Ministry of Energy, 2020). Pakistan hosts 1,211 captive power plants (CPPs), with 849 under Sui Southern Gas Company Limited (SSGCL) and 362 under Sui Southern Gas Pipeline Limited (SNGPL). These CPPs consume 34.9% of the gas supply to the power sector, totaling around 415 MMCFD (210 MMCFD on SSGCL and 205 MMCFD on SNGPL). Halting gas supplies to these power plants, as occurred in 2021 and 2022, results in significant economic losses, especially as 610 of these CPPs belong to export units [4].

Transitioning from natural gas to indigenous renewable sources is a long-term solution. However, immediate attention to energy efficiency is crucial. Saving an MMBTU of gas through cost-effective measures is more sustainable than importing RLNG. Thus, assessing the performance of gas-fired CPPs, identifying energy losses, and recommending efficiency measures is vital. This study aimed to assess the overall performance of different gas-fired captive power plants, identify efficiency gaps, recommend energy-saving measures, reduce auxiliary power consumption, enhance net heat rate, and establish benchmarks through comparative analysis.

MATERIALS AND METHODS

In this section, we outline the methodology employed for the assessment of cogeneration-based Captive Power Plants (CPPs) in this study, covering data collection, instrumentation, calculations, results analysis, and recommendations.

Data Collection

Our study focuses on cogeneration-based CPPs, which were categorized based on installed capacity (<5 MW and >5 MW), the type of prime mover (gas generator, gas turbine), and the type of waste heat recovery (WHR) systems (e.g., WHR boilers, WHR chiller, engine jacket WHR, and double section WHR units). A graphical representation of the selected CPPs, areas of work, data types, parameters analyzed, and key results are provided in Figure 2.1.

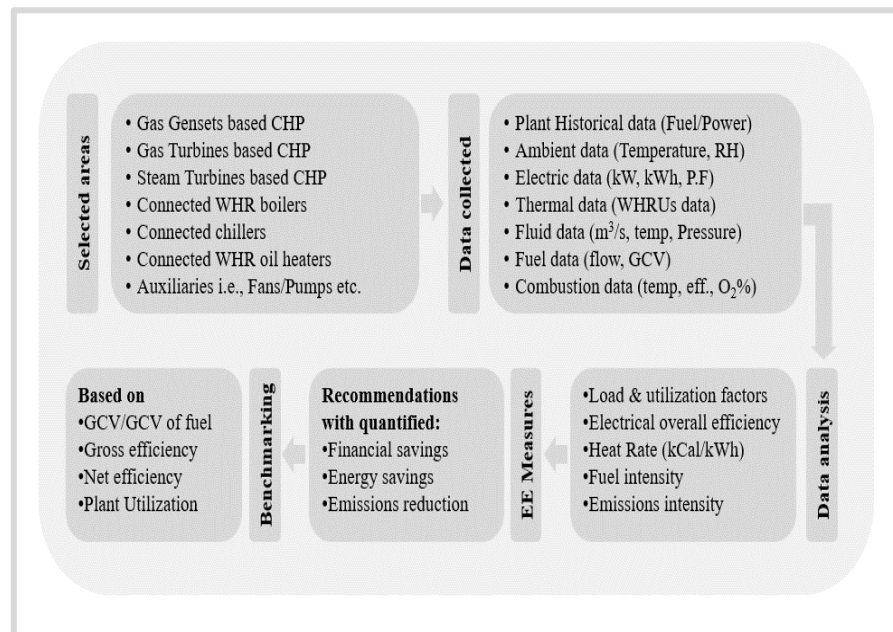


Figure Error! No text of specified style in document.96: Graphical presentation of this study

Collecting and Scrutinizing Pre-Assessment Data

The initial step involved gathering historical data on fuel consumption, power generation, operating hours, annual average load factor, and heat recovery from various gas-fired CPPs. The purpose was to understand plant layout and energy flow patterns. Historical trends of fuel consumption in plant versus industrial processes and energy demand from the onsite plant versus the national grid were visualized through pie charts.

Instrumented Energy Audit

To measure and improve energy efficiency, operational data of cogeneration plants was collected using state-of-the-art auditing equipment. Data related to ambient conditions, fuel consumption, power generation, exhaust gas conditions, and heat recovery through WHR systems was essential. Equipment such as power quality analyzers, flue gas analyzers, thermal imagers, flow meters, thermometers, and other specialized tools provided by the Center for Industrial and Building Energy Audits (CIBEA) were employed.

Data Compilation and Calculations

Pre-assessment historical data and onsite instrumented data were compiled into Excel files for further analysis. This data was used to calculate various performance parameters of cogeneration plants, such as electrical efficiency, thermal efficiency, heat rate, utilization factor, and more. Different configurations of prime movers and attached waste heat recovery systems were considered. Formulas were utilized to quantify and compare these parameters.

Results Analysis and Graphical Presentation

After data compilation and performance parameter calculation, preliminary results were analyzed. The key performance parameters included electrical efficiency, thermal efficiency, heat rate, and utilization factor. Both net and gross calorific values were considered. These results, trends, and energy flows were presented using various graphical representations, including bar graphs, heat balance diagrams, and Sankey diagrams.

Identifying Gaps and Recommending Energy Conservation Measures (ECMs)

Comparative assessments of design and operational parameters allowed us to identify gaps. Various ECMs were recommended to minimize thermal inefficiencies and energy losses, including tuning combustion air, improving load factor, and reducing stack temperature. Detailed analyses were performed to assess the benefits of these ECMs, including fuel consumption reduction, fuel cost minimization, and GHG emission reduction.

Benchmarking of All CPPs

After individual analyses of each CPP, a comparative thermal efficiency assessment was conducted. Internal benchmarking based on the net and gross calorific value of fuel revealed performance trends for gas-fired CPPs with different configurations, capacities, and load factors.

RESULT AND DISCUSSION

Comparison summary

The key performance parameters are compared for the audited CPPs. The comparison of all the assessed parameters is summarized in Table 1.

The graphical comparison of electrical efficiency, thermal efficiency, heat rate, stack losses, and other performance parameters is presented in the subsequent sections.

Comparison of efficiencies

The chart given below in Figure depicts the comparison of electrical and thermal efficiencies of the audited CPPs. The overall efficiencies of all the CPPs are in the acceptable range. CPP-3, with the lowest stack losses of 7% and the highest waste heat recovery potential of 39% has the highest overall efficiency among all.



Table 1: Comparative performance of the audited CPPs.

| Parameters assessed | CPP-1 | CPP-2 | CPP-3 | CPP-4 |
|---|--------|--------|----------|---------|
| Capacity (MW) | 6.32 | 12.2 | 1.067 | 48 |
| The power produced (MW) | 4.08 | 7.71 | 0.587 | 27.2 |
| Load factor (%) | 64.34 | 63.2 | 55 | 56.7 |
| Annual generation (MWh/yr.) | 25,522 | 60,353 | 4,745.90 | 208,894 |
| Auxiliary power (kW) | 205.5 | 410.6 | 42.7 | 2,100 |
| Auxiliary consumption (MWh/yr.) | 728 | 3,293 | 189.8 | 14,321 |
| Share of auxiliary kWh (%) | 2.86 | 5.4 | 4 | 6.59 |
| Electrical efficiency (%) _{GCV} | 32.8 | 36.5 | 34.2 | 34.8 |
| Jacket waste heat recovery (%) _{GCV} | 14.9 | 17.0 | 21.2 | 0.0 |
| Exhaust waste heat recovery (%) _{GCV} | 15.15 | 11.1 | 18.4 | 27.3 |
| Combined thermal efficiency (%) _{GCV} | 30.0 | 28.1 | 39.6 | 27.3 |
| Gross overall efficiency (%) _{GCV} | 62.8 | 64.57 | 73.8 | 62.1 |
| Net overall efficiency (%) _{GCV} | 61.51 | 63.42 | 71.99 | 60.14 |
| Gross plant heat rate (kCal/kWh) _{GCV} | 2,621 | 2,357 | 2,514 | 2,475 |
| Net plant heat rate (kCal/kWh) _{GCV} | 2,728 | 2,433 | 2,648 | 2,622 |
| Stack losses (%) _{GCV} | 8.9 | 13.5 | 7 | 26.8 |
| Overall losses (%) _{GCV} | 37.2 | 35.4 | 26.2 | 37.9 |
| Current net efficiency | 61.5 | 63.4 | 71.9 | 60.1 |

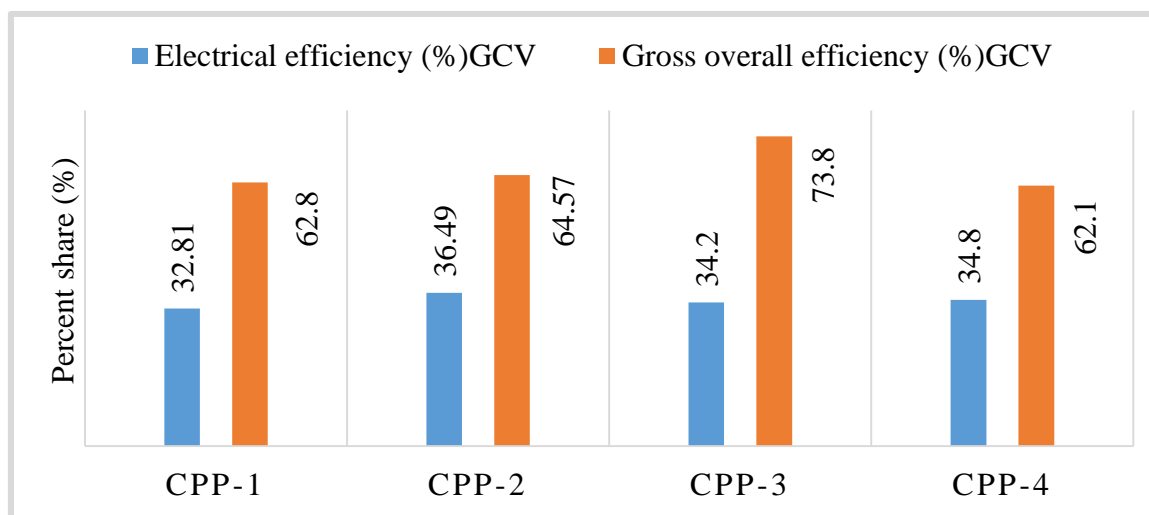


Figure 2: Electrical vs overall efficiency of the audited CPPs

Comparison of heat rates

Figure 3 shows the comparison of gross and net heat rates of the audited CPPs. Heat rate is the measure of chemical energy (in kCal) required to produce 1 kWh of electricity. CPP-2 with efficient gas engines (36.5% operational electrical efficiency) has the lowest heat rate among all.

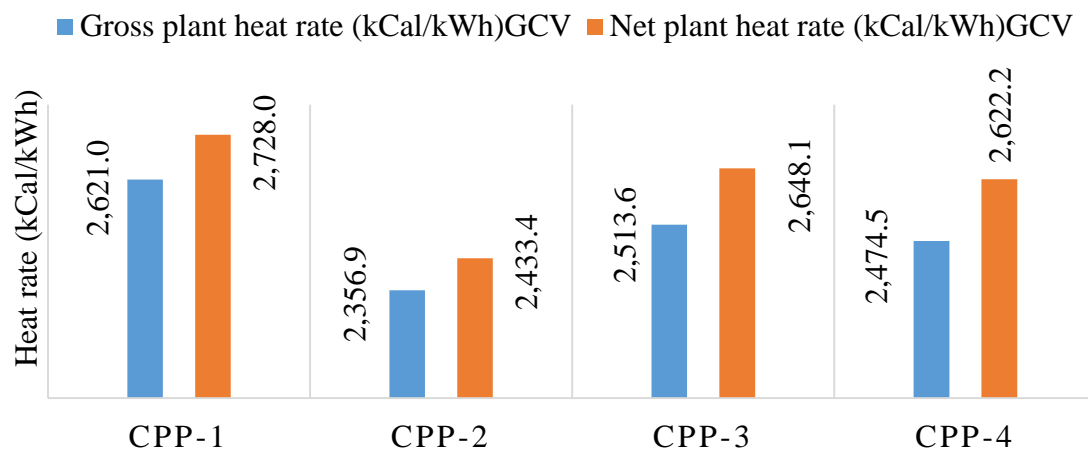


Figure 3: Net and gross heat rates of the audited CPPs.

Benchmarking of current, required, and achievable efficiencies

Despite significant losses, the assessed CPPs were running at good efficiency. The comparison of current efficiency, the minimum required efficiency, and the maximum achievable efficiency of the assessed CPPs is shown in Figure .

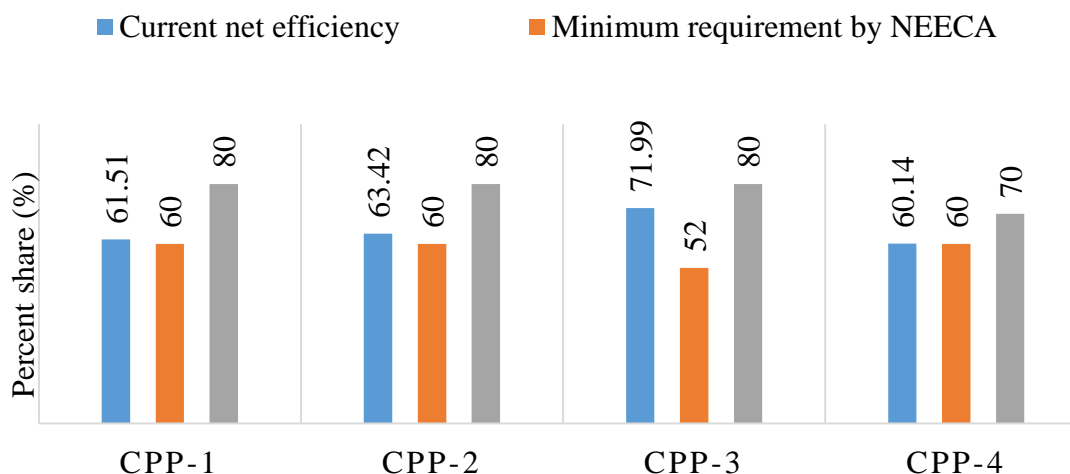


Figure 4: Current, the min required, and max achievable efficiency of the CPPs

Comparison of losses

The efficiency of the audited CPPs is much lower than the maximum achievable efficiency of similar combined heat and power units. The gap can be minimized if certain losses like stack losses and insulation losses in WHR units are addressed. A summary of these losses is displayed in Figure .

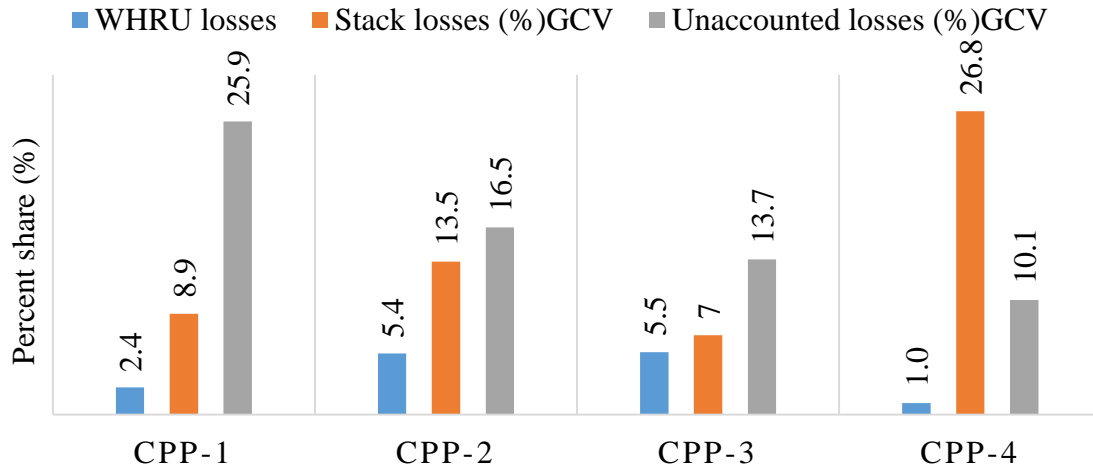


Figure 5: Stack losses, WHRU losses, and unaccounted losses in the audited CPPs

Comparison of quantified benefits

To minimize the above-mentioned losses in the audited CPPs, a few ECMs were recommended including installing waste heat recovery systems, tuning air to fuel ratio of prime movers, and improving insulation to reduce heat transfer losses. The quantified benefits in the form of fuel savings and carbon footprint savings are shown in Figure and Figure below.

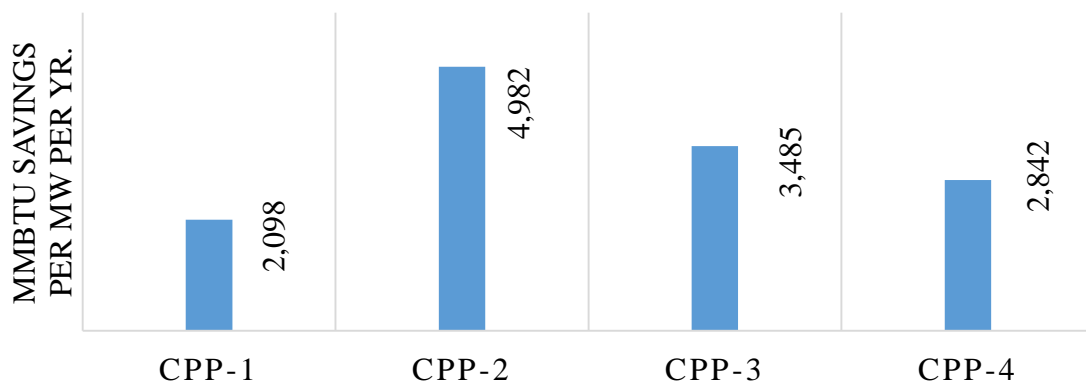


Figure 6: Identified MMBtu savings per MW per yr. for the audited CPPs

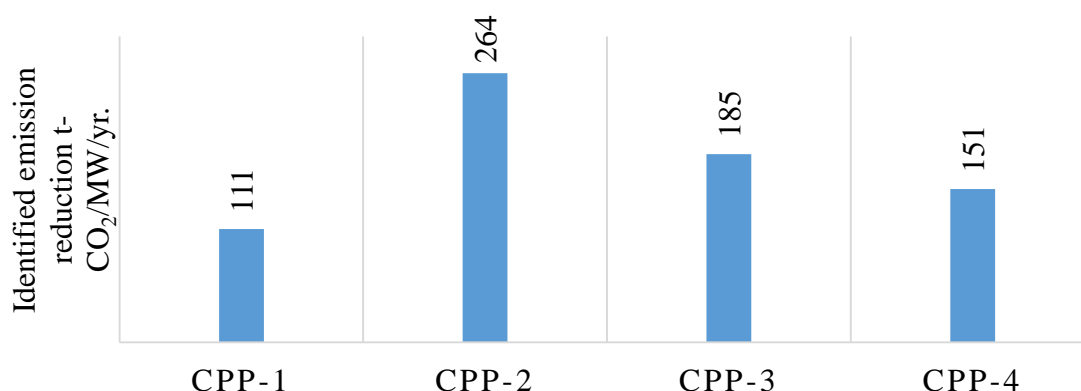


Figure 7: Identified emission reduction potential in the audited CPPs

CONCLUSION

Four cogeneration captive power plants were assessed in this study, and it was found that the assessed cogeneration plants were running at good thermal efficiency ranging from 60% to 72%. Waste heat recovery losses and stack losses (dry flue gas losses, wet flue gas losses) were the most prominent losses identified during the energy assessment of sample cogeneration plants. Due to the higher flue gas temperature associated with a gas turbine, CPP-4 has the highest percentage of stack losses i.e., 27% of the input fuel energy. Reciprocating engines based on the LEANOX technology having operational electrical efficiency of 36% were the most efficient system among all. Tuning the air-to-fuel ratio and installing a condensing heat recovery exchanger on the exhaust were the most promising energy conservation measures identified in this study. Overall fuel savings of 214,157 MMBtu/yr. and emission reduction of 11,350 t-CO₂/yr., for the 4 CPPs, were identified in this study.

ACKNOWLEDGEMENTS

I would like to thank my supervisor and mentor Prof. Dr. Mohammad Abdul Aziz Irfan for his coherent support and guidance throughout this research work. Besides this, I am indebted to the National Energy Efficiency and Conservation Authority (NEECA) and the Center for Industrial and Building Energy Audits (CIBEA) for providing me with all the financial and technical assistance needed throughout this work.

REFERENCES

- [1] Prospects of renewable penetration in the energy mix of Pakistan. Farooqui, S. K. 2014. 2014, Renew. Sustain. Energy Rev., Vol. 29, pp. 693–700
- [2] Ministry of Finance. 2021. Pakistan Economic Survey 2020-21. s.l. : Finance Division GoP, 2021
- [3] Farid, Nida Rizwan. 2013. Energy Efficiency Database. [Online] 2013. [Cited: June 01, 2022.] <https://www.energyefficiencydatabase.com/energy-flow-diagram.php>
- [4] Petroleum Division. 2020. Development Plan for Pakistan, Oil & Gas Industry. s.l. : Ministry of Energy, 2020

Paper ID: ICSET-2336

A COMBINED APPROACH OF COMPUTATIONAL FLUID DYNAMICS AND EXPERIMENTAL STUDY ON AIR JET INTERACTION

Engr. Nadeem ur Rehman*, Dr. Kareem Akhtar

Department of Mechanical Engineering, University of Engineering and Technology, Peshawar

**Corresponding author*

Email: nadeem.rehman@uetpeshawar.edu.pk

ABSTRACT

This work investigates the dynamics of rising air jets and bubbles in vertical water channels, investigating discontinuous and continuous air jets with the help of a submerged needle and a combined experimental and numerical approach. For experimental studies, high-speed digital camera technology (Casio EXILIM EX-FH20) with slow-motion capabilities up to 1000 frames per second is used.

Prior studies, as reported in [10] [11], have demonstrated that small bubbles, especially those with a radius of less than approximately 0.81 mm, usually follow a straight path. This behavior is changed, though, when a submerged needle is added, resulting in spiral trajectories under different flow circumstances.

Air jet flow characteristics in a vertical water channel are analyzed by numerical simulations carried out in a 2D framework using the volume of fluid (VOF) approach, which replicates the dimensions of the experimental setup. The simulations show that the bubbles do, in fact, travel in a spiral pattern, and that the jet likewise tends to follow the trajectory under the effect of the submerged needle, which is consistent with experimental findings.

Moreover, the numerical simulations demonstrate how the submerged needle affects the rising jets' track at the intake by introducing disruptions. Remarkably, the Shear-Stress Transport (SST) turbulence model performs better in precisely describing and capturing the observed events than the k- ϵ turbulence model. This thorough study offers insightful information about how to control air bubble generation in vertical water channels in an energy-efficient manner.

INTRODUCTION

A lot of researchers have been interested in studying the course of free rising bubbles through experiments. Taylor flow in micro channels by patching and T-junction techniques was investigated by M. said [1]. Numerical simulations show that both approaches perform satisfactorily, but that the patching method performs more computationally efficiently. The study advances our knowledge of the hydrodynamics of Taylor flows in micro channels. The transition of the straight-rising, zigzagging, and swirling course of bubbles is caused by the tainting of the liquids in many studies. The route and wake of a free rising air bubble in ultra-clean water were explored by A.W.G. de Vries [2]. The jet wake is linked to the rising bubble path in ultra-clean water. A double-threaded wake is seen for jets moving in a non-rectilinear manner. The lift force is responsible for the bubbles' swirling and zigzagging patterns. It is not due to vortex shedding, which is what happened when jets rose in contaminated water.



Y. Cordova [3] investigates the use of direct discharge for effective steam condensation in swimming pools. The important importance of nozzle diameter and mixing percentage on jet behavior is revealed by experimental findings on air/steam combinations, which have valuable applications in a variety of sectors.

B. Ho [4] investigates the effects of constantly submerged jets on a stationary wall using Computational Fluid Dynamics simulation and the Wray-Agarwal turbulence model. The findings demonstrate that the jet structure is dependent on impact height regardless of Reynolds number. A constant pressure distribution, increased jet diffusion, and decreased velocity are the results of increasing impact height. These observations provide useful advice for technical applications.

According to A.W.G. de Vries' observations [2], the majority of the zigzagging bubbles were observed to be between 0.81-0.88 mm and 1.00-1.10 mm in size.

M. Xiang [5] investigates the mechanics of three different flow patterns created by high-speed submerged gas jets in the water. The research evaluates pressure distributions, vortex structures, and gas-liquid interface profiles with accuracy using a compressed multiphase model. It also predicts shedding processes. The results offer important new understandings of flow properties and modes-to-mode changeover mechanisms.

Y Zhou [6] numerically analyzed submerged steam jet condensation using non-condensable gas in subcooled. Heat transfer coefficients are impacted when the shape of the steam plume changes and static pressure peak values decrease due to an increase in air content. The findings show that the properties of heat transmission, air concentration, and water turbulence interact intricately.

Air bubble ascent and movement have been extensively investigated both theoretically and empirically. When bubbles with a diameter of 0.7 mm or less rise through water, they exhibit a spherical shape and a rectilinear ascent [3]. Large bubbles, on the other hand, follow a helical or zigzag pattern and have an ellipsoidal form and wobble [7] [8].

A little bubble travels in a straight line. According to experiments, bubbles with a radius of less than 0.81 mm rise rectilinearly, as demonstrated by [9].

A bubble's zigzag rise usually happens in frothy flows. The primary sources of turbulence in bubbly flows are thought to be the jet's wake and oscillatory vortices that shed behind a jet. Thus, they cause an alternating lift force to form [10].

Ellingsen and Risso [11] came to the conclusion that bubble motion is zigzag-like, transitioning into helical motion following the acceleration stage. The creation of sets of hairpin vortices, which depict the structure of the vortex in the jet wake, is connected to the jet's trajectory. The zigzag motion is caused by their alternating shedding [12], and the zigzag turns into a spiral jet [2] when helical structure is present.

Similar to Saffman [3], Aybers and Tapucu [13] [14] also observed a transition; however, in contrast to Saffman's conclusion [3], spiraling bubbles were only seen at $0.67 \text{ mm} < \text{req} < 1.0 \text{ mm}$. This indicates that there is a peculiar occurrence in this range that needs to be investigated further. Additionally, it was determined that the shape of the jets was spherical up to $\text{req} = 0.42 \text{ mm}$, ellipsoidal up to 1.0 mm, and oscillatory for larger jet sizes.

Air-water two-phase flow regimes were experimentally studied by P. Hanafizadeh et al. [15] using a high-speed camera operating at 1200 fps in a vertical micro pipe. They used image processing techniques in order to obtain sharp photos of jets. These methods set up the jets for post-processing and additional analysis, such as diameter, area, perimeter, and velocity calculations.

Using the ultrasonic transit time approach and a high-speed camera, T. R et al. [16] conducted experiments to study the rose of in zigzag patterns. They came to the conclusion that at the trajectory's



reversal points, the bubble's diameter is, at most, 30% bigger than the deq equivalent diameter. Additionally, the bubble's diameter shrinks as it gets farther away from the reversal spots.

The rising bubble trajectory was numerically explored by M. Abid Akhtar et al. [17]. They deduced that the behavior of small bubbles, measuring 2–6 mm, is meandering. Bubbles larger than 6 mm exhibit oscillations from side to side. Bubbles with a diameter of 10–20 mm rise in the shape of jellyfish. Bubbles with a diameter of 30 mm flapped like the wings of a bird.

Using the Lattice Boltzmann method, Z. L. Yang et al. [18] performed a numerical analysis of bubble movement and verified the results for various physical parameters. They also looked into flow regime transitions. They came to the conclusion that body force had a significant influence on bubble motion and surface tension had minimal effect on the change in flow regime. Since bubbles of the same size do not merge, the flow regime will continue in this scenario.

A single bubble in water was numerically studied by M. T. Islam et al. [19] using the level set (LS) approach in both the rectangular and trapezoidal domain volume of fluid (VOF) methods. They noticed that a column's shape affects the bubble's velocity. The bubble velocity in the rectangular domain is greater than the one in the trapezoidal domain. This demonstrates that the trapezoidal domain exhibits wall effect. Additionally, the bubble deforms more in the trapezoidal domain due to the push of the primary and secondary vortices than it does in the rectangular domain.

Using the volume of fluid method, H K et al. [20] investigated the effect of height and Reynolds number in convergent-divergent channels. They found that the oscillation amplitude of the bubble traveling within the channels increases with increasing h and Re . Many applications, particularly those involving small-scale flows, can benefit from the enhanced mixing caused by the oscillation of the bubble shape and its convoluted route.

Afshin Ahmadi and Ebrahim Shirani [21] conducted a numerical study on the effects of several surface tension models on interfacial flows. Surface tension force is the main reason for the difficulty of simulating interfacial flows. When one of the two fluids is liquid, surface tension force is always present at the contact. There are certain interfacial flows where surface tension force is significant.

In order to mimic the ascent of bubbles, I. Chakraborty et al. [22] numerically investigated the impacts of coupled technique in conjunction with fluid volume (CLSVOF). While achieving mass conservation, the linked technique estimates interfacial geometric parameters more precisely.

The velocity of the bubble in reducing pipe with water was studied numerically by Wenqi Yuan et al. [23]. Their primary conclusions were that when the fluid goes through the reducer's junction, the air-water interface has a tendency to become wavy and concave. It results from an uneven rise in gas and liquid velocities brought on by a smaller pipe diameter. The non-uniform wall shear stress increases noticeably as a result.

With an emphasis on the impact of a submerged needle, this research uses both experimental (2D and 3D) and numerical (2D and 3D) methods to conduct a thorough investigation into the rising behavior of air jets in a vertical water channel. Through both experimental and numerical analyses in various planes, the research attempts to characterize the flow dynamics of single, linked, four, and row configurations of air jets, as well as continuous and discontinuous jets. Furthermore, by using numerical simulations based on Reynolds-Averaged Navier-Stokes (RANS) methods in conjunction with experimental high-speed digital camera observations, the study aims to investigate the impact of the submerged needle on the trajectory of ascending jets.

MATERIALS AND METHODS

Experimental Setup

Water tanks made of acrylic glass are used for the experiments. The length of the water tank was 80 mm in the x, 200 mm in the y, and 80 mm in the z directions. In the x-axis, a 2 mm hole is drilled in the middle of the water tank. An air injector with a length of 30 mm and diameter of 2mm is placed into the water tank through this aperture. Air is injected into the tank via the air injector using an air storage and captured using high speed camera.



Figure 1: Experimental Setup

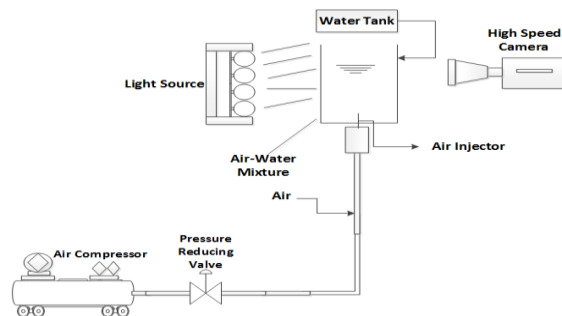


Figure 2: Experimental Setup schematics

Methodology

Water is added into the tank up to 200 mm. Through air injector, air is being injected into water tank. A valve for lowering pressure is used to change the air flow rate. Images are obtained from both planes (x-y, y-z) to get a precise sense of the jets' rising characteristics.

The digital high-speed camera Casio EXILIM EX-FH20, which can capture slow motion footage, is utilized to capture crisp footage of the water jets rising. The frame rate of the camera was adjusted to 420 fps. Adobe Premier Elements is then used to turn the film into individual frames in order to create the photos. Additional tools such as VLC, Frame Shots, and others can also be used for this. Twenty frames per image was the frame rate that was chosen for each example. After that, the obtained images are used as inputs for image processing methods. The final binary images produced by the image processing methods are then

used for post-processing, such as jet trajectory analysis. Following the picture processing, the final image has the same appearance as the figure 3.

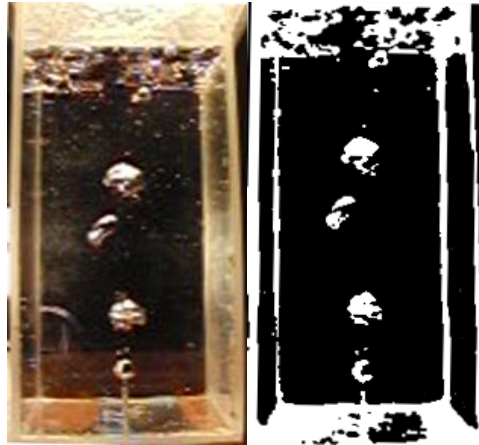


Figure 3: Image before and after image processing via matlab

Finite Element Analysis

The water tank used in the numerical simulations (2D) has the same dimensions as the experimental one. The water tank measured 80 mm in the x and 200 mm in the y directions. In order to verify the interface behaviour, an additional 100mm domain is designed on top of the channel. The water tank's center has a 2 mm hole planned at a distance of 39 mm along the x-axis. A buried 2mm diameter needle with a length of 30 mm is intended to be inserted through this hole into the water tank. The idea of multi-domain is applied here. The water tank is meshed using Ansys 14 ICEM-CFD and imported to FLUENT 19.2 to examine various scenarios of the air jets' rising characteristics in water. Air is used to initialize the top domain while water is used to initialize the bottom domain. The needle is used to inject air at a predetermined mass flow rate.

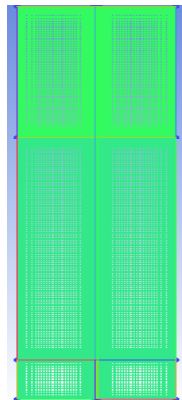


Figure 4: Numerical Mesh in ICEM

RESULT AND DISCUSSION

Experimental Results and Discussion



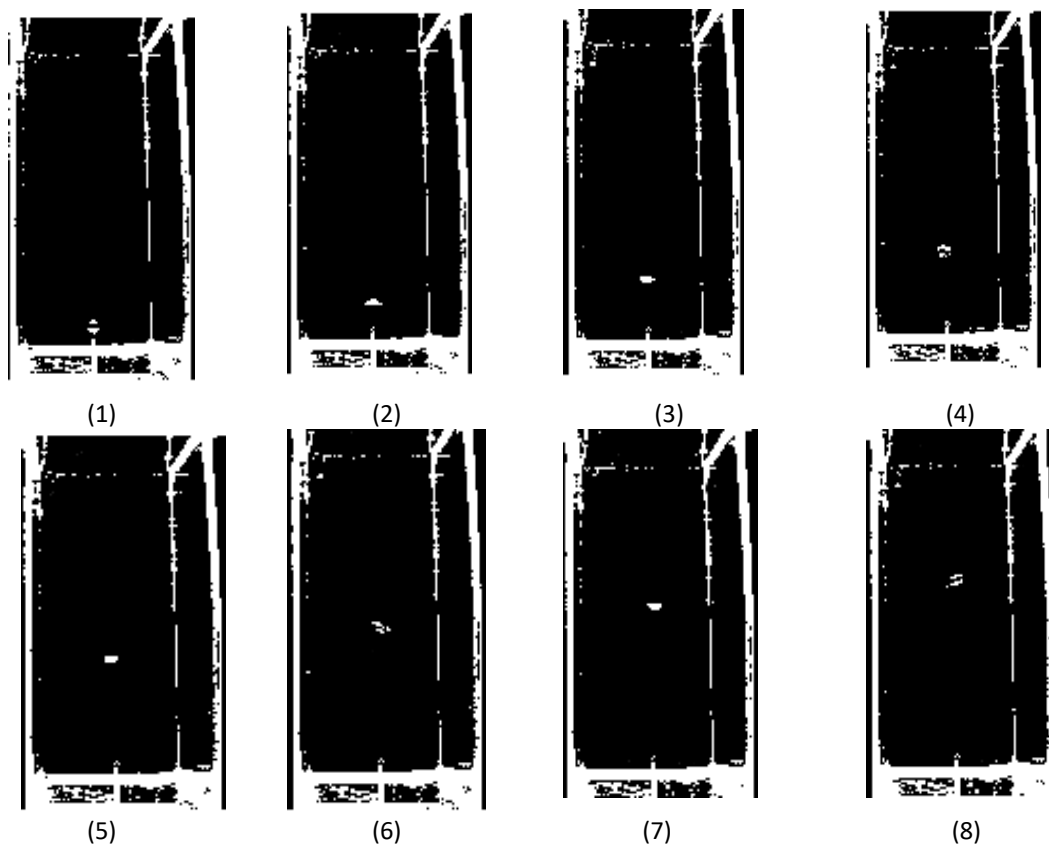
In the plane (x-y), three different jet scenarios are taken into consideration, each changing the air storage's flow rate. Table 1 lists the many cases that were taken into consideration.

Table 1: Different Bubble/Jet Cases

| | | |
|---------------|-------------------------------|---|
| Case 1 | Single bubble | Only one air bubble at a time was injected into the water tank due to the extremely low flow rate. |
| Case 2 | Large Number (row) of bubbles | In Case 2, a high quantity (row of bubbles) of air bubbles were injected into the water tank by increasing the flow rate once more. |
| Case 3 | Discontinuous Jet | The water tank was then injected with a discontinuous jet by increasing the flow rate. |

Case 1 (Single Bubble (X-Y) Plane)

In order to examine the rising characteristics of the first case, the flow rate was kept extremely low, allowing for the injection of only one air bubble at a time into the water tank. The bubble in water's post-processing findings are displayed in Figure 5(1–14). The air bubble does not ascend straight; rather, it spirals, as Figure 5(15 & 15) makes evident.





ICSET-23



UET Peshawar

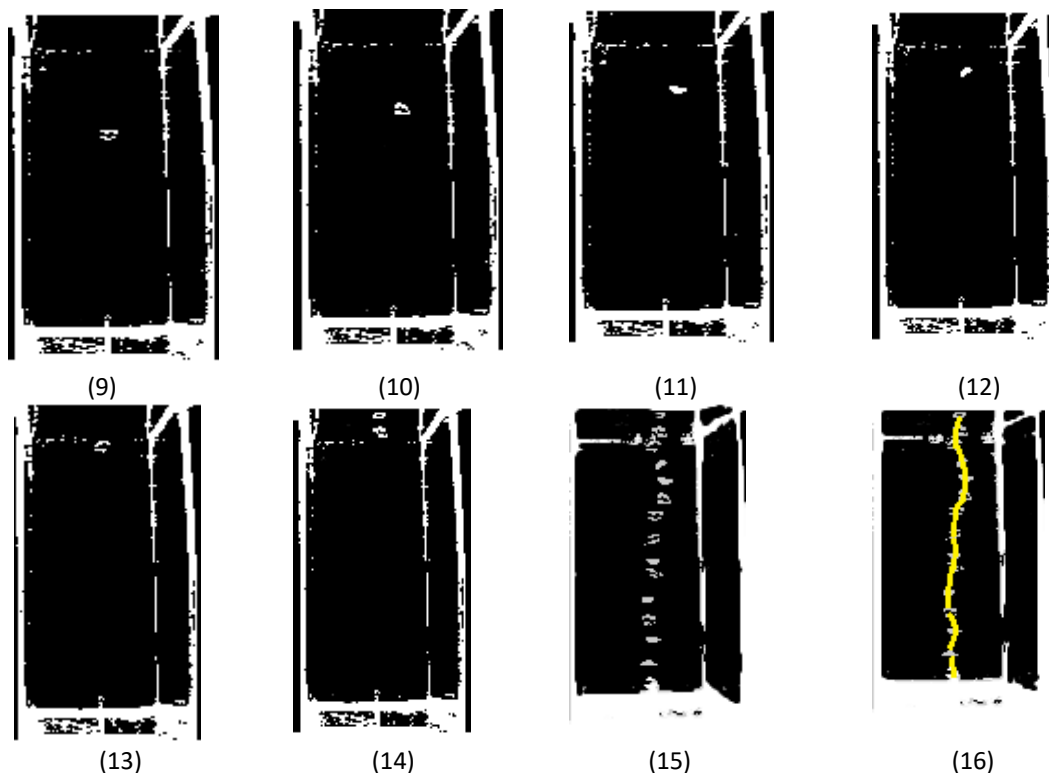
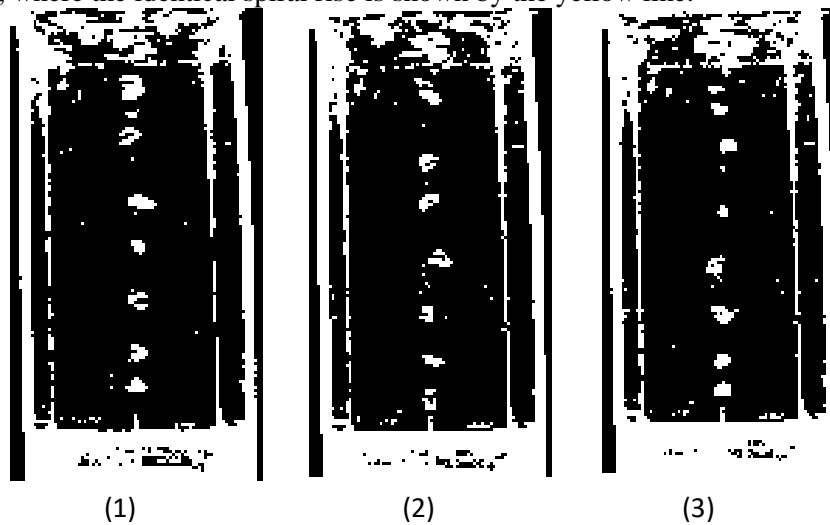


Figure 5: (1-14) a bubble following a spiral course. (15) An overlay of Figure 5 (1–14). (16) The trajectory is superimposed into an image

Case 2 (Large Number (Row) of Bubbles)

Case 2 produced the row of jets shown in Figure 6 (1-3) when the flow rate was increased further. In this instance, the frame rate was maintained at 20 frames every picture. The jets' trajectory is depicted in Figure 6 (4–6), where the identical spiral rise is shown by the yellow line.



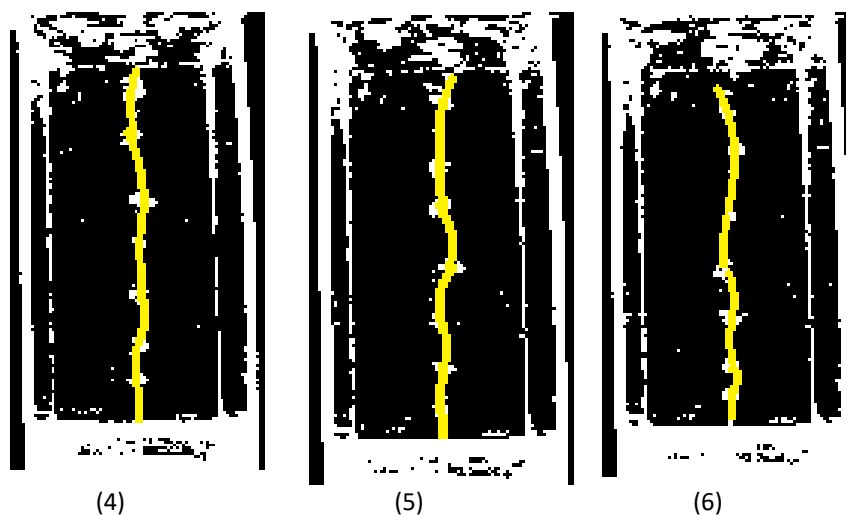
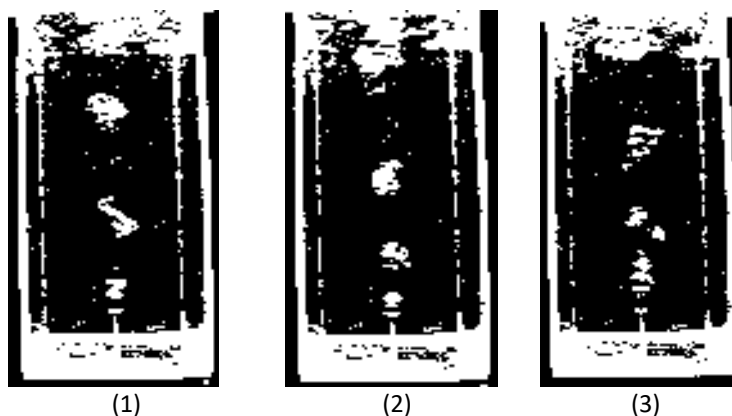


Figure 6: (1-3) a row of bubble following a spiral path while maintaining a frame rate of 20 frames each picture. The bubble trajectory is indicated by the yellow line in (4-6)

Case 3 (Discontinuous Jet)

Subsequently, the flow rate was raised to a specific number once again in order to get the discontinuous jet ascending in Figure 7(1-3) below, which shows results after image processing. The spiral growth of the jet is clearly visible, as seen in Figure 7 (4-6).



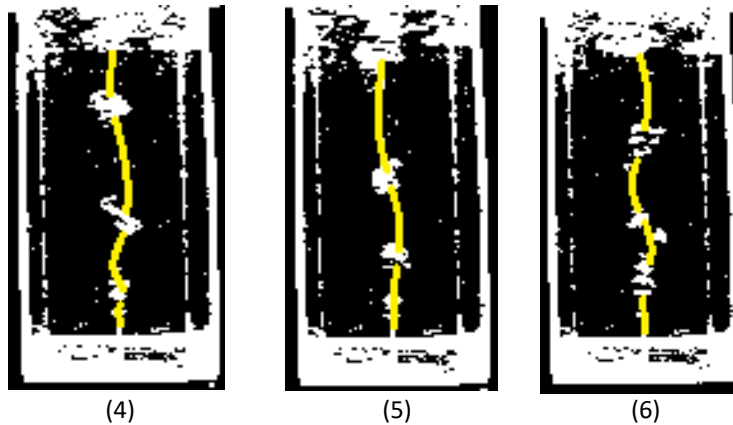


Figure 7: Discontinuous (1-3) After 20 frames apiece, a jet rises in the water while traveling in a spiral pattern in the x-y plane. The yellow line in (4–6) depicts the jets' course

Numerical Results and Discussion

In the (x-y) plane, three distinct air jet scenarios with varied flow rates are taken into consideration. Table 2 lists the many cases taken into consideration.

Table 2: Air mass flow rate

| Case 1: Single Bubble | Case 2: Row of Bubbles | Case 3: Discontinuous Jet |
|--------------------------|--------------------------|---------------------------|
| 0.0000036 kg/s(In Pulse) | 0.0009095 kg/s(In Pulse) | 0.12 s (Continuous) |

Case 1 (One bubble)

At the air mass flow rate of 0.0000036 Kg/s at the inlet of the nozzle, we got one air bubble rise in the channel. Pictures are captured at various angles. The blue color shows the air vlume fraction and the red color shows the water volume fraction. The air volume fraction of red zone is zero and water volume fraction of red zone is one.The findings of the bubble in water derived from the tec plot are displayed in Figure 9(1-15). The overlaid image of the bubble rising in water is seen in Figure 9 (15). The track of the air bubble rise in water is shown by the yellow line in Figure 9(16). Figure 9(15 & 16) makes it evident that the air bubble travels in a spiral pattern.

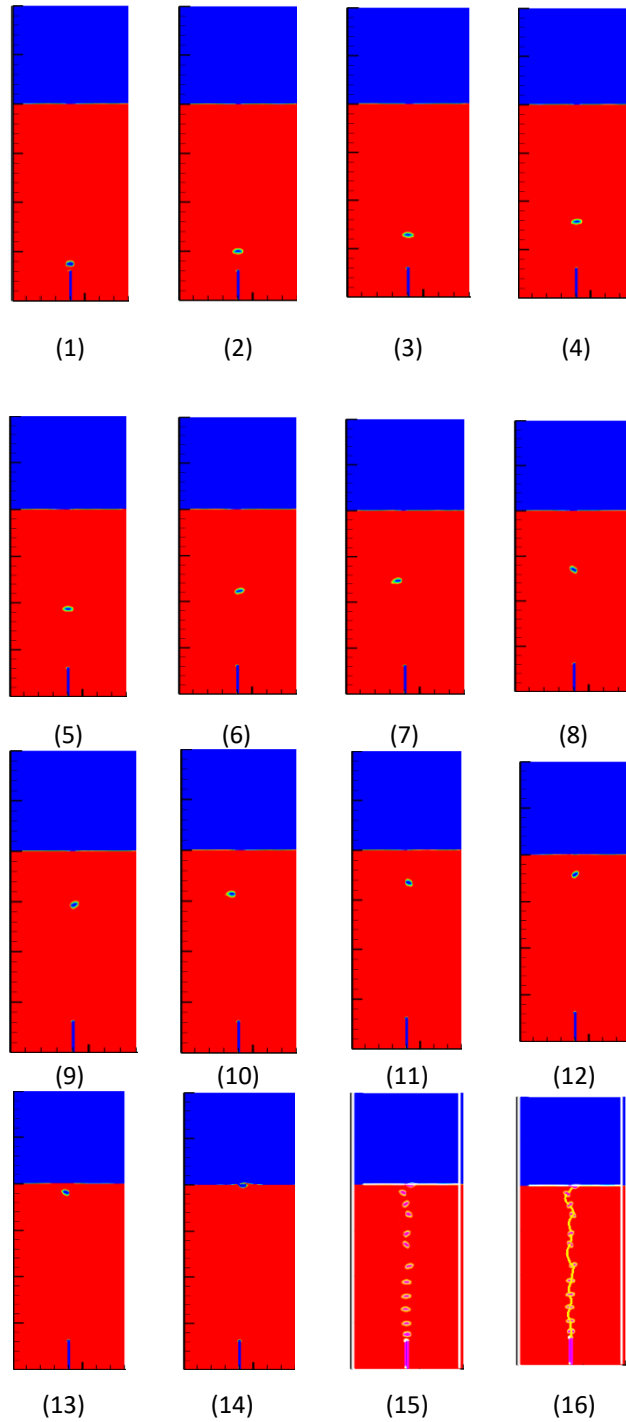


Figure 9: A Bubble travelling in spiral path (1–14). (15) An image of Figure 9 superimposed (1–14). (16) Overlaid picture of a bubble, with the bubble's trajectory shown by the yellow line

Case 2 (Row of Bubbles)

For Case 2, the mass flow rate was increased to 0.0009095 kg/s. With increasing mass flow rate of air at the inlet of the nozzle we get a row of bubbles seen in Figure 10(1-2). The bubbles' trajectory is depicted in Figure 10(3-4), where the same spiral ascend is shown by the yellow line. The bubbles follow a spiral pattern which clearly validate the numerical results with the experimental results which also shows the spiral pattern of bubble in case of submerged needle in water channel. All the bubbles after following a specific pattern to the top burst at the top surface of the water as shown in figure 10 (4).

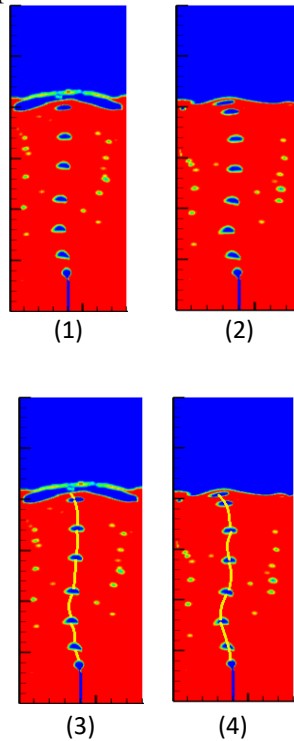


Figure 10: (1 & 2) A series of ascending bubbles that are spiraling through the water. The yellow line in (3 & 4) depicts the jets' course

Case 3 (Discontinuous Jet)

Following that, At the air mass flow rate of 0.0012 Kg/s at the inlet of the nozzle, we get a discontinuous jet that is raising in the water channel, as seen in Figure 11(1 & 2) below. As seen in Figure 11(3 & 4), a jet was also seen after spiral increase, much like in the earlier occurrences and perfectly resembles the experimental results. The numerical results clearly shows that with increasing the mass flow rate of the air injected at the inlet of the nozzle shifts the formation of bubbles into jets. Further increase in air mass flow rate will form a more continuous and confined jet.

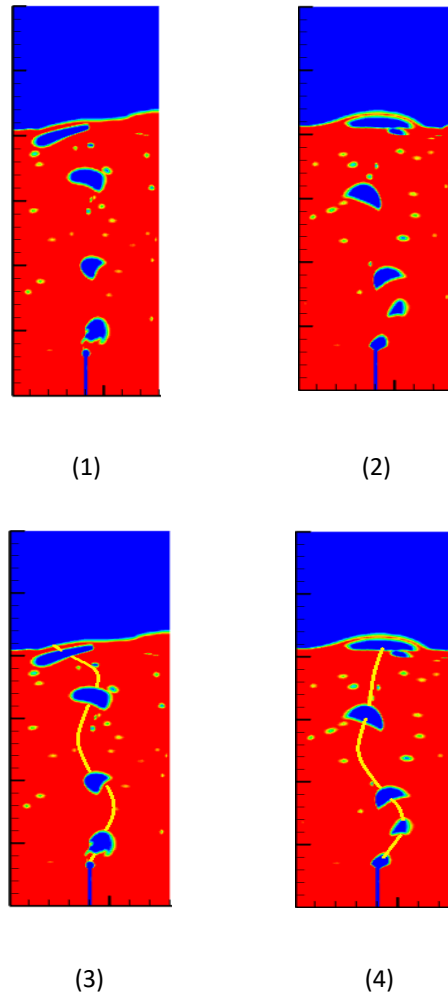


Figure 11: Discontinuous (1 & 2) Jet ascending in the plane of $x-y$ on a spiral path through the water. The yellow line in (3 & 4) depicts the jets' course

CONCLUSION

Significant insights into the behavior of the air bubbles and jets in vertically channels of water, especially in the case of a submerged needle, are obtained from a thorough review of experimental and computational data. The results of the experiment show that the climb is not as straight as expected; instead, it continuously follows a spiral path. This divergence is explained by the air rise's adoption of a spiral trajectory due to the destabilizing effect of the immersed needle at the intake. Surprisingly, the air rises regardless of changes in flow rate, highlighting the importance to the submerged needle's effect on trajectory.

Air rise tends to follow a spiral path instead of a straight one, as confirmed by numerical models that match experimental findings. The destabilizing effect of the submerged needle at the intake is maintained within the numerical domain, supporting the idea that it is crucial in determining the air jets'



ICSET-23



UET Peshawar

trajectory. Moreover, the numerical outcomes confirm that jet rise is independent of flow rate variations. Interestingly, the precise predictions obtained using the Transition SST model are in contrast to the inadequate jet behaviour forecast by the k- ϵ turbulence model. The study's credibility is strengthened by the agreement between computational and experimental results, which highlights the usefulness of these results for the management of water resources and related sectors.

ACKNOWLEDGEMENTS

I am appreciative to Allah Ta'ala for giving me the ability to conduct this research. I appreciate the cooperation, inspiration, and direction I received from Supervisor Associate Professor Dr. Kareem Akhtar, of the Mechanical Department at the UET, Peshawar.

We would especially like to thank the USPCASE University of Engineering and Technology in Peshawar's Dr. Khurshid Ahmad, Dr. Hassan, Engr. Saad Rehan, and Engr. Fahad for their assistance with the numerical investigation.

REFERENCES

- [1] M Said, N. N. Bouda and S Harmand, "A Comparative Study of Two Numerical Methods Applied for 3D Liquid-Liquid Taylor Flow in a Microchannel, *Journal of Applied Fluid Mechanics*, vol. 17, pp. 1-18, and 2023.
- [2] A. W. G. d. Vries, *Path and Wake of a Rising Jet*, the Netherlands, 2001.
- [3] Y. Cordova, Y. Rivera, *Experimental Investigation of Submerged Horizontal Air–Steam Mixture Jets into Stagnant Water*, WIT Transactions on Engineering Sciences, Vol 128, ISSN 1743-3533, 2020.
- [4] Bo Ho "A Numerical Study of a Submerged Water Jet Impinging on a Stationary Wall" *Journal of Marine Science and Engineering*, vol. 10, no. 2, pp. 228-242, 2022.
- [5] M. Xinng "Transient dynamic analysis for the submerged gas jet in flowing water," *European Journal of Mechanics - B/Fluids*, vol. 85, pp. 351-360, 2021.
- [6] Y. Zhou, "Numerical investigation on submerged steam jet condensation in subcooled water flow in a restricted channel with the presence of non-condensable gas," *International Journal of Thermal Sciences*, vol. 170, no. 4, pp. 251-263 2021.
- [7] I. E. J. Magnaudet, "The Motion of High-Reynolds-Number Jets in Inhomogeneous Flows," *Annual Review of Fluid Mechanics*, vol. 32, pp. 659-708, 2000.
- [8] H. S.-I. H. TSUGE, "The onset conditions of oscillatory motion of single gas jets rising in various liquids," *Journal of Chemical Engineering of Japan*, vol. 10, no. 1, pp. 66-68, 1977.
- [9] T. B. Benjamin, "Hamiltonian theory for motions of jets in an infinite liquid," *Journal of Fluid Mechanics*, vol. 181, pp. 349-379, 1987.
- [10] M. A. Y. K. M. M. M. Nakagawa, "Identification of Aerodynamic Coefficients of Zigzag Rising Jets," *Proceedings of 15th International Conference on Nuclear Engineering*, 2007.
- [11] F. R. KJETIL ELLINGSEN, "On the rise of an ellipsoidal jet in water: oscillatory paths and liquid-induced velocity," *Journal of Fluid Mechanics*, vol. 440, pp. 235-268, 2001.
- [12] M. W. Erin Kelley, "Path instabilities of rising air jets in a Hele-Shaw cell," *PHYSICAL REVIEW LETTERS*, vol. 79, no. 7, p. 1265, 1997.



ICSET-23

*Proceedings of the 5th International Conference on Sustainable
Energy Technologies (ICSET 2023) Peshawar, Pakistan
14-15 December 2023*



UET Peshawar

- [13] N. M. A. Tapucu, "The motion of gas jets rising through stagnant liquid," *Heat and Mass Transfer Wärme- und Stoffübertragung*, vol. 2, no. 2, p. 118–128, 1969.
- [14] N. M. A. Tapucu, "Studies on the drag and shape of gas jets rising through a stagnant liquid," *Heat and Mass Transfer Wärme- und Stoffübertragung*, vol. 2, no. 3, p. 171–177, 1969.
- [15] M. S. A. N. G. S. G. P. Hanafizadeh, "Experimental investigation of air–water, two-phase flow regimes in vertical mini pipe," *Scientia Iranica*, vol. 18, no. 4, p. 923–929, 2011.
- [16] K. E. X. Y. S. O. T. Richter, "Measuring the diameter of rising gas jets by means of the ultrasound transit time technique," *Nuclear Engineering and Design*, vol. 291, p. 64–70, 2015.
- [17] M. T. V. P. M. Abid Akhtar, "Single and Multiple Jet in Jet Column Reactors," *Process Systems Computations Laboratory, Department of Chemical Engineering, Perth, Western Australia*.
- [18] B. P. B. S. Z.L. Yang, "Numerical simulation of bubbly two-phase flow in a narrow channel," *International Journal of Heat and Mass Transfer*, vol. 45, no. 3, p. 631–639, 2002.
- [19] P. G. J. N. S. M. N. U. A. M. M. T. Islam, "A SINGLE AIR JET IN WATER: A CFD STUDY," *Mechanical Engineering Research Journal*, vol. 9, pp. 1-6, 2013.
- [20] M. K. T. K. C. S. Harsha Konda, "Jet motion in a converging-diverging channel," *Journal of Fluids Engineering*, vol. 138, no. 6, 2016.
- [21] E. S. Afshin Ahmadi Nadooshan, "Numerical Simulation of a Single Air Jet Rising in Water with Various Models of Surface Tension Force," *International Journal of Aerospace and Mechanical Engineering*, vol. 2, no. 1, 2008.
- [22] G. B. P. G. I. Chakraborty, "A coupled level-set and volume-of-fluid method for the buoyant rise of gas," *International Journal of Heat and Mass Transfer*, vol. 58, no. 1-2, p. 240–259, 2013.
- [23] S. L. S. L. T. T. K. X. Wenqi Yuan, "Numerical Simulation of Jet Motion in," *Engineering Applications of Computational Fluid*, vol. 5, no. 4, pp. 517-529, 2011.

Paper ID: ICSET-2337

ANALYSIS ON HOMER SOFTWARE FOR ENERGY MODELLING AND FORECASTING: A CASE STUDY

Umair Akhtar, Waqas Javid*, Aqib, Ahmed Nawaz, Shahid Iqbal, Atif Niaz, Mehmood Ul Hassan Amjad
Mechanical Engineering Department, Wah Engineering College, University of Wah, Pakistan

**Corresponding author*

Email: waqas.javid@wecuw.edu.pk

ABSTRACT

The generation of ON-grid power utilizing sustainable power source innovations has turned into a more dependable source to address the issues of provincial territories at a restricted level without thinking about regular assets. The primary aim of this research was to develop a cost-effective and well-optimized hybrid energy project for producing electricity for an educational institution located in the Rawalpindi district of Taxila (Wah Cantt), Punjab province. Additionally, electrical load data for one of the educational institutions in the Taxila region was gathered. Technical-economic analyses is used to determine the proper load fulfilment using the hybrid PV configuration, the hybrid renewable energy optimization model was employed. The analysis using the hybrid PV potential and solar irradiance data by the educational institution was carried out using a data analysis expert software. Sensitivity analyses were used to further refine the results taken from the software, which yielded the current total net cost (NPC) and the cost of electricity (COE). Sensitivity parameters that have been used in sensitivity analysis include PV price, solar irradiation, and load variation. Cost analysis for the combination of 23kW and 29kW of 30 kW capacity convertor and 675 and 850kW PV modules was a better solution for this contextual analysis, with a starting capital venture of approximately PKR 3M and an overall net present cost (NPC) of PKR 4.48M. Since the cost of power from a lattice is 18 PKR/kWh for commercial purposes, this cross-breed framework provides power to the buyers for 15.5 PKR/kWh with little to no effort and saves about 2.5 PKR/kWh, after comparing the system attainment, this analysis demonstrates that, given the current net cost and energy cost, the system is technically and economically feasible.

KEYWORDS: Renewable Energy, Hybrid Energy System, HOMER, Sensitivity Analysis, Pakistan

INTRODUCTION

Pakistan has been dealing with a terrible electricity crisis that has an impact on many other sectors in addition to business, industry, and agriculture, since 2007. Pakistan's GDP has decreased from 8% to 2% over the past ten years due to this, with the agriculture sector accounting for 20% of the total GDP [1]. Pakistan is recognized to be the fourth-largest groundwater consumer just for irrigation in agriculture, with a vast area dedicated to farming. As a result, the country's third-largest user of electricity for irrigation is the agricultural sector. Pakistan's industrial sector accounts for 24% of GDP. Its major industries, which produce 40% of the country's employed labour force and 66% of its merchandise, are cotton, textile, and apparel manufacture. For this reason, Pakistan is regarded as the world's second-largest consumer of electricity [1]. Industrial manufacturing and agricultural irrigation systems are severely impacted by the consistently extreme shortfall. Because there is a continuous, long-term lack of electricity to power the



irrigation systems, it is impractical to provide water to the crops. It can occasionally last longer than sixteen hours [2]. Besides, the majority of these frameworks based on inexhaustible sources have contradictory supply problems compared to traditional sources due to irregular qualities under variable climate conditions, which affect the vitality creation. These frameworks based on endless sources can be coupled with developments in energy storage or other non-sustainable frameworks to solve this issue and offer energy supply in dependable ways. Immense research on such independent and cross-breed frameworks has been done before, incorporating at least two kinds of sustainable sources and capacity apparatuses. Analysts and vitality modelers have been assessing the performance and reliability of these frameworks through the use of distinctive instruments or projects for display. One of these instruments for displaying vitality that the analyst uses for demonstration and streamlining is HOMER. The cost and framework-improving, Half and Half Streamlining Model for Electric Renewables (HOMER), developed by NREL (National Renewable Energy Laboratory, USA), is used for determining the feasibility of any task. This instrument can perform hourly recreations and handle a variety of emerging innovations, such as photovoltaics (PV), wind, hydropower, and energy components. This device has been used for the planet's off-network control framework investigations as well as pre-feasibility studies. For the half-and-half framework in Newfoundland that uses hydrogen as a source of energy [3]. Karakoulidis et al. (2007), Barsoum (2009), and Giatrakos et al. (2005) investigated the half-breed electric power framework based on the photovoltaic-diesel engine that distinguishes that cross frame is financially smart than that of a 50-watt sun-based array with storage. This study is actually based on little household things having peak load on 40 W and 5W based. Furthermore, this does not characterize the beneficial use of vitality since it concentrates only the fundamental needs [4-6].

Munuswamy S. et al. (2011) conducted a survey on the cost of supply the power module used by the HOMER programming. This investigation has deduced that the power. However, cost correlation research was conducted simply by taking variety of biomass quantities supply of the network is less expensive than that of a network-based source in case it has exceeded 44 km. This investigation was conducted by a small substance but not by a provincial group [7]. As a result, Anand Singh et al. (2015) reproduced the upfront cost using HOMER programming for a solar, biomass and power-based module considering half and half of the vitality point for the Bhopal energy center. This test was performed for the essential heap of 101kWh / day using components oriented to the sun, biomass and energy without taking into account the required changes and the hydrogen fuel used as a feed device [8]. Hafez O et al. (2012) took into consideration the cross-scale network infrastructure in view of the breeze, hydroelectric power, Renewable and conventional power for the 1183 kW peak stack and the accumulation of 600 bases in the group of countries. This investigation was completed by providing oversized assumptions impossible for the framework [9]. Smruti et al. (2013) introduced a cost analysis based on the cross-biomass-biomass structure for a small peak space of 3.6 kW in a remote territory using biomass excreta. This framework was financially experimented with deference to the traditional matrix scheme and the period of recovery of the investment was around 12 years. However, this test was also performed for a 95-year-old house, not even at the group level [10]. Luiz et al. (1998) has presented a pre-feasibility report for a half-field FV-diesel frame for a small town of 100 families. This half-breed framework must be financially intelligent than the diesel-based framework that lowers the cost of fuel utilization [11].

It is evident that the central focus in the field of sphere of the before mentioned studies was electrification of rural and urban areas seeking for the domestic intensity ignoring the electricity requirement that never ends for agriculture as for irrigation purposes. Programmed the law in the direction of the sober knowledge of the author, very seeks the appearance of rejection to the captious side together to the techno-economic colon so based on HOMER of such renewable energy systems angry convincing part of Pakistan.



ICSET-23



UET Peshawar

Disposition of an underdeveloped country, Pakistan is economically contingent, to include a superior agricultural sector which produces in a defective manner due to the proximity of the damage caused by the electricity always from a decade. With regard to the part, 61.74% endless makes some place come to your home from the community of rural areas, the prohibition of access for 46% keeps reroute instead of the electric network [12, 13]. Little by little, the basic objective to establish the balance and the precision of proportioning and optimizing to first level part is to have a realistic realist who belongs to the property of electrification of the income and advertising of rural areas. More information about Pakistan somewhere in the electricity network not available. A rest, the tactics just before preparing these objectives, the load of electricity, biomass and the informer on the superior solar radiation was of fashion of second-hand supervision of technical-economic analysis of restlessness through simulations based on HOMER without including the sensitivities of collapse renewable energy technologies are considered to be essential component in the economic progress of country.

METHODOLOGY

The HOMER program, created by NREL (National Renewable Energy Laboratory, USA), is the most efficient way to design a hybrid solar/biomass system and evaluate its techno-economic viability and accessibility. When the target function is reduced to its constraints, the best possible system configuration is improvised. The target function for this analysis is Net Present Cost (NPC), which is the system's current cost minus gross receipts. Maintenance of power balance, batteries and cells, and other technological constraints are some of the limitations. Every operating hour's energy balance is produced by the HOMER software, which simulates the system configuration and determines the hourly electric and thermal loads required to run the system [14]. This analysis elaborates on the importance of renewable incursions and filling on the NPC and COE. Optimization and feasibility analysis can be done by HOMER before the installation of microgrid systems. Commonly, HOMER can perform three major tasks i-e simulation of the system, optimization of simulation, and sensitivity analysis [15]. In order to create a pre-HOMER analysis, the actual loads required by the institute are checked before proceeding with the HOMER-based analysis of hybrid biomass or solar systems in general. Subsequently, the computed load data is entered into the HOMER software interface, enabling analysis of the hybrid micro-grid system through the use of the software's accessible hardware. The load, grid, and components of hybrid renewable systems are the three main pieces of equipment. Different electric loads are included in this study's load, and components include batteries, power generators, photovoltaic cells, and converters. [16] After this study, the HOMER model builds an equipment's capacity based on the needs of the operational system. Valuable constraints are used for sensitivity analysis based on life cycle cost analysis and system requirements. To arrive at a final decision regarding the market energy cost value, a post-analysis was conducted following the completion of the HOMER-based analysis. Pakistan has set market energy prices, including cost supply tariffs, through MEPCO, LESCO, and NTDC. The feasibility analysis approach is elaborated in the fig below.

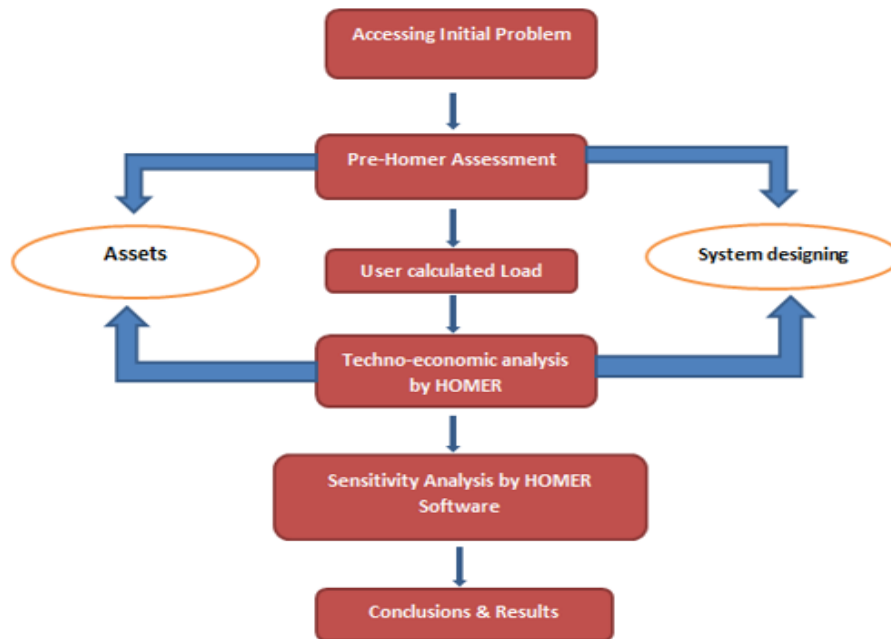


Fig 1. Methodology adopted for analysis

User Load Assessment

This hybrid On-grid system is actually designed to meet the electricity needs of education institutes. In the current situation, demand is considerably high due to the consumption of High electricity equipment 'like Electric cattle, Air conditioners, Motors, and other Lab apparatuses. The evaluation of the electrical load has been carried out carefully considering the load requirements for peak season for energy needs. Load calculations are listed in Table 1 and Table 2 respectively.

The peak load of load requirement is calculated at approximately 2256.2056kWh and 2841.449kWh respectively. The daily electric load and peak load profile including seasonal effect as shown in figure 2 (a) and (b). The electric load profiles show clearly the load variation through 24 hours of the day, the maximum load requirement is the mid of the day and the minimum at the night of the day. During the day, most of the electric equipments are used in labs therefore maximum load occur at that time i.e., 12:00 am. The lab schedule is mostly in between 9:00 a:m to 4:00 p:m of the week which maximizes the peak load during the day times.



ICSET-23

Proceedings of the 5th International Conference on Sustainable
Energy Technologies (ICSET 2023) Peshawar, Pakistan
14-15 December 2023



UET Peshawar

Table 1: Electric load calculation

| Time: | JAN | FEB | MARCH | APRIL | MAY | JUNE | JULY | AUG | SEP | OCT | NOV | DEC |
|---------------|------------|------------|------------|------------|-----------|-------------|------------|------------|-------------|-------------|-------------|----------|
| 01 (12:00 am) | 94.9785 | 103.6485 | 111.5235 | 117.5235 | 126.067 | 122.72145 | 118.18925 | 112.42225 | 105.70225 | 102.38225 | 97.28225 | 95.716 |
| 02 (01:00 am) | 94.9785 | 103.6485 | 111.5235 | 117.5235 | 126.067 | 122.72145 | 118.18925 | 112.42225 | 105.70225 | 102.38225 | 97.28225 | 95.716 |
| 03 (02:00 am) | 94.9785 | 103.6485 | 111.5235 | 117.5235 | 126.067 | 122.72145 | 118.18925 | 112.42225 | 105.70225 | 102.38225 | 97.28225 | 95.716 |
| 04 (03:00 am) | 94.9785 | 103.6485 | 111.5235 | 117.5235 | 126.067 | 122.72145 | 118.18925 | 112.42225 | 105.70225 | 102.38225 | 97.28225 | 95.716 |
| 05 (04:00 am) | 94.9785 | 103.6485 | 111.5235 | 117.5235 | 126.067 | 122.72145 | 118.18925 | 112.42225 | 105.70225 | 102.38225 | 97.28225 | 95.716 |
| 06 (05:00 am) | 93.9544 | 95.1544 | 96.2544 | 97.3244 | 98.881 | 98.121 | 97.3345 | 96.6455 | 96.4115 | 96.1985 | 95.8418223 | 95.716 |
| 07 (06:00 am) | 93.9544 | 95.1544 | 96.2544 | 97.3244 | 98.881 | 98.121 | 97.3345 | 96.6455 | 96.4115 | 96.1985 | 95.8418223 | 95.716 |
| 08 (07:00 am) | 154.368 | 161.348 | 169.804 | 179.248 | 187.348 | 178.00447 | 170.66447 | 166.33147 | 162.77147 | 159.44947 | 155.55947 | 153.148 |
| 09 (08:00 am) | 1103.1632 | 1053.7005 | 1355.33523 | 1775.902 | 1836.234 | 1785.670733 | 985.250733 | 980.918513 | 976.585213 | 1357.020643 | 1146.566143 | 1167.412 |
| 10 (09:00 am) | 1093.0781 | 1032.72377 | 1393.17937 | 1893.52367 | 1938.98 | 1798.56 | 988.126 | 982.8008 | 979.2342 | 1379.8008 | 1189.4708 | 1154.186 |
| 11 (10:00 am) | 1108.647 | 1043.877 | 1444.427 | 1914.767 | 1945.843 | 1810.94643 | 990.71343 | 985.49143 | 981.24723 | 1411.91323 | 1211.59123 | 1145 |
| 12 (11:00 am) | 1114.1958 | 1084.1958 | 1505.4413 | 2115.6736 | 2256.2056 | 2121.30885 | 1009.97685 | 997.42335 | 990.09935 | 1440.83705 | 1225.83705 | 1194.33 |
| 13 (12:00 pm) | 1097.3547 | 1094.9347 | 1455.2647 | 1905.698 | 1996.238 | 1876.028 | 990.34911 | 987.14911 | 981.81589 | 1382.27119 | 1199.97119 | 1103.09 |
| 14 (13:00 pm) | 1130.01027 | 1118.01027 | 1468.57627 | 2069.04 | 2139.04 | 2088.3967 | 1001.94236 | 998.48636 | 993.92636 | 1333.92636 | 1183.58186 | 1139.696 |
| 15 (14:00 pm) | 1133.60068 | 1128.35512 | 1439.13512 | 1939.57512 | 2050.153 | 1949.8074 | 999.4544 | 997.22 | 990.4514465 | 1280.451447 | 1170.001447 | 1148.71 |
| 16 (15:00 pm) | 685.5912 | 659.0252 | 819.7252 | 1120.2922 | 1240.97 | 1130.63 | 730.63 | 719.286 | 710.7416 | 821.0866 | 760.6566 | 697.248 |
| 17 (16:00 pm) | 303.248311 | 306.81621 | 376.81621 | 407.61 | 458.26 | 414.693 | 294.23734 | 281.78074 | 275.30274 | 335.86874 | 314.29174 | 301.92 |
| 18 (17:00 pm) | 110.8274 | 109.5944 | 126.9244 | 155.3644 | 166.71 | 159.1311 | 110.5544 | 106.321 | 102.222655 | 133.2002655 | 113.2132655 | 111.416 |
| 19 (18:00 pm) | 109.45155 | 105.77355 | 113.77355 | 134.12655 | 143.03 | 132.475 | 105.01944 | 102.71944 | 101.26444 | 121.96444 | 110.62044 | 109.528 |
| 20 (19:00 pm) | 112.2741 | 114.1441 | 137.4773 | 167.1543 | 195.722 | 177.15522 | 136.47692 | 131.01116 | 122.46116 | 168.11816 | 117.61816 | 113.81 |
| 21 (20:00 pm) | 94.9785 | 103.6485 | 111.5235 | 117.5235 | 126.067 | 122.72145 | 118.18925 | 112.42225 | 105.70225 | 102.38225 | 97.28225 | 95.716 |
| 22 (21:00 pm) | 94.9785 | 103.6485 | 111.5235 | 117.5235 | 126.067 | 122.72145 | 118.18925 | 112.42225 | 105.70225 | 102.38225 | 97.28225 | 95.716 |

Table 2: Electric load calculation

| Time: | JAN | FEB | MARCH | APRIL | MAY | JUNE | JULY | AUG | SEP | OCT | NOV | DEC |
|---------------|-----------|-----------|------------|------------|------------|----------|----------|----------|----------|----------|----------|-----------|
| 01 (12:00 am) | 142.141 | 138.906 | 159.029 | 175.126 | 183.804 | 191.81 | 185.348 | 171.694 | 157.128 | 168.56 | 163.668 | 151.264 |
| 02 (01:00 am) | 142.141 | 138.906 | 159.029 | 175.126 | 183.804 | 191.81 | 185.348 | 171.694 | 157.128 | 168.56 | 163.668 | 151.264 |
| 03 (02:00 am) | 142.141 | 138.906 | 159.029 | 175.126 | 183.804 | 191.81 | 185.348 | 171.694 | 157.128 | 168.56 | 163.668 | 151.264 |
| 04 (03:00 am) | 142.141 | 138.906 | 159.029 | 175.126 | 183.804 | 191.81 | 185.348 | 171.694 | 157.128 | 168.56 | 163.668 | 151.264 |
| 05 (04:00 am) | 142.141 | 138.906 | 159.029 | 175.126 | 183.804 | 191.81 | 185.348 | 171.694 | 157.128 | 168.56 | 163.668 | 151.264 |
| 06 (05:00 am) | 142.141 | 138.906 | 159.029 | 175.126 | 183.804 | 191.81 | 185.348 | 171.694 | 157.128 | 168.56 | 163.668 | 151.264 |
| 07 (06:00 am) | 111.627 | 109.196 | 111.332 | 115.811 | 119.432 | 120.141 | 116.688 | 114.501 | 112.182 | 118.614 | 115.374 | 113.062 |
| 08 (07:00 am) | 111.627 | 109.196 | 111.332 | 115.811 | 119.432 | 120.141 | 116.688 | 114.501 | 112.182 | 118.614 | 115.374 | 113.062 |
| 09 (08:00 am) | 1664.7645 | 1611.5555 | 1882.2305 | 2312.8315 | 2614.5065 | 2746.658 | 1296.118 | 1225.227 | 1164.927 | 1831.272 | 1765.672 | 1716.6615 |
| 10 (09:00 am) | 1686.1526 | 1645.7176 | 1926.2026 | 2376.9896 | 2667.7546 | 2778.713 | 1318.059 | 1257.609 | 1198.703 | 1865.563 | 1796.942 | 1736.6956 |
| 11 (10:00 am) | 1613.717 | 1563.953 | 1859.861 | 2270.647 | 2591.193 | 2665.88 | 1215.315 | 1168.335 | 1106.657 | 1757.057 | 1698.607 | 1666.175 |
| 12 (11:00 am) | 1698.81 | 1668.27 | 1968.571 | 2469.465 | 2780.122 | 2841.449 | 1340.795 | 1261.141 | 1206.265 | 1906.807 | 1860.899 | 1784.241 |
| 13 (12:00 pm) | 1422.8543 | 1362.4013 | 1713.1663 | 1963.7333 | 2214.4093 | 2373.287 | 1172.726 | 1098.226 | 1052.444 | 1633.053 | 1572.177 | 1483.3043 |
| 14 (13:00 pm) | 1470.6805 | 1405.2475 | 1745.8145 | 2047.2465 | 2338.0115 | 2418.524 | 1198.026 | 1127.681 | 1071.701 | 1652.25 | 1584.263 | 1511.5775 |
| 15 (14:00 pm) | 1297.6315 | 1239.0465 | 1579.8585 | 1790.5035 | 2021.0465 | 2166.499 | 1121.829 | 1054.028 | 1002.362 | 1443.152 | 1391.443 | 1354.0615 |
| 16 (15:00 pm) | 918.65625 | 878.11325 | 1108.76625 | 1299.53125 | 1470.18525 | 1539.946 | 829.046 | 797.376 | 766.906 | 1068.715 | 1009.175 | 962.46625 |
| 17 (16:00 pm) | 357.407 | 351.729 | 382.405 | 425.861 | 452.65 | 497.2 | 366.609 | 351.177 | 340.644 | 400.187 | 387.623 | 374.077 |
| 18 (17:00 pm) | 275.574 | 271.806 | 293.592 | 305.357 | 326.924 | 349.752 | 309.317 | 296.861 | 280.318 | 311.215 | 295.326 | 282.45 |
| 19 (18:00 pm) | 147.447 | 143.438 | 184.198 | 192.095 | 196.884 | 205.78 | 160.215 | 154.648 | 148.883 | 170.558 | 157.998 | 152.101 |
| 20 (19:00 pm) | 142.141 | 138.906 | 159.029 | 175.126 | 183.804 | 191.81 | 185.348 | 171.694 | 157.128 | 168.56 | 163.668 | 151.264 |
| 21 (20:00 pm) | 142.141 | 138.906 | 159.029 | 175.126 | 183.804 | 191.81 | 185.348 | 171.694 | 157.128 | 168.56 | 163.668 | 151.264 |
| 22 (21:00 pm) | 142.141 | 138.906 | 159.029 | 175.126 | 183.804 | 191.81 | 185.348 | 171.694 | 157.128 | 168.56 | 163.668 | 151.264 |
| 23 (22:00 pm) | 142.141 | 138.906 | 159.029 | 175.126 | 183.804 | 191.81 | 185.348 | 171.694 | 157.128 | 168.56 | 163.668 | 151.264 |
| 24 (23:00 pm) | 142.141 | 138.906 | 159.029 | 175.126 | 183.804 | 191.81 | 185.348 | 171.694 | 157.128 | 168.56 | 163.668 | 151.264 |



ICSET-23

*Proceedings of the 5th International Conference on Sustainable
Energy Technologies (ICSET 2023) Peshawar, Pakistan
14-15 December 2023*



UET Peshawar

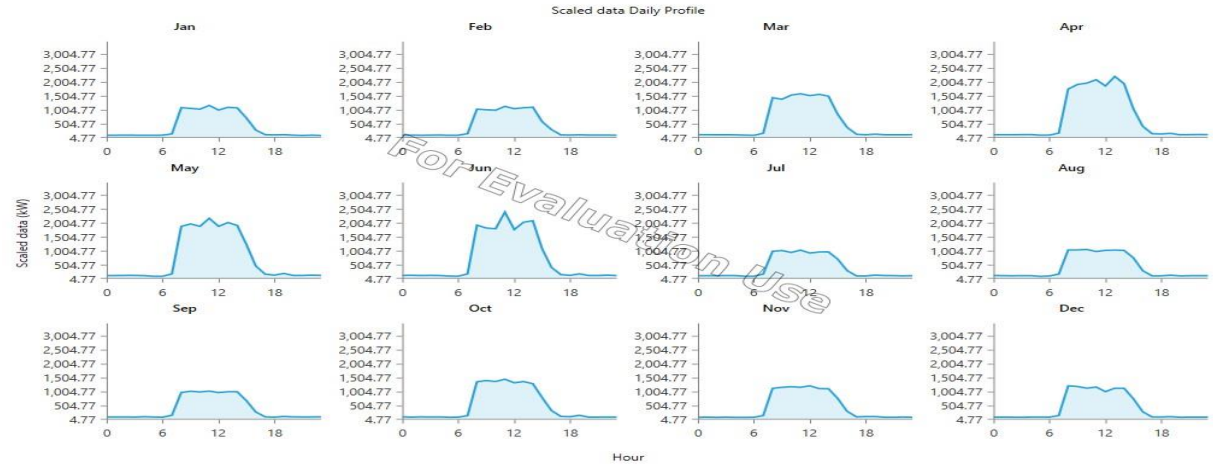


Figure 2 (a): Load profile for educational institute

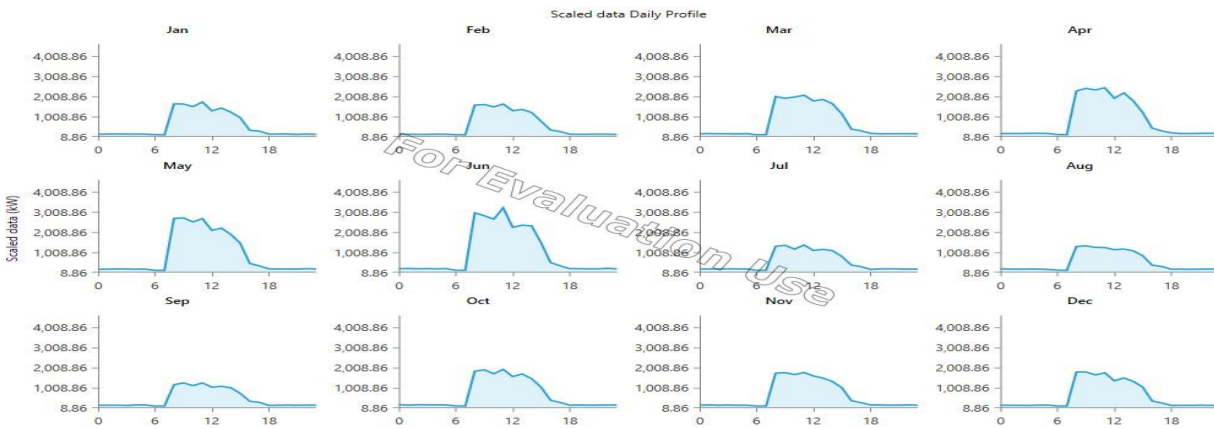


Figure 2 (b): Peak Load profile for educational institute

Available Resources Assessment

The full details and evaluation of the resources and hybrid solar system are provided below for the specific case in which it is being considered.

Available Solar Radiation

Data on solar radiation was obtained using the HOMER software for the position "Wah Cantt, Taxilla" of latitude 31°13, 6'N and longitude 70°57, 1'E from "Surface Meteorology and Solar from NASA Energy database. "The annual average solar radiations were 5.18 kwh/m²/day and the maximum solar

radiation was 7.43 kwh/m²/day. The data show that the position has a good solar potential and can efficiently produce energy using photovoltaic panels (PV) as shown in Fig. 3 and 4.

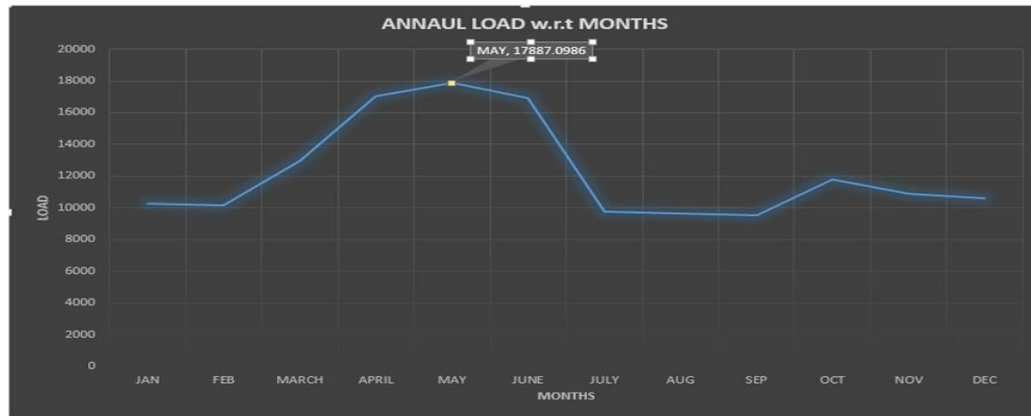


Figure 3: Monthly average load profile.

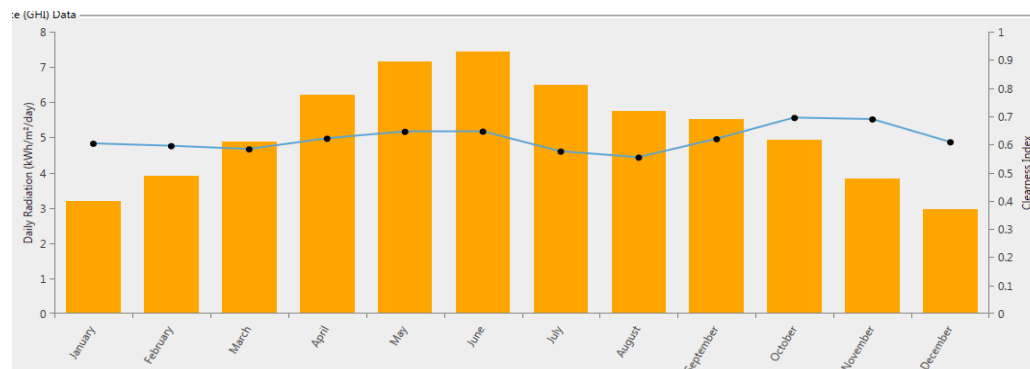


Figure 4: Solar radiations profile

Design and View Point

In this system electricity generation system outside the PV-solar network, two main components include photovoltaic (PV) panels, converter, and storage batteries. To present the pre-feasibility report for the hybrid system, a system consisting of 675 KW and 850 kW photovoltaic modules and converter has been designed as shown in figures 5 and 6.

Solar Module

In order meet the load requirement during the days of maximum lab load for experiment purposes. A list of all the solar modules used in the current system can be found in Table 3.

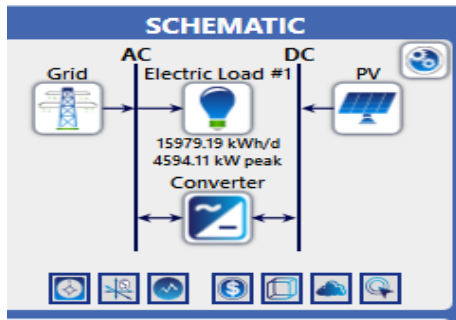


Figure 6: Configuration of hybrid PV system

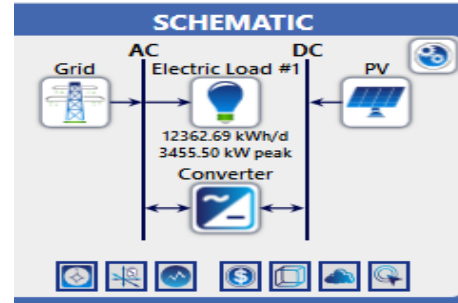


Figure 5: Configuration of hybrid PV system

Table 3: Solar Modules Cost and technical parameters

| Sr. No | Parameters | Units | Values |
|--------|------------------------------|----------|---------|
| 01 | Capital cost | PKR/kW | 9260000 |
| 02 | Replacement cost | PKR/kW | 4500000 |
| 03 | Operation & Maintenance cost | PKR/year | 6800000 |
| 04 | De-Rating Factor | % | 83 |
| 05 | Rated power | W | 250 |
| 06 | Life time | years | 25 |
| 07 | Slope | Degree | 24.5 |
| 08 | Maximum power voltage | V | 30.3 |
| 09 | Maximum power current | A | 8.21 |
| 10 | Open circuit voltage | V | 35.5 |
| 11 | Short circuit current | A | 8.75 |

Converter

The direct current that comes from the solar panel is changed into alternating current using a converter. A converter is typically assessed based on the chosen solar modules' power and an 80% average converter efficiency, such as;

$$\text{Converter} = P_{\text{array}} \times 100/80$$

$$\text{Converter} = 26 \text{ kW} \times 1.16$$

$$\text{Converter} = 30.16 \approx 30.0 \text{ kW}$$

The consumption of electricity purpose that covers the maximum load the curve is during peak hours (9: 00 a:m - 4: 00 p:m) and the hybrid system is being built outside the network. The primary goal of the hybrid system is to maximize PV during the day by sharing the load during peak hours. For the 675kW photovoltaic field, 23 converters with a 30kW capacity were chosen after taking into account the load distribution during peak hours. Similarly, 29 converters with a 30kW capacity were chosen for an 850kW



photovoltaic field. It was estimated that the converter's efficiency was 90% and that its initial cost per kW was 3, 250,00 PKR.

Table 4: Solar Modules Cost and technical parameters

| Sr. No | Parameters | Units | Values |
|--------|--------------------------------|----------|----------|
| 01 | Capital cost | PKR/kW | 45900000 |
| 02 | Replacement cost | PKR/kW | 22950000 |
| 03 | Operation and Maintenance cost | PKR/year | 9300000 |
| 04 | De-Rating Factor | % | 83 |
| 05 | Rated power | W | 250 |
| 06 | Life time | Years | 25 |
| 07 | Slope | Degree | 24.5 |
| 08 | Maximum power voltage | V | 30.3 |
| 09 | Maximum power current | A | 8.21 |
| 10 | Open circuit voltage | V | 35.5 |
| 11 | Short circuit current | A | 8.75 |

Analysis

The primary goal of software is to reduce the net cost and system operating based on input sensitivity. This is because the software is helpful to give system designers the viability and economic relationship of the system at the design stage, to verify the profitability of the systems. The project's 25-year duration and a 15% annual discount rate were taken into account for the economic analysis. The HOMER program was then used to simulate the system configuration in accordance with the load requirements. In order to assess the system's operating costs for the various daytime loads, the photovoltaic panels' capacities have been adjusted from 675–690 kW and 845-870 kW.

RESULTS AND DISCUSSIONS

In this research's PV hybrid system was created to satisfy the requirements. The HOMER program was used to simulate the system in order to optimize its configuration, which was created in accordance with the load profile. Taking into account a distinct sensitivity parameter, the system has been examined and optimized.

Results

For this reason, the technical-financial example is that these are essential factors controlling the framework, which are powerful in the performance of the framework and operating costs of the framework. The structure is sustainable and vulnerable, for example, the surveillance of the supply of biomass and the progressions in the radiation directed to the sun have been considered for the examination of the emotional capacity. The measurement of the sun-oriented radiation is different for each type of impact on the economy of the frame and the sun-oriented radiation differed from 5.19-7.43 kWh/m²/day. The results from the investigation of the emotional capacity of the vehicle and the chassis medium are shown in figure 7 (a) and

(b), which shows the margin of the net cost, energy cost (COE), the costs of the activities due to the quantity in the supply of PV solar and in the radiation solar. On the basis of the feet, we can see that expanding the surveillance of biomass and thinking about variations in solar radiation, also increase current and labor cost.





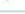
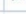

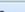








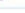
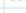



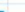





| Sensitivity | | | | Architecture | | | | | | Cost | | | | |
|-------------------------|---------------------------|--|--------------------------------|---|---|---|------------|--------------|-------------------|----------|-------------|-------------|---------------------------|-------------------------|
| Power Price (Rs/kWh) | Sellback Rate (Rs/kWh) | Solar Scaled Average (kWh/m ² /day) | Temp Scaled Average (°C) |  |  |  | PV (kW) | Grid (kW) | Converter (kW) | Dispatch | COE (Rs) | NPC (Rs) | Operating cost (Rs/yr) | Initial capital (Rs) |
| 18.0 | 11.0 | 7.43 | 20.4 |  |  |  | 675 | 999,999 | 675 | CC | Rs15.83 | Rs926M | Rs68.0M | Rs46.6M |
| 18.0 | 11.0 | 7.43 | 22.0 |  |  |  | 675 | 999,999 | 675 | CC | Rs15.88 | Rs928M | Rs68.2M | Rs46.6M |
| 18.0 | 13.0 | 5.19 | 20.4 |  |  |  | 675 | 999,999 | 675 | CC | Rs16.58 | Rs968M | Rs71.3M | Rs46.6M |
| 18.0 | 13.0 | 5.19 | 22.0 |  |  |  | 675 | 999,999 | 675 | CC | Rs16.62 | Rs970M | Rs71.4M | Rs46.6M |
| 18.0 | 13.0 | 7.43 | 20.4 |  |  |  | 675 | 999,999 | 675 | CC | Rs15.83 | Rs926M | Rs68.0M | Rs46.6M |
| 18.0 | 13.0 | 7.43 | 22.0 |  |  |  | 675 | 999,999 | 675 | CC | Rs15.87 | Rs928M | Rs68.2M | Rs46.6M |
| 20.0 | 11.0 | 5.19 | 20.4 |  |  |  | 675 | 999,999 | 675 | CC | Rs18.13 | Rs1.06B | Rs78.3M | Rs46.6M |
| 20.0 | 11.0 | 5.19 | 22.0 |  |  |  | 675 | 999,999 | 675 | CC | Rs18.17 | Rs1.06B | Rs78.5M | Rs46.6M |

Figure 7 (a): Sensitivity results for the hybrid PV system.

| Sensitivity | | | | Architecture | | | | Cost | | | | System | | PV | | |
|-------------------------|--|--------------------------------|--|--------------|------------|--------------|-------------------|----------|-------------|-------------|---------------------------|-------------------------|-----------------|----------------------|----------------------|------------------------|
| Power Price (Rs/kWh) | Solar Scaled Average (kWh/m ² /day) | Temp Scaled Average (°C) | | | PV (kW) | Grid (kW) | Converter (kW) | Dispatch | COE (Rs) | NPC (Rs) | Operating cost (Rs/yr) | Initial capital (Rs) | Ren Frac (%) | Total Fuel (L/yr) | Capital Cost (Rs) | Production (kWh/yr) |
| 18.0 | 5.19 | 20.4 | | | 850 | 999,999 | 850 | CC | \$16.63 | \$1,268 | \$92.8M | \$58.7M | 21.9 | 0 | 45,900,000 | 1,349,422 |
| 18.0 | 5.19 | 22.0 | | | 850 | 999,999 | 850 | CC | \$16.67 | \$1,268 | \$93.0M | \$58.7M | 21.7 | 0 | 45,900,000 | 1,337,443 |
| 18.0 | 7.43 | 20.4 | | | 850 | 999,999 | 850 | CC | \$15.92 | \$1,218 | \$88.9M | \$58.7M | 25.8 | 0 | 45,900,000 | 1,594,396 |
| 18.0 | 7.43 | 22.0 | | | 850 | 999,999 | 850 | CC | \$15.96 | \$1,218 | \$89.1M | \$58.7M | 25.6 | 0 | 45,900,000 | 1,580,074 |
| 20.0 | 5.19 | 20.4 | | | 850 | 999,999 | 850 | CC | \$18.19 | \$1,388 | \$102M | \$58.7M | 21.9 | 0 | 45,900,000 | 1,349,422 |
| 20.0 | 5.19 | 22.0 | | | 850 | 999,999 | 850 | CC | \$18.23 | \$1,388 | \$102M | \$58.7M | 21.7 | 0 | 45,900,000 | 1,337,443 |
| 20.0 | 7.43 | 20.4 | | | 850 | 999,999 | 850 | CC | \$17.41 | \$1,328 | \$97.6M | \$58.7M | 25.8 | 0 | 45,900,000 | 1,594,396 |
| 20.0 | 7.43 | 22.0 | | | 850 | 999,999 | 850 | CC | \$17.45 | \$1,328 | \$97.9M | \$58.7M | 25.6 | 0 | 45,900,000 | 1,580,074 |

Figure (b): Sensitivity results for the hybrid PV system

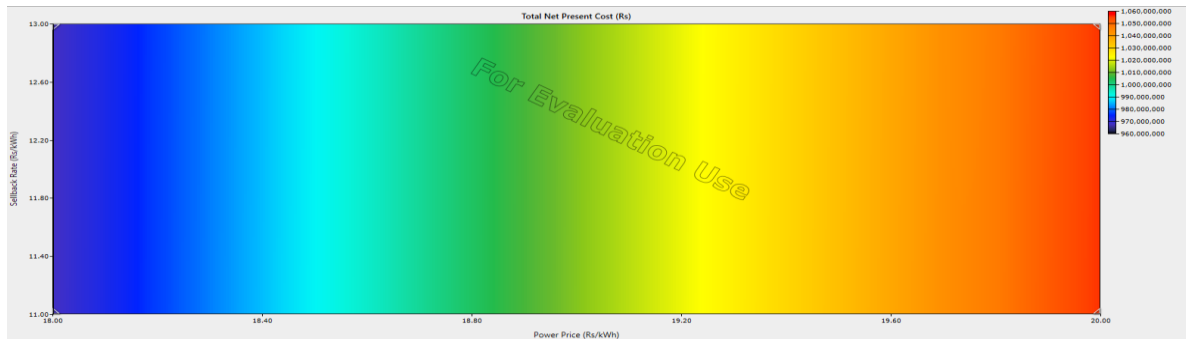


Figure (c). Sensitivity results for the hybrid PV system

The cost of energy (COE) produced by the cross structure is plotted at first sight diagram superimposed on the net real cost (NPC), as shown in Figure 8 (a). The plot shows that with the increase in



ICSET-23

*Proceedings of the 5th International Conference on Sustainable
Energy Technologies (ICSET 2023) Peshawar, Pakistan
14-15 December 2023*



UET Peshawar

solar radiation, the net production of PV-PV energy increases and the cost of viability have decreased. In this line, it can be said that at least the variable of affectivity, the limit and the generation of energy of the distinctive parts of the frame increase even more. In this sense, a photovoltaic structure can be more efficient than other regular structures due to its variety with characteristic vital resources. By changing the photovoltaic system's capacity, the HOMER software has simulated a hybrid PV system with sensitivity inputs to find the most efficient and cost-effective setup. In order to optimize the system that meets the electrical load, the photovoltaic flow range in the HOMER research space has been adjusted between 675 and 810 kW. As indicated in Figure 7 (a) and (b), the best optimized and financially simulated option for the hybrid system design in the current study is a 30 kW converter along with various renewable components selling 675 kW and 850 kW matrixes. Since HOMER offers these optimized outcomes, they are arranged according to NPC, COE, and initial capital investment. The PV that has been optimized has a total net cost (NPC) of 45,900,000 PKR and a cost of electricity (COE) of 15.5 PKR per kWh. Different sizes of equipment can be used to meet the same electricity load in configurations with higher initial cost of capital, coefficient of exchange, and current net cost. Fig. 8(a) and (b) make it clear that the photovoltaic modules are arranged coherently by the bio-gas generator's power. The photovoltaic modules produce 1,266,138 kWh / year with a limit factor of 25%. The age of control of photovoltaic modules is reduced due to the inaccessibility of radiation based on the sun in the middle of most peak hours (6:00-18:00). In addition, the framework is compliant with energy usage of 65,372 kWh/year with an abundance of energy, which can be used for some valid reason or can be saved. The average monthly electricity generation and consumption are exactly equal, as can be seen by comparing Figures 8 (a) and (b).

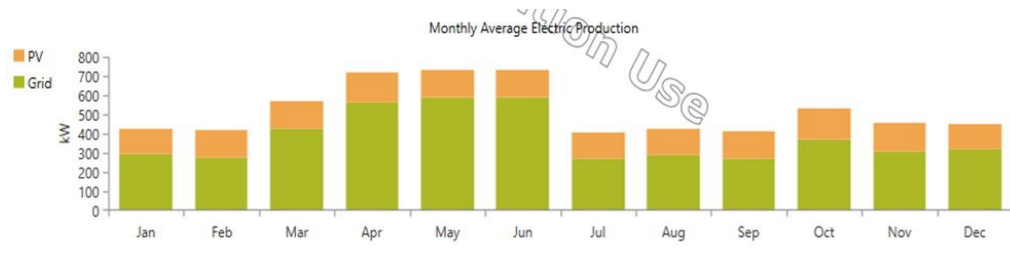


Figure 8 (a). Monthly average electricity production from the hybrid system

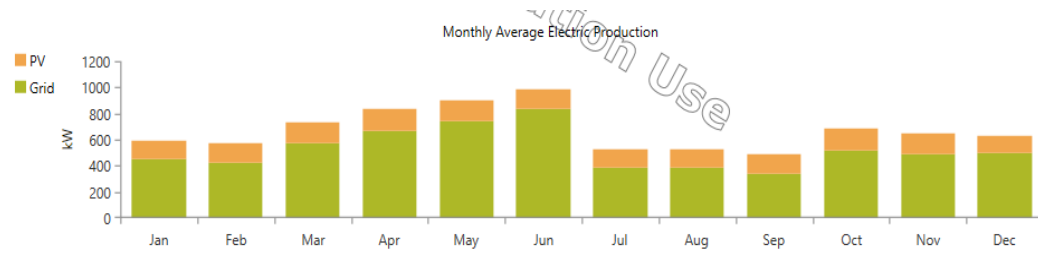


Figure 8 (b): Monthly average electricity production from the hybrid system

CONCLUSIONS

This evaluation introduces a techno-monetary assessment of different ON-Grid arrangements for the provincial universities and colleges of Pakistan. Distinctive framework arrangements of PV parameters were examined in HOMER by reproducing a dynamic mixture show. According to the results of the cost analysis, the combination of 23kW and 29kW of 30 kW capacity convertor and 675 and 850kW PV modules was a better solution for this contextual analysis, with a starting capital venture of approximately PKR 3M and an overall net present cost (NPC) of PKR 4.48M. Since the cost of power from a lattice is 18 PKR/kWh for commercial purposes, this cross-breed framework provides power to the buyers for 15.5 PKR/kWh with little to no effort and saves about 2.5 PKR/kWh. The annual production of this hybrid system is approximately 1,266,138 kWh. This framework also reduces the carbon emission in the atmosphere of about 2,098,415kg/yr. The framework has Sensible present cost for the projection time of 25 years and assessed 4.1 payback time. These half breed inexhaustible frameworks are more compelling and solid wellspring of vitality; the administration of Pakistan can assume a critical part to conquer vitality emergencies by encouraging rustic regions with such frameworks. Besides, the present supporting enactment for the use of such frameworks incorporates just assessment decreases or exclusions, which isn't adequate for the low wage groups to utilize these frameworks. The government may alter its financing arrangements, provide incentives for the framework's operation, and launch a national charge program. In order to eliminate networks from the remote rural areas, this investigation's combination infinite source-based system can be applied.



ICSET-23



UET Peshawar

ACKNOWLEDGEMENTS

All the Authors are thankful to Mechanical Engineering Department, Wah Engineering College for their support.

REFERENCES

- [1] Mahmood, A. and Akhtar, N., 1996. The export growth of Pakistan: a decomposition analysis. *The Pakistan Development Review*, 693-702.
- [2] Shahzad, M.K., Zahid, A., ur Rashid, T., Rehan, M.A., Ali, M. and Ahmad, M., 2017. Techno-economic feasibility analysis of a solar-biomass off grid system for the electrification of remote rural areas in Pakistan using HOMER software. *Renewable energy*, 106, 264-273.
- [3] Karakoulidis, K., Mavridis, K., Bandekas, D.V., Adoniadis, P., Potolias, C. and Vordos, N., 2011. Techno-economic analysis of a stand-alone hybrid photovoltaic-diesel-battery-fuel cell power system. *Renewable Energy*, 36(8), 2238-2244.
- [4] Barsoum, N.N. and Vacent, P., 2007, March. Balancing cost, operation and performance in integrated hydrogen hybrid energy system. In *First Asia International Conference on Modelling & Simulation (AMS'07) (14-18)*. IEEE.
- [5] Giatrakos, G.P., Tsoutsos, T.D., Mouchtaropoulos, P.G., Naxakis, G.D. and Stavrakakis, G., 2009. Sustainable energy planning based on a stand-alone hybrid renewableenergy/hydrogen power system: Application in Karpathos island, Greece. *Renewable Energy*, 34(12), 2562-2570.
- [6] Givler, T. and Lilienthal, P., 2005. Using HOMER software, NREL's micropower optimization model, to explore the role of gen-sets in small solar power systems; case study: Sri Lanka (No. NREL/TP-710-36774). National Renewable Energy Lab.(NREL), Golden, CO (United States).
- [7] Munuswamy, S., Nakamura, K. and Katta, A., 2011. Comparing the cost of electricity sourced from a fuel cell-based renewable energy system and the national grid to electrify a rural health centre in India: A case study. *Renewable Energy*, 36(11), 2978-2983.
- [8] Singh, A., Baredar, P. and Gupta, B., 2015. Computational simulation & optimization of a solar, fuel cell and biomass hybrid energy system using HOMER pro software. *Procedia Engineering*, 127, 743-750.
- [9] Hafez, O. and Bhattacharya, K., 2012. Optimal planning and design of a renewable energy based supply system for microgrids. *Renewable Energy*, 45, 7-15.
- [10] Pradhan, S.R., Bhuyan, P.P., Sahoo, S.K. and Prasad, G.S., 2013. Design of standalone hybrid biomass & PV system of an off-grid house in a remote area. Smruti Ranjan Pradhan et al *Int. Journal of Engineering Research and Applications*, 3(6), 433-437.
- [11] Valente, L.C.G. and de Almeida, S.C.A., 1998. Economic analysis of a diesel/photovoltaic hybrid system for decentralized power generation in northern Brazil. *Energy*, 23(4), 317-323.
- [12] Tradingeconomics.com. (2016). Rural population (% of total population) in Pakistan. <http://www.tradingeconomics.com/pakistan/rural-population501-percent-of-total-population-wb-data.html>.
- [13] Palit, D. and Chaurey, A., 2011. Off-grid rural electrification experiences from South Asia: Status and best practices. *Energy for sustainable development*, 15(3), 266-276.
- [14] Ghasemi, A., Asrari, A., Zarif, M. and Abdelwahed, S., 2013. Techno-economic analysis of stand-alone hybrid photovoltaic-diesel-battery systems for rural electrification in eastern part of Iran—



ICSET-23

*Proceedings of the 5th International Conference on Sustainable
Energy Technologies (ICSET 2023) Peshawar, Pakistan
14-15 December 2023*



UET Peshawar

A step toward sustainable rural development. Renewable and Sustainable Energy Reviews, 28, 456-462.

- [15] Farret, F.A. and Simões, M.G., 2006. Integration of alternative sources of energy (Vol. 504). Piscataway, NJ, USA: IEEE press.
- [16] Lambert, T., Gilman, P. and Lilienthal, P., 2006. Micropower system modeling with HOMER. Integration of alternative sources of energy, 1(1), 379-385.

Paper ID: ICSET-2338

Sustainable Wheels In Motion: Eco- Transit A Review Of Three-Wheeler Reverse Trike Fun Utility Vehicle Innovation

Mehmood ul Hassan Amjad*, Waqas Javid, Muhammad Sameer Jamil, Ahmed Shakeel, Ansar Malik

Department of Mechanical Engineering, Wah Engineering College, 47000, Wah Cantt, Pakistan.

**Corresponding author*

Email: mehmoodmoodi18@gmail.com

ABSTRACT

This review paper is dedicated to an in-depth exploration of the world of three-wheeled reverse trike vehicles, with a particular emphasis on safety, suspension systems, and lightweight body design. The primary focus of this review is to elevate the standards of safety features, optimize suspension systems, and introduce cutting-edge lightweight materials in three wheelers. In alignment with Sustainable Development Goals this research is committed to fostering a Low Carbon Economy by championing energy-efficient transportation solutions through innovative designs and environmentally conscious materials, while advancing the field of Energy Economics and Modeling to pave the way for a sustainable future in transportation.

KEYWORD: Three –Wheeler, Reverse Strike, Suspension System, Aerodynamics, Economic, Light Weight Chassis, MS Body

HISTORICAL BACKGROUND

The first car with an internal combustion engine that was used for daily transportation was created in 1885 by German mechanical engineer Karl Benz. Internal combustion engine power propelled the three-wheeled vehicle.

The history of cars is a remarkable journey spanning over a century. It all began in the late 19th century with Karl Benz's invention of the Motorwagen, the first gasoline-powered vehicle. Early development saw pioneers like Ford, Daimler, and Renault producing automobiles, but they were often reserved for the wealthy. Production was revolutionized and cars became more affordable with Henry Ford's invention of the assembly line in the early 20th century. The post-war boom in the 1950s brought about stylish and powerful vehicles. In the 1970s, environmental concerns and oil crises shifted focus to fuel efficiency. Computers and safety features became prominent in the 1980s, paving the way for hybrid and electric vehicles in the late 20th century. The 21st century marked the rise of autonomous and connected vehicles, with a growing emphasis on sustainability and electric cars. The history of cars is a testament to human innovation, continually evolving to meet the demands of a changing world.



INTRODUCTION

The purpose of working on project of a tri-wheeler is due to its evolution in recent area and to provide safety factor an economic zone to the driver with high speed. A reverse trike can be engineered to have a lower center of gravity, improving stability and reducing the risk of rollovers. PMVs (Personal Mobility Vehicles) -Tri Wheelers are considered a new category of transportation devices that can offer solutions for mobility issues faced by developing low-carbon transportation, the elderly, and revitalizing downtown [1].

A Reverse Trike

It is a vehicle which has two wheels up front and one in the back. In most cars, the front wheels are handled by the steering while the engine powers the rear wheels. The reason for discussing safety factors and goals is that the number of accidental deaths has been on the rise from 2003 to 2012, with a 51.8% increase in 2012 over 2002. Three-wheelers may be the way of the future for the automotive industry because they are extremely safe to drive and unlikely to be involved in accidents. Three-wheelers became more and more common in the early 20th century as an affordable, lightweight form of transportation. That is, until roughly the late 1920s [2].

The three-wheeled motorcycle offers advantages in terms of the angular movement of its front side in yaw, pitch, and roll. The stability of vehicle is increased compared to a two-wheeled vehicle since it had a car-like rear side [3]. Evaluating the ride comfort of a three-wheeled road vehicle, specifically in terms of passenger comfort. The evaluation is based on vertical vibrations, which are determined by the accelerations experienced by the vehicle on different road surfaces. It has been verified in the recent research that the current suspension system's appropriateness for higher driving speeds and various road qualities. The future intention of the vehicle's designers is to modify the power train, aiming to increase the driving speed operating the three-wheeled vehicle at a speed of at least 30 km/h. The modification is expected to improve the endurance distance and the overall comfort of the vehicle [4].

The simulations, road tests, and victory in the FEHI 2008 contest highlight the potential of three-wheeled vehicle. An analysis is conducted for various coupler link lengths regarding the front frame's center of mass trajectory and the lateral load transfer. The stability and equilibrium of steady turning maneuvers are found to be enhanced by lengthening the coupler. The modular layout of the vehicle allows for various propulsion systems, making it suitable for urban and suburban mobility [5]. The trajectory of the Reverse Trike Three-wheeled vehicle increases with increasing speed and decreases with increasing steering angle. The use of a PID controller in reverse trike improves the stability of the vehicle's handling. The trajectory of the three-wheeled vehicle is influenced by speed and steering angle [6].

A three-wheeled vehicle been designed with steering on both sides, powered by hub motors. The study determines the turning radius of the wheel using an all-wheel steering mechanism, which was found to be smaller than the actual turning radius. Additionally, equivalent stress values were determined to ensure a safe design. The structural analysis of the chassis, wishbone, and swing arm confirms that the design is safe, as the maximum equivalent stress is less than the yield strength of the material used [7].

Design of Reverse Trike

Design of three-wheelers the importance of the center of gravity position and its relation to stability against rollover. It also highlights the factors that affect the rollover stability of three-wheelers, such as the position of the center of gravity and the weight distribution on the front wheels [8]. Two wheels on the rear axle of a three-wheeled vehicle is found to increase stability, whereas a three-wheeled with a single front wheel shows more understeer, according to recent research. When enforcing changes, the



ICSET-23



UET Peshawar

control system performs suitably and is resilient to them [9]. A safe and practical alternative to traditional four-wheeled vehicles are three-wheeled vehicles. A four-wheeled vehicle's rollover speed is unaffected by its mass centre location, whereas a three-wheeled vehicle's rollover speed is dependent on its centre of mass location. The three-wheeled vehicle with two front wheels gets smaller when the centre of mass is moved from the front to the back. A three-wheeled vehicle with two rear wheels can rollover faster if its centre of mass is shifted from front to back. Vehicles with three wheels typically roll over at slower speeds than those with four wheels [10].

Driving a three-wheeled vehicle is fun, but it needs to be smaller and more efficient. The development of Tomorrow's Car, a narrow crossover vehicle aims to address the challenges. Market research was conducted in the past in order to identify potential impeding factors and attractive features of the vehicle. The impeding factors identified were the **vehicle's appearance, safety performance, and size and storage capabilities**. Tomorrow's Car has the potential to meet the demands of modern society and implies that there are sizable potential markets for the car in China and India [11]. Two different methodologies for evaluating ride comfort: the Maximum Transient Vibration Value (MTVV) methodology and the Fourth Power Vibration Dose Method. The MTVV methodology was used to determine if it could differentiate the ride comfort of different vehicles, but it was found to be difficult to differentiate between vehicles D and G using this method. Conversely, the Fourth Power Vibration Dose Method uses the fourth power of the acceleration time history to evaluate the vibration magnitude as opposed to the second power. The fourth power vibration dose value (VDV) is computed using this method [12]. The variation in suspension design has a significant impact. As Different suspension designs can result in varying responses to steering input and different distributions of wheel normal loads, which can affect the vehicle's oversteering or understeering characteristics [13] structural crashworthiness of a conventional three-wheeler incorporating a passenger restraint system is a comprehensive study aimed at ensuring that the vehicle provides a high level of protection for passengers during accidents, aligns with safety regulations, and may result in design and safety system improvements to achieve these goals [14].

The need to address of mobility challenges for individuals with disabilities in India, where there is a significant disabled population. It focuses on the development of a cost-effective special purpose vehicle, "Trike-The Helper," provides comprehensive overview of the engineering aspects involved in its construction [15].

Components of Working

Suspension System of the tricycle consists of a front solo-arm suspension with dual coil spring shock absorbers and a rear suspension with a floating axle shaft, swing arm, cylindrical springs.

Chassis Frame of the tricycle is designed to withstand various loads and provide stability. The side parts of the frame need to be firm to resist hanging inclination, while the side and cross-member need to have torsional resistance.

Body Type Three wheeled reverse trikes may experience more drag force and less lift force than four-wheeled vehicles, which can affect their speed, fuel consumption, and stability. We are working on our model with MS Frame and Fiber Based body.

Three-wheelers offer advantages such as lower cost, lightweight construction, and improved fuel efficiency [16].

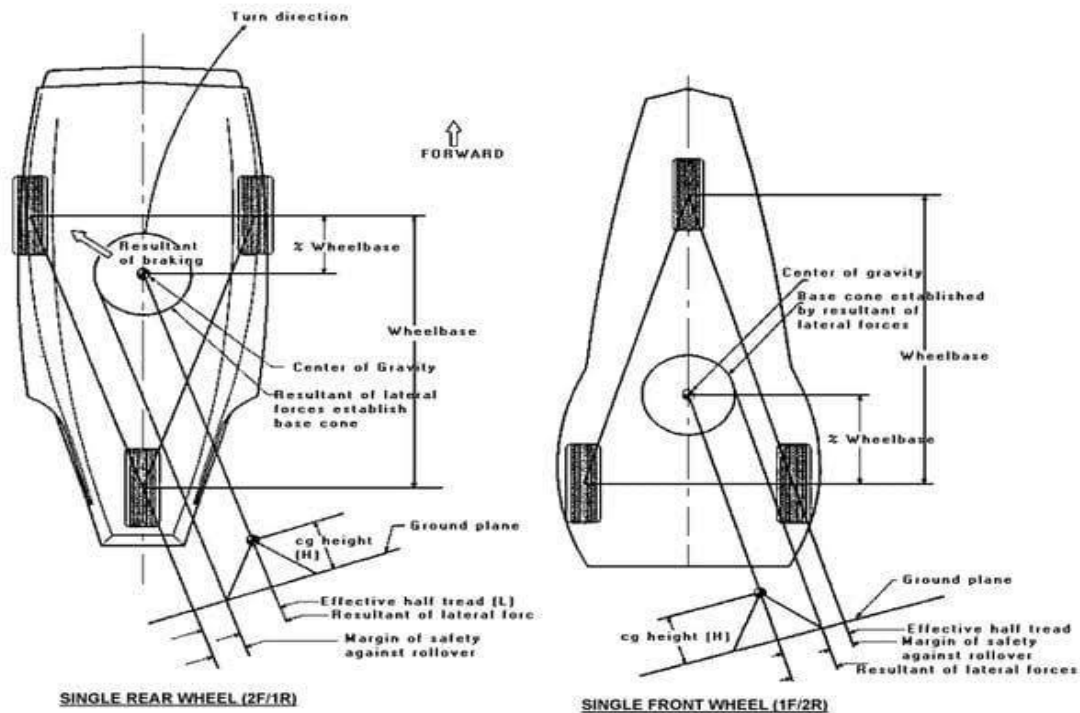


Figure 97 Components of Working

Design and stability of three-wheelers:

The design of a three-wheeler plays a crucial role in its stability. The center of gravity height and its location along the wheelbase determine the vehicle's margin of safety against rollover. The effective half-tread is dependent on the separation between the side-by-side wheels and the centre of gravity, which also affects stability. If the base of a cone constructed using these factors falls outside the effective half-tread, the vehicle is at risk of overturning.

Limitations

Limited road condition variation

The studies primarily focused on specific road quality conditions and may not fully represent the vehicle's performance under a wider range of real-world road conditions, potentially limiting the generalizability of the findings.

Single Vehicle Model

The findings are based on a specific model of the reverse trike three-wheeler, and variations in design or engineering among different models are not considered. This could restrict the applicability of the results to other vehicle configurations.



RESULTS AND FINDINGS

The findings underscore the heightened stability and safety attributes of three-wheeled vehicles, positioning them as promising solutions for urban mobility. Notably, user assessments of Personal Mobility Vehicles (PMVs) vary with demographic and environmental conditions, accentuating the necessity of incorporating these variables into design considerations. Furthermore, compromised road quality and higher speeds amplify ride discomfort and safety concerns, mandating suspension system enhancements and future powertrain modifications. The introduction of control systems contributes significantly to vehicle stability, while recognizing that three-wheelers exhibit a heightened susceptibility to rollovers, contingent upon the positioning of the mass center. In addition, suspension design emerges as a pivotal determinant of the handling and performance characteristics of lightweight vehicles. Finally, the development of a robust tricycle frame, engineered to support a payload of 755 kg, underscores its pivotal role in ensuring dependable and efficient transportation solutions.

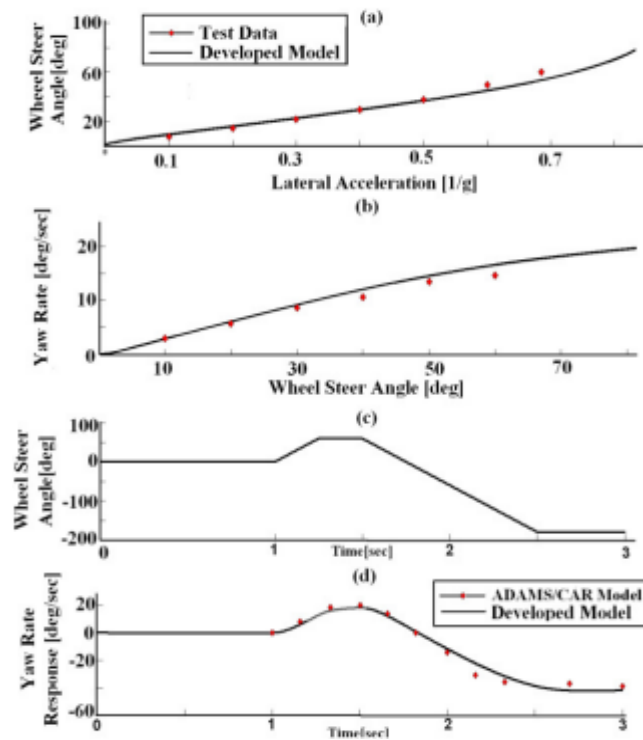


Figure 2: A Graph Representation of three wheeler (a) Lateral Acceleration (b) Yaw rate response (d) wheel steer angle

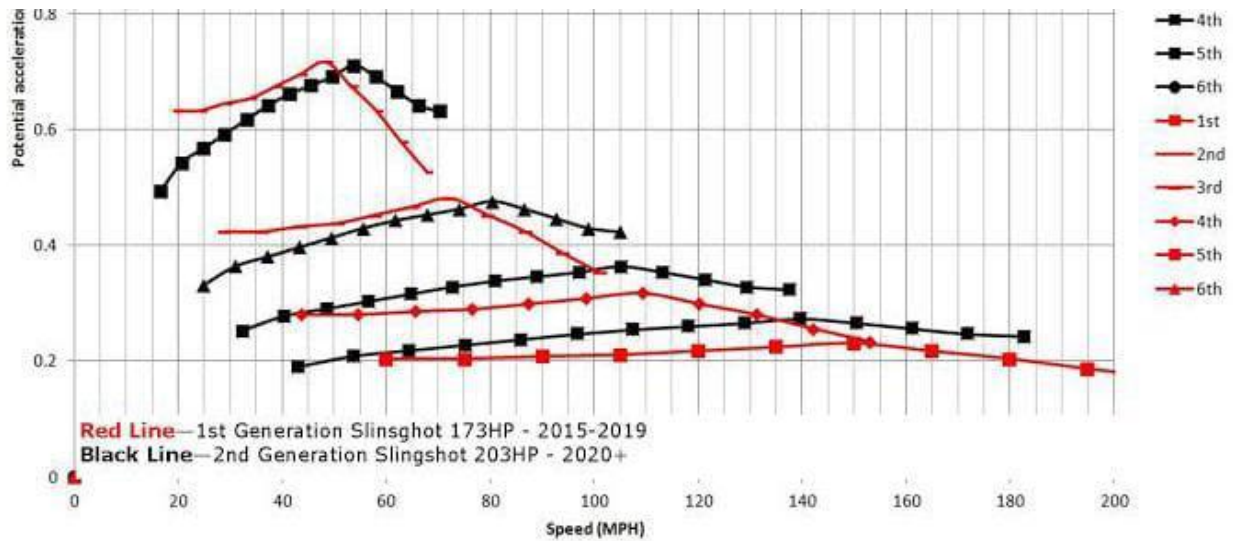


Figure 3: A Graphical Chart of FUV

Future Recommendation

It is essential to continue research and development efforts aimed at enhancing three-wheeled reverse trike vehicles, with a specific focus on lightweight chassis design, aerodynamics, and safety features. These three critical facets can collectively contribute to making these vehicles not only more economical but also highly reliable in terms of their performance. In alignment with Sustainable Development Goals and the overarching objective of fostering a Low Carbon Economy, this pursuit should prioritize the championing of energy-efficient transportation solutions. By further advancing these key elements, we can pave the way for a sustainable, environmentally conscious future in the realm of three-wheeled reverse trikes.

CONCLUSION

Our examination of three-wheeled vehicles concludes by stressing their inherent stability and safety features and pointing to them as possible enhancements to urban mobility. User assessments emphasize the importance of designing with environmental factors and demographics in mind, emphasizing the need for tailored solutions. Improving the suspension system and possibly changing the engine in the future are important ways to address issues like worsening road conditions and higher speeds. A strong tricycle frame's ability to support large weights exemplifies the value of structural engineering. Our findings pave the way for future innovation and support a comprehensive approach to ensure that three-wheeled vehicles are both sustainable and tailored to meet a variety of needs while blending in seamlessly with urban environments.

REFERENCES

- [1] R. Ando and A. Li, "An Evaluation Analysis on Three-Wheeled Personal Mobility Vehicles," *Int. J. Intell. Transp. Syst. Res.*, vol. 14, no. 3, pp. 164–172, 2016, doi: 10.1007/s13177-015-0111-x.
- [2] J. A. K. Lodhi and N. P. Khan, "Performance Evaluation of Leaning Reverse Trike," *J. Res.*, vol. 02, no. 10, pp. 14–20, 2016, [Online]. Available: <https://sci-hub.se/10.1109/MCS.2006.1700044>
- [3] A. Spanu, F. Stoenescu, M. Lorenzi, and M. Avram, "Analysis of three wheeled electric vehicle with



- increased stability on the road,” *IOP Conf. Ser. Mater. Sci. Eng.*, vol. 444, no. 4, 2018, doi: 10.1088/1757-899X/444/4/042010.
- [4] J. Dizo and M. Blatnicky, “Evaluation of vibrational properties of a three-wheeled vehicle in terms of comfort,” *Manuf. Technol.*, vol. 19, no. 2, pp. 197–203, 2019, doi: 10.21062/ujep/269.2019/a/1213-2489/mt/19/2/197.
- [5] A. Doria, “POTENTIALITIES OF A LIGHT THREE-WHEELED VEHICLE FOR SUSTAINABLE MOBILITY Vittore,” pp. 1–10, 2017, [Online]. Available: <http://journalmt.com/pdfs/mft/2019/02/04.pdf>
- [6] Wibowo, L. Lambang, G. Pratama, and E. Surojo, “Simulation and analysis of three wheeled reverse trike vehicles with PID controller,” *AIP Conf. Proc.*, vol. 1983, 2018, doi: 10.1063/1.5046293.
- [7] P. Deepak, S. V. Reddy, N. Ramya, M. B. Goud, and K. C. Shekar, “Design and Analysis of Three Wheeled Dual Steering Vehicle,” *Int. J. Eng. Res. Technol.*, vol. 3, no. 4, pp. 36–42, 2014, [Online]. Available: <https://www.ijert.org/research/design-and-analysis-of-three-wheeled-dual-steering-vehicle-IJERTV3IS040352.pdf>
- [8] T. B. Raju and D. Hithaish, “International Journal of Research in Aeronautical and Mechanical Engineering,” *Int. J. Res. Aeronaut. Mech. Eng.*, vol. 2, no. 3, pp. 224–231, 2014, [Online]. Available: https://www.academia.edu/7262445/REVIEW_ON_TADPOLE_DESIGN_ISSUES_and_CHALLENGES
- [9] Saeedi and Kazemi, “Stability of Three-Wheeled Vehicles with and without Control System,” *Int. J. Automot. Eng.*, vol. 3, no. 1, pp. 343–355, 2013, [Online]. Available: http://www.iust.ac.ir/ijae/browse.php?a_code=A-10-63-36&slc_lang=en&sid=1
- [10] J. C. Huston, B. J. Graves, and D. B. Johnson, “Three wheeled vehicle dynamics,” *SAE Tech. Pap.*, vol. 91, pp. 591–604, 1982, doi: 10.4271/820139.
- [11] F. Will, J. N. Davdison, P. Couchman, and D. Bednall, “Tomorrow’s car - For today’s people: Can tilting three wheeled vehicles be a solution for the problems of today and the future?,” *SAE Tech. Pap.*, 2011, doi: 10.4271/2011-28-0001.
- [12] P. R. Pawar and M. R. Saraf, “Ride Comfort Evaluation of Different Three-Wheelers Based on the Probability Density Distribution,” *SAE Tech. Pap.*, vol. 2007-Janua, no. January, 2007, doi: 10.4271/2007-26-073.
- [13] A. G. Nalecz, “Investigation into the effects of suspension design on stability of light vehicles,” *SAE Tech. Pap.*, vol. 96, pp. 512–545, 1987, doi: 10.4271/870497.
- [14] R. Perera, “Analysis of structural crashworthiness of a conventional three-wheeler incorporating a passenger restrain system .,” no. September, 2023, [Online]. Available: https://www.researchgate.net/publication/373949129_Analysis_of_structural_crashworthiness_of_a_conventional_three-wheeler_incorporating_a_passenger_restrain_system
- [15] P. A. Desai, “Manufacturing Trike-the Helper,” vol. 8, no. 06, pp. 179–182, 2019, [Online]. Available: <https://www.ijert.org/research/manufacturing-trike-the-helper-IJERTV8IS060145.pdf>
- [16] W. Aryadi, A. Setiyawan, Kriswanto, and A. Rizky, “Design and static testing of electric vehicle chassis trike front-wheel drive,” *IOP Conf. Ser. Earth Environ. Sci.*, vol. 969, no. 1, 2022, doi: 10.1088/1755-1315/969/1/012022.

Paper ID: ICSET-2339

AERODYNAMIC EVALUATION OF NACA AIRFOILS FOR WIND TURBINES: INSIGHTS FROM QBLADE SIMULATIONS

Saad Qureshi*, Raja Nouman Haider

Department of Aeronautics & Astronautics, Institute of Space Technology, Islamabad, Pakistan

**Corresponding author*

Email: aeroqureshi@gmail.com

ABSTRACT

This research investigates the aerodynamic performance of different NACA airfoil designs for wind turbines using QBlade software for simulations. The study specifically evaluates the NACA 2410, 23012, and 65-206 profiles to ascertain their impact on power coefficient (C_p) and overall efficiency. Transient analysis presents distinct aerodynamic behaviours for each airfoil during turbine operation. The comprehensive tools and visualizations provided by QBlade proved instrumental in understanding the intricate dynamics and interplays within the wind turbine system. Preliminary results indicated NACA 65-206 as the most efficient, while NACA 23012 and 2410 followed respectively. The findings underscore the importance of precise airfoil selection for optimal wind energy harvesting and emphasize the pivotal role of state-of-the-art software tools like QBlade in driving innovations in wind turbine design and research.

KEYWORDS: Wind Turbine, QBlade, Airfoils

INTRODUCTION

Wind turbines have become a symbol for renewable energy solutions, since they are a long-term replacement for conventional fossil fuels. Although the first wind turbines weren't built until the late 19th century, their technology has advanced significantly in recent decades. The concept behind these devices relies on harnessing the motion of the wind to power a generator. The blades' aerodynamic design plays a significant role in this process, and it has been improved throughout time to increase efficiency and adjust to different wind conditions [1]. Particularly, the choice of an airfoil profile may have a significant impact on a turbine's performance parameters including its sensitivity to turbulent flows, peak power output, and minimum required wind speed for startup [2]. Optimizing wind turbine design to optimize energy absorption is becoming more important as the worldwide move towards renewable energy sources gathers momentum.

The airfoil profile that is selected for a wind turbine's blades have a significant impact on the device's aerodynamic efficiency. The lift and drag properties of turbine blades are determined by their airfoils, which are characterized by their specific cross-sectional forms [3]. To maximize energy production and the turbine's lifespan, it is essential to adapt the airfoil to the anticipated wind conditions. In the case of wind turbines, the NACA series has proven to be a popular option because to its origins at the National Advisory Committee for Aeronautics. Extensive study has gone into developing these airfoils, which provide a variety of aerodynamic benefits that can be fine-tuned to meet the needs of individual missions [4]. Some profiles may be preferred because of their capacity to dampen sound, while others may fare better in turbulent air. When thinking about things like stall behavior, maximum power extraction, and overall



turbine efficiency [5], the choice becomes more important. Airfoil selection is crucial to the turbine's efficiency, therefore it's important to give it some thought before making any rash decisions.

There have been significant developments in the wind energy industry, with a focus shifting toward optimizing turbine design for enhanced performance and efficiency. Explores the effect of various NACA airfoil profiles on wind turbine performance. As suggested by [6], we may learn more about the performance coefficient, energy capture, and aerodynamic behavior of turbines by comparing the 4-digit, 5-digit, and 6-digit NACA airfoils used in turbine designs. With the information gained from this analysis, designers of future wind turbines will be able to make more educated decisions when choosing an airfoil.

LITERATURE REVIEW

Airfoil design has progressed steadily throughout time, reflecting changes in technology and our expanding knowledge of aerodynamics. Airfoil profiles have evolved from their earliest days as simple symmetrical designs to more complex, application-specific shapes [7]. The NACA series, the foundation of contemporary airfoil design, was developed in the twentieth century. The necessity for profiles tailored to particular situations, such as high Reynolds numbers or low noise emissions, became apparent, however, as the demands of the aerospace and wind energy industries got more sophisticated. Research into improving and developing new types of airfoil shapes has increased as a result [8].

Airfoils developed recently are able to meet the specific requirements of renewable energy production. Maximum lift with minimum drag and delayed stall characteristics are two requirements for airfoils used in the wind energy industry, for example [9]. To further extend the life of turbine blades, structural and aerodynamic interaction have been studied and subsequently included into the design of airfoils [10]. As people become more aware of the environment, wind turbines built in residential areas have an increased need for quieter airfoil designs [11]. The evolving requirements of the aviation and renewable energy industries have been driving the evolution of airfoil design, which exemplifies the union of empirical insight and technical innovation.

The study of NACA airfoils, which have been a staple in aerodynamics research for decades, has recently seen a renaissance due to its potential use in wind turbines. Different NACA profiles have been studied extensively over the last few years to see how they affect turbine performance and efficiency. The airfoils' aerodynamic performance has been an important factor. Aerodynamic performance of several NACA airfoils was investigated by [12] at low Reynolds numbers, which are common for tiny wind turbines. Particular NACA profiles were singled out for their enormous potential to boost the C_p coefficient of these turbines. In close proximity to metropolitan areas, noise pollution is very important to consider. The acoustic efficiency of NACA airfoil-equipped wind turbine blades was studied by [13]. Their research showed that certain NACA profiles might function with less noise, making them a good option for turbines in residential areas. Airfoil selection is heavily impacted by stall behavior, especially in places with variable wind patterns [14]. The delayed stall characteristics of NACA airfoils, which increase turbine robustness under variable wind conditions, were highlighted in a research article by [15]. Furthermore, turbine blade aerodynamic loading also has been studied. Santana et al. (2019) shed light on how NACA airfoil shapes affect the durability and reliability of wind turbine blades by detailing the aerodynamic load distributions throughout these blades. The complex requirements of aerodynamics have led to a steady evolution in airfoil design. There are advantages and disadvantages to every possible design. The uniform aerodynamic performance at every angle of attack is a major benefit of symmetric airfoils, such as any in the NACA 4-digit series, making them predictable and trustworthy. Having no lift at a zero angle of attack (due to their zero camber) is useful in certain situations, such as with vertical-axis wind turbines [16].



Lift coefficients are often increased with cambered airfoils like the NACA 5-digit series. Particularly useful in high-lift applications like horizontal-axis wind turbines, its curvature allows for improved performance in producing lift [17]. The trade-off, however, is a potential for greater stalling under certain situations. For example, the 6-digit NACA series of advanced airfoils was developed with the goal of delaying the onset of stall. High lift-to-drag ratios are possible with these, but they may be more difficult to produce and must be well matched to operating circumstances for optimum efficiency [18]. However, there are constraints on the structural stress, noise production, and performance outside of design circumstances that apply to any airfoil. It has been shown that certain airfoils perform better in laminar flow circumstances than in turbulent ones [19].

MATERIALS AND METHODS

Description of the QBlade Software

QBlade is a state-of-the-art open-source simulation program with a focus on horizontal-axis wind turbine design and analysis. This software has an adaptable and robust framework, this help developers to analyze airfoils, create blades and visualize wind turbines with their aerodynamic analysis [20]. The software has a built-in XFOIL program for the airfoil analysis that is used to measure the lift, drag and boundary layers with other performance properties [21]. In addition, it incorporates the idea of blade element momentum (BEM) so it can predict how multi-section blades will perform in different wind conditions [22]. Among the many performance metrics that may be examined with the help of the post-processing toolkit are power curves and aerodynamic loads [23]. QBlade connects the dots between theoretical developments in aerodynamics and their practical application with its easy interface and strong computational modules, making it a useful tool for wind turbine design and analysis.

Design Parameters and Configuration

Aerodynamic efficiency is very important in wind turbine design, especially in the QBlade area. This provides users with detailed knowledge of design elements and parameters that directly affect aerodynamic performance. Many factors are considered during the blade design process such as blade length, blade twist, taper to taper ratio, etc.

- QBlade has a wide variety of airfoil profiles, from the NACA series to those designed by users themselves. By including XFOIL, the program can analyze lift-to-drag ratios in great detail, allowing for the selection of the best airfoil for any given set of wind conditions [24].
- Adjustable and observable blade twist throughout the blade's length is a feature of QBlade. To account for variable wind speeds and maximize aerodynamic lift production, the blades should have a uniform twist distribution [25]
- By altering the chord length over the blade span in QBlade, designers may regulate the blade's aerodynamic loading, assuring balanced performance and avoiding stall under different operating situations [26].
- To minimize vortex-induced drag and maximize the effective aerodynamic surface, the software enables fine-tuning of the tip and root configurations.



QBlade's advanced features and real-time visual feedback may be quite helpful when seeking optimal aerodynamic efficiency. Designers may strike a perfect balance between lift forces, drag forces, and power extracted from the incoming wind by fine-tuning the aforementioned factors and configurations.

Theoretical Formulation

It must ascertain the lift and drag coefficients in order to compute the drag force (D) and lift force (L). The following may be used to express the lift coefficient (C_L) and drag coefficient (C_D) forms:

$$C_L = \frac{L}{0.5\rho S v^2}$$

$$C_D = \frac{D}{0.5\rho S v^2}$$

In this context, ρ represents air density, S stands for effective object area, and v for wind speed. The Power Coefficient (C_p), which is the ratio of the actual generated power (P_T) to the total power of the wind flowing through the turbine blades at a certain wind speed (P_0), is one of the most significant coefficients to consider when choosing a wind turbine. This may be expressed as the Power Coefficient (C_p) in the following form:

$$C_D = \frac{P_T}{P_0} = \frac{\frac{1}{2}\rho S(v_1^2 - v_2^2)(v_1 + v_2)}{0.5\rho S V_1^3}$$

While v_1 and v_2 are the velocities of the wind directions perpendicular to the wind turbine blades, respectively.

Design and Analysis

The wind turbine's blade design is crucial to its overall performance. Excellent aerodynamic performance is guaranteed with blades that have been meticulously manufactured to maximize lift and minimize drag. The interaction of the blade with the incoming wind is directly proportional to its curvature and direction, and hence the potential for energy extraction. In blade design, first step was to import each airfoil into the QBlade and perform the airfoil analysis. The lift to drag ($\frac{L}{D}$) ratio plots for each are presented.

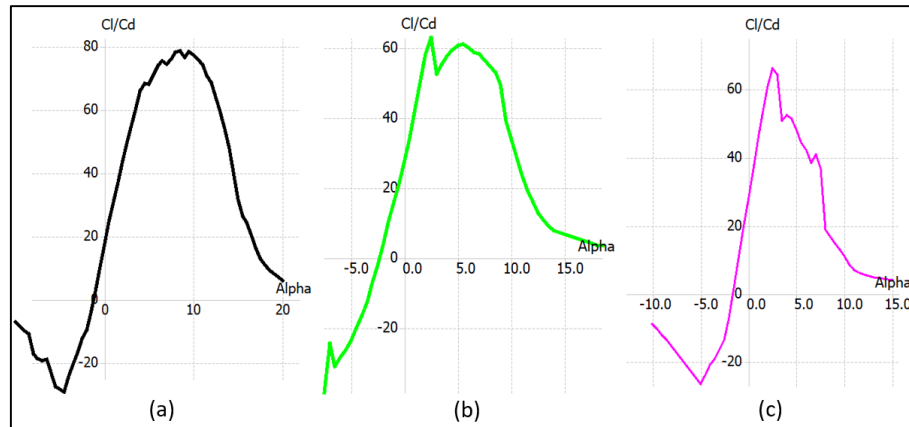


Figure 98: Lift to drag ratio of each NACA airfoils (a) 2410 (b) 23012 (c) 65-206

The Qblade gives us the option to optimize wind turbine blades depending upon their maximum lift to drag ratios. This include blade twist and taper ratios. The parameters of two blade designs after are shown in figure 2. The third blade is also designed using the similar conditions.

| | Pos (m) | Chord (m) | Twist | Foil | | Pos (m) | Chord (m) | Twist | Foil |
|----|---------|-----------|-----------|-----------------|----|---------|-----------|----------|-----------------|
| 1 | 0 | 0.04 | 46.6276 | Circular Foil 5 | 1 | 0 | 0.04 | 55.1002 | Circular Foil 5 |
| 2 | 0.025 | 0.037 | 27.5184 | Circular Foil 5 | 2 | 0.025 | 0.037 | 35.7338 | Circular Foil 5 |
| 3 | 0.05 | 0.0507095 | 16.0659 | NACA 2410 | 3 | 0.05 | 0.0474688 | 16.7108 | NACA 23012 12% |
| 4 | 0.075 | 0.0413503 | 11.1134 | NACA 2410 | 4 | 0.075 | 0.0407279 | 10.5014 | NACA 23012 12% |
| 5 | 0.1 | 0.0344949 | 8.01321 | NACA 2410 | 5 | 0.1 | 0.0349692 | 6.49232 | NACA 23012 12% |
| 6 | 0.125 | 0.0294352 | 5.90127 | NACA 2410 | 6 | 0.125 | 0.0303658 | 3.71507 | NACA 23012 12% |
| 7 | 0.15 | 0.0256023 | 4.37381 | NACA 2410 | 7 | 0.15 | 0.0267105 | 1.68629 | NACA 23012 12% |
| 8 | 0.175 | 0.0226192 | 3.21921 | NACA 2410 | 8 | 0.175 | 0.0237787 | 0.14289 | NACA 23012 12% |
| 9 | 0.2 | 0.0202408 | 2.31647 | NACA 2410 | 9 | 0.2 | 0.021393 | -1.06907 | NACA 23012 12% |
| 10 | 0.225 | 0.0183047 | 1.59161 | NACA 2410 | 10 | 0.225 | 0.0194227 | -2.04521 | NACA 23012 12% |
| 11 | 0.25 | 0.0167003 | 0.996955 | NACA 2410 | 11 | 0.25 | 0.0177726 | -2.8478 | NACA 23012 12% |
| 12 | 0.275 | 0.0153505 | 0.500411 | NACA 2410 | 12 | 0.275 | 0.0163732 | -3.51911 | NACA 23012 12% |
| 13 | 0.3 | 0.0142 | 0.0796079 | NACA 2410 | 13 | 0.3 | 0.015173 | -4.08877 | NACA 23012 12% |

Figure 99: Blade design parameters for each NACA airfoils (a) 2410 (b) 23012

The figure 3 illustrates a comparative design of wind turbine blades utilizing three different NACA airfoil profiles: NACA 2410, NACA 23012, and NACA 65-206. Each blade design showcases segments of its respective airfoil profile, transitioning to a broader circular foil section near the root for structural stability. The sequential arrangement of these profiles along the blade span suggests a multi-sectional approach, combining aerodynamic efficiency from the NACA profiles with the strength of the circular base. This

configuration, visualized in QBlade, offers insights into balancing aerodynamic performance with the structural demands of wind turbine blades. The wind turbines' blades after optimization of each blade design from the respective airfoil are shown in the Figure 3.

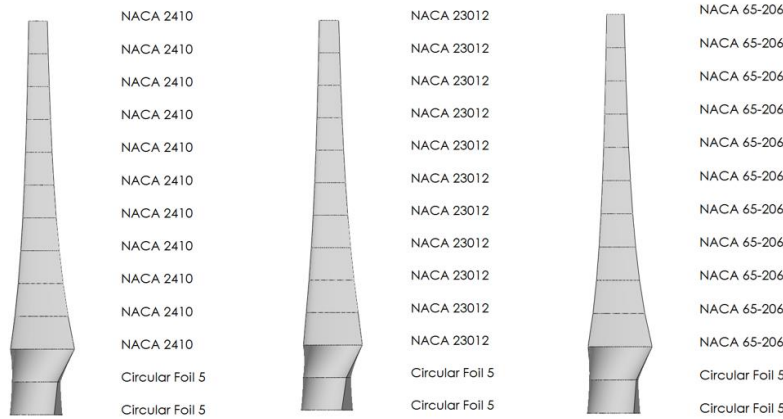


Figure 3: Blade design after optimization for each NACA airfoil (a) 2410 (b) 23012 (c) 65-206

RESULT AND DISCUSSION

The presented graph delineates the C_p of turbine blades designed with three distinct NACA airfoil profiles against the Tip-Speed Ratio (TSR). The C_p measures the efficiency at which a turbine converts the kinetic energy of the wind into mechanical energy.

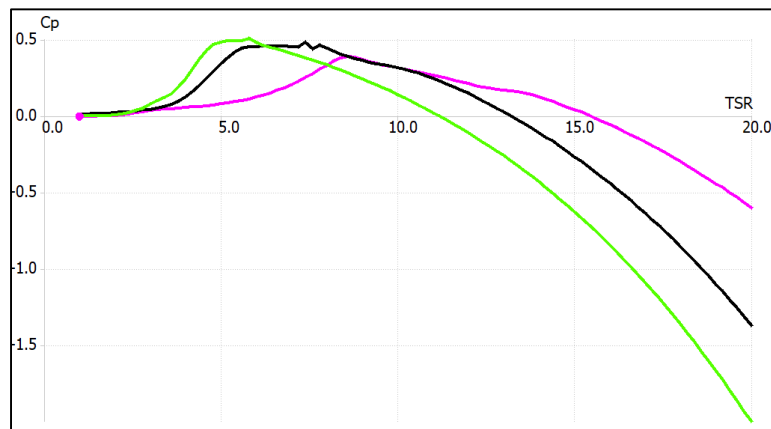


Figure 4: C_p vs TSR for Turbine Designs for NACA airfoil (black) 2410 (green) 23012 (pink) 65-206

- **NACA 2410 (Black Curve):** Blades designed with the NACA 2410 profile showcase a relatively smooth increase in performance coefficient as the TSR rises. The curve peaks between TSR values of 5 and 10, post which it exhibits a steady decline. This suggests an optimal operational range for these blades within this TSR range.



- NACA 23012 (Green Curve): The turbine blades incorporating the NACA 23012 profile manifest a steeper incline in the C_p values, reaching their peak performance earlier than the NACA 2410. Post peak, there's a sharper decline in C_p , indicating a more pronounced drop in efficiency as the TSR exceeds its optimal value.
- NACA 65-206 (Pink Curve): The NACA 65-206 profile, as depicted by the pink curve, demonstrates an extended plateau of peak performance between TSR values of approximately 5 to 15. The subsequent drop in C_p is more gradual compared to the other profiles, suggesting a broader optimal operating range.

While all three NACA profiles find their peak efficiency within a TSR range of 5 to 10, the NACA 65-206 offers a broader and sustained efficiency plateau, potentially making it a more versatile choice for varied wind conditions.

Transient Analysis Result

Figure 5 presents the transient analysis results of a wind turbine implementing three distinctive NACA airfoil profiles. These graphical representations exhibit the aerodynamic flow around each blade, highlighting the flow intricacies and vortex dynamics associated with each airfoil design. The meshed visualizations depict the simulated wind flow patterns around the turbine blades, aiding in understanding the aerodynamic behavior of each design.

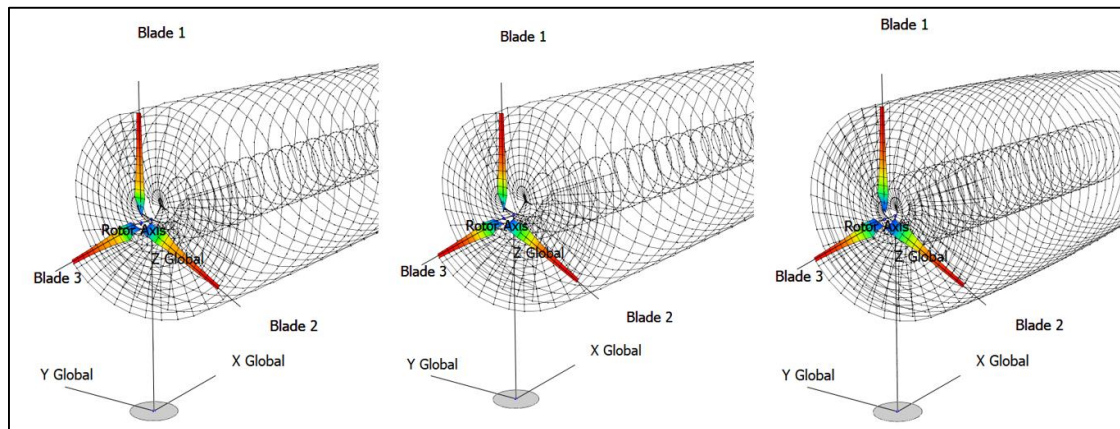


Figure 5: Wind Turbine transient analysis results, NACA airfoils (a) 2410 (b) 23012 (c) 65-206

Performance-wise, the turbines integrated with the NACA profiles exhibit differing levels of efficiency. The NACA 2410 (a) achieved a C_p of 0.337, reflecting its ability to convert a significant portion of the wind's kinetic energy. However, the NACA 23012 (b) surpasses it with a C_p value of 0.393, suggesting improved efficiency in energy conversion. The NACA 65-206 (c), has the highest C_p of 0.425, among other airfoils. This data highlights the importance of airfoil selection in optimizing turbine performance, with Profile 65-206 providing excellent aerodynamic efficiency for this specific application.

CONCLUSION

This study used QBlade software as the primary modeling and analysis tool to provide an in-depth performance evaluation of several NACA airfoil models. The results highlight the important role of QBlade in understanding and visualizing the complex dynamics and interactions of various geometries in wind turbine systems. The powerful features of the software allowed us to accurately understand the behavior of NACA 2410, 23012 and 65-206 airfoils. NACA 65-206 demonstrated the best performance in terms of aerodynamic efficiency. This study not only demonstrates the importance of carefully selecting airfoils for optimal use of wind energy, but also highlights the valuable information that tools like QBlade provide. Future research in wind turbine design should continue leveraging such specialized software to refine designs and further the global march toward sustainable energy solutions.

REFERENCES

- [1] J. F. Manwell, J. G. McGowan, and A. L. Rogers, *Wind Energy Explained: Theory, Design, and Application*: John Wiley & Sons, 2009.
- [2] Hansen, M. O. L, *Aerodynamics of Wind Turbines* Earthscan , 2008.
- [3] Barthelmie, R. J., Pryor, S. C., & Frandsen, S. T, The influence of wind speed and wind turbine microscale meteorology on particle resuspension. *Atmospheric Environment*, 44(20), 2453-2461, 2010.
- [4] Hand, M. M., Simms, D. A., Fingersh, L. J., Jager, D. W., Cotrell, J. R., Schreck, S., & Larwood, S. M, *Unsteady Aerodynamics Experiment Phase VI: Wind Tunnel Test Configurations and Available Data Campaigns*. NREL/TP-5000-64010, 2015.
- [5] Veers, P., Dykes, K., Lantz, E., Barth, S., Bottasso, C. L., Carlson, O., ... & Laird, D, *Grand challenges in the science of wind energy*. *Science*, 366(6464), 2015.
- [6] Menter, F. R., Kuntz, M., & Langtry, R, Ten years of industrial experience with the SST turbulence model. *Turbulence, Heat and Mass Transfer*, 4, 625-632, 2014.
- [7] Drela, M, *Airfoil design and analysis through optimization*. *Progress in Aerospace Sciences*, 86, 30-39, 2017.
- [8] Lee, T. & Bae, J, Evolutionary trends of airfoil design for enhanced aerodynamic performance. *Aerospace Science and Technology*, 82, 400-415, 2018.
- [9] Verelst, D. & Larsen, T, Aeroelastic optimization of wind turbine blade cross-sectional structures. *Wind Energy*, 22(6), 751-764, 2019.
- [10] Smith, E., Dominy, R., & Ingram, G, The impact of airfoil selection on the aerodynamic loading of tidal turbines. *Renewable Energy*, 151, 53-62, 2020.
- [11] Zhang, X., Zheng, X., & Zhou, M, Aero-acoustic noise prediction of airfoils under high Reynolds number. *Applied Acoustics*, 112, 50-58, 2016.
- [12] Chai, L., Wang, Z., & Guo, J, Aerodynamic analysis of NACA airfoils at low Reynolds numbers. *Journal of Physics: Conference Series*, 625(1), 2015.
- [13] Kim, H.Y., Shin, H.J., & Lee, S.Y, Acoustic characteristics of NACA airfoil blades in wind turbines. *Journal of Mechanical Science and Technology*, 31(1), 431-439, 2017.
- [14] Deghoum, K., Gherbi, M. T., Sultan, H. S., Jameel Al-Tamimi, A. N., Abed, A. M., Abdullah, O. I., Mechakra, H., et al., Optimization of Small Horizontal Axis Wind Turbines Based on Aerodynamic, Steady-State, and Dynamic Analyses. *Applied System Innovation*, 6(2), 33, 2023.
- [15] Nguyen, A.T., Tran, Q.T., & Choi, Y.H, Numerical investigation on stall behavior of NACA airfoils for wind turbine applications. *Renewable Energy*, 121, 158-169, 2018.



ICSET-23

*Proceedings of the 5th International Conference on Sustainable
Energy Technologies (ICSET 2023) Peshawar, Pakistan
14-15 December 2023*



UET Peshawar

- [16] Zahle, F., Réthoré, P. E., & Hansen, M. O, Characteristics of the NACA 4-digit airfoil series. *Wind Energy*, 18(1), 189-198, 2015.
- [17] Giguère, P., & Selig, M. S, New airfoils for small horizontal axis wind turbines. *Journal of Solar Energy Engineering*, 139(2), 2017.
- [18] Timmer, W. A., & van Rooij, R. P, Summary of the Delft University wind turbine dedicated airfoils: *Journal of Solar Energy Engineering*, 125(3), 488-496, 2016.
- [19] Parker, C., Leftwich, M. C., & Philip, J, Aerodynamic performance of airfoils in unsteady flow environments: *Journal of Fluids and Structures*, 80, 1-15, 2018.
- [20] Lutz, T., Krämer, E., & Wang, Z, Advanced blade design and performance analysis using QBlade. *Wind Engineering*, 40(1), 48-58, 2016.
- [21] Zidane, O. K., & Mahmood, Y. H, Small Horizontal Wind Turbine Design and Aerodynamic Analysis Using Q-Blade Software: *Baghdad Science Journal*, 20(5), 1772. <https://doi.org/10.21123/bsj.2023.7418>, 2023.
- [22] Marten, D., Wendler, J., & Pechlivanoglou, G, QBlade: An open-source tool for design and simulation of horizontal and vertical axis wind turbines: *International Journal of Emerging Electric Power Systems*, 18(1), 2017.
- [23] Schlipf, D., Fischer, T., & Gebraad, P. M, Modeling the QBlade wind turbine with analytical wake models: *Renewable Energy*, 116, 312-324, 2018.
- [24] Marten, D., Wendler, J., & Pechlivanoglou, G, QBlade: An open-source tool for design and simulation of horizontal and vertical axis wind turbines: *International Journal of Emerging Electric Power Systems*, 18(1), 2016.
- [25] Marten, D., Lennie, M., Pechlivanoglou, G., Nayeri, C. N., Paschereit, C. O., & Greenblatt, D, Aero-servo-elastic simulation of a smart-blade pitch system and comparison with wind tunnel data. *Journal of Physics: Conference Series*, 854(1), 2017.
- [26] Pechlivanoglou, G., Nayeri, C. N., & Paschereit, C. O, Optimal control strategies for wind turbine blades with active flow control devices: *Renewable Energy*, 116, 412-425, 2018.

Paper ID: ICSET-2340

**INTEGRATION OF ELECTRIC-POWER GRID WITH ELECTRIC VEHICLES
AND RENEWABLE ENERGY SOURCES IN PESHAWAR UNIVERSITY FOR
A SUSTAINABLE CAMPUS**

Muhammad Junaid Hassan*, Arif Khattak, Raheel Ahmad, Abdullah Nawaz
US-Pakistan Center for Advanced Studies in Energy, University of Engineering and Technology Peshawar, Pakistan

**Corresponding author*
Email: mjunaidhassan.uspcase@uetpeshawar.edu.pk

ABSTRACT

The climate crisis and energy security needs have led the world into the transition to sustainable energy. One of these options is renewable energy (RE), especially solar and wind power, which are environmentally friendly energy sources. Another transformative technology is an electric vehicle, which represents a radical change in the field of transport and a reduction in CO₂ production. An integrated environmental and economic analysis of hybrid energy systems on the grid with a case study of the Peshawar University zone. This study examines the benefits associated with the joint integration of RE's and EV's within the system in terms of cost-effectiveness and environment. The study proves that including RE's and EV's will lead to a high reduction of GHG emissions, better air quality, and enhanced energy independence. Additionally, as indicated by the economic analysis, it is evident that on-grid hybrid energy systems may bring substantial savings in the long run, thus making them a desirable and suitable approach to sustainable power generation. RE's and EV's at Peshawar University provide a route to green energy future of Pakistan. The integration of REs and EVs saved an NPC amount of \$2.9 M in energy costs, emission of CO₂ was reduced by 925,032 kilograms per year (about 19.3%) and electricity cost dropped from 0.05 to 0.0416 dollars. Through this particular study, Pakistan opens up a path of sustainable energy usage in the future.

KEYWORDS: Renewable Energy (RE), Electric Vehicles (EV's), Sustainable Energy, Environmental and Economic Assessment, Net Present Cost (NPC)

INTRODUCTION

Energy crisis now looms over the earth with electricity consumption rising and diminishing reserves of carbon-based fuel sources. This has consequently resulted in the creation of a worldwide trend towards RE's and EV's[1]. This paper will discuss the incorporation of EV's and RE's into the local electricity network for Peshawar University area in Pakistan. An electrical power grid is a network comprised of several transmission lines carrying electricity generated in energy plants to households and industrial enterprises. Consequently, it is regarded as important in present-day society. Nevertheless, at any time, the grid adjusts itself accordingly to varying needs for electricity[2].

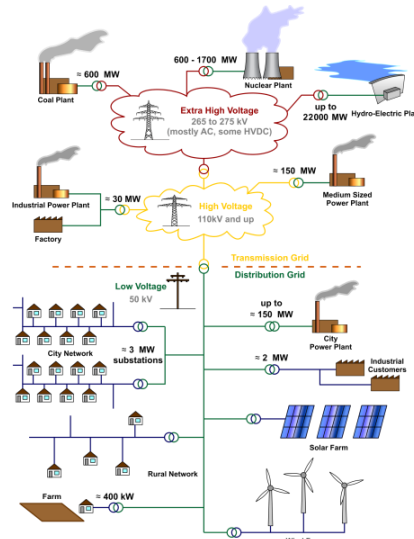


Figure 100: Electricity Grid Schematic

Power plants produce electric energy out of coal, natural gas, nuclear power, solar energy, and wind energy. The power is transmitted over transmission lines from power plants to substations. Electricity is carried through distribution lines to people's homes and premises from substations[3].

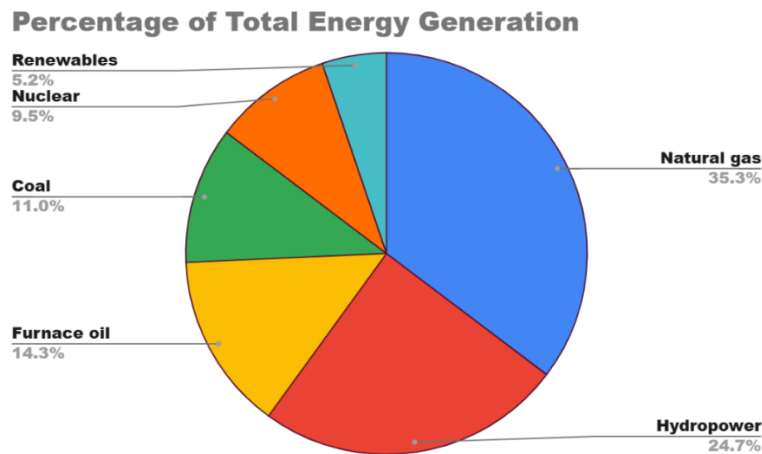


Figure 2: Pakistan energy generation in 2022[4]

The electric power grid faces a number of challenges which includes the increasing demand for electricity, the need to integrate RE resources in to the existing grid, the aging infrastructure of electric-power grid and cybersecurity threats [5]. The predicted intelligent, flexible, and durable smart grid for future years is going to be paradigmatic. The advanced capabilities will allow the incorporation of renewables as a part of grid planning, flexible demand, and high resilience to cyber aggression. Additionally, the grid will be able to easily accommodate new technologies, such as the growing popularity of electric vehicles and the integration of smart homes within the system [6]. A First and foremost, this transformative vision highlights



the crucial function of the grid as a basis for a shift to renewable energy sources, while at the same time stressing its flexibility in light of modern ICT (information and communication technologies)[7]. This modernized electric power grid is called a keystone for future energy infrastructure. This shows their dedication to providing an intelligent energy grid, which is exactly what the new society needs.

An electrical vehicle is a car that uses electric energy rather than petrol and diesel. Batteries store electricity that is used to drive a motor to make these units operable. The zero tailpipe emissions that are characteristic of EV's make them much more environmentally friendly than conventional gasoline vehicles. Since EV's have no tailpipe emissions, air quality is enhanced, and greenhouse gas emissions are decreased. Compared to gasoline-powered cars, electric vehicles have higher energy efficiency. Up to 80% of the electrical energy coming from the grid can be converted by them into power for the wheels. Conversely, only 12%–30% of the energy contained in gasoline is converted into power for the wheels of a gasoline-powered vehicle[8]. EV's operate significantly more silently than cars that run on gasoline. In cities, this can be very advantageous. It is because they do not have mobile engines to rotate and emit harmful gases. EV's require less maintenance because they have fewer moving parts than cars that run on gasoline[9].

The term "renewable energy sources" (RE'S) describes energy sources that, in human perception, naturally replenish over time. These kinds of energy sources include biomass, geothermal, hydropower, wind, and solar energy. In contrast to fossil fuels, renewable energy sources (RE'S) have an effect on climate change.

Table 35: Comparative Analysis of Renewable Energy Generation (in GWh) Over a Decade[4]

| Year | Solar Power (GWh) | Wind Power (GWh) | Hydropower (GWh) | Geothermal Power (GWh) | Biomass Power (GWh) | Total Renewable Energy Generation (GWh) |
|------|-------------------------|------------------------|---------------------|------------------------------|---------------------------|---|
| 2010 | 340 | 590 | 2200 | 110 | 260 | 3500 |
| 2011 | 420 | 650 | 2300 | 120 | 280 | 3770 |
| 2012 | 510 | 720 | 2400 | 130 | 300 | 4060 |
| 2013 | 620 | 810 | 2500 | 140 | 320 | 4390 |
| 2014 | 750 | 920 | 2600 | 150 | 340 | 4760 |
| 2015 | 910 | 1050 | 2700 | 160 | 360 | 5180 |
| 2016 | 1090 | 1210 | 2800 | 170 | 380 | 5650 |
| 2017 | 1320 | 1390 | 2900 | 180 | 400 | 6190 |
| 2018 | 1580 | 1600 | 3000 | 190 | 420 | 6790 |
| 2019 | 1900 | 1830 | 3100 | 200 | 440 | 7470 |

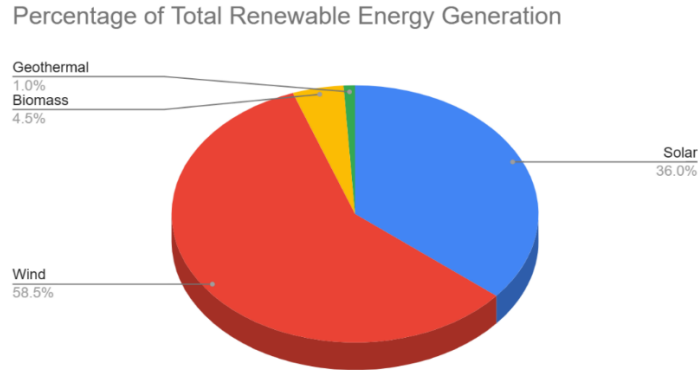


Figure 3: Pakistan Renewable energy generation in 2022[4]

The integration of EV's into the power grid together with RES offers great advantages to the society and environment without any cost to consumers. Integration of EV's into the grid enhances its flexibility and reduces dependence on fossil fuels as depicted in a graph by arrows signifying the connection between EV's, RES and the grid[10]. In fighting against climate change it reduces the emissions as well as improves the air quality[10]. Lastly, it boosts economic growth by manufacturing jobs within the renewable energy industry which leads to low power prices for consumers represented by a man installing a solar panel. Embracement of EVs and RES provide us with the path toward a clever, neat, and wealthy tomorrow.

Table 2Error! No text of specified style in document.: Review of related literature and system design

| Reference | Location | Grid | System Architecture | Software |
|-----------|-------------|---------|--|-----------|
| [11] | Switzerland | On-grid | PV/ battery | PYTHON |
| [12] | UK | On-grid | PV/ battery | MATLAB |
| [1] | Iran | On-grid | PV/ WT/ battery/ diesel generator/ fuel cell/ electrolyzer / hydrogen tank | HOMER PRO |

MATERIALS AND METHODS

Homer Pro software is used in the simulations, and it is known for its many possibilities of integration. The software had been developed into a custom form to suit our needs in this particular research context. In particular, a 1 MW solar power plant was linked to the selected grid in our facility. We also effortlessly added an EV fleet of at least 100 units. Using a converter to convert DC to AC that complies with our operation parameters for a successful meeting of the project's requirements concerning energy conversion. However, a very careful choice and assembly of components were conducted to achieve maximum effectiveness and correspondence with research goals.

System Architecture

The simulation process was carried out with the utmost care using the mentioned dataset. Special care was taken to make sure each parameter, variable, or input contained in the targeted data is reflected in the proposed simulation framework.

Table 3 *Error! No text of specified style in document.: Name, size and unit of Proposed Model*

| Component | Name | Size | Unit |
|------------------|-----------------------|----------------------|---------|
| PV | Generic flat plate PV | 1,000 | kW |
| Storage | Generic 100kWh Li | 100 | strings |
| System converter | System Converter | 434 | kW |
| Grid | Grid | Uninterrupted source | kW |

This was done in an effort to ensure that our analysis was as accurate as possible; hence, a clear picture of how the system behaved under those exact circumstances could be obtained.

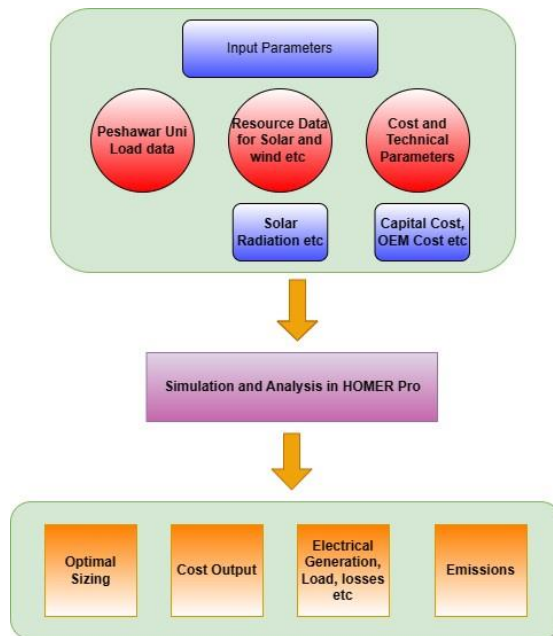


Figure 4: HOMER software's optimization workflow

Load Profile

According to concerned grid (Peshawar University Grid Sub-Station), the maximum demand is in the month of January which is 1350 kW. The Average Scaled Energy Consumption is 21600 kWh/day.

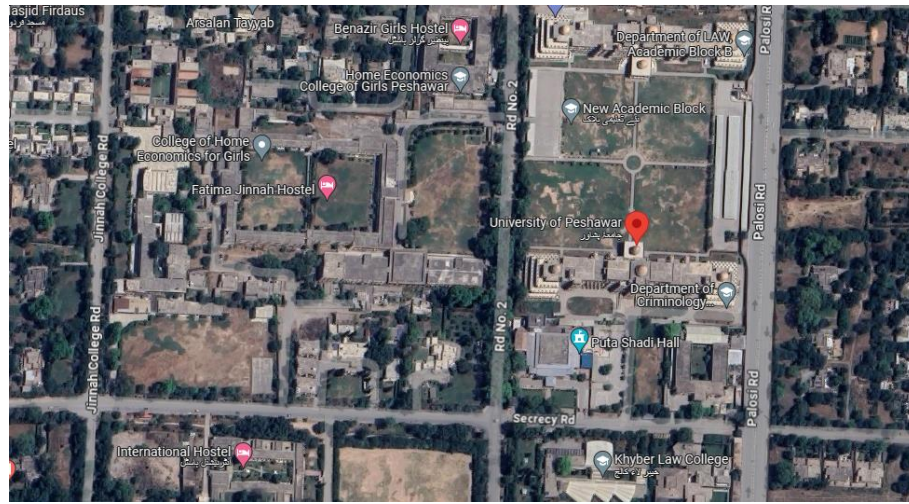


Figure 5: Satellite view of Peshawar University

Average Demand (kW) of each hour in the month of January is given in Table 4. This data is provided by the concerned grid station (Peshawar University Grid Sub Station)

Table 4: January Average Load of each hour [13]

| Hours | Load (kW) | Hours | Load (kW) |
|-------|-----------|-------|-----------|
| 0 | 700 | 12 | 1,200.00 |
| 1 | 700 | 13 | 1,185.00 |
| 2 | 735 | 14 | 1,124.00 |
| 3 | 786 | 15 | 1,112.00 |
| 4 | 798 | 16 | 1,084.00 |
| 5 | 804 | 17 | 1,079.00 |
| 6 | 810 | 18 | 1,063.00 |
| 7 | 821 | 19 | 1,046.00 |
| 8 | 825 | 20 | 1,032.00 |
| 9 | 836 | 21 | 1,020.00 |
| 10 | 843 | 22 | 918 |
| 11 | 867 | 23 | 879 |

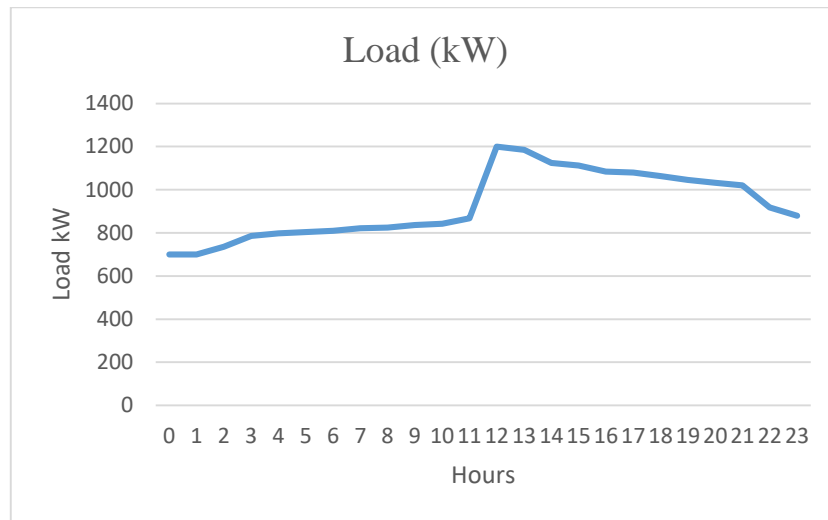


Figure 6: Graph presenting average load kW per hour in January [13]

The block diagram integrating 100 units of EV's, 1MW system of RE (Photo-Voltaic according to the site of Peshawar University Selected), Converter, Load and Grid in HOMER PRO is simulated below:

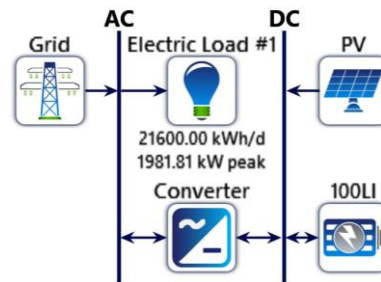


Figure 7: Schematic of Integration

Environmental Data

System element design and environmental factors influence the power output of the majority of renewable energy sources. For instance, solar radiation and ambient temperature play a significant role in determining the solar PV output. As input GHI resources in the proposed HES, monthly average solar radiation, clearness index, and ambient temperature data for a year, respectively, are used. The NREL store contains a huge amount of data necessary for renewable sources and RES studies, as this data is taken from the National Renewable Energy Laboratory (NREL). This data is related to the specific site selected, i.e., the Peshawar University Campus area. The discussion of environmental factors influencing solar generation is done in Table 3-3, that focuses on solar radiation and temperature.



Table 5: Solar irradiance, atmospheric clarity index, and temperature levels at the designated site

| Month | Solar Radiation (kWh/m ² /day) | Clearness Index | Temperature °C |
|-------|--|--------------------|----------------|
| Jan | 0.577 | 3.032 | 7.410 |
| Feb | 0.580 | 3.808 | 9.080 |
| Mar | 0.560 | 4.670 | 14.350 |
| Apr | 0.575 | 5.762 | 20.320 |
| May | 0.610 | 6.770 | 26.610 |
| Jun | 0.610 | 7.028 | 31.290 |
| Jul | 0.577 | 6.506 | 31.520 |
| Aug | 0.552 | 5.731 | 29.550 |
| Sep | 0.616 | 5.470 | 26.310 |
| Oct | 0.639 | 4.517 | 20.480 |
| Nov | 0.610 | 3.374 | 14.650 |
| Dec | 0.521 | 2.523 | 9.700 |

A Centre for Research on Energy and Clean Air (CREA) report indicates that the emission factor in Pakistan averaged 0.61 kg/kWh. In 2021, it was reduced from 0.65 kilograms of CO₂ per kWh in 2019.

Table 6: Emission Factor of each pollutant/kWh in Pakistan

| Pollutant | Emission factor (g/kWh) |
|-----------------|-------------------------------|
| CO ₂ | 610 |
| CO | 0.2 |
| CH ₄ | 0.01 |
| SO ₂ | 0.4 |
| NO _x | 0.2 |

RESULTS AND DISCUSSIONS

Integrating Electric Vehicles and Renewable Sources especially Solar Energy in to the existing grid gives us astonishing results in terms of economics and environment. Our next generation will breathe the clean air and will be able to purchase energy at cheap price.

Cost Summary

Cost summary of this integration of RE's and EV's is based on their Net Present Cost. These Simulations were the result of high interest rate (22% as of now) and high Inflation rate (22.9 %) according to State Bank of Pakistan.

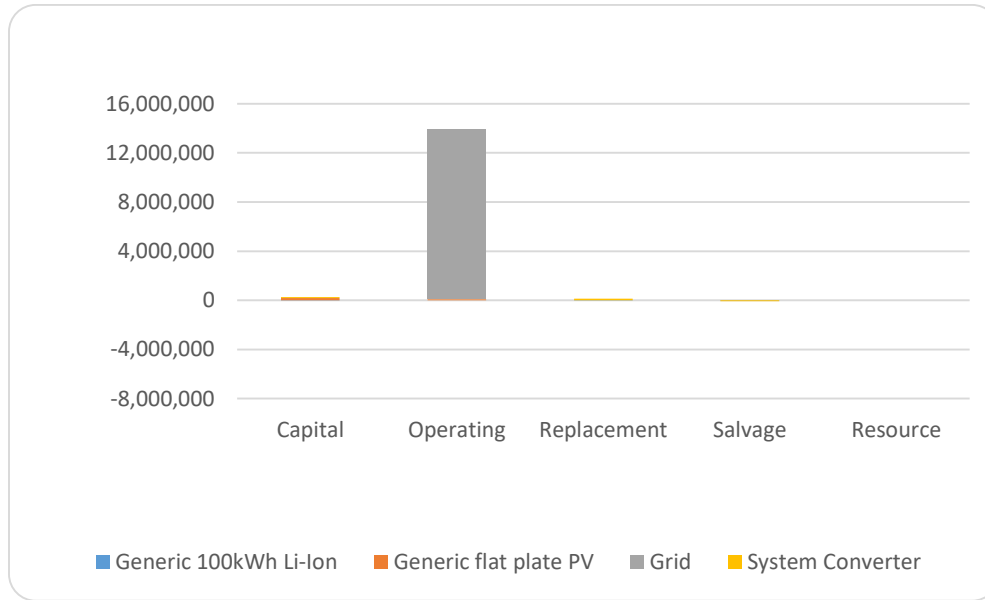


Figure 8: Graph Representing Share cost of each Term

Table 7: Net Present Costs (for 25 years)

| Name | Capital | Operating | Replacement | Salvage | Resource | Total |
|-----------------------|-----------|-----------|-------------|-----------|----------|-----------|
| Generic flat plate PV | \$196,500 | \$86,829 | \$0.00 | \$0.00 | \$0.00 | \$283,329 |
| Grid | \$0.00 | \$13.8M | \$0.00 | \$0.00 | \$0.00 | \$13.8M |
| System Converter | \$73,810 | \$0.00 | \$133,242 | -\$65,847 | \$0.00 | \$141,204 |
| System | \$270,310 | \$13.9M | \$133,242 | -\$65,847 | \$0.00 | \$14.2M |

Electrical Summary

Table below, provide detailed information regarding unmet and surplus electric load, PV output overview, grid purchases, and consumption data as part of the electrical summary. This table-based format conforms to professional standards, assuring that electrical engineering data is available for adequate analysis and interpretation to offer necessary information.



Table 8: Excess and Unmet

| Quantity | Value | Units |
|---------------------|-------|--------|
| Excess Electricity | 2,210 | kWh/yr |
| Unmet Electric Load | 0 | kWh/yr |
| Capacity Shortage | 0 | kWh/yr |

These tables present the relevant electrical data in an elaborate and orderly way to facilitate systematic analysis of circumstances with excessive load demands, PV performance, difficulties with grid purchases, and the general consumption patterns.

Table 9: Production Summary

| Component | Production (kWh/yr) | Percent |
|-----------------------|---------------------|---------|
| Generic flat plate PV | 1,625,093 | 20.3 |
| Grid Purchases | 6,367,554 | 79.7 |
| Total | 7,992,646 | 100 |

Table 10: Consumption Summary

| Component | Consumption (kWh/yr.) | Percent |
|-----------------|-----------------------|---------|
| AC Primary Load | 7,884,000 | 100 |
| DC Primary Load | 0 | 0 |
| Deferrable Load | 0 | 0 |
| Grid Sales | 710 | 0.00901 |
| Total | 7,884,710 | 100 |

PV: Generic flat plate PV

Subsequent tables and charts provide comprehensive details on various parameters like maximum output, PV penetration, hours of operation, or total kilowatt-hour (kWh) production for different PV panels. They show a very close look at the way in which photovoltaic systems are operating, with detailed information about KPIs.

Table 11: Generic flat plate PV Electrical Summary

| Quantity | Value | Units |
|--------------------|---------|--------|
| Minimum Output | 0 | kW |
| Maximum Output | 1,020 | kW |
| PV Penetration | 20.6 | % |
| Hours of Operation | 4,382 | hrs/yr |
| Levelized Cost | 0.00402 | \$/kWh |

Table 12: Generic flat plate PV Statistics

| Quantity | Value | Units |
|------------------|-----------|--------|
| Rated Capacity | 1,000 | kW |
| Mean Output | 186 | kW |
| Mean Output | 4,452 | kWh/d |
| Capacity Factor | 18.6 | % |
| Total Production | 1,625,093 | kWh/yr |

Figure 9 below shows the output in kW from the proposed Model of RE (1MW solar power plant). The x-axis shows the period of time in days for one year while y-axis shows the hours of each day. Graph clearly shows power comes during the day time. Furthermore, the other figure shows the intensity of power delivered in kW.

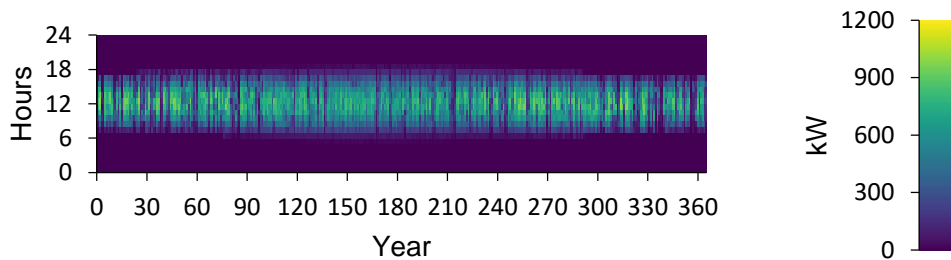


Figure 9: Generic flat plate PV Output (kW)

Grid

This part gives an in-depth view of energy trades consisting of purchased kWh, kWh for sale, monthly energy charge, and cumulative yearly energy expenses.

Table 13: Energy kWh data for the whole year

| Month | Energy Purchased (kWh) | Energy Sold (kWh) | Net Energy Purchased (kWh) | Energy Charge |
|-----------|------------------------|-------------------|----------------------------|---------------|
| January | 544,486 | 60.4 | 544,426 | \$27,223 |
| February | 476,430 | 0 | 476,430 | \$23,822 |
| March | 560,775 | 123 | 560,652 | \$28,036 |
| April | 521,021 | 80.9 | 520,940 | \$26,049 |
| May | 513,002 | 116 | 512,886 | \$25,647 |
| June | 518,348 | 77.1 | 518,271 | \$25,915 |
| July | 527,270 | 0 | 527,270 | \$26,364 |
| August | 564,707 | 96.3 | 564,610 | \$28,233 |
| September | 518,923 | 0 | 518,923 | \$25,946 |
| October | 525,564 | 141 | 525,424 | \$26,275 |
| November | 521,723 | 0 | 521,723 | \$26,086 |
| December | 575,304 | 15.4 | 575,288 | \$28,765 |
| Annual | 6,367,554 | 710 | 6,366,843 | \$318,360 |

Figure 10 shows the output in kW from the concerned grid (Peshawar University Grid Sub-station). The x-axis shows the period of time in days for one year while y-axis shows the hours of each day. Graph clearly shows power has been delivered all the day. Furthermore, the other figure shows the intensity of power delivered in kW.

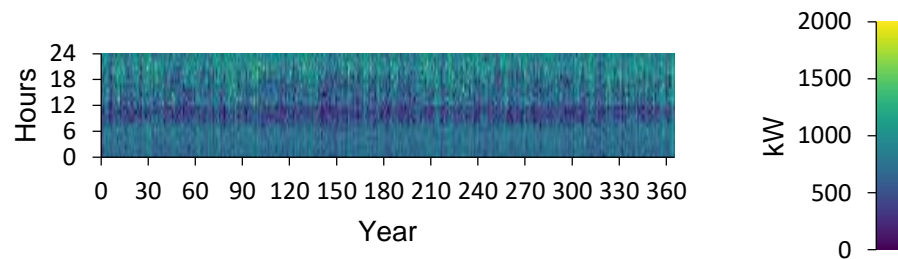


Figure 10: Energy Purchased from Grid (kW)

Figure 11 shows the energy sold in kW to the concerned grid (Peshawar University Grid Sub-station). The x-axis shows the period of time in days for one year while y-axis shows the hours of each day. Graph clearly shows power has been delivered in small amount. Furthermore, the other figure shows the intensity of power delivered in kW.

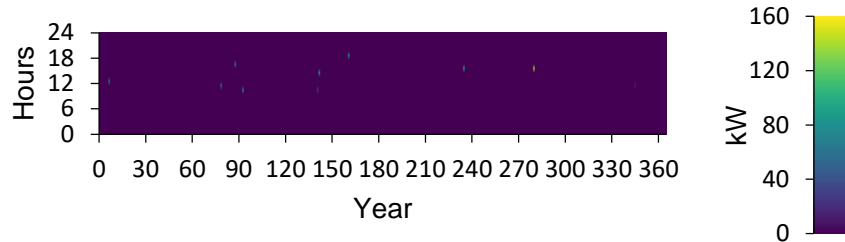


Figure 11: Energy Sold to Grid (kW)

Comparing Economics

Financial indicators of the project suggest an investment possibility. An IRR of 27.0%, which far exceeds the usual required rate of return on most investments, shows that the project is likely to yield good profits. The other thing is that the capital recovery period for this investment project is 3.35 year, which makes it comparably shorter payback period. Additionally, the simple payback period of 3.66 years is short enough to make certain that the project is an appreciable venture. Generally speaking, the financial ratios indicate that this is an advantageous investment project, providing for rapid profits accumulation in the short-term.

Table 14: Comparison between proposed and base system for 25 years

| | Base System (Grid Only) | Proposed System |
|-------------------------|-------------------------|-----------------|
| Net Present Cost | \$17.1M | \$14.2M |
| CAPEX | \$0.00 | \$270,410 |
| OPEX | \$394,200 | \$321,914 |
| LCOE (per kWh) | \$0.0500 | \$0.0416 |

Comparing Emissions

The Proposed Model having integrated RE's and EV's with the concerned grid has reduced the emissions of GHG's (Green House Gases) such as CO₂, SO₂, Unburnt Hydrocarbons, NO_x, and CO. We have compared the Proposed Model (Grid, EV's and RE's) with the base Model (Only Grid) and the results are huge satisfying regarding clean and green future.

Table 15: Comparing Emissions between Proposed and Base Model

| Proposed Model (Grid, EV's and RE's) | | | Base Model (Only Grid) | | |
|--------------------------------------|-----------|--------|------------------------------|-----------|--------|
| Quantity | Value | Units | Quantity | Value | Units |
| Carbon Dioxide | 3,884,208 | kg/yr. | Carbon Dioxide | 4,809,240 | kg/yr. |
| Carbon Monoxide | 1,274 | kg/yr. | Carbon Monoxide | 1,577 | kg/yr. |
| Unburned Hydrocarbons | 63.7 | kg/yr. | Unburned Hydrocarbons | 78.8 | kg/yr. |
| Particulate Matter | 0 | kg/yr. | Particulate Matter | 0 | kg/yr. |
| Sulfur Dioxide | 2,547 | kg/yr. | Sulfur Dioxide | 3,154 | kg/yr. |
| Nitrogen Oxides | 1,274 | kg/yr. | Nitrogen Oxides | 1,577 | kg/yr. |

CONCLUSION

Integration of EVs and RE sources in the Peshawar University Grid Substation shows great economic and environmental advantages. NPC for the twenty-five-year project is now \$2.9 M (two point nine million dollars) less than its budget value of \$17.1 M (seventeen point one million dollars) hence the savings of about 17 percent. Furthermore, the company has managed to cut down on operational expenses by lowering their electricity cost from \$0.05 to as low as \$0.0416 per kilowatt-hour.

In addition, the coupling of vehicles with renewables has produced significant environmental gains as well. The annual CO₂ emissions reduced by 19.3% (from 4,809,240 kg/yr to 3,884,208 kg/yr). The emissions of carbon monoxide (CO) decreased by 19.2%, from 1,577kg/yr down to 1,274kg/yr. The reduced emissions of unburnt hydrocarbons (HCs) are 19.1% (from 78.8kg/yr, to 63.7kg/yr). The emissions of SO₂ have decreased by 19.5% – from 3,154 kg/yr to 2,547 kg/yr. Eventually, NO_x releases have gone down by twelve percent (19.2%) with a drop from one thousand five hundred and seventy-seven kilogram per annum to a thousand two hundred and seventy-four kilograms each year.

The above findings show that incorporating EVs and REs in a current grid system may be an ideal platform for not only achieving economic needs but also environmental goals as well. This is an example on how Peshawar University has successfully implemented this project that any institution or company willing to cut its costs and reduce environmental impact should borrow.

ACKNOWLEDGEMENTS

Finally, I appreciate a lot of assistance which was provided by my supervisor Dr Arif Khattak for the study. Without his knowledge, tolerance and good attitude, I would not have reached an advanced level of education and a developed career. Thirdly, I would like to thank my friends, Raheel Ahmad and Abdullah



Nawaz, as their contributions have been priceless to me as well. We highly appreciate their support in providing information for data collection, data analysis, and in preparing manuscripts. Lastly, I would like to acknowledge my parents' commitment and undying love during my academic journey. It has consistently been one source of inspiration that drives me.

REFERENCES

- [1] A. Singh and P. Baredar, "Techno-economic assessment of a solar PV, fuel cell, and biomass gasifier hybrid energy system," *Energy Reports*, vol. 2, pp. 254–260, Nov. 2016, doi: 10.1016/j.egy.2016.10.001.
- [2] J. Tant, F. Geth, D. Six, P. Tant, and J. Driesen, "Multiobjective Battery Storage to Improve PV Integration in Residential Distribution Grids," *IEEE Trans Sustain Energy*, vol. 4, no. 1, pp. 182–191, Jan. 2013, doi: 10.1109/TSTE.2012.2211387.
- [3] W. Su, H. Eich, W. Zeng, and M. Y. Chow, "A survey on the electrification of transportation in a smart grid environment," *IEEE Trans Industr Inform*, vol. 8, no. 1, pp. 1–10, Feb. 2012, doi: 10.1109/TII.2011.2172454.
- [4] "Our World in Data." Accessed: Nov. 24, 2023. [Online]. Available: <https://ourworldindata.org/>
- [5] K. Vijay Kumar and T. Bharath Kumar, "Optimal scheduling of micro grid for Plug-in Electrical Vehicle," *International Journal of Engineering and Technology(UAE)*, vol. 7, pp. 558–564, 2018, doi: 10.14419/IJET.V7I2.7.10882.
- [6] W. Tushar, C. Yuen, S. Huang, D. B. Smith, and H. V. Poor, "Cost minimization of charging stations with photovoltaics: An approach with EV classification," *IEEE Transactions on Intelligent Transportation Systems*, vol. 17, no. 1, pp. 156–169, Jan. 2016, doi: 10.1109/TITS.2015.2462824.
- [7] E. I. Obeagu and T. A. Owunna, "Overview of Smart Grid Technology as a Renewable Energy Source," *Article in Journal of Energy Research and Reviews*, vol. 12, no. 3, pp. 6–15, 2022, doi: 10.9734/jenrr/2022/v12i3239.
- [8] A. N. Siddiqui and M. S. Thomas, "Techno-Economic Evaluation of Regulation Service from SEVs in Smart MG System," *Technology and Economics of Smart Grids and Sustainable Energy*, vol. 1, no. 1, pp. 1–10, Dec. 2016, doi: 10.1007/S40866-016-0016-Z/TABLES/5.
- [9] V. Monteiro, J. G. Pinto, and J. L. Afonso, "Operation Modes for the Electric Vehicle in Smart Grids and Smart Homes: Present and Proposed Modes," *IEEE Trans Veh Technol*, vol. 65, no. 3, pp. 1007–1020, Mar. 2016, doi: 10.1109/TVT.2015.2481005.
- [10] F. Mwasilu, J. J. Justo, E.-K. Kim, T. D. Do, and J.-W. Jung, "Electric vehicles and smart grid interaction: A review on vehicle to grid and renewable energy sources integration," *Renewable and Sustainable Energy Reviews*, vol. 34, pp. 501–516, Jun. 2014, doi: 10.1016/j.rser.2014.03.031.
- [11] A. Pena-Bello, E. Barbour, M. C. Gonzalez, M. K. Patel, and D. Parra, "Optimized PV-coupled battery systems for combining applications: Impact of battery technology and geography," *Renewable and Sustainable Energy Reviews*, vol. 112, pp. 978–990, Sep. 2019, doi: 10.1016/j.rser.2019.06.003.
- [12] R. D. Bingham, M. Agelin-Chaab, and M. A. Rosen, "Whole building optimization of a residential home with PV and battery storage in The Bahamas," *Renew Energy*, vol. 132, pp. 1088–1103, Mar. 2019, doi: 10.1016/j.renene.2018.08.034.
- [13] "WAPDA - Water and Power Development Authority." Accessed: Nov. 24, 2023. [Online]. Available: <https://www.wapda.gov.pk/>

Paper ID: ICSET-2341

MODELLING OF SOLID-STATE TRANSFORMER FOR OFFSHORE WIND TURBINE AND HIGH VOLTAGE DC TRANSMISSION

Muhammad Shahab Uddin*, Haris Alam, Muhammad Muneeb Ullah
Electrical Engineering, UET Peshawar, Peshawar 25120, Pakistan

**Corresponding author*

Email: 18pwele5265@uetpeshawar.edu.pk

ABSTRACT

This research focuses on the modelling of Solid-State Transformer for Off-shore wind turbine and its High Voltage Direct Current (HVDC) transmission. Wind power is clean, renewable and in plentiful amount. The proposed wind energy systems using Solid State Transformer (SST) can effectively eradicate the problem of synchronization of generated Alternating Current (AC) gathered from different wind turbines. SST is an AC to AC converter having two Direct Current (DC) links. Among the DC-DC converter topologies for SST, Dual Active Bridge (DAB) topology is implemented. This project also describes the use of HVDC technology, overcoming a number of major technical challenges in shape of Corona, Skin effect, Proximity effect, etc. For consumers, Dual Bridge Inverter is being utilized to have AC supply for AC loads and local distribution. (With the help of wind turbines each connected to rectifier, resulting in a constant DC source. The DC-DC convertor utilized in a Dual Active Bridge with a PWM generating unit for transistor switching and a control unit to maintain the output. The PWM unit generating produce a unipolar waveform obtain by comparing two sine waves with a 180-degree phase shift. This phase shift drives the Dual Bridge inverter designed for the voltage level of 135 kV. A PWM switching scheme is implemented and simulated to yield accurate and precise results. The Total Harmonic Distortion (THD) analysis, value of 2.03% in AC waveform for local loads. Overall, the system demonstrates effective power conversion from wind turbine to a stable high voltage DC output with controlled switching and reduced harmonic distortion.

KEYWORDS: SST, HVDC, Off-shore Wind Turbine

INTRODUCTION

Solid State Transformer (SST) is also known as Power Electronic Transformer (PET). It replaces the conventional low frequencies transformer (LFT) by a high frequency transformer (HFT) and some power electronic circuitry. SST converts an input of low frequency (LF) into High frequency (HF) power through the switching circuits and regenerates a low frequency power at the output terminals. SSTs are also utilized in other power distribution aspects, such as Var compensation, active filtering, FACTS, fault isolation, and current limiting [1]. Basically, SST is an AC to AC converter having two DC links, one of high voltage (HVDC) link and one of low voltage (LVDC) link. SST has less weight and volume than conventional transformers. In comparison to the traditional 50/60 Hz transformer, it is predicted to have 1/1000 the volume at 100 kHz [2].

Typically, transmission to grid station is achieved through HVAC transmission lines. Corona effect, skin effect, proximity effect and capacitive effect causes major power losses in the system. Thus, transmitting bulk power through HVAC is not suitable. So, it needs an alternative. The best option for maximizing energy transfer, dependability and stability is HVDC technology [3]. A high voltage direct current (HVDC) also called a power super highway or an electrical super highway uses DC for the transmission of an electric current. HVDC eliminates the losses being faced in the HVAC transmission. Successful operation of Matiari-Lahore Bipolar HVDC Transmission line having rating ± 660 kV has pushed the planners to take account HVDC transmission to integrate Hydel Power Resource of Northern areas into National grid [4].

The aim of this project is to efficiently interface the SST with wind turbines. It also focuses on the HVDC transmission of the power generated by wind turbines, eliminating the HVAC transmission losses.

If thesis statement is achieved, the architecture for wind farm based on SST will be according to the future demand, economical and having improved power quality (a smaller number of conversion stages are required, harmonic filtration and reactive power compensation property of SST). Hence, the power system infrastructure will become efficient and more reliable.

Figure 1 shows the complete structure of this project. In first step, output of wind turbine is rectified from AC to DC. This DC output is supplied to LVDC link of SST which is stepped up to HVDC. The HVDC is transmitted through HVDC transmission. At the end, HVDC is inverted through inverter before supplying it to the grid station.

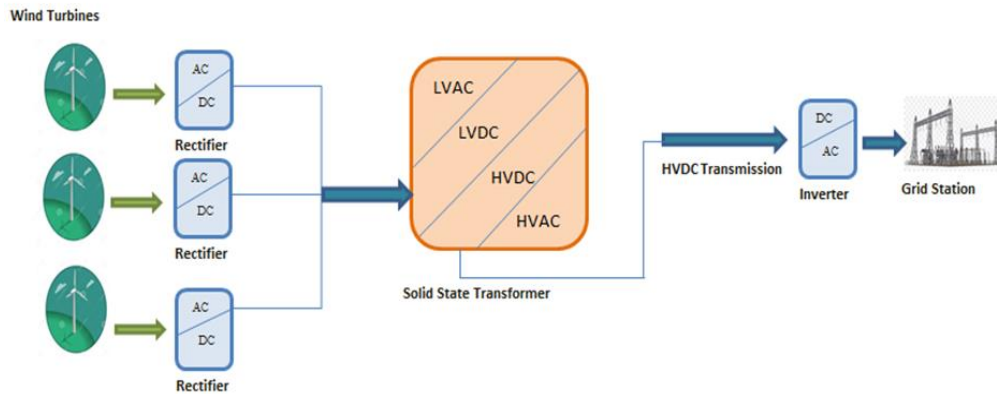


Figure 101: Modeling of SST for off-shore wind turbine and HVDC Transmission

MATERIALS AND METHODS

The initial focus is on the turbine, where the conversion of wind kinetic energy into electrical energy is discussed. Following this, the second step involves the interfacing of a rectifier with the Solid-State Transformer (SST), and the chapter concludes with a discussion on High Voltage Direct Current (HVDC) transmission.

With the aim of lowering energy costs and reducing dependence on fossil fuels, wind turbines are extensively employed. Preferred one is an off-shore wind turbine due to higher wind speeds compared to on-shore locations. The off-shore wind turbine is considered a constant DC source within this project.



The Solid-State Transformer (SST) is a high-frequency transformer with various topologies. As the SST is the combination of a powered electronic circuit and a HF transformer, the voltage regulation, voltage dip/sag protection, fault segregation and DC output are some of its main features [5]. The selected stage topology for this project is the three-stage configuration with links at both ends. Within the three-stage topology, the rectifier stage takes the spotlight as the interface between incoming AC and the DC link of the SST. The second stage involves a DC to DC converter, a critical component playing a vital role in voltage regulation, volume reduction, and losses reduction, as depicted in Figure 3. The final stage of this topology is the inverter, responsible for converting incoming DC into highly sinusoidal and regulated AC.

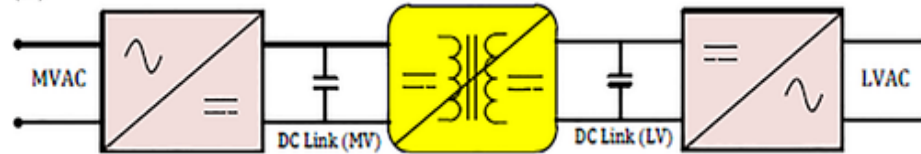


Figure 102: Three Stages SST Topology

The chosen three-stage topology offers several advantages. Firstly, it provides both HVDC and LVDC links, enhancing flexibility in power transmission. Additionally, this topology allows for a reduction in the transformer's size, leading to a corresponding decrease in core size and, consequently, a reduction in core losses. Notably, it facilitates the seamless integration of renewable energy sources, such as solar and wind energy, into the power station. Moreover, the DC link at the output serves a dual purpose by enabling the charging of backup DC supply in the grid station. Furthermore, the three-stage topology proves effective in suppressing harmonics and ensuring voltage regulation. Importantly, it allows for power factor correction within the system.

The rectified output from the off-shore wind turbine is directed to the Solid-State Transformer (SST). The SST, in turn, steps up the LVDC input to HVDC output for transmission through the HVDC transmission line. Finally, an inverter is employed to convert the incoming DC back to AC, completing the power transmission process.

The primary emphasis is on the DC to DC converter stage, where various topologies are considered for DC-DC conversion. The chosen one is the Dual Active Bridge converter. The Dual Active Bridge converter is characterized by a high-frequency transformer in the middle and two H-bridges at both ends, as depicted in Figure 3 and simulated in MATLAB. In this configuration, an 11kV LVDC input is supplied to the Dual Active Bridge converter, which efficiently converts it into a 135kV HVDC output. This HVDC is then transmitted through the HVDC transmission line, representing a crucial stage in the overall project.

HVDC transmission offers several advantages. In contrast to AC lines, HVDC transmission exhibits zero inductance for the DC line, minimizing the impact of inductance-related issues. The capacitive effect present in DC systems is essentially an open circuit, eliminating the capacitive reactance that contributes to $I^2 R$ losses in AC systems. HVDC systems require fewer conductors compared to HVAC systems, leading to the use of smaller transmission towers. Furthermore, the power flow in a DC system can be controlled by adjusting delay angles at the terminal, providing a level of control not achievable in AC systems where power flow is contingent on system generation and load. Additionally, HVDC transmission allows for the connection of two AC systems with different frequencies via a DC link, offering flexibility and synchronization independence between systems.

The Full-Bridge Inverter is represented by a single-phase circuit depicted in Figure 3, which includes four power switches. This configuration is employed in applications requiring higher power ratings. The associated operations are elucidated in Table 1, detailing the switching states and corresponding output of the inverter.

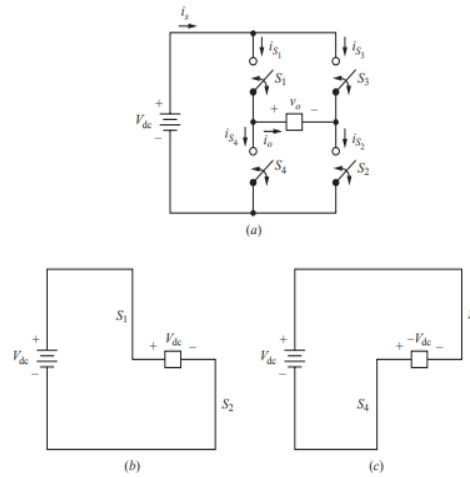


Figure 3: Full Wave Bridge Inverter [6]

Table 1: Switching States and Output Voltage of Full Bridge Inverter

| Switches Closed | Output Voltage V_o |
|-----------------|----------------------|
| S_1 and S_2 | $+V_{dc}$ |
| S_3 and S_4 | $-V_{dc}$ |
| S_1 and S_3 | 0 |
| S_2 and S_4 | 0 |

The focus is on evaluating the quality of the AC output voltage or current generated by the inverter, which utilizes a DC voltage source to power an AC load. To quantify the quality of a non-sinusoidal wave, Total Harmonic Distortion (THD) is employed. Harmonic distortion is defined as the ratio of harmonics to the fundamental frequency or the deviation of a wave from a theoretically pure sine wave. The THD equations are provided in terms of both output voltage (Equation 3.1) and current (Equation 3.2), offering a comprehensive assessment of the inverter's performance.

$$THD = \sqrt{\frac{\sum_{n=2}^{\infty} (V_{n,rms})^2}{V_{1,rms}^2}} = \frac{\sqrt{V_{rms}^2 - V_{1,rms}^2}}{V_{1,rms}} \dots\dots\dots 3.1$$

$$THD = \sqrt{\frac{\sum_{n=2}^{\infty} (I_{n,rms})^2}{I_{1,rms}^2}} = \frac{\sqrt{I_{rms}^2 - I_{1,rms}^2}}{I_{1,rms}} \dots\dots\dots 3.2$$



The Sinusoidal Pulse Width Modulation (SPWM) is a technique that generates variable-width pulses by comparing a triangular carrier signal with a sinusoidal reference waveform. This modulation method includes two types: Unipolar and Bipolar SPWM techniques. Unipolar Sinusoidal Pulse Width Modulation (SPWM) is favoured for this research for several reasons. Unipolar PWM inverters demonstrate superior efficiency and lower Total Harmonic Distortion (THD) compared to bipolar PWM inverters. Additionally, the unipolar SPWM technique requires a smaller filter to produce a sine wave, contributing to a reduction in THD.

RESULT AND DISCUSSION

Two Wind Turbines coupled with each Rectifier is considered as a constant DC source. Each source of 5.5kV is connected in series to get a constant DC voltage of 11kV.

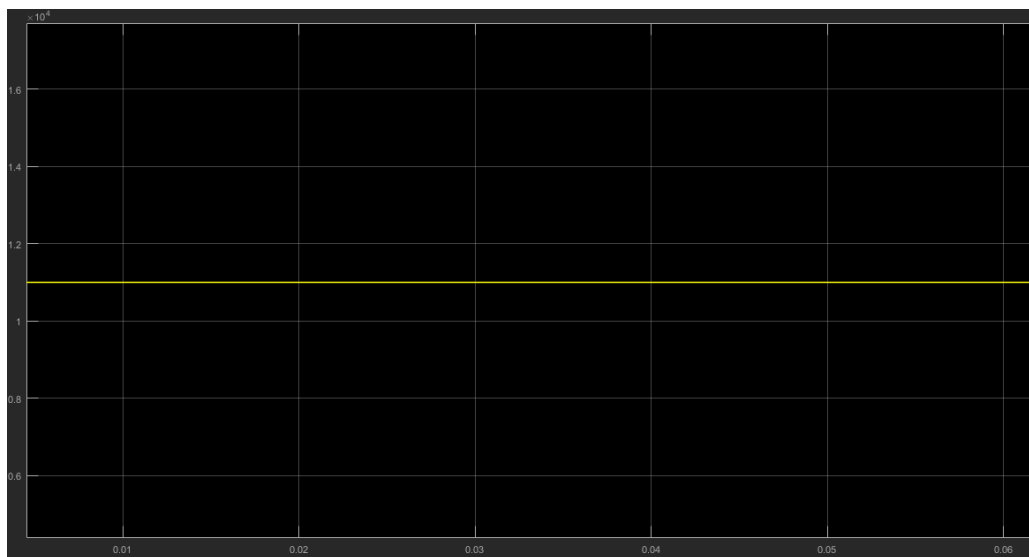


Figure: 4: Graph of Input to DAB

The DC-DC Converter used in this model is Dual Active Bridge. A PWM generating unit is there to create a switching signal for the transistors used in DAB. Moreover, there is a control unit to maintain the output voltage. DAB after processing and switching with extra high frequency, boost the voltage into 135kV. At the output of DAB, there is a little overshoot in the transient response. However, Steady State response is firm and desired one. At the other end, a Pulse Width Modulator is installed to observe its AC properties like Total Harmonic Distortion. THD of the output waveform is 2.03%.

The graph of PWM generating unit is also obtained shown in Figure 5. A Unipolar Wave is obtained from the unit after comparing two sine waves of having 180 degrees' phase shift. The comparator operator will examine the level of both.

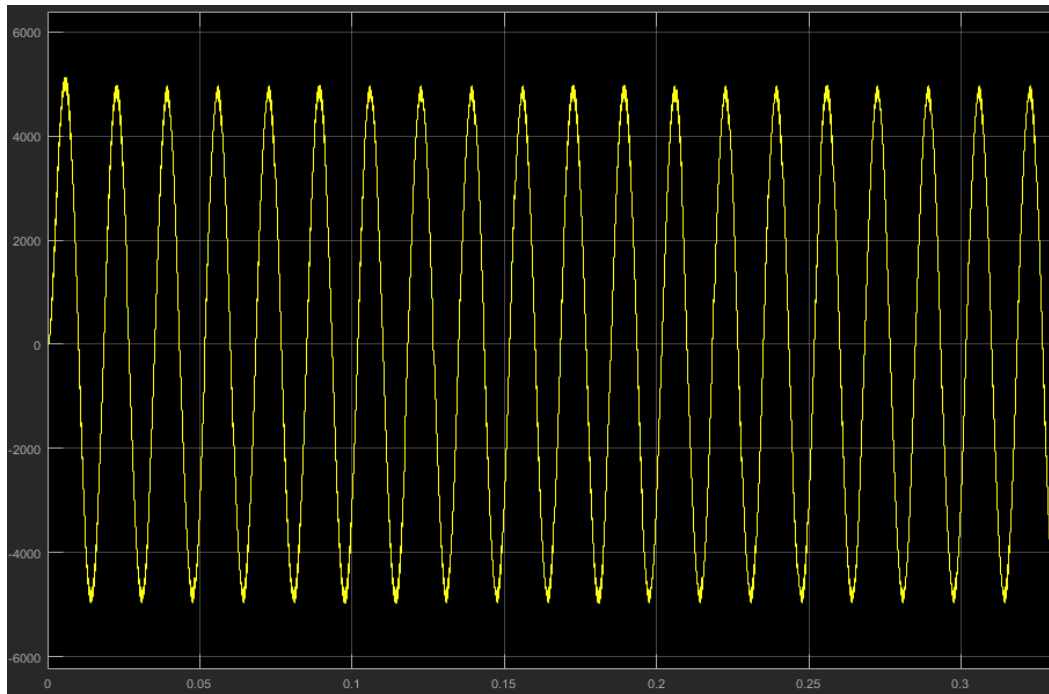


Figure 5: Output Current level of Inverter

PWM switching scheme is being implemented and simulated to give accurate results and precise value (THD= 2.03%). Moreover, THD plays a vital role in AC waveforms regarding the performance and efficiency. Its value is reduced to the standard region of IEEE. THD value can be noticed in Figure 6.

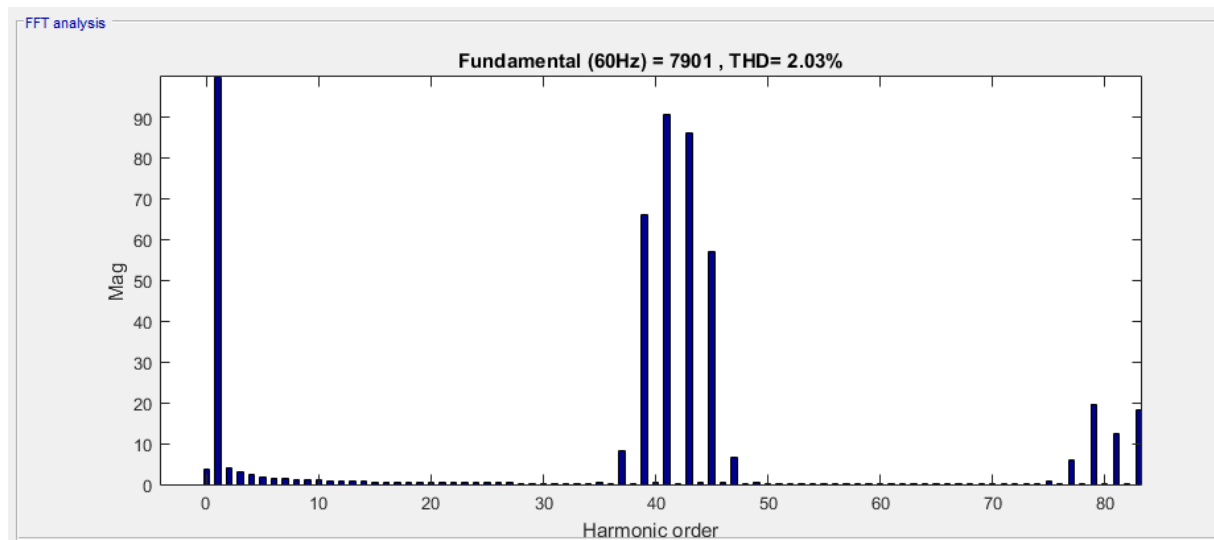


Figure 6: Graph of PWM

CONCLUSION

In this paper, the application of SSTs in the context of offshore wind turbines is demonstrated. The ability of SSTs to provide voltage regulation, power quality improvement, and integration with HVDC systems will introduce a new paradigm in offshore energy transmission.

Wind Turbine coupled with rectifiers to provide 11kV input to Solid State Transformer. The boost Voltage on output is observed to be 132kV. This HVDC is transmitted with two lines of 400 Ohms resistance. At the end, a PWM inverter is installed for utility loads. THD is observed to be 2.03%. This research not only highlights the technical aspects of the SST but also emphasizes its potential to revolutionize the dynamics of offshore wind energy production, paving the way for a greener and more sustainable energy landscape.

ACKNOWLEDGEMENTS

We would like to extend our gratitude to our project supervisor, Prof. Dr. Syed Waqar Shah for their patient supervision, enthusiastic encouragement, resourceful knowledge and useful critiques for this project. Also, we would like to thank our parents for believing in us and for their sincere and unfeigned prayers without which it could not be possible.

REFERENCES

- [1] Solid-State Transformer-Based DC Power Distribution Network for Shipboard Applications by Abdelrahman Ismail, Mahmoud S. Abdel-Majeed, Mohamed Y. Metwly, Ayman S. Abdel-Khalik , ,Mostafa S. Hamad,Shehab Ahmed 4,Eman Hamdan 5 and Noha A. Elmalhy , Feb 2022
- [2] N. Kimura, T. Morizane, I. Iyoda, K. Nakao, T. Yokoyama: “Solid State Transformer Investigation for HVDC transmission from Offshore Wind Turbine”, 6th International Conference on Renewable Energy Research and Application (2017).
- [3] N M Kirby, M J Luckett, L Xu, W Siepmann, “HVDC Transmission for Large Offshore Wind farms”, AC-DC Power Transmission, Nov.2001.
- [4] Future Prospective of HVDC System in Pakistan by Maaz Ahmad; Muhammad Yousaf Ali Khan; Ehtasham Mustafa; Nazar Hussain Baloch; Muhammad Ali Khan, published in 4th International Conference on Computing, Mathematics and Engineering Technologies (iCoMET),2023
- [5] Comprehensive Review of Solid-State Transformers in the Distribution System: From High Voltage Power Components to the Field Application by Abdur Rehman, Malik Imran-Daud , Syed Kamran Haider , Ateeq Ur Rehman , Muhammad Shafiq and Elsayed Tag Eldin, Sept 2022
- [6] Daniel W. Hart, Power Electronics, New York, McGraw-Hill, 2010.

**Paper ID: ICSET-2342****DESIGN, ANALYSIS AND FABRICATION OF LONG ENDURANCE HYBRID
DELTA WING UAV**

M. Fasih Shahzad¹, Nadeem Ur Rehman^{1,*}, Nadir Ullah¹, Fahad Ullah Zafar², Muhammad Saad Rehan²

¹Department of Mechanical Engineering, University of Engineering and Technology, Peshawar

²US-Pakistan Center for Advanced Studies in Energy, University of Engineering and Technology Peshawar,
Pakistan

**Corresponding author*

Email: nadeem.rehman@uetpeshawar.edu.pk

ABSTRACT

The study aims to develop an efficient UAV capable of enhanced-range missions. To design, analyze and fabricate long endurance delta wing UAV which can be used for various social and military purposes. The endurance of the UAV is given special consideration in this work.

UAV's are built significantly nowadays for surveillance, emergency protocols, and videography and for entertainment, and delivery purposes. Ever increasing demand requires sustainability too. Autonomous, low aspect ratio UAV's, and fully solarized UAV's are continuously been built. This study addresses a unique wing design incorporated with solar cells.

The design includes a hybrid system comprising of an electric motor and a battery that powers a pusher propeller. The RC plane was fabricated after CAD model and CAE tests. Plane was successful and took flights appropriately. UAV operates on 5200mAh battery and on three light weight flexible solar cells, each weighing 70g. The airframe except its landing gears is made of Jumbolon foam, attached with balsa wood at crucial locations for structural integrity, which makes it lightweight and strong.

The results of the testing showed that the UAV is capable of a maximum endurance of 35.01 minutes, with an operational altitude of 3-150 meters directly depending on connected frequency of RC.

KEYWORDS: UAV, Endurance, AOI, ESC, Delta wing.

INTRODUCTION

The primary goal of this research was to alter the way unmanned aerial vehicles (UAVs) are currently designed. Based on these modifications, a light-weight UAV will be designed, built, and flown for the purposes of surveillance and reconnaissance.

Unmanned Air Vehicles (UAVs) are a type of aerial vehicle that can be self-piloted with a gyroscope or remotely controlled by an operator using a radio transmitter. Radio flight control is possible for self-piloting aircraft with the use of an autopilot system. Transmitter and receiver is used in Piloting that operate radio-controlled (RC) aircraft. The receiver receives the signals from transmitter and send to the installed servos to execute the command, which then sends them through the installed servos. Servos controls the Control surfaces like elevators, rudders and ailerons. [1] [2]. Unmanned Aerial Vehicles (UAVs) are gaining importance in the aerospace industry due to their versatility in tasks. The advancement of nanotechnologies and the application of diverse materials in these endeavours are intimately associated [3].



Many real-life applications are examined in [4], including some related to logistics, reconnaissance, and surveillance. Solid Works was utilised to model the design. The XFLR5 v6 numerical programme was utilised for the wing and airfoil analysis since it is essential for data generation and analysis in the aerospace industry [5]. The design simulations were performed in ANSYS 2019 R2 (Academic) and ANSYS 2019 R3.

Design Process

It was found that the design procedure for remote-controlled aircraft is time-consuming due to the high level of aerodynamics knowledge required. Our intention was to modify the existing design process to make it more practical and easy to use in everyday settings. As a result, we modified the process that was advised in [6] and applied it in order to develop our aircraft [7]. The design steps used are as;

Step 0: Pre-design (knowing the concept of stability)

Step 1: Determine the need, and then base different design goals on it.

Step 2: Choosing the geometry type (wing type, airfoil, etc.)

Step 3: Determine the weight that was pre-planned.

Step 4: Wing design.

Step 5: Designing the control surfaces and fuselage.

Step 6: Manufacturing the plane's component pieces.

Step 7: Selecting an appropriate propulsion mechanism.

Step 8: Ground and Aerial Tests, which test our aircraft.

THE PLANE'S STABILITY:

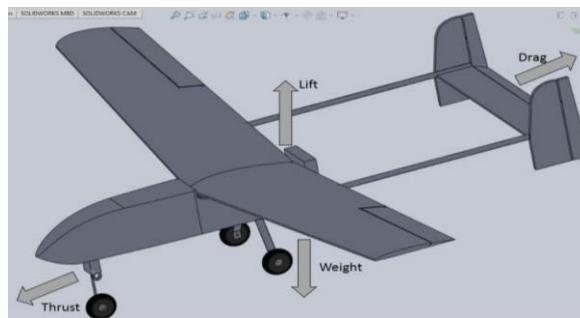


Figure 1: Number of forces on a plane, Retrieved from [8]

A plane is subject to four forces in total: lift, weight, drag, and thrust. The upward force or the aerodynamic force component perpendicular to the wind is referred to as lift. The weight force, or the force that pulls the plane downward due to gravity, opposes it. The opposing force that the plane experiences while it is in the air is called drag force. The thrust force, which is produced by the plane's propulsion system, opposes drag. The forces must be balanced in order to preserve stability; otherwise, the plane will become unbalanced and gravitate toward the stronger force. [9] [10]



An aircraft has three main axes: the roll, pitch, and yaw axes. The yaw axis runs parallel to the direction of the wings. The vertical stabilizer (rudder) has control over movement along this axis. The plane's up-and-down movement is caused by the pitch axis, which is the axis parallel to the wing. The horizontal stabilizer, also known as the elevator, regulates the movement around it. The roll axis, like the pitch axis, is in charge of the plane's up and down motion. The Alerions on the wings are in charge of it. All three axes must be in balance for the flight to be controlled and stable; otherwise, the flight will be unstable. [11]

Assuming the aircraft's weight at the beginning of the design process is a good idea because it plays a major role in the design of the aircraft, more so than it does in any other engineering design process [12].

By estimating the weight, we can also choose the right wing span and wing cord for the aircraft, which in turn helps us determine the plane's wing area—another crucial design component. This is achieved by selecting an appropriate value for 3D wing loading or wing cube loading. The weight of the aircraft divided by the wing area to the power of 1.5 is the wing cube loading, or "C."

$$C=W/(A_w)^{1.5} \quad \dots (1)$$

Whereas C=Cube Wing Loading; W= Total Weight of the Wings; A_w=Wing Area For the RC Planes Wing cube loading should be around 12 or most probably less than 12. Considering, our design requirements it was chosen to be 11.5 [13].

Following investigation, it was decided to use "ClarkY" airfoil. Its superior C_L/C_D ratio, better lift coefficient at zero angle of attack, and overall suitability for low speed UAVs with Reynold Numbers less than 10^6 , or $Re < 10^6$, are the main reasons it was selected. [14] [15]

MATERIALS AND METHODS

A delta wing is a type of wing which is triangular when seen from the top or bottom view. Cropped delta wing is chosen as it has more area than any other and has maximum lift during take-off. Additionally, it can glide if propulsion system fails during flight which can avoid damage to the UAV when it hits the ground. The acute angle formed between the longitudinal axis of the aircraft and the chord line of the wing is referred to as the angle of incidence (AOI) or wing setting angle. This UAV is of high wing configuration which gives good angle of incidence (AOI). These all combines to give a safer landing with elegant flight. For enhancing endurance, we introduced flexible light weight solar cells above the wings and made their connection with battery to make the operation hybrid.

We took general idea, from the constraints of international sport chaired by Switzerland called Aeromodelling by **Fédération Aéronautique Internationale (FAI)**. Fuse Length: 70% of wing span, Horizontal Stab Area: 20% - 25% of the wing area, Elevator Area: 20% - 25% of the horizontal stab chord, Rudder Area: 30% - 50% of the vertical stab chord, Vertical Stab Area: 7% -12% of the wing area.

Configurations

The particular configurations of the plane are shown in Table 1, 2, 3, 4, 5 and Table 6.

Table 1: Wing configuration

| Number of wings | Wing location | Wing type |
|------------------|---------------------|-------------|
| Mono | High wing | Delta |
| High-lift device | Sweep configuration | Shape |
| Plain flap | Fixed wing | Fixed shape |

Table 2: Tail configuration

| Aft or forward | Horizontal and vertical tail | Attachment |
|-----------------------|------------------------------|------------|
| Aft conventional tail | Conventional | Fixed tail |

Table 3: Propulsion system configuration

| Power type | Power Source location |
|-------------------------|-----------------------|
| Motor-powered (Tractor) | In front of nose |

Table 4: Landing gear configuration

| Landing gear mechanism | Landing gear type |
|------------------------|--------------------------|
| Fixed and faired | Tri cycle (tail dragger) |

Table 5: Fuselage configuration

| Largest internal Division | Pressure system |
|---------------------------|-------------------|
| Cabin | Pressurized Cabin |

Table 06: Subsystem configuration

| Primary control surfaces | Secondary control surfaces | Battery Location |
|---|----------------------------|------------------|
| Conventional (i.e., elevator, aileron, and rudder) | None | Inside fuselage |
| Storage | | |
| Payloads | | |

Structural Formation

The cropped delta high mono-wing configuration is chosen to ensure stable and controllable three-dimensional movements, achieved by increasing the aspect ratio more than that of conventional wings. The wing span of the selected plane is greater than that of typical delta wings. The aircraft has to be designed optimally by considering subsequent weight & maximum power output from battery.

The optimal battery for our Delta wing Plane is chosen as a 3-cell LiPo battery of 5200mAh, placed at the nose section of the plane. An Electronic Speed Controller (ESC) is a purpose-built device designed for controlling the speed of an electric motor. Using a specialised combination of hardware and firmware, ESCs drive motors to a commanded speed. They maintain motor speed under various circumstances, such as the dynamic load of a propeller. ESC with a rating of 40A is used to drive the motor's operation at 9400 rpm.

The weight in grams and balance of Centre of Gravity(CoG) along with x and y axes in inches, of components are as follows, Fuselage Frame 500g, 17.25x, 0y; Batteries 650g, 4.25x, 0y; Motor 120g, -0.75x, 0y; Propeller 36.8g, -1.95x, 0y; ESC (Electronic speed controller) 57.1g, 9.3x, 0y; Cables and Connectors 35g, 3.2x, 0y; Servos and pushrods 60g, 25x, 0.8y, -0.8y; Front landing Gear 121g, 9x, -9y.

Key Dimensions, CAD and CAE

Root chord 18 in, Wing span 54 in, Wing tip chord 7.5 in,

$$\text{Average chord} = \frac{\text{Root chord} + \text{Tip chord}}{2} = \frac{18 + 7.5}{2} = 12.75 \text{ in}$$

Wing Area = wing span x average chord

Wing Area = 54in x 12.75. This makes, Wing Area = 688.5 in².

One plate area = 14 x 9.5= 133 in²

Nose Length= 20% x Fuselage Length = 9.2in

Tail Length = 40% x Fuselage Length = 18.4in

Fuselage Height is 5.5 in, Fuselage Internal width is 3.75 in, Fuselage external width is 5 in, Fuselage length is 56 in, Horizontal stabilizer length is 27.56 in, Horizontal stabilizer tip is 3 in, Vertical stabilizer height is 10.00 in, Vertical stabilizer tip is 4 in, Wing gear tire is 3 in, Tail gear is 0.75 in. The control surfaces and body parts of the plane covering fuselage, airfoil, wings, empennage, rudder and elevators are shown in CAD views below. Hot wire cutting was used for smooth finishing and accurate dimensions.

The wing total area is 688 in², one plate area is = 14 x 9.5= 133 in².

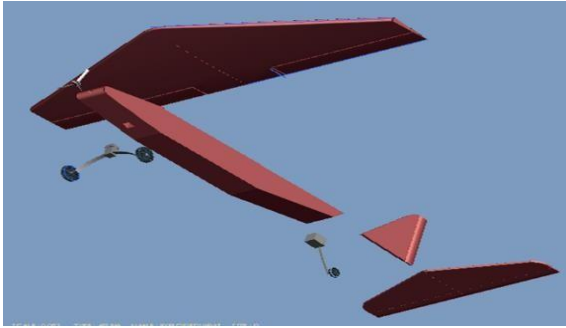


Figure 2 (a): Isometric View

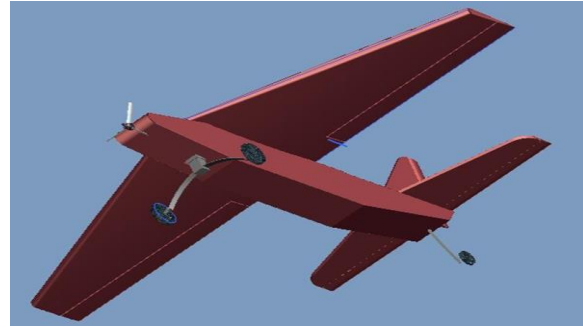


Figure 2 (b): Exploded View

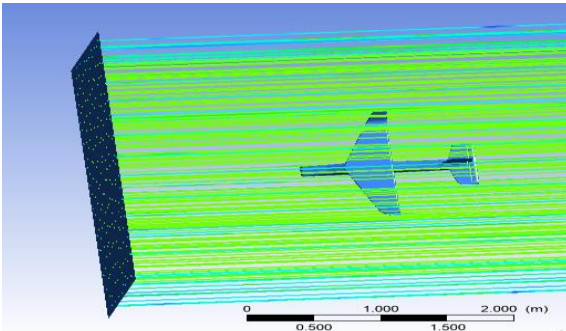


Figure 3: Velocity Outlet

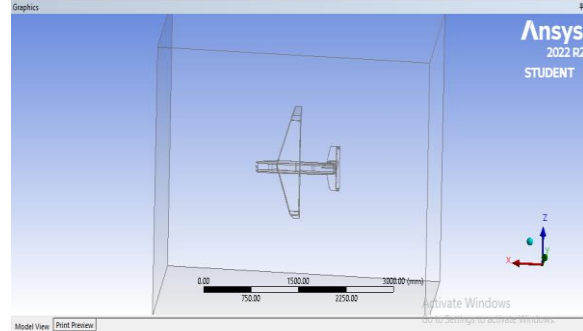


Figure 4: CFD Analysis

Power

One plate voltage is 2V and amperes is 2 amps. In series, voltage from 3 plates = $2+2+2 = 6\text{ V}$.

As the solar plates are connected in series and one solar plate has 2 Ampere and 2 Volts. So, voltage adds in series circuit so the power from three plates would be, $P = VI$

Power from one plate = $2 \times 2 = 4\text{ W}$.

As the solar plates are connected in series and voltage adds while current remains constant in series circuit so the power from three plates would be, $P = (2+2+2) \times 2 = 12\text{ W}$.

Our battery energy is 5200mAh or 5.2 Ah. This shows that it will provide 5.2 A of current for one hour. Hence, we got the required voltage at the output. The connection of solar plates with the other components is shown below,

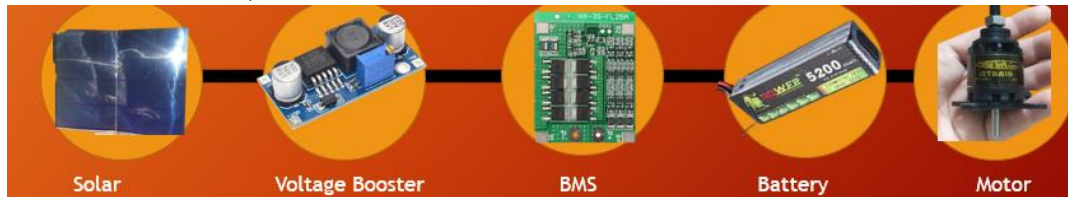


Figure 5: Hierarchy of Power Devices



ICSET-23



UET Peshawar

To increase the voltage at the required level, voltage booster is used. The positive terminal of plates is connected with the positive of voltage booster and negative with negative of voltage booster. Hence due to specified circuitry of voltage it increases the voltage to the required level at output.

Battery Management System(BMS) is used to equally charge the cells of the battery so that no cell remains un-charged. The positive terminal of voltage booster from other side is connected with the 12V terminal of the BMS and negative of voltage booster with the ground(0V). Hence, required 12V is gained at the output terminal of BMS and then connected with the battery to equally charge the cells of the battery.

The idea is very straightforward, furnished with the solar cells skinning its wing; it recovers vitality from sun keeping in mind the end goal to gives energy.¹⁰ The final plane along with solar cells installed is shown below,



Figure 6: Final Plane

RESULT AND DISCUSSION

Aircraft Flight Tests Results:

Time Calculation of First flight (dry test without Solar):

Take off = 7.80sec, Flight = 16 min, 26 sec, Approaching for Landing = 7.98sec, Landing = 4.66sec, Additional ground time = 18.00 sec, Battery Usage = 16 min, 44 sec.

Time Calculation of Second flight (dry test without Solar):

Take off = 7.74sec, Flight = 5 min, 37 sec, Approaching for Landing = 22.17sec, Landing = 2.55sec, Additional ground time = 2.05 sec, Battery Usage = 6 min, 12 sec.

Total of first and second flight (without Solar):

Total time = 16min, 44sec + 6min, 12sec = 22min, 56sec, Total battery usage = 65% battery usage. This was known by using a battery indicator. A device which shows how much battery is discharged.

So, the battery consumed per minute = $65\% / 22.93$

Battery consumed per minute = 2.83%

We can found how much percentage of battery can be consumed if we fly our plane for any given number of minutes. So, if we want to fly our Plane for 30 minutes

Battery % consumed = $2.83\% \times 30\text{min} = 84.90\%$

Third Flight with Solar:

After 1st and 2nd dry flight test there was 35% battery remaining with voltage of 9.0V. This time we have induced 3 solar plates on a delta wing plane for the test flight. We did our first flight by introducing three solar plates each of 70g. We introduced three solar plates so,

$70 \times 3 = 210\text{g}$ (total weight of solar plates)

Take off = 8.18sec, Flight = 26 min, 30 sec, Approaching for Landing = 25.91sec, Landing = 5.79sec,
Additional ground time = 9.11 sec, Battery Usage = 68.1%,

So, battery consumption per minute = $68.1\% / 26\text{min}, 30\text{sec}$

= $68.1\% / 26.5\text{min}$

= 2.57% So, now if we want to fly our Plane for 30 minutes

Battery % consumed = $2.57\% \times 30\text{min}$

= 77.10%

Table 7: Power Consumption before and after in percentage

| Time | 2.83% battery consumed per minute (without solar) | 2.57% battery percentage consumed per minute(with solar) |
|------|--|---|
| 5 | 14.15% | 12.85% |
| 10 | 28.30% | 25.70% |
| 15 | 42.45% | 38.55% |
| 20 | 56.60% | 51.40% |
| 25 | 70.75% | 64.25% |
| 30 | 84.90% | 77.10% |
| 35 | 99.05% | 89.95% |
| | | |

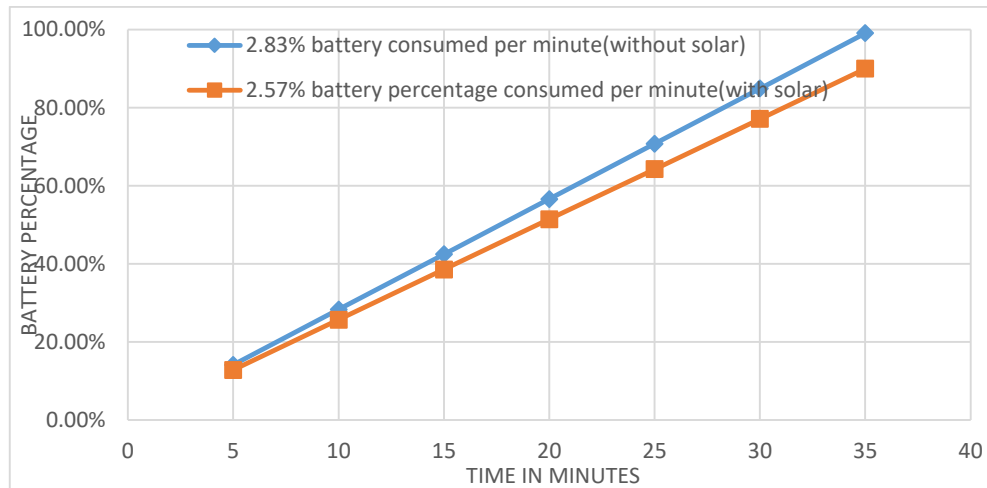


Figure 7: Comparison of Endurance with and without Solar cells

Checking Endurance

Now to check how much endurance is enhanced if we use the battery to certain amount of consumption. Let us say that certain percentage consumed is 90% as this is the safe consumption until which a UAV can be flown in air,

So, 90% without solar plates = $90\% / 2.83\% = 31.80$ min

90% with solar = $90\% / 2.57\% = 35.01$ min

Enhanced endurance = 90 % battery consumption with solar – 90% battery consumption without solar

Enhanced endurance = 3.22 min = 3 min, 13 sec

Table 8: Time taken by Flights with and without solar cells

| 90% battery consumed without solar cells | 90% battery consumed with solar cells |
|--|---------------------------------------|
| 31.8 | 35.01 |

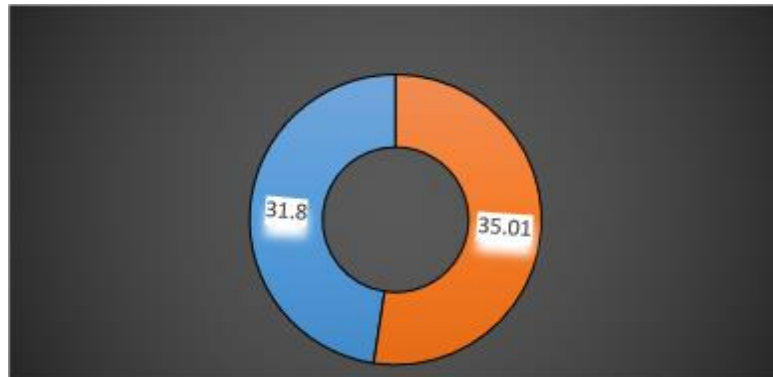


Figure 8: Time taken by Flights with and without solar cells

Hence, by inducing 3 solar plates on our plane, we have enhanced its endurance by 3.22 min (3 min, 13 sec). For Efficiency, it is increased as follows, Efficiency = $3.22 / 31.80 \times 100 = 10.12\%$

CONCLUSION

The particular Cropped-delta wing provides more speed and significant lift. To increase the endurance of UAV installation of solar cells proved magnificent. The material used for fabricating plane is jumbolon having density of 35kg/m^3 . This material was chosen due to its light weight and structural stability. This plane was fully operational. It also went into wears and tears during flight tests. CAD design of final plane was made and after the successful analysis tests plane was made and had a cropped-delta wing. The advantage of delta wing was its maximum area relative to the rectangular wing so that the solar cells can easily be incorporated.

The flight tests of delta wing UAV were successful. UAV was operated on 5200mAh Li-Po battery. To increase the flight time we used the light weight flexible solar cells. Five cells could have been installed on the wing according to the wing area but only three cells of area 133in^2 were induced to reduce



ICSET-23



UET Peshawar

the failure chances. We used epoxy glue to attach the solar plates. Flight was done with solarized wings and our project achieved overall 10.1% of efficiency. Flight tests with solarized wings were a success, hence, we achieved the goal of enhanced endurance on our unique design.

Along with this objective we achieved some additional objectives as it was supposed to carry out its designated tasks efficiently in a variety of scenarios while offering significant benefits in terms of sustainability. The UAV developed has the capability to drop payloads, is lightweight, agile and requires shorter landing and take-off runways as of its counterparts. It plays a crucial role of being environmental friendly as none carbon emitting agents and other hazardous things are used.

Future Recommendations

Further work can be done on its Aerodynamics. Aerodynamic efficiency and stability during flight can be improved by optimising the design of hybrid delta wing unmanned aerial vehicles (UDVs) by making adjustments to the wing form, control surfaces, and propulsion systems. Advances in autonomous technology could enable these unmanned drones to do ever-more complex jobs and operate in a range of environments. Developments in energy storage technologies are critical to extending the lifespan as well as range of (UAVs). Solar energy is one among the cleanest sources of energy with the most potential for growth in the near future. Advances in technology for communication can lead to improved connectivity and control for hybrid delta wing unmanned aerial vehicles. Artificial intelligence (AI) has the potential to enhance flight performance, detect and assess targets, and automate processes. It may enable intelligent control systems that enhance range and efficiency.

REFERENCES

- [1] S.N Logu, "Design and fabrication of RC Plane with flexible wings," International Journal of advance engineering research and development, 2021.
- [2] M. K. Jane, Unmanned aerial veicles and targets, Jane's Publishing Corporation, 2000.
- [3] M. B. Vasile Prisacariu, "Design and construction of flying wing unmanned aerial vehicle," in International Conference on Military Technology, 2018.
- [4] John E. Peters, "Unmanned aircraft systems for logistics applications," RAND Coroporation, 2017.
- [5] Lasantha Kurukularachchi, "Stability and control analysis in twin boom vertical stabilizer, unmanned air vehicle," International Journal of Scientific and Research Publications, 2019.
- [6] M. H. Sadraey, Aircraft Design_A System Engineeing Approach, A John Wiley and Sons Ltd Publishers, 2013.
- [7] Shreyas S Hegde, "A systematic approach for designing, analyzing and building a model RC Plane," International Journal of Engineering Research and Technology (IJERT), 2014.
- [8] N. Hall, "Forces On an Airplane," 5 May 2015. [Online]. Available: <http://www.grc.nasa.gov/www/k-12/airplane/forces.html>.



ICSET-23

*Proceedings of the 5th International Conference on Sustainable
Energy Technologies (ICSET 2023) Peshawar, Pakistan
14-15 December 2023*



UET Peshawar

- [9] Dr Murat Vural, "Estimating RC Model Aerodynamics and Performance," Illionois Institute of Technology, Illionois, 2009.
- [10] William Owens, "A Method for inflight adjustment of wings dihedral with folding wings and tail," New Jersey's Governor's School of Engineering and Technology, New Jersey, 2018.
- [11] N. Hall, "Aircraft Rotations," 5 May 2015. [Online]. Available: <http://www.grc.nasa.gov/www/k-12/airplane/rotations.html>.
- [12] E. Schatzberg, Wings of Wood, Wings of Metal: Culture and technical choice in american airplane materials 1914-1945, Princeton, NJ: Princeton University Press, 1956.
- [13] F. Reynolds, "Model Design and Technical Stuff," 1989. [Online]. Available: <http://www.theampeer.org/CWL/reynolds.htm>.
- [14] Karthik MA, "Analysis and Selection of Airfoils for low speed UAV's," International Journal of Latest Engineering Research and Applications, pp. 40-49, 2018.
- [15] Marchman III, "Clark-Y Airfoil performance at low Reynolds Number," in AIAA 22nd Aerospace Sciences Meeting, Nevada, 1984.

Paper ID: ICSET-2343

PRODUCTION IMPROVEMENT AND ENHANCEMENT IN A MANUFACTURING UNIT BY IMPLEMENTING OVERALL EQUIPMENT EFFECTIVENESS

Tayeed Wahab^{1,*}, Prof. Dr. Misbah Ullah¹, Dr. Imran Ahmad¹, Dr. Rehman Akhter¹, Sajid Ahmad¹,
Muhammad Waseem²

¹Department of Industrial Engineering, University of Engineering and Technology, Peshawar, Pakistan

²University of Virginia, USA

**Corresponding author*

Email: engrdarwesh3439@gmail.com

ABSTRACT

Overall Equipment Effectiveness (OEE) is important in manufacturing industries as it provides a comprehensive metric for evaluating and monitoring the efficiency and productivity of equipment and processes. It enables companies to optimize operations, enhance production output, and reduce costs. This study focuses on utilizing Overall Equipment Effectiveness (OEE) to monitor manufacturing effectiveness and address six significant losses: setup, breakdowns, minor stoppages, reduced speed, start-up rejects, and production rejects. Relevant data were collected from local industry in Pakistan, where PET bottle production processes were examined. The initial analysis determined the current OEE, and the results were used to develop a process improvement plan, enhancing productivity and reducing costs. Moreover, countermeasures such as Planned Downtime Management, Management Routines, Six Sigma, and 5S Workplace Organization were implemented to address individual losses identified by OEE. Each countermeasure targeted specific aspects of OEE and was applied separately. Furthermore, notable improvements were achieved in the three major blocks of OEE: availability increased from 85.62% to 86.12%, performance improved from 82.33% to 90.9%, and quality rose from 81.73% to 85.68%. Applying these countermeasures individually and in combination optimized manufacturing system effectiveness, resulting in an overall improvement in OEE from 57.59% to 66.68%. The study highlights the importance of using OEE as a monitoring tool in manufacturing industries and demonstrates that targeted countermeasures can optimize operations, enhance production efficiency and reduce costs.,

KEYWORDS: Availability, Manufacturing, Overall Equipment Effectiveness (OEE), Performance, Production System, and Quality.

INTRODUCTION

Overall Equipment Effectiveness (OEE) is a powerful tool to gauge equipment effectiveness in any industrial setting. The OEE is characterized as a measure of execution of total equipment to perform a task as required. The term OEE was initially depicted by Nakajima in 1988 [1], [2]. Equipment effectiveness could be easily measured. Distinguishing components that cause manufacturing losses are characterized into six noteworthy groups of OEE. The six groups recognize and measure primary manufacturing losses [3],

[4]. It centres around availability losses, Performance losses, and quality losses, which compute the current proficiency of the manufacturing unit. It is the best technique to increment and upgrade the capability of different machines, manufacturing units, production systems, and assembly lines. OEE is a measure of the proficiency and adequacy of the manufacturing processes. A normal OEE score of around 60% for most organizations, industries, and manufacturing units enhancing a world-class OEE value would mean a colossal improvement in productivity and profitability [5], [6]. Al-Hafiz Crystoplast (Pvt) Ltd (AHCP) initially had an OEE of 57%. However, by promulgating, a variety of countermeasures has achieved notable improvements, and OEE has risen to 66.68%, which is considered quite suitable. Notable enhancements have been observed in the three main components of OEE: availability increased from 85.625 to 86.12%, performance improved from 82.33% to 90.9%, and quality rose from 81.73% to 85.68%. By implementing these countermeasures individually, OEE optimized from 57.59% to 66.68%. AHCP's management has recognized the significance of OEE as a tool to enhance and monitor the production of PET bottles. It is one of the vital measurements in TPM (total productive maintenance) and lean manufacturing tasks to measure TPM and particular activities by giving an overall way to make sufficiency of the production and assembling procedure [1], [2]. In OEE, improvement opportunities for everyone, including heads, support staff, bargain specialists, designers, engineers, chiefs, and managers. It is superior to different strategies on the grounds of competitiveness, gigantic profit from the venture, get the best performance from hardware, expanded process quality, exceptionally viable to carry out, etc. [7], [8].

METHODOLOGY

During the visit to Al-Hafiz Crystoplast (Pvt) Ltd (AHCP), we exhaustively considered all processes involved in manufacturing PET bottles. The required data were collected, and analysis was performed to determine the current OEE and the three blocks of OEE. Overall Equipment Effectiveness (OEE) is one of the effective tools. It primarily focuses on availability losses, performance losses, and quality losses, which calculate the current efficiency of manufacturing units or industries. OEE in percentage can be calculated by two methods. Firstly, dividing actually produced items by theoretical produced items. Second, by multiplying quality, availability, and performance [2], [5], [9 – 12]. OEE is determined by utilizing Equation.

$$OEE = A \times P \times Q \quad (1)$$

Whereas OEE=Overall Equipment Effectiveness
A=Availability, P=Performance, Q=Quality

Moreover, productivity loss is of three types and is associated with the three factors of OEE, which are downtime loss, speed loss, and quality loss. The objective is to tenaciously work towards eliminating OEE Losses. These three major losses are further subdivided into OEE six big losses [13 – 15].

Table 1. OEE Losses Category

| Availability | Performance | Quality |
|------------------|-------------|---------------------|
| Planned Downtime | Minor Stops | Production Rejects |
| Breakdowns | Speed Loss | Rejects on Start up |



Availability is the time for which a machine is available, known as production planned time, and the time which is not available is downtime, which combines all the significant and minor stoppages [16], [17].

$$\text{Availability} = \frac{\text{Operating Time}}{\text{Planned Production Time}} \quad (2)$$

The availability losses that occur during production are Setup/Planned Down Time and Breakdowns [18]. Setup time is the one in which an organization or equipment is arranged or planned for executing the operations [19], [20], [36]. It includes changeover, material, operator shortages, major adjustments, and warm-up time. The breakdown is one of the major losses among six big losses and is affecting the availability of machines. It is because of equipment, tooling failure, unplanned maintenance, and general breakdowns.

Table 2. Availability losses in OEE

| Availability Losses (Minutes) | | | |
|-------------------------------|-----------------------|-----|---------|
| SETUP | planned maintenance | PM | 15 |
| | warm up Time | WT | 18.375 |
| Breakdown | Equipment Failure | EF | 14.375 |
| | Tooling Failure | TF | 35.0833 |
| | General Breakdowns | GB | 15 |
| | Unplanned Maintenance | UPM | 5.8333 |

It depicts availability loss in AHCP, whereas tooling failure constitutes a major loss of 35%, and then a warm up time of 18% counts towards total availability loss. Hence, availability by calculating came out 85%. However, by implementing the planned downtime technique, availability increased to 86%, as shown in (6).

Performance is defined as the performance of a machine during its operation stage.

$$\text{Performance} = \frac{\text{Actual Operating Time}}{\text{Planned Operating Time}} \quad (3)$$

Performance losses are divided into two major categories: Minor Stops and Reduced Speed [22] [23]. Minor stoppages are defined as events that interfere with the production flow without really failing the machine used for production. The losses associated with minor stops are Components Jams, Miss Feeds, and Cleaning/Checking [24]. Reduced speed or speed loss is due to the slowness of the process. The losses associated with speed loss are Rough Running and Equipment Wear [25].

Table 3. Performance losses in OEE

| Performance Losses (minutes) | | | |
|------------------------------|---------------------|----|--------|
| Minor stops | Components Jam | CJ | 51.166 |
| | Cleaning / Checking | CC | 28.5 |
| Reduce Speed | Rough Running | RR | 16.575 |
| | Equipment Wear | EW | 17.5 |

It portrayed the performance loss in AHCP. Where Components Jam constitutes 51% as the major loss, and then Cleaning and Checking comprises 28% of the total performance loss. Therefore, with losses, the performance was 82%. However, implementing the Management Routine technique performance increased to 90.9%, as shown in table 6.

Quality is the ratio of good pieces to total pieces produced.

$$Quality = \frac{Good\ pieces}{Total\ Pieces} \quad (4)$$

Furthermore, the two major classifications of quality losses are recognized as Start-up Rejection and Production Rejects [26]. Start-up rejects are rejects during warm-up, start-up, improper setup, or other early production of the items. These are further classified as scrap, rework, in-process damage, in-process expiration, and incorrect assembly. The production rejects include the items that are lost during steady-state production. These are further classified as scrap, rework, in-process damage, in-process expiration, and incorrect assembly.

Table 4. Quality losses in OEE

| Quality Losses (minutes) | | | |
|--------------------------|-------------------|-----|--------|
| Start-up Rejects | In-process Damage | IPD | 22.916 |
| | Scrap | SC | 0 |
| Production Rejects | In-Process Damage | IPD | 55.208 |
| | Scrap | SC | 17.583 |

It shows the quality loss in AHCP where Production Rejects in-process damage covers 55% of total quality loss. The scrap during production (production rejects scrap) is 17 %, and start-up rejects in-process damage covers 22%. Hence, the quality determined was 81.7%. However, promulgating Six Sigma and 5S Workplace Organization techniques, quality reached 85.68%, as shown in table 6.

Practically, Overall Equipment Effectiveness is handily determined by utilizing various software. The manufacturing industry is to be chosen to take out losses for improving and upgrading production by utilizing OEE.

Countermeasures for improving OEE are the following.

Several countermeasures were implemented to improve the OEE of Al-Hafiz Crystoplast (Pvt) Ltd (AHCP). These countermeasures include management routines, planned downtimes, Six Sigma, and 5S Workplace Organization. Management routines involve setting up daily, weekly, and monthly routines to monitor production and identify any issues that may arise [18], [27], [28]. Planned downtimes were implemented to ensure maintenance and repairs were conducted on machines, preventing breakdowns and reducing downtime [21], [25]. Six Sigma methodologies were used to improve the quality of production, reduce defects, and enhance overall efficiency.

The Six Sigma DMAIC process (Define, Measure, Analyse, improve, control) is a framework for the development of existing methods falling under detail and looking for gradual improvement [29], [30]. Six

Sigma is a prepared, data-driven technique and strategy for discarding defects. The major canterers of Six Sigma are to decrease process variety [31], [32]. In many organizations, quality loss is considered the smallest of the OEE losses. Six Sigma is a proportional system that might be important to keep up the spotlight on quality upgrades [22], [23], [33].

The steps for six Sigma is,

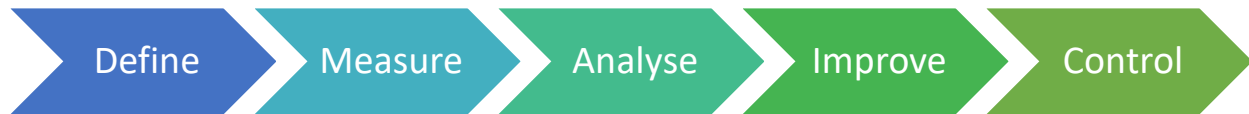


Figure 1 DMAIC Cycle

Additionally, the 5S Workplace Organization was implemented to create a more organized and efficient workspace as shown in figure 2. The combination of these countermeasures has had a significant impact on the OEE of AHCP, improving the effectiveness of the manufacturing process and ensuring that the company remains competitive in the market. It is associated with normalized cleanup. Nonetheless, it is something other than cleanup. 5S is the system to manage and form the work area and smooths the work stream to accomplish capability by taking out and limiting the waste, upgrading the waste, and decreasing the methodology that causes shortcomings of the assembling unit [Vamshi K. Katukoori]. Process for applying 5S in an organization. It is also a constant enhancement cycle [Vamshi K. Katukoori]. Ongoing plan for improving the manufacturing process.

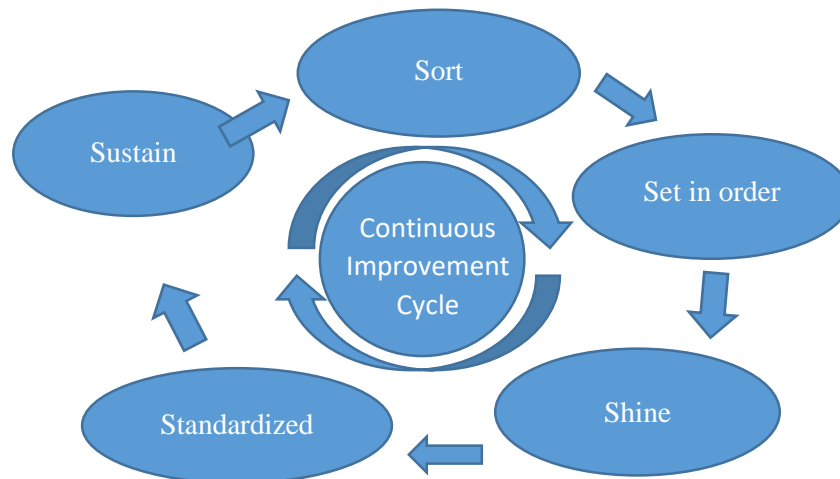


Figure 2. 5s Workplace Organization Cycle

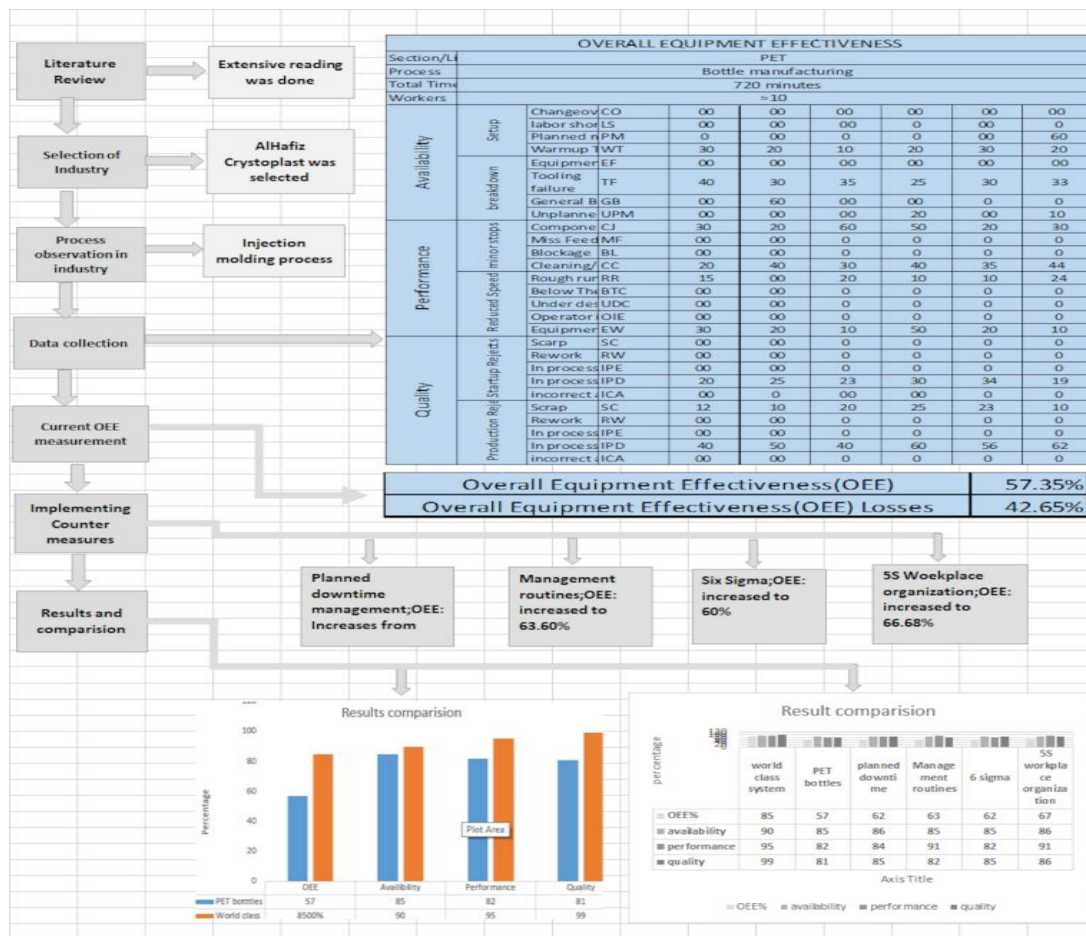


Figure 3. Flow Chart of Methodology

To tackle the individual losses, various countermeasures are being applied to improve the structure blocks of OEE. Each countermeasure will be utilized separately to improve specific areas of the manufacturing process, ultimately resulting in an increase in overall OEE from 57% to 68% and the effectiveness of the manufacturing system. The Methodology can be perfectly portrayed as shown in figure 3.

RESULTS & DISCUSSION

The estimation of the current OEE of Al-Hafiz Crystoplast (Pvt) Ltd (AHCP) manufacturing industry revealed that it is currently operating at 57%. The correlation of the results showed that significant improvement was necessary to achieve a world-class system. As a result, various countermeasures were carried out to improve the availability of machines, upgrade performance, and enhance the quality of production. These efforts resulted in an increase in the OEE of the manufacturing unit to 66.68%. Consistent improvement and workers' training were scheduled and executed to obtain the necessary results. These efforts resulted in a significant improvement in the OEE of the manufacturing unit, bringing it closer to the world-class standard. The implementation of these improvements will ensure that AHCP remains competitive in the market and can continue to provide high-quality products to its customers.

(a) Losses with countermeasures

Table 5. Losses with Countermeasures

| Losses | Previous observed | After Improvement | | | | Improvement |
|--------|-------------------|-------------------|---------------------|-----------|------|-------------|
| | | Planned down time | Management routines | Six sigma | 5S | |
| PM | 15.0 | 13.0 | 15.0 | 15.0 | 15.0 | 13.0 |
| WT | 18.0 | 15.0 | 18.0 | 18.0 | 18.4 | 15.0 |
| EF | 14.0 | 14.0 | 144.0 | 14.4 | 14.4 | 15.0 |
| TF | 35.0 | 35.0 | 35.0 | 35.1 | 35.1 | 35.1 |
| GB | 15.0 | 15.0 | 15.0 | 15.0 | 15.0 | 15.0 |
| UPM | 5.8 | 5.8 | 5.8 | 5.8 | 5.8 | 5.8 |
| CJ | 51.0 | 51.0 | 30.0 | 51.0 | 30.0 | 30.0 |
| CC | 29.0 | 29.0 | 10.0 | 28.5 | 10.0 | 10.0 |
| RR | 17.0 | 17.0 | 8.0 | 17.0 | 8.0 | 8.0 |
| EW | 18.0 | 18.0 | 7.0 | 17.5 | 7.0 | 7.0 |
| IPD | 23.0 | 23.0 | 23.0 | 23.0 | 22.9 | 22.9 |
| IPD | 55.0 | 55.0 | 55.0 | 27.6 | 27.6 | 27.6 |
| SC | 18.0 | 18.0 | 18.0 | 8.8 | 8.8 | 8.8 |

Losses that are considered in each scenario to be addressed with the aid of countermeasures are presented. The countermeasures are then assessed to determine the extent to which they reduce these losses.

(b) Improvement with countermeasure

Table 6. Improvements with Countermeasures

| | Previous | Planned Downtime | Management Routine | Six Sigma | 5S |
|----------------------|----------|------------------|--------------------|-----------|--------|
| OEE % | 57% | 61.95% | 63.60% | 62% | 66.68% |
| Total available time | 720 | 720 | 720 | 720 | 720 |
| prayer time | 60 | 60 | 60 | 60 | 60 |
| Schedule | 710 | 710 | 710 | 710 | 710 |
| Availability | 103.67 | 98.288 | 103.67 | 104 | 103.66 |
| actual production | 607.96 | 611.71 | 607.96 | 608 | 607.96 |
| Availability | 85.62 | 86.15 | 85.62 | 85.6 | 85.62 |
| Theoretic output | 607.96 | 611.71 | 607.96 | 608 | 607.96 |
| Performance | 109.66 | 109.66 | 55 | 110 | 55 |
| Actual output | 498.29 | 513.42 | 552.96 | 498 | 552.96 |
| packing(min) | 2 | 2 | 2 | 2 | 2 |
| Performance | 82.33 | 83.93 | 90.9 | 82.3 | 90.9 |
| Weight/ kg | 2 | 2 | 2 | 2 | 2 |
| Predicted Boxes | 249.14 | 256 | 249.14 | 256 | 276.48 |
| Weight/ kg | 498.04 | 512 | 498.04 | 498 | 572 |
| Wastage(kg) | 72.79 | 36.39 | 54 | 36.4 | 36.39 |
| Productive | 407.29 | 438.74 | 407.29 | 439 | 438.74 |
| Actual boxes | 203.65 | 219.36 | 203.65 | 219 | 246 |
| Boxes loss | 45.5 | 36.64 | 45.5 | 37 | 30.479 |
| Quality% | 81.737 | 85.68 | 81.74 | 85.7 | 85.68 |

The summary of improvements with countermeasures renders a comprehensive understanding of how OEE is calculated in the AHCP and the outcomes of implementing these countermeasures.

(c) Comparison of OEE of AHCP with World class system

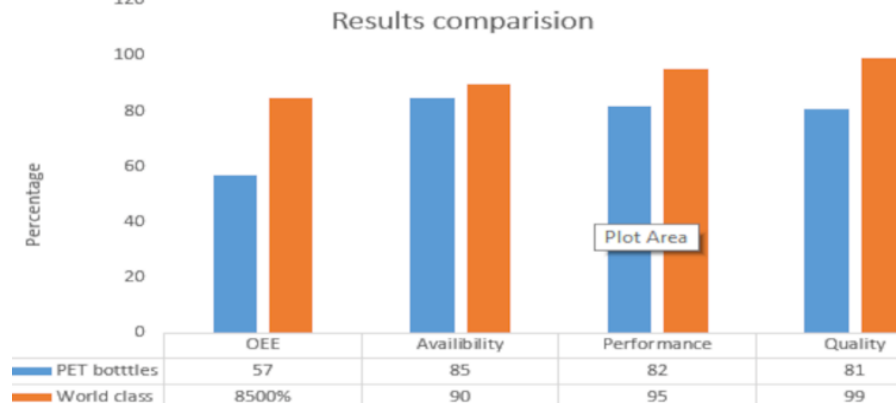


Figure 4. Comparison of OEE with World Class

Comparing the current OEE, availability, performance, and quality of the AHCP with a world-class system reveals notable differences. The analysis of the results indicates that significant improvements in ongoing OEE are required to attain the level of excellence associated with a widely recognized world-class system

(d) Comparison of OEE of (AHCP) PET bottles with World class system and with Countermeasures

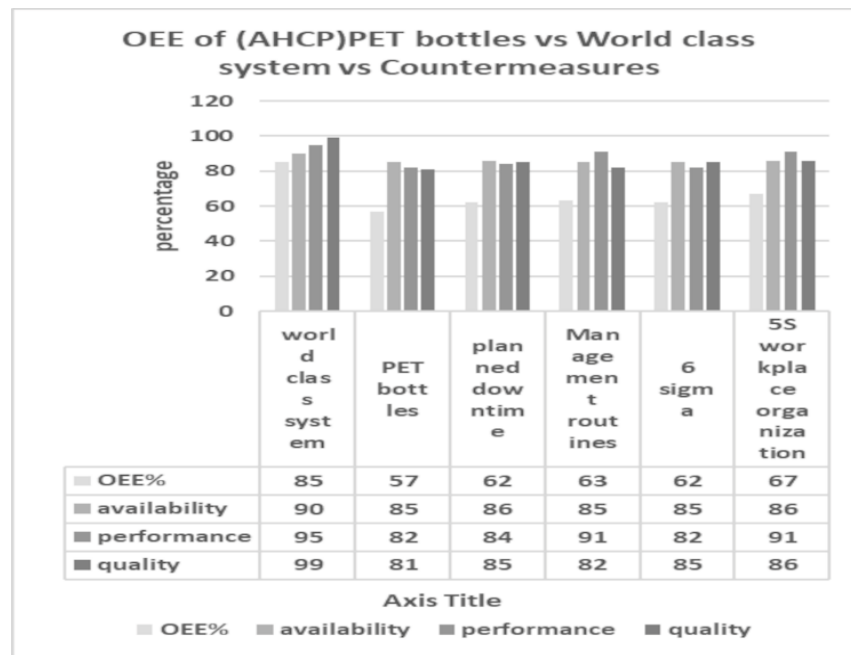


Figure 5. Comparison of OEE with Countermeasures and with World-class system

The application of countermeasures to enhance the current system is evaluated and benchmarked against global standards. This graph portrayed to compare the outcomes of these countermeasures with the existing state of the AHCP.



CONCLUSION

It is observed that the majority of industries and manufacturing units have an OEE of 60%; however, at Al-Hafiz Crystoplast (Pvt) Ltd (AHCP), it was only 57%. The implementation of countermeasures has proven to have a significant impact on the OEE. By applying these countermeasures, the OEE at AHCP increased to 66.68%, bringing it closer to the industry standard. By utilizing OEE as a tool, AHCP can continue to improve its manufacturing process and stay competitive in the market.

Overall, the utilization of OEE and the countermeasures outlined in this study will provide a roadmap for improving the manufacturing process, enhancing productivity, and increasing profitability. Hence, Al-Hafiz Crystoplast (Pvt) Ltd can remain competitive in the marketplace and continue to provide high-quality products to its customers.

ACKNOWLEDGEMENT

I would like to express my sincere gratitude for the invaluable support provided by UET Peshawar that made this research possible. The generous assistance was instrumental in the successful completion of this work.

REFERENCES

- [1] Neely A, Gregory M, and Platts K. (2020, Dec.). Performance measurement system design: A literature review and research agenda. *International Journal of Operations Production Management*. 25 (12), pp. 1228-1263.
- [2] Puvanasvaran A. P, Mei C. Z, and Alagendran V. A. (2013). OEEM Improvement Using Time Study in an Aerospace Industry. *International Tribology Conference Malaysia*. [Online]. 68, pp. 271-277. Available: <http://www.sciencedirect.com/science/article/pii/S187770581302033X>
- [3] Shaikh A, S., et al. (2017), Implementation of 5S in an industrial inventory store. Lista A.D. International Corporation. (2017). Implementing 5S Workplace Organization Methodology Programs in Manufacturing Facilities. [Online]. Available: <http://www.epa.gov/lean/thinking/fives.htm>
- [4] David A.G. and Chris V. (2021). Overview: Overall Equipment Effectiveness. Overview: Overall Equipment Effectiveness (OEE). IQity Solutions. [Online]. Available: <http://www.iqitysolutions.com>
- [5] Amir Azizi. (2015, Feb.). Evaluation improvement of production productivity performance using Statistical Process Control, OEE and Autonomous Maintenance. *International Materials, Industrial and Manufacturing Engineering Conference*. 2, pp. 186-190
- [6] Gomes C. F., Yasin M. M. In addition, Lisboa J. V. (2004. Sept.). A literature review of manufacturing performance measures and measurement in an organizational context: a framework and direction for future research. *Journal of Manufacturing Technology Management*. 15(6), pp. 511-530.
- [7] Joel C. G. (2004). Six Sigma Systems Principles Module 2.1. MIT Engineering Systems Learning Center.
- [8] Chandrajit Ahire P. and Anand Relkar S. (2012). Correlating Failure Mode Effective Analysis (FMEA) and Overall Equipment Effectiveness (OEE). *International Conference on Modeling*



ICSET-23

*Proceedings of the 5th International Conference on Sustainable
Energy Technologies (ICSET 2023) Peshawar, Pakistan
14-15 December 2023*



UET Peshawar

- Optimization and Computing. [Online]. 38, pp. 3482-3486. Available: <http://www.sciencedirect.com/science/article/pii/S1877705812023156>
- [9] Hammer D.M. (2020). Process management and the future of six sigma's. IEEE Journal Engineering Management Review. 30(4), pp. 55-56.
- [10] Dale Bester field H., "Quality Control", Seventh Edition, pp. 1-3.
- [11] Daniel Sheu D. (2006). Overall Input Efficiency and Total Equipment Efficiency. IEEE Transactions on Semiconductor Manufacturing. 19, pp. 496-501.
- [12] De Carlo F., Tucci M. In addition, Borgia O. (2013). Bucket brigades to increase productivity in a luxury assembly line. International Journal of Engineering and Business Management. 5, pp. 59-68.
- [13] Filippo De Carol, Maria Antonietta and Mario T. OEE evaluation of a paced assembly line: A case study in Pharmaceutical Environment. International Journal of Engineering and Business Management, Special Issue: Innovations in Pharmaceutical Industry.
- [14] Inductive Automation. How to reduce downtime and raise OEE [Online] pp. 1-15 Available: <https://inductiveautomation.com>
- [15] Inductive Automation. How to reduce downtime and raise OEE[Online] pp. 2 Available: <https://inductiveautomation.com>
- [16] Iron Mountain White Paper. The business case for disaster recovery planning: Calculating the cost of downtime. [Online]. pp. 7-10. Available: www.ironmountain.com
- [17] Kevin L., Zaheer S. R. G., Srilata C. (2003). Six Sigma: A goal-theoretic perspective. Journal of Operations Management. 21(2), pp. 193-203.
- [18] Parast M. M., (2011). Effect of six sigma projects on innovation and firm performance. International Journal of Project Management. 29(1), pp. 45-55.
- [19] Raisinghani M. S., Ette H. In addition, Pierce R. (2005). Six Sigma: Concepts, tools and applications. Journal Industrial Management and Data Systems. 105(4), pp. 491-505.
- [20] Raisinghani M. S., Ette H., Pierce R., Cannon G. In addition, Prathima D. Six Sigma: Concept, tools and application. [Online]. pp. 491-504. Available: www.emeraldinsight.com/
- [21] Tabikh M., "Downtime cost reduction analysis: Survey results," M.S thesis, Innovative Production, IDT KPP231.
- [22] Anantharaman N. In addition, Nachiappan R. M. (2006). Evaluation of OLE in a continuous product line manufacturing system. Journal of Manufacturing Technology Management. 17(7), pp. 987-1008.
- [23] Production Automation Corporation. 5S/Visual Workplace Handbook: Building the foundation for continuous improvement. [Online]. Available: www.bradyid.com/visualworkplace.
- [24] Productivity Dev. Team. (1999, July). OEE for operators: Overall Equipment Effectiveness. Productivity Press. pp. 4-7.
- [25] Ziemerink R. A. and Bodenstein C. P. (1998, July) Utilizing a LonWorks control network for factory communication to improve Overall Equipment Effectiveness. IEEE International Symposium on Industrial Electronics. 2, pp. 684-689.
- [26] Schroeder R. G., Linderman K. In addition, Liedtkeet C. (2008). Six Sigma: Definition and underlying theory. Journal of Operations Management. 26(4), pp. 536- 554.
- [27] Hansen R. (2001). Overall Equipment Effectiveness (OEE): A powerful production and maintenance tool. Industrial Press
- [28] Report by Bloomberg. (2012, Nov.). [Online]. Available: <http://tribune.com.pk/story/615853/fmcgs-biscuit-industry-shows-impressive-figures/>



ICSET-23

*Proceedings of the 5th International Conference on Sustainable
Energy Technologies (ICSET 2023) Peshawar, Pakistan
14-15 December 2023*



UET Peshawar

- [29] Robert C. Hansen. (2001, Dec.). Overall Equipment Effectiveness. Industrial Press. pp. 1-20.
- [30] Subramaniam S. K., Husin S. H., Yusop Y. and Hamidon A. H. Machine efficiency and manpower utilization on the production line. WSEAS International Conference on Electronics, Hardware, Wireless and Optical Communication. pp. 70-75.
- [31] Nakajima S. (1988). Introduction to TPM: Total Productive Management. Productivity Press Portland. OR.
- [32] Nakajima S. (1989). Introduction to Total Productive Maintenance. Productivity Press.
- [33] Tangen S. (2005, Jan.). Demystifying productivity and performance. International Journal of Production Performance Management. 54(1), pp. 34- 46.
- [34] Sowmya, K. and Chetan N., (2016) a review on effective utilization of resources using overall equipment effectiveness by reducing six big losses. International Journal of Scientific Research in Science, Engineering and Technology. 2(1): p. 2394-4099
- [35] Tom Pherson. (2006, June). Overall Equipment Effectiveness and Real Time Visual Management Critical Lean Tools. Intelligent Manufacturing Solutions. pp. 1-18.
- [36] Vamshi K. Katukoori. "Standardizing Availability Definition", pp. 4. Vamshi K. Katukoori. "Standardizing Availability Definition", pp. 5-12.



Paper ID: ICSET-2344

TECHNO-ECONOMIC ANALYSIS OF LARGE-SCALE SOLAR POWER PLANT IN PESHAWAR

Raheel Ahmad*, Arif Khattak

US-Pakistan Center for Advanced Studies in Energy, University of Engineering and Technology Peshawar, Pakistan

**Corresponding author*

Email: raheelahmad.uspcase@uetpeshawar.edu.pk

ABSTRACT

In this paper, a detailed analysis of large-scale solar PV power plant of 1 MW is studied. Peshawar being a warm region has a great potential of generating energy using solar power. A pre-selected area Hayatabad phase 6 is brought under study, for A solar power plant installation is being considered.

Moreover, according to the topographic and geographic location of Peshawar, use of solar power, as a main power source for vast vacant area is discussed. Simulations, results, and output graphs are also discussed based on various factors. 10 plots each of 5446 ft² is considered, on each plot 184 panels (of 545W each) will be installed, giving total production of 1 MW and inverter of 110 kW is selected. A detailed cost analysis based on the selection of PV Modules and inverter cost of Rs 128.160 Million, site selection, labor cost of Rs 2.4 Million, cost of H-Beam is Rs 27.6 Million and maintenance and operation cost of Rs 3 Million for the use of solar power plant / panels is also discussed.

Some of the possible problems and their solutions is also discussed while considering different cases.

KEYWORDS: PV Modules; Inverter; PV Arrays.

INTRODUCTION

A lot of research has been carried out in this new trending area, European countries and eastern countries like Iran has also designed a power plant [1] of 5 MW for fifty cities, using RET screen software and effort was done to obtain the mean capacity factor of 22.27%. Now a have built many large solar PV modules and a lot of work has been done on their design and upgradation and modification of the design of the batteries too. Efficient optimization and quick evaluation through along with a thorough study, a computer programme was also created for a 35-kW hybrid PV-diesel power plant project. and study of all topographical features and a subjective analysis of the battery in southern Algeria [2]. Another fruitful investigation was carried out to examine the possibility of solar power plants in the Gulf Corporation Council (GCC) nations [5] and research showed that existing lower tariff was a cost-effective option highly costly PV system. One of the huge solar power plants of 12 MW in the kingdom of Bahrain [6] was erected at two buildings' windows and roofs giving a revenue generation of 4,800,000£ per annum. Similar research of a solar power plant of 1 MW in Serbia [7] was conducted and it was concluded that CdTe solar modules generated higher amount of electricity. Likewise, in one of the recent studies the solar PV electricity was the most effective way to satisfy future energy demands [8] in the six main Indian cities up to the year 2025. Most of the other recent researches also [9, 10]. Thus to address upcoming difficulties with energy security and environmental sustainability, the development of solar energy should be taken into consideration.



Peshawar has pledged to enhance the proportion of renewable energy in this area by reintroducing PV modules.

Many researches and papers have been published worldwide. It may be determined that the manufacturing and installation of large solar power plants is the best technically possible solution to supply the electricity demand in the present and in the future after analyzing the effectiveness and technical viability of Solar PV power plants. The worldwide solar power industry had increased at a rate of 30% per year from 1996 to 2001, hence increasing the electricity production over four times. [11]

MATERIALS AND METHODS

As we are working in region of Peshawar which is hot area and sun shines at its high. So, the best renewable source we have is Solar Energy. Most of research is going on solar energy and Photovoltaic cells to increase their efficiency.

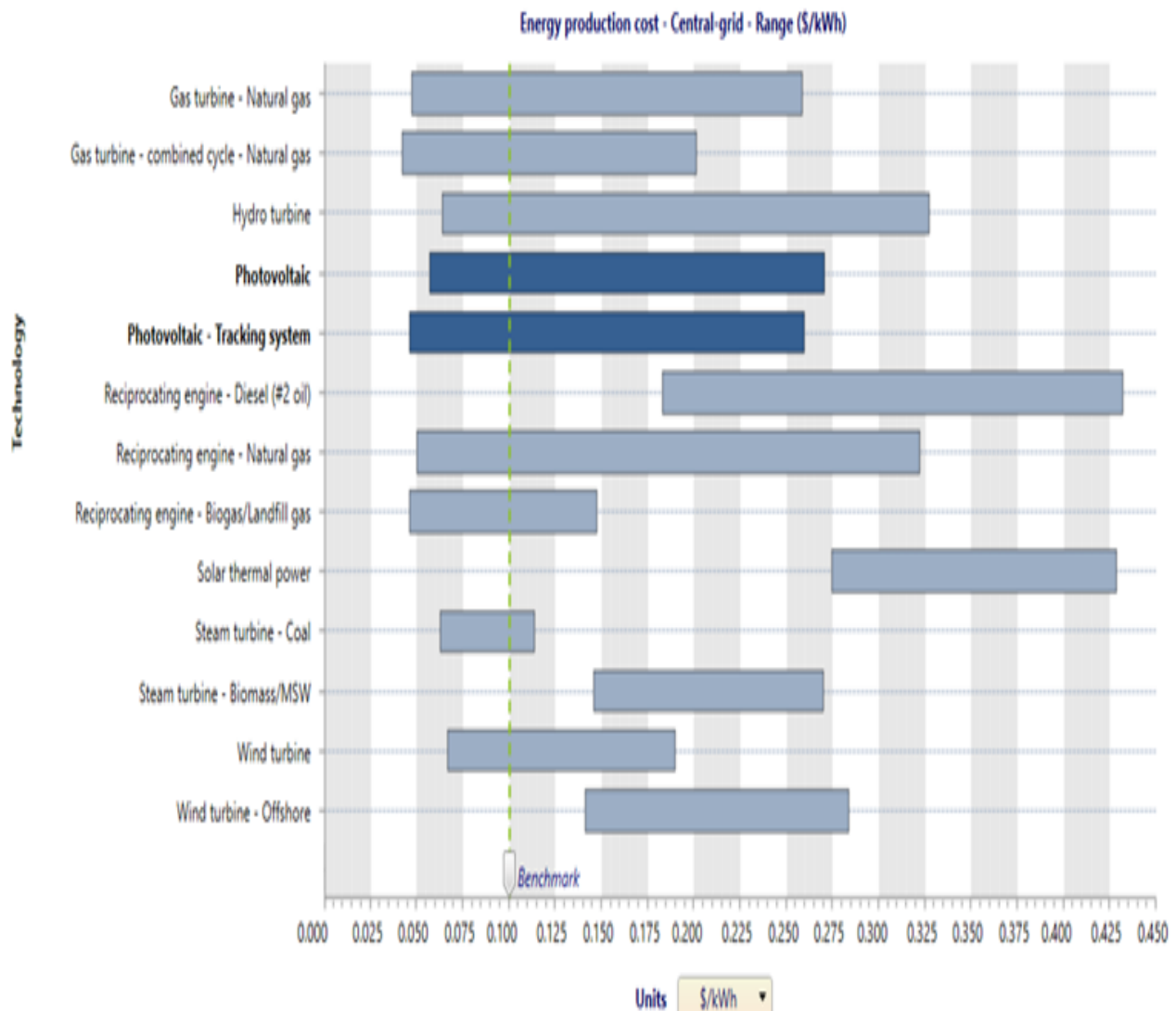


Figure 1: Comparison of different technologies used to produce Electrical energy



As its clear from Figure 1 that by comparing different types of technologies / ways for the production of electrical energy in area like Peshawar, having unique topographical features, Photovoltaic Technology is the most suitable and economical and is the best option to be considered. The amount of solar energy reaching the surface of the planet is so great that in one year it is roughly twice as much as will ever be obtained from all of the non-renewable resources of coal, oil, natural gas, and mined uranium combined. The Earth receives 174 peta watts (PW) (1015 watts) of incoming solar radiation at the upper atmosphere.

Table 1: Geographical Parameters of Hayatabad Phase 6, Peshawar

| | Unit | Climate data Location | Facility Location |
|------------------------------------|------|-----------------------|-------------------|
| Latitude | | 34.0 | 34.0 |
| Longitude | | 71.4 | 71.5 |
| Climate Zone | | 28-Hot- Dry | |
| Elevation | m | 0 | 345 |
| Heating design temperature | °C | 4.8 | - |
| Cooling design temperature | °C | 41.4 | - |
| Earth Temperature amplitude | °C | 27.4 | - |

Figure 2: Topographical features of the selected Area in Peshawar

| Month | Air temperature °C | Relative humidity % | Precipitation mm | Daily solar radiation - horizontal kWh/m ² /d | Atmospheric pressure kPa | Wind speed m/s | Earth temperature °C | Heating degree-days 18 °C °C-d | Cooling degree-days 10 °C °C-d |
|---------------|-----------------------|------------------------|---------------------|---|--------------------------------|-------------------|-------------------------|---|---|
| January | 11.2 | 43.6% | 26.04 | 3.08 | 97.6 | 1.7 | 7.4 | 211 | 37 |
| February | 12.9 | 48.3% | 63.84 | 4.03 | 97.4 | 1.9 | 9.9 | 143 | 81 |
| March | 17.4 | 46.7% | 66.65 | 4.99 | 97.1 | 1.9 | 15.8 | 19 | 229 |
| April | 23.2 | 40.0% | 48.60 | 6.11 | 96.7 | 2.0 | 22.4 | 0 | 396 |
| May | 28.6 | 26.1% | 23.56 | 7.15 | 96.3 | 2.2 | 29.9 | 0 | 577 |
| June | 33.1 | 21.8% | 21.60 | 7.24 | 95.7 | 2.2 | 35.5 | 0 | 693 |
| July | 32.3 | 37.5% | 57.04 | 6.55 | 95.7 | 2.4 | 35.5 | 0 | 691 |
| August | 30.7 | 46.3% | 62.00 | 5.98 | 95.9 | 2.2 | 32.9 | 0 | 642 |
| September | 28.9 | 37.8% | 29.40 | 5.43 | 96.4 | 1.8 | 28.9 | 0 | 567 |
| October | 23.7 | 28.4% | 20.77 | 4.55 | 97.0 | 1.7 | 21.6 | 0 | 425 |
| November | 17.6 | 28.8% | 15.90 | 3.73 | 97.4 | 1.7 | 14.5 | 12 | 228 |
| December | 12.5 | 37.1% | 22.32 | 3.02 | 97.6 | 1.7 | 9.1 | 171 | 78 |
| Annual | 22.7 | 36.8% | 457.72 | 5.16 | 96.7 | 1.9 | 22.0 | 555 | 4,644 |

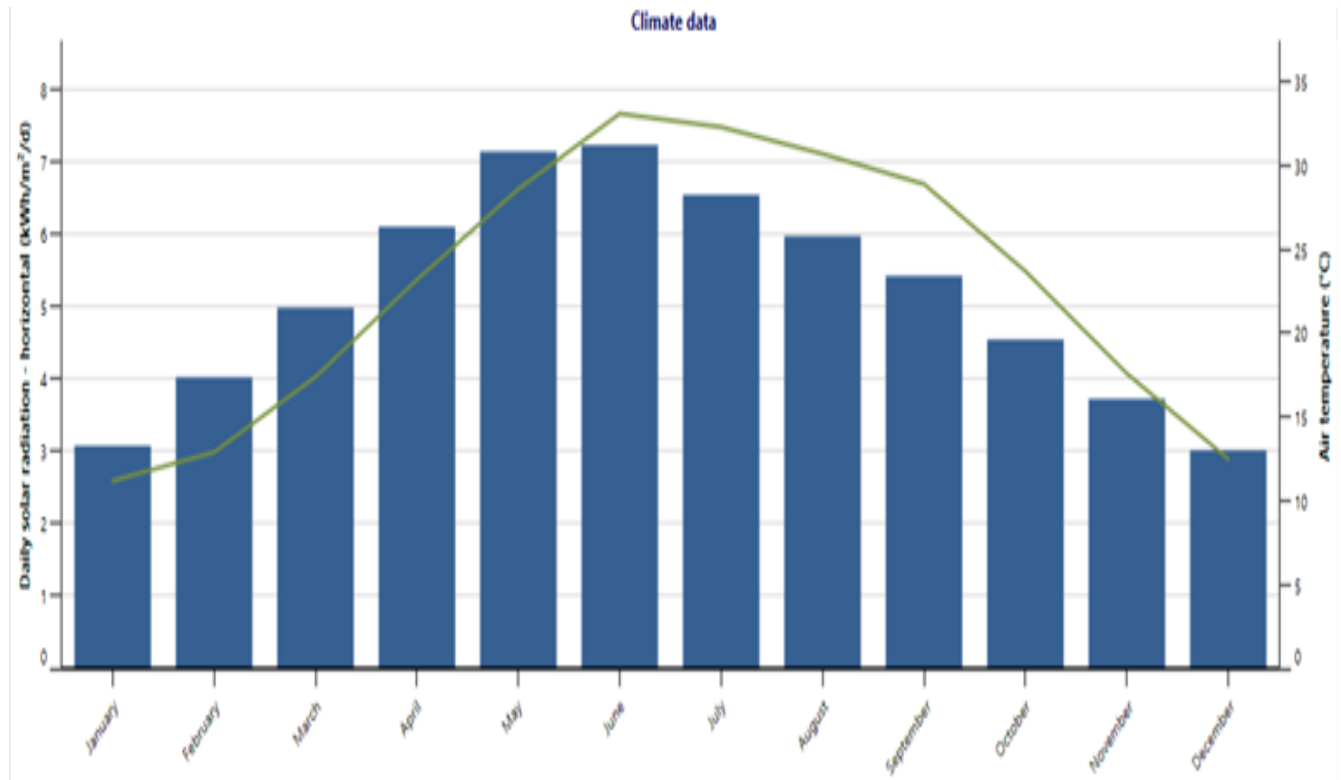


Figure 3: Daily Horizontal Solar Radiation

LONGI 545 watts PV Panels is my consideration for my research. Calculating required area is also required to analyse our placement cost as well. One LONGI 545 watts PV Panel is (7.4 ft x 3.8 ft). I need 1840 LONGI 545 watts PV Panels, so my required dimension becomes (51740.8 ft²). All the specifications of 545W LONGI Panel are described in Table 2, the data for which is collected from the data sheet of the panel available in market. [9]

Table 2: Data Sheet (Electrical Characteristic) of LONGI 545W Panel

| Testing Condition | STC | NOCT |
|--|-------|-------|
| Maximum Power (Pmax/W) | 545 | 407.0 |
| Open Circuit Voltage (Voc/V) | 49.65 | 46.55 |
| Short Circuit Current (Isc/A) | 13.92 | 11.25 |
| Voltage at Maximum Power (Vmp/V) | 41.80 | 38.92 |
| Current at Maximum Power (Imp/A) | 13.04 | 10.46 |
| Module Efficiency | 21.3 | |
| STC (Standard Testing Condition): Irradiance 1000W/m ² , Cell Temperature 25°C, Spectra at AM 1.5 | | |
| NOCT (Nominal Operating Cell Temperature): Irradiance 800 W/m ² , Ambient Temperature 20°C, Spectra at AM1.5, Wind at 1 m/s | | |

PV Panels Output

PV panels output depends upon light intensity and light intensity is directly proportional to Temperature of given area. As weather averages discussed below, output of 545W PV panel for one day is given in Figure 4 and annually is given below in form of graph illustrated in Figure 5, the mentioned topographical data of the region is taken from the online data available. [15]

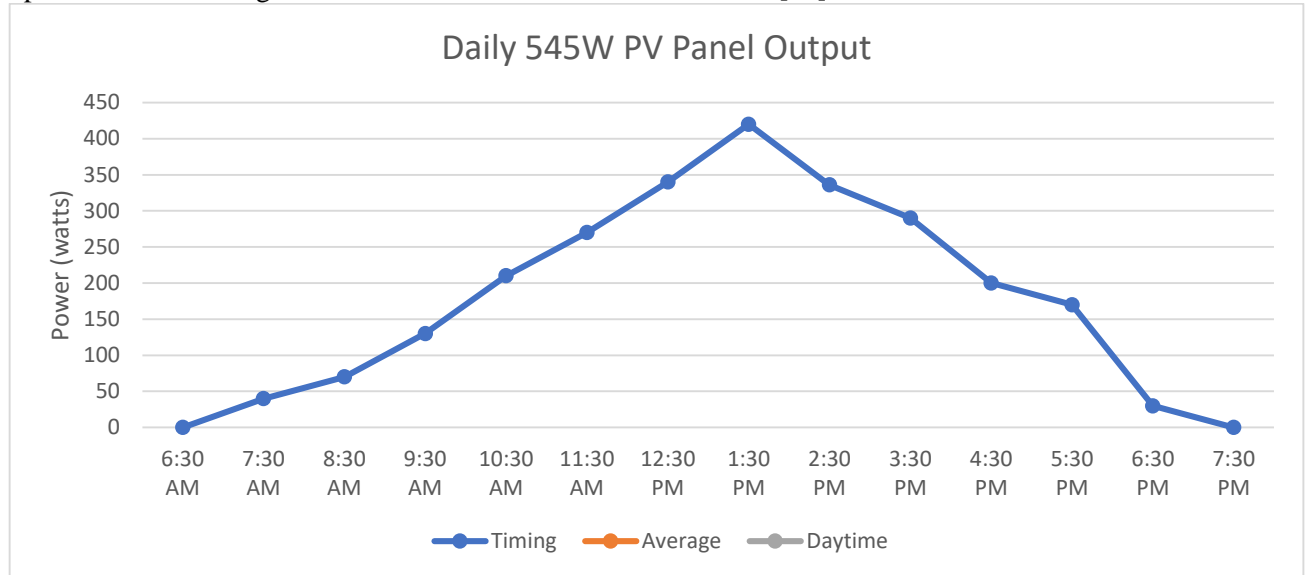


Figure 4: Output Power vs Time Graph of a Single PV Panel

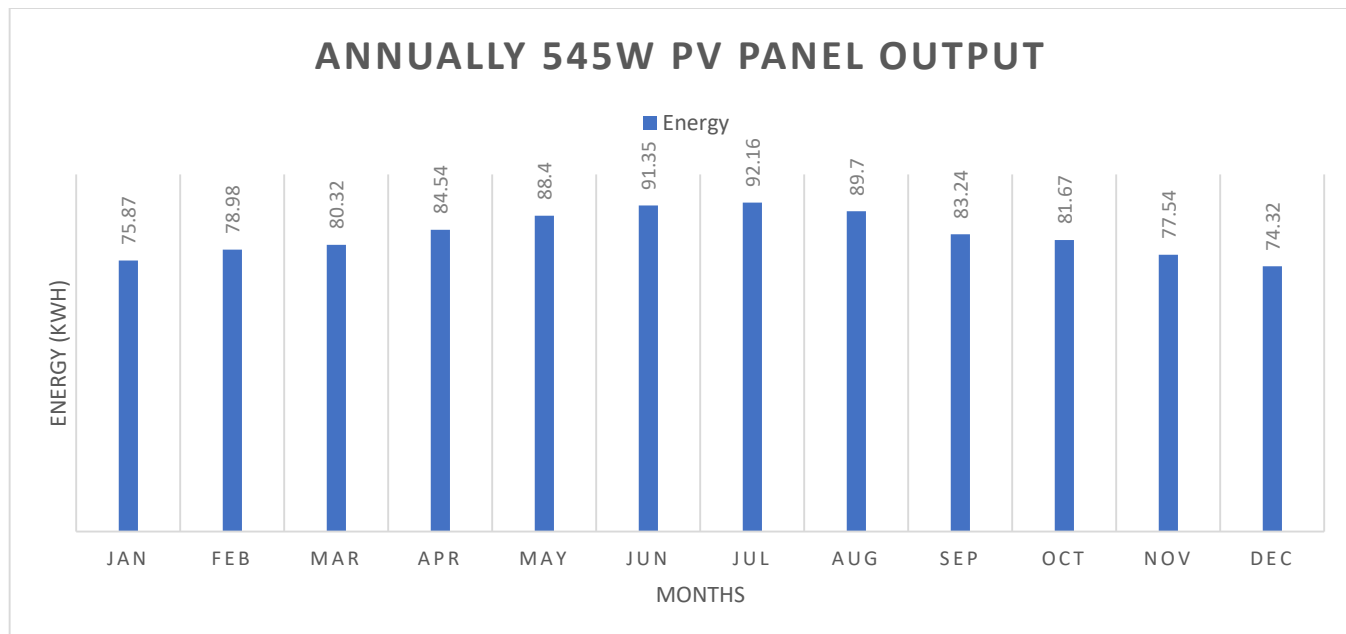


Figure 5: Average Monthly Output of a Single PV Panel



Electrical power ranges from 50W to 500W in a single PV panel. So, their price increases with their quality and power efficiency. Market survey from different areas across Khyber Pakhtunkhwa and Pakistan is given below in Table 3.

Table 3: Cost Comparison of different types of Solar Panels

| Type | Watts | Price (PKR) |
|---|-------|-------------|
| Canadian Mono Panel | 400 | 55200 |
| Jinko Mono Solar Panel | 535 | 57220 |
| Jinko Mono Crystalline Solar Panel | 545 | 58290 |
| MaxPower Half Cut Poly-Perc Solar Panel | 340 | 36360 |
| MaxPower Half Cut Mono-Perc Solar Panel | 400 | 42780 |
| SunMaxx Mono Solar panel | 170 | 18180 |
| Trina half Cut Mono Perc Solar panel | 450 | 48130 |
| Trina half Cut Mono Perc Solar panel | 540 | 57750 |
| LONGI Mono PERC | 545 | 57750 |
| Canadian Mono Perc Solar panel | 445 | 47600 |
| Max Power Poly Solar Panel | 330 | 35290 |

From the table above, it is too much clear that mono-crystalline PV panels are much efficient than the rest ones. So, i must prefer mono-crystalline PV panel for our research analysis. I will be preferring LONGI Mono PERC panels of 545 W for this research.

PWM is old technology, mostly used in industrial load while MPPT is new technology and is best for PV charge controlling. For the power coming from PV panels, we need PV charge controller and batteries of same capacity as combined cars have (2000 kWh). PV charge controller of 5940 A (287.11 kW & 48 V) is not available in the market. Maximum availability is 100 Amps PV charge controllers. Which means that one PV charge controller can withstand 11 PV panels of 435 watts (48 V & 9 Amps). So, we need 60 PV charge controllers (MPPT) of 100 Amps each to cover 660 PV panels of 435 watts (48 V & 9 Amps). Cost of one MPPT charge controller is PKR 4700/-, so cost of 60 MPPT charge controllers is Rs 282,000.

From the concern selected Hayatabad Phase 6 area, i have pre-selected data of the specific area. After analysing data, i have extracted and deduced some of the important results and the data in the form of load of concerned geographical region which is given below:

- Selected Load is 1 MW.
- To be divided among the land areas available in the form of pre-built houses and rooftops would be utilized to produce some kW.
- Total kW to be calculated by the summation of all available

Table 4: Comparison of Solar Radiation Vs Electricity Export per Each Month

| Month | Daily Solar radiation. Horizontal (kWh/m ² /d) | Daily Solar radiation. Tilted (kWh/m ² /d) | Electricity export rate (\$/kWh) | Electricity exported to grid (MWh) |
|-----------|---|---|----------------------------------|------------------------------------|
| January | 3.08 | 1.35 | 0.10 | 3.901 |
| February | 4.03 | 2.22 | 0.10 | 5.697 |
| March | 4.99 | 3.52 | 0.10 | 9.787 |
| April | 6.11 | 4.98 | 0.10 | 13.054 |
| May | 7.15 | 6.42 | 0.10 | 16.941 |
| June | 7.24 | 6.74 | 0.10 | 16.912 |
| July | 6.55 | 6.02 | 0.10 | 15.732 |
| August | 5.98 | 5.15 | 0.10 | 13.564 |
| September | 5.43 | 4.08 | 0.10 | 10.421 |
| October | 4.55 | 2.75 | 0.10 | 7.429 |
| November | 3.73 | 1.57 | 0.10 | 4.212 |
| December | 3.02 | 1.15 | 0.10 | 3.287 |
| Annual | 5.16 | 3.84 | 0.10 | 120.937 |

Total No. of panels = No. of panels for one plot × No. of plots (of 20 Marlas)
 $= 184 \times 10$
 $= 1840$

our maximum load is not more than 100kW for each individual plot, we need 10 inverters to cover that required maximum load.

Price of one inverter = 2190000 PKR
 so price for 10 inverters = 21900000 PKR

I have selected a string consisting of 46 panels in each string. Each panel in the string is of 545 W, 24V. Total there are 4 strings connected, each of 46 panels in series with each other. The four strings are connected parallel with each other.

Area occupied by 1 Marla plot (Full rooftop available) = 272.3 ft²

Dimensions of 1 panel = 7.4 ft × 3.8 ft = 28.12 ft²

Area required for 1 panel (545 W) = 28.12 ft²

Area required for 1 W = $\frac{28.12 \text{ ft}^2}{545 \text{ W}}$

Now, Total Area required for 1 MW = $\frac{28.12 \text{ ft}^2}{545 \text{ W}} \times 1000000$
 $= 51596.3 \text{ ft}^2$

51596.3 ft² = 189.5 Marlas ≈ 190 Marlas

But as we know that there must be 1 inch gap in between two panels and same 1 inch gap between the two arrays (vertically also)

This makes area required for panel as:

Area for 1 panel = 7.5ft × 3.9ft = 29.25 ft²

So, 545 W panel = 29.25 ft²



ICSET-23

*Proceedings of the 5th International Conference on Sustainable
Energy Technologies (ICSET 2023) Peshawar, Pakistan
14-15 December 2023*



UET Peshawar

$$\begin{aligned}\text{Area required for 1 MW system} &= \frac{29.25 \text{ ft}^2}{545 \text{ W}} \times 1000000 \\ &= 53670 \text{ ft}^2\end{aligned}$$

Requirement of land for 1 MW system = 197.14 Marlas \approx 198 marlas

Available Area

In my research, the available area is in the form of available plots in the Hayatabad phase 6, and all the roof tops area easily available for the installation of each and everything of the solar PV system like arrays, wiring, inverter etc.

I divided the 1 MW system into 10 equal parts.

Each part is

Area of 1 Marla Land = 272.3 ft²

Area of 20 Marlas land = 5446 ft²

$$\begin{aligned}\text{No. of 545 W panels to be installed at land of 20 Marla Plot} &= \frac{5446 \text{ ft}^2}{272.3 \text{ ft}^2} \\ &= 193 \text{ Panels}\end{aligned}$$

I take No. of panels = 184

Which gives total production = 100.3 kW

$$\begin{aligned}\text{Total No. of panels} &= \text{No. of panels for one plot} \times \text{No. of plots (of 20 Marlas)} \\ &= 184 \times 10 \\ &= 1840\end{aligned}$$

$$\begin{aligned}\text{Land required for 184 panels} &= \text{area of one panel} \times \text{total no. of panels} \\ &= 28.12 \text{ ft}^2 \times 184 \\ &= 5174.08 \text{ ft}^2\end{aligned}$$

$$\begin{aligned}\text{Spare area in each plot} &= 5446 \text{ ft}^2 - 5174.08 \text{ ft}^2 \\ &= 271.92 \text{ ft}^2 \\ &\approx 1 \text{ marla}\end{aligned}$$

This area is left for cabling, inverter placement and stands placement etc.

RESULT AND DISCUSSION

Cost of 1 PV Panel (LONGI 545W) = Rs 57750

Total No. of PV panels required for 1MW PV System = 1840

$$\begin{aligned}\text{Total cost of PV 1840 panels} &= 1840 \times \text{Rs } 57750 \\ &= \text{Rs } 106,260,000 = \text{Rs } 106.26 \text{ M}\end{aligned}$$

Cost of 1 Inverter of 100kW (Huawei) = Rs 2190000

Total Number of inverters needed for 1MW PV system = 10

$$\begin{aligned}\text{Total cost of 10 inverters} &= \text{Rs } 2190000 \times 10 \\ &= \text{Rs } 21,900,000 = \text{Rs } 21.9 \text{ M}\end{aligned}$$

$$\begin{aligned}\text{Now, Total Cost of Inverter + PV Modules} &= \text{Rs } 106,260,000 + \text{Rs } 21,900,000 \\ &= \text{Rs } 128,160,000\end{aligned}$$

Design Engineering and management cost

This includes the main physical structure cost including the Beam cost, designing and selection of the material from which the beam, that is the main supporting structure for the PV modules is made.



ICSET-23



UET Peshawar

Now for mounting structures H-Beam Girders are selected as they are potentially strong, structurally really feasible and potentially supportable. The Selected H-Beam structure is manufactured by the Mughal Girders, which is a local and easily available manufacturer in Pakistan / Peshawar, thus the availability of the Mounting structure becomes more easily available. These H-Beam Girders of Mughal Manufacturers have lifetime more than 25 years, which is also a potentially feasible advantage of these structures.

Nowadays, According to Market survey,

The cost of H-Beam Girders per panel = Rs 15000

Total No. of panels needed = 1840

Total cost of the H-Beam for full 1MW PV system = $1840 \times \text{Rs } 15000$
= Rs 27,600,000

Installation / labor cost

The installation cost includes the cost of DC cables / wires required for the full connection of the system. The DC circuit breakers and other safety equipment also including all type of installation accessories.

Installation labor costs = Rs. 200 per man-hour,

with a man-hour requirement of 12 hours for each kW of PV power

The total labor costs for installing a 1 MW PV power plant = PKR 2,400,000.

Maintenance and Operation Cost

Fixed Operation and Maintenance cost = 2,000,000 PKR

Variable Operation and Maintenance cost = 1,000,000 PKR

Financial Analysis

Financial Cost analysis includes the total cost of the panels installed, structural support expenses, wiring costs, inverter costs, transport and luggage cost and all minor expenditures, that are necessary for the building and setting up of the desired structure. The current cost analysis mentioned is in accordance with the current market rates, as per prices fluctuation, all types of expenditures may vary.

Table 5: Module Cost Analysis

| Parameter | Cost |
|--------------------|---------------|
| Module Cost | 106260000 PKR |
| Supports Cost | 27600000 PKR |
| Inverter | 21900000 PKR |
| Wiring | 10000000 PKR |
| Transport/Mounting | 5000000 PKR |
| Total Investment | 170760000 PKR |

CONCLUSION

A thorough analysis of the technical and economic viability of a sizable solar photovoltaic power plant with a 1 MW capacity has been conducted in a KPK region Peshawar. The overall system is divided into 10 parts, each as a production unit of 100 kW independently and giving a total generation of 1000kW (1MW). Each 100kW solar PV system is installed on a 20 Marla Area. For this huge power generation mega power plant with 46 modules in each row, a total of 18,400 solar PV modules are required. A total of 200 Marlas (1.25 acres) of land is needed to accommodate ten Huawei inverters, each of which has a 100kW capacity.

The string design, area calculations, installation and labor cost, operation and maintenance cost, design engineering and management cost, inverter sizing and selection, PV module selection and calculations, inclination and orientation of PV modules and a detailed topographical and geographical features and contents of the selected region are studied.

Financial and economic performance indicators are also evaluated and calculated. So this type of huge solar power plant will add significant amount of energy to the area like Peshawar and its most optimum to install it due to the area's most suitable geographical and topographical features.

ACKNOWLEDGEMENTS

I would like to thank my research supervisor, Dr. Arif Khattak, for helping to guide me through my research and for his support.

He never merely put up with me; no matter what the issue, he was always able to provide me with wise counsel. He helped me a lot and provide me guidance and shared his experience in a fruitful way. I would also thank my friends, who helped me a lot in collecting the relevant data and carrying out literature review.

REFERENCES

- [1] S. M. P. R. V. G. D. Y. & S. E. Besarati, "The potential of harnessing solar radiation in Iran: Generating solar maps and viability study of PV power plants," *Renewable energy*, , vol. 53, pp. 193-199., 2013.
- [2] A. T. A. B. M. & A. A. H. Khelif, "Feasibility study of hybrid Diesel-PV power plants in the southern of Algeria: Case study on AFRA power plant.," *International Journal of Electrical Power & Energy Systems*,, vol. 43(1), pp. 546-553, 2012.
- [3] R. H., "On the value of decentralized PV systems for the GCC residential sector," *Energy Policy*, vol. 39, pp. 2020-7, 2011.
- [4] F. Alnaser NW, "Potential of making—over to sustainable buildings in the Kingdom of Bahrain.," *Energy Build*, vol. 40, pp. 1304 - 23, 2008.



ICSET-23

*Proceedings of the 5th International Conference on Sustainable
Energy Technologies (ICSET 2023) Peshawar, Pakistan
14-15 December 2023*



UET Peshawar

- [5] M. D. A. M. Pavlovic T, “Possibility of electricity generation using PV solar plants in Serbia.,” *Renew Sustain energy*, vol. 20, pp. 201-18, 2013.
- [6] S. R. A. Mekhilef S, “A review on solar energy use in industries,” *Renew sustain Energy*, vol. 15, pp. 1777-90, Rev 2011.
- [7] G. S., “Scope for solar energy utilization in the Indian textile industry,” *Sol Energy*, vol. 42, pp. 311-8, 1989.
- [8] G. MA., “Recent developments in photovoltaics,” *Solar Energy*, Vols. 76(1-3), pp. 3-8, 2004.
- [9] [Online]. Available: <http://www.energiasolarphb.com>.
- [10] D. P. J. & K. P. Moya, “Technical, financial, economic and environmental pre-feasibility study of geothermal power plants by RETScreen–Ecuador's case study.,” *Renewable and Sustainable Energy Reviews*, vol. 92, pp. 628-637, 2018.
- [11] M. El-Shimy, “Viability analysis of PV power plants in Egypt.,” *Renewable energy*, vol. 34(10), pp. 2187-2196, 2009.
- [12] A. M. S. Muneer T, “Sustainable production of solar electricity with particular reference to the Indian economy,” *Renew suatain energy Rev*, vol. 9, pp. 444-73, 2005.
- [13] T. G. Nawaz I, “Embodied energy analysis of photovoltaic (PV) system 569,” *Energy Policy*, vol. 34(17), pp. 3144-52, 2006.
- [14] “European photovoltaic industry association and green peace.,” *Solar generation*, 2008.
- [15] [Online]. Available: <http://www.accuweather.com>.

Paper ID: ICSET-2345

Implementation/Impact of Solar Energy System on a Power Grid System

Sanam Ijaz^{1,*}, Dr. Amjad Ullah², Rehmat Hadi³

¹Electrical Engineering, UET Peshawar, Peshawar 25120, Pakistan

²Electrical Engineering, UET Peshawar, Peshawar 25120, Pakistan

³Renewable Energy Engineering, UET Peshawar, Peshawar 25120, Pakistan

**Corresponding author*

Email: sanam.ijaz23@gmail.com

ABSTRACT

In Pakistan, the demand for energy is increasing quickly due to urbanization and industrialization. In order to prevent the climate change consequences of greenhouse gas emissions and reduce dependence on fossil fuels, clean, sustainable energy is becoming more and more important than conventional energy sources. This study is aimed to investigate the use of large-scale solar photovoltaic (SPV) integration in Power Grids in underdeveloped networks of a developing nation in order to meet the demand for power and reap the benefits of improved stability. The application of large-scale grid integrated solar photovoltaic SPV of weak power networks is examined in this research to improve the power, Voltage and frequency stability and possibilities of raising the level of large-scale SPV penetration into the power Grid system. The theoretical and mathematical model for the software simulation circuit was developed and simulated using Homer Pro and SIMULINK, with subsequent analysis of the results. The reserve power from SPV power plant is utilized to regulate the SPV micro grid power in case of any intermittencies. SPV Energy with conventional energy sources minimize active power imbalance in power Grids, enhancing the operation's security and reliability of the grid. Additionally, it reduces the operating cost of the system by allowing the traditional energy to operate at their lower limits and using less reserve for the active power balancing services. The results for centralized and dispersed SPV generation compared and achieved a better and sustainable power stability for the system at Large Scale Power Grid. Therefore, this work provides a baseline insight and results on the potential application of large-scale SPV integration in weak grids to address the power sustainability problems in the power system while utilizing the abundant solar resource as green energy that meets the increasing energy demand.

KEYWORDS: PV Energy, Power Grid System, Primary Control, Reactive Power Balance, Active Power Balance

INTRODUCTION

Both in industrialized and emerging nations, the proportion of renewable energy in total energy generation is rising quickly. Additionally, a lot of nations have lofty goals for changing their power industry to renewable sources. As a result, expenditures in and development of renewable energy conversion technologies have significantly increased globally. The two main renewable energy sources that can be used to produce huge amounts of grid-compatible electricity are wind and solar. Currently, there are 1,185



ICSET-23

*Proceedings of the 5th International Conference on Sustainable
Energy Technologies (ICSET 2023) Peshawar, Pakistan
14-15 December 2023*



UET Peshawar

gigawatts (GW) of installed PV capacity worldwide. In addition, the design and development of grid inter connected solar PV (SPV) systems are growing as utility-scale grid-connected SPV replaces the more traditional small-scale rooftop SPV. However, the lack of research on the benefits of improving voltage stability by integrating large amounts of SPV into fragile grids in developing nations has made the present study necessary. Access towards green, clean, consistent, and cheap energy required for basic human needs at household level, and for their economic productive uses to improve economic problems represent the minimum levels required to improve livelihoods in the emerging countries and to drive local economic development on a sustainable basis. The author in this paper emphasized that Green energy can improve livelihood and economic growth of poor countries [1]. Author elaborated that a lot livelihood is affected by no access to clean energy which is the challenge also facing in Pakistan. Where more than 25% of rural people do not have access to electricity and water [2]. The high reliance on conventional and centralized generation hastens the depletion of fossil fuel sources and environmental degradation, as well as increasing the potential for global warming, posing a threat to civilization [3]. The author in this paper relate Gadoon industrial area of Pakistan. Pakistan, being an emerging country, is beset by energy shortages. Distributed generation using locally accessible renewable energy resources is proven to be the most viable method for resolving the energy issue without sacrificing the environment [4]. As fuel prices in Pakistan is increasing daily the energy produce from fuel is costly. Renewable energy resources are used when conventional energy sources are depleted and oil prices rise [5]. Furthermore, the high reliance on conventional and centralized generation has the depleted the fossil fuel sources and causes environmental degradation, as well as increasing the potential for global warming, posing a threat to civilization [6]. The rising integration of renewable energy sources is impeding the reliable and secure operation of the power grid. When the Power grid is running in stand-alone mode, these problems get worse. In order to sustain an uninterrupted flow of electricity, a micro grid is composed of coordinated scattered energy sources, energy storage systems, and loads that are connected to the distribution level of the main power system network at a single point of connection known as the point of common coupling (PCC). The frequency of the micro grid, which is unstable due to the variability of renewable energy sources, is directly connected with its dependability and security [7]. In response to the rise in demand for Solar PV and Battery bank technologies applications, a detailed investigation is being done to select a suitable generator/Grid for a SPV and Battery provides a thorough comparison of synchronous and asynchronous generators for use in PV farms [8]. The fundamental benefit of asynchronous machines is that, because to their variable speed operation, they can maximize SPV power while minimizing fluctuations [9]. The advantages of battery energy storage for an isolated SPV system are covered in [10]. With increasing penetration levels of RES, micro grid instability problems occur and the load frequency control and automatic voltage regulation techniques are discussed and compared with other standalone designs and results of fully sustainable micro grids' performance are discussed in [11]. Technically speaking, incorporating renewable energy sources into the electric power grid is subject to substantial limitations. The two primary renewable energy sources, solar and batteries bank, are significantly impacted by the weather. These resources are highly unpredictable and fundamentally alter how power is generated. Intermittent availability (i.e., not always present; for example, solar generation is not present at night) and volatility are two crucial properties of renewable energy sources. Backup generation has previously been considered by system designers as a means of lowering generation variability to assist the efficient integration of renewable energy sources. Examples of quick-response backup generation systems that frequently offer a quick response to generation changes include hydro units, gas units, demand management, and energy storage systems. There is a risk that in these circumstances the backup generation installation's true value won't be realized because it is frequently used for the primary purpose of coordinating the renewable generating. It raises more concerns about the deployment's economic



sustainability because its cost will be added to the capital cost of the renewable energy resource, which is already high. The primary aspect is that according to these supplies' variable generation, they are unable to properly make up for a disruption in the utility grid's ability to produce electricity. In other words, if employed alone, these resources cannot provide generation reliability. A micro grid can be used to replace backup generation while preserving reliability. When these two factors are considered jointly, the following is true [12-15]. Power grids, which are operated, faces problems of the low power and voltage trapping due to imbalance in supply and demand. The principal problem in this scenario is power instability, and to control the power balancing, the Power grid has to be supplied with backup power from conventional generating units. This raises operating expenses and has a negative impact on the environment. To solve this issue, it is required to integrate the reserve power from the non-conventional generating units such as SPV power plant and the Hydrogen ion or any Battery bank. This will reduce the dependency on the conventional power plant units and increases reliability of the system operation. [16-19].

MODELING OF SPV MICRO GRID FOR THE POWER GRID

MATLAB SIMULINK is used to simulate the Power Grid problem. This design is intended for a large scale power Grid in which we incorporate solar and battery backup power to solve the power issue. The sources incorporated in the system consist of large scale Solar PV Farm, Battery Energy system power plant that operates as a base-load provider. These sources and their load ratings are detailed in Table 1. The renewable resources in this power grid are not always available, which can cause fluctuations in the power system's frequency when there is more demand for power than supply.

This research explores how to inject large scale solar PV and Battery bank Power as reserve power into the Power Grid system to serve as reserves for meeting increased active power or reactive power needs. Solar PV farm are designed to serve as a source. while battery bank power server both as source and load. They act as a source through the Battery to Grid (B2G) topology and as a load through the grid-to-Battery (G2B) topology. The SIMULINK (MATLAB) model representing the proposed Power Grid is shown in Figure 1.

Solar Photovoltaic Farm

A solar photovoltaic (PV) farm stands as a testament to the surging advancements in renewable energy. Diverging from other sustainable sources, solar PV technology is making significant strides. Two prominent technologies in this realm are solar concentrators and photovoltaic (PV), with a focus on Concentrated Solar Power (CSP). In contrast to alternative renewable energy sources, solar energy technologies are experiencing rapid growth. Among these, solar concentrators and photovoltaic (PV) technology, specifically Concentrated Solar Power (CSP), stand out as the most widely recognized.

$$S = 3/2 (V \times I^*) \quad (1)$$

In the proposed framework, solar energy is converted into apparent power according to equation (1). Equation (2) subsequently defines the DC voltages, which are then used to calculate the DC currents based on apparent The current-controlled voltage sources receive DC currents in a three-phase setup to directly produce three-phase power for the MG. In Figure 2, the solar irradiance graph is depicted, while Figure 3 shows the 24-hour wind profile.

$$V_1 = 1/3 (V_{ab} - a^2 \times V_{bc}) \quad (2)$$

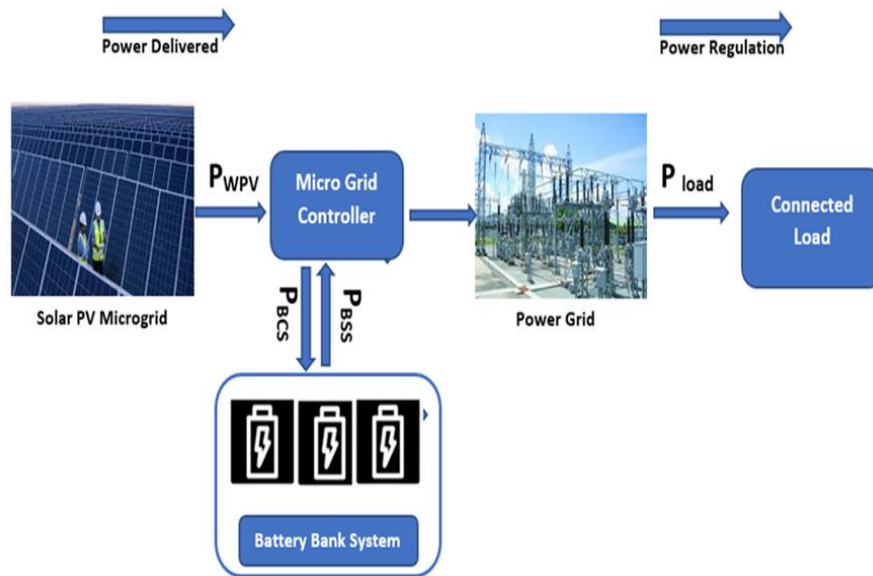


Figure 1: Complete Micro Grid of Proposed Model

Loads Across Power Grid

The load linked to the proposed Power Grid comprises residential, industrial, and entirely resistive elements rated at 10MW, 5MW, and 5MW, respectively. Residential demand fluctuates throughout the day, varying with time, as illustrated in Figure 3, displaying the residential load profile over a 24-hour period. Industrial consumption is time-specific, aligned with the industry's designated schedules. A significant portion of our load comprises pure resistance, with a 5MW resistive load integrated into the MG. Industrial equipment demands a substantial amount of reactive power. Residential loads exhibit a mixed nature, involving resistive, capacitive, and inductive elements.

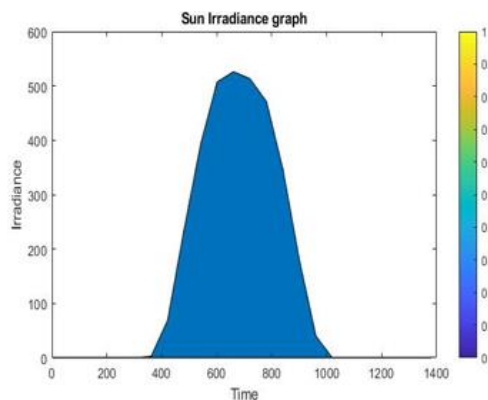


Figure 2: SPV Farm Irradiance

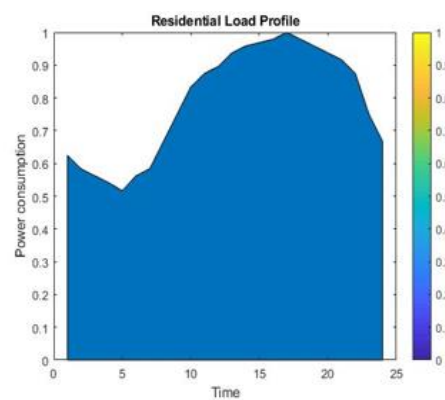


Figure 3: Domestic Load Representation



Battery Energy System to Grid

The introduction of battery energy sources involves a strategic synchronization process, allowing for optimized energy flow and distribution. By harnessing advanced technologies, these systems contribute to the grid's resilience by storing excess energy during periods of low demand and releasing it during peak demand, thereby promoting a balanced and sustainable energy supply. Battery Energy System (BESs) are incorporated into the envisioned power Grid as a versatile load, capable of functioning both as an active power source and a load as per the necessity. When the system frequency drops below the preset nominal value, Battery Backup systems with ample charge storage switch to a regulatory mode, acting as a source through B2G topology. They cater to the active power demand, thereby restoring the frequency as well as voltage control. Conversely, when renewable energy generation exceeds the load, causing the frequency to rise, the Battery system are placed on charge mode via the battery charge controller. This action, utilizing the B2G topology, consumes the surplus active power, maintaining the rated voltage and frequency. The author integrated 100 Batteries into the Power Grid. Figure 3 displays the battery system.

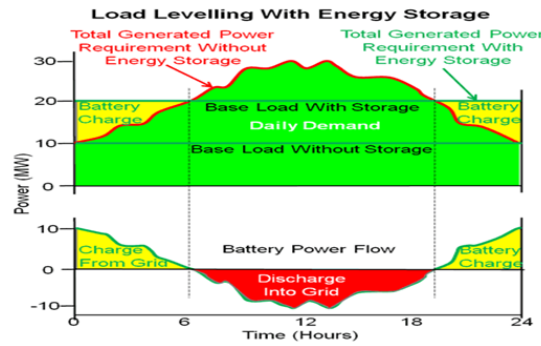


Figure 4: Battery Energy system as reserve power

Large Scale Power Grid Control Algorithm

The control algorithm defines the operational characteristics of any system, responding to real-time system operator requirements and predefined conditions. In the proposed Power Grid, the primary constraints are the system power and various generation capacities (solar PV farm and Battery Backup system). When generation matches demand, the system power aligns with the predetermined nominal value. In cases where generation fail to meet load demand due to their intermittent nature, the Power Grid experiences fluctuations in frequency and voltage. To regulate the frequency and voltage, the paper titled "Implementation/Impact of Solar Energy system on a power Grid system" introduces a method involving active and reactive power balancing between supply and load using Conversely, when the system frequency and voltage and power exceeds the nominal value, Batteries are linked to the Power Grid to absorb extra power and restore the frequency Power and voltage to its set value through G2B topology. If, during B2G operation, the BESS of lacks reserve power, the MG implements load shedding in certain areas, as determined by ΔP in equation 6. Similarly, in G2B operation, when the BESS of batteries lacks the capacity to draw additional power, PV plant is adjusted to a lower operating point using governor control. For the proper functioning of the Power Grid, certain conditions must be met.

$$P_G = P_L \quad (3)$$

$$P_G - P_L = 0 \quad (4)$$

$$P_G \neq P_L \quad (5)$$

$$P_G - P_L = \pm \Delta P \quad (6)$$

SOLAR PV & POWER GRID SIMULATION RESULTS AND DISCUSSION

Following the 24-hour simulation of the proposed Solar PV Incorporation into Power Grid in SIMULINK/MATLAB, the results were obtained. To validate these findings, three distinct events were generated within the 24-hour span, coinciding with instances of frequency dropping below its nominal value. These events occurred as follows:

1. Initiation of the industrial load's connection to the Power Grid.
2. Occurrence of partial shading on the solar panels at noon, lasting for 300 seconds.
3. Shutdown of the solar PV turbine at 6:00 pm due to sundown surpassing the acceptable range.

During these events, the power Grid frequency voltage and power experienced a decline, prompting the Battery to enact an initial response to regulate the frequency and voltage. Figure 5 illustrates the generations and loads over the 24-hour period. Furthermore, the combined generation graph in figure 6 reveals that as renewable resource generation increases its output, prioritizing the renewables to supply the load.

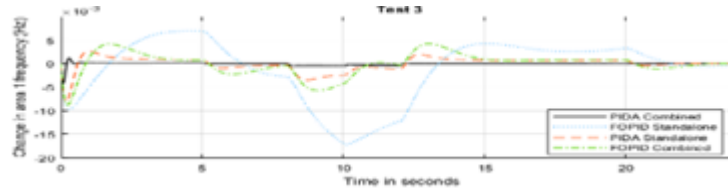


Figure 5: Event 01(The oscillation and control of frequency, voltage and Power)

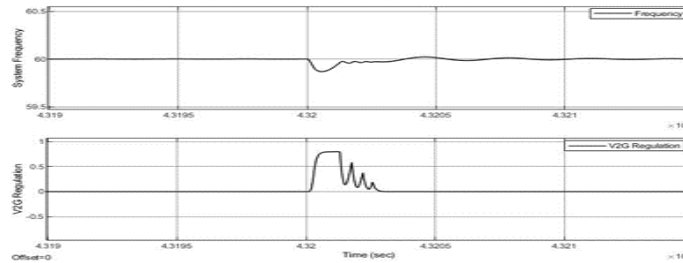


Figure 6: Event 02(The oscillation and control of frequency, voltage and power)

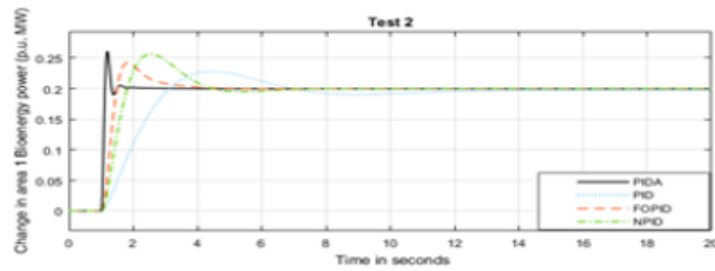


Figure 7: Event 03(The oscillation and control of frequency, voltage and power)

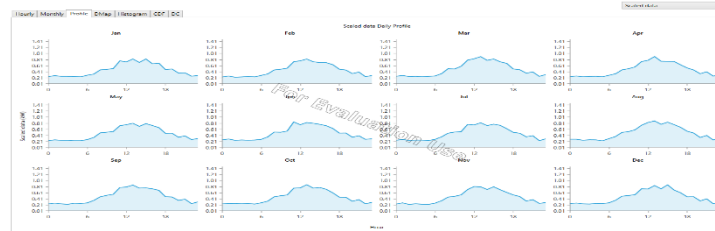


Figure 8: Homer pro Results

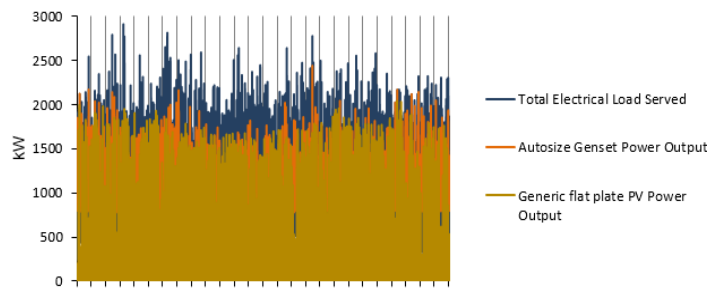


Figure 9: Homer pro SPV and Grid Profile

Figures 6,7 distinctly illustrate that when frequency power and voltage fluctuations occur due to heightened demand for active power and reactive power surpassing generation capacity, Solar PV and Battery system play a crucial role in supporting this demand and stabilizing the frequency and voltage back to its nominal value. Figure 8 and 9 shows the Homer pro software simulation of large scale SPV grid incorporation into Power system Grid.

CONCLUSION

This research concluded on Power Grid system (PGS) that incorporates large scale solar photovoltaic farm and Battery sources, in addition to a power system grid acting as a steady provider with the ability to manage unexpected situations, particularly those stemming from industrial power needs. Solar and Solar alone, as sustainable source, align with the demand based on their specific generation patterns. Battery power is especially useful as a backup power source to help keep the frequency and voltage stable. When the frequency deviates from its nominal value, it triggers events. The elements can either regulate or charge, depending on the frequency deviations seen in the simulation results. During times of fluctuating frequency and voltage, Solar and battery energy system serve as the primary response mechanism. In the conclusion,



ICSET-23



UET Peshawar

simulation is made and Battery charge controller is improved with extra data constraints which increased efficiency of Solar PV and Battery power with the Power grid system, led to better regulation in voltage.

REFERENCES

- [1] Ullah, K.; Basit, A.; Ullah, Z.; Albogamy, F.R.; Hafeez, G. Automatic Generation Control in Modern Power Systems with Wind Power and Electric Vehicles. *Energies* 2022, 15, 1771. <https://doi.org/10.3390/en15051771>
- [2] Barik, A.K.; Das, D.C. Expedition frequency control of solar photovoltaic/biogas/biodiesel generator based isolated renewable microgrid using grasshopper optimisation algorithm. *IET Renew. Power Gener.* 2018, 12, 1659–1667.
- [3] Bai, C.; Sarkis, J. The Water, Energy, Food, and Sustainability Nexus Decision Environment: A Multistakeholder Transdisciplinary Approach. *IEEE Trans. Eng. Manag.* 2019, 3, 656–670.
- [4] Rasul, M.G.; Ault, C.; Sajjad, M. Bio-gas mixed fuel micro gas turbine cogeneration for meeting power demand in Australian remote areas. *Energy Proc.* 2015, 75, 1065–1071.
- [5] Renewable Energy Policy Network for the 21st CENTURY Annual Report 2017. Available online: <https://www.ren21.net>.
- [6] Liguori, V. Numerical investigation: Performances of a standard biogas in a 100 kWe MGT. *Energy Rep.* 2016, 2, 99–106.
- [7] Abdalla, O.H.; Fayek, H.H.; Abdel Ghany, A.G.M. Secondary and Tertiary Voltage Control of a Multi-Region Power System. *Electricity* 2020, 1, 37–59.
- [8] Corsi, S. *Voltage Control and Protection in Electrical Power Systems: From System Components to Wide-Area Control*; Springer: New York, NY, USA, 2015.
- [9] Fayek, H.H.; Kotsampopoulos, P. Central Tunicate Swarm NFOPID-Based Load Frequency Control of the Egyptian Power System Considering New Uncontrolled Wind and Photovoltaic Farms. *Energies* 2021, 14, 3604.
- [10] Abdalla, O.H.; Ghany, A.M.A.; Fayek, H.H. Coordinated PID secondary voltage control of a power system based on genetic algorithm. In *Proceedings of the 2016 Eighteenth International Middle East Power Systems Conference (MEPCON)*.
- [11] Micev, M.; Calasan, M.; Oliva, D. Fractional Order PID Controller Design for an AVR System Using Chaotic Yellow Saddle Goatfish Algorithm. *Mathematics* 2020, 8, 1182.
- [12] Pahadasingh, S.; Jena, C.; Panigrahi, C.K. Load frequency control incorporating electric vehicles using FOPID controller with HVDC link. In *Innovation in Electrical Power Engineering*,



ICSET-23

*Proceedings of the 5th International Conference on Sustainable
Energy Technologies (ICSET 2023) Peshawar, Pakistan
14-15 December 2023*



UET Peshawar

Communication, and Computing Technology; Sharma, R., Mishra, M., Nayak, J., Naik, B., Pelusi, D., Eds.; Lecture Notes in Electrical Engineering; Springer: Singapore, 2020; Volume 630.

- [13]. Fayek, H.H. Load Frequency Control of a Power System with 100% Renewables. In Proceedings of the 2019 54th International Universities Power Engineering Conference (UPEC), Bucharest, Romania, 3–6 September 2019; pp. 1–6.
- [14] Fayek, H.H. 5G Poor and Rich Novel Control Scheme Based Load Frequency Regulation of a Two-Area System with 100% Renewables in Africa. *Fractal Fract.* 2021, 5, 2.
- [15] Fayek, H.H.; Mohammadi-Ivatloo, B. Tidal Supplementary Control Schemes-Based Load Frequency Regulation of a Fully Sustainable Marine Microgrid. *Inventions* 2020, 5, 53.
- [16] Abdalla, O.H.; Fayek, H.H.; Abdel Ghany, A.M. Secondary Voltage Control Application in a Smart Grid with 100% Renewables. *Inventions* 2020, 5, 37.
- [17] Barik, A.K.; Das, D.C. Coordinated regulation of voltage and load frequency in demand response supported biorenewable cogeneration-based isolated hybrid microgrid with quasi-oppositional selfish herd optimisation. *Int. Trans. Electr. Energ. Syst.* 2020, 30, e12176.
- [18] Nahas, N.; Abouheaf, M.; Sharaf, A.; Gueaieb, W. A Self-Adjusting Adaptive AVR-LFC Scheme for Synchronous Generators. *IEEE Trans. Power Syst.* 2019, 34, 5073–5075.
- [19] Goswami Mishra Goswami, K.; Mishra, L. Load Frequency and Voltage Control of Two Area Interconnected Power System using PID Controller. *IJERT* 2017, 4, 301–315.

Paper ID: ICSET-2346

MACHINE LEARNING BASED SCHEDULING AND LOAD FORECASTING OF ENERGY MANAGEMENT SYSTEM FOR PROSUMER

Zia Ul Islam*, Sheraz Khan
Electrical Engineering Department, UET Mardan, Pakistan

**Corresponding author*
Email: zia2987@gmail.com

ABSTRACT

The low impact that renewable energy sources (RES) have on the environment has made them more desirable to people. Among the RESs, wind and solar are more readily available. Due to the intermittent nature of RESs, the energy management system (EMS) of the Smart Grid (SG), an improved version of the traditional grid, must be more intelligent. For both typical customers and prosumers, it is desirable to balance the supply and demand of power. In this paper, K-Nearest Neighbor (KNN), Random Forest (RF) and Multiple Linear Regression (MLR) machine learning techniques are utilized to forecast the quantity of energy generated by RESs and the electricity demand of customers. Before applying machine learning algorithms, key features are extracted from a particular data set and the data is partitioned into training and testing data. These machine learning techniques are then used to obtain predicted results of Load forecasting, price forecasting and generation forecasting. The performances of the EMS are evaluated by applying KNN, RF and MLR, using MSE, RMSE and R2 performance matrices. The simulation results show that for Load forecasting the MLR has shown the least values for MSE, RMSE and R2 i.e. 0.76, 0.87 and 0.99 whereas for price forecasting the values of MLR noted to be 8.42×10^{-6} , 0.002 and 0.99 respectively for MSE, RMSE and R2 and for generation forecasting MLR has shown the least values for MSE 9279, RMSE 96.33 and R2 0.49.

KEYWORDS: Energy management system (EMS), K-Nearest Neighbors (KNN), Multiple Linear Regression (MLR), Random Forest (RF), Multiple Linear Regression (MLR), Renewable energy sources (RES), Smart Grid (SG).

INTRODUCTION

The more adoption of renewable energy resources (RES) in the energy system and the upgrade of the old electric grid into a smarter, more adaptable, and correlative one, has increased the importance of electric load forecasting in smart grid design and operation. Figuring out the electric load is a complex task because it varies a lot and is impenetrable to predict, whether it affects one family or the entire system. Load forecasting can help optimize the use of RES, reduce greenhouse gas emissions, improve grid reliability and security, and lower operating costs and electricity prices [1].

Electricity load forecasting is a vital process that helps the power industry to plan and manage the power system efficiently. Usually, a strategy utilized by power or vitality supply companies to foresee the power/energy required to meet the supply and request adjust. Forecasting accuracy is critical for a power company's operational and managerial workload. Based on the time horizon, forecasting of electricity load



ICSET-23



UET Peshawar

can be divided into three categories: short- forecasting (MTF), long-term forecasting (LTF), and short-term forecasting (STF). Medium-term and long-term power stack estimating have gotten to be a vital require due to extreme climate alter effect on power utilization and unused patterns in keen networks (such as the utilize of renewable assets and the approach of prosumers and vitality commons). Such estimates back the plans and choices that assess the capacity of centralized and decentralized control era frameworks, execute request reaction techniques, and control the operation. Electricity load forecasting can be influenced by various factors such as weather, economic parameters, household lifestyle, historical energy consumption, and stock indices [2].

One of the key concerns for electricity utility businesses is load forecasting. It is crucial for pricing, operations, scheduling, customer satisfaction, system security, and decision-making. This enables smart utility businesses to supply services more efficiently and monitor their operations to maximize performance. Different techniques have been discussed: KNN, MLR, RF. Load forecasting is the technique of predicting the power or energy needed to always balance the supply and demand. Among the various methods for load forecasting, machine learning (ML) methods have picked up ubiquity due to their capacity to learn complex and nonlinear relationships from data and generalize to unseen cases [3]. Predicting future electricity consumption patterns based on past data is an important and emerging research area. This provides a framework that combines feature selection, extraction, and regression techniques to perform electric load prediction, which can aid in striking a balance between the electric load and demand, which frequently vary significantly [4].

Prosumer is a concept that involves consumers who also produce and sell energy from renewable sources. This can have positive impacts on the environment, society, and economy, such as lower carbon emissions, more renewable energy use, new market opportunities, better energy access in cities, and enhanced resilience for developing communities. However, prosumers also challenge the existing energy system and its stakeholders and may create problems for the electricity grid due to the variability of renewable energy generation [5].

To cope with the increasing use of variable and uncertain energy sources, energy management is essential for ensuring system flexibility. Demand Response (DR) programs increase demand adaptability by informing the end-consumer of the energy market price fluctuations [6].

Colab is a platform that enables AI and data science researchers to share their experiments and insights in a reproducible way. It also offers a great opportunity for students to learn about these fields in a hands-on manner. One of the main advantages of Colab is that it provides students with enough computational power to run interactive AI applications, without requiring them to install any software or dependencies on their own devices [7].

ML appears to be a tool to process the significant amount of data generated in the electrical network.

Machine learning algorithms (MLA) are methods that learn from data and make predictions or decisions based on learned models.

MLA features include price and load forecasting, outage detection, power generation, and optimal future scheduling in the event of a data breach. [8,9, 10].

Following a review of recent forecasting scenarios in the literature, the motivation behind the work intended is that management of these energy resources, keeping in view the energy demand is challenging task and remains open for research. Machine learning-based algorithms is a potential candid to regulate the system's performance.

A new method to improve the effectiveness and precision of the EMM method by combining machine learning (ML) and Gaussian Process Regression (GPR). This method uses ML to select the most relevant features for the EMM model, and GPR to estimate the unknown parameters of the model. The advantages



of this approach are demonstrated through numerical experiments and real data applications [11]. Estimated the hourly electricity consumption of the Greek system for the next 24 hours using two types of dependable and standard artificial neural networks with forward links. It employs data on electric load and weather variables that are open to the public [12]. A new EMS that forecasts weather and load using a hybrid machine learning method has been proposed. The method combines ANFIS, MLP ANN, and RBF for accurate and reliable forecasts. The EMS uses the forecasts to schedule and operate the PMGs optimally [13]. The optimization of the μ G components, such as battery storage, diesel generator, and grid connection, based on the forecasted load demand and renewable energy production, is the main goal of the EMS strategy presented in this paper. The EMS strategy can lower the operational cost and enhance the self-consumption of an institutional microgrid (μ G) from green distributed generators (DGs) [14]. A data-driven approach to forecast the total and flexible load of a retail building using ML models has been made. The ML models are designed to meet the criteria of reliability, computational efficiency, and scalability for deployment purposes. Data preprocessing, training test dataset preparation, cross validation, algorithm selection, hyperparameter optimization, feature ranking, model selection, and model evaluation are performed according to ML model development best practices.

ML models are compared to time-series sustainability models based on selected performance metrics. The results show that ML models can achieve higher accuracy and reliability for daily and weekly load forecasting for retail buildings. [15]. Using historical load data for two years from IEEE data port, this paper compares stochastic and deterministic methods for STLF. The methods are exponential smoothing, SVM, ensemble, ANN, CNN, LSTM and CNN-LSTM. The best method is chosen by the coefficient of correlation (R) [16]. A novel methodology that combines the benefits of state-of-the-art deep learning algorithms, especially Convolution Neural Nets (CNN), for time series forecasting. The key feature of our methodology is the use of the statistical properties of each time series dataset to optimize the hyperparameters of the neural network and to transform the dataset into a form that maximizes the CNN algorithm's performance [17]. Using machine learning approaches such as support vector machine (SVM) and RF, and deep learning techniques such as non-linear auto-regressive exogenous (NARX) neural network and recurrent neural networks (Long Short-Term Memory—LSTM), the author aims to create and evaluate accurate models for forecasting the electrical load demand at the district level [18]. Compared four methods for forecasting electricity demand: MLR, RF, artificial neural networks (ANNs), and automatic regression integrated moving average (ARIMA), applied these methods to a dataset of electricity consumption in Dubai and evaluate their performance [19]. Many existing studies in the broader literature have examined Electrical load forecasting and scheduling of Energy management system for prosumer using machine learning Techniques but certain short coming and limitations yet to be addressed. The work in presented in this paper aims to apply different techniques for load forecasting, price forecasting and forecasting the generation of electricity. KNN, MLR and RF often appear in the existing literature.

However, research and analysis are needed to compare the performance of the system under consideration using these techniques. KNN is a simple and intuitive method that assigns a new data point to the class of its k closest neighbors. MLR is a statistical technique that uses a linear equation to model the connection between a dependent variable and one or more independent variables. RF is an ensemble technique that generates more reliable and accurate predictions by combining several decision trees. The performance of these techniques on a real-world dataset of electricity load demand from a utility company. Various accuracy and error metrics such as mean square error (MSE), root mean squared error (RMSE), and coefficient of determination(R^2) are required to evaluate the results.



ICSET-23



UET Peshawar

Our contribution consists of data acquiring from the datasets from a credible and reliable source. Acquiring data from datasets is not a simple task. It requires careful planning, execution, evaluation, and maintenance. However, if done properly, it can bring significant value and benefits to the work. Data preprocessing is another essential step to ensure the quality and vitality of data and improve the performance and accuracy of the model. The selection of appropriate ML algorithm adds more value to the training and testing of models in our scenario we have selected the fundamental ML Algorithms namely KNN, RF and MLR. Performance Evaluation is the process of measuring and assessing how a model or system perform on a given task or objective. An understanding of a model's strengths and limitations and their optimization can be achieved with the aid of performance evaluation. In our paper we are using the three of most prestigious performance Evaluation metrics i.e. RMSE, MSE and R2.

Section 1 of this work is devoted to the introduction and literature review. Section 2 consists of System Model, ML Algorithms, Performance Evaluation and Predictions. Results have been discussed in section 3 and 4.

MATERIALS AND METHODS

We followed a methodical and rigorous approach to obtain the outcomes we aimed for. We divided the process into several stages, each with a clear objective and a set of criteria to evaluate the progress. We documented the results and challenges of each stage and used them to inform the next steps. This way, we ensured the quality and validity of our work, and addressed any potential issues or limitations along the way.

Our system model consists of the following five processes as shown in Fig. 1. First, load data of residential houses is obtained from dataset stored by UMass repository. Second, in the processing Electric load, price and generation data has been considered and pre-processed. Third, Feature Engineering comprised of important features and discarding rest of all. Fourth, applying algorithms for each forecasting. KNN which conventionally uses proximity to make predictions. Application of the random Forest technique which combines the output of several decisions to reach a single result. Linear regression pragmatized that is based on variable based on the value of another variable outperformed in our predicts. Finally, performance evaluators are used to evaluate the performances of KNN, RF, and MLR algorithms applied for the forecasting.

One of the sources of data for studying residential electricity consumption is the UMass smart dataset repository, which provides high-resolution meter readings from several homes in Western Massachusetts. This paper uses the HomeA-2016 dataset from this repository to examine how different households use electricity over time. The HomeA-2016 dataset contains 9454 observations and 16 variables and covers the period from 01/01/2016 12:00:00 am to 15/07/2016 11:30:00 pm.

Data preprocessing is an essential step in machine learning, as real-world data often contains noise, missing values, or is in an unsuitable format. By cleaning and preparing the data for a machine learning model, data preprocessing not only makes the data usable, but also enhances the model's performance and effectiveness. The missing values have been searched, then made it in usable format then we check date and time accordingly the data which is suited accordingly in half hours. Arranged values for Example 1:00 to 1:30 if the values are given for 1 minute or 2 minutes are processed for 1:28 to 1:29 we arranged them according to half hours. Then used libraries for processing purpose. The code relies on the NumPy Python library for any mathematical operation. NumPy is the fundamental Python package for scientific computing. It also supports large, multidimensional arrays and matrices. The Pandas library handles the import and

management of the datasets. It is a popular and powerful Python library for data analysis and manipulation. The target columns are use [KW] and gen [KW], which are extracted from the dataset for feature extraction. To ensure the validity and accuracy of our ML algorithms, we followed the standard practice of dividing our data into train and test sets. We have allocated 80% of the data for training and 20% for testing, resulting in 7563 training rows and 1891 testing rows. The ML algorithms learned from the training data and made predictions on the test data.

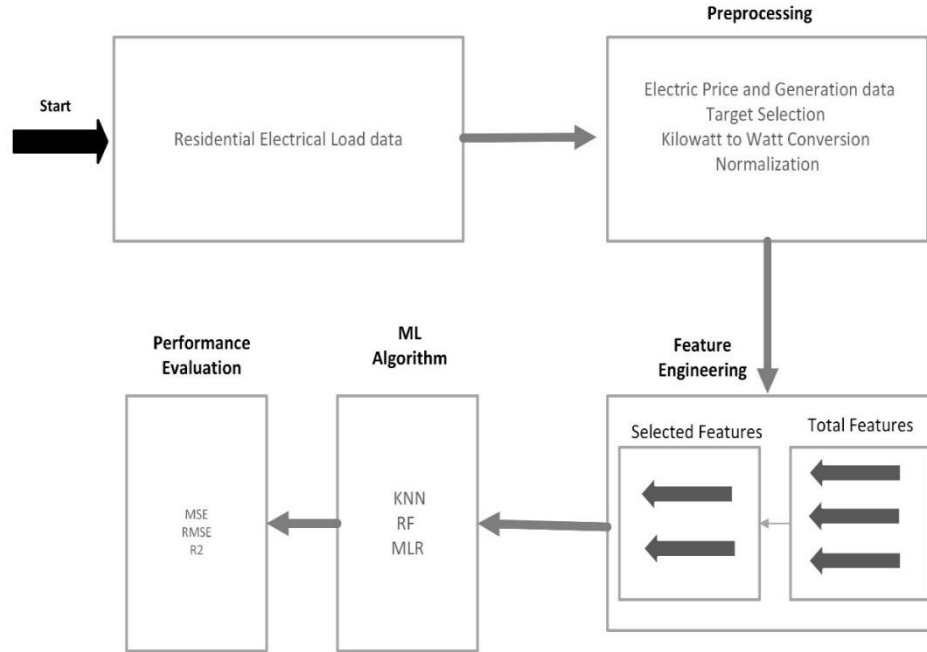


Figure 1: System flow Diagram

The Performance Evaluation metrics, namely MSE, RMSE and R2, were used to assess the performance of the above models. These metrics measure the accuracy and fit of the models to the data. A lower MSE and RMSE indicate a smaller error, while a higher R2 indicates a better fit.

ML Algorithms

Three different algorithms, namely K-Nearest Neighbors (KNN), Random Forest (RF) and Multiple Linear Regression (MLR), were applied to a dataset of historical power usage.

To classify or regress a new data point using the k-nearest neighbors' algorithm (KNN), the algorithm finds the k closest data points to it in a feature space and assigns it to the most common class among them. The algorithm was first introduced by Evelyn Fix and Joseph Hodges in 1951, and it is a simple and popular supervised learning method. The algorithm requires two user-defined parameters: k, which is the number of neighbors to consider, and a distance metric, which is a function that measures the similarity between data points. Some common distance metrics are Minkowski, Manhattan, and Euclidean, which are defined by the following equations:

$$\text{Minkowski: } M_k = (\sum_{i=1}^n |x_i - y_i|)^{1/p} \quad (1)$$

$$\text{Manhattan: } M_h = \sum_{i=1}^n |x_i - y_i| \quad (2)$$

$$\text{Euclidean: } \varepsilon_{\mu} = \sqrt{\sum_{t=1}^n |x_i - y_i|^2} \quad (3)$$

The performance of the KNN algorithm depends on the choice of k and the distance metric. A small value of k can cause overfitting, while a large value of k can cause under fitting. Similarly, different distance metrics may be more suitable for different types of data and problems [20,21,22].

Random forests (RFs) are a type of machine learning technique that combines multiple decision trees to perform classification or regression tasks. Each tree is trained on a random subset of the data and features, which ensures low correlation among the trees and reduces the variance of the predictions. The final output is obtained by averaging or voting over the trees in the forest. RFs have many advantages, such as being missing values and imbalanced data, and being easy to use and interpret [23].

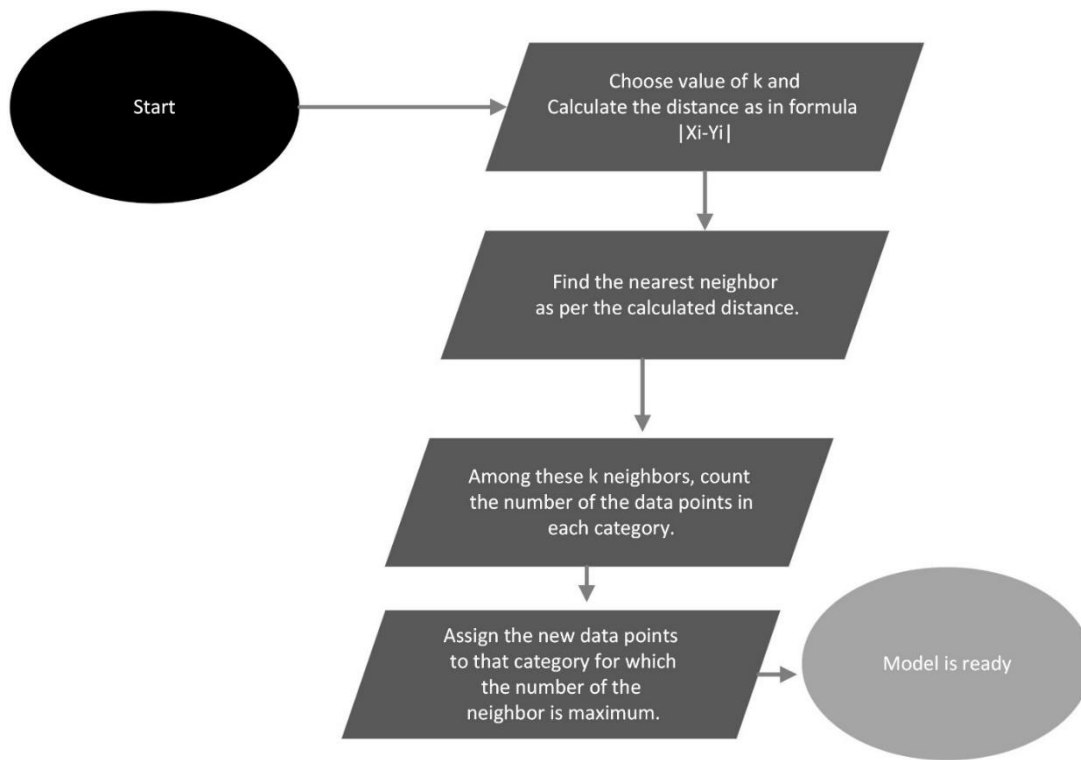


Figure 2: KNN Algorithm Flow Chart

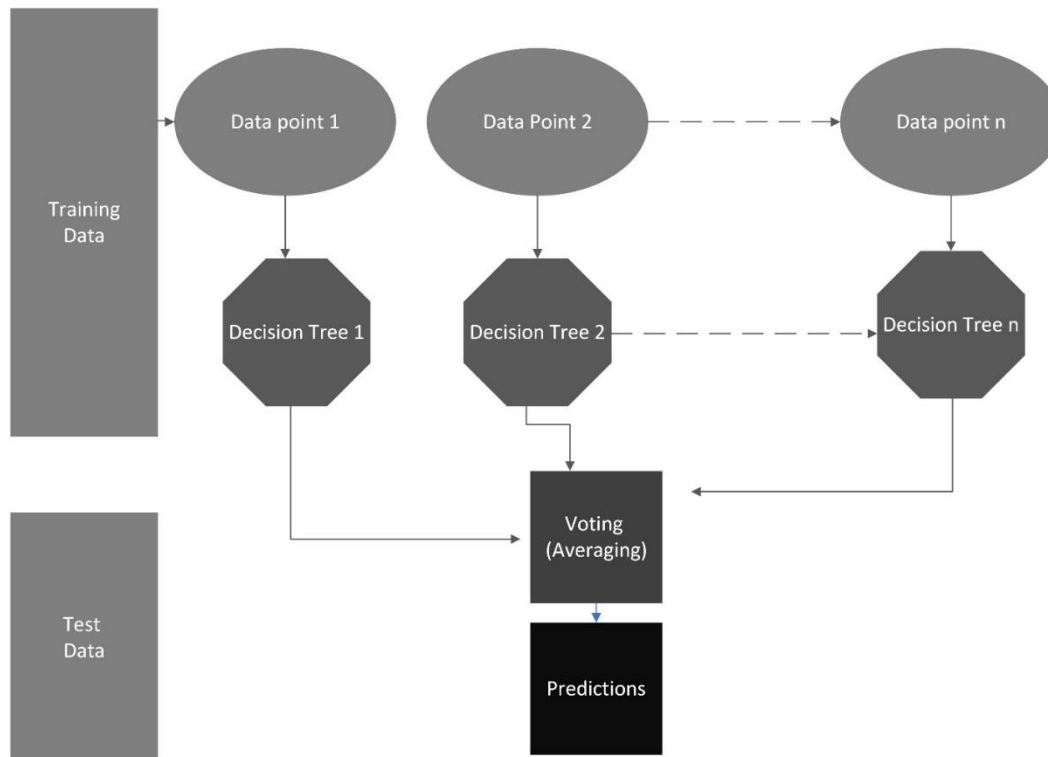


Figure 3: RF Algorithm

Regression analysis is a statistical method that allows us to examine how a dependent variable (y) changes with one or more independent variables (x_1, x_2, \dots, x_k). The purpose of regression analysis is to find a function that best describes the relationship between the variables, so that we can predict the value of y for any given values of x. One type of regression analysis is multiple linear regression, which assumes that the dependent variable is a linear combination of the independent variables plus an error term. The error term (ε) represents the random variation in y that is not explained by the independent variables. It accounts for the fact that the relationship between y and x may not be perfect or deterministic. The equation for multiple linear regression is:

$$y = \beta_0 + \beta_1 x_1 + \beta_2 x_2 + \dots + \beta_k x_k + \varepsilon \quad (4)$$

where y is the dependent variable, x_1, x_2, \dots, x_k are the independent variables, $\beta_0, \beta_1, \beta_2, \dots, \beta_k$ are the regression coefficients, and ε is the error term. The regression coefficients ($\beta_0, \beta_1, \beta_2, \dots, \beta_k$) are the parameters that measure the effect of each independent variable on the dependent variable [24,25].

Performance Evaluation

Performance of the above models assessed using the following Performance Evaluation metrics namely MSE, RMSE and R2.

Mean squared error (MSE) is a statistical metric that quantifies the difference between the actual and predicted values of a variable. It is calculated by taking the average of the squared errors, which are the

deviations of the predictions from the observations. Squaring the errors has two benefits: it removes any negative signs, and it gives more weight to larger errors. MSE is always positive and lower values indicate better model performance. The formula for MSE is:

$$MSE = \frac{1}{n} \sum_{i=1}^n (y_i - \hat{y}_i)^2 \quad (5)$$

Root Mean Square Error (RMSE) is a common metric for measuring the accuracy of a predictive model. It is calculated by taking the square root of the mean square of the difference between the predicted value and the actual value. A lower RMSE indicates a better fit of the model to the data.

$$RMSE = \sqrt{\frac{\sum_{i=1}^n (y_i - \hat{y}_i)^2}{n}} \quad (6)$$

R-Squared is a statistical measure that indicates how well a model fits the observed data. It is calculated as the ratio of the explained variance to the total variance. The explained variance is the amount of variation in the data that can be accounted for by the model. The total variance is the amount of variation in the data without any model. R-Squared ranges from 0 to 1, with higher values indicating a better fit. R-Squared can be used to compare different models and assess their performance.

$$R^2 = 1 - \frac{\sum_{t=1}^n (y_i(t) - \hat{y}^*(t))^2}{\sum_{t=1}^n (y_i(t) - \hat{y}^*(t))^2} \quad (7)$$

RESULTS

Data is obtained for the proposed scheme from the UMass smart dataset repository. The Western Massachusetts homes' individual electricity consumption is being maintained by the UMass dataset repository. In this research work HomeA-2016 data has been taken containing 9454 rows and 16 columns from 01/01/2016 12:00:00 am to 15/07/2016 11:30:00 pm. This data set contains 4727 hours' data. Data is further divided into training and testing. There are 16 attributes in the dataset including target attribute [26].

Table 136: All Features.

| Date & Time | Gen [kW] | Furnace HRV [kW] |
|--------------------------|----------------------|----------------------|
| Cellar Outlets [kW] | Washing Machine [kW] | Fridge Range [kW] |
| Disposal Dishwasher [kW] | Kitchen Lights [kW] | Bedroom Outlets [kW] |
| Bedroom Lights [kW] | Bedroom Lights [kW] | Master Outlets [kW] |
| Master Lights [kW] | Duct Heater HRV [kW] | use [kW] |

It is mandatory to first train and test data for algorithms; therefore, we have split data into train and test dataset into 80% and 20%. we have split 7563 for training and 1891 rows for testing. When we trained and tested our model for KNN regression. We have selected k value as 3.



Load Forecasting

Electrical load forecasting is a technique used by power companies to predict the future demand for electricity. It helps them plan their generation, transmission, and distribution of electricity efficiently and economically. Different factors affect the electricity consumption patterns, such as weather, economic conditions, household lifestyle, and historical data. The Fig. 4 here shows the predicted load after applying KNN regression, RF and MLR algorithm on our data. In this graph we have Load in Watt/half-hour on the y-axis and x-axis shows half-hours data. The graph is based on use Load(actual) and KNN (predicted Load). The green-colored lines show the actual load whereas red colored lines show Linear regression algorithm prediction graph, blue color graphs unveil RF algorithm prediction graph and yellow color gives us KNN algorithm prediction graph. For RF regression we have used n-estimators=100 and random state = 42. MLR is applied on both training and testing data. where a graph is plotted Load(watt/half-hour) vs time (Half-hours). A comparison of all three algorithms (i.e. KNN, RF, LR) have been illustrated.

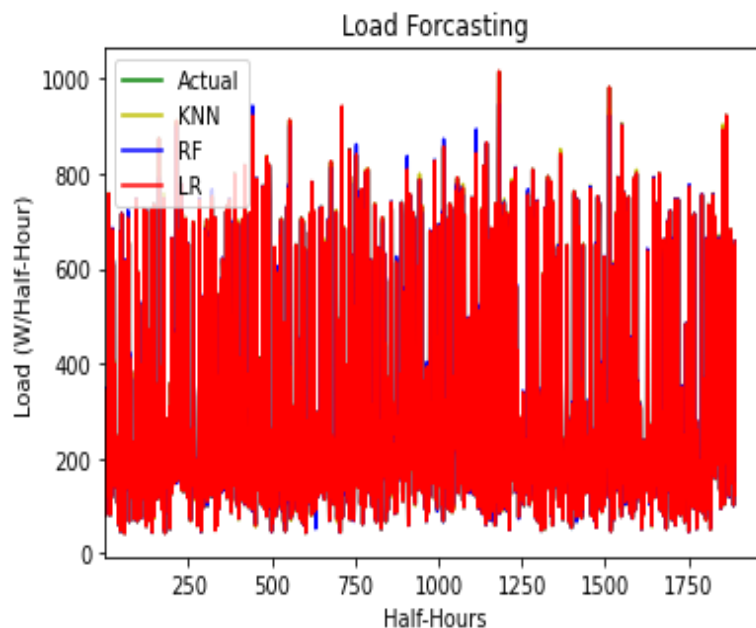


Figure 4: Load forecasting

Price Forecasting

The process of price forecasting of electrical load is estimating the future demand and supply of electricity in each market. It is a vital tool for planning, operation, and optimization of power systems. Customer satisfaction, reliability and costs can be enhanced, improved, and reduced by it. Fig.5 draws a comparison of price forecasting predictions of all three algorithms. It can be seen from the graph that as the consumption of electric load rises as the KW/half-hours also increases. The green-colored lines show the actual load whereas red colored lines show Linear regression algorithm prediction graph, blue color graphs unveil RF algorithm prediction graph and yellow color gives us KNN algorithm prediction graph.

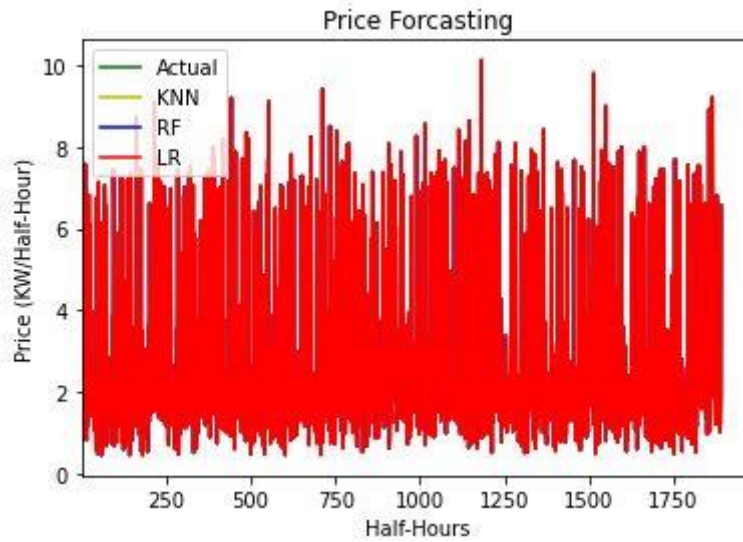


Figure 5: Price forecasting

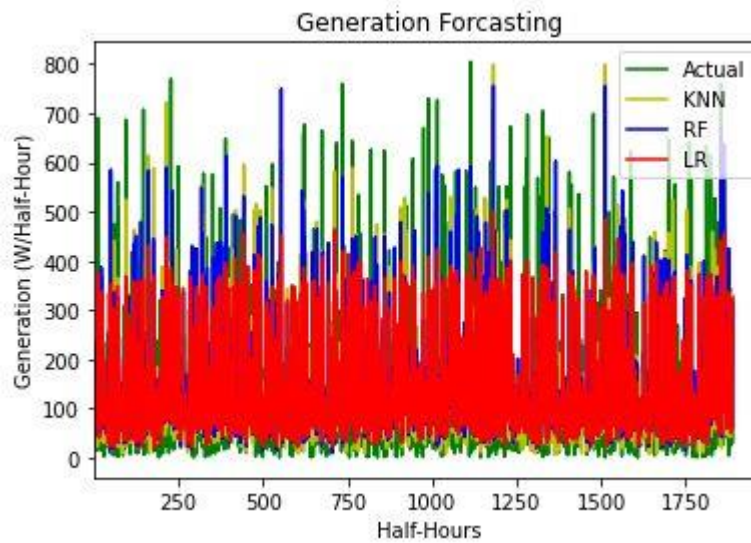


Figure 6: Generation forecasting

Generation Forecasting

Generation forecasting methods can be classified into two categories: deterministic and probabilistic. Deterministic methods use historical data and mathematical models to predict the load curve, while probabilistic methods account for the uncertainty and variability of load patterns and other factor. Generating forecasting in Fig.6 shows the actual to predictions graphs. The green color shows the actual values while red, blue and yellow color shows the predictions using ML algorithms. The difference between the green and other colors denotes the demand that we need to fulfill from national grid. The red, blue, and yellow color denotes the generation load that prosumer has generated using any source and their predictions

using ML algorithms. Fig.6 also demonstrates a comparison of generation predictions of all three ML algorithms.

DISCUSSION

Table 2 shows the performance evaluation metrics of the Load forecasting predictions of KNN, RF and MLR here. MLR has shown the best results in the below table. MLR has shown least MSE, RMSE and R².

Table 2: Load forecasting Results

| ML Algorithm | MSE | RMSE | R ² |
|--------------|--------------------|--------------------|--------------------|
| KNN | 56.12562430225043 | 7.491703698241838 | 0.998554862384178 |
| RF | 87.53118215758059 | 9.355810074898944 | 0.997746223664042 |
| MLR | 0.7696439043458515 | 0.8772935109447986 | 0.9999801830024916 |

Table 3 shows the performance evaluation metrics of price forecasting predictions of all three ML algorithms applied. MLR once again has shown the least MSE, RMSE and R².

Table 3: Price forecasting Results

| ML Algorithm | MSE | RMSE | R ² |
|--------------|---------------------|---------------------|-------------------|
| KNN | 0.00012922766785679 | 0.01136783479193805 | 0.999966727606015 |
| RF | 8.7178224581546e-05 | 0.00933692800558868 | 0.999977554123793 |
| MLR | 8.4208144867690e-06 | 0.0029018639676540 | 0.999997831883358 |

In the generation forecasting the results of KNN, RF and MLR as shown here in the Table 4 below MLR has shown the results with least MSE, RMSE and R² values.

Table 4: Generation forecasting Results

| ML Algorithm | MSE | RMSE | R ² |
|--------------|--------------------|--------------------|--------------------|
| KNN | 12179.920441859096 | 12179.920441859096 | 0.3385960478827954 |
| RF | 11206.142879907715 | 105.8590708437766 | 105.8590708437766 |
| MLR | 9279.857413466312 | 96.33201655455113 | 0.4960776305847595 |

CONCLUSION

In this paper short term load forecasting, price forecasting and generation forecasting of a dataset obtained from UMASS Smart dataset repository using Machine Learning Algorithms such as KNN, RF and MLR. The forecasts based on the historical data. The predictions performed with python code in the Google Collaboratory for best performance and equipping with the enhanced features. As discussed in the result section MLR has shown less error values in Load forecasting i.e. for MSE, RMSE and R2 with values 0.769, 0.877 and 0.99 whereas for price forecasting the values noted 8.42×10^{-6} , 0.002 and 0.99 respectively for MSE, RMSE and R2. While in generation forecasting MLR has also surged to values for 9279.85, 96.33 and 0.49 for given performance Evaluation metrics.

REFERENCES

- [1] N. Andriopoulos, A. Magklaras, A. Birbas, A. Papalexopoulos, C. Valouxis, S. Daskalaki, M. Birbas, E. Housos, and G.P. Papaioannou. 2021. "Short Term Electric Load Forecasting Based on Data Transformation and Statistical Machine Learning" *Applied Sciences* 11, no. 1: 158.
- [2] S. Navid, A. Nizami, M. Khazen, and M. Nik-Bakht. 2021. "Medium-Term Regional Electricity Load Forecasting through Machine Learning and Deep Learning" *Designs* 5, no. 2: 27.
- [3] H. A. Sayed, A. William, and A.M. Said. 2023. "Smart Electricity Meter Load Prediction in Dubai Using MLR, ANN, RF, and ARIMA" *Electronics* 12, no. 2: 389.
- [4] E. A. Madrid, and N. Antonio. 2021. "Short-Term Electricity Load Forecasting with Machine Learning" *Information* 12, no. 2: 50.
- [5] K. Kirsi, L.F.Walter, A.A. Marisa, B. Luciana, Ö. P. Gökcin, W.Tony 2019, "Energy Prosumers' Role in the Sustainable Energy System Affordable and Clean Energy" Springer International Publishing ISBN 978-3-319-71057-0
- [6] K. Derck, N. Sadat-Razavi, and W. Ketter. 2017. "Machine Learning for Identifying Demand Patterns of Home Energy Management Systems with Dynamic Electricity Pricing" *Applied Sciences* 7, no. 11: 1160.
- [7] B. Ekaba, "Google Colaboratory". In: *Building Machine Learning and Deep Learning Models on Google Cloud Platform*. Apress, Berkeley, CA.
- [8] N. Christof & F. Stefan. (2020). Forecasting electricity prices with machine learning: predictor sensitivity. *International Journal of Energy Sector Management*. ahead-of-print. 10.1108/IJESM-01-2020-0001
- [9] S. Simon & W. Andreas. (2020). Electricity Price Forecasting with Neural Networks on EPEX Order Books. *Applied Mathematical Finance*. 27. 1-18. 10.1080/1350486X.2020.1805337.
- [10] C. Zeynep & G. Murat. (2017). Machine learning based electricity demand forecasting. 412-417. 10.1109/UBMK.2017.8093428.
- [11] W. Ahmed et al., "Machine Learning Based Energy Management Model for Smart Grid and Renewable Energy Districts," in *IEEE Access*, vol. 8, pp. 185059-185078, 2020, doi: 10.1109/ACCESS.2020.3029943
- [12] G. Stamatellos, and T. Stamatelos. 2023. "Short-Term Load Forecasting of the Greek Electricity System" *Applied Sciences* 13, no. 4: 2719.
- [13] F. Jamal & K. Abbas & H. Hashemi-Dezaki & S. Miadreza & C. Joao. (2020). Optimal Day-Ahead Self-Scheduling and Operation of Prosumer Microgrids Using Hybrid Machine Learning-Based Weather and Load Forecasting. *IEEE Access*. PP. 1-1. 10.1109/ACCESS.2020.3019562.



- [14] K.A. Muqet, & A. Ahmad. (2020). Optimal Scheduling for Campus Prosumer Microgrid Considering Price Based Demand Response. IEEE Access. PP. 1-1. 10.1109/ACCESS.2020.2987915.
- [15] K. Gautham, and A. Kiprakis. 2020. "A Machine Learning Pipeline for Demand Response Capacity Scheduling" *Energies* 13, no. 7: 1848.
- [16] K. Shahare, A. Mitra, D. Naware, R. Keshri, H.M. Suryawanshi, Performance analysis and comparison of various techniques for short-term load forecasting, *Energy Reports*, Volume 9, Supplement 2023, Pages 799-808, ISSN 2352-4847.
- [17] N. Andriopoulos, A. Magklaras, A. Birbas, A. Papalexopoulos, C. Valouxis, S. Daskalaki, M. Birbas, E. Housos, and G.P. Papaioannou. 2021. "Short Term Electric Load Forecasting Based on Data Transformation and Statistical Machine Learning" *Applied Sciences* 11, no. 1: 158.
- [18] S. Navid, A. Nizami, M. Khazen, and M. Nik-Bakht. 2021. "Medium-Term Regional Electricity Load Forecasting through Machine Learning and Deep Learning" *Designs* 5, no. 2: 27.
- [19] H. A. Sayed, A. William, and A.M. Said. 2023. "Smart Electricity Meter Load Prediction in Dubai Using MLR, ANN, RF, and ARIMA" *Electronics* 12, no. 2: 389.
- [20] M. Purlu and B. E. Turkay, "Estimating the Distributed Generation Unit Sizing and Its Effects on the Distribution System by Using Machine Learning Methods", *ELEKTRON ELEKTROTECH*, vol. 27, no. 4, pp. 24-32, Aug. 2021.
- [21] A. Moradzadeh, B. Mohammadi-Ivatloo, M. Abapour, A. Anvari- Moghaddam and S. S. Roy, "Heating and Cooling Loads Forecasting for Residential Buildings Based on Hybrid Machine Learning Applications: A Comprehensive Review and Comparative Analysis," in *IEEE Access*, vol. 10, pp. 2196-2215, 2022, doi: 10.1109/ACCESS.2021.3136091.
- [22] T. Alquthami, M. Zulfiqar, M. Kamran, A. H. Milyani and M. B. Rasheed, "A Performance Comparison of Machine Learning Algorithms for Load Forecasting in Smart Grid," in *IEEE Access*, vol. 10, pp. 48419-48433, 2022, doi: 10.1109/ACCESS.2022.3171270.
- [23] Dudek, Grzegorz. (2015). Short-Term Load Forecasting Using Random Forests. 10.1007/978-3-319-11310-4_71.
- [24] N. Amral, C. S. Ozveren and D. King, "Short term load forecasting using Multiple Linear Regression," 2007 42nd International Universities Power Engineering Conference, Brighton, UK, 2007, pp. 1192-1198,
- [25] J. Kim, S. Cho, K. Ko and R. R. Rao, "Short-term Electric Load Prediction Using Multiple Linear Regression Method," 2018 IEEE International Conference on Communications, Control, and Computing Technologies for Smart Grids (SmartGridComm), Aalborg, Denmark, 2018, pp. 1-6.
- [26] B. Khan, R. Khalid, M. U. Javed, S. Javaid, S. Ahmed, and N. Javaid, "Short-Term Load and Price Forecasting based on Improved Convolutional Neural Network," 2020 3rd International Conference on Computing, Mathematics and Engineering Technologies (iCoMET), Sukkur, Pakistan, 2020, pp. 1-6, doi: 10.1109/iCoMET48670.2020.9074080.

Paper ID: ICSET-2347

LIFE CYCLE ASSESSMENT AND ECONOMICS SUSTAINABILITY OF RENEWABLE ENERGY RESOURCES

Aamir Hamza*, Dr. Zaheer Ahmad

Department of Industrial Engineering, University of Engineering and Technology, Taxila, Pakistan

**Corresponding author*

Email: aamirhamza815@gmail.com

ABSTRACT

There is an immediate demand for decentralized power-generating solutions because a significant portion of the world's population still lacks access to consistent energy. In places without centralized networks, this study analyses the advantages of hybrid energy systems over standalone choices like biogas, solar, and wind, with an emphasis on the areas of KPK Province. To enhance clean energy generation while reducing harmful emissions, the project intends to design a hybrid power system that strikes a compromise between technological feasibility and economic viability. It will achieve this by carefully examining the life cycles (LCAs) of biogas, wind, and solar energy. The Wana case study offers important information about how to choose the hybrid system configuration that will save the most expense. Additionally, an extensive cost analysis is conducted, taking into consideration many variables including capital expenditures, salvage value, fuel expenses, operating and maintenance costs, and replacement costs. The outcome of the research is a carefully designed hybrid power system that can meet local needs. The results of the study show the distribution of energy in various areas: While Abbottabad primarily relies on photovoltaic (PV) sources, Bannu and D.I. Khan show differing levels of reliance on PV and wind energy. Waziristan Wana depends equally on PV and wind turbines. The potential for future wind and solar projects is shown by an analysis of the distribution of energy sources in other locations, including Dir, Haripur, Kohat, Lucky Marwat, Mardan, Mansehra, Miranshah, Murree, Nowshera, Shawal, Swabi, and Zarmula. NASA provides temperature, wind speed, and global horizontal insolation (GHI) data that are used in this research. With a particular focus on meeting the electricity needs of the Province of Khyber Pakhtunkhwa (KPK), the research suggests installing solar and wind turbine systems as feasible options to satisfy the region's energy needs.

KEYWORDS: Energy infrastructure, integrated energy, lifespan evaluation of the environment, ecological balance, power generation from sustainable sources, ecological footprint, and financial assessment.

INTRODUCTION

The challenge in providing clean and cheap electricity to the world's population—especially to the over a billion people who lack access to it—remains a significant concern in this era of fast economic and technological growth. Solutions for decentralized power generation are crucial, especially among humans



ICSET-23



UET Peshawar

disconnected from local or national power networks. Following collaborative efforts, the number of people living without electricity has been effectively lowered to around one billion [1]. It is essential to have accessibility to critical data, grid interaction modeling optimization strategies, and geographic approaches in order to maximize the accuracy of Life Cycle Assessments (LCAs) [2]. These strategies efficiently attenuate the unpredictable behavior of discrete energy sources, thereby augmenting economic and ecological efficacy [3]. For instance, it has been shown that integrating wind turbines with solar panels produces a more constant electrical energy manufacturing, which enhances grid integration. Hybrid systems have been shown to have economic benefits; a \$5 million project in western Minnesota connected solar energy to a wind turbine inverter is one such example. Stunning example of how solar panels and wind turbines are used to provide power include Guangzhou's Pearl River Tower [4]. Life cycle assessment, sometimes known as LCA, is a detailed methodology that evaluates a product's environmental effect at every stage of its lifespan. The establishment of objectives and scope, inventory analysis, impact assessment, and interpretation are all included in the LCA process [5]. Though system variables and data limitations may lead to disparities in LCA research, these variations add up to a significant body of knowledge that decision-makers may use [6]. A survey of the literature around photovoltaic (PV) integration has revealed shortcomings in thorough system design and performance assessment. Energy management techniques and different hybrid renewable energy system configurations have been examined in large part through the HOMER software. An examination of the literature in the field of photovoltaic (PV) integration found knowledge gaps in the areas of thorough system design and performance assessment. Energy management methods and several hybrid renewable energy system designs were evaluated with the help of HOMER software. The integration of solar photovoltaic technology into energy systems is referred to as "photovoltaic (PV) integration" in the context given. A literature review is a systematic analysis of the body of knowledge previously produced on a certain topic. In this case, the review's primary objective was to analyse studies, publications, and research papers pertaining to the integration of photovoltaic systems into energy production. "Knowledge gaps"—domains where knowledge or research on comprehensive system design and performance evaluation is deficient—were discovered during the literature study. This implies that some components of the integration of PV systems into the energy [7 – 10].

RESEARCH METHODOLOGY

This study uses an amalgam of both quantitative and qualitative methods of research, including survey responses and an in-depth review of the literature. The research utilizes life cycle assessment (LCA) and economic analysis to assess the sustainability and financial viability of renewable energy sources in Pakistan. The literature review summarizes the state of the art in Pakistani research on biomass, solar, and wind energy, with an emphasis on social benefits and economic viability. Every renewable energy source is put through a thorough life cycle evaluation to figure out how it will affect the environment at every stage of its existence. The economic study looks at a number of factors related to renewable energy projects in Pakistan, including income, incentives, operating costs, and investment. A life cycle assessment (LCA) is a systematic examination of the environmental impacts of a process, product, or service throughout the course of its entire being. Its main goal is to assess and measure the possible negative effects on the environment and environmental elements of a process or product from the point at origin until disposal. This comprehensive investigation helps with decision-making on sustainability and reducing harmful.

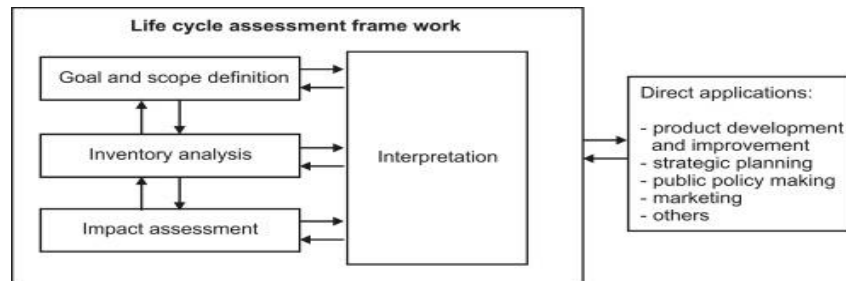


Figure 1: **Represent LCA Farm work**

The life cycle assessment (LCA) of wind, biogas, and photovoltaic (PV) energy systems looks at the environmental effects of each system across its whole duration, considering factors like resource extraction, production, operation, and end-of-life management to find out how environmentally sound each system is. The decisions made on the use of renewable energy are significantly impacted by those assessments. Carefully gathering data on energy use from 100 households—data that was obtained from reliable sources such as NASA and the Pakistan Meteorological Department—was essential in the selection of the research region (Wana). The goal of the work was to create a hybrid energy system that would fulfill Pakistan's varied communities' needs for power. These 100 residences in the Primary and peak loads in the Wana Region were 625.05 kWh and 68.59 kW peak, respectively, depending to load estimates based on actual electricity bills. The collection also included information on the production of biogas from 100 goats and 100 cows—one goat and one cow per household—as well as meteorological data like wind speed and sun radiation. Homer software was employed to do simulations using these large datasets. A 25-year-long "Generic Flat PV" system with a 10-kW capacity, 13% efficiency, and "Generic 1 kWh Lead Acid" energy storage system are shown in the research schematic. It also features a 10-kW "EOCYCLE EO10" wind turbine and includes data on electrical load for a thorough performance evaluation in a range of climatic situations. Additionally, the summer had the most electrical demand, while the winter had the lowest, as per the average electrical load calculation. Over the course of a year, a maximum electric load of 70 kW was recorded; the baseline electrical demand was approximately 625.05 kWh per day, with a peak load of 68.59 kW. Figure 2 shows the daily load profile for the month of January figure 2.



ICSET-23

*Proceedings of the 5th International Conference on Sustainable
Energy Technologies (ICSET 2023) Peshawar, Pakistan
14-15 December 2023*



UET Peshawar

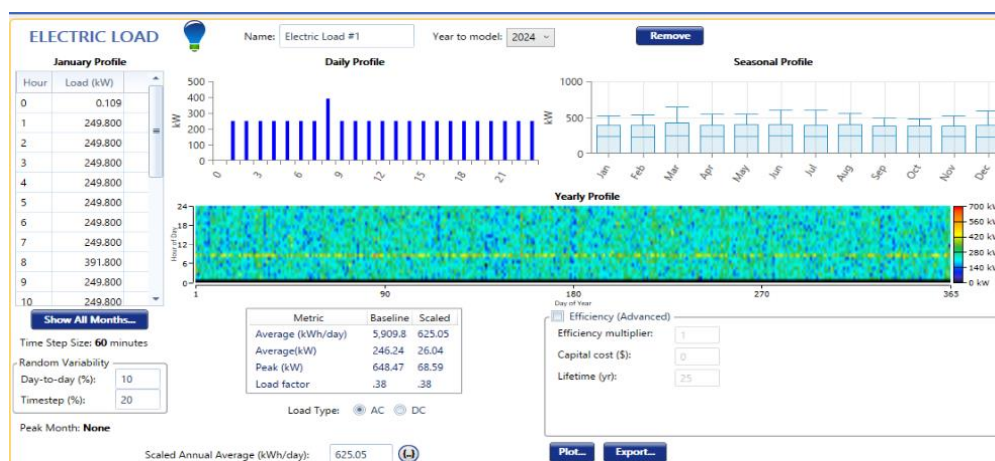


Figure 2: Represent Daily Load Profile, seasonal Profile, and Day of Year

The 10 kW rated capacity Wind Turbine (Eocycle E010) has an initial capital cost of \$6,000 and a \$5,000 replacement cost. The Biogas Genset requires a \$1,000 initial capital investment and a \$1,000 replacement cost. It has a density of 0.720 kg/m³, a lower heating value of 5.5 MJ/kg, and a carbon content of 5.0%. Its 10 kW rated capacity is the same as the wind turbine's. The PV (Photovoltaic) system has a \$500 replacement cost and an initial capital cost of \$600. Its rated capacity is 10 kW, and its temperature coefficient is -0.5. The cost of a lead acid battery is \$250 for the original capital expenditure plus another \$250 for replacement. Its rated capacity is 10 kW, and its string size is 2. Each cow (there are 100 total) produces 4.38 tons of manure annually per head, whereas each buffalo (there 50 total) produces 3.285 tons of dung annual per head.

RESULT AND DISCUSSION

An extensive Life Cycle Assessment (LCA) of each of the three energy sources: biomass, wind turbines, and solar panels, has been performed. The review comprised an extensive examination of each energy source's performance and effects on the environment during all phases of its life cycle, including installation, operation, disposal, and generation. After that, to have a deeper I looked at the LCA data to get an insight into the overall efficiency and environmental sustainability of different energy sources data.

Contribution of Life Cycle periods to Environmental impacts: The following illustration shows the relative impacts of the Manufacturing, Transportation, Installation, Operation, and Decommissioning stages of the life cycle on the environmental effects associated with solar PV systems, wind turbines, and biogas. The graph's bars each indicate the extent to which a certain phase affects each energy source's overall environmental effects. For example, the graph below shows how the manufacturing process adds to the overall environmental footprint of each energy-generating source, with the bars labelled 'Manufacturing'.

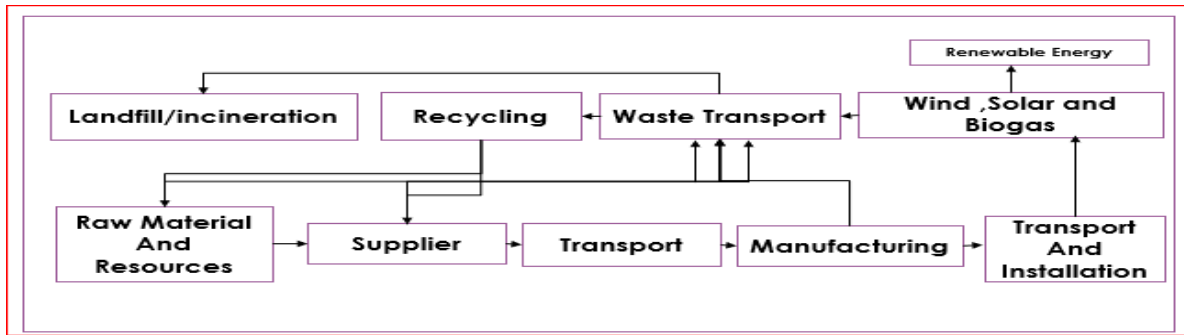


Figure 3: LCA Framework of Wind, Solar, and Biomass

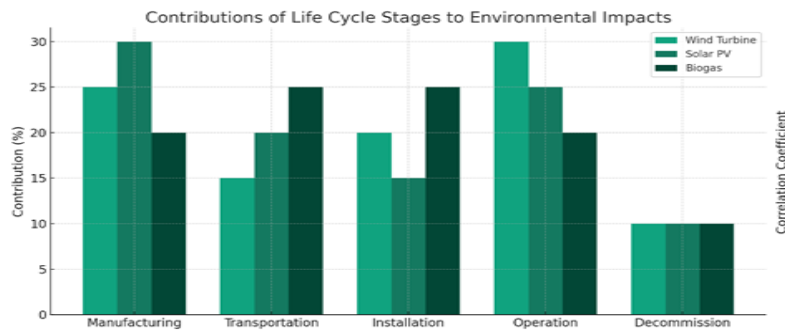


Figure 4: Contributions of Life Cycle Stages to Environmental Impacts

The qualitative environmental effects of wind, solar, and biomass energy are shown in the chart below, taking into consideration factors like air pollution, soil impact, biodiversity and human health, noise pollution, thermal pollution, and visual impact. An outline of the effects related to each component is provided by several colored lines which represent the various energy sources.

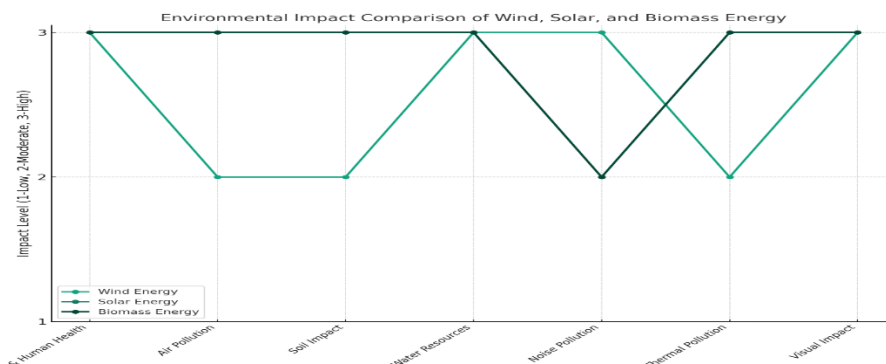


Figure 5: Environmental Impact Comparison of Wind, Solar, and Biomass Energy

Three main components are included in the optimization results: system designs, cost evaluations, and different system variables. Every element—Wind, Solar, Biogas, and Battery—has received a thorough assessment. It's crucial to remember that the initiative, which concentrates on the Waziristan Wana Region, is intended to last for 25 years.

Hybrid System with Wind Biogas and PV:

The combined effects of the Wana region's PV, biogas, and wind installations are shown in this section. As shown in Figure 6, the Net Present Cost (NPC) for wind, biogas, and PV is \$823,052, while operational expenses come to \$30,507 total. Kilowatts (kW) are the unit of measurement for solar panel capacity. The capacity of another energy source, the wind turbine, can be represented by E010 (kW), meaning it's similarly expressed as kilowatts. The capacity of the system's biomass energy component, expressed in kilowatts, is indicated by the symbol bio (kW). Additionally, 1 kWh LA (kW) could also relate to a battery's or storage system's capacity when 1 kWh of energy is discharged. A converter (kW) is a unit of measure used to express a unit's kilowatt capacity for energy conversion (e.g., DC to AC). The word "dispatch" defines the system's operational strategy, such as load following (LF) or cycle charging (CC). Net Present Cost, represented by the syntax NPC (\$), is the system's lifetime total cost adjusted for current value. The average cost per kilowatt-hour of energy delivered throughout the duration of a system's lifecycle is known as the Levelized Cost of Energy, or LCOE (\$/kWh). The operating cost (\$/yr) indicates the annual expenditures related to operating the system.









| Architecture | | | | | | | | | | Cost | | |
|---|---|---|---|------------|------|-------------|----------------|-------------------|----------|-------------|------------------|---------------------------|
|  |  |  |  | PV (kW) | EO10 | Bio (kW) | 1kWh LA (#) | Converter (kW) | Dispatch | NPC (\$) | LCOE (\$/kWh) | Operating cost (\$/yr) |
|  |  |  |  | 194 | 15 | 500 | 814 | 71.7 | LF | \$823,052 | \$0.279 | \$30,507 |

Figure 6: Optimization Result of Hybrid Power System (PV, Wind, Biogas) Using Homer Software

Hybrid system with Wind and PV:

Here we study only PV and wind if someone installs only these two then the total cost is NPC cost is \$852,244 and the operating cost is 28,620 as shown in figure 7.








| Architecture | | | | | | | | | | Cost | | |
|---|---|---|---|------------|------|-------------|----------------|-------------------|----------|-------------|------------------|---------------------------|
|  |  |  |  | PV (kW) | EO10 | Bio (kW) | 1kWh LA (#) | Converter (kW) | Dispatch | NPC (\$) | LCOE (\$/kWh) | Operating cost (\$/yr) |
|  |  |  |  | 283 | 16 | | 798 | 66.8 | CC | \$852,244 | \$0.289 | \$28,620 |

Figure 7: Optimization Result of Hybrid Power System (PV, Wind) Using Homer Software

Hybrid System with Solar and Biogas:

Here we study only PV and Biogas and NPC cost is \$1.1M and operating cost is \$51,973 as shown in figure 8.










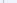





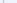






| Architecture | | | | | | | | | | Cost | | | |
|---|---|---|---|---|---|--|--|---|--|--|--|---|--|
|  |  |  |  |  | PV (kW)  | EO10  | Bio (kW)  | 1kWh LA (#)  | Converter (kW)  | Dispatch  | NPC (\$)   | LCOE (\$/kWh)   | Operating cost (\$/yr)   |
|  |  |  |  |  | 304 | | 500 | 928 | 76.5 | LF | \$1.11M | \$0.375 | \$51,973 |

Figure 8: Optimization Result of Hybrid Power System (PV, Biogas) Using Homer Software

Hybrid System with Solar:

Here we study only PV and NPC cost is \$1.24M and operating cost is \$47,372 as shown in figure 9.







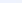

| Architecture | | | | | | | | | | Cost | | | |
|---|---|---|---|---|---------|------|----------|-------------|----------------|----------|----------|---------------|------------------------|
|  |  |  |  |  | PV (kW) | EO10 | Bio (kW) | 1kWh LA (#) | Converter (kW) | Dispatch | NPC (\$) | LCOE (\$/kWh) | Operating cost (\$/yr) |
|  | | |  |  | 501 | | | 1,220 | 82.5 | CC | \$1.24M | \$0.420 | \$47,372 |

Figure 9: Optimization Result of Hybrid Power System(PV) Using Homer Software

Hybrid System with Wind and Biogas:

Here we study only P wind and Biogas and NPC cost is \$1.3M and operating cost is \$64,769 as shown in figure 10.

| Architecture | | | | | | | | | | Cost | | | |
|---|---|---|---|---|---------|------|----------|-------------|----------------|----------|----------|---------------|------------------------|
|  |  |  |  |  | PV (kW) | EO10 | Bio (kW) | 1kWh LA (#) | Converter (kW) | Dispatch | NPC (\$) | LCOE (\$/kWh) | Operating cost (\$/yr) |
| |  |  |  |  | 34 | 34 | 500 | 960 | 216 | LF | \$1.34M | \$0.453 | \$64,769 |

Figure 10: Optimization Result of Hybrid Power System (Wind, Biogas) Using Homer Software

Hybrid System with Wind:

Here we study only wind and NPC cost is \$1.34M and operating cost is \$64,769 as shown in the figure 11.







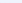

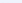

| Architecture | | | | | | | | | | Cost | | | |
|---|---|---|---|---|---------|------|----------|-------------|----------------|----------|----------|---------------|------------------------|
|  |  |  |  |  | PV (kW) | EO10 | Bio (kW) | 1kWh LA (#) | Converter (kW) | Dispatch | NPC (\$) | LCOE (\$/kWh) | Operating cost (\$/yr) |
|  |  |  |  |  | 34 | 34 | 500 | 960 | 216 | LF | \$1.34M | \$0.453 | \$64,769 |

Figure 11: Optimization Result of Hybrid Power System (Wind) Using Homer Software

Electrical Perspective:

The system's electrical statistics are shown in Figure 12. To meet the energy demand, the system generates 1.31% from biogas, PV 71.3%, and Wind turbines 27.4%. Furthermore, the system generates 2.69% more electricity than it needs. The renewable fraction of the total load, which is 534742KWh/yr., indicates that 98% of the load is provided by renewable sources, such as solar, wind, and batteries.



ICSET-23

Proceedings of the 5th International Conference on Sustainable
Energy Technologies (ICSET 2023) Peshawar, Pakistan
14-15 December 2023



UET Peshawar

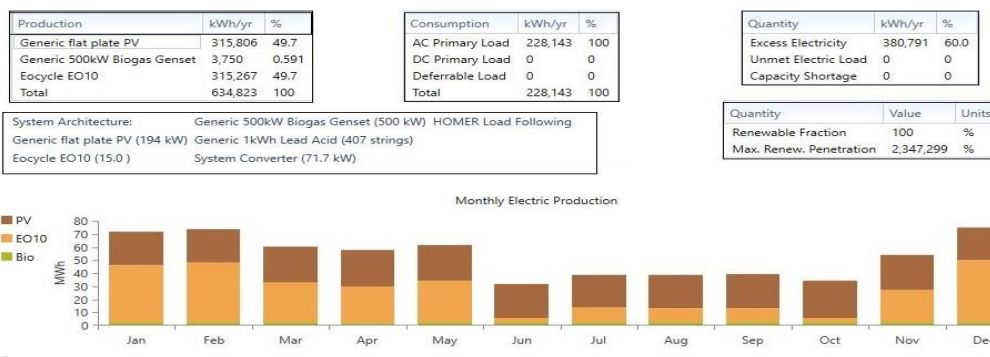


Figure 12: Electrical Statistics (Year, Monthly, Electric Production, Consumption, Quantity) KWh

CONCLUSION

The research indicates that a hybrid system utilizing solar, biogas, wind, and battery technologies is the most environmentally and financially sustainable method to power Wana. A 15–25-year return on investment is anticipated, with salvage value held all through that time. Actual testing, battery storage optimization, comprehensive environmental impact studies, economic analysis, research on additional renewable energy sources, and the development of decentralized microgrids are among the topics of study that follow. To meet Wana's energy needs, the hybrid system makes use of a range of energy sources. It gets electricity from wind turbines (27.4%), photovoltaic (PV) systems (71.3%), and methane (1.31%). The net present cost (NPC) of wind, biogas, and PV combined is \$823,052, with an operational cost of \$30,507. Given the abundance of renewable resources in Pakistan, With Pakistan's availability of renewable resources, the goal of this research is to improve self-sufficiency in isolated areas while lowering reliance on conventional fossil fuels. Additionally, the distribution of energy across the Province of KPK highlights the potential for future power production with the installation of solar and wind turbine projects. With an emphasis on meeting electrical demands, NASA has given data on temperature, wind speed, and global horizontal irradiance (GHI).

REFERENCES

1. Khoja, A. H., et al., *An analysis of Pakistan's energy policies and how they affect the growth of bioenergy*. Article 101246 in *Sustainable Energy Technologies and Assessments*, (2021), 46.
2. Combs, C.; Guenther, E.; Jordaan, S.M. *Life cycle evaluation of electricity generation: A thorough review of spatiotemporal methodologies*. *Scientific and Industrial Progress*, (2021), vol. 3, pp.100-58.
3. Al-Antaki, A. M., Kuvshinov, V. V., Krit, B. L., Al-Rufae, F. M., Aldali, L. M., & Morozova, N. V. *Research on hybrid solar and wind energy systems for the Iraqi energy sector*. 56(4) *Applied Solar Energy*, (2020), pp.284-290.
4. Shin, C., Cho, Y., Kim, H., Chowdhury, O., & Park, J. *HOMER-Based Hybrid Renewable Energy System Optimization*. *Ubiquitous Computing and Advances in Computer Science*, (2015), pp. 93–99.
5. M. Brunsseau *Alternatives to Global Change and Pollution: Sustainable Development*. *Environmental and Pollution Science*, Cambridge, MA, USA: Academic Press, (2019), pp. 585–603.



ICSET-23

*Proceedings of the 5th International Conference on Sustainable
Energy Technologies (ICSET 2023) Peshawar, Pakistan
14-15 December 2023*



UET Peshawar

6. Goglio, P.; Williams, A.; Huisingh, D.; Zhang, Z.; Tavoni, M.; Balta-Ozkan, N.; Harris, N.; Williamson, P. *Life cycle assessment (LCA) of greenhouse gas removal technologies: advancements and problems in the battle against climate change*. Cleaner Production Journal, (2020), 244, 118896.
7. Hertwich, E.G. and Arvesen, A. *An evaluation of current knowledge and research requirements is conducted to assess the life cycle environmental implications of wind power*. Reviews of Sustainable and Renewable Energy, (2012), 16, 5994–6006.
8. Galil, B. S., Panov, V., and Nehring, S. *The impact of globalization and climate change on rivers as highways for invasion Biological Invasion*. Springer. (2008), Pp. 59–74
9. Jabeen, A., Ahmad, M., Zafar, M., & Ahmad, F. Khan, M. A. *Indigenous peoples of Islamabad, Pakistan's Margalla Hills National Park make use of commercially significant plants*. Journal of Biotechnology in Africa, (2009), 8 (5).
10. D. M. Kabiye *An assessment of a hybrid mini-grid system's performance. doctoral dissertation*, University of Makerere. (2021), pp-21-22